Energy, Mines and
Resources Canada

Énergie, Mines et
Ressources Canada

CANMET

Canada Centre
for Mineral
and Energy
Technology

Centre canadien
de la technologie
des minéraux
et de l'énergie

POTASH MINING PROJECT

PROJET D'EXPLOITATION DE LA POTASSE

[illegible]ERAUX

USE OF BACKFILL IN NEW BRUNSWICK POTASH MINES

VOLUME 1

EXECUTIVE SUMMARY

May, 1987

Final Report By:

DENISON-POTACAN POTASH COMPANY
Sussex, New Brunswick

Prepared by:

MRAZ PROJECT CONSULTANTS LTD
Saskatoon, Saskatchewan

Work on the Project was conducted under the auspices of the Canada Centre for Mineral and Energy Technology, Energy, Mines and Resources Canada, funded as part of the Canada/New Brunswick Mineral Development Agreement.

DSS FILE NO: 14SQ.23440-5-9031

DSS CONTRACT SERIAL NO: OSQ85-00208

CANMET PROJECT NO: 1.4.09.05

CANMET SCIENTIFIC AUTHORITY: Dr. G. Herget

70 pp

MICROMEDIA

ACKNOWLEDGEMENTS

The contribution of various organizations and their personnel in accomplishing the work performed during this research project is duly recognized.

The participants included various Denison-Potacan personnel who assisted in the project, in particular, the geology and mining departments whose manpower and equipment were often utilized during the in-situ testing.

The staff and WATSALT laboratory of the University of Waterloo provided much needed testing facilities and technical expertise in the testing, analysis and interpretation of collected samples. In addition, their computer modelling and numerical analysis capabilities have served to establish a working computer model for the Denison-Potacan mine.

The staff of Mraz Project Consultants Ltd were actively involved in the design and supervision of the test program and provided analytical expertise.

A special thanks is extended to Dr. G. Herget, the Scientific Authority, and to the Canada Centre for Mineral and Energy Technology (CANMET)/New Brunswick Mineral Development Agreement through which a large portion of the field test program was funded under the project name of "Use of Backfill in New Brunswick Potash Mines".

LIST OF REFERENCES

1. Waugh, D.E.C., and Urquhart, B.R., "The Geology of Denison-Potacan's New Brunswick Potash Deposit", Sixth International Symposium on Salt, 1983, Vol. 1, Toronto, pp 85-98.

2. Ibid., p 89.

3. Ibid., p 94.

USE OF BACKFILL IN NEW BRUNSWICK POTASH MINES

VOLUME 1
EXECUTIVE SUMMARY

TABLE OF CONTENTS

1.0 SUMMARY

2.0 INTRODUCTION

3.0 RESEARCH OBJECTIVES

4.0 INTACT ROCK SPECIMEN TESTING
4.1 INTACT ROCK CREEP TESTING
4.2 BRITTLE YIELD TESTING
4.3 ELASTIC MODULUS DETERMINATION
4.4 PROPERTY CRITERIA FOR NUMERICAL MODELLING
4.4.1 MECHANICAL PROPERTIES
4.4.2 RHEOLOGICAL PROPERTIES

5.0 BACKFILL MATERIALS TESTING
5.1 GRAIN SIZE
5.2 MINERALOGICAL
5.3 MOISTURE CONTENT
5.4 SPECIFIC GRAVITY
5.5 BACKFILL PLACEMENT DENSITY LABORATORY TESTING
5.6 BACKFILL PLACEMENT DENSITY SURFACE TESTING (FULL SCALE EQUIPMENT)

6.0 BACKFILL CONSOLIDATION TESTING
6.1 CONSOLIDATION TEST RESULTS

7.0 BACKFILL TRIAXIAL TESTING

8.0 CALIBRATION OF SASKATCHEWAN RESEARCH COUNCIL (SRC) WAFER CELL

9.0 IN-SITU TESTING

10.0 INTACT ROCK BEHAVIOURAL MODEL

11.0 PREDICTION OF LONG TERM RESPONSE OF DENISON-POTACAN STOPES

12.0 EXCESS TAILINGS VOLUME STORAGE

13.0 CONCLUSIONS

LIST OF FIGURES

FIGURE 2.1 GEOLOGY OF MONCTON SUBBASIN IN NEW BRUNSWICK

FIGURE 2.2 SCHEMATIC OF CASSIDY LAKE FORMATION POTASH MEMBER

FIGURE 5.4 CREEP LAW USED IN MODELLING

FIGURE 10.1 RANGES OF BEHAVIOUR FOR A SALT ROCK OPENING

FIGURE 11.1 STOPE/BACKFILL INTERACTION PREDICTION, DPPC BACKFILL DENSITY VS. TIME

LIST OF TABLES

TABLE 5.1 PLACEMENT METHODS: RANGES OF EXPECTED POROSITY

TABLE 5.2 SURFACE TRIALS: BACKFILL DENSITY

TABLE 7.1 BRITTLE YIELD TRIAXIAL TESTING RESULTS FOR BACKFILL SAMPLES CONSOLIDATED TO 90%

TABLE 11.1 DENISON-POTACAN 4 M X 42 M STOPE, BACKFILL DENSITY VS. TIME

TABLE 11.2 DENISON-POTACAN 12.5 M X 42 M STOPE, BACKFILL DENSITY VS. TIME

TABLE 11.3 DENISON-POTACAN 30 M X 42 M STOPE, BACKFILL DENSITY VS. TIME

SECTION 1.0

1.0 SUMMARY

Denison-Potacan Potash Company, jointly with the University of Waterloo (U of W) and Mraz Project Consultants Ltd (MPC), submitted a proposal dated July, 1985, in response to the Department of Supply and Services Canada's (DSS) request for proposal for the use of backfill in New Brunswick potash mines.

The joint proposal of Denison-Potacan, U of W and MPC was accepted by DSS and Contract No. 0SQ85-00208, entitled "Use of Backfill in New Brunswick Potash Mines" was initiated.

This Final Report is submitted in compliance with the terms of the contract.

SECTION 2.0

2.0 INTRODUCTION

The Denison-Potacan Potash Company mine site is located southwest of Sussex, New Brunswick, as shown in Figure 2.1. The company's Clover Hill deposit was first identified by surface exploratory drilling in 1973 conducted under the direction of the New Brunswick Department of Natural Resources. In 1975, the Government of New Brunswick granted International Minerals and Chemical Corporation (IMC) the right to explore and develop the Clover Hill property. IMC conducted a surface exploration drilling program which defined approximately 200 million tonnes of potash ore grading 28% K_2O. In 1979, Denison Mines Limited purchased the Clover Hill property and, in 1980, formed a partnership with Potash Company of Canada. An extensive underground exploration program led to a decision in 1983 to develop the property into a producing mine capable of producing 1.3 million tonnes of product per year. Potash production commenced in July, 1985.

The Clover Hill potash deposit is part of the Cassidy Lake Evaporite Formation of the Windsor Group. The deposit is confined to the Marchbank Syncline, which is the most southerly major structural feature of the Moncton Subbasin (see Figure 2.1). The evaporite interval has been subdivided into four members:

1. Basal Halite;
2. Middle Halite;
3. Potash;
4. Upper Halite.

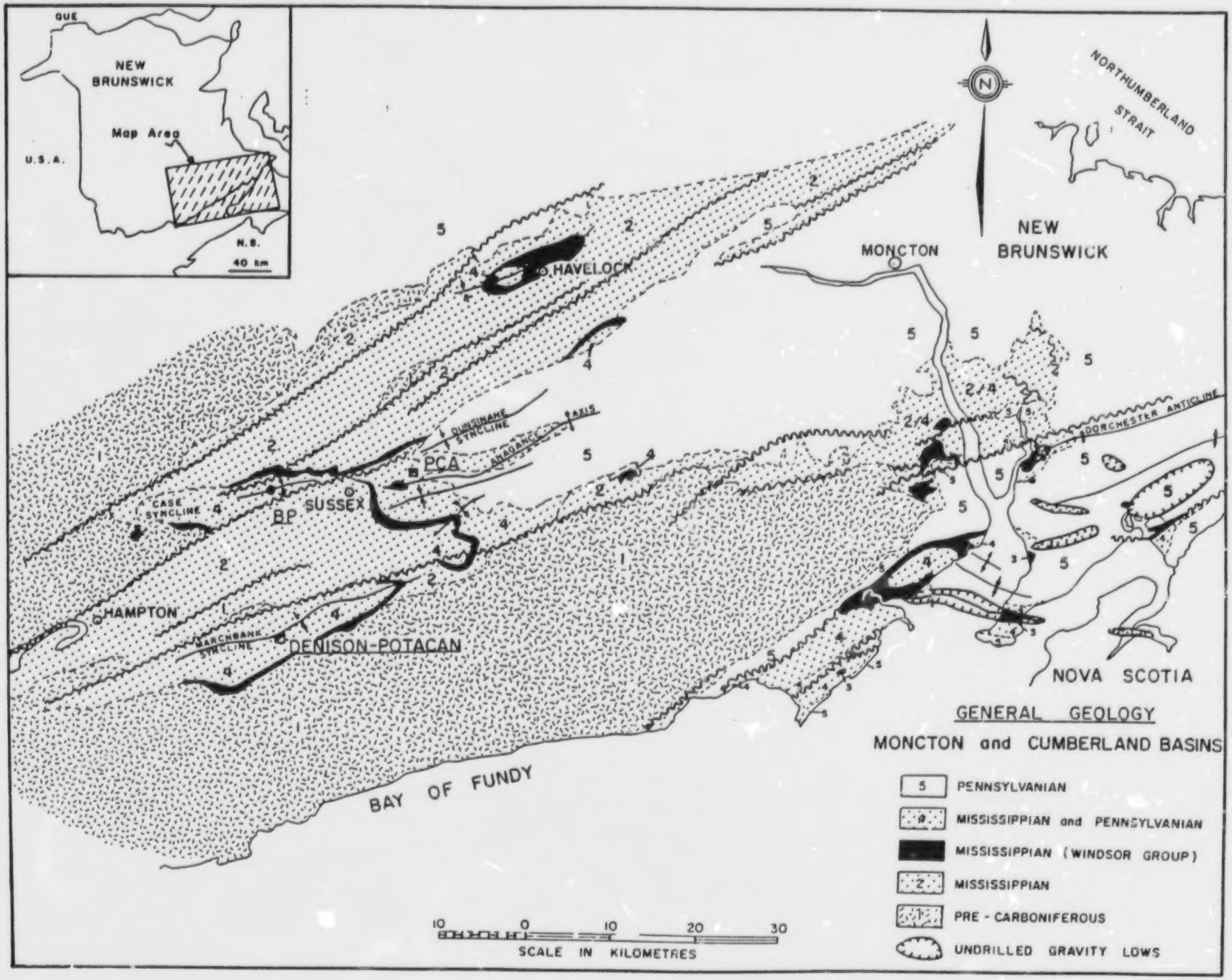
QUE
NEW BRUNSWICK
Map Area
U.S.A.
N.S.
40 km
NORTHUMBERLAND STRAIT
NEW BRUNSWICK
MONCTON
HAVELOCK
SUSSEX
BP
PCA
DUNSINANE SYNCLINE
ANAGANCE AXIS
CASE SYNCLINE
HAMPTON
MARCHBANK SYNCLINE
DENISON-POTACAN
DORCHESTER ANTICLINE
NOVA SCOTIA
BAY OF FUNDY
1
2
2/4
4
5
GENERAL GEOLOGY
MONCTON and CUMBERLAND BASINS
5 PENNSYLVANIAN
4 MISSISSIPPIAN and PENNSYLVANIAN
MISSISSIPPIAN (WINDSOR GROUP)
2 MISSISSIPPIAN
1 PRE - CARBONIFEROUS
UNDRILLED GRAVITY LOWS
10 0 10 20 30
SCALE IN KILOMETRES

FIGURE 2.1

GEOLOGY OF THE MONCTON SUBBASIN IN NEW BRUNSWICK (Reference 2)

The potash member consists of the Lower Gradational Bed and the Sylvinite Bed. The Lower Gradational Bed is comprised of medium to fine-grained brown to orange halite with sylvite clusters being present. The Sylvinite Bed is composed of fine-grained sylvite and halite.

The Sylvinite Bed is subdivided into five generally distinct zones based on mineralization, percent insolubles and colour. These have been designated from oldest to youngest as the A, B, C, D and E zones with the B and C zones comprising the main ore bed (see Figure 2.2). The geology of the Clover Hill deposit has been previously documented in detail by Waugh and Urquhart (Reference 1).

The Denison-Potacan potash deposit is approximately 10 kilometres long with a maximum width of 3.5 kilometres and is generally found at a depth of 850 metres. The grade of the deposit is one of the world's highest with an average content of 28% K_2O.

The room and pillar method of mining, with delayed backfilling, is being employed using both continuous mining and drill and blast techniques. A conveyor belt system is used for transporting ore from the mining areas to an underground storage bin and then to the production shaft where ore is hoisted to the surface in 25 tonne skips.

The continuous mining technique being employed in the mine using primarily twin rotor Marietta mining machines has been well established in the potash mines in Saskatchewan.

At present, drill and blast methods and equipment are being used on a developmental basis where there are varying geological conditions. Initial results from this program have been very encouraging.

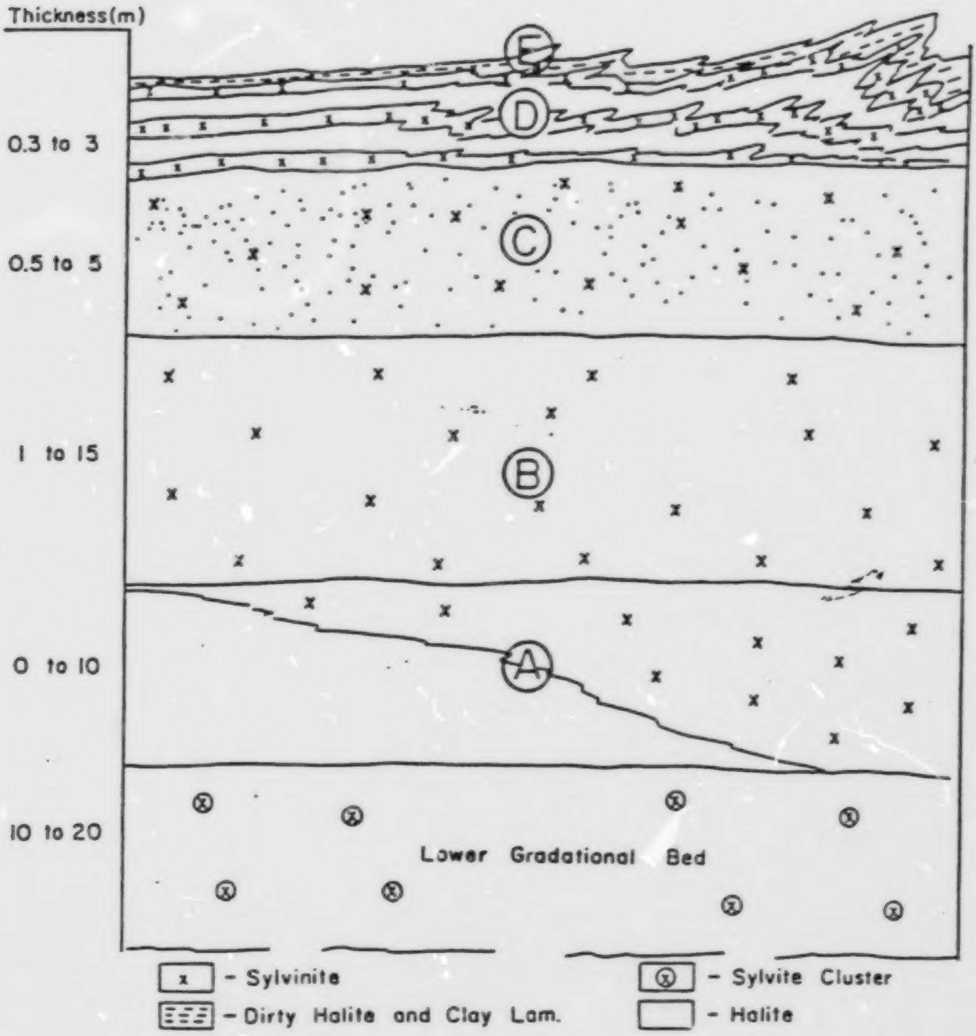
Thickness(m)
0.3 to 3
0.5 to 5
1 to 15
0 to 10
10 to 20
E
D
C
B
A
Lower Gradational Bed
x - Sylvinite
Dirty Halite and Clay Lam.
Sylvite Cluster
Halite

Figure 2.2

Schematic of Cassidy Lake Formation
Potash Member

(Reference 3)

An important component of mine operations at Denison-Potacan is the placement of tailings backfill in the mined out underground workings. The placement of tailings backfill underground allows for an environmentally safe tailings disposal method, as well as, the potential increased recovery of potash resources due to secondary pillar recovery.

The Denison-Potacan mine is the second potash mine to begin operations in the Province of New Brunswick. The Potash Company of America (PCA) mine currently uses tailings backfill in its mining operations principally as an aid to the mining cycle and not as a means for secondary pillar recovery. No other potash mine in Canada practices backfilling underground in any significant quantity.

Thus, in planning for the placement of tailings backfill in the mined out underground workings, a number of technical questions and issues required solving prior to the commencement of backfilling.

Recognizing the critical nature of these questions and issues raised and their relevance to other potash mines in New Brunswick and Canada, Denison-Potacan retained the services of Mraz Project Consultants Ltd (MPC) of Saskatoon, Saskatchewan to submit a proposal for a research program into the use of backfill that would be partially funded by the provincial government of New Brunswick and CANMET.

Thus, in July 1985, a proposal was submitted to the Minister of Supply and Services bearing an overall title of "Use of Backfill in New Brunswick Potash Mines Proposal". This was jointly submitted by Denison-Potacan, MPC and the Department of Earth Sciences, University of Waterloo in response to a Request for Proposal from the Department of Supply and Services.

The stated goal of the research program was to accomplish basic scientific research in backfill from the plant tailings stream that would be returned to mined out rooms so as to:

i) Accomplish an environmentally desirable method of tailings disposal;

ii) Provide support and stabilization to the mine structure leading to increased resource recovery mining methods.

A contract was awarded to Denison-Potacan to proceed with the research work and was subsequently entitled "Phase I - Use of Backfill in New Brunswick Potash Mines".

The following is a Final Report of the work performed under DSS Contract Serial No. 0SQ85-00208/CANMET Project No. 1.4.09.05.

SECTION 3.0

3.0 RESEARCH OBJECTIVES

In the simplest of terms, the research project was designed to provide a technical basis for the use of tailings backfill material underground in the mined out areas of the Denison-Potacan mine, to dispose of the tailings material in an environmentally acceptable manner and to improve the total reserve recovery in the mine.

By backfilling, the mine openings and pillars would be stabilized to enable a second stage mining operation to recover a portion of those pillars that had been left behind in the first stage mining operation and, hence, improve the total reserve recovery.

The research project included a number of work components to achieve these objectives:

- The collection and laboratory analysis of intact rock samples.
- The collection and laboratory analysis of backfill material.
- The installation and monitoring of in-situ rock mechanics instrumentation.
- The development of various constitutive laws for the interactive stress behaviour of backfilled mine openings.

Active participants in the research work were the engineering, geological and operations staff at Denison-Potacan, various faculty and student members working with Dr. M.B. Dusseault of the University of Waterloo and various staff of the consulting firm, MPC, under the direction of D. Mraz.

SECTION 4.0

4.0 INTACT ROCK SPECIMEN TESTING

The primary objective of the intact rock specimen testing program was to provide material, mechanical and rheological properties for input to the computational analyses that would be representative of in-situ conditions at the Denison-Potacan mine.

4.1 INTACT ROCK CREEP TESTING

A substantial database for Sylvinite Bed, Upper Halite and the Lower Gradational Bed material was established. In total, 36 creep tests were performed that established the steady state strain rate for these materials at various stress differences.

4.2 BRITTLE YIELD TESTING

Again, a substantial database for Sylvinite Bed, Upper Halite and the Lower Gradational Bed was established. In total, 14 brittle yield tests were performed that established the brittle yield criteria for these materials under various vertical and confining stresses.

4.3 ELASTIC MODULUS DETERMINATION

The modulus of elasticity was determined through unload/reload testing. The differences in stress on the curves were divided by the appropriate difference in strain to determine the modulus.

Unload/reload tests were performed on all three saltrock materials to determine the modulus of elasticity.

4.4 PROPERTY CRITERIA FOR NUMERICAL MODELLING

Based on the laboratory testing summarized previously and described in detail in Volume 2 of the Final Report, the following criteria have been established for intact rock in the numerical modelling exercise.

4.4.1 MECHANICAL PROPERTIES

Sylvinite Bed:

Unconfined compressive strength	26.25 MPa
Modulus of elasticity	5.462 GPa
Tensile strength	1.65 MPa

Upper Halite:

Unconfined compressive strength	29.22 MPa
Modulus of elasticity	10.210 GPa
Tensile strength	2.00 MPa

Lower Gradational Bed:

Unconfined compressive strength	28.40 MPa
Modulus of elasticity	6.908 GPa
Tensile strength	1.48 MPa

The failure envelopes plotted through brittle yield testing were fitted to an empirical expression developed by Rothenburg:

$$\sigma_1 = \frac{\sigma_c}{2}\left[(1 - MR) + \sqrt{(1 + MR)^2 + 4m\frac{\sigma_3}{\sigma_c}}\right]$$

$$R = \frac{\sigma_T}{\sigma_c}$$

Where:

σ_1	.....	maximum principal stress
σ_3	.....	minimum principal stress
σ_C	.....	unconfined compressive strength
σ_T	.....	tensile strength
M	.....	empirical constant

The following values give the best fit equation to the laboratory data:

	R	M
Sylvinite Bed	0.0629	53.8
Upper Halite	0.0684	500.0
Lower Gradational Bed	0.0521	34.2

4.4.2 RHEOLOGICAL PROPERTIES

The power law fit of Denison-Potacan test data was determined by the linear regression method. Because the measured in-situ strain rates were two to three orders of magnitude lower than those tested in the labortory, it was decided to use the power law of the normalized form:

$$\dot{\epsilon}_{ss} = \dot{\epsilon}_k \left\{ \frac{\Delta\sigma}{2K} \right\}^n$$

Where:

$\dot{\epsilon}_{ss}$	.....	steady state strain rate
$\dot{\epsilon}_k$	.....	steady state strain rate at Prandtl Limit
K	.....	Prandtl Limit
$\Delta\epsilon$	.....	principal stress difference
n	.....	empirical constant

The rationale for this approach is explained in Volume 4, as is the method of determining the Prandtl Limit. The magnitudes of exponent n above the stress level of 2K was accepted as determined by the power law fit and the magnitudes of $\dot{\epsilon}_k$ was derived from extensometer readings in the test room and the test stope. The magnitude of exponent n below the stress level of 2K was estimated. Following are the properties used in numerical modelling (Figure 5.4):

	2K (MPa)	$\dot{\epsilon}_k$ (s^{-1})	$\Delta\sigma^{n}_{\geq 2K}$	$\Delta\sigma^{m}_{<2K}$
Sylvinite Bed	17.6	3×10^{-11}	6.0	1.0
Upper Halite	20.0	3×10^{-11}	4.5	1.0
Lower Gradational Bed	18.8	3×10^{-11}	4.8	1.0

The results of the program calibration runs, as described in Volume 5, support the validity of the approach used.

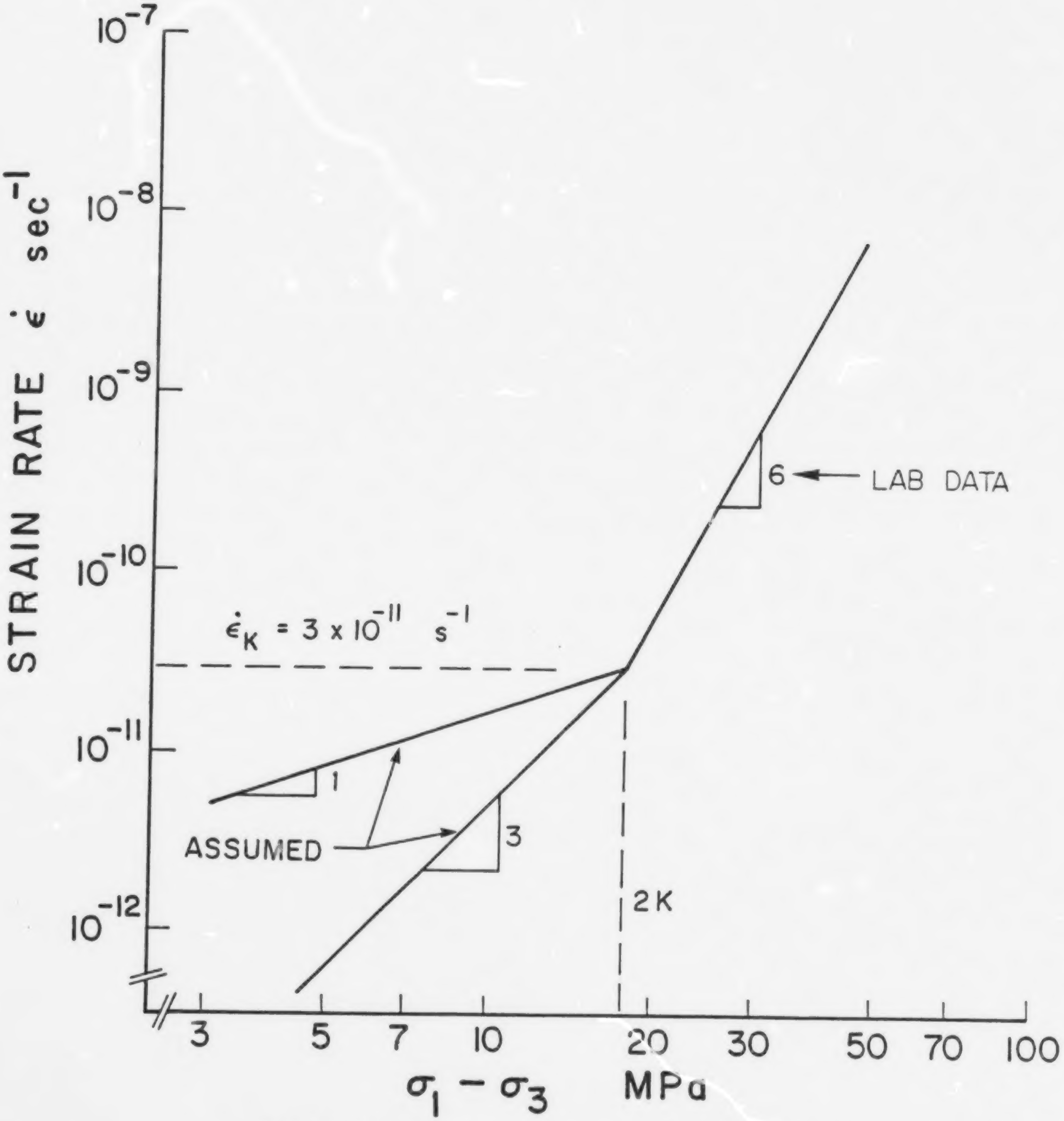

CREEP LAW USED IN MODELLING

FIGURE 5.4

SECTION 5.0

5.0 BACKFILL MATERIALS TESTING

The primary objective of the backfill laboratory testing program was to provide material properties for input to the computational analyses that would be representative of in-situ conditions at the Denison-Potacan mine.

The backfill material will be expected to densify during placement and closure of the mine openings until it provides structural support for the overburden during the second stage or pillar mining phase of Denison-Potacan's mining operation.

5.1 GRAIN SIZE

In comparison to conventional hard rock tailings backfill material, the Denison-Potacan backfill material:

i) is characteristically coarser;
ii) is similarly graded;
iii) contains negligible slimes materials (sizes less than 200 mesh or 0.075 mm).

In comparison to the Rocanville salt tailings backfill material tested by others, the Denison-Potacan backfill is considerably finer in grain size distribution.

5.2 MINERALOGICAL

Only two mineral types were detected in the backfill samples, halite and sylvite. In general, the amount of sylvite was less than 5%, the balance being made up of primarily clear and colored halite.

No discernible insoluble component exists in the backfill, although trace amounts of clays were visible in the tailings pond area.

5.3 MOISTURE CONTENT

The average uncorrected moisture content is 7.53% corresponding to a corrected moisture content of 7.8%. However, it should be noted that the backfill drains readily and a long term moisture content of 2.5% was used for numerical modelling purposes.

It should be noted here that the mass balance information derived by Kilborn for the operation of the process plant actually anticipated a somewhat higher moisture content corresponding to 8.6% by weight.

5.4 SPECIFIC GRAVITY

The calculated average specific gravity of the proposed backfill is 2.15.

5.5 BACKFILL PLACEMENT DENSITY LABORATORY TESTING

Table 5.1 is a summary and reference table of values to illustrate the porosity percentages to be expected in various mining room heights assuming various achievable backfill densities and placement methods.

TABLE 5.1

PLACEMENT METHODS: RANGES OF EXPECTED POROSITY

LABORATORY PLACEMENT METHOD	SPECIFIC GRAVITY (Dry)	POROSITY (dry) %	AVERAGE POROSITY PERCENTAGES 10m High %	15m High %	20m High %	30m High %
Loose Or Flinger Placement	1.00	53.7	58.33	56.79	56.02	55.25
	1.10	49.1	54.17	52.47	51.62	50.77
	1.20	44.4	50.00	48.15	47.22	46.30
Rodding Placement	1.30	39.8	45.83	43.83	42.82	41.82
Slurry sed'n, Vibro-Comp'n	1.40	35.2	41.67	39.51	38.43	37.35
	1.50	30.6	37.50	35.19	34.03	32.87
Bomag Dual-Drum Comp.*	1.60	25.9	33.33	30.86	29.63	28.40
	1.70	21.3	29.17	26.54	25.23	23.92
	1.80	16.7	25.00	22.22	20.83	19.44
	1.90	12.0	20.83	17.90	16.44	14.97
	2.00	7.4	16.67	13.58	12.04	10.49
	2.10	2.8	12.50	9.26	7.64	6.02
Solid Rock-Salt	2.16	0.0	10.00	6.67	5.00	3.33

NOTE: In all cases it is assumed that fill will be placed at an average density as shown to within 1 metre of the back.

* Achieved in surface trials at mine site.

5.6 BACKFILL PLACEMENT DENSITY SURFACE TESTING (FULL SCALE EQUIPMENT)

A surface test was designed using a Wagner ST-8A scooptram vehicle to construct various lift heights of backfill of from 0.45 m to 1.2 m with vehicle travel effects from compaction of the fill under the tires.

To evaluate the potential of auxiliary compaction using vibratory roll equipment, a Bomag dual drum vibratory compaction machine, model BW655 was used, compacting lifts of 0.18 m and 0.25 m of backfill.

The results of these trials are summarized in Table 5.2.

The test results from the surface trials supported the trend shown in the laboratory testing, i.e. vibro-compaction provides an effective auxiliary means of achieving higher backfill density.

TABLE 5.2

SURFACE TRIALS:
BACKFILL DENSITY

TEST METHOD	LIFT HEIGHT (m)	DRY DENSITY (t/m³)	
ST-8A	0.45	1.324	Average
ST-8A	1.20	1.470	1.379 t/m³
ST-8A	0.45*	1.296	
ST-8A	1.20*	1.425	
Bomag	0.18	1.631	Average
Bomag	0.25	1.591	1.611 t/m³

* Indicates density measured one day after compaction.

SECTION 6.0

6.0 BACKFILL CONSOLIDATION TESTING

The objective of the backfill consolidation testing was twofold:

i) To establish a support function;

ii) To establish the failure criterion for the fill at less than 100% consolidation.

The support function will be interactive with the intact rock stress function, such as to modify the stress conditions around the mine opening and thereby affect closure rates by some amount.

The failure criterion needed to be established so as to predict the limits of closure velocity associated with brittle failure of the consolidated backfill.

The emphasis of this research work was placed on the testing and assessment of the properties of highly consolidated samples containing porosity, for example, of only 5% to 20% by volume. This porosity will approximate much more closely the condition of the backfill at the time when second stage mining will occur.

6.1 CONSOLIDATION TEST RESULTS

Two characteristics of importance have been derived from the testing results:

i) Initial consolidation occurs rapidly from a loosely packed condition;

ii) At constant uniaxial stress conditions, consolidation continues to occur at significant rates at typical densities achievable by practical placement methods.

Consolidation testing over a period of ninety days supported the initial hypothesis that the emplaced backfill will have limited support capability prior to almost complete elimination of porosity in the fill during the closure history of the backfilled openings.

The function used to model the stiffness or support characteristics of the backfill in the numerical modelling exercise is a non-linear elastic function. As stress increases in the backfill, the modulus of elasticity increases and, hence, the backfill is simulated to become "stiffer".

Additional testing is proposed for this area.

SECTION 7.0

7.0 BACKFILL TRIAXIAL TESTING

The objective of the backfill triaxial testing was to develop brittle yield failure envelopes for the backfill material.

Table 7.1 is a summary and reference table of results to date.

These results are insufficient to enable the development of brittle yield failure envelopes and additional testing, beyond the scope of Phase I of the research project, is required.

TABLE 7.1

BRITTLE YIELD TRIAXIAL TESTING RESULTS FOR BACKFILL SAMPLES CONSOLIDATED TO 90%

SAMPLE NUMBER	TIME OF PREPARATION (hrs)	UNCONFINED STRENGTH (psi)	(MPa)
1-90	36	1009.8	6.96
2-90	36	972.8	6.71
3-90	1	407.1	2.81
4-90	1	645.0	4.45

SECTION 8.0

8.0 CALIBRATION OF SASKATCHEWAN RESEARCH COUNCIL (SRC) WAFER CELL

There were twenty-one SRC wafer cells used in the in-situ testing at the Denison-Potacan mine to verify stress conditions. Calibration runs on two wafer cells were carried out in the laboratory. The results of these tests indicate that the in-situ stress measurements obtained with wafer cells are reasonably accurate. Within the range of stresses of 10.0 to 20.0 MPa, the mean deviation of measured stress was 0.37 MPa or 2.4%

Additional work is recommended to calibrate these cells for a full range of stress conditions.

SECTION 9.0

9.0 IN-SITU TESTING

The significance and value of collecting and analyzing in-situ rock mechanics data was recognized and acted upon by Denison-Potacan as early as 1982, leading to the establishment of the Rock Mechanics Station (Test Room) in February, 1983.

An extensive underground exploration program led to a decision in 1983 to develop the property into a producing mine capable of producing 1.3 million tonnes of product per year. Potash production commenced in July, 1985.

During this time, and to the present day, Denison-Potacan have installed, monitored and analyzed in detail the data from the following sites:

- Rock Mechanics Station (Test Room) first established February 7, 1983;
- Test Stope Station, first established January 8, 1984;
- Stope 1105 Station, first established August 6, 1986.

These Rock Mechanics Stations were established recognizing that, in order to optimize the extraction ratio for the Denison-Potacan deposit, in-situ rock mechanics information was essential.

This included determining the stress and strain distributions around both active mining and test room sites, as well as defining basic material properties. The installation of appropriate rock mechanics instrumentation allowed both stress and strain data to be collected.

The collection of the appropriate rock mechanics field data and the determination of basic material properties were fundamental in developing and calibrating a representative computer analysis (through numerical modelling) of mining and backfilling alternatives.

The results of the in-situ testing work carried out both before and during the project conducted under the auspices of CANMET/New Brunswick Mineral Development Agreement are described in detail in Volume 3 of the Final Report.

SECTION 10.0

10.0 INTACT ROCK BEHAVIOURAL MODEL

Volume 4 of the Final Report describes the development of the behavioural model used in the numerical modelling carried out to simulate the behaviour of the openings which Denison-Potacan have excavated and instrumented.

The behavioural model approach used is justified with reference to the literature on crystal physics and examples given of how the model corresponds to the actual behaviour in the field.

The material model used has the following major elements:

a) Below a specific activation shear stress (Prandtl Limit), deformation processes are diffusion controlled and the relationship between the effective stress and the rate of strain is through a power law of exponent 1.0.

b) The turning point in the behavioural law is specified by two parameters; the Prandtl Limit and the Prandtl Strain Rate, both of which were measured or estimated in the laboratory and in the field through use of a test room.

c) The behavioural law above the Prandtl Limit, but below the rupture criterion, is assumed to be a simple relationship for analytic simplicity. The actual function relating strain rate and effective stress is a complex one which includes effects of the normal stress and the non-linear rate at which dislocations are generated in a medium experiencing cracking and crack healing. For the present, a simple power law is assumed with an exponent between 4.5 and 6.0. Future refinements are expected in this formulation.

d) The upper limit to the steady state creep regime is the Mohr-Coulomb rupture criterion which is a conventional strain weakening behaviour evidenced when laboratory salt rock specimens are strained at a sufficiently rapid rate and under a sufficiently low confining stress as to exhibit rupture.

All of the regimes and the parameters are explained in Volume 4 in terms of reasonable physical mechanisms which have been documented in the crystal physics and materials science literature.

The ranges of behaviour are shown in Figure 10.1.

Where:

σ ... normal stress

τ ... shear stress

K ... Prandtl Limit (activation shear stress required to activate crack growth/healing creep mechanism)

UCS ... uniaxial compressive strength

Y ... brittle yield criterion

r ... radial distance

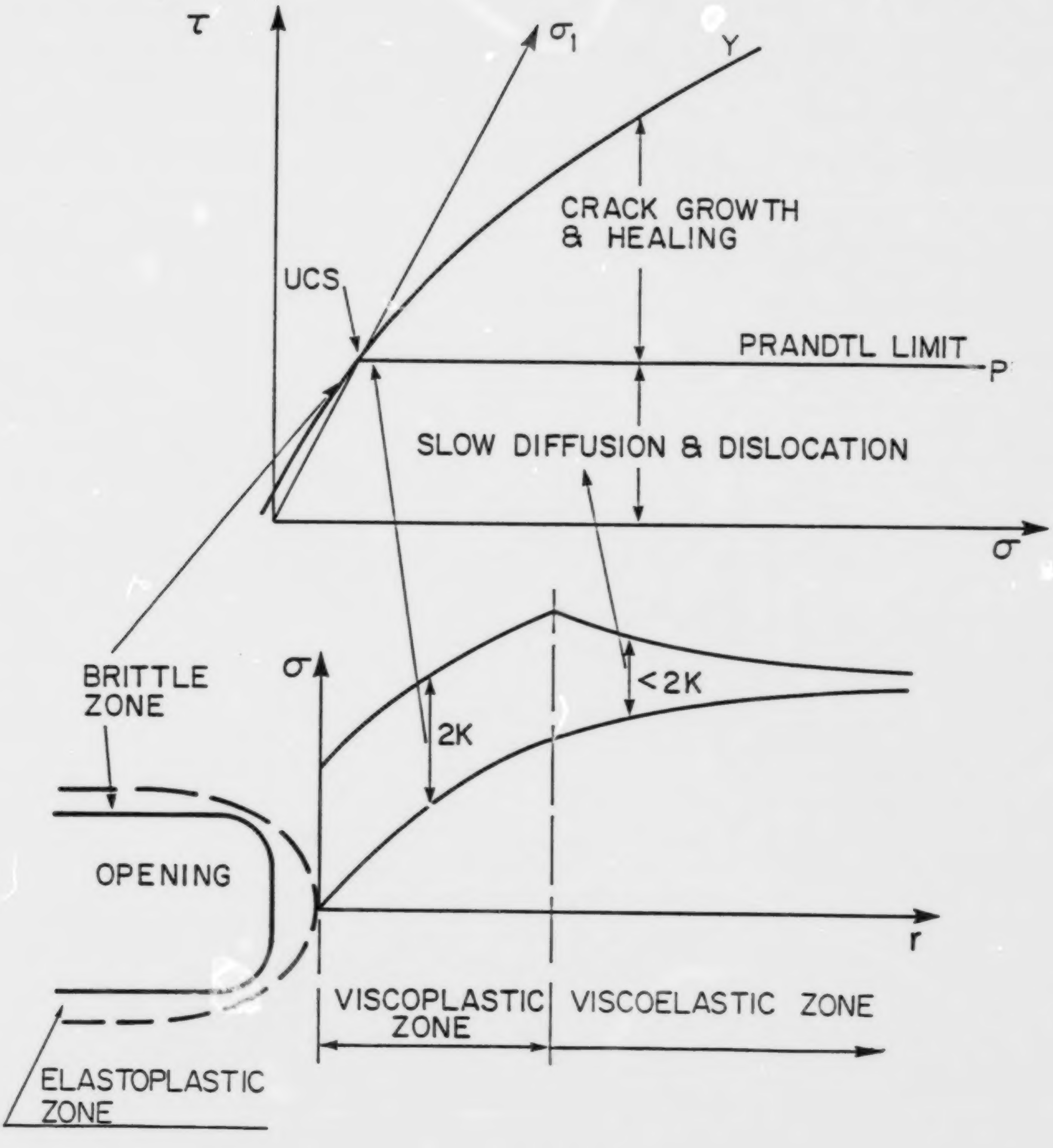
τ
σ1
Y
CRACK GROWTH & HEALING
UCS
PRANDTL LIMIT
P
SLOW DIFFUSION & DISLOCATION
σ
BRITTLE ZONE
σ
<2K
2K
OPENING
r
VISCOPLASTIC ZONE
VISCOELASTIC ZONE
ELASTOPLASTIC ZONE

RANGES OF BEHAVIOUR FOR A SALTROCK OPENING

FIGURE 10.1

SECTION 11.0

11.0 PREDICTION OF LONG TERM RESPONSE OF DENISON-POTACAN STOPES

It was not anticipated that the backfill would substantially slow down the convergence of the stopes. However, as can be seen in Volume 5, the computer runs do indicate that there will be a substantial slow down in convergence that will aggravate, to some extent, the problem associated with delayed compaction and, hence, the ability (or suitability) of the backfill to support the overburden.

Based on the numerical modelling predictions, the following tables 11.1, 11.2 and 11.3 have been developed to calculate the changes in emplaced backfill as stope closure occurs.

The assumptions used are:

- Top 0.5 m of stope is filled at 1.0 S.G.
- Next 1.5 m of stope is filled at 1.4 S.G.
- Balance of stope is filled at 1.6 S.G.

The use of different specific gravities reflects the different methods of backfilling that may be utilized.

Based on these calculations, the changes in backfill density have been plotted against time, as shown in Figure 11.1.

TABLE 11.1

DENISON-POTACAN 4 M X 42 M STOPE
BACKFILL DENSITY VS. TIME

YEAR	ROOF TO FLOOR CLOSURE (M)	WALL TO WALL CLOSURE (M)	NEW ROOF/FLOOR DIMENSION (M)	NEW WALL/WALL DIMENSION (M)	STOPE X-SECT. AREA (M^2)	BACKFILL X-SECT. AREA .5M @ 1.0 DENSITY (M^2)	BACKFILL X-SECT. AREA 1.5M @ 1.4 DENSITY (M^2)	BACKFILL X-SECT. AREA 2.0M @ 1.6 DENSITY (M^2)	TOTAL BACKFILL AREA (M^2)	BACKFILL IN-SITU MASS (000'S KG)	AVERAGE BACKFILL DENSITY (G/C.C)
STOPE AT TIME OF BACKFILLING			4.00	42.00	168	21	63	84	168	244	1.45
0	0.17	0.00	3.83	42.00	161				161	244	1.52
5	0.44	0.12	3.56	41.88	149				149	244	1.64
10	0.60	0.18	3.40	41.82	142				142	244	1.72
15	0.72	0.22	3.28	41.78	137				137	244	1.78
20	0.80	0.24	3.20	41.76	134				134	244	1.82
25	0.86	0.26	3.14	41.74	131				131	244	1.86
30	0.88	0.28	3.12	41.72	130				130	244	1.88
35	0.90	0.29	3.10	41.71	129				129	244	1.89

TABLE 11.2

DENISON-POTACAN 12.5 M X 42 M STOPE
BACKFILL DENSITY VS. TIME

YEAR	ROOF TO FLOOR CLOSURE (M)	WALL TO WALL CLOSURE (M)	NEW ROOF/FLOOR DIMENSION (M)	NEW WALL/WALL DIMENSION (M)	STOPE X-SECT. AREA (M^2)	BACKFILL X-SECT. AREA .5M @ 1.0 DENSITY (M^2)	BACKFILL X-SECT. AREA 1.5M @ 1.4 DENSITY (M^2)	BACKFILL X-SECT. AREA 10.5 M @ 1.6 DENSITY (M^2)	TOTAL BACKFILL AREA (M^2)	BACKFILL IN-SITU MASS (000'S KG)	AVERAGE BACKFILL DENSITY (G/C.C)
STOPE AT TIME OF BACKFILLING			12.50	42.00	525	21	63	441	525	815	1.55
0	0.20	0.02	12.30	41.98	516				516	815	1.58
5	0.66	0.28	11.84	41.72	494				494	815	1.65
10	1.04	0.43	11.46	41.57	476				476	815	1.71
15	1.30	0.54	11.20	41.46	464				464	815	1.76
20	1.54	0.63	10.96	41.37	453				453	815	1.80
25	1.74	0.70	10.76	41.30	444				444	815	1.84
30	1.90	0.75	10.60	41.25	437				437	815	1.86
35	2.10	0.81	10.40	41.19	428				428	815	1.90

TABLE 11.3

DENISON-POTACAN 30 M X 42 M STOPE
BACKFILL DENSITY VS. TIME

YEAR	ROOF TO FLOOR CLOSURE (M)	WALL TO WALL CLOSURE (M)	NEW ROOF/FLOOR DIMENSION (M)	NEW WALL/WALL DIMENSION (M)	STOPE X-SECT. AREA (M^2)	BACKFILL X-SECT. AREA .5M @ 1.0 DENSITY (M^2)	BACKFILL X-SECT. AREA 1.5M @ 1.4 DENSITY (M^2)	BACKFILL X-SECT. AREA 28.0 M @ 1.6 DENSITY (M^2)	TOTAL BACKFILL AREA (M^2)	BACKFILL IN-SITU MASS (000'S KG)	AVERAGE BACKFILL DENSITY (G/C.C)
STOPE AT TIME OF BACKFILLING			30.00	42.00	1,260	21	63	1,176	1,260	1,991	1.58
0	0.30	0.08	29.70	41.92	1,245				1,245	1,991	1.60
5	1.04	0.64	28.96	41.36	1,198				1,198	1,991	1.66
10	1.54	0.90	28.46	41.10	1,170				1,170	1,991	1.70
15	2.00	1.12	28.00	40.88	1,145				1,145	1,991	1.74
20	2.36	1.30	27.64	40.70	1,125				1,125	1,991	1.77
25	2.70	1.44	27.30	40.56	1,107				1,107	1,991	1.80
30	3.04	1.56	26.96	40.44	1,090				1,090	1,991	1.83
35	3.32	1.68	26.68	40.32	1,076				1,076	1,991	1.85

STOPE/BACKFILL INTERACTION PREDICTION

DPPC BACKFILL DENSITY V. TIME

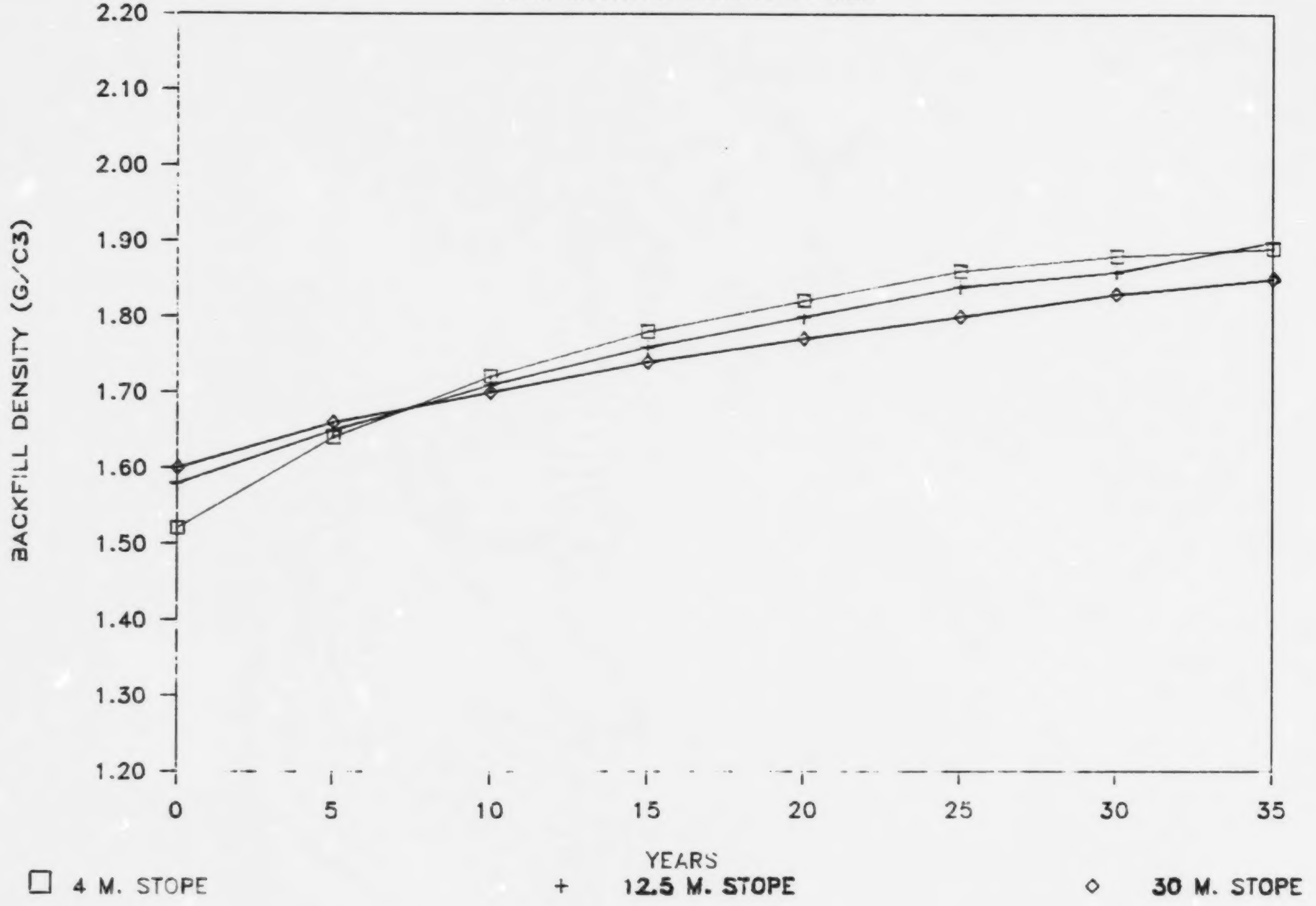

FIGURE II.1

It would appear from these results that the backfill placed will not reach the density necessary to provide adequate support to the overburden within the required time frame.

Since a target of ten years or less has been set from the time of complete backfilling of two adjacent stopes to the time that second stage mining takes place in the intervening pillar, other measures may have to be taken to accelerate the process of backfill consolidation and, hence, support.

SECTION 12.0

12.0 EXCESS TAILINGS VOLUME STORAGE

At backfill placement specific gravity of 1.4, it is calculated that a net imbalance of mass inflows would exist such that excess tailings will accumulate and have to be stockpiled on surface.

At a backfill placement specific gravity of 1.4 and the predicted production and recovery rates forecast for the Denison-Potacan mine, these excess tailings are estimated to be in the order of 0.78 million tonnes per year.

At a backfill placement specific gravity of 1.5, these excess tailings are estimated to be in the order of 0.57 million tonnes per year.

If backfilling efficiency could be improved to 100% at average backfill specific gravity of 1.4, the mass flow imbalance would be reduced to 0.49 million tonnes per year.

If the backfill specific gravity could be improved from 1.4 to 1.6, the mass flow imbalance would be virtually eliminated and there would be no need to stockpile tailings on surface.

SECTION 13.0

13.0 CONCLUSIONS

The Potash Company of America (PCA) mine currently uses tailings backfill in its operation as an integral part of the mining cycle. The Denison-Potacan mine is the second potash mine to begin operations in the Province of New Brunswick. No other potash mine in Canada practices backfilling underground in any significant quantity.

There were numerous technical questions and issues to resolve to enable mine planning and backfilling to commence in the Denison-Potacan mine. Discovering the best methods of backfill placement and consolidation were the primary objectives of Phase I of the research project.

As a result of Phase I of this research project, the following conclusions have been reached with respect to the proposed backfill material characteristics and placement densities:

- The proposed backfill material consists of less than 2 millimetre size halite tailings crystals.

- The backfill material is of a permeable and free draining characteristic and the pumping facilities in the mine, with an installed capacity of 370 to 400 L/min, should be adequate for brine removal from the mine.

- The anticipated placement density achievable with this material is strongly governed by the placement method used.

- Placement density in-situ has a possible limit of 1.5 specific gravity, which will best be achieved by mechanical spreading means with incidental compaction. Auxiliary vibro-compaction of the backfill could achieve in-place specific gravities in the range of 1.5 to 1.6.

- Emplaced backfill will have limited support capability prior to almost complete elimination of porosity in the fill during the closure history of the backfilled openings. Using Phase I base case criteria and preliminary functions established for stress, strain rate and support capability, the elapsed time before second stage mining can begin would be unacceptable.

- The primary methods of reducing the elapsed time to second stage mining for Denison-Potacan will be:

    a) Placement of backfill to as high a density as is practical and as high a filling efficiency as possible.
    b) Acceleration of closure rates as the last step of first stage mining, or as an intermediate operation without compromising the safety of workers and integrity of mine stability.
    c) Devising novel backfill density improvement methods, such as brine recirculation or engineered backfill.

- Intentional closure rate acceleration of mined openings will have a close correlation with gross subsidence and mining induced seismicity over the mining area. Denison-Potacan's Rock Mechanics Program should ensure that subsidence in the overburden will consist of low magnitude energy release events which will not endanger the safety of the mine or its workers.

- Given the probable placement density and backfilling inefficiency scenario of the base case in the Phase I study, a net mass flow imbalance will accumulate on surface.

Backfilling operations commenced at the Denison-Potacan mine as of February, 1987. Compaction has been by means of scooptram distribution and, hence, packing under the weight of the machine.

However, the following aspects remain to be addressed:

a) The development and analysis of a backfill support function with respect to backfill density, extraction and stope geometry.

b) The characterization and analysis of method(s) to introduce closure rate acceleration.

c) The characterization and evaluation of alternate backfill density improvement methods.

d) The development of failure criteria for backfill as functions of density.

e) The optimization of backfill density and mining geometry to achieve safe and cost efficient recovery of reserves through second stage mining.

f) The characterization and evaluation of the impact of closure rate of mined openings with respect to gross subsidence, mining induced seismicity over the mining area and, hence, impacts on the safety of the mine and its workers.

It is proposed that this area of the technology of potash mine backfilling be researched in Phase II of the research project.

Volume
2

Energy, Mines and Resources Canada
Énergie, Mines et Ressources Canada

CANMET
Canada Centre for Mineral and Energy Technology
Centre canadien de la technologie des minéraux et de l'énergie

POTASH MINING PROJECT

PROJET D'EXPLOITATION DE LA POTASSE

[illegible] LES MINÉRAUX
[illegible] MINIÈRE

USE OF BACKFILL IN NEW BRUNSWICK POTASH MINES

VOLUME 2

LABORATORY TESTING

May, 1987

Final Report By:

DENISON-POTACAN POTASH COMPANY
Sussex, New Brunswick

Prepared by:

MRAZ PROJECT CONSULTANTS LTD
Saskatoon, Saskatchewan

- and -

M.B. DUSSEAULT and C. FORDHAM
Dept. of Earth Sciences, University of Waterloo
Waterloo, Ontario

Work on the Project was conducted under the auspices of the Canada Centre for Mineral and Energy Technology, Energy, Mines and Resources Canada, funded as part of the Canada/New Brunswick Mineral Development Agreement.

DSS FILE NO: 14SQ.23440-5-9031

DSS CONTRACT SERIAL NO: 0SQ85-00208

CANMET PROJECT NO: 1.4.09.05

MICROMEDIA

266 pp

CANMET SCIENTIFIC AUTHORITY: Dr. G. Herget

USE OF BACKFILL IN NEW BRUNSWICK POTASH MINES

VOLUME 2

LABORATORY TESTING

TABLE OF CONTENTS

1.0 SUMMARY

2.0 INTRODUCTION

3.0 INTACT ROCK SPECIMEN TESTING
3.1 SAMPLE COLLECTION: 100 MM DIAMETER CORES
3.2 SAMPLE PREPARATION AND TESTING
3.3 INTACT ROCK CREEP TESTING RESULTS
3.4 BRITTLE YIELD TESTING RESULTS
3.5 ELASTIC MODULUS DETERMINATION
3.6 PROPERTY CRITERIA FOR NUMERICAL MODELLING
3.6.1 MECHANICAL PROPERTIES
3.6.2 RHEOLOGICAL PROPERTIES

4.0 BACKFILL MATERIALS TESTING
4.1 SAMPLE COLLECTION AND CHARACTERIZATION
4.2 GRAIN SIZE
4.3 MINERALOGICAL
4.4 MOISTURE CONTENT
4.5 SPECIFIC GRAVITY

5.0 BACKFILL PLACEMENT DENSITY TESTING
5.1 PLACEMENT BY SPREADING ONLY
5.2 PLACEMENT BY SLURRY SEDIMENTATION
5.3 PLACEMENT BY RODDING METHODS
5.4 PLACEMENT BY FLINGER METHODS
5.5 PLACEMENT BY VIBRO-COMPACTION METHODS
5.6 SURFACE TRIALS: FULL SCALE EQUIPMENT

6.0 BACKFILL CONSOLIDATION TESTING
6.1 CONSOLIDATION TESTING
6.2 CONSOLIDATION TEST RESULTS

7.0 BACKFILL TRIAXIAL TESTING

8.0 WAFER CELL CALIBRATION

APPENDIX A

APPENDIX B

APPENDIX C

APPENDIX D

APPENDIX E

LIST OF FIGURES

FIGURE 3.1 STRESS DIFFERENCE VERSUS STRAIN RATES

FIGURE 3.2 DPPC BRITTLE YIELD TEST RESULTS

FIGURE 3.3 DPPC SYLVINITE BED FAILURE ENVELOPE

FIGURE 3.4 DPPC UPPER HALITE FAILURE ENVELOPE

FIGURE 3.5 DPPC LGB FAILURE ENVELOPE

FIGURE 3.6 UNCONFINED COMPRESSIVE STRENGTH TEST DG9

FIGURE 3.7 UNCONFINED COMPRESSIVE STRENGTH TEST UH10

FIGURE 3.8 UNCONFINED COMPRESSIVE STRENGTH TEST LGB48

FIGURE 3.9 STRESS DIFFERENCE VS. STRAIN RATE

FIGURE 4.1 GRAIN SIZE ANALYSES, BULK SAMPLES

FIGURE 4.2 GRAIN SIZE ANALYSES, SCROLL AND SLIMES TAILINGS

FIGURE 4.3 GRAIN SIZE ANALYSIS: TYPICAL TAILINGS

FIGURE 6.1 CONSOLIDOMETER TEST, 17 DAYS AT ROOM TEMPERATURE, 5 MPa

FIGURE 6.2 CONSOLIDOMETER TEST, 17 DAYS AT 35 DEGREES C, 5 MPa

FIGURE 6.3 CONSOLIDATION TESTS, DPPC TAILS, 2.5% Wc

FIGURE 7.1 PROPOSED BRITTLE FAILURE TESTING ON SALT BACKFILL

FIGURE 8.1 PHOTOGRAPH OF SAMPLE WITH TEST CELL

FIGURE 8.2 SRC WAFER CELL RESPONSE

FIGURE 8.3 SAMPLE LGB 44 WAFER CELL RESPONSE (AXIAL STRESS 5 MPa)

FIGURE 8.4 SAMPLE LGB 45 WAFER CELL RESPONSE (AXIAL STRESS 5 MPa)

FIGURE 8.5 SAMPLE LGB 45 WAFER CELL RESPONSE (AXIAL STRESS 3 MPa)

FIGURE 8.6 SRC WAFER CELL RESPONSE

LIST OF TABLES

TABLE 3.1 DENISON-POTACAN INTACT ROCK CREEP TEST DATA

TABLE 3.2 DENISON-POTACAN BRITTLE YIELD TEST DATA

TABLE 4.1 INITIAL MOISTURE CONTENT DETERMINATIONS

TABLE 4.2 COMBINED STREAM TAILINGS MOISTURE CONTENT SAMPLES

TABLE 5.1 PLACEMENT METHODS: RANGES OF EXPECTED POROSITY

TABLE 5.2 SURFACE TRIALS: BACKFILL DENSITY

TABLE 7.1 BRITTLE YIELD TRIAXIAL TESTING RESULTS FOR BACKFILL SAMPLES CONSOLIDATED TO 90%

TABLE 8.1 ULTIMATE RESPONSE OF SRC WAFER CELL

TABLE 8.2 LINEAR REGRESSION CONSTANTS FOR SRC WAFER CELL CALIBRATION

TABLE 8.3 STATISTICAL ANALYSIS OF CALIBRATION STAGES

LIST OF APPENDICES

APPENDIX A	"TRIAXIAL TESTING OF CREEP AND YIELD BEHAVIOUR OF INTACT SALT ROCKS"; C. J. Fordham, M. B. Dusseault, D. Mraz.
	"TRIAXIAL TESTING OF INTACT SALT ROCKS: PRESSURE CONTROL, PRESSURE SYSTEMS, CELL AND FRAME DESIGN; J. R. Baleshta, M. B. Dusseault
	"TEST PROCEDURES FOR SALT ROCK"; M. B. Dusseault, D. Mraz, J. Unrau, C. Fordham.
APPENDIX B	BACKFILL SAMPLING AT DENISON-POTACAN; S. Munroe
APPENDIX C	COMPACTED TAILINGS DENSITIES: M. Frayne
APPENDIX D	MECHANICAL PROPERTIES OF HALITE TAILINGS FROM THE DENISON-POTACAN POTASH MINE, SUSSEX, NEW BRUNSWICK; C. J. Fordham; PART I: CHARACTERIZATION OF MATERIALS; PART II: MOISTURE/DENSITY RELATIONSHIPS
APPENDIX E	FIELD DENSITY TESTING OF BACKFILL MATERIAL AT DENISON-POTACAN; S. Munroe

SECTION 1.0

1.0 SUMMARY

This volume describes laboratory testing work and the results obtained at the University of Waterloo WATSALT facility.

Intact rock specimen testing was performed to establish basic physical property data for the Sylvinite Bed materials in their solid form.

The combined tailings stream, or backfill material, was tested to enable an evaluation of the physical properties of the material.

Backfill placement density trials were designed and executed in the laboratory in order to evaluate the suitability of various placement densities from the standpoint of achieving maximum packing density or consolidation.

Backfill consolidation testing was performed so as to establish a support function and the failure criterion for the fill at less than 100% consolidation.

Preliminary brittle yield triaxial testing was performed on the backfill so as to enable the development of brittle yield failure criteria.

A series of calibration tests were performed on two wafer pressure cell units with the objective to calibrate and verify in-situ data obtained with these pressure cells.

The testing methods, apparatus and results are described, as well as the data which have been used to derive input parameters to the computer analysis used to analyze mining and backfilling alternatives.

SECTION 2.0

2.0 INTRODUCTION

Laboratory testing was performed on intact rock samples that were obtained from the Denison-Potacan mine during a July, 1986 coring program.

Laboratory testing was also performed on backfill materials obtained from the combined tailings refuse stream at Denison-Potacan.

The objectives were such as to determine the physical properties of these materials to provide parameters for the modelling of various mining and backfilling alternatives.

This volume describes the laboratory testing program, data collection and analyses used with the research work to evaluate the use of backfill in New Brunswick potash mines.

SECTION 3.0

3.0 INTACT ROCK SPECIMEN TESTING

A primary objective of the research program was to develop a sound basis for analyses to be performed on the intact rock and the backfill materials. A significant amount of laboratory work was therefore required to establish basic physical property data for both the sylvinite and the halite materials in their solid form.

The work program required cutting 100 mm diameter cores in-situ for subsequent testing at the University of Waterloo. A description of the work follows.

3.1 SAMPLE COLLECTION: 100 MM DIAMETER CORES

An attempt was made to cut 100 mm diameter cores using air flushing for cooling of the core bit and removal of the chips. A tractor drill rig was adapted to drive a 500 mm long thin-walled tube using tungsten carbide inserts at the cutting edge.

The core recovered was severly fractured into a series of discs, between 10 mm and 15 mm thick.

It was decided, as a result of this trial, to abandon the attempt to drill dry cores. Subsequent core drilling was performed using Denison-Potacan's geological exploration drill, which uses brine flushing and conventional coring tools.

The Model 200 Superdrill coring drill rig was used with a Craelius T6S 131 mm x 1500 mm core barrel, part no. 8392027903. A Corborit tungsten carbide bit was obtained for drilling in the Sylvinite Bed.

Using this equipment, the 100 mm core samples were obtained during the week of July 7 - 11, 1986. The cores were logged and shipped to the University of Waterloo to initiate the laboratory testing program of the intact rock specimens.

3.2 SAMPLE PREPARATION AND TESTING

The WATSALT laboratory at the University of Waterloo is equipped with specially designed and built testing equipment for performing triaxial creep testing on 50 mm and 100 mm diameter rock cores. A systematic methodology has also been developed for working with viscoelastic materials, such as slyvinite and rock salt.

Three papers, included in Appendix A, describe the testing equipment and methods in use at the laboratory:

- Fordham, et al., Triaxial testing of creep and yield behaviour of intact saltrocks;

- Baleshta and Dusseault, Triaxial testing of intact saltrocks: pressure control, pressure systems, cell and frame design;

- Dusseault, et al., Test procedures for saltrock.

3.3 INTACT ROCK CREEP TESTING RESULTS

The intact rock triaxial creep testing program was completed for Phase I of the research program in March, 1987.

A substantial database for Sylvinite Bed, Upper Halite and Lower Gradational Bed material has been established.

The results obtained from the intact rock creep testing program are summarized on Table 3.1 and plotted graphically in Figure 3.1.

TABLE 3.1

DENISON-POTACAN INTACT ROCK CREEP TEST DATA

SAMPLE NO.	σ_1 (MPa)	σ_3 (MPa)	σ_1-σ_3 (MPa)	σ_{oct} (MPa)	τ_{oct} (MPa)	ϵ_{ss} (sec^{-1})
SYLVINITE BED:						
1944A	26.00	6.30	19.70	12.87	9.29	5.97×10^{-9}
	30.00	10.00	20.00	16.67	9.43	6.08×10^{-9}
	27.90	7.70	20.20	14.43	9.52	5.65×10^{-9}
	28.20	7.90	20.30	14.67	9.57	5.55×10^{-9}
	30.30	9.70	20.60	16.57	9.71	6.08×10^{-9}
	30.10	8.90	21.20	15.97	9.99	6.29×10^{-9}
1948	30.00	10.00	20.00	16.67	9.43	2.27×10^{-9}
1960A	28.70	5.00	23.70	12.90	11.17	1.08×10^{-8}
	32.50	7.50	25.00	15.83	11.79	9.10×10^{-9}
	32.70	7.40	25.30	15.83	11.93	1.09×10^{-8}
	36.80	10.90	25.90	19.53	12.21	1.14×10^{-8}
1960B	28.30	3.50	24.80	11.77	11.69	2.65×10^{-8}
	37.80	10.20	27.60	19.40	13.01	2.60×10^{-8}
	33.20	6.80	26.40	15.60	12.45	2.93×10^{-8}
1961A	28.80	3.20	25.60	11.73	12.07	1.15×10^{-8}
	33.50	6.50	27.00	15.50	12.73	1.13×10^{-8}
1910	29.80	10.00	19.80	16.60	9.33	1.60×10^{-9}
	25.80	6.30	19.50	12.80	9.19	1.70×10^{-9}
	30.70	9.00	21.70	16.23	10.23	3.94×10^{-9}
	26.20	5.50	20.70	12.40	9.76	4.26×10^{-9}
	26.40	5.30	21.10	12.33	9.95	3.94×10^{-9}
	29.20	6.30	22.90	13.93	10.80	8.10×10^{-9}
	31.40	7.90	23.50	15.73	11.08	8.00×10^{-9}
	32.10	6.60	25.50	15.10	12.02	2.93×10^{-8}
UPPER HALITE:						
UH3	49.70	23.20	26.50	32.03	12.49	3.93×10^{-9}
UH13	37.20	5.40	31.80	16.00	14.99	3.90×10^{-9}
	34.40	6.80	27.60	16.00	13.01	1.93×10^{-9}
UH12	41.00	15.50	25.50	24.00	12.02	3.42×10^{-9}
	41.70	15.20	26.50	24.03	12.49	3.75×10^{-9}
	40.30	15.90	24.40	24.03	11.50	1.22×10^{-9}
LOWER GRADATIONAL BED:						
LGB30	41.70	15.20	26.50	24.03	2.49	7.86×10^{-9}
	43.80	14.10	29.70	24.00	4.00	1.45×10^{-8}
	39.60	16.20	23.40	24.00	11.03	2.12×10^{-9}
LGB31	33.00	7.50	25.50	16.00	12.02	3.08×10^{-9}
	34.40	6.80	27.60	16.00	13.01	3.84×10^{-9}
	35.80	6.10	29.70	16.00	14.00	3.98×10^{-9}

σ_1 ... Ram stress

σ_3 ... Confining stress

σ_{oct} ... Octahedral stress

τ_{oct} ... Octahedral shear stress

$\dot{\epsilon}_{ss}$ ... Steady state strain rate

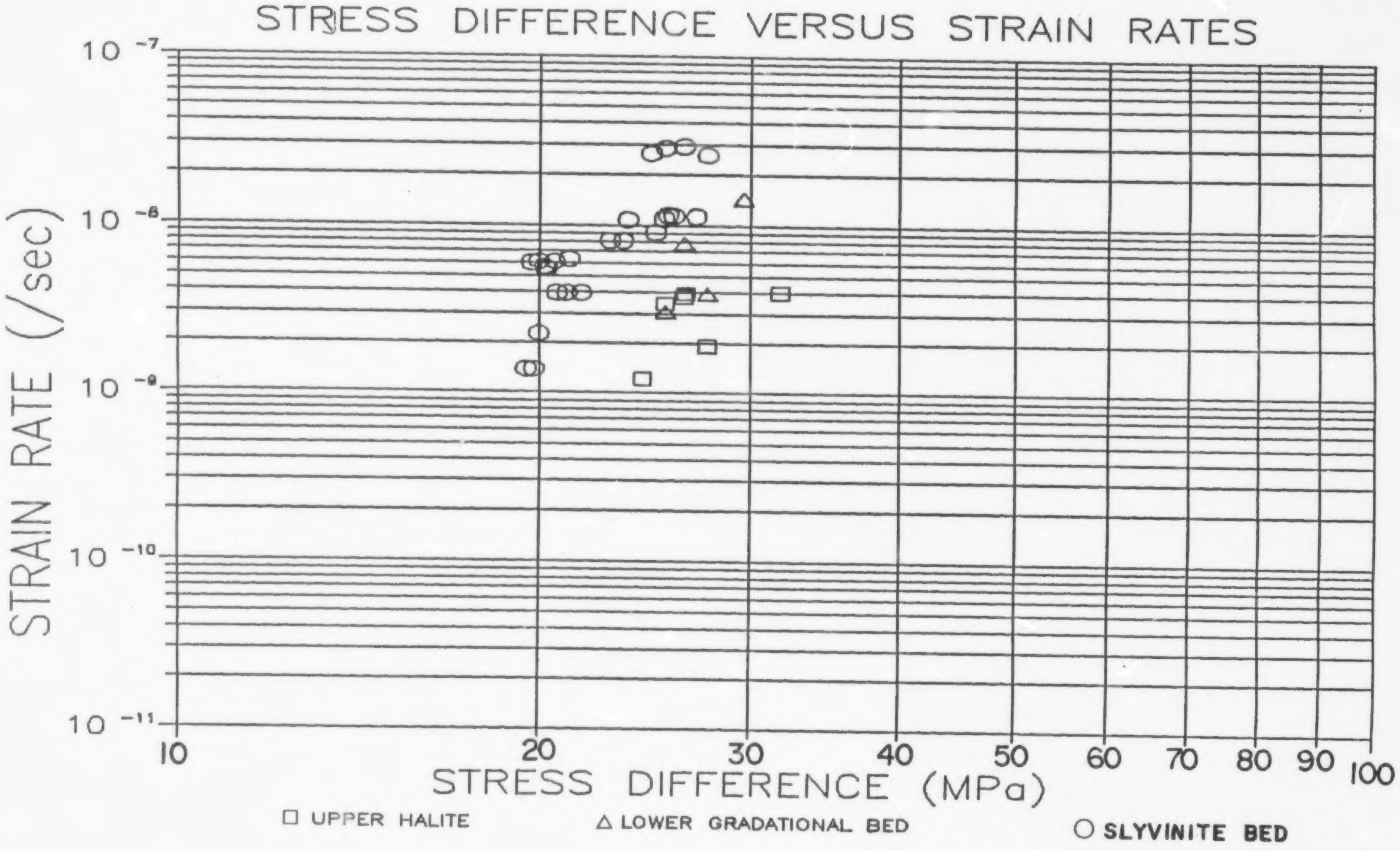
STRESS DIFFERENCE VERSUS STRAIN RATES

FIGURE 3.1

3.4 BRITTLE YIELD TESTING RESULTS

The brittle yield testing program was completed for Phase I of the research program in March, 1987.

Again, a database for the Sylvinite Bed, Upper Halite and Lower Gradational Bed material has been established.

The results obtained from the brittle yield testing program are summarized on Table 3.2 and plotted graphically on Figure 3.2. The individual graphs for each material are shown Figures 3.3, 3.4 and 3.5.

Where:

R ... σ_T / σ_C

σ_T ... tensile strength

σ_C ... unconfined compressive strength

M ... empirical constant

σ_1 ... maximum principal stress

σ_3 ... minimum principal stress

TABLE 3.2

DENISON-POTACAN BRITTLE YIELD TEST DATA

TEST NO.	σ_3 (MPa)	σ_1 (MPa)	$\dot{\epsilon}$ (/sec^{-1})
SYLVINITE BED:			
B2	-1.65	0.00	1.0×10^{-3}
UCS1	0.00	26.25	1.0×10^{-3}
1955	1.00	41.21	1.1×10^{-5}
1941B	2.50	50.95	1.8×10^{-5}
1952AA	5.00	70.44	1.7×10^{-3}
1950	7.50	86.64	3.7×10^{-3}
UPPER HALITE:			
UH10B	-2.00	0.00	1.0×10^{-4}
UH10	0.00	29.22	1.0×10^{-4}
UH5	1.00	49.89	2.0×10^{-4}
UH9	1.50	65.81	2.0×10^{-4}
LOWER GRADATIONAL BED:			
LGB48B	-1.48	0.00	1.0×10^{-4}
LGB48	0.00	28.40	1.0×10^{-4}
LGB47	0.50	36.40	2.0×10^{-4}
LGB46	1.00	39.20	2.0×10^{-4}

σ_3 .... Confining stress

σ_1 .... Vertical stress

$\dot{\epsilon}$ .... Strain rate

DPPC BRITTLE YIELD TEST RESULTS

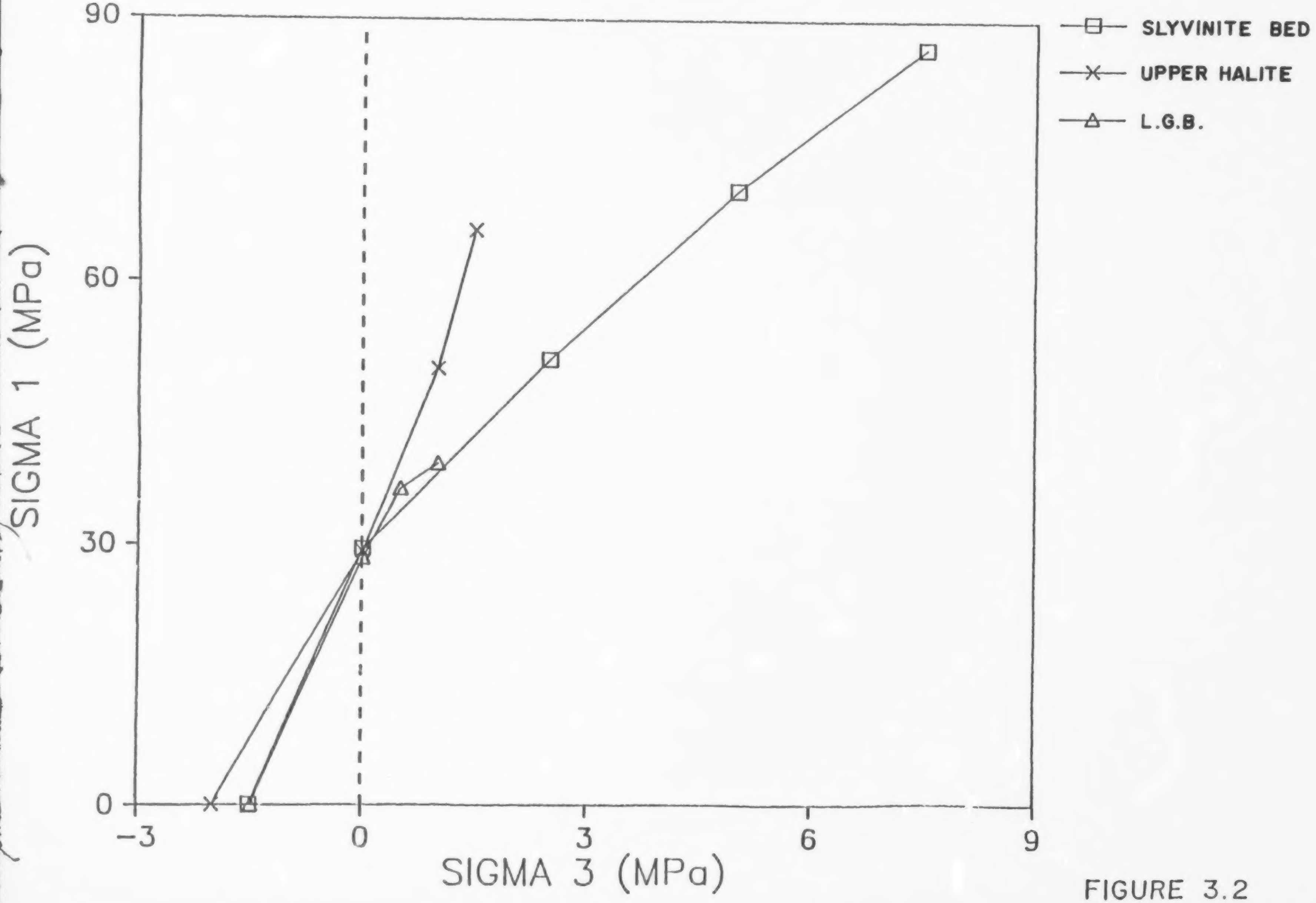

FIGURE 3.2

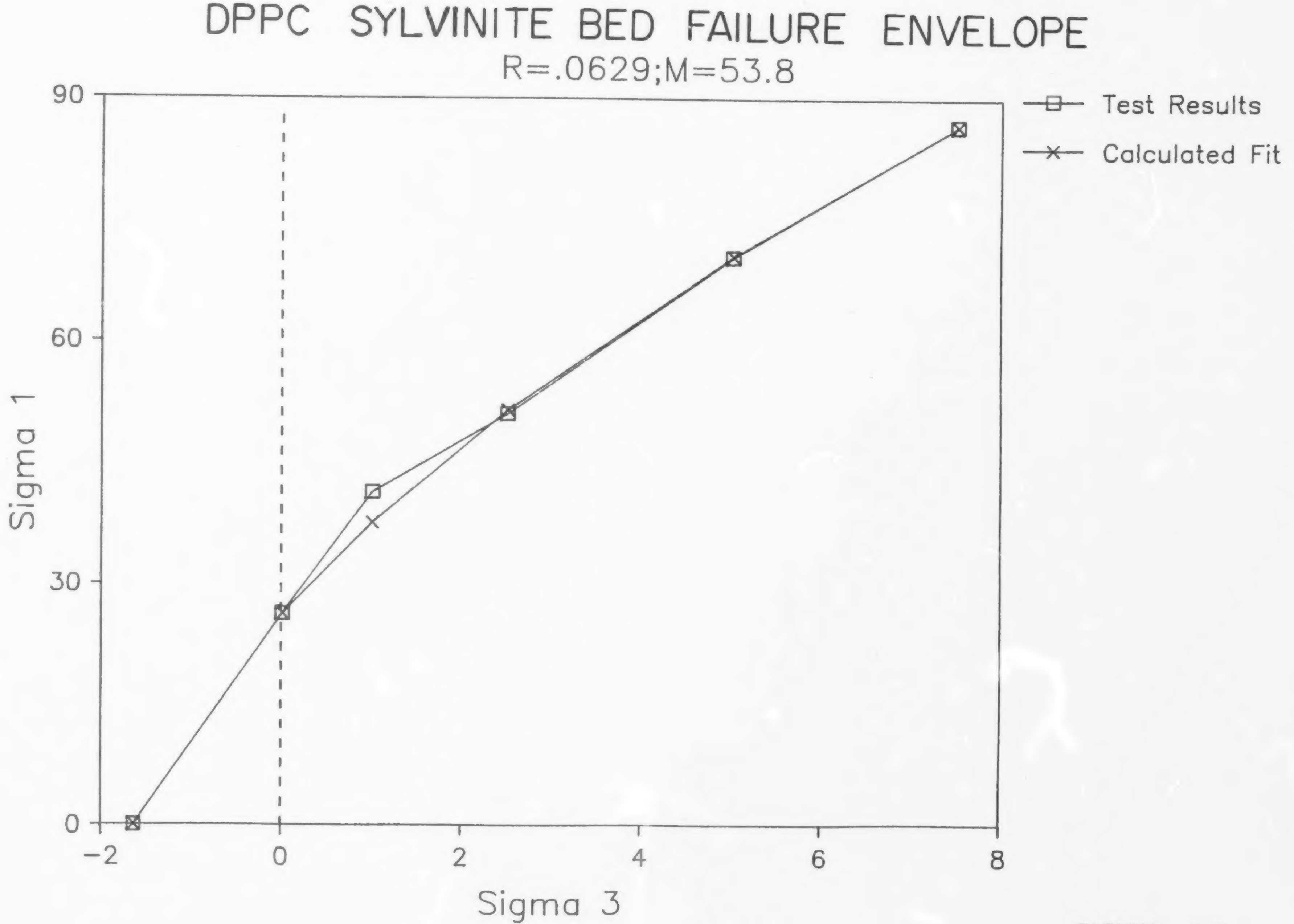
DPPC SYLVINITE BED FAILURE ENVELOPE
R=.0629;M=53.8
Test Results
Calculated Fit
Sigma 1
90
60
30
0
Sigma 3
-2
0
2
4
6
8

FIGURE 3.3

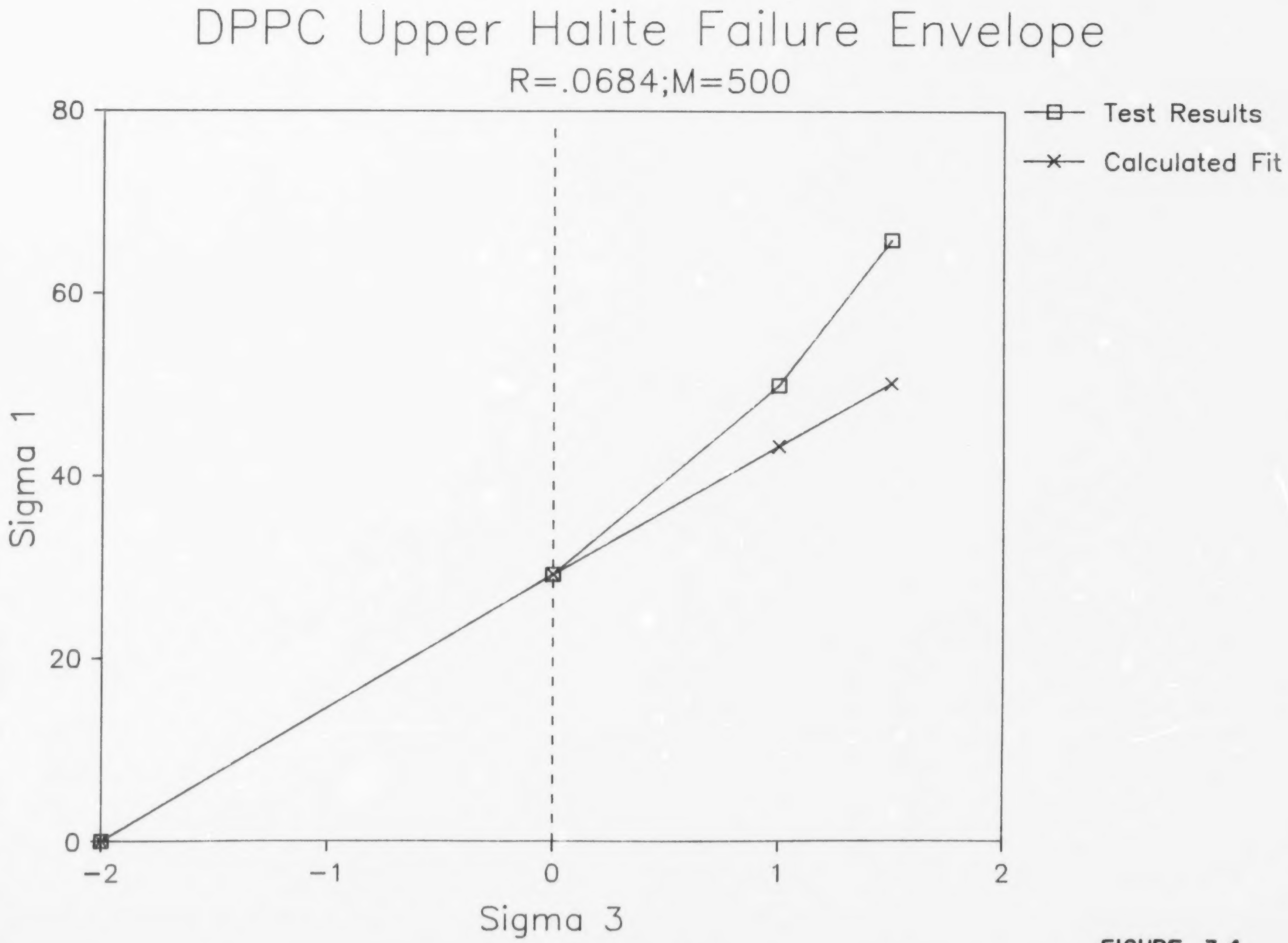
DPPC Upper Halite Failure Envelope
R=.0684;M=500
Sigma 1
80
60
40
20
0
-2
-1
0
1
2
Sigma 3
Test Results
Calculated Fit

FIGURE 3.4

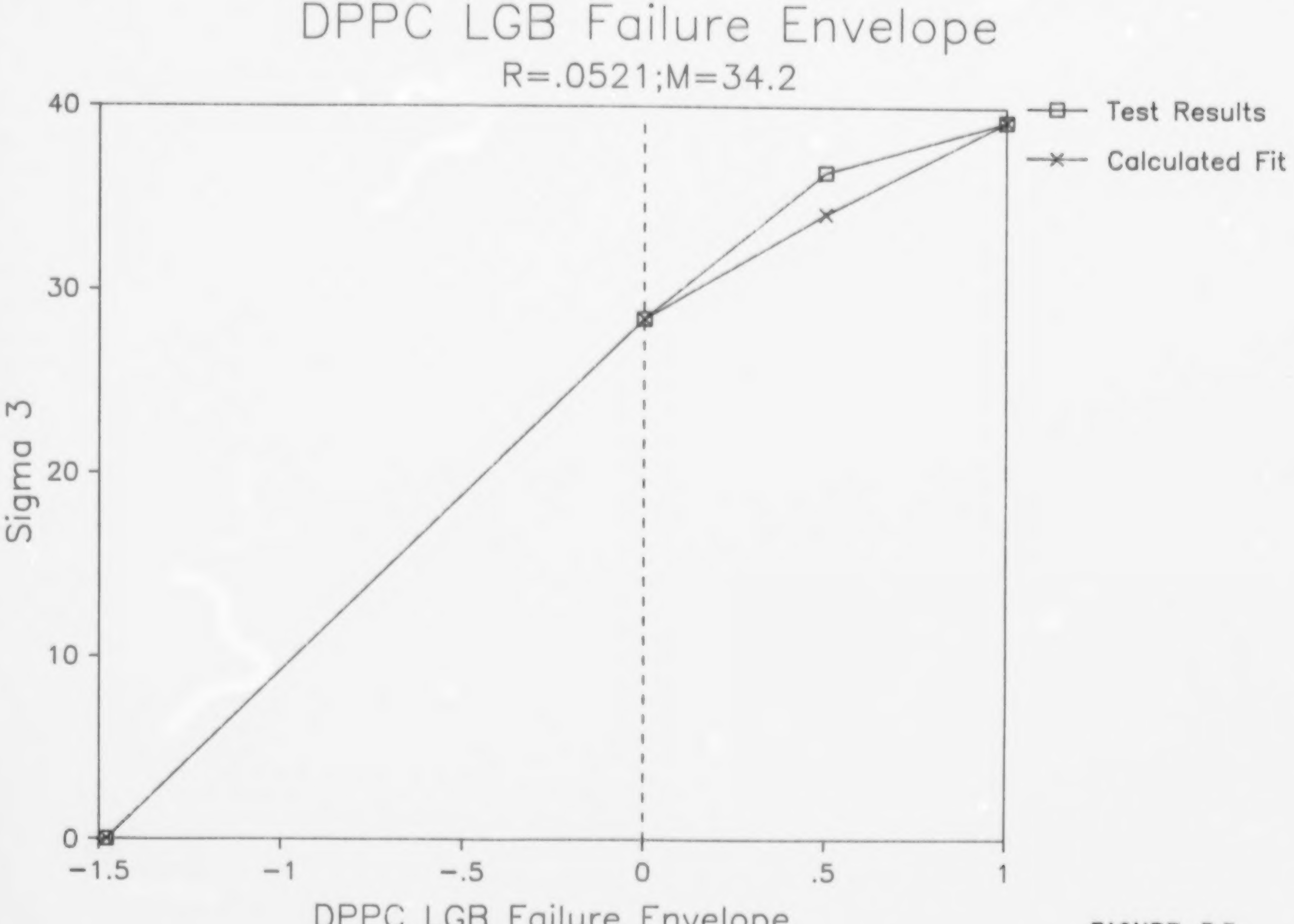
DPPC LGB Failure Envelope
R=.0521;M=34.2
Test Results
Calculated Fit
Sigma 3
40
30
20
10
0
-1.5
-1
-.5
0
.5
1
DPPC LGB Failure Envelope

FIGURE 3.5

3.5 ELASTIC MODULUS DETERMINATION

Young's modulus is usually measured directly on the loading curve.

This procedure is inadequate in determining a short term elastic response of salt rock. Instead, it is an unload/reload modulus that is generally used for modelling elastic behaviour of salt rock. Unload/reload curves (2) are generated when the stresses are removed from the sample and then re-applied.

To determine the elastic modulus, a curve is drawn tangent to the unload/reload curve. Points are marked near the top and bottom of the tangent line. The difference in stress between these two points is measured along the Y-axis of the graph. The difference in strain is measured along the X-axis of the graph. The difference in stress is divided by the difference in strain to determine the modulus.

Using this procedure, the elastic moduli of Denison-Potacan rocks were determined as follows:

MATERIAL	TEST #	MODULUS (GPa)	FIGURE
Sylvinite Bed	DG9	5.462	3.6
Upper Halite	UH10	10.210	3.7
Lower Gradational Bed	LGB48	6.908	3.8

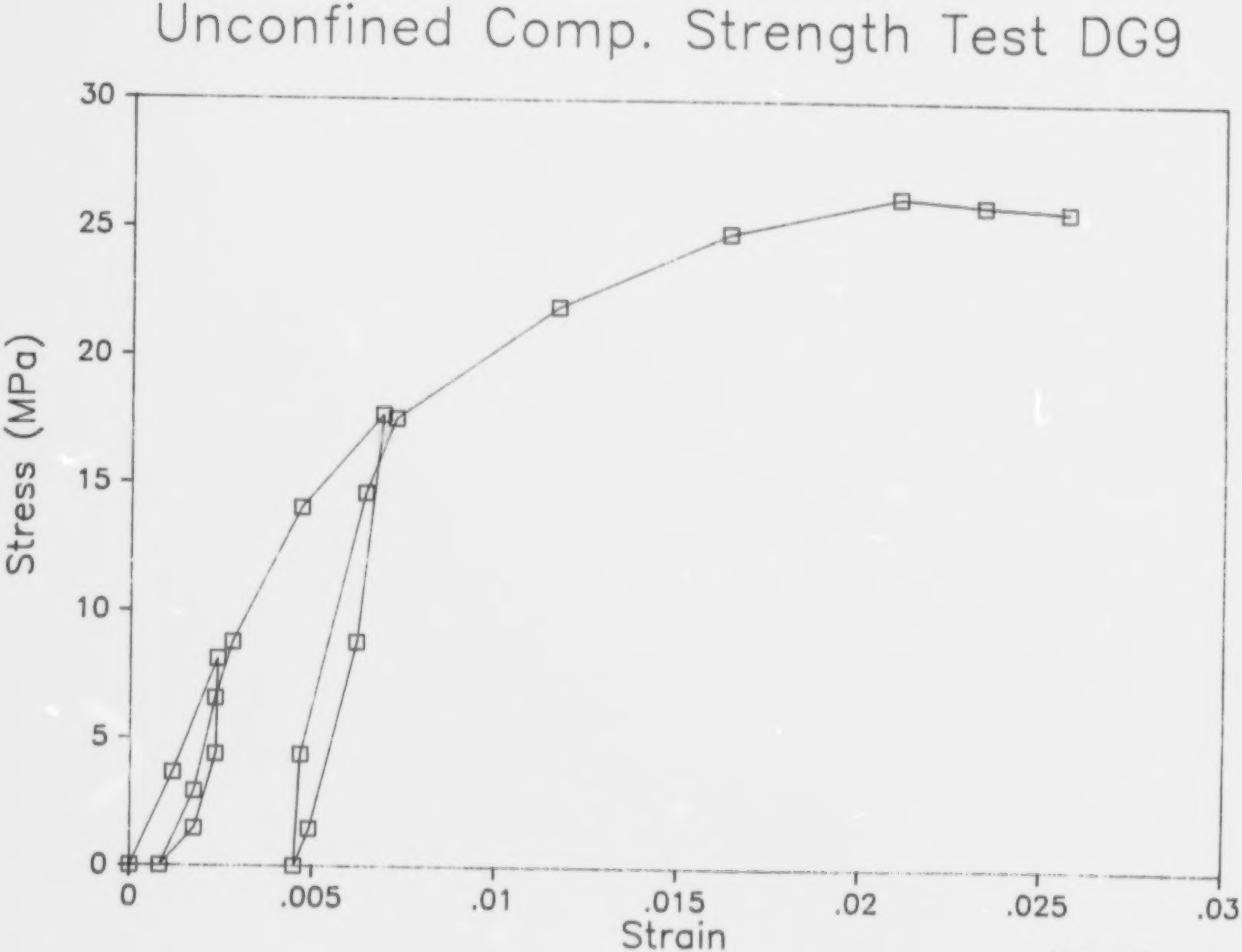
Unconfined Comp. Strength Test DG9
Stress (MPa)
30
25
20
15
10
5
0
0
.005
.01
.015
.02
.025
.03
Strain

FIGURE 3.6

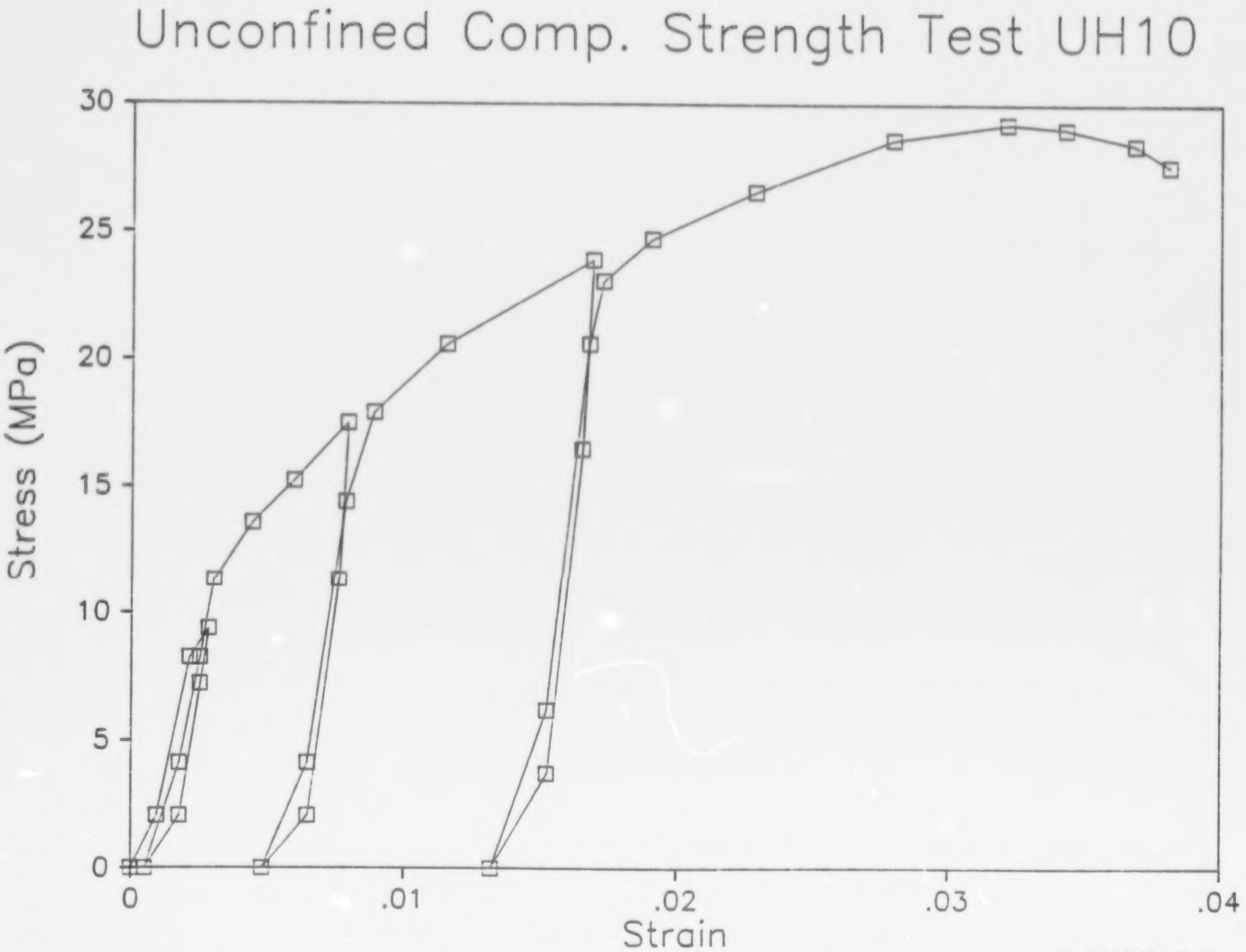
Unconfined Comp. Strength Test UH10
Stress (MPa)
30
25
20
15
10
5
0
0
.01
.02
.03
.04
Strain

FIGURE 3.7

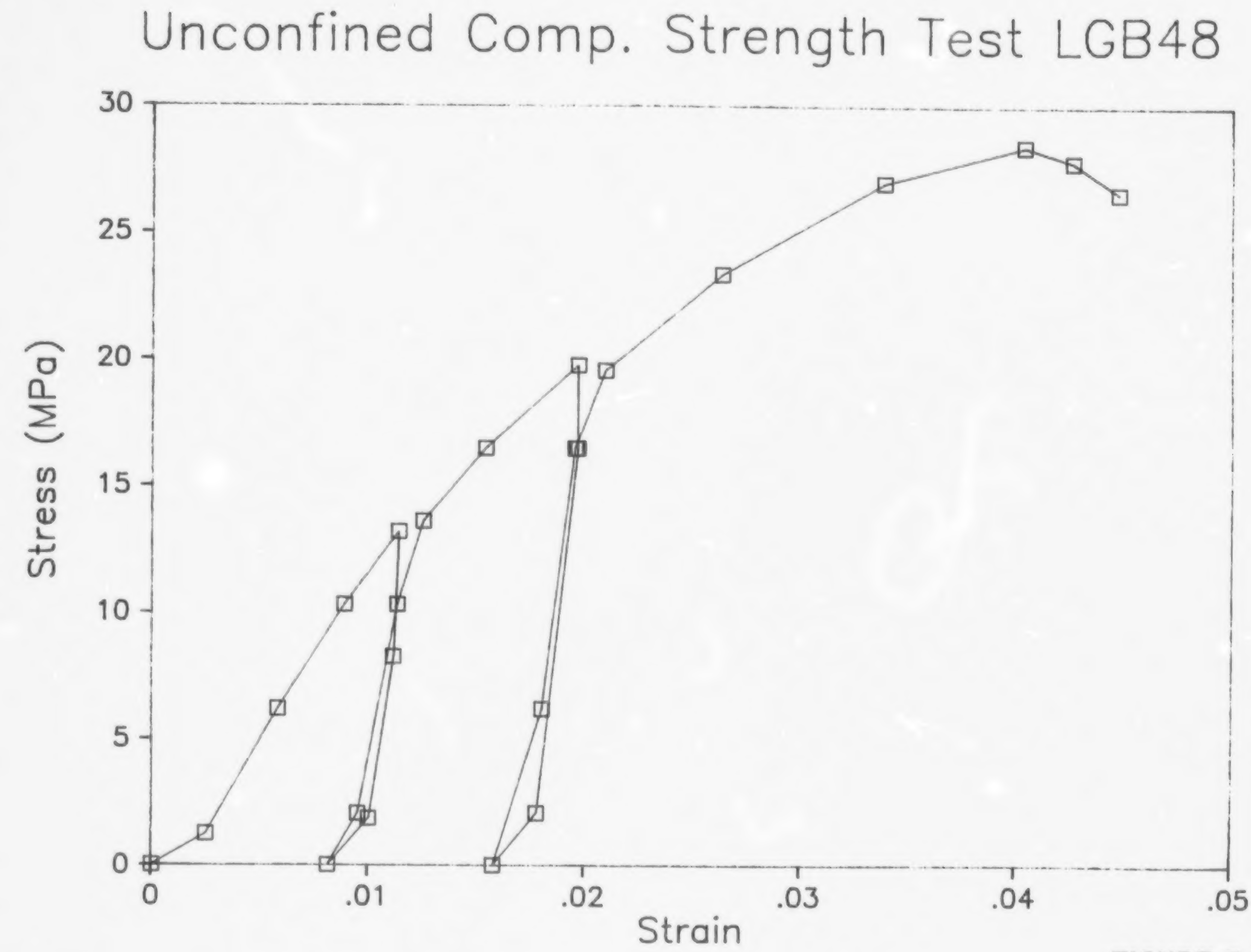
Unconfined Comp. Strength Test LGB48
30
25
20
15
10
5
0
Stress (MPa)
0
.01
.02
.03
.04
.05
Strain

FIGURE 3.8

3.6 PROPERTY CRITERIA FOR NUMERICAL MODELLING

Based on the laboratory testing described previously, the following criteria have been established for intact rock in the numerical modelling exercise:

3.6.1 MECHANICAL PROPERTIES

Sylvinite Bed:
Unconfined Compressive Strength: 26.25 MPa
Modulus of Elasticity: 5.462 GPa
Tensile Strength: 1.65 MPa

Upper Halite:
Unconfined Compressive Strength: 29.22 MPa
Modulus of Elasticity: 10.21 GPa
Tensile Strength: 2.00 MPa

Lower Gradational Bed:
Unconfined Compressive Strength: 28.40 MPa
Modulus of Elasticity: 6.908 GPa
Tensile Strength: 1.48 MPa

The failure envelopes plotted in Figures 3.2, 3.3 and 3.4 can be fitted to an empirical expression developed by Rothenburg:

$$\sigma_1 = \frac{\sigma_c}{2}\left[\left(1 - MR\right) + \sqrt{\left(1 + MR\right)^2 + 4M\,\frac{\sigma_3}{\sigma_c}}\right]$$

$$R = \frac{\sigma_T}{\sigma_c}$$

σ_1 ... maximum principal stress

σ_3 ... minimum principal stress

σ_c ... unconfined compressive strength

σ_T ... tensile strength

M ... empirical constant

The following values give the best fit equation to the experimental data:

	R	M
Sylvinite Bed	0.0629	53.8
Upper Halite	0.0684	500.0
Lower Gradational Bed	0.0521	34.2

3.6.2 RHEOLOGICAL PROPERTIES

The isothermal steady state creep data are usually fitted to the power law of the form:

$$\dot{\epsilon}_{ss} = A \Delta\sigma^{n}$$

$\dot{\epsilon}_{ss}$ ... steady state strain rate

$\Delta\sigma$ ... principal stress difference

A, n ... empirical constants

The power law fit of Denison-Potacan test data was determined by linear regression method, as shown in Figure 3.9. It is obvious that the power law fit does not provide an adequate tool for estimating the rock behaviour to below the level of strain rates tested. A limited time frame did not allow testing of the rocks at strain rates of less than 1×10^{9} s^{1}, but the measured and expected strain rates in-situ are about two to three orders of magnitude lower. In order to overcome this difficulty, it was decided to use the power law of the normalized form:

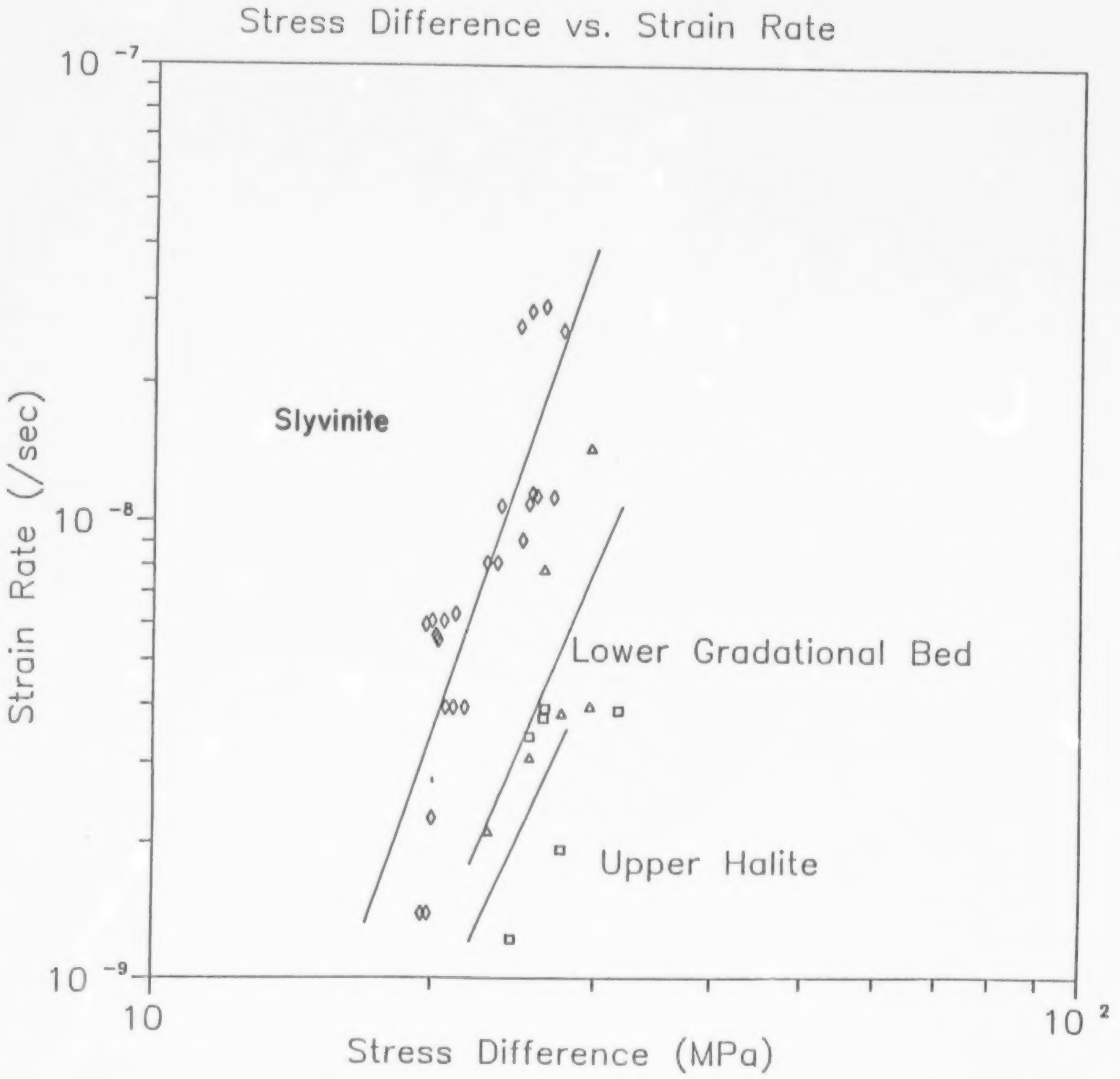
Stress Difference vs. Strain Rate
10 -7
10 -8
10 -9
Strain Rate (/sec)
10
10 2
Stress Difference (MPa)
Slyvinite
Lower Gradational Bed
Upper Halite

FIGURE 3.9

$$\dot{\epsilon}_{ss} = \dot{\epsilon}_{K}\left(\frac{\Delta\sigma}{2K}\right)^{n}$$

K ... Prandtl Limit

$\dot{\epsilon}_{K}$ ... steady state strain rate at Prandtl Limit

The rationale for this approach is explained in Volume 4, as is the method of determining the Prandtl Limit. The magnitudes of exponents n above the stress level of 2K were accepted as determined by the power law fit and the magnitudes of $\dot{\epsilon}_{K}$ were derived from extensometer readings in the Test Room and the Test Stope. The magnitude of exponent m below the stress level of 2K was estimated as explained in Volume 4. Following are the properties used in numerical modelling:

	2K (MPa)	$\dot{\epsilon}_{K}$ (s^{-1})	n $\Delta\sigma \geqq 2K$	m $\Delta\sigma < 2K$
Sylvinite Bed	17.6	3×10^{-11}	6.0	1.0
Upper Halite	20.0	3×10^{-11}	4.5	1.0
Lower Gradational Bed	18.8	3×10^{-11}	4.8	1.0

The authors would have preferred different formulation of the constitutive law, but a more traditional approach was used in order to avoid controversy. However, the results of the program calibration runs, as described in Volume 5, support the validity of the approach used.

SECTION 4.0

4.0 BACKFILL MATERIALS TESTING

The backfill material for the Denison-Potacan potash mine is the combined tailings refuse stream from the beneficiation process. The material is relatively fine grained, consisting primarily of the halite component of the Sylvinite Bed.

The backfill material will be expected to densify during placement and closure of the mine opening until it provides structural support for the overburden during the second stage, or pillar mining, phase of Denison-Potacan's mining operation.

To enable an evaluation of physical properties, samples of the tailings materials were collected and shipped to the University of Waterloo. A broad range of tests were planned to enable the backfill materials to be fully characterized.

4.1 SAMPLE COLLECTION AND CHARACTERIZATION

The backfill samples were collected by Denison-Potacan staff during normal operation of the process plant.

The procedure for sampling the backfill materials is described in Denison-Potacan's report in Appendix B. Process brine was also sampled.

In all respects, the sampling procedure was designed to recognize all potential influences which could have produced non-representative samples, such as:

1. The mill feed ore was judged to represent an average daily condition in terms of the type of ore being processed.

2. The mill was judged to be operating at steady state conditions prior to sample collection, and all of the beneficiation steps were operating normally.

3. Moisture sampling was done prior to and during the course of collecting the sample materials, to detect whether steady state conditions were in effect during the sampling interval.

4. The individual coarse (scroll filter) and fine (string filter) components were sampled, as was the combined tailings sample which constitutes the proposed backfill material.

5. The samples were collected and placed into sealed epoxy-lined steel drums immediately so as to prevent moisture loss. At the University of Waterloo, the samples were repacked into 19 litre plastic pails from the drums to prevent any corrosion effects affecting the samples.

6. A number of the tests at the University of Waterloo were done to compare selected properties from the top, middle or bottom of the sample drums, to ensure that representative sampling was done from the bulk samples collected.

Additional samples were collected from the tailings pond area by Denison-Potacan personnel to evaluate the characteristic density of the natural sedimentation process. These samples were collected and tested as per Denison-Potacan's report in Appendix C. The naturally sedimented material at less than 1% moisture content had experienced both natural drainage and evaporation processes for an indeterminate length of time, but otherwise was representative of backfill as it would be placed underground, if slurry transportation and sedimentation were used as the placement means.

4.2 GRAIN SIZE

The grain size distribution of the particles of the backfill materials was determined at the University of Waterloo using the methods discussed in their report contained in Appendix D.

Samples of the slimes fraction, the coarse fraction, and the combined tailings stream (which is the proposed backfill material) were tested, producing the characteristic grain size distribution curves as in Figures 4.1 and 4.2.

Figure 4.3 is a reproduction of Figure 4.1 for the combined or bulk sample, but showing additional plots of typical mill tailings and backfill materials used, or proposed to be used, at other mines. In comparison to conventional hardrock tailings backfill material, the Denison-Potacan backfill material:

i) is characteristically coarser;
ii) is similarly graded;
iii) contains negligible slimes material (sizes less than 200 mesh or .075 mm).

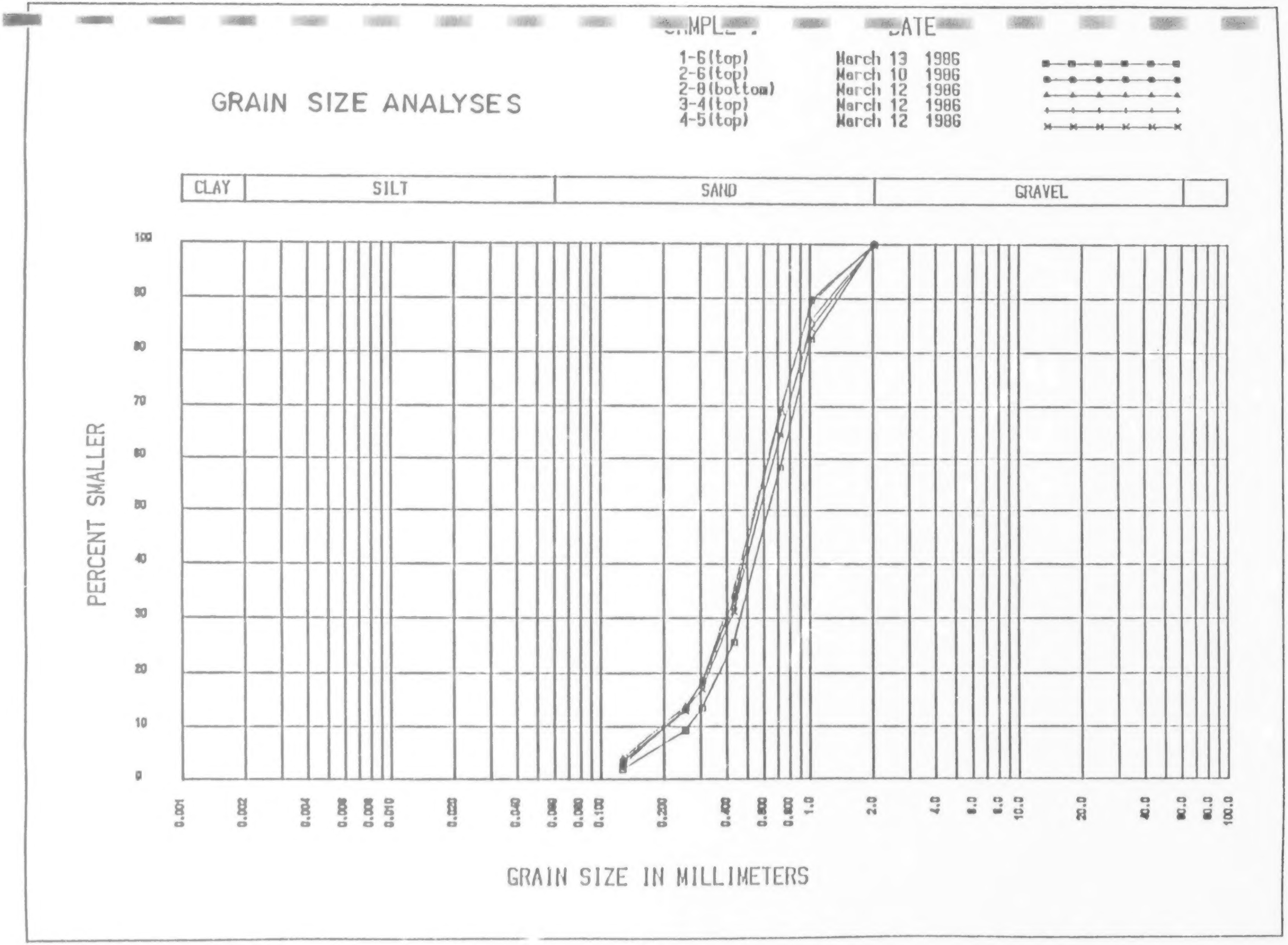

Grain Size Analyses, Bulk Samples

FIGURE 4.1

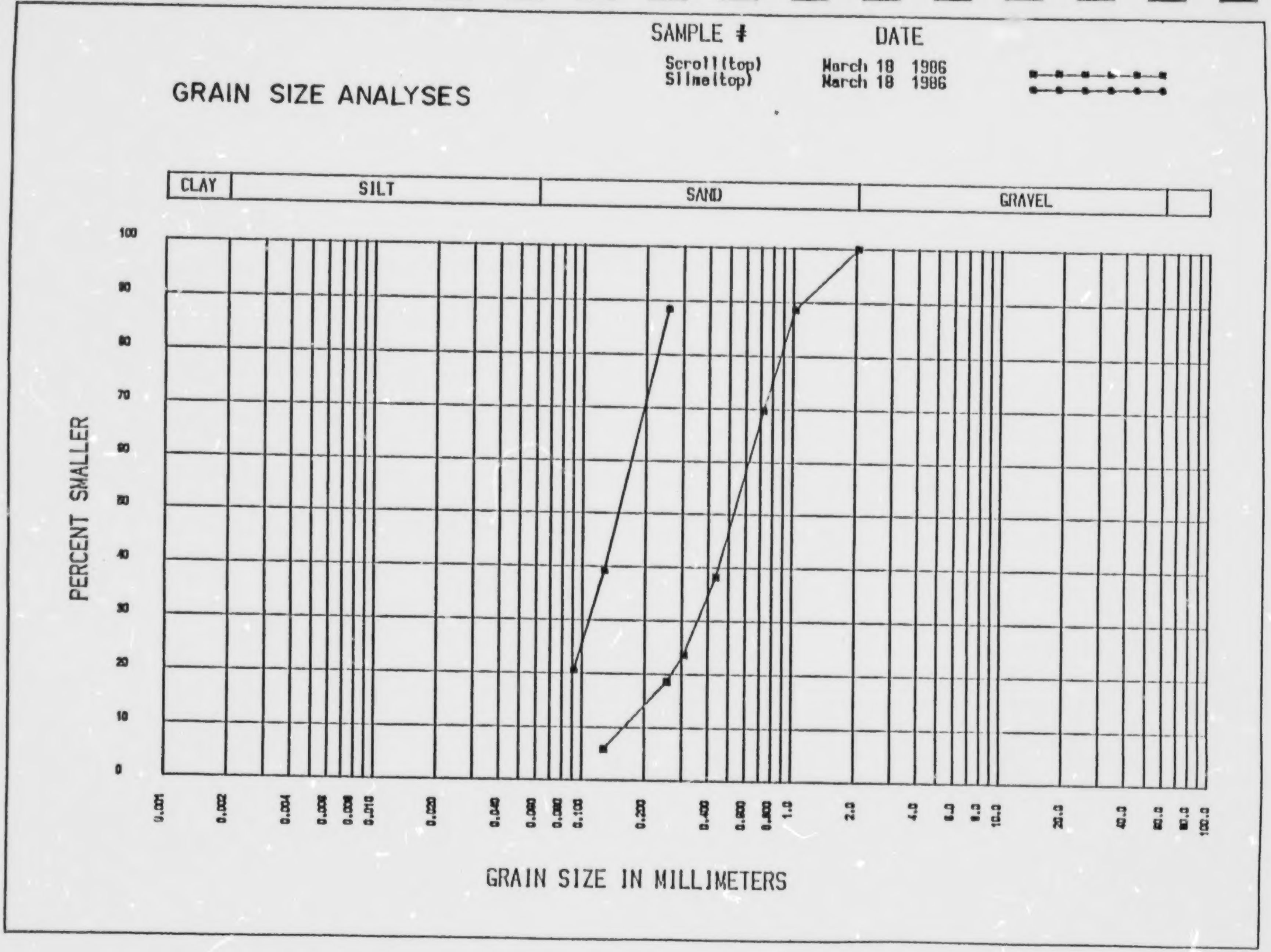

Grain Size Analyses, Scroll and Slimes Tailings

FIGURE 4.2

GRAIN SIZE ANALYSIS : TYPICAL TAILINGS

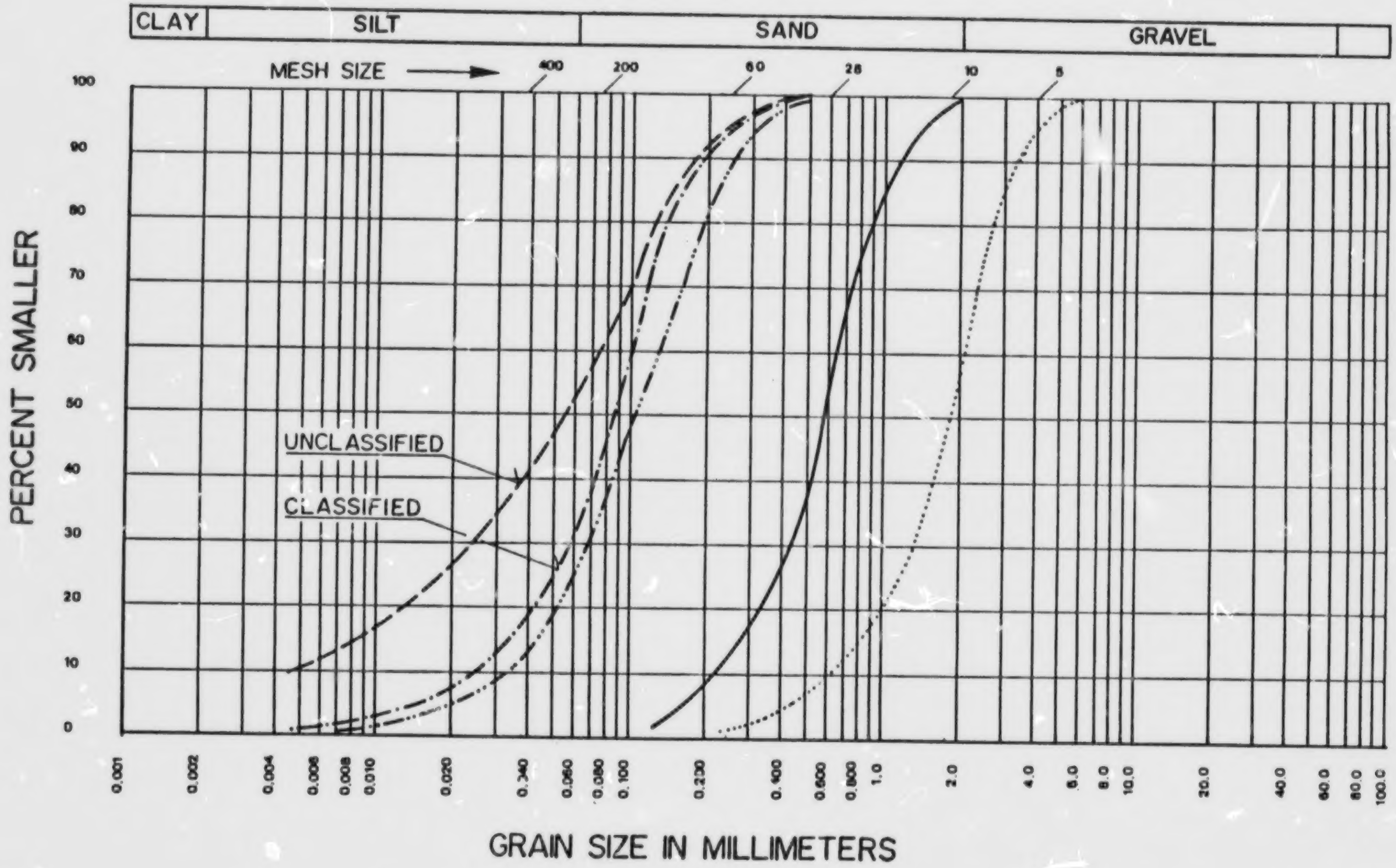

A - CURVE — — — — UNCLASSIFIED NICKEL - COPPER TAILINGS; REF. 1, p. 114.
B - CURVE —·—·—·— CLASSIFIED NICKEL - COPPER TAILINGS, REF. 1, p. 114.
C - CURVE —··—··—·· UNSPECIFIED MILL TAILINGS; REF. 1, p. 118.
D - CURVE ———— DENISON - POTACAN COMBINED TAILINGS STREAM.
E - CURVE ·············· ROCANVILLE SALT TAILINGS, REF. 2, p. 12.

FIGURE 4.3

In comparison to the proposed Rocanville salt tailings backfill material, the Denison-Potacan backfill is considerably finer in grain size distribution.

4.3 MINERALOGICAL

The mineralogical testing of the Denison-Potacan material was performed at the University of Waterloo using the procedures and equipment described in their report in Appendix D.

Only two mineral types were detected in the backfill samples; halite and sylvite. In general, the amount of sylvite was less than 5%; the balance being made up primarily of clear and coloured halite.

In contrast to prior work on Saskatchewan tailings, no discernible insoluble component exists in the backfill, although trace amounts of clays were visible in the tailings pond area. Denison-Potacan personnel expressed the opinion that the insoluble component probably was not captured in the tailings circuit due to its fineness. It would, therefore, be retained in the process brine circuit, and would eventually be discarded with the excess process brine.

4.4 MOISTURE CONTENT

Typically, moisture content values determined and reported at an operating potash plant are calculated from a weighing/oven drying/weighing procedure, which does not take into account the precipitation of halite and sylvite solids during the oven drying step.

A correction must be made to enable meaningful mass balance calculations for dry solids and drainage brine volumes/masses during backfilling. The correction procedure and calculations are contained in Appendix D in the University of Waterloo's report.

Table 1, from the University of Waterloo report is reproduced here to show the relative values of the uncorrected moisture content, Wc, and the corrected values, Wct. It can be seen here that a reported moisture content of 20% will actually have about 22% brine content prior to evaporation of the water.

Reproduced from University of Waterloo report:

TABLE 4.1
INITIAL MOISTURE CONTENT DETERMINATIONS

DRUM	LOCATION	Wc(%)	Wct(%)
1	top	1.75	1.77
	middle	10.85	11.38
	bottom	19.95	21.85
2	top	2.32	2.34
	middle	5.23	5.35
	bottom	20.61	22.64
3	top	2.54	2.57
	middle	6.06	6.22
	bottom	18.19	19.75
4	top	2.16	2.18
	middle	6.02	6.18
	bottom	21.69	23.94
Scroll	middle	2.89	2.92
Slimes	middle	35.70	42.24*

* Slimes samples arrived saturated.

Table 3 from Denison-Potacan's report in Appendix B is reproduced here as a measure of the average moisture content of the proposed backfill material. The average uncorrected moisture content is 7.53%, corresponding to a corrected moisture content of 7.8%. This value will be used for all subsequent calculations.

Reproduced from Denison-Potacan's report:

TABLE 4.2
COMBINED STREAM TAILINGS MOISTURE
CONTENT SAMPLES

SAMPLE TIME	% MOISTURE
4A (10:51)	6.8
4B (11:07)	7.5
4C (11:13)	6.5
1A (11:23)	6.9
1B (11:38)	7.7
1C (11:47)	8.7
3A (12:48)	7.3
3B (13:02)	7.7
3C (13:15)	8.0
2A (13:23)	8.0
2B (13:37)	7.8
2C (13:51)	7.5
AVERAGE	7.53%

It should be noted here that the mass balance information derived by Kilborn for the operation of the process plant actually anticipated a somewhat higher moisture content corresponding to 8.6% by weight.

4.5 SPECIFIC GRAVITY

The specific gravity of the proposed backfill material was calculated at the University of Waterloo based upon the mineralogical composition of the sylvinite/halite mixture. The calculated average specific gravity is 2.15.

SECTION 5.0

5.0 BACKFILL PLACEMENT DENSITY TESTING

The placement density testing methods and results are contained in the University of Waterloo's report in Appendix D, and in Denison-Potacan's report in Appendix E.

The laboratory placement density trials were designed to evaluate the suitability of various practical placement methods, from the standpoint of achieving maximum packing density. As noted in the discussions following, each laboratory test has an approximate corresponding practical equivalent for actual in-situ placement.

The goal of maximizing placement density has two desirable benefits:

i) Maximize the disposal of plant tailings in the mine;

ii) Minimize porosity in the backfill to improve its potential ability to stabilize the mine openings.

Table 5.1 presented here is a summary and reference table of values to illustrate the porosity percentages to be expected in various room heights assuming various achievable backfill densities.

5.1 PLACEMENT BY SPREADING ONLY

Appendix D contains the graphical results of the laboratory density testing at various moisture conditions and compaction conditions.

The initial density of salt tailings backfill material loosely placed in a mine stope can be inferred from the test results and the literature as having a lower boundary of about 1.0 equivalent specific gravity (dry basis). The calculated porosity would be 53.7% on a volume basis.

TABLE 5.1

PLACEMENT METHODS: RANGES OF EXPECTED POROSITY

LABORATORY PLACEMENT METHOD	SPECIFIC GRAVITY (Dry)	POROSITY (dry) %	AVERAGE POROSITY PERCENTAGES			
			10m High %	15m High %	20m High %	30m High %
Loose Or Flinger Placement	1.00	53.7	58.33	56.79	56.02	55.25
	1.10	49.1	54.17	52.47	51.62	50.77
	1.20	44.4	50.00	48.15	47.22	46.30
Rodding Placement	1.30	39.8	45.83	43.83	42.82	41.82
Slurry sed'n, Vibro-Comp'n	1.40	35.2	41.67	39.51	38.43	37.35
	1.50	30.6	37.50	35.19	34.03	32.87
Bomag Dual-Drum Comp.*	1.60	25.9	33.33	30.86	29.63	28.40
	1.70	21.3	29.17	26.54	25.23	23.92
	1.80	16.7	25.00	22.22	20.83	19.44
	1.90	12.0	20.83	17.90	16.44	14.97
	2.00	7.4	16.67	13.58	12.04	10.49
	2.10	2.8	12.50	9.26	7.64	6.02
Solid Rock-Salt	2.16	0.0	10.00	6.67	5.00	3.33

NOTE: In all cases it is assumed that fill will be placed at an average density as shown to within 1 metre of the back.

* Achieved in surface trials at mine site.

5.2 PLACEMENT BY SLURRY SEDIMENTATION

The sedimentation density results reported in the Denison-Potacan testing in Appendix C are at best an approximation for two reasons:

i) The natural evaporation process for the tailings pond samples will introduce an error such that the true dry density average value will be lower than reported here;

ii) The self-weight consolidation forces which would be present in an actual stope may, in fact, have the effect of compacting the backfill to a higher value than reported here.

There being no means of estimating the trade-off between these two opposing effects, an average dry density value of 1.33 g/cc will be assigned to the natural sedimentation process. The calculated porosity in this case will be 38.4% on a volume basis.

5.3 PLACEMENT BY RODDING METHODS

The standard Proctor Test, which involves a procedure of filling a cylindrical mould in lifts with rodding/compaction of the sample, produced a dry specific gravity of 1.3 independent of initial moisture content. This corresponds to a porosity ratio of 39.8% on a volume basis.

This placement test would approximately simulate compaction of lifts of backfill in a stope by a sheeps-foot roller.

5.4 PLACEMENT BY FLINGER METHODS

The laboratory drop tests simulate placement by conveyor flinger or pneumatic means in the mine stope. Various energy levels of particle impact were achieved by dropping the sample material through a tube at variable heights into the sample container.

In this test, the range of dry specific gravity achieved was from 0.86 to 1.14. Moisture content had a significant effect, as did total drop height, in achieving higher compaction density.

The lack of large, massive particles in the size distribution of the backfill limits the ultimate packing density achievable by this mechanism to the lowest density achieved of any of the methods tested. The corresponding porosity range will be from 60.7% to 47.2% by volume.

5.5 PLACEMENT BY VIBRO-COMPACTION METHODS

The test procedure for this method consisted of placing various reaction weights on the upper surface of a loosely filled sample in a cylindrical mould, which was then vibrated on a vibrating table for various lengths of time. This test simulates, from a laboratory viewpoint, the vibro-compaction effort of typical civil construction machinery used for foundations and/or road construction.

Densities achieved demonstrated a beneficial effect from higher moisture content and from higher specific pressure. The specific gravity achieved at 7.36 kPa and 12% moisture was about 1.4. The corresponding porosity ratio would be 35.2% by volume.

5.6 SURFACE TRIALS: FULL SCALE EQUIPMENT

A series of tests were performed by Denison-Potacan personnel at the plantsite to evaluate potential densities achievable by actual mining/construction equipment. The test procedures and results are contained in Appendix E of this report. These tests provide a valuable insight into the performance potential of actual equipment without the scaling uncertainty of laboratory data.

Backfilling practise at the Potash Company of America's (PCA) New Brunswick potash mine involves the use of LHD vehicles to spread the backfill. Compaction under the tires of the vehicle is an incidental, but real, mechanism of compaction. Since this would be a viable method of backfill distribution in the Denison-Potacan mine, a surface test was designed using a Wagner ST-8A scooptram vehicle to construct various lift heights of backfill of from 0.45 to 1.2 m with vehicle travel effects from compaction of fill under the tires.

Auxiliary compaction of the backfill using vibratory roll equipment, such as is common in road construction work, would also be viable underground at Denison-Potacan. To evaluate the ultimate potential of this method, a Bomag dual drum vibratory compaction machine, model BW65S, was used to compact lifts of 0.18 m and 0.25 m of placed backfill in a surface tailings storage area at the Denison-Potacan plantsite.

The ASTM sand cone method was used to determine backfill density achieved in both cases. The results of these trials are summarized in Table 5.2.

TABLE 5.2

SURFACE TRIALS: BACKFILL DENSITY

TEST METHOD	LIFT HEIGHT (m)	DRY DENSITY (t/m^3)	
ST-8A	0.45	1.324	
ST-8A	1.2	1.470	
ST-8A	0.45 *	1.296	Average 1.379 t/m^3
ST-8A	1.2 *	1.425	
Bomag	0.18	1.631	Average 1.611 t/m^3
Bomag	0.25	1.591	

* Indicates density measured one day after compaction.

The test results from the surface trials support the trend of the results of the lab trials; vibro-compaction provides an effective auxiliary means of achieving higher backfill density.

The expected porosity of the backfill spread by the scooptram with incidental compaction by the tires is 36.1% by volume.

The expected porosity of the backfill which has auxiliary vibro-compaction densification is 25.4% by volume.

SECTION 6.0

6.0 BACKFILL CONSOLIDATION TESTING

The backfill consolidation tests done at the University of Waterloo used the full stream tailings as the proposed backfill material. The testing facilities and the testing methods are described in the University of Waterloo's reports in Appendix A.

The purpose of the backfill consolidation testing was at least two-fold; to establish a support function and the failure criterion for the fill at less than 100% consolidation. The support function will be interactive with the intact rock stress function, such as to modify the stress conditions around the mine opening by some amount, and to thereby affect closure rates by some amount. The failure criterion will be established so as to predict the limits of closure velocity associated with brittle failure of the consolidated backfill.

6.1 CONSOLIDATION TESTING

During the course of the research program, it became clear that the physical characteristics of loosely consolidated backfill materials would be of little relevance for the Denison-Potacan situation.

Rather, the emphasis in this research work was to test and assess the properties of highly consolidated samples preferably containing porosity, for example, of only 5% to 20% by volume. This porosity will approximate much more closely the condition of the backfill at the time when second stage mining may be appropriate.

Consolidation tests have been completed using loosely packed samples at relatively low consolidation pressures. Also, highly consolidated samples were prepared and tested at high uniaxial stress levels and strain rates in triaxial testing.

6.2 CONSOLIDATION TEST RESULTS

The consolidation curves in Figures 6.1 and 6.2 illustrate two characteristics of importance:

i) initial consolidation occurs rapidly from a loosely packed initial condition;

ii) at constant uniaxial stress conditions, consolidation continues to occur at significant rates at typical densities achievable by practical placement means.

The actual densities achieved at a uniaxial (confined) stress condition of 5 MPa over a seventeen-day period increased from an initial 1.16 g/cc value to a value in the range of 1.4 to 1.5 g/cc. During the test, the strain rate (equal to volumetric reduction rate in this case) was in the range of 1% to 3% per day.

Actual equilibrium strain rates of the mine openings at Denison-Potacan are in the order of only 0.0004% per day; almost four orders of magnitude slower.

The results of further consolidation testing over a period of 90 days, shown in Figure 6.3, of the Denison-Potacan tailings at 2.5% moisture content and varying uniaxial (confined) stress conditions support the initial hypothesis that the emplaced backfill will have limited support capability prior to almost complete elimination of porosity in the fill during the closure history of the backfilled openings. Nevertheless, due to the intergranular friction, it will slow down the closure which may further extend the time required to achieve the required support capability.

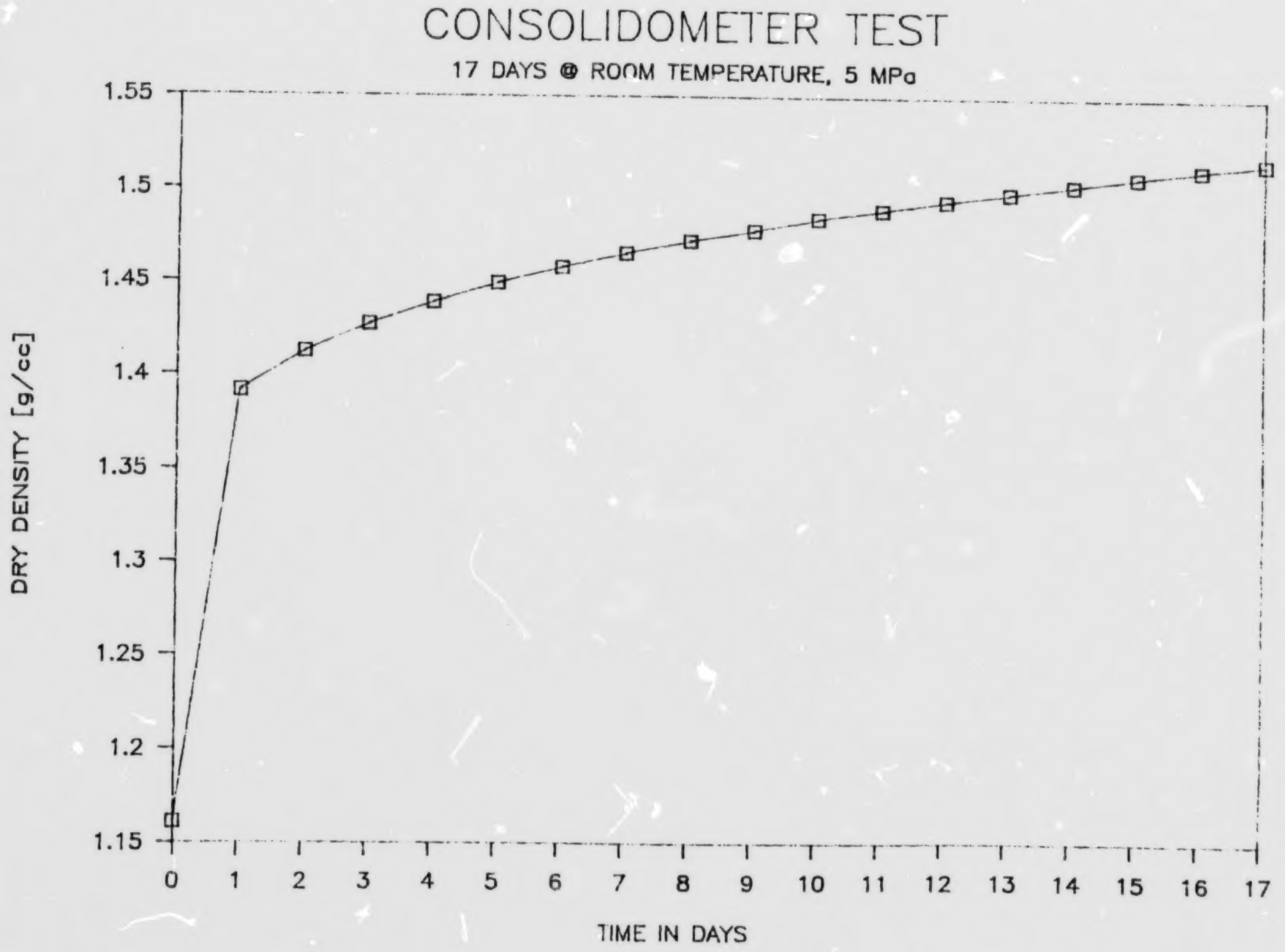
CONSOLIDOMETER TEST
17 DAYS @ ROOM TEMPERATURE, 5 MPa
DRY DENSITY [g/cc]
1.55
1.5
1.45
1.4
1.35
1.3
1.25
1.2
1.15
0
1
2
3
4
5
6
7
8
9
10
11
12
13
14
15
16
17
TIME IN DAYS

FIGURE 6.1

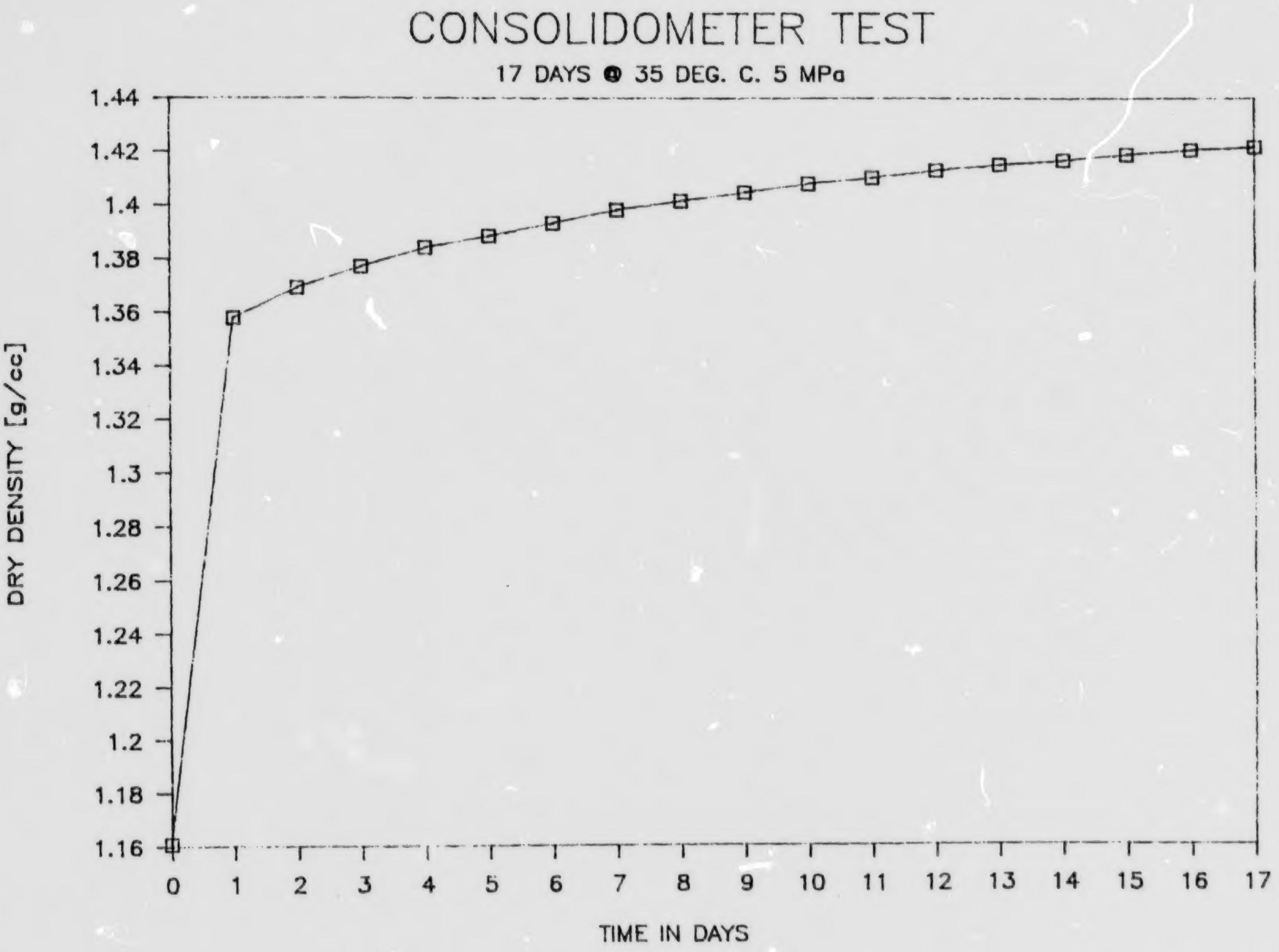
CONSOLIDOMETER TEST
17 DAYS @ 35 DEG. C. 5 MPa
DRY DENSITY [g/cc]
1.44
1.42
1.4
1.38
1.36
1.34
1.32
1.3
1.28
1.26
1.24
1.22
1.2
1.18
1.16
0
1
2
3
4
5
6
7
8
9
10
11
12
13
14
15
16
17
TIME IN DAYS

FIGURE 6.2

Figure 6.3 shows that the greater the initial confinement stress on the backfill, the more rapid the initial compaction which then, as time progresses, slows to similar rates no matter what the confinement stress value.

This suggests that, at the beginning of compaction, the "open" voids are closed more rapidly as a direct function of confinement stress and, hence, the rise of the curves is quite varied, but with advancing compression another mechanism takes over, that of intergranular friction.

It has been suggested that this is due to the fact that not all of the halite tailings grains are involved in the load transmission and they slow down the compaction by their intergranular friction.

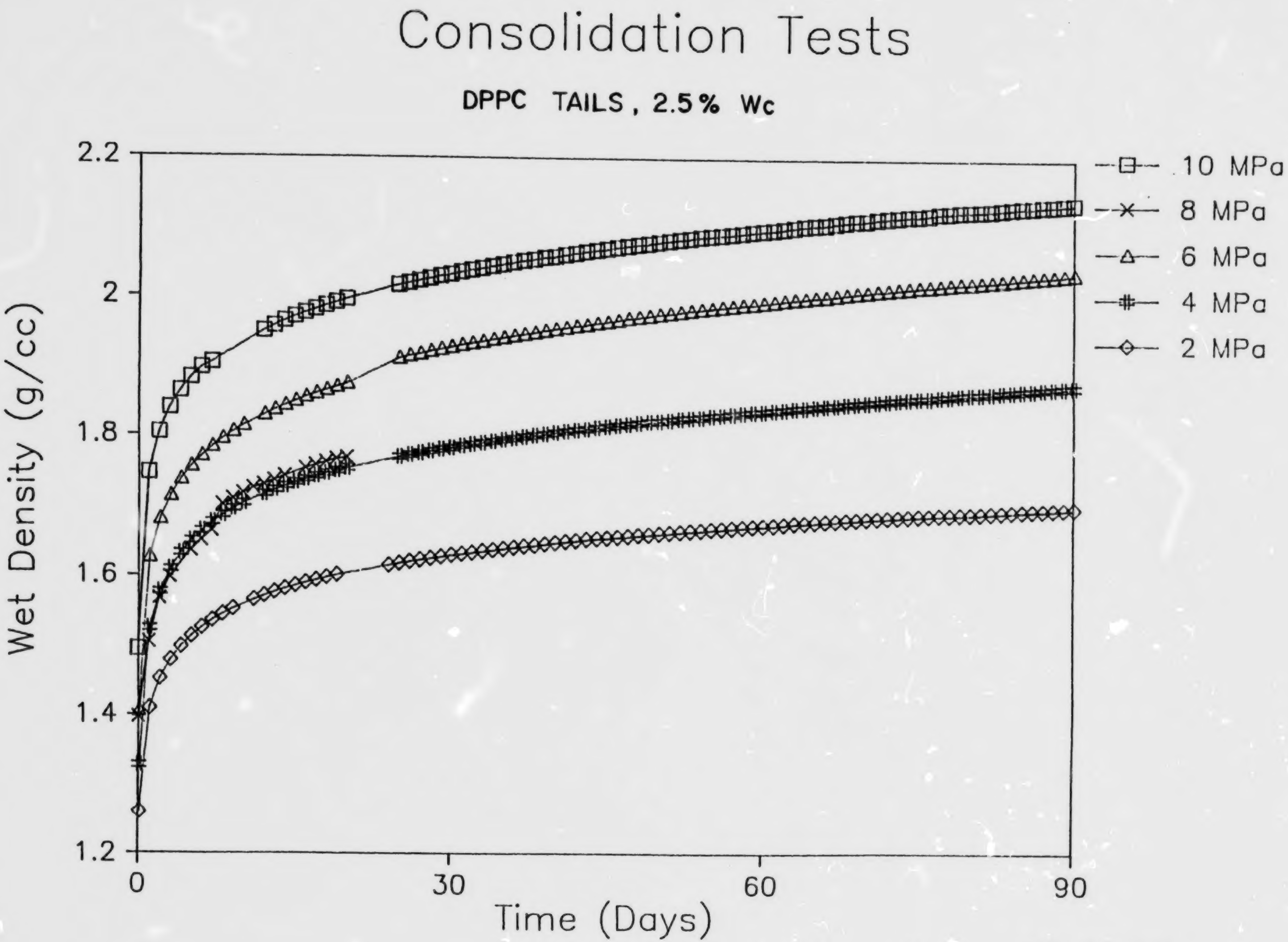
Consolidation Tests
DPPC TAILS, 2.5% Wc
Wet Density (g/cc)
2.2
2
1.8
1.6
1.4
1.2
0
30
60
90
Time (Days)
10 MPa
8 MPa
6 MPa
4 MPa
2 MPa

FIGURE 6.3

SECTION 7.0

7.0 BACKFILL TRIAXIAL TESTING

The brittle yield triaxial testing was performed at the University of Waterloo using the full stream tailings as the proposed backfill material. The testing facilities and the testing methods are described in the University of Waterloo's reports in Appendix A.

The purpose of the backfill triaxial testing was to enable the development of brittle yield failure envelopes for the backfill material, such as are suggested by the curves in Figure 7.1

Table 7.1, presented here, is a summary and reference table of results to date:

TABLE 7.1

BRITTLE YIELD TRIAXIAL TESTING RESULTS FOR BACKFILL SAMPLES CONSOLIDATED TO 90%

SAMPLE NUMBER	TIME OF PREPARATION (hrs)	UNCONFINED (psi)	STRENGTH (MPa)
1-90	36	1,009.8	6.96
2-90	36	972.8	6.71
3-90	1	407.1	2.81
4-90	1	645.0	4.45

These results are insufficient to enable the development of brittle yield failure envelopes and additional testing, beyond the scope of Phase I of the research project, is required.

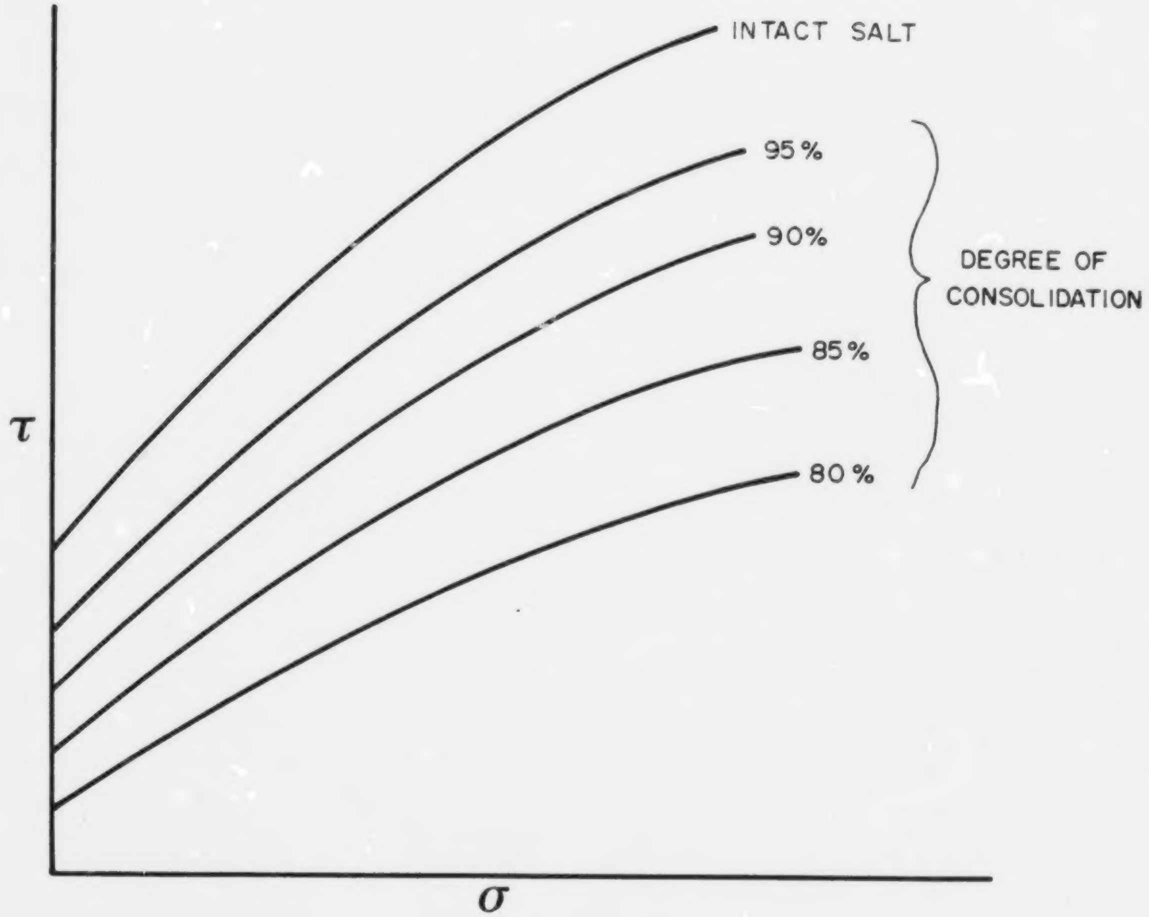

τ - SHEAR STRESS
σ - NORMAL STRESS

PROPOSED BRITTLE FAILURE TESTING ON SALT BACKFILL.

FIGURE 7.1

Should further research proceed, then additional samples will be made at the higher ranges of consolidaton, for example, with porosity in the range of 5% to 20% corresponding to the specific gravity range of 2.0 to 1.7.

The samples would be made at very high uniaxial pressures over very short periods of time. It is expected that these samples will be weaker than the actual in-situ case, since the re-healing mechanism may operate more effectively under in-situ conditions. The results, in this case, would be conservative.

SECTION 8.0

8.0 WAFER CELL CALIBRATION

The Saskatchewan Research Council (SRC) wafer cell was calibrated in the WATSALT Test Facility at the University of Waterloo in samples of Lower Gradational Bed salt (Samples 44 and 45). Two specially constructed wafer cells were tested. Each was 15.25 cm (6 in) long by 5.2 cm (2 1/8 in) wide. Cells used as in-situ instrumentation are 25.0 cm long by 5.2 cm wide.

To calibrate the wafer cells, creep test samples were prepared. They were then to be cored axially by a 5.7 cm coring bit. This proved difficult, however, as the samples were only 10.2 cm in diameter and tended to fracture during drilling. It was then decided to create a slot for the wafer cells by drilling a series of small holes across the diameter of the salt specimen.

A 1.3 cm carbide bit was specially sharpened to drill the holes. Three holes were drilled; the first down the center of the sample and two more at about 2.5 cm on either side of the central hole. The material between the holes was carefully cut out and the faces of the slot smoothed with a file and fine grit sandpaper. The final slot size was approximately .8 cm larger than the wafer cell.

The wafer cell was placed in the slot equidistant from the ends of the sample and a brine grout poured between the salt and the wafer cell. As the grout was poured, the salt sample was vibrated lightly on a vibrating table to ensure that no air bubbles were trapped. The grout was then left to cure for one week (Figure 8.1).

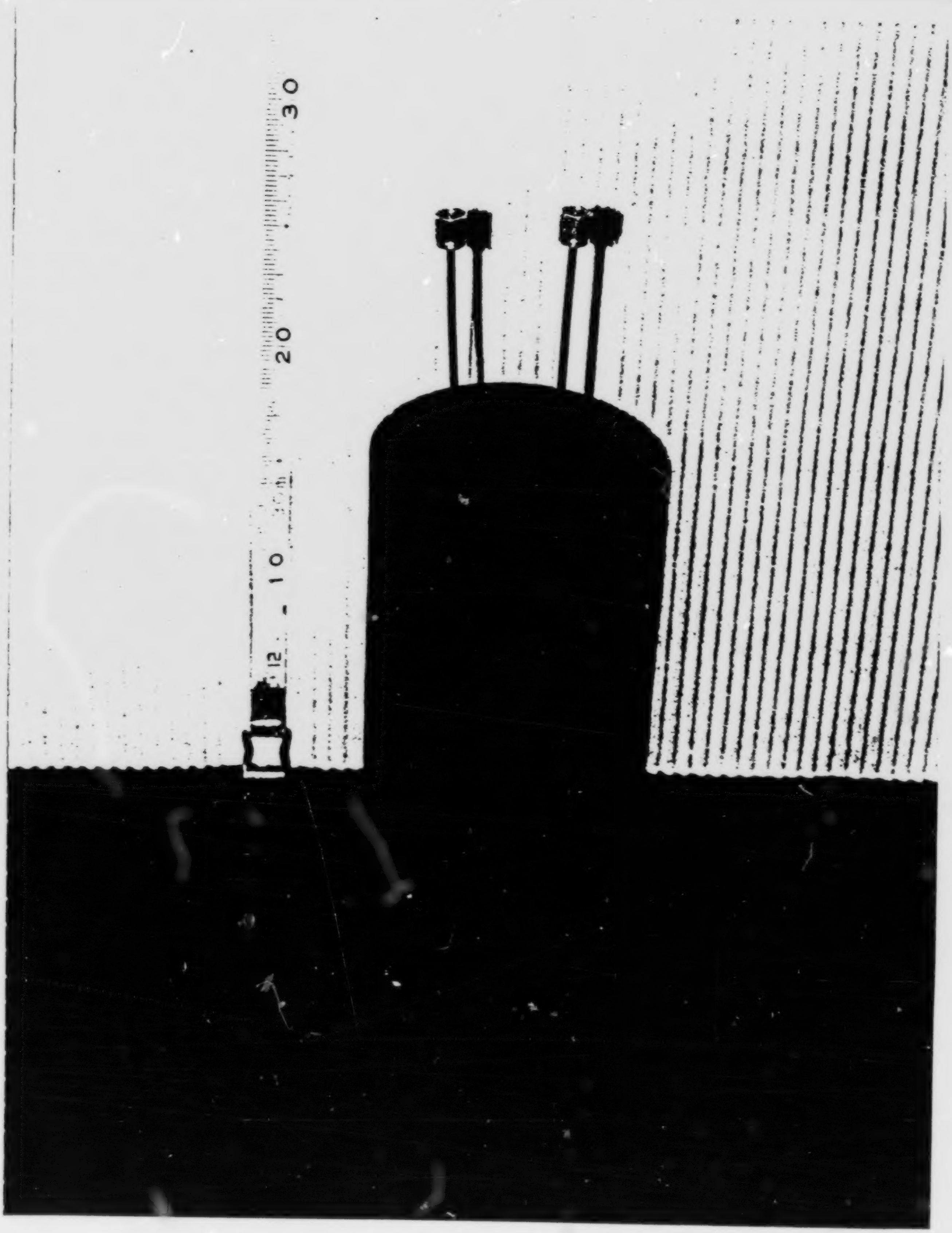

FIGURE 8.1

When the grout was cured, the ends of the salt sample were again sanded with fine sandpaper to ensure a smooth interface betwen the salt and the loading platen. The sample was mounted in a triaxial cell with the two wafer cell oil lines (feed and bleed) exposed through a specially constructed axial platen. A 34.5 MPa (5,000 psi) pressure transducer was placed in the oil feed line to monitor the wafer cell's response to stress. Oil was then pumped in through the feed line of the wafer cell until it began flowing out the bleed line. The bleed line was capped and the temperature chamber replaced around the triaxial cell. The feed line was left open and connected to the oil pump during the 24 hour temperature adjustment period to assure that no internal pressures would build up with the temperature increase. The temperature was raised to 26 degrees celsius.

When the triaxial cell temperature had equilibrated (after about 24 hours) the feed line to the wafer cell was closed and the axial and confining pressures were raised to 5 MPa (hydrostatic). The set up was again left for 24 hours to ensure that all hydraulic connections were leak free and that the wafer cell itelf remained intact.

In-situ, SRC wafer cells are often pre-stressed to speed up the response time. The effect of pre-stressing is to force the contents of the borehole (wafer cell and grout) against the surrounding rock. The stress caused by the wafer cell on the surrounding rock dissipates with time and the true in-situ stress is felt by the wafer cell. In the laboratory, pre-stressing is unnecessary and impractical. The imposed stress (confining stress) is applied close to the cell; no stress relieved zone develops as it does around a borehole underground. As well, pre-stressing would probably cause the sample to undergo hydrofracture.

To calibrate the wafer cell, the stress normal to the face of the wafer, the confining stress, was increased and the oil pressure in the wafer monitored. The first stage of calibration was begun by raising the confining stress in the triaxial cell to 10 MPa. It responded very slowly and only reached peak response after about six days. Its peak response was about 7.7 MPa. It was decided that the stress conditions in the triaxial cell (5 MPa axial stress, 10 MPa confining stress) did not create high enough shear stresses within the sample to allow it to creep onto the wafer cell effectively. Essentially, the shear stress in the sample was below the 2K limit.

The next stage of calibration was performed at 20 MPa confining stress; the axial stress remained unchanged. The response at this stress was considerably faster (1.5 days) and a much better representation of the confining stress was measured by the wafer cell (19.52 MPa). The confining stress was then dropped in 2 MPa increments and the wafer cell response measured. The complete response/time curve can be seen in Figure 8.2. Table 8.1 shows the ultimate response of the wafer cell and the time to ultimate response at various confining stresses.

The second wafer cell was prepared and mounted exactly as the first. However, the first stage of calibration was performed at a confining stress of 20 MPa and an axial stress of 5 MPa. After four calibration stages, the axial stress was reduced to 3 MPa and the confining stress cycled from 20 MPa to 10 MPa and back up to 20 MPa. It was decided that 24 hours between calibration stages allowed adequate response time for the wafer cell.

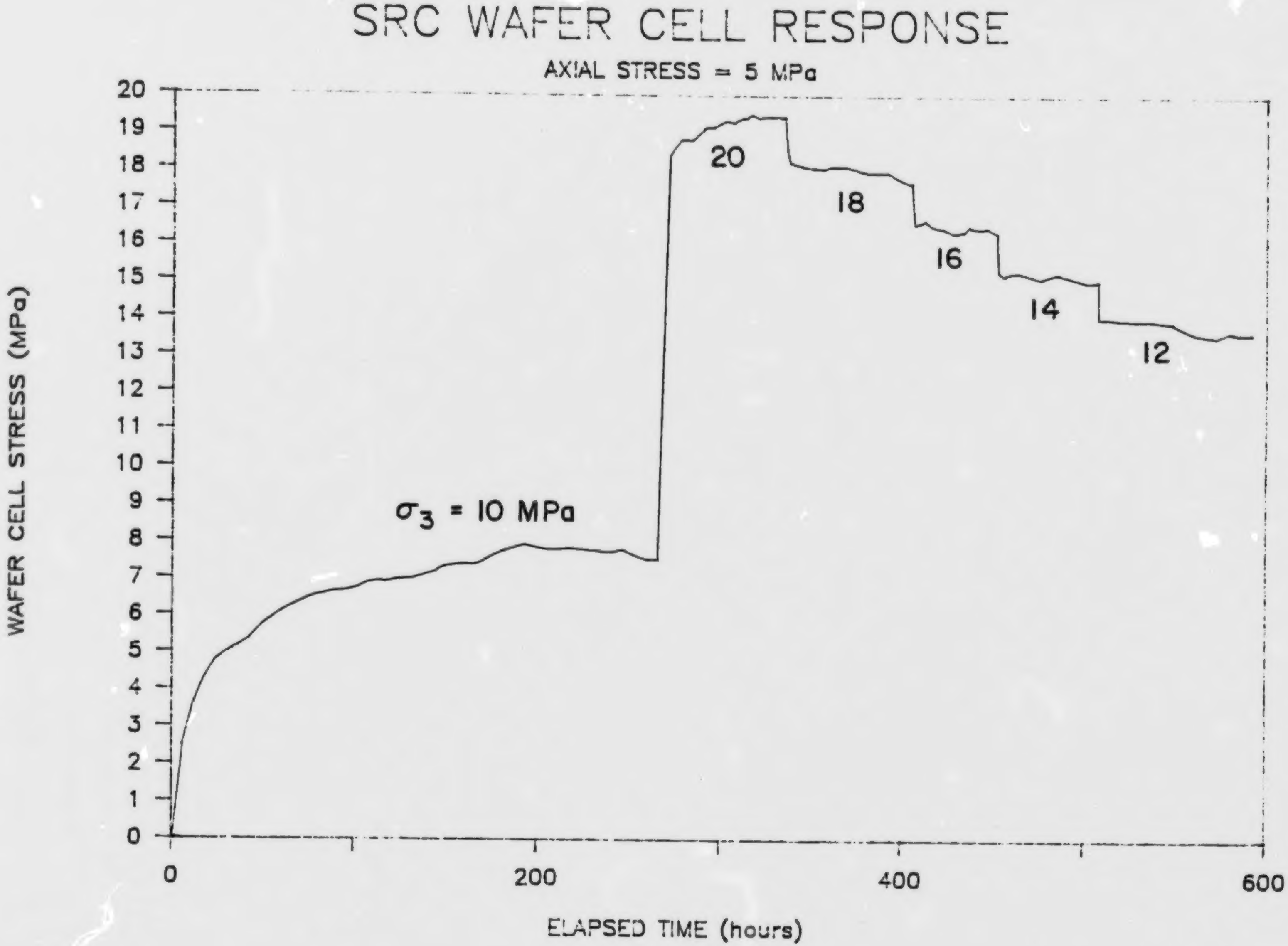
SRC WAFER CELL RESPONSE
AXIAL STRESS = 5 MPa
WAFER CELL STRESS (MPa)
20
19
18
17
16
15
14
13
12
11
10
9
8
7
6
5
4
3
2
1
0
ELAPSED TIME (hours)
0
200
400
600
σ_3 = 10 MPa
20
18
16
14
12

FIGURE 8.2

TABLE 8.1

ULTIMATE RESPONSE OF SRC WAFER CELL

AXIAL STRESS (MPa)	CONFINING STRESS (MPa)	WAFER CELL RESPONSE (MPa)	DIFFERENCE (MPa)	TIME TO ULTIMATE RESPONSE (hrs)
SAMPLE LGB 44				
5	10	7.68	-2.32	144
5	20	19.52	-0.48	36
5	18	17.62	-0.38	22
5	16	16.30	0.30	9
5	14	15.04	1.04	23
5	12	13.51	1.51	16
SAMPLE LGB 45				
5	20	17.09	-2.91	65
5	18	15.84	-2.16	**
5	16	14.75	-1.25	**
5	14	13.72	-0.28	**
3	20	18.22	-1.78	72
3	18	17.20	-0.80	**
3	16	16.07	0.07	**
3	14	15.10	1.10	**
3	12	13.71	1.71	**
3	10	12.25	2.25	**
3	12	13.09	1.09	**
3	14	14.26	-0.26	**
3	16	15.26	-0.74	**
3	18	16.13	-1.87	**
3	20	17.90	-2.10	**
Mean	15.62	15.25	-0.37	

** 24 Hour Stages

Regression analyses were performed on the wafer cell responses (Table 8.2, Figures 8.3, 8.4, 8.5 and 8.6). Regression was performed on each calibration run (Sample LGB 44, Sample LGB 45 5 and 3 MPa axial stress). A linear regression was performed on:

a) All results

b) All results, except the first test (10 MPa confining stress, 7.7 MPa wafer cell response).

It was felt that this result was spurious, as the sample was under very low shear stresses. The only other response at 10 MPa confining (12.25 MPa @ 3 MPa axial stress) was achieved by relaxing the confining stress rather than increasing it to 10 MPa. This allowed the salt to creep rapidly (transient creep) away from the wafer cell, allowing a more accurate wafer cell response more quickly.

Because the effect of axial stress appears to be minimal, mean wafer cell responses and standard deviations were calculated for each confining stress. The results are shown in Table 8.3.

Average deviation from the mean was 0.37 MPa or 2.4% (Table 3.1).

TABLE 8.2

LINEAR REGRESSION CONSTANTS FOR SRC WAFER CELL CALIBRATION

SAMPLE	AXIAL STRESS (MPa)	SLOPE	INTERCEPT (MPa)
LGB 44	5	1.04	-0.65
LGB 44*	5	0.73	4.72
LGB 45	5	0.56	5.83
LGB 45	3	0.57	6.61
Bulk 1**		0.70	4.29
Bulk 2***		0.58	6.36

* All stages, except first stage calibration

** All calibration results

*** All calibration results, except first stage calibration

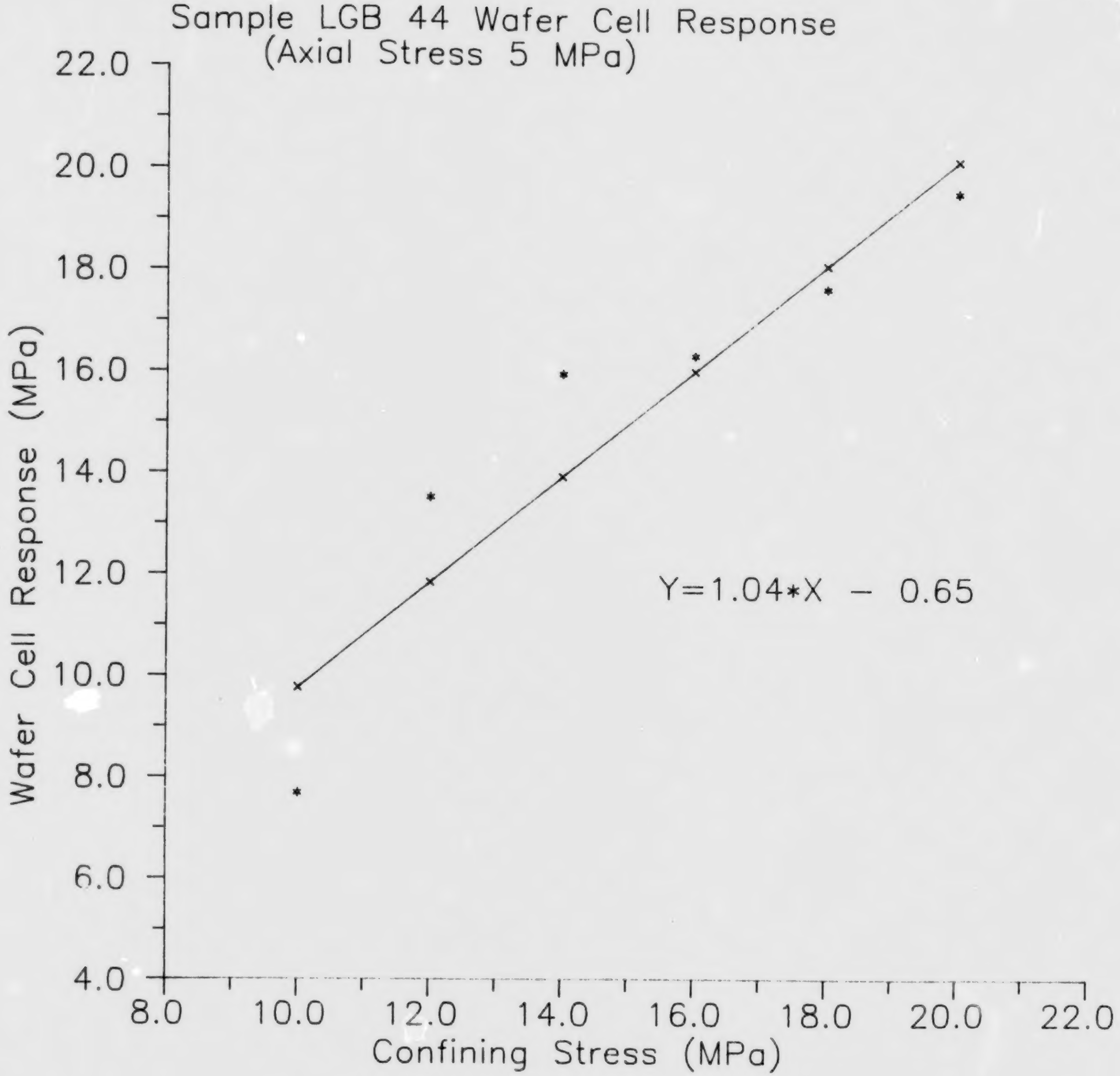
Sample LGB 44 Wafer Cell Response
(Axial Stress 5 MPa)
Wafer Cell Response (MPa)
22.0
20.0
18.0
16.0
14.0
12.0
10.0
8.0
6.0
4.0
Y=1.04*X - 0.65
8.0
10.0
12.0
14.0
16.0
18.0
20.0
22.0
Confining Stress (MPa)

FIGURE 8.3

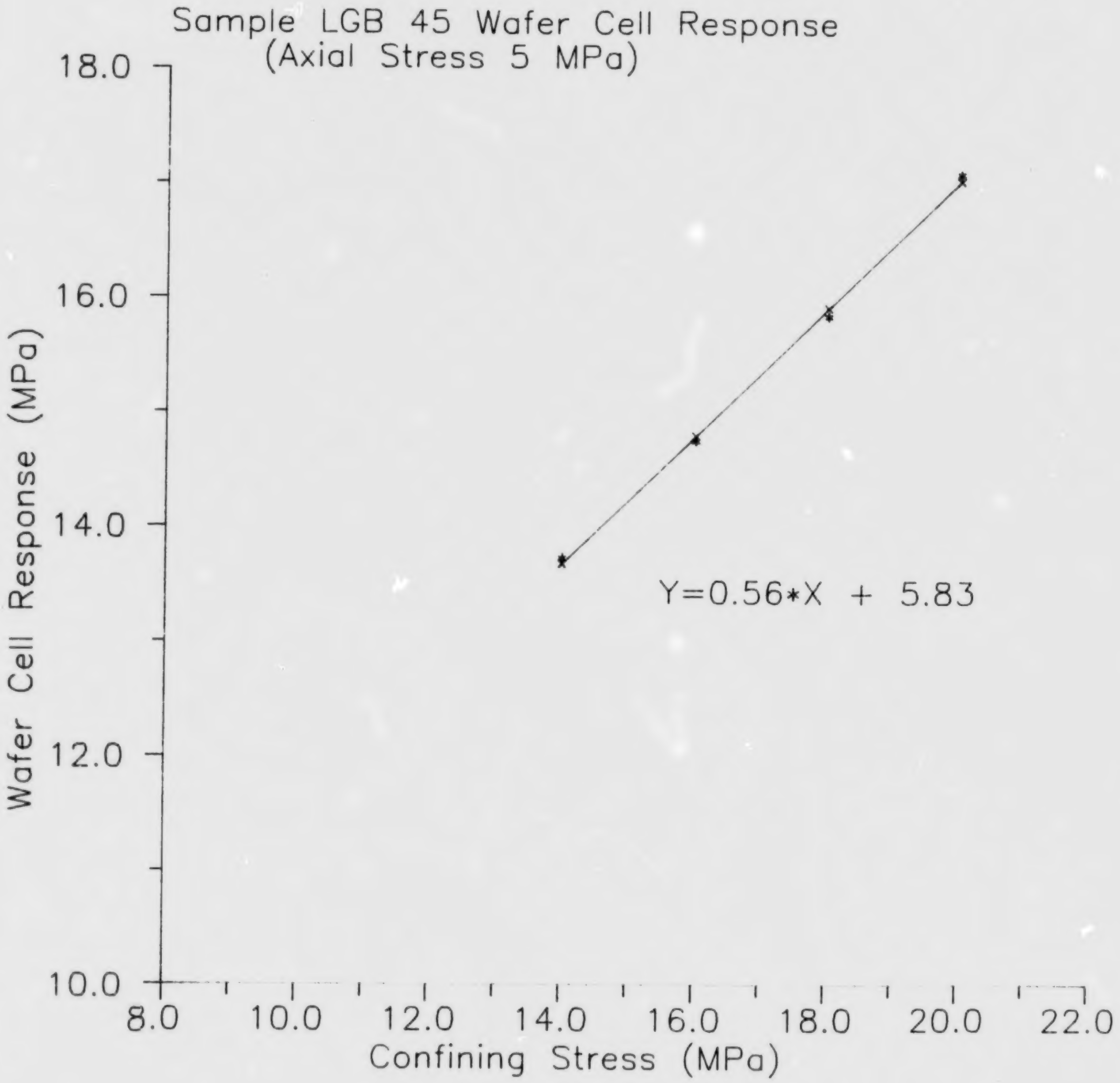
Sample LGB 45 Wafer Cell Response
(Axial Stress 5 MPa)
18.0
16.0
14.0
12.0
10.0
Wafer Cell Response (MPa)
Y=0.56*X + 5.83
8.0
10.0
12.0
14.0
16.0
18.0
20.0
22.0
Confining Stress (MPa)

FIGURE 8.4

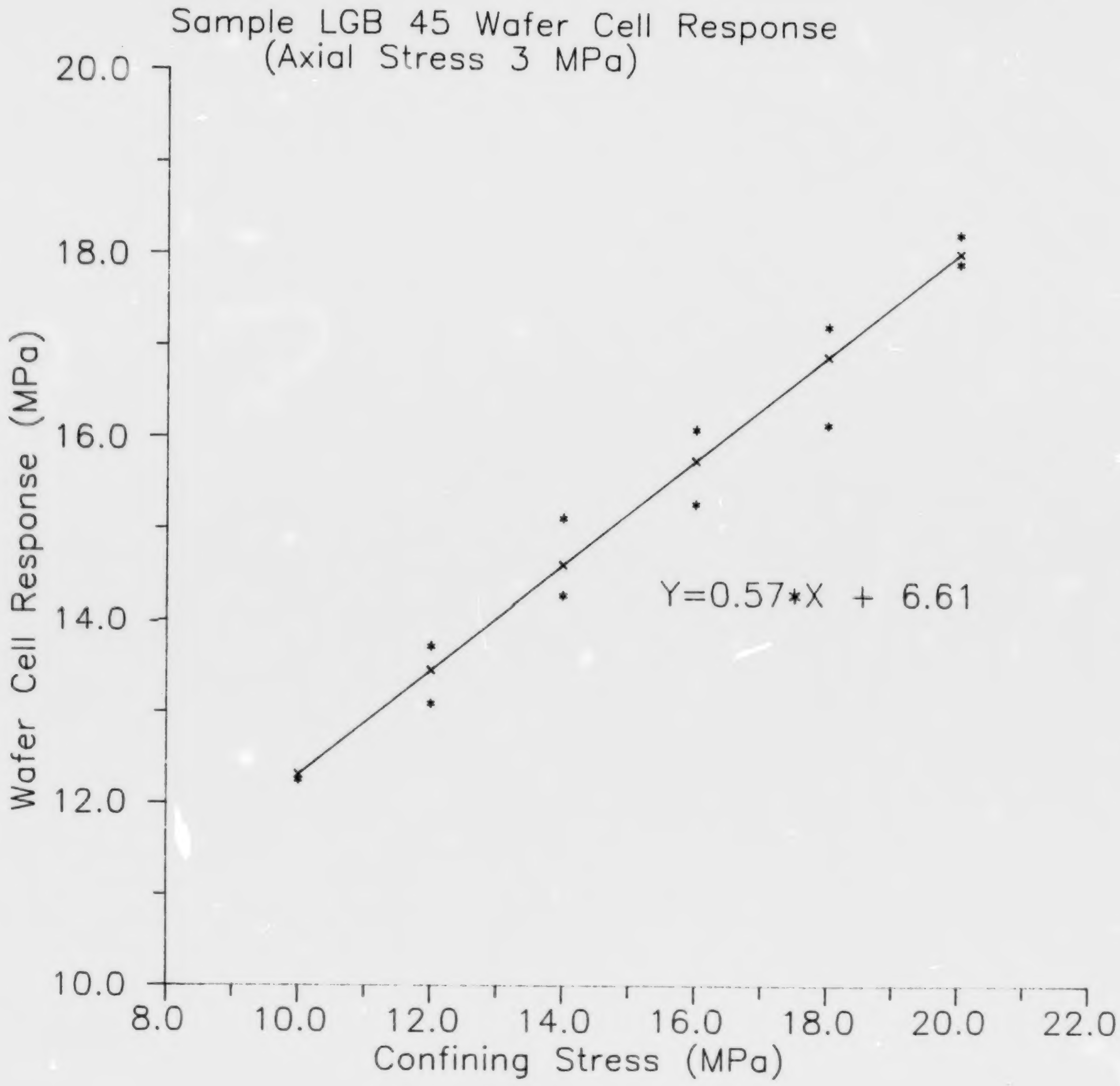
Sample LGB 45 Wafer Cell Response
(Axial Stress 3 MPa)
Wafer Cell Response (MPa)
20.0
18.0
16.0
14.0
12.0
10.0
8.0
10.0
12.0
14.0
16.0
18.0
20.0
22.0
Confining Stress (MPa)
Y=0.57*X + 6.61

FIGURE 8.5

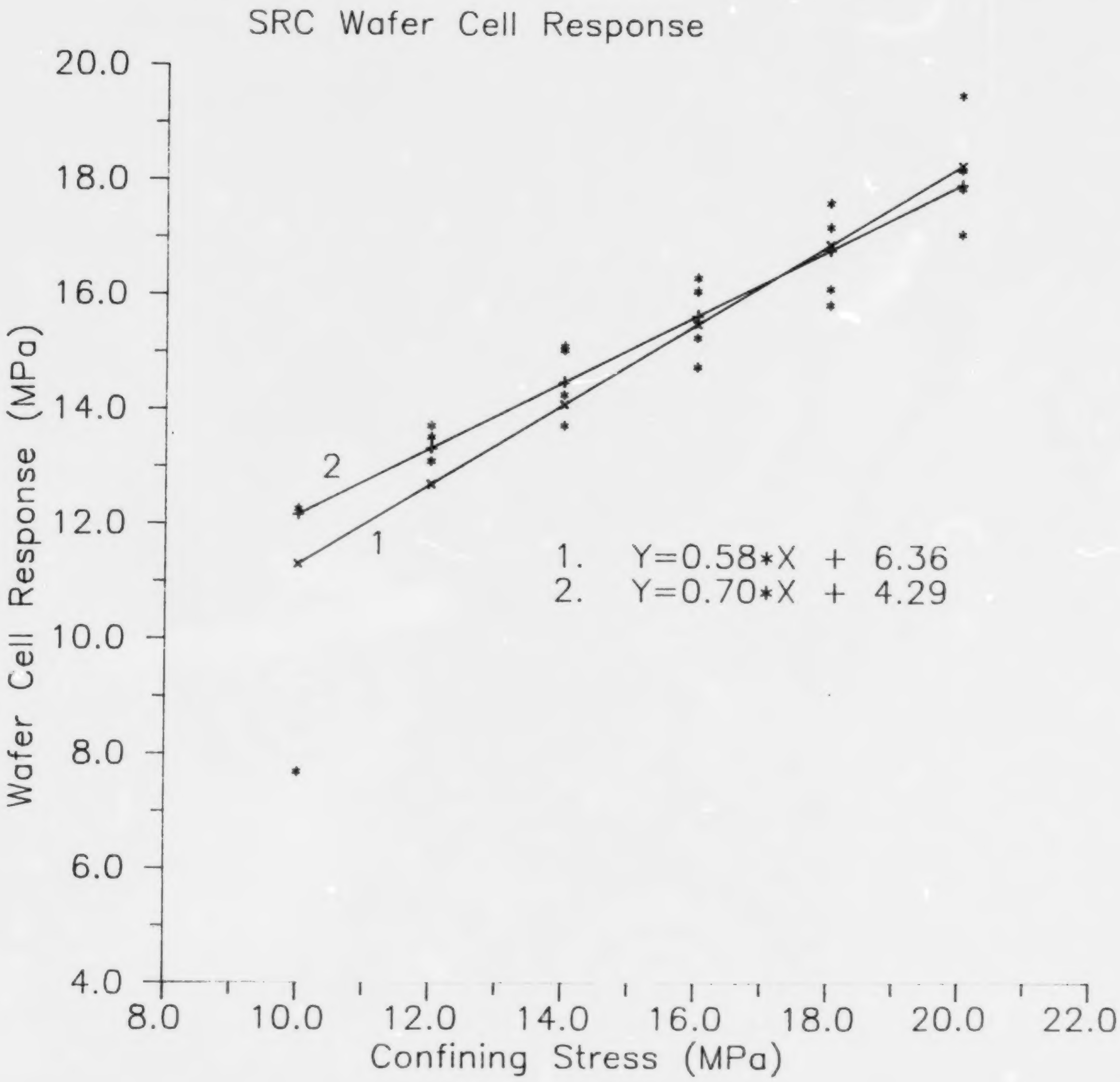
SRC Wafer Cell Response
Wafer Cell Response (MPa)
20.0
18.0
16.0
14.0
12.0
10.0
8.0
6.0
4.0
8.0
10.0
12.0
14.0
16.0
18.0
20.0
22.0
Confining Stress (MPa)
2
1
1. Y=0.58*X + 6.36
2. Y=0.70*X + 4.29

FIGURE 8.6

TABLE 8.3

STATISTICAL ANALYSIS OF CALIBRATION STAGES

CONFINING STRESS (MPa)	MEAN WAFER CELL RESPONSE (MPa)	STANDARD DEVIATION	NUMBER OF OBSERVATIONS
10	9.965	2.285	2
12	13.437	0.258	3
14	14.530	0.573	4
16	15.595	0.622	4
18	16.697	0.735	4
20	18.183	0.875	4

APPENDIX A

Triaxial Testing of Creep and Yield Behavior of Intact Salt Rocks

C.J. Fordham, M.Sc.
Department of Earth Sciences, University of Waterloo

M.B. Dusseault, Ph.D., P.Eng.
Department of Earth Sciences, University of Waterloo

D. Mraz, M.Sc.,P.Eng.
Mraz Project Consultants Ltd., Saskatoon

ABSTRACT

Laboratory derived behavioral parameters can be used for salt rock mine design only when they have been determined from rational test procedures. High quality test specimens and test equipment must be used in conjunction with a good understanding of the parameters which are required. The laboratory parameters must then be confirmed with appropriate in situ measurements.

KEYWORDS: Creep, Yield, Octahedral Stress, Prandtl Limit, Constant Strain Rate

1.0 INTRODUCTION

Behavioral parameters for design of underground openings in salt rocks (potash, halite) can be obtained in the laboratory. It is important that high quality specimens are available and appropriate test methodology used to assure that the results are applicable. It is also important to understand what parameters are required and why they are critical to design. A valid and appropriate design approach must be available to use the laboratory information correctly, and this design approach should be used by experienced personnel. Finally, laboratory parameters and designs must be confirmed by appropriate measurements in situ. This paper describes one aspect of design; an approach to triaxial testing of salt rocks to obtain parameters describing their creep and yield behavior.

2.0 BACKGROUND

Two types of tests are commonly performed to assess the mechanical behavior of salt rocks; standard rock mechanics tests, and creep tests. Standard rock mechanics tests include Brazilian tests, uniaxial compression tests, and load rate controlled triaxial tests for mapping of yield criteria. Creep tests are performed under conditions of constant stress, constant strain rate, or stress relaxation, to asses the rheological behavior of the material.

Standard rock mechanics methods were developed for testing geological materials which can be modeled more or less acceptably by elastic theory and brittle yield concepts. Salt rocks do not deform elastically; their time dependent behavior must be modeled as visco-elastic or visco-elasto-plastic. Deformations are both stress and strain rate dependent and all viscous deformations are non-recoverable.

Results from standard rock mechanics tests on salt rocks are dependent on test conditions. It has been noted (1,2) that uniaxial and triaxial tests performed at two different loading rates yield two Mohr's envelopes (Figure 1). It should also be noted that above a confining stress of about 1500 psi, both curves become almost parallel to the σ axis, indicating a change in mechanism from frictional yield of a polycrystalline material to perfectly plastic flow with no frictional component. Tests performed at several constant strain rates will also give a family of Mohr's envelopes (3) and will show different strains to peak strength.

Creep testing is performed to assess deformation characteristics of a salt rock with time. Two types of creep are measured; transient and steady state. A curve is often fit to the results in an effort to use laboratory data as a predictive tool.

A typical formulation used to predict axial strain based on laboratory data is given (4):

$$\varepsilon_1 = A \cdot t^n \cdot \Delta\sigma^m \cdot T^p$$

where: ε_1 is the axial strain
A is a laboratory derived constant
t is time
$\Delta\sigma$ is the principal stress difference
T is temperature
n, m, p are curve fit parameters to laboratory data

This formulation predicts a continuously decreasing strain rate with time (strain hardening), implies no effect of the mean confining stress and does not recognize the existence of a discrete initiation stress (Prandtl limit) required to initiate more rapid dislocation creep (5,6). It demonstrates the danger in using an empirical formulation, even if testing is of superior quality.

3.0 CREEP TESTING OF SALT ROCKS

At least 8 variables influence the creep characteristics of salt rocks in the laboratory. Four are external variables, the others are material dependent parameters. These include:

External Variables	Material Variables
Stress State	Mineralogy
Percent Strain	Grain Size
Time	Impurities
Temperature	Moisture

In order to carry out meaningful laboratory creep tests, as many variables as possible must be kept constant or monitored during the test. The writers are of the opinion that constant stress creep testing methods are superior to others and easier to interpret.

Material variability must be controlled by careful and consistent choice of high quality test specimens. Care is required during core collection, transportation, and storage. Test specimens must be free from shear planes or fractures which could give spurious results. The sample should be representative of the deposit as a whole, containing no clay seams or other noticeable impurities. The crystal size to sample diameter ratio should be at least 10:1, preferably higher. The sample should be kept wrapped until the time it is to be tested to maintain the moisture content.

External variables are monitored or kept constant with high quality test equipment. Stresses need to be kept constant, but the axial load is periodically adjusted as the sample deforms (7). Temperatures should be kept to within 1 degree C, as salt rock strain rates are extremely temperature sensitive (8).

Time and strain are monitored continuously during a creep test to determine the strain rate (creep rate). Initially, a set of stresses is applied to a specimen and the strain rate monitored. After steady state creep is achieved, stresses are adjusted, and the strain rate is monitored until a new steady state creep is achieved. This staged creep test approach is valid for salt rocks but must be terminated when 7.5% to 10% total axial strain is achieved (Figure 2).

3.1 Interpretation of Creep Test Results

The isothermal compressive creep and yield behavior of salt rocks are outlined in Figure 3. Constant stress creep tests are used to map the zone between the Prandtl limit and the lower yield surface (Y2). A number of constant strain rate tests are used to determine the location of the yield surfaces.

The major objective of a creep testing program is to study the relationship between stress and steady state creep. This can be done be either applying stresses to a test specimen and measuring the strain rate or applying a constant strain rate and measuring the stresses. Regardless of the approach, it is important that all creep tests be allowed to reach steady state conditions. To achieve this condition, stresses may need to be maintained for 15 to 20 days or more.

Different combinations of shear (τ_{oct}) and normal (σ_{oct}) stresses can yield similar strain rates. The stress change required to maintain a constant strain rate depends on the strain rate and the material. When the octahedral stress diagram has been mapped sufficiently (about 9 to 16 points) the points of equal strain rate can be joined (Figure 4). The resulting lines are known as isovelocity lines.

Within the range of stresses encountered in many potash and salt mines (σ_{oct}= 8 to 40 MPa) the isovelocity lines are inclined to the normal stress axis. At higher normal stresses these lines may become horizontal. The angle between the normal stress axis and the isovelocity lines is a function of the strain rate; the higher the strain rate, the higher the angle between the isovelocity line and the normal stress axis. Extending the lowest angle isovelocity line to the σ_{oct} axis gives a good approximation of the Prandtl limit, K .

The Prandtl limit is a line parallel to the σ_{oct} axis (Figure 3) and is therefore independent of confining stress level. The strain rate associated with the Prandtl viscous limit on the order of 10^{-11} /sec. This is not dislocation creep but diffusion or pressure solution/recrystallization creep. The existence of the horizontal Prandtl limit, the slight dependence of creep rate on normal stress above this limit, and the strain rate associated with the limit have all been confirmed experimentally and by in situ monitoring (6), therefore this is a useful interpretive scheme based on fact, not an empirical formulation or theoretical construct.

As tests are conducted at higher shear stress levels approaching the lower yield surface, there is potential for another deformation mechanism; stable crack growth involving crack extension and annealing due to high flow rates at stress concentrations associated with crack tips. It should be noted that this is a different process than stable crack growth associated with 'conventional' rocks. Once a covalent bond is ruptured under normal engineering stress and temperature, it cannot be 'healed', as an energy barrier exists. This is not the case for ionically bonded materials; bonds can be re-established by dislocation slip and flow. Consequently, even at engineering stress levels, there can be true steady state creep due to crack growth, rotation, and annealing, with no strain deterioration, merely deformation. At any stress conditions below Y2, a salt rock will continue to creep at a constant rate, provided material properties and boundary conditions do not change.

4.0 STRENGTH OF SALT ROCKS

Yield in salt rocks is unlike yield in most other geologic materials. Under uniaxial stress or low confining stresses and high strain rates, salt rocks yield in a classic strain-weakening manner (brittle failure). At high confining stresses, salt rocks do not yield at all; rather they display almost perfectly plastic behavior and can 'flow' rapidly with no loss of strength. At intermediate confining stresses, a gradual loss of strength is displayed.

Laboratory tests for determination of the strength of salt rocks must be performed under the following conditions:

1: All tests should be done under triaxial stress conditions. *In situ*, most material in a pillar is confined, very little is in a uniaxial stress field.

2: Confining stresses are kept constant, axial stresses are monitored during the test.

3: Axial stresses should be applied using a constant axial strain rate.

4: No sample should be tested to more than 10% axial strain as this is seldom encountered in the field and, at excessive strain rates, can alter material properties.

5: Temperature is not as important a factor during individual yield tests as they are relatively short term. However, laboratory temperatures should be maintained constant throughout a test program and as close to *in situ* as possible. This is merely good experimental practice.

A constant strain rate approach for the determination of yield behavior in salt rocks is the only configuration where all major variables important in salt rock deformation can be controlled fully. Constant load rate tests may apply a reasonably constant strain rate during initial stages of a test, but as the sample begins to weaken, the strain rate must increase dramatically to maintain the constant load rate. This leads to increased damage of the internal structure of the sample, weakening it further, forcing it to fail. It appears that at about 7.5% to 10% strain the integrity of a sample has been altered to the point where it begins to show changes in mechanical behavior, hence we do not recommend testing beyond 10% strain.

Four types of data are required from yield tests to determine a complete yield criterion for a salt rock; confining stress, axial stress at failure (for the determination of τ_{oct} and σ_{oct}), strain rate, and percent strain at peak stress. In order to limit the number of tests, a confining stress/strain rate mapping scheme has been developed based on two assumptions;

1. The higher the strain or displacement rate, the more likely failure is to occur, and
2. The higher the confining stress, the less likely the specimen is to fail.

The test grid containing all confining stresses and strain or displacement rates is drawn up prior to testing. Note that because this is just a grid of the tests to be performed, the axes need not be linear (Figure 5). The confining stress/displacement rate space is mapped backwards from the highest confining stress and displacement rate. The initial displacement rate is chosen to come as close to Y2 as possible. The choice of an initial confining stress is less critical. If the first test shows no yield by 10% strain, the next test is performed at a lower confining stress but at the same displacement rate. If yield occurs during this test, the next test is performed at the same confining stress but at a slower displacement rate, ie. no yield - move horizontally left on the grid, yield - move vertically down the grid. Once the confining pressure that allows a sample to yield at a certain displacement rate is determined, no further tests are necessary performed at that displacement rate. It can be assumed that tests at any lower confining stresses will all yield although probably at smaller strains, and tests at all higher confining stresses will show no yield. Extrapolations among tests will fill in the gaps effectively.

4.1 Interpretation of Strength Test Results

Yield tests are performed to determine the boundaries of the yield zone between Y2 and Y1. Y2 represents failure by 10% strain at infinite time. Y1 represents failure at minimal strain at time equals zero. Both are impossible to achieve in reality, but are approximated in the laboratory. However, by choosing suitable starting points on the confining stress/strain rate grid before beginning a test program, the yield zone can be mapped quite accurately.

Initial strain rates for yield testing should come as close to Y2 as the test equipment will allow. This will assure that the test program will cover all in situ conditions. A good starting strain rate is 10-3 to 10-4/sec. The choice of an initial confining stress is not as important; if a confining stress lower than expected in the pillar is chosen and no failure occurs, it can be assumed that no failure will occur in that zone in the pillar where the stresses are the same. Note that the assumption of a uniform load distribution in the pillar is not even close to reality (6).

Yield testing at a constant axial strain rate is essentially an accelerated creep test. Diffusion and dislocation creep are still occurring; however, above Y2 the material can no longer heal the internal microcracks as fast as they are created. This leads to a loss of strength and eventually failure, a phenomenon which has previously been referred to as tertiary creep. Tertiary creep is characterized by accelerating deformations which ultimately lead to failure. It is the third phase of the conventional three phase creep curve which includes a period of

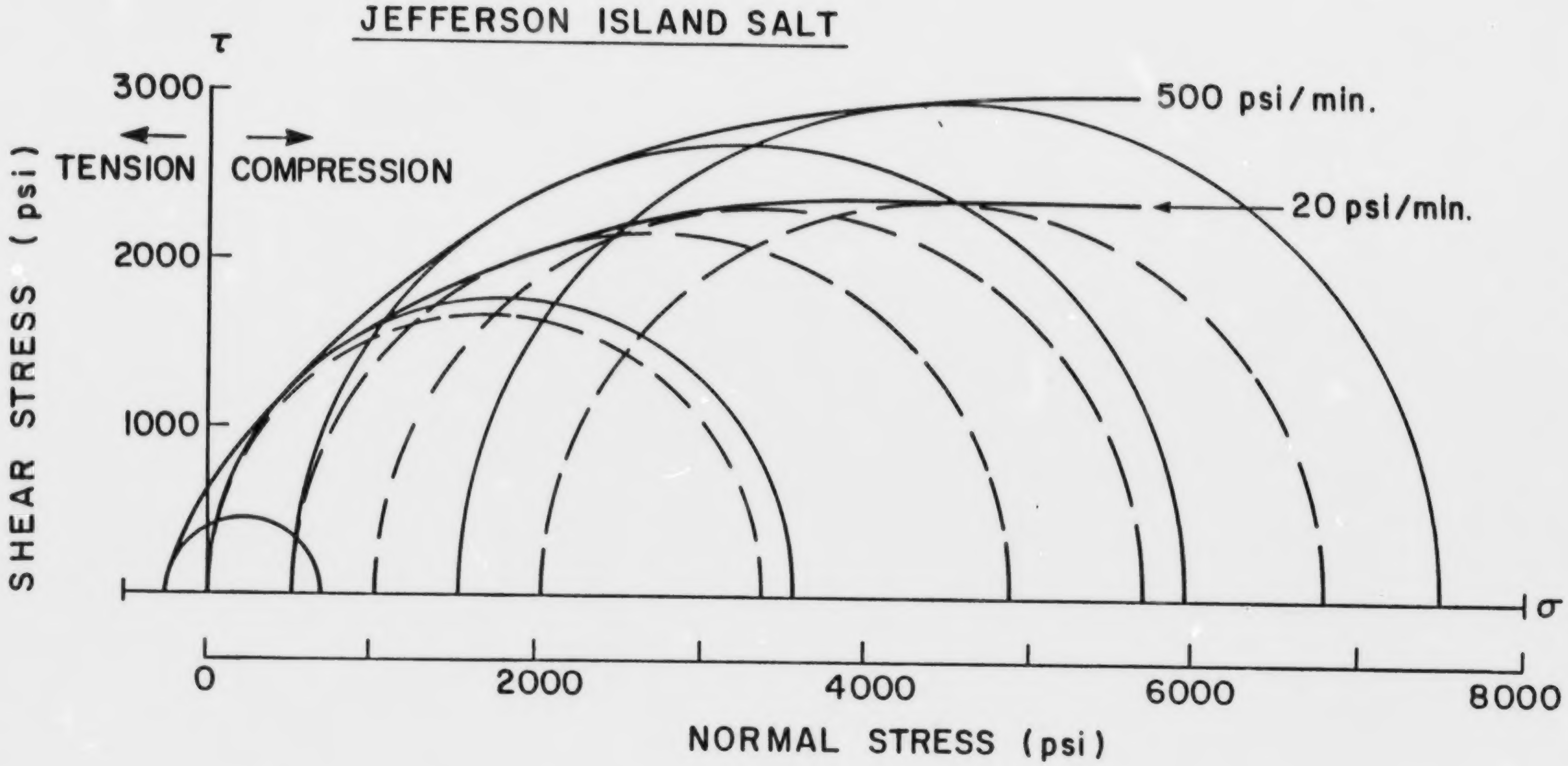
JEFFERSON ISLAND SALT
τ
3000
2000
1000
SHEAR STRESS (psi)
TENSION
COMPRESSION
500 psi/min.
20 psi/min.
σ
0
2000
4000
6000
8000
NORMAL STRESS (psi)

Figure 1

primary or transient creep and a period of secondary or steady state creep. At constant stresses below Y2 and within 0 to 10% strain, the three phase creep curve will not develop. These comments and concepts apply only to salt rocks, not to 'conventional' geological materials.

If stress conditions exceed Y2, a sample should experience a transitional creep phase followed directly by a phase of accelerating creep leading to failure without entering into steady state deformation (Figure 6a). If stress conditions are below Y2, a sample will proceed from transition creep into steady state creep and continue to deform at a constant rate; it will not fail unless material properties or boundary conditions are altered (Figure 6b).

5.0 CONCLUSIONS

Two types of behavioral parameters are required for salt rock mine design; creep characteristics and yield conditions. Both parameters can be accurately determined in the laboratory provided a rational test program is carried out.

A test program must incorporate high quality test equipment and specimens with a thorough understanding of the variables important to salt rock deformational behavior. Each variable must be accounted for during a test by either keeping it constant or by monitoring its variation.

Creep tests are performed to study the effects of stress on the steady state strain rate of a sample. The results are used to map the zone between the Prandtl limit and the lower limit of the yield zone, Y2. Joining the points of equal strain rate generates the isovelocity lines along which, regardless of stresses, the strain rate is the same.

The strength of a salt rock must be studied under conditions of constant strain rate. Constant load rate tests force the material to fail while they do not take into account the effects of strain rate. A series of constant strain rate tests starting at as high a strain rate as possible allow the mapping of the yield zone between Y1 and Y2 by a novel step-wise method.

REFERENCES

(1) Hansen, F.D.,"Case History Rock Mechanics Investigation of the Jefferson Island Salt Mine: II. Laboratory Evaluation of Strength and Creep Deformation Characteristics of Dome Salt under Confining Pressure," Technical Memorandum Report RSI-0057, Re/Spec Inc, Rapid City, S.D. Prepared for the Office of Waste Isolation, Oak Ridge, Tenn., 1977.

(2) Rokahr, R.B., and Staudtmeister, K., Proceedings of the Sixth International Symposium on Salt, B.C. Schreiber and H.L. Harner Eds., Salt Institute, Alexandria, VA., pp. 455-462, 1981.

(3) Farmer, I.W., and Gilbert, M.J., Proceedings of the First Conference on the Mechanical Behavior of Salt, H.R. Hardy and M.Langer Eds., Trans Tech, Germany, pp. 3-18, 1981.

(4) Hansen, F.D., and Mellegarde, K.D., Creep of 50 mm Diameter Specimens of Domal Salt from Avery Island, Louisiana. Office of Nuclear Waste Isolation Report ONWI-104, Battelle Memorial Laboratory, Columbus, OH, 63 p., 1980.

(5) Dusseault, M.B., and Mraz, D., Potash '83, Saskatoon, Saskatchewan, pp. 311-319, 1983.

(6) Mraz, D., and Dusseault, M.B., Proceedings of the Twenty-Seventh U.S. Symposium on Rock Mechanics, Tuscaloosa, Ala., 1986.

(7) Hansen, F.D., and Carter, N.L., Proceedings of the First Conference on the Mechanical Behavior of Salt, Trans Tech, Germany, pp. 53-70, 1981.

(8) Carter, N.L., and Heard, H.C., American Journal of Science, Vol. 269, October, 1970, p.193-249.

Figure Captions

Figure 1: Mohr's envelopes for Jefferson Island domal salt loaded at two axial load rates (1).

Figure 2: Typical stage load creep test results for New Brunswick potash ore.

Figure 3: Octahedral stress diagram used to map creep and yield in salt rocks.

Figure 4: Mapping the octahedral stress diagram with stresses and strain rates determined from the stage load test shown in Figure 2.

Figure 5: Typical yield map and yield testing results for New Brunswick potash ore.

Figure 6: a) Primary creep leading directly to failure. b) Primary creep leading to steady state creep.

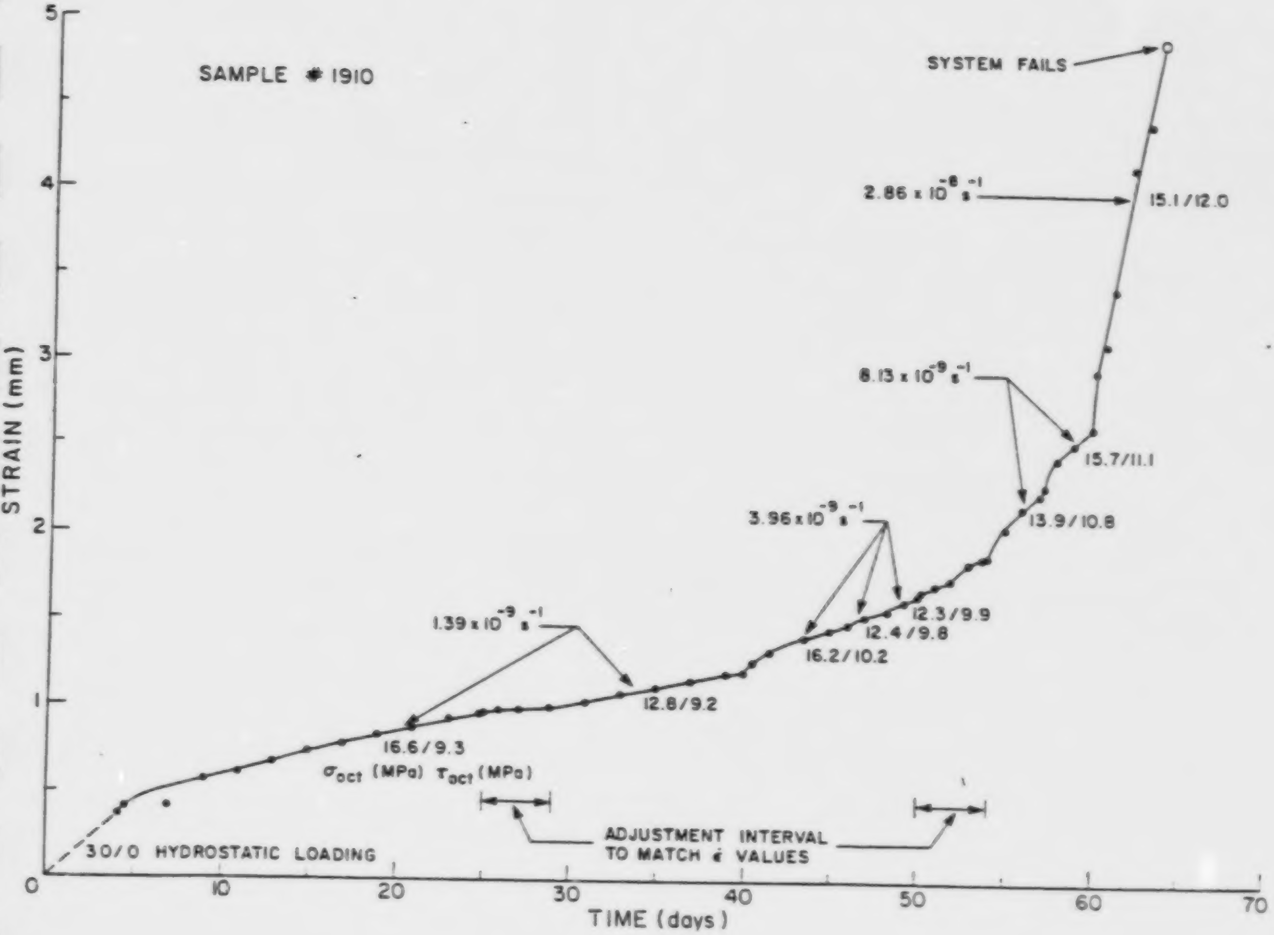
SAMPLE # 1910
SYSTEM FAILS
2.86 x 10^{-8} s^{-1}
15.1 / 12.0
8.13 x 10^{-9} s^{-1}
15.7 / 11.1
13.9 / 10.8
3.96 x 10^{-9} s^{-1}
12.3 / 9.9
12.4 / 9.8
16.2 / 10.2
1.39 x 10^{-9} s^{-1}
12.8 / 9.2
16.6 / 9.3
σ_{oct} (MPa) τ_{oct} (MPa)
ADJUSTMENT INTERVAL TO MATCH $\dot{\epsilon}$ VALUES
30/0 HYDROSTATIC LOADING
STRAIN (mm)
0
1
2
3
4
5
TIME (days)
10
20
30
40
50
60
70

Figure 2

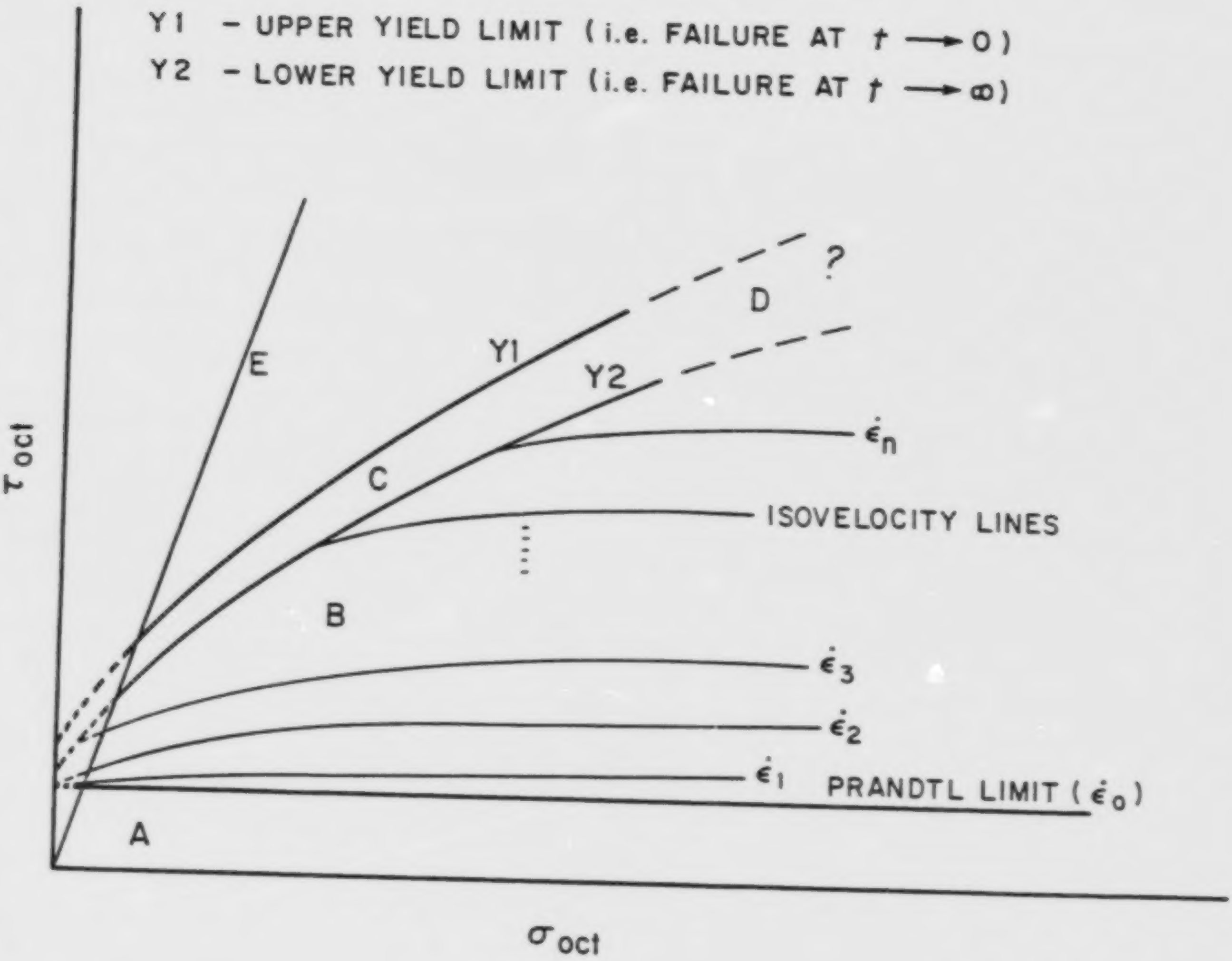
Y1 - UPPER YIELD LIMIT (i.e. FAILURE AT $t \longrightarrow 0$)
Y2 - LOWER YIELD LIMIT (i.e. FAILURE AT $t \longrightarrow \infty$)
?
D
E
Y1
Y2
$\dot{\epsilon}_n$
C
ISOVELOCITY LINES
B
$\dot{\epsilon}_3$
$\dot{\epsilon}_2$
$\dot{\epsilon}_1$
PRANDTL LIMIT ($\dot{\epsilon}_0$)
A
τ_{oct}
σ_{oct}

REGION A : TIME - DEPENDENT BEHAVIOR DUE TO DIFFUSION ONLY
PRANDTL LIMIT : ONSET OF DISLOCATION MECHANISMS
REGION B : STEADY - STATE CREEP REGIME
REGION C : STRESS REGIMES WHICH LEAD TO YIELD
REGION D : YIELD (STRAIN WEAKENING) UNDEFINEABLE, PLASTIC SHEAR
REGION E : UNEQUIVOCALLY UNSTABLE REGION

Figure 3

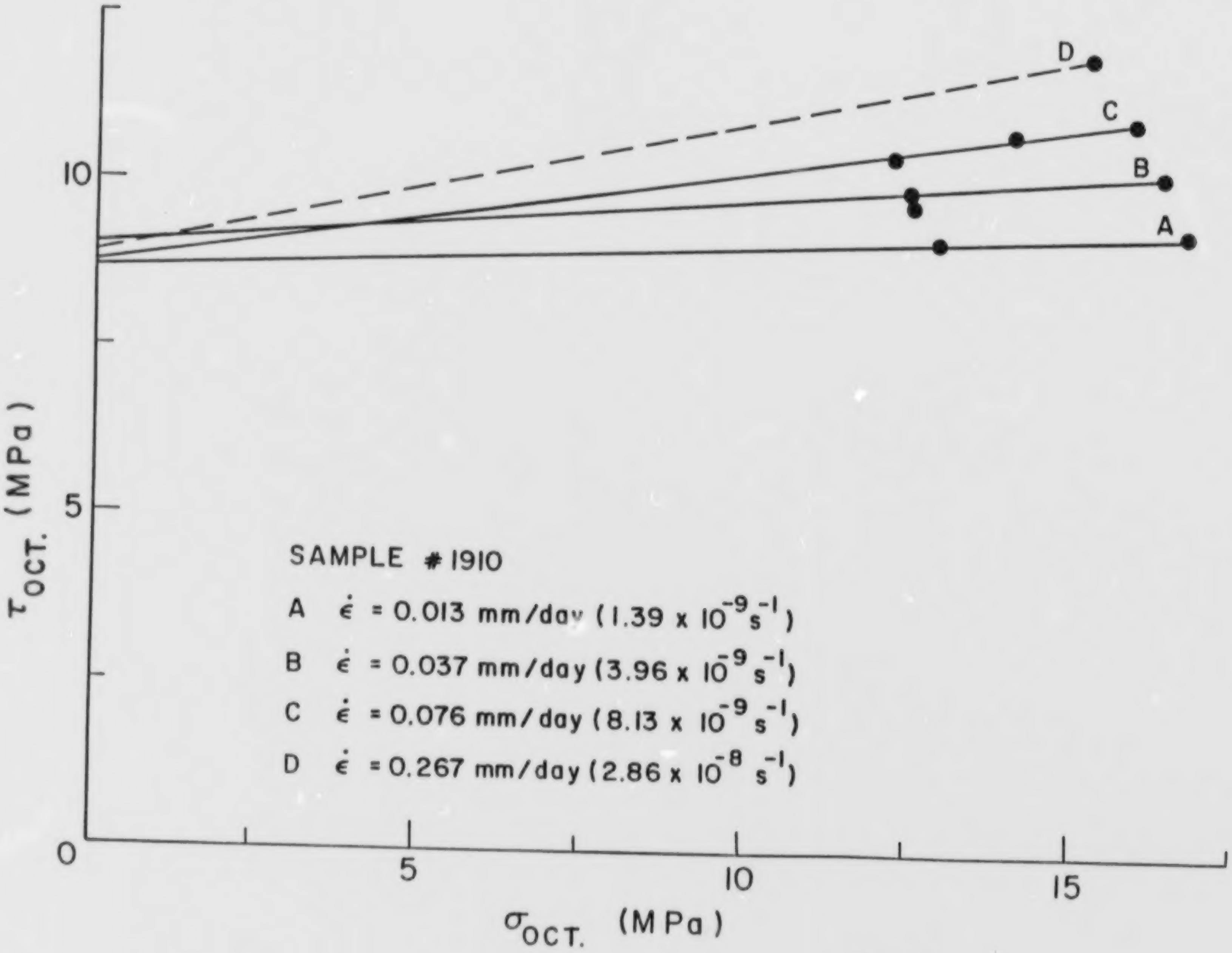
D
C
B
A
10
5
0
5
10
15
$\tau_{OCT.}$ (MPa)
$\sigma_{OCT.}$ (MPa)
SAMPLE # 1910
A $\dot{\epsilon}$ = 0.013 mm/day (1.39 x $10^{-9} s^{-1}$)
B $\dot{\epsilon}$ = 0.037 mm/day (3.96 x $10^{-9} s^{-1}$)
C $\dot{\epsilon}$ = 0.076 mm/day (8.13 x $10^{-9} s^{-1}$)
D $\dot{\epsilon}$ = 0.267 mm/day (2.86 x $10^{-8} s^{-1}$)

Figure 4

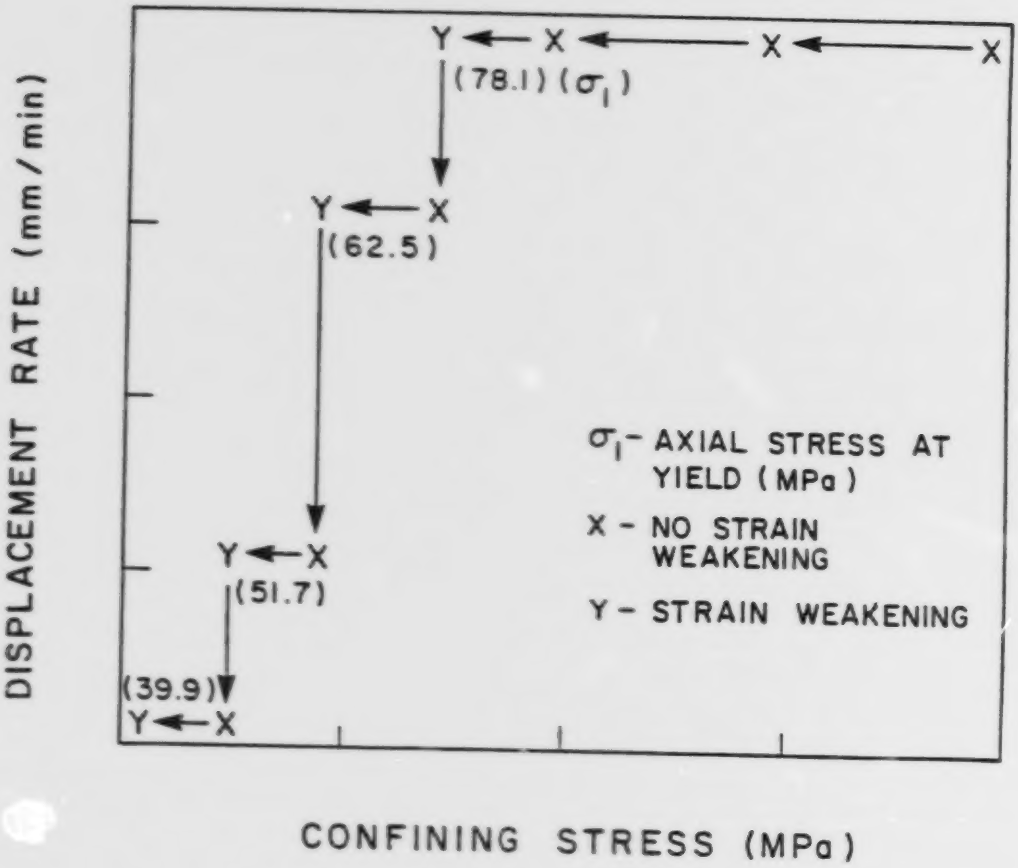

DISPLACEMENT RATE (mm / min)
CONFINING STRESS (MPa)
Y ← X ← X ← X
(78.1) (σ_1)
Y ← X
(62.5)
Y ← X
(51.7)
(39.9)
Y ← X
σ_1 - AXIAL STRESS AT YIELD (MPa)
X - NO STRAIN WEAKENING
Y - STRAIN WEAKENING

Figure 5

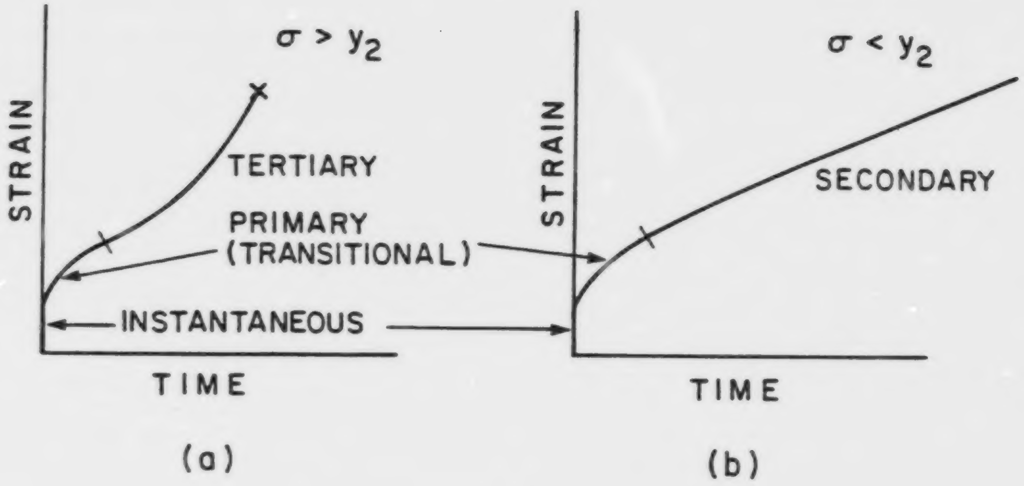

$\sigma > y_2$
STRAIN
TERTIARY
PRIMARY
(TRANSITIONAL)
INSTANTANEOUS
TIME
(a)
$\sigma < y_2$
STRAIN
SECONDARY
TIME
(b)

Figure 6

TRIAXIAL TESTING OF INTACT SALT ROCKS: PRESSURE CONTROL, PRESSURE SYSTEMS, CELL AND FRAME DESIGN

Baleshta, J.R. and Dusseault, M.B.
University of Waterloo, Waterloo, Ontario, Canada

ABSTRACT

An extensive laboratory for intact salt rock behaviour research (the WATSALT Laboratory) was conceived at the University of Waterloo in 1982, and by 1984 was producing results of high quality. At present, six high capacity test stations for creep behaviour are operating on a continuous basis. The designs were generated in-house to meet the requirements of long term, constant pressure, environmentally stable creep work. Some innovative systems have been developed, which are performing effectively. This paper describes the approach to design, the triaxial cell and axial load frame configuration, an alternate internal axial piston cell, temperature and pressure control systems, instrumentation and data acquisition. The long term accuracy and stability characteristics of these systems are also provided.

KEYWORDS: Triaxial Cells, Loading Frames, Temperature Control, Pressure Control, Data Acquisition, Salt

INTRODUCTION

This paper describes the design, development, and systematic use of triaxial equipment related to potash and salt research at the University of Waterloo. Extensive triaxial testing on intact salt specimens required the design of specialized research equipment and the implementation of several supportive appurtenances.

Laboratory studies of creep behavior tend to be long-term projects. Tests on an individual specimen can extend to periods of over 6 months. Creep strain over this period can be as much as 15%. For the 48 mm to 102mm diameter specimens tested at L/D ratios of 2:1, this translates to axial shortening of 14 to 31 mm. In addition, previous experience indicated that normal laboratory temperature fluctuations of ± 2°C can create a 0.5 MPa confining pressure deviation in a cell. The design procedure required addressing these issues, solving the problems of stability for long-term tests, and generating an economic design.

DESIGN APPROACH

In light of the design constraints suggested, above a general approach or "philosophy of design" was conceived. The major components required for each complete test system were divided into the following sub-groups: the triaxial cell itself, the axial load frame, axial and lateral pressure control, temperature control, instrumentation and data acquisition.

In the design approach to each of the above sub-groups, personnel safety is the primary concern. It was therefore imperative to minimize the pressurized volumes, to use competent materials with ample reserves of strength beyond the working stresses, and to design proper electrical and pressure circuits.

The next most important design criterion was versatility so that the equipment can be adapted readily to other modes of testing upon completion of the present creep research. To enhance this versatility, each system or creep station required an axial stress capability of 200 MPa, and a confining pressure capability of 70 MPa. Because tests are lengthy, it was also desirable to reduce the possibility of losing a specimen in the midst of several months of testing, due to the failure of one component in the system. A rather straightforward, though crucial point which had to be considered at the earliest stage of design was the limits of the machine shop facilities which would construct the equipment.

Design for extended test duration included an automated data acquisition system (with electronic instrumentation) and some 'closed loop' form of process control to regulate temperatures and pressures. Finally, the complete system was to be compact, and as economical as possible - using materials at hand or those readily available on the market, with no unnecessary peripherals. An effort would be made during design to create a simple system with the highest likelihood of successful operation, returning the most performance for the limited funding available. Emulation of large industrial servo-controlled frames was not a possibility.

TRIAXIAL CELL DESIGN

Separate triaxial cells were designed to test 44, 48 and 54 mm specimens. These cells were designed to withstand confining pressures to 70 MPa. A sectional view of a typical cell is shown in Figure 1.

Confining pressure was applied to cylindrical test specimens in the conventional manner (eg. Hoek-Franklin Cell [1]), with the use of hydraulic oil. The specimens were isolated from the pressurized fluid by a neoprene sleeve. If manufactured properly these sleeves are oil resistant, leak proof, and reusable. Although the inner diameter is set by the mandrel diameter on which it was made (plus 0.7% typical shrinkage), the outer diameter of the membrane can be ground to tolerances of about ± 0.4mm. For specimen diameters of 54 mm and smaller, our experience is that the optimum urethane durometer rating for use in these cells is 70.

Monobloc 4340 steel was used to construct the pressure cylinders. It was machined to approximate size, heat treated to a Rockwell C hardness of 30-32, then machined to final dimensions. The heat treatment imparted a greater uniformity in material properties, refines the grain size and increased the strength of the vessel [2]. The Rockwell C value specified for the 4340 steel brought its ultimate strength to 960 MPa and its yield strength to 825 MPa, while maintaining durability.

The vessels were designed to achieve minimum inner diameter, taking lateral specimen expansion (as high as 8% at 15% axial strain) into account. The reasons for this were threefold: a reduced inner diameter reduces the pressurized fluid volume and enhanced safety; a smaller inner diameter reduced the outer diameter required for sufficient tangential strength; and these two together reduced the overall vessel weight and manufacturing cost. The margin of safety employed for the working stress of the vessels was in accordance with Section 8 of the ASME Pressure Vessel Code [3].

The seals used in the vessels are of the positively actuated lip, or cup seal geometry. By proper arrangement of this type of seal a vessel which may have required 4 to 8 O-rings could be sealed with a total of two seals each one serving multiple purposes. The seals are located between the bore of the vessel and the enclosing membrane and kept hydraulic oil from penetrating the specimen, exiting the vessel through the enclosure, or seeping through the clearance at the axial piston. The machining of seal installation chamfers and selection of a bevelled edge style seal greatly facilitated cell assembly.

The seal retainers were implemented so that specimens could be changed without draining the hydraulic oil. This was intended to save the user time and trouble. However, with induced creep strains of 15% encountered in our work, the membranes conformed to the bulged specimens and have to be removed from the vessel. For lower strain levels (5%-8%), direct specimen removal is often possible.

Threaded end caps were used to enclose the vessel. With the use of hook spanner wrenches the vessels could be assembled and disassembled easily. The lip seal did not require an initial torque for sealing. Given sufficient engagement length, the strength of a class 2 thread can be equivalent to the pitch diameter of an unthreaded component [4]. Hence with threads on the outer diameter of the vessel, the enclosures can be very strong when used for static low cycle purposes. However, studies have shown that stress concentrations in threads can be as much as of 3.85 . and this was accounted for in design [8].

The ram and lower platen which contact the specimen were constructed of 304 or 316 stainless steel. One system has been modified to include flow-through capability. To deal with sample end non-parallelism, a spherical seat was incorporated as the bottom platen. To reduce side friction and binding, a guide length of 1½ times the piston diameter was provided on the upper enclosure. The tolerance between the ram and guide surface was set as a close sliding fit, but it was in no way intended as a pressure seal. A second spherical seat was used outside the vessel to account for any non-parallelism between the axial piston and the load frame actuator.

The surfaces of the piston and lower platen which contact the specimen were always sprayed with a thin layer of dry lubricant. This minimized the end restraint created by platen friction and reduced the amount of barrelling.

LOADING FRAME

Compressional load frames were required to apply axial load to the triaxial cells described in the previous section. These frames were designed to be as versatile and economical as possible. They can be constructed of inexpensive and readily available materials and are adjustable to accommodate various sizes of triaxial cells or other devices requiring a reaction frame.

The alternative selected as best suited to these purposes was a bolted frame design using standard structural steel. Design analysis followed the provisions of the structural steel CSA Standard S16.1 [8]. The design used stiffened 200mm x 200mm wide flange sections for the upper and lower beam members and two 100mm x 100mm wide flange sections as columns.

Steel plates, 25mm x 200mm, were welded to the column members for additional stiffness. The assembly was connected by bolting these sections to similar sized plates, welded to the ends of the beam members. Two rows of three 16mm class 5 bolts were used at each connection. Additional bolt holes were drilled to provide a range of height adjustment. The bolted connections were designed so that friction between the sandblasted plates was sufficient to withstand full actuator load. This prevented slippage during testing and avoided the possibility of applying excess shear to the first bolt to come into bearing. As an additional precaution, the design was such that the shear plane would not intersect the threads of the bolts. Transverse and 45° oriented stiffening plates were added to prevent web crippling, local flange buckling and shearing of the beam members, and to resist moment induced thrust in the columns.

Compact commercially available hydraulic cylinders were used to supply the compressive load. These actuators were attached to the top beam with a metal ring. On the lower beam a 200 mm circular hardened steel disk was attached as a platen. The facing flange surfaces of the beams were machined flat to ensure parallelism between the platen and the ram. Concentric grooves spaced at radial distances of 15 mm were machined into the surface of the platen for alignment of test specimens or cells. The platen and ring also acted as bearing plates and distributed the vertical load applied to the beams. This increased the local bearing resistance of the flange they rested on. To complete the design, angular sections were bolted to the outer column flanges to prevent toppling.

A small laboratory hoist was used to position the members during assembly. Tapped holes for the attachment of eye hooks were provided on the heavier components.

Following assembly, the frames were readied for testing with an initial cycling to full load capacity. To calibrate the hydraulic cylinders, load cells were inserted in the frames to precisely determine the relation between applied hydraulic pressure and resulting axial force. Finally, dial gauges were used to check frame stiffness by determining the deflections due to the combined effects of column extention and bending of the beam members. At full capacity a maximum deflection of 0.6mm was found.

In the completed form, the frames are 1150 mm "bench top" units capable of applying 450kN of compressive force, with an adjustable inner working space of 430 mm x 530 mm. Two frames were constructed in this fashion. A third frame was later constructed of larger members but same overall design for 900kN capacity. All frames are semi-portable and can be completely dismantled. Figure two shows an example 450kN frame remove, with temperature chamber and triaxial cell.

INTERNAL PISTON CELL

In 1985 an expanding program of laboratory research required the construction of 3 additional creep stations for testing 100mm diameter intact salt specimens. At this time an alternative cell/frame system was developed. Instead of the usual triaxial cell with an external compression frame providing axial load reaction, these cells were designed to incorporate both the axial load and confinement pressure capability in a compact integral unit. This simplified device meant savings in materials, labour, implementation time and space requirements in the laboratory. The vessel was designed to be capable of applying 210 MPa axial stress and 70 MPa confinement stress on 100 mm x 200 mm cylindrical specimens.

In most respects, the upper portion of the device was similar to the triaxial cell described earlier (albeit upside-down) in that the membrane, spherical seat, and sealing method were retained. The membrane thickness was 3.2 mm as before; however, for the larger 100 mm diameter, a urethane durometer of 80 was used.

Since every triaxial cell requires enclosures and some form of fastening arrangement, it was relatively straight-forward to incorporate an additional chamber with an internal axial load piston at the lower end of the cell. The larger diameter (178 mm) of this chamber was required to achieve the desired 1750 kN axial force under a hydraulic actuation pressure of 70 MPa. The axial load piston was constructed of aluminum for reduction in weight, and ease of machining. The tall profile of this piston was designed to reduce side loading. Wear rings and a low friction lip seal were also incorporated to keep the break-away friction stick-slip to a minimum. As a result the piston moves quite readily, requiring only about 7 kPa to initiate movement. This created a responsive system which quickly adjustes to creep movement. The piston has a stroke length of 40 mm which can accommodate up to 19% strain in the specimen. The system was calibrated by inserting a load cell in place of the upper (confinement) chamber and determining the relationship between actuation pressure and axial force.

A single set of end plates enclose both vessels, and a series of ten threaded tie rods (32 mm diameter) holds the entire system together. An intermediate ring has the multiple functions of separating the two chambers, providing cylinder alignment, seal seating and additional bearing for the piston, as well as protecting the tie rods from errant lateral blows during assembly. Materials for the vessel included 4340 steel for the enclosures and cylinders (again heat treated to HRC 30), and a cold worked steel called 'stressproof' for the tie rods. Where the ram and platen contact the specimen, stainless steel coated with a thin layer of dry lubricant was again used.

Three cells were built in this fashion (figure 3). They form compact 355 mm (diameter) by 760 mm units and require about 40% less laboratory space than an equivalent external frame system (figure 4). The cost savings in construction for this integral type of creep station over the former were approximately 25%.

PRESSURE APPLICATION AND CONTROL

Fluctuation of lateral and axial pressures are induced by changes in air temperature, minute leaks through fittings, and by creep deformation of the specimen. Due to the 24 hours/day extended nature of testing it was apparent that continuous manual pressure adjustment would be difficult. Hence an automated system was required to control hydraulic pressures. As with all components in the system, an economical though effective design was desired. The risk of failure of the pressure system (effecting a corresponding loss of perhaps several weeks of testing) was to be minimized.

The first component developed to reduce these pressure deviations is referred to as an intensifier-accumulator. This device is an accumulator since it stores a quantity of compressed nitrogen to buffer pressure fluctuations induced by changes in the pressurized volume. It is also an intensifier because the output hydraulic oil pressure side of the device is boosted from the 2.0 MPa nitrogen pressure to 70 MPa due to a cross-sectional reduction of the bore.

A major objective in the design of this device was to reduce the break-away friction and drag during operation. To achieve this a rolling diaphragm seal was used at the low pressure, nitrogen end. This seal confines the nitrogen in a 100 mm diameter bore, and can take working pressures to 2.0 MPa. At the high pressure end of the intensifier-accumulator a 17.5 mm rod transmits the force applied by the compressed nitrogen and pressurizes the hydraulic oil. A low friction lip seal is used to contain the high pressure oil. The volume of oil stored is set by the stroke length of the diaphragm seal and diameter of the high pressure bore. The volumes are 48 cc for a 35 MPa output version and 24 cc for a 70 MPa design. An outside indicator on the intensifier-accumulator reveals the rod location. The hydraulic system was configurated in such a way that when the piston has completed 90-95% of its stroke, the intensifier-accumulator can be restroked (using a small hydraulic hand pump) in 45 seconds or less, without loss of system pressure. A sectional view of our intensifier-accumulator is shown in figure 5.

Following the implementation of the intensifier-accumulator a further improvement was conceived. This was the application of a simple closed-loop or self-regulating pressure control system to automatically adjust the input nitrogen pressure. The pressure is monitored by a pressure transducer at the high pressure, hydraulic oil end of the system. This is a direct indication of the axial force or confinement pressure being applied during a test. The pressure transducer signal is fed back to either an analogue control unit or a microprocessor, and is compared to a selected reference. If the pressure is low a solenoid valve in line with the nitrogen source opens to increase system pressure. Alternatively, if pressure is excessive a second solenoid valve opens to vent some nitrogen gas to the atmosphere, which lowers the system pressure. Needle valves are placed in series with the solenoid valves to throttle (buffer) the amount of nitrogen flow into or out of the system to give it a high degree of stability. Typically, a single bottle of nitrogen lasts for six months of continuous testing.

Two complete pressure control systems are required for each creep station, one to control axial load and the other to regulate confining pressure. They are capable of controlling to better than ±0.1% of the maximum operating pressure. Since 1983 fifteen of these systems, including intensifier-accumulators, have come into use at the University of Waterloo. Twelve of these systems are used to control the six creep stations in the WATSALT Laboratory. A dual pressure control system for one creep station is shown in figure 6.

The design of the pressure system explicitly sacrifices rapid loading capability. The most rapid reasonable strain rate which can be applied by controlling the pressure system with a microprocessor is about 10^{-5} sec^{-1}, and this would require relatively frequent recharging by hand. However, the savings generated by the current design as compared to a commercial servo-controlled system are on the order of $30,000.00 to $100,000.00, depending on which system is purchased.

Because the system uses pistons of the same diameter as samples, triaxial extension tests can be carried out with almost trivial ease. Also, microprocessor pressure control permits programming any stress path, providing strain rates are relatively slow.

TEMPERATURE CONTROL

As stated earlier, experience has shown that changes in temperature can cause significant hydraulic pressure fluctuation in the test cells. Separate temperature chambers were built for the six creep stations, each with individual temperature control.

The temperature boxes are constructed of 50 mm of extruded polystyrene foam insulation with interior and exterior aluminum sheet casing. They are typically $0.13 m^3$ in volume. The units for the external frame/cell systems are detachable in two components (Figure 2), whereas the boxes for the internal piston cells are single units and are lowered directly onto the cell (Figure 7). All boxes are light in weight, and can be attached by hand.

The heaters for these chambers are two 100 watt light bulbs. A thermistor monitors the interior temperature and an analogue control unit turns the light bulbs on to heat the box as required. A squirrel cage fan circulates the air in the chamber when the light bulbs are on. Temperatures are adjustable to 40°C with this simple device, and are controlled to ± 0.1°C. Replacing the bulbs with higher wattage devices or direct heating coils would allow the chambers to operate up to a design limit of 75-80°C.

Room temperature air (typically 20 ±2°C in the laboratory) is used as the cooling medium. However, one design has incorporated a cooling unit consisting of thermal-electric modules and can lower the chamber temperature to 10°C if desired.

A dual plexiglass window is included in each chamber for visual monitoring of the test cperation without removal of the temperature chamber. Hydraulic hoses and electrical cables which run into the box are sandwiched between layers of soft foam rubber to provide a thermal seal.

INSTRUMENTATION AND DATA ACQUISITION

Data required routinely from each creep station includes axial and confining pressures, specimen axial deformation and cell temperature. Electronic instrumentation is used to monitor these parameters, and their output signals are automatically recorded at regular intervals with a data acquisition device.

The transducer used in the pressure control loops are also the indicators of axial and confining pressure, indicative of σ_1 and σ_3. These pressure transducers were selected for their ability to withstand long term pressure application as opposed to quick cycling or fatigue. Our work has shown that strain-gaged, welded metal diaphragm style transducers tend to be well suited to this purpose.

The axial deformation of the specimens is monitored by a single linear variable displacement transducer (LVDT) mounted inside the temperature controlled environment. Efforts were made to ensure that the LVDTs were measuring only specimen deformation and not some other information such as the extention of the load frame, etc. The LVDTs were mounted directly to the cell piston so to be as unaffected as possible by any deflection in the system other than the contraction of the specimen. Aluminum dummy specimens were tested in each cell to determine the extent of equipment effect so it could be subtracted from the actual readings. The LVDTs used were of the range ± 25mm to cover the entire range of specimen deformation during an extended test. Currently, work is being done using a ± 1.3 mm LVDT in addition to the longer stroke unit, for enhanced resolution. This shorter stroke LVDT can be reset as required. At present, the LVDT system is extremely stable because of the lack of vibration and the constant temperature. Displacements of a few microns in a day can be detected easily. The systems have been monitoring creep tests at strain rates below 10^{-10} sec^{-1} with no serious problems.

The data acquisition device selected for use in the WATSALT Laboratory was selected for its compatability to triaxial testing. It contains an integral screen for multi-channel output. The complete data for each creep station can be displayed on the screen as a "page" of information containing all relevant channels. It is possible to configure the input voltages so they read in the direct units desired: eg. MPa for the pressure transducers. Another design feature of this data acquisition system is its capability of internally providing both power source and signal conditioning for the

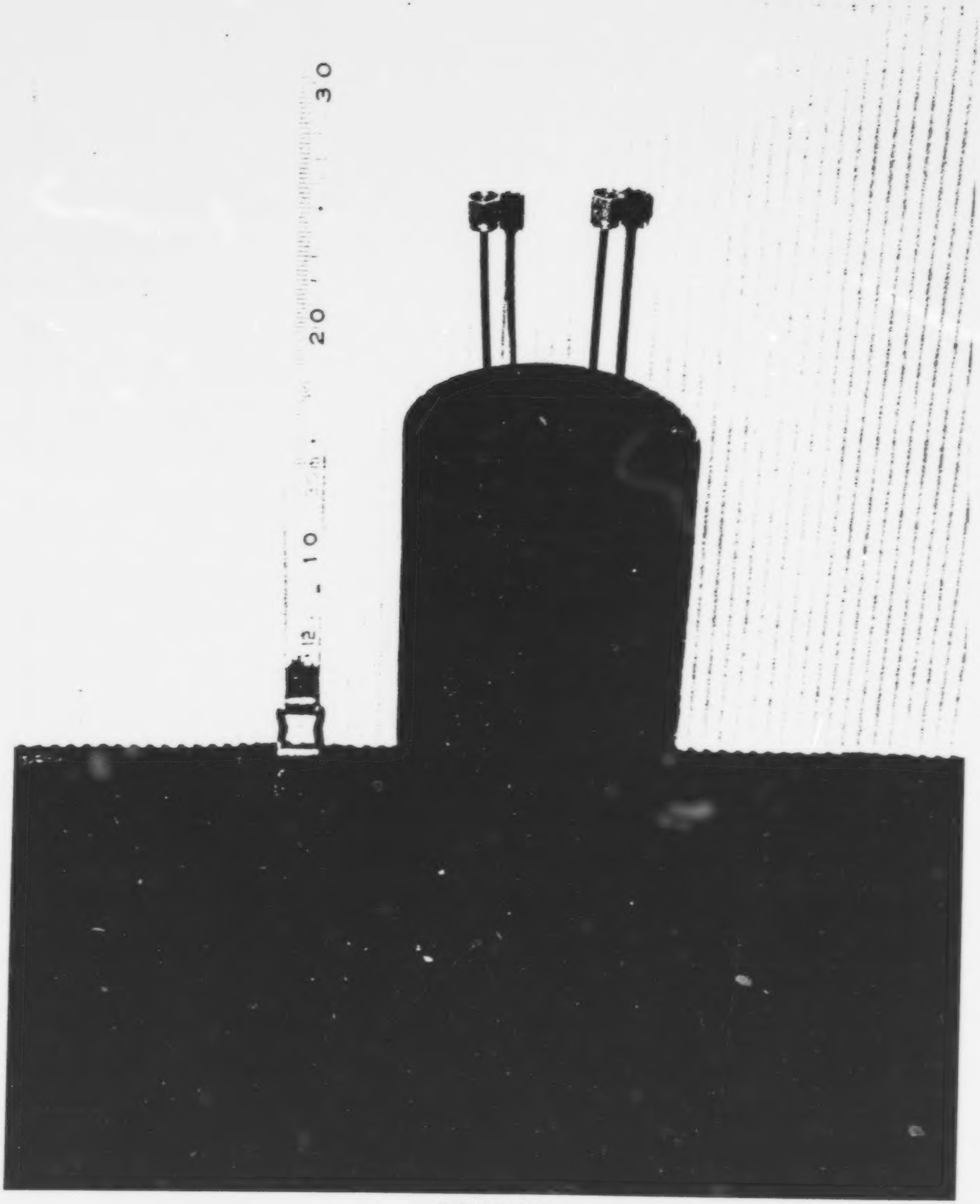

FIGURE 8.1

instruments. Hence only a single cable for each instrument is necessary to send power and return the output signal. This eliminates the costs for power supplies, additional connectors and amplifiers, reduces installation labour and decreases the possibility of poor electrical connections. In the extensive equipment configuration of the WATSALT Laboratory, reducing the myriad of wires which typically surrounds a multi-channel electronically instrumented system allows a more efficient operation and reduces the likelihood of damage.

Finally, the output readings for each system are sent through a RS-232 port on the data acquisition system to both a hardcopy printer and a microcomputer at continuous 4 hour intervals.

Figure 8 is a schematic diagram which depicts the major components for an individual creep station.

SUMMARY

An extremely compact and economical system for triaxial creep testing of cylindrical specimens has been designed and is in continous use. It provides most of the capabilities of much larger systems at literally a fraction of the cost through several novel design concepts. The precision and reliability of the system is very high, and the entire assembly has been shown to be stable for months.

ACKNOWLEDGEMENTS

The authors would like to thank researchers John Unrau and Mike Souliere for their work in implementing the designs and systems described in this paper. The authors also appreciate the work and advice of machinists Heinz Birkenhauer and Jacques Pronovost, and Arie DeGroot of Mechanical Engineering at the University of Waterloo. Thanks is extended to Sue Andrews and Nadia Bahar for preparation of the manuscript and figures. Financial support from the Natural Sciences and Engineering Research Council of Canada is gratefully acknowledged, and thanks are extended to Mr. D. Mraz, of MPC Limited, for getting us involved in the first place.

REFERENCES

[1] Hoek, E. and Franklin, J.A., 1968. A simple triaxial cell for field and laboratory testing of rock. Trans. Inst. Mining and Metallurgy, (G.B.), Vol. 77, pp.A22-A26.

[2] Jastrezebski, Z.D. 1976. The nature and property of engineering materials, 2nd ed., Wiley, New York, 1976, p.317-320.

[3] ASME Boiler and Pressure Vessel Code, American Society of Mechanical Engineers, New York 1974, Section VIII Division I.

[4] Shigely, J.E. and Mitchell L.D., 1983. Mechanical Engineering Design, 4th ed., McGraw Hill, New York, p.359.

[5] Harvey, J.F., 1974. Theory and design of modern pressure vessels, 2nd ed., Van Nostran Reinhold, New York, p.351-353.

[6] CISE, 1977. Limit States Design Steel Manual, 1st ed., Gilmor, M.I., Ed., Canadian Institute of Steel Construction, Toronto.

LIST OF FIGURES

Figure 1: Triaxial Creep Cell, Sectional View.

Figure 2: Example of a 450 kN frame, with Triaxial Cell and Temperature Chamber
A. Compression frame B. Triaxial Cell
C. Temperature Chamber

Figure 3. Internal Piston Creep Cell, Sectional View

Figure 4. Three Internal Piston Cells in the Laboratory

Figure 5. Intensifier-Accumulator.

Figure 6. Pressure Control System for an Individual Creep Station
A. Intensifier-Accumulator B. Hydraulic Hand Pump
C. Solenoid Valves D. Pressure Transducers

Figure 7. Internal Piston Cells with Temperature Control Chambers in Place

Figure 8. Major Components of an Individual Creep Station.

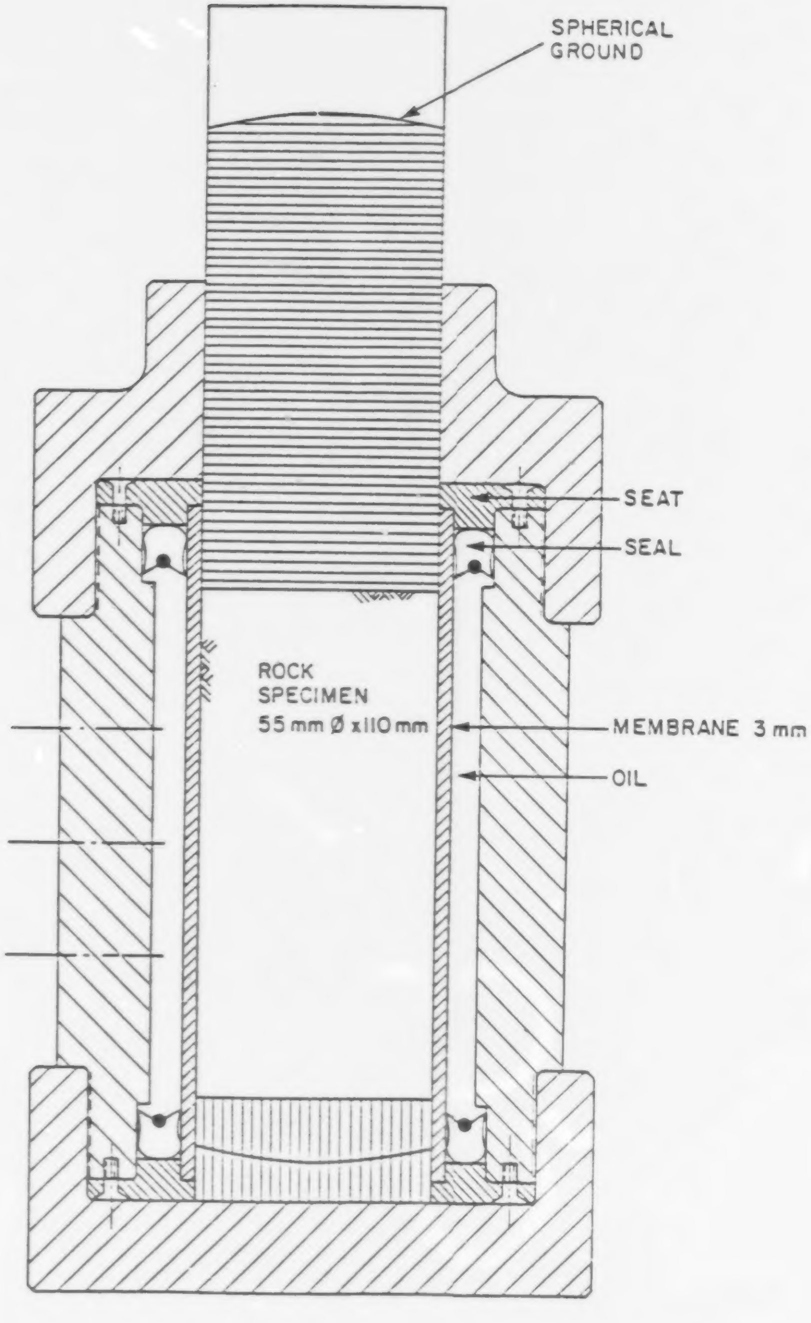
SPHERICAL GROUND
SEAT
SEAL
ROCK SPECIMEN 55 mm Ø x110 mm
MEMBRANE 3 mm
OIL

FIG. 1

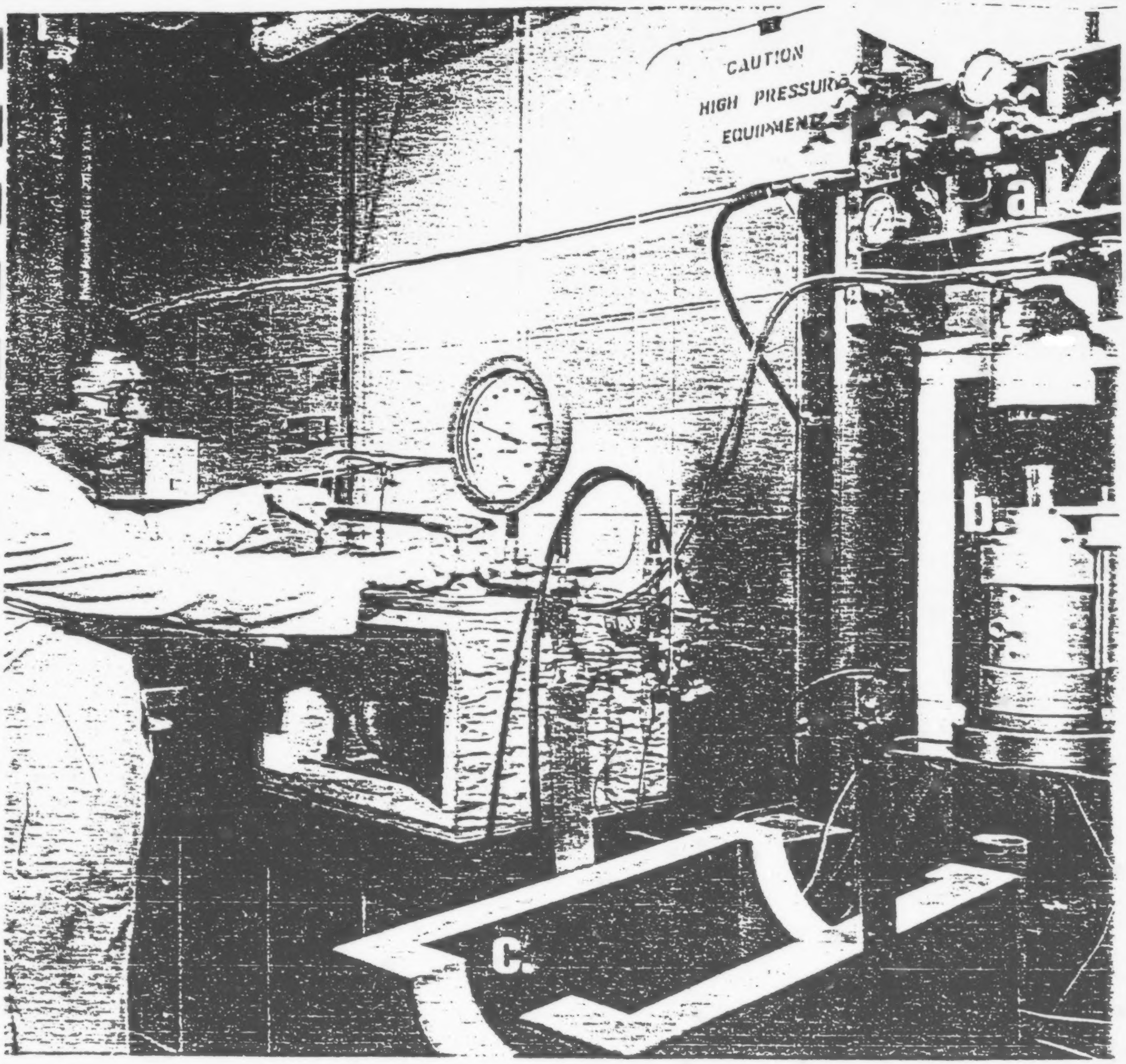
CAUTION
HIGH PRESSURE
EQUIPMENT
a
b.
c.

FIG 2.

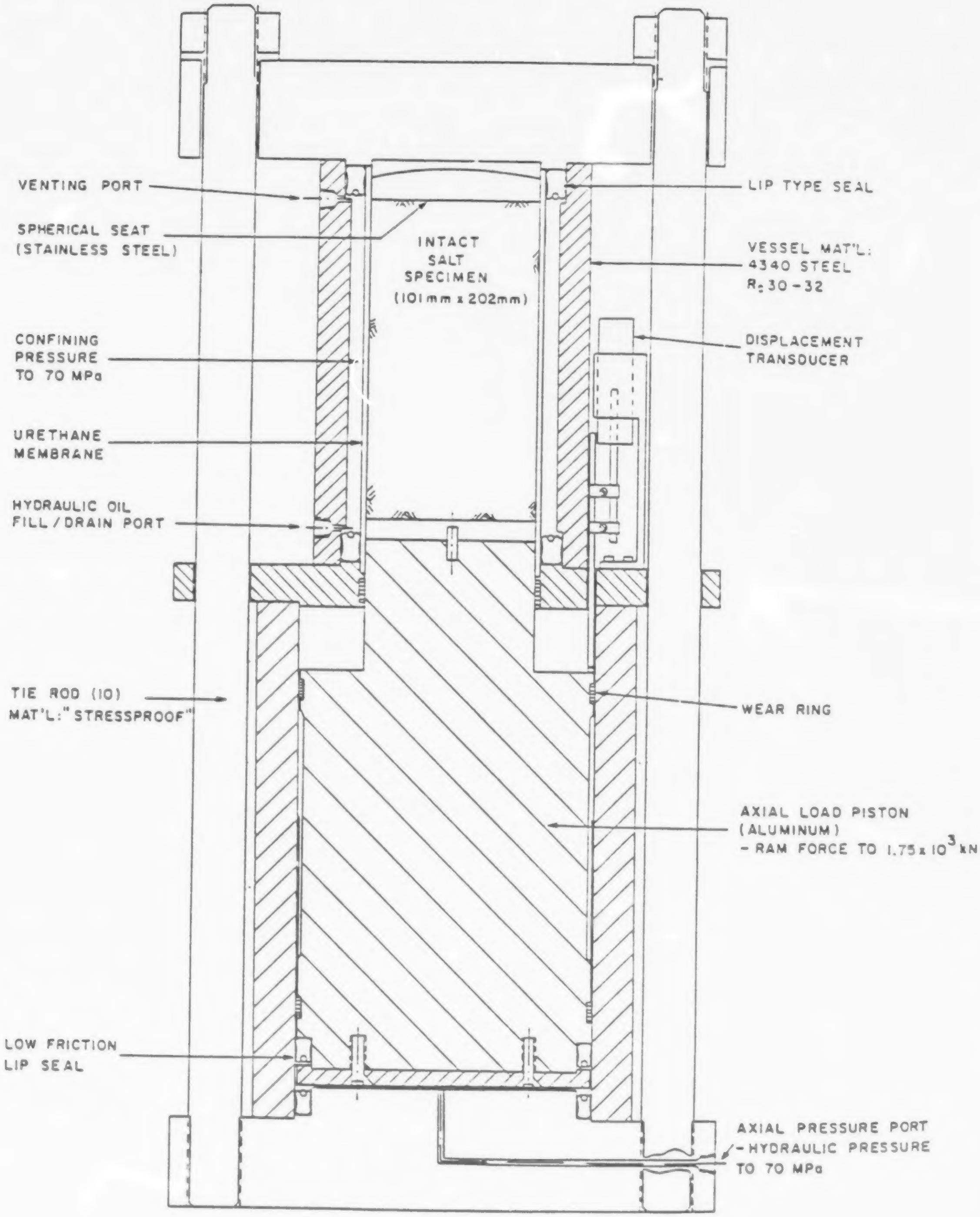
VENTING PORT
SPHERICAL SEAT
(STAINLESS STEEL)
INTACT
SALT
SPECIMEN
(101mm x 202mm)
CONFINING
PRESSURE
TO 70 MPa
URETHANE
MEMBRANE
HYDRAULIC OIL
FILL / DRAIN PORT
TIE ROD (10)
MAT'L: "STRESSPROOF"
LOW FRICTION
LIP SEAL
LIP TYPE SEAL
VESSEL MAT'L:
4340 STEEL
Rc 30 - 32
DISPLACEMENT
TRANSDUCER
WEAR RING
AXIAL LOAD PISTON
(ALUMINUM)
- RAM FORCE TO 1.75 x 10³ kN
AXIAL PRESSURE PORT
- HYDRAULIC PRESSURE
TO 70 MPa

FIG3.

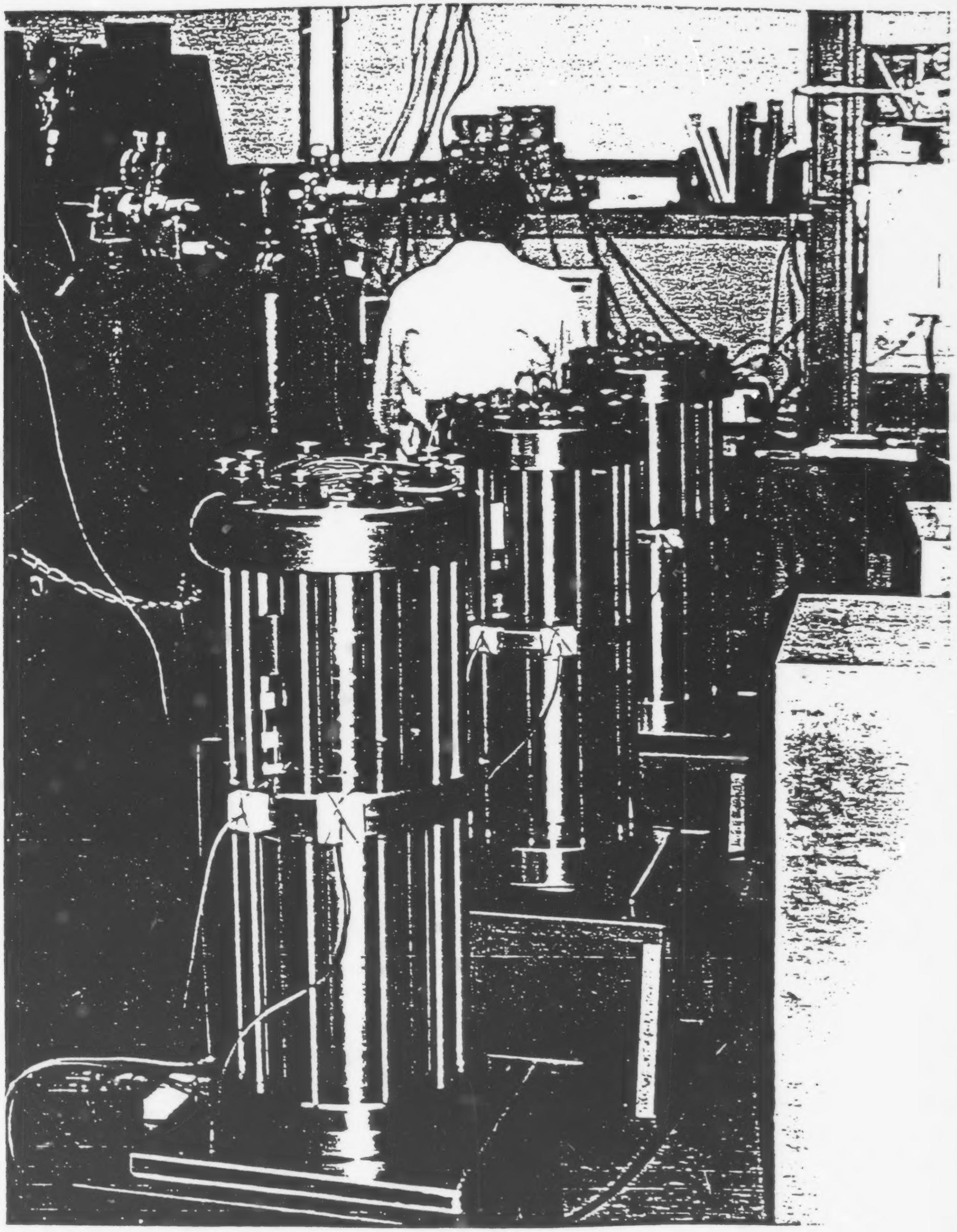

FIG. 4.

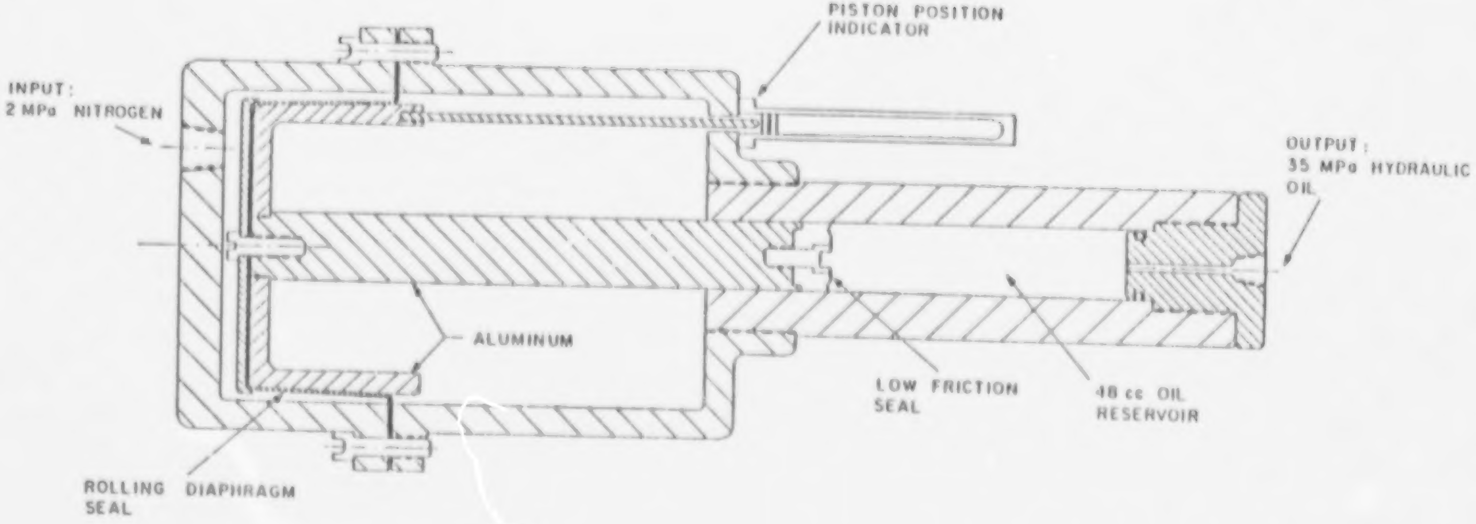
PISTON POSITION INDICATOR
INPUT: 2 MPa NITROGEN
OUTPUT: 35 MPa HYDRAULIC OIL
ALUMINUM
LOW FRICTION SEAL
48 cc OIL RESERVOIR
ROLLING SEAL
DIAPHRAGM

FIG. 5.

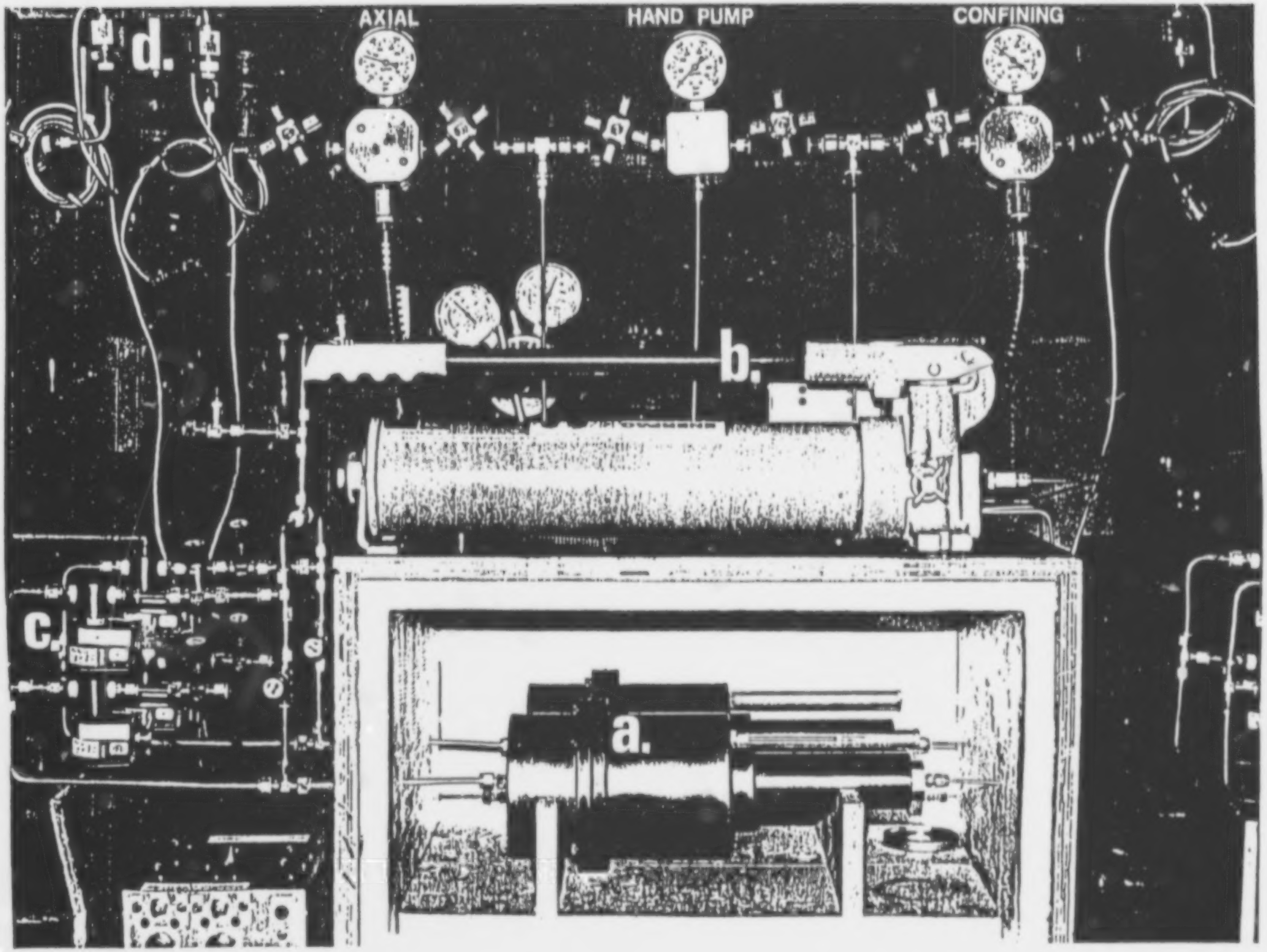
d.
AXIAL
HAND PUMP
CONFINING
b.
c.
a.

FIG 6.

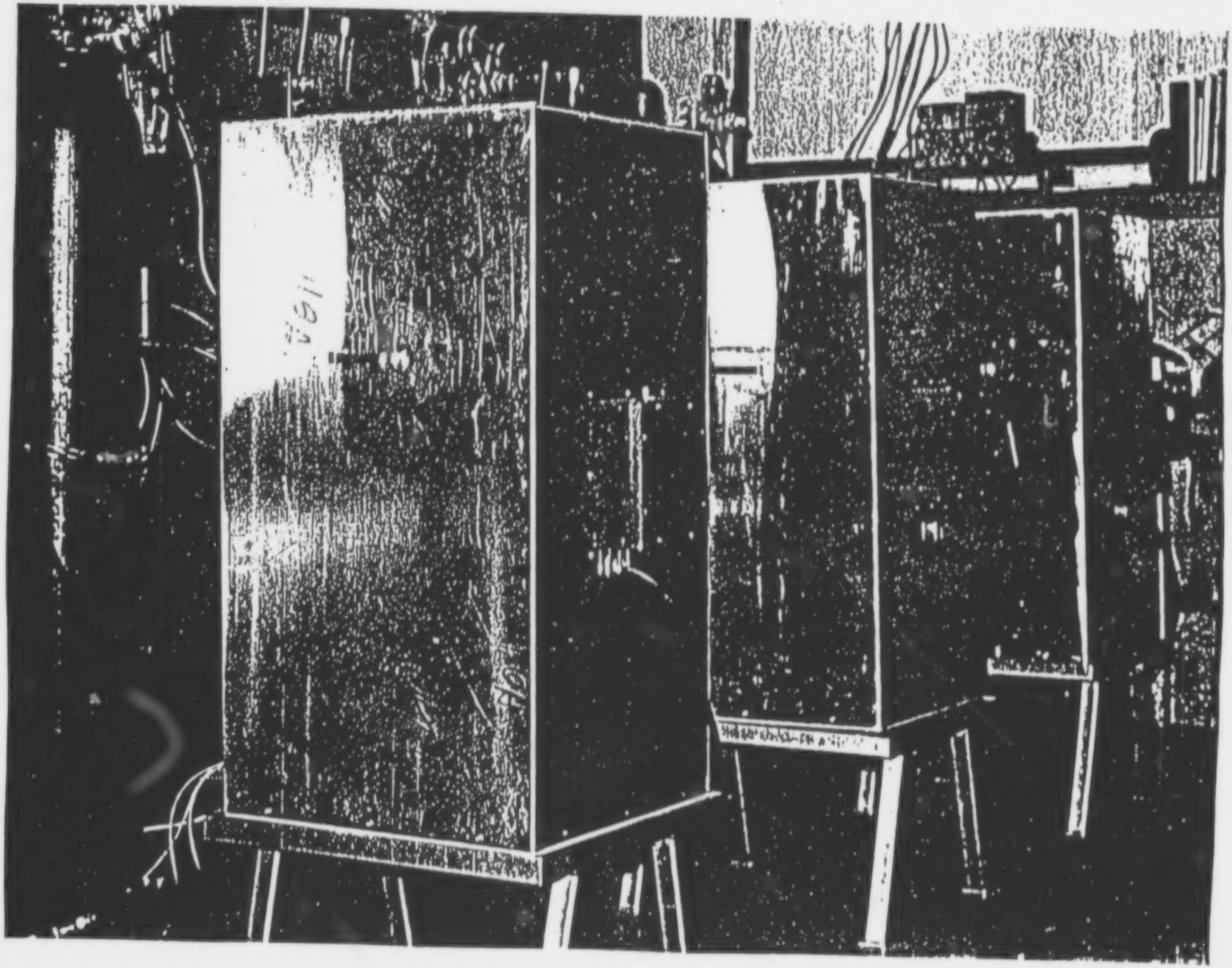

FIG 7

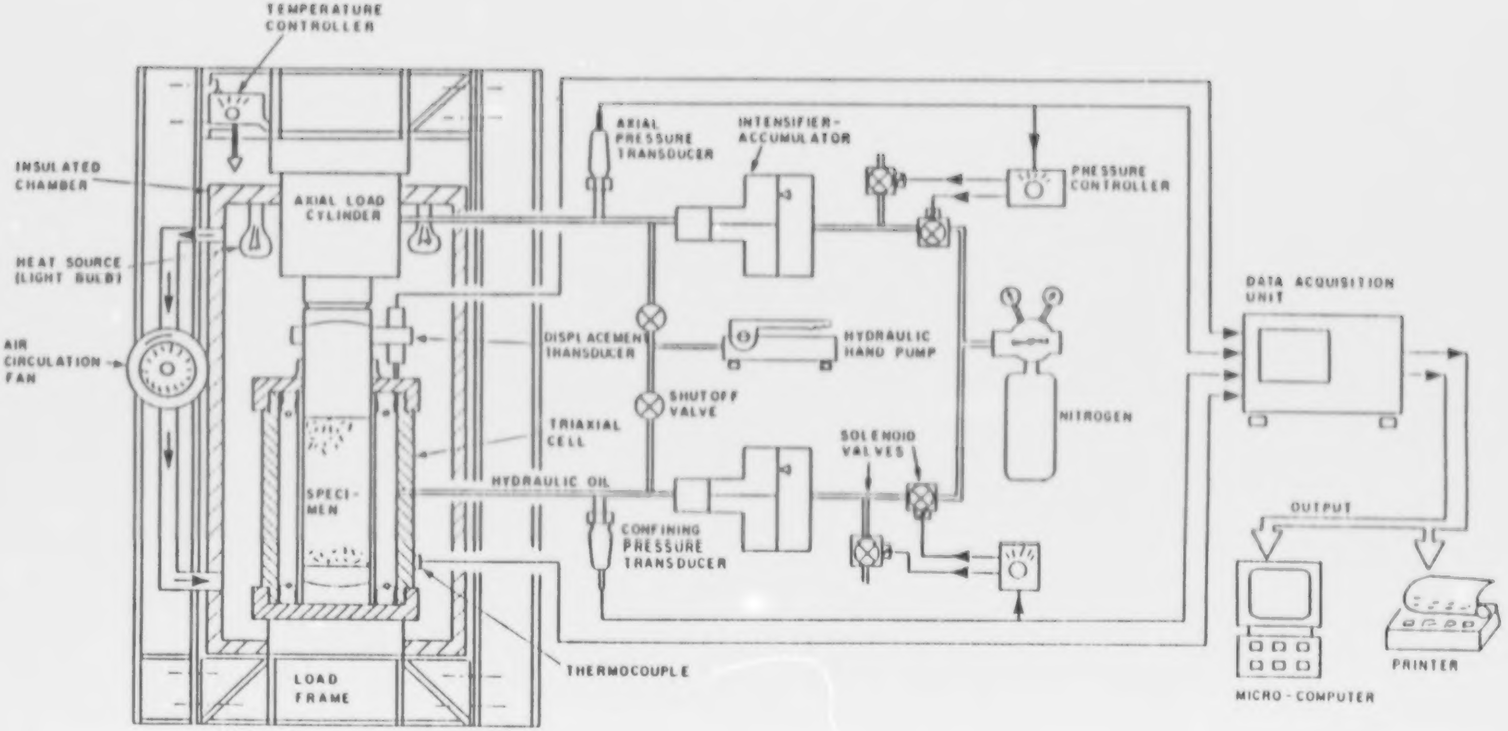
TEMPERATURE CONTROLLER
INSULATED CHAMBER
HEAT SOURCE (LIGHT BULB)
AIR CIRCULATION FAN
AXIAL LOAD CYLINDER
SPECI-MEN
LOAD FRAME
THERMOCOUPLE
TRIAXIAL CELL
HYDRAULIC OIL
DISPLACEMENT TRANSDUCER
SHUTOFF VALVE
AXIAL PRESSURE TRANSDUCER
CONFINING PRESSURE TRANSDUCER
INTENSIFIER-ACCUMULATOR
HYDRAULIC HAND PUMP
SOLENOID VALVES
PRESSURE CONTROLLER
NITROGEN
DATA ACQUISITION UNIT
OUTPUT
MICRO-COMPUTER
PRINTER

FIG. 8

26th US Symposium on Rock Mechanics / Rapid City, SD / 26-28 June 1985

Test procedures for salt rock

M.B.DUSSEAULT
University of Waterloo, Ontario, Canada
D.MRAZ
Mraz Project Consultants, Saskatoon, Saskatchewan, Canada
J.UNRAU & C.FORDHAM
University of Waterloo, Ontario, Canada

ABSTRACT

Potash mining, salt mining, design of solution caverns in salt rocks, disposal of waste in salt repositories, and the use of granular halite backfill in underground salt rock mines are all mining activities which are practised or contemplated for the near future. Whatever the purpose, the need for high quality design parameters is evident.

We have been testing salt rocks in the laboratory in a number of configurations for some time. Great care has been given to the quality of sample preparation and test methodology. This paper will describe the methods, present the elements of equipment design, and show some typical results.

1. INTRODUCTION

Intact salt rocks and granular halite tailings for use as mine backfill are materials which display time dependant deformation. Testing is essential if a rational, economic design procedure is to be achieved for a wide range of times, materials, and mine geometries. We present our methods for testing these materials. Other techniques, such as hollow cylinder tests or plane strain tests, are not discussed, as they do not fall into the realm of routine testing. Rather, they are simulations of in situ geometries, and, while extremely valuable in their own right, are not amenable to the provision of large quantities of data for design purposes.

2. INTACT SALT ROCK TESTING

The creation of an underground opening in salt rock (Figure 1) causes redistribution of the stresses which were carried by the material in the opening to the surrounding material. Several types of data are required.

1. It may be necessary for purposes of modelling or evaluation of instrumentation to know the "instantaneous" deformational behaviour of material as expressed by a pair of moduli (K and G or E and *) for a linear elastic assumption;
2. Because certain parts of the roof and wall of the material adjacent

to the opening are subjected to extremely high deviatoric stresses, the failure behaviour of the salt rock is required; and, most important;

3. The creep behaviour at appropriate stress levels is required to assess the redistribution of stress and the rates of deformation of walls and pillars for medium and long-term mine design.

Three different approaches are used to determine the relevant data. Triaxial cells are used in all cases. We do not believe that classical shear box testing of salt rocks is of value for strength data. Boundary stress conditions must be thoroughly understood before salt rock tests can be performed. Classical shear box tests allow measurement of only two stresses; the horizontal stress perpendicular to movement is unknown. Rigorous control of boundary conditions is essential.

3. SAMPLING AND SAMPLE PREPARATION

To ensure high quality test results from intact salt specimens, undisturbed core must be obtained. Core samples should be obtained from at least two metres beyond a free face. Drilling should be performed using brine or, preferably, air in conjunction with either a continuous flight, hollow stem auger or a conventional diamond core barrel. Suitable lengths of core are carefully dried, wrapped in cellophane, and placed in a rigid, air-tight, storage chamber for shipping. Core specimens taken deep within a wall are preferred over block specimens obtained at the face of the wall as the latter have been observed to contain shear planes caused by post-excavation stress relief.

We prepare samples for triaxial testing to an L/D ratio of at least 2.0. Sample ends are carefully dry ground with 600 grit. It is important that the ratio of crystal size to sample diameter be at least 1:10. We can test samples up to 15 cm in diameter or samples with crystal sizes up to 15 mm. Ultrasonic velocity tests are performed on all specimens to determine the dynamic elastic moduli.

A high pressure, high temperature MoS_2 dry lubricant is applied to sample ends and highly polished, stainless steel endcaps. This technique has resulted in a dramatic reduction of laboratory strain-hardening, especially during long term triaxial tests. Even after repeated load stages, cylindrical deformation (barrelling) remains uniform.

The sample is placed in the confining membrane and attached to the endcaps with gear clamps. To minimize the effects of moisture diffusion and membrane stresses, hydraulic oil and special neoprene membranes are used in the triaxial cells.

4. TRIAXIAL TESTING OF INTACT SALT SPECIMENS

We perform three types of triaxial tests on intact salt specimens;

1. bulk modulus tests to determine instantaneous deformation characteristics;
2. brittle yield tests to determine failure criteria under various stresses; and,
3. creep tests to determine time-dependant behaviour.

Our salt rock testing facility incorporates an economical, self-regulating pressure control system with a data acquisition system for long term monitoring (Figure 2). The same test configuration is used for all intact salt rock tests.

4.1 Bulk modulus testing

We use bonded foil strain gauges (60 mm) mounted in vertical and horizontal directions at the midpoint of a piece of core. This is the only test configuration in which we use bonded strain gauges, because total strains are very low. Strain gauges are applied using an epoxy adhesive and the leads are taken out along the side of the specimen. The flexible neoprene membrane attached to the endcaps by gear clamps has proven to be a satisfactory seal against oil entering the specimen. Special exit seals allow the leads to be taken out of the cell. The sample is mounted in a conventional fully triaxial rock cell (not a Hoek-Franklin cell), placed in a reaction frame to hold the ram, and subjected to stress through pressurized oil acting against the membrane (Figure 3).

The test is carried out by "instantaneously" raising the oil pressure to perhaps 35 MPa from an initial low stress state of about 0.5 MPa. Strains are recorded immediately and continuously until deformation ceases. This takes about 3-7 days using potash from New Brunswick.

The pressure is then dropped to its initial value with continuous recording. The cycle may be repeated at different stresses. Figure 4 shows data from two tests performed on one sample. The instantaneous strain represents "elastic" material deformation, but it also has a component of microcrack closure. The deformation continues for several days because the core samples, or any samples of salt rock for that matter, are disturbed due to the microcracks which open along grain boundaries because of stress relief. In the potash specimens we have tested, halite/sylvite grain boundaries show crack development and evidence of microscopic stress cracks (Dusseault and Mraz, 1983). These result from differential strain arising from unequal bulk moduli of the two constituent minerals.

4.2 Brittle yield and creep testing

Samples for brittle yield testing are placed in a triaxial cell and mounted in a frame which can be displacement controlled up to 4.5 mm/min. Lateral stresses are maintained constant throughout the test while axial stresses are monitored. For lateral stresses of less than 5 MPa, brittle yield is easily achieved. Upon disassembly, clear conical failure surfaces are usually found. For tests at confining stresses greater than 10 MPa, specimens do not undergo brittle yield. Rather, the specimens reach a stress plateau and simply continue to yield. In other words, at high confining stresses, salt rocks do not rupture under high deviatoric stresses, they simply yield rapidly. The transition range for the New Brunswick potash ore is from 5 to 10 MPa.

Samples for creep testing are placed in a triaxial cell and hydrostatically stressed to 30 MPa for about 72 hours to reverse post-sampling stress and strain relief. First stage axial and lateral stresses are then applied and creep is allowed to stabilize. After 7-14 days of steady state creep, stress levels are altered to maintain first stage creep rates under the new stresses. This may be repeated for up to six stages and two or three different strain rates (Figure 5). Typical data plotted in stress space (q vs.p) are shown in Figure 6. Note that only two or three points adequately define a constant strain rate tangent. The slope of each tangent or the angle of internal yield friction (ϕ^{o}) is then plotted against creep rate (Figure 7).

5. HALITE BACKFILL TESTING

Granular halite waste from flotation or gravity separation processes used to recover sylvite is being considered as backfill in potash mines. Two fundamentally different processes are involved in evaluating and modelling halite backfill performance. First, near the backfill face behind the active longwall the backfill (Figure 8) may shear or buckle if insufficiently supported. This cannot be permitted in a potash mine with high pressure water above the rock. Therefore it is a shear strength problem, not a creep problem.

The other issue is the coupled closure/support-stress/creep strain problem further away from the backfill face (Figure 8) where shear failure is not an issue. Tests are performed to assess the time-stress-strain behaviour of the backfill to predict long term closure, to predict stress in abandoned panel development adits, and to do stress analysis in abutment and guard pillars for mine security. This is a creep-consolidation issue, not a backfill shear strength issue.

5.1 Approach to variations in initial material parameters

In order to reduce as much as possible the number of tests performed for the client, careful preplanning is required. First, the placement density in the backfill must be estimated so that the initial test density can be standardized. Gravity drop tests, relating velocity of impact to density can be performed to assess blower or flinger efficiency, but ultimately real data from a prototype operation are required. We strongly recommend that the range of placement specific densities for initial testing be specified within ± 0.05 g/cc. Second the halite backfill reaches placement at a certain moisture content, and drainage may occur. We recommend testing at the no-load free-draining moisture content of the process tailings achieved in the test cell, then testing in either a fully drained or fully undrained mode. Temperature of testing should be equal to the mine temperature. Other factors such as mineralogical variations, grain size, and so on, must be handled by careful representative sample preparation during sampling and blending.

Fundamentally, our approach is to carefully control all extrinsic factors to assure that we test the right material under the right initial conditions. We can then concentrate on determining the full constitutive behaviour over the appropriate stress ranges.

5.2 Creep-consolidation testing

Figure 9 shows the major elements of the test cell apparatus. Axial stress is controlled externally, either held constant or changed at some some pre-determined rate, by an analogue system controlling solenoids on the low pressure side of an intensifier. Because the actuator is built into the cell, a large load frame is not required. The cell construction is entirely of brass and stainless steel to resist corrosion, and full provision is made for liquid drainage from the base. It was decided that double drainage was not an issue in this load configuration, therefore only basal drainage using a sintered porous stainless steel disk is employed. Vertical deformation is monitored electronically on the downward movement of the actuator piston. Five cells are used simultaneously in a chamber which is temperature controlled to ±

0.5° C to ensure environmental constancy.

Salt rocks creep readily, therefore it is essential to directly measure lateral stress development with time under the constant axial stress load conditions. A novel strain gauge yoke load cell of 2 cm diameter lies flush with the cell wall and gives a reasonable estimate of lateral stress. Calibration of the load cell and determination of ram stick/friction is performed with water in the cell.

5.3 Triaxial strength of halite backfill

Samples for triaxial testing are assembled by a standard compactive effort in 2-3 cm lifts within a latex membrane in a 75 x 150 mm brass mold. A brass top cap is affixed and the sample is placed in a lucite cell reinforced with fiberglass bands to withstand 3 MPa. A sintered stainless steel plate in the bottom cap allows for drainage. For long term tests (greater than 2-3 hours) oil is used as a cell fluid. Water is used to apply the confining stress for short term tests. Testing is carried out at a constant axial strain rate after a very brief period of consolidation under the desired confining stress.

Triaxial testing of halite backfill involves a parameter not normally considered in frictional granular material testing. Because creep-consolidation is occuring at all times during the test, the element of time is critical. We therefore test a particular material over a wide range of confining stresses and deformation rates. Roof closure can be slow or rapid, so a wide range of axial deformation rates are used. Figure 10 shows a Mohr-Coulomb plot for halite backfill. Like intact potash, halite backfill will only display strain-weakening behaviour when subjected to high strain rates and low lateral stresses.

It is also critical to know the void ratio of the solid phase at any time, therefore great care must be exercised to determine lateral and axial strain and fluid status, from which back calculations can be carried out.

6. CONCLUSIONS

High quality results from intact salt rocks can only be achieved when undisturbed sampling is combined with careful sample preparation and rigorous control of boundary conditions. Such control can only be maintained under triaxial conditions. Data required include "instantaneous" deformational characteristics, failure criteria, and time dependant behaviour.

Before granular halite backfill can be tested, initial conditions such as density, water content, and grain size must be determined. Once these parameters have been determined, tests must be performed to determine shear strength of the unsupported material near the backfill face and creep-consolidation characteristics for regions further away from the backfill face.

REFERENCES

Dusseault, M.B. and Mraz, D., 1983. Salt rock constitutive behavior. Proceedings, Potash '83, editor: R.M. McKercher, Saskatoon, Sask., pp.311-320.

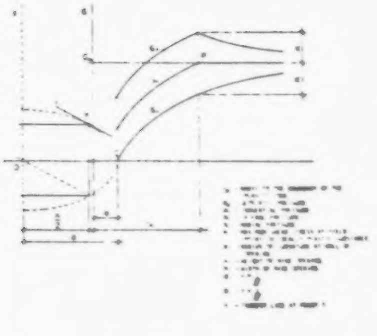

Figure 1: Stress distribution around an underground opening.

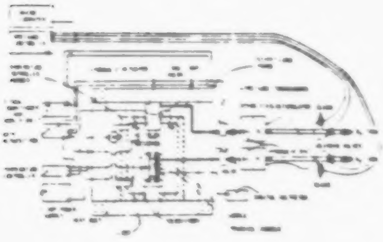

Figure 2: Triaxial cell configuration.

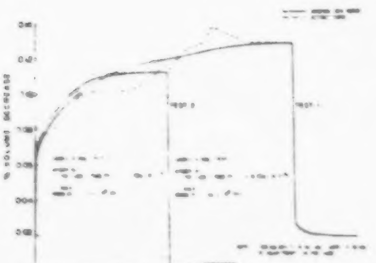

Figure 3: Bulk modulus data for two hydrostatic loading stages.

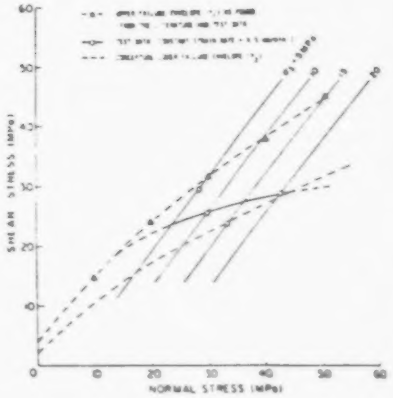

Figure 4: Brittle failure data.

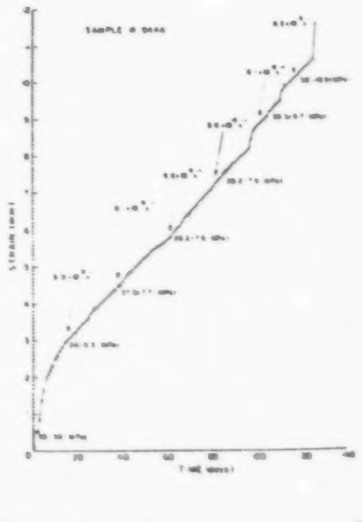

Figure 5: Stage creep testing of potash at different stress levels.

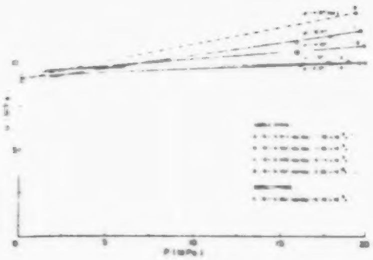

Figure 6: Creep data in terms of mean shear stress (Q) and mean normal stress (P).

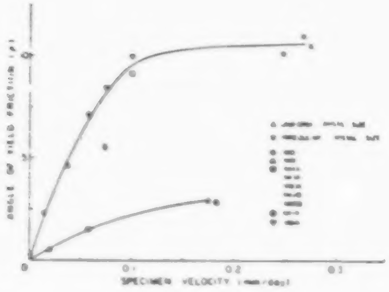

Figure 7: Angle of internal yield friction for different creep rates.

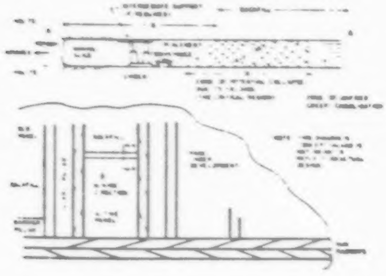

Figure 8: Halite backfill in longwall mining operations.

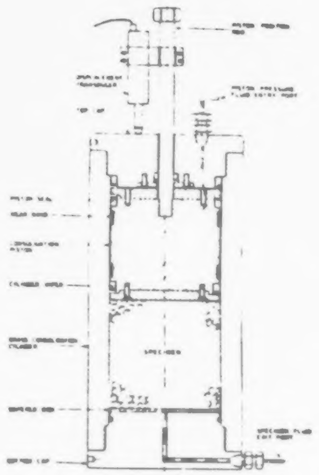

Figure 9: Halite backfill consolidometer.

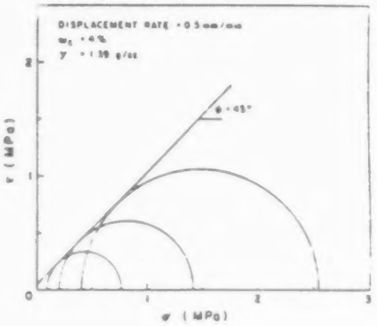

Figure 10: Mohr-Coulomb plot for halite backfill.

APPENDIX B

BACKFILL SAMPLING AT
DENISON-POTACAN POTASH COMPANY

Prepared By:

SHAWN MUNROE
Denison-Potacan Potash Company

April, 1986

TABLE OF CONTENTS

Page

LIST OF FIGURES AND TABLES ii

1.0 SUMMARY 1

2.0 INTRODUCTION 2

3.0 BACKFILL PREPARATION 3

- 3.1 COARSE ORE STORAGE 3
- 3.2 FEED PREPARATION 4
- 3.3 FLOTATION 4
- 3.4 TAILINGS PREPARATION 4
- 3.5 TAILINGS FILTRATION AND DISPOSAL 5

4.0 BACKFILL SAMPLING 6

- 4.1 SCROLL AND DRUM FILTER SAMPLING 6
- 4.2 COMBINED STREAM TAILINGS SAMPLING 7
- 4.3 PROCESS BRINE SAMPLING 7
- 4.4 PACKAGING AND SHIPMENT OF SAMPLES 7

5.0 FACTORS EFFECTING BACKFILL COMPOSITION 8

- 5.1 CHANGES IN THE ORE 8
- 5.2 PROCESS CHANGES 8
- 5.3 TAILINGS MATERIALS 9

6.0 CONCLUSIONS 10

7.0 LIST OF REFERENCES 11

8.0 APPENDIX 12

LIST OF FIGURES AND TABLES

LIST OF FIGURES

Page

FIGURE 1. BACKFILL PREPARATION FLOWSHEET 13

LIST TO TABLES

TABLE 1. PRELIMINARY MOISTURE CONTENT ANALYSIS 14

TABLE 2. SCROLL FILTER AND STRING DRUM FILTER MOISTURE CONTENT SAMPLES 14

TABLE 3. COMBINED STREAM TAILINGS MOISTURE CONTENT SAMPLES 15

1.0 SUMMARY

Tailings from the Denison-Potacan Potash Company surface process plant will be utilized for backfill in mined out underground workings. The placement of tailings underground allows for an environmentally safe disposal method as well the possible increased recovery of potash resources with subsequent pillar recovery.

In order to investigate the material characteristics and properties of the tailings, backfill laboratory testing is required. Tailings samples were collected in January, 1986 from the surface process plant for testing at the University of Waterloo.

2.0 INTRODUCTION

An important component of mine operations at Denison-Potacan Potash Company (DPPC) is the placement of tailings backfill in mined out underground workings. The placement of tailings backfill underground allows for an environmentally safe tailings disposal method as well as the possible increased recovery of potash resources due to pillar recovery. Pillar recovery will be attempted after backfilled rooms have been allowed to support the overlying weight of overburden.

The backfill material to be used at DPPC is comprised of the waste salt tailings from the surface process plant. At present the tailings materials are slurried and then pumped to a surface tailings storage area. Initiation of mine backfilling operations is scheduled to begin during 1986. The tailings from the surface tailings storage area will gradually be reclaimed for use as mine backfill. In order to investigate the beneficial effects of backfilling on mine stability and on the increased recovery of potash resources, various testing on tailings materials is required.

Laboratory testing to determine the tailings material characteristics, packing densities under various circumstances and the strength and deformation properties of the backfill material is scheduled to be conducted at the University of Waterloo. The testing will take place in the Department of Earth Sciences under the guidance of Dr. Maurice Dusseault. The testing program is partially funded by CANMET (Department of Energy, Mines and Resources) under the contract entitled "Use of Backfill in New Brunswick Potash Mines". (1)[1]

This report will briefly describe the backfill preparation process at DPPC and the methods used to collect the tailings samples required for the laboratory testing program. If more detailed information is required on the backfill preparation processes, the KILBORN LIMITED Process Plant Reports should be consulted. (2, 3, 4)

[1] Underlined numbers in parentheses refer to items in the List of References.

3.0 **BACKFILL PREPARATION**

A simplified flowsheet of the backfill preparation process is presented in the Appendix.

3.1 COARSE ORE STORAGE

The potash ore is transported to surface from underground in the production headframe in 24 tonne ore skips. A 6000 tonne storage bin between the production shaft and the mill provides 12 1/2 hours of constant throughput at the designed feed rate of 475 tonnes per hour.

The ore is withdrawn from the storage bin and conveyed to the concentrator building where it is screened. Screen oversize is fed to a reversible impactor which reduces the ore to approximately seven millimeters. The screen undersize and impactor discharge are combined, slurried, and pumped to the secondary circuit.

3.2 FEED PREPARATION

The slurry from the primary circuit is fed over 24 double-stage sieve bend wet sizing screens. The screen oversize is recycled in closed circuit to reversible impactors. This allows size reduction to minus 2.36 mm in order to fully liberate the sylvite crystals.

The wet sizing screen undersize feeds 24 double-stage sieve bend feed preparation screens. The feed preparation screens split the coarse and fine fractions into approximately equal portions.

The undersize from the feed preparation screens is pumped to twenty 254 mm diameter desliming cyclones. The cyclone overflow feeds the slimes thickener while the cyclone underflow passes to the fines reagentizing tanks. The oversize from the feed preparation screens feeds the coarse reagentizing drum.

3.3 FLOTATION

The fines flotation circuit consists of a rougher, cleaner, and recleaner bank of cells. The underflow from the desliming cyclones feeds five 8.5 m^3 rougher cells. The rougher concentrate feeds a bank of five 8.5 m^3 cleaner cells. The cleaner concentrate is further upgraded by a bank of four 8.5 m^3 recleaner cells. Two screen bowl centrifuges are used to debrine the leached recleaner concentrate prior to drying.

The tailings from the fines rougher cells feed the tailing cyclones. The tailings from the cleaner and recleaner cells pass to the regrind rougher flotation cells.

The coarse reagentizing drum feeds a double bank of five 5.1 m^3 coarse rougher cells. The coarse rougher concentrate feeds two single-stage sieve bend screens for debrining and removal of entrained fine salt. The screen undersize concentrate passes to the fines cleaner cell bank for further upgrading. The screen oversize concentrate feeds the coarse concentrate leaching tank. A screen bowl centrifuge is used to debrine the leached coarse rougher concentrate prior to drying.

The screen bowl centrifuge effluents are pumped to a bank of five 254 mm diameter cyclones. The cyclones recover coarse particles if the centrifuges have worn or broken screens. The cyclone overflow feeds a bank of six 2.8 m^3 scavenger flotation cells. The scavenger cell concentrate feeds a string discharge drum filter. The scavenger cell tailings discharge to the slimes thickener.

3.4 TAILINGS PREPARATION

The tailings from the coarse rougher cells discharge to six single stage sieve bend tails screens. The screen undersize feeds the tailings cyclones. The screen oversize feeds a 2896 mm diameter x 3656 mm ball mill in closed circuit with six double-stage sieve bend tails regrind screens. The tails regrind screen undersize is pumped to four 254 mm diameter cyclones where insoluables liberated during grinding are removed.

The regrind cyclone overflow feeds the slimes thickener. The regrind cyclone underflow and the tailings from the fines cleaner and recleaner flotation cells feed five 8.5 m^3 regrind rougher flotation cells. The regrind rougher concentrate discharges to the fines cleaner flotation cells. The regrind rougher tailings are pumped to the tailings cyclones.

3.5 TAILINGS FILTRATION AND DISPOSAL

The tailings cyclone cluster, comprised of sixteen 254 mm diameter cyclones, is used to separate the fine and coarse fractions of the tailings at 200 mesh. The cyclone underflow (coarse fraction) feeds two 6706 mm diameter horizontal scroll discharge filters. The scroll filter cake at approximately seven percent moisture is discharged to a reversible belt conveyor for disposal.

The tailings cyclone overflow (fines fraction) feeds a 18.30 m diameter slimes thickener lamella tank. The overflow from the desliming cyclones, regrind desliming cyclones and the tailings from the scavenger flotation cells also feed the slimes thickener. The thickener underflow is pumped to a 3505 mm diameter x 4877 mm string discharge drum filter. The drum filter cake at 10-15 percent moisture is discharged to a reversible belt conveyor where it mixes with the coarse tailings from the scroll filters for disposal.

The tailings cake at approximately seven percent moisture will be conveyed to the service headframe for disposal as mine backfill. Alternatively, the tailings cake can be repulped with brine for disposal by pipeline to the surface tailings pond. Tailings from the surface tailings pond will gradually be reclaimed for disposal as mine backfill.

4.0 BACKFILL SAMPLING

The following samples were required for testing by the University of Waterloo:

1. Horizontal scroll discharge filter tailings
2. String drum filter tailings
3. Combined stream scroll filter and drum filter tailings
4. Process brine

The mill circuit had to be in normal operation at least two hours prior to sample collection.

4.1 SCROLL AND DRUM FILTER SAMPLING

The scroll filter and string drum filter samples were collected on January 27, 1986. Moisture content samples were taken prior to sample collection to determine if typical samples would be obtained. The moisture contents were determined to be satisfactory and sampling commenced. The presampling moisture content results are presented in the Appendix.

The scroll filter tailings samples were obtained using a sampling scoop and were collected at a sampling port in the scroll filter discharge chute. Six 20 litre plastic pails of scroll filter samples were collected; three from each of the scroll filters.

The string drum filter slimes samples were obtained using a shovel to collect the cake discharge from the drum filter. A total of five 20 litre plastic pails of slimes samples were collected.

For all of the scroll filter and string drum filter samples, a moisture content sample was taken during the collection of each pail of material. The results of the moisture content analyses were forwarded to the University of Waterloo and are presented in the Appendix.

4.2 COMBINED STREAM TAILINGS SAMPLING

The discharge from the two scroll filters and the string drum filter combine on a reversible belt conveyor prior to their disposal. At present, the combined stream tailings discharge to the tailings slurry tank where they are repulped and pumped to the surface tailings pond.

The combined stream tailings were collected at the discharge end of the belt conveyor prior to being slurried. The samples were obtained using a shovel to catch the belt conveyor discharge. Access to the enclosed belt conveyor was gained through an observation door located at the end of the belt conveyor.

Four 200 litre steel barrels of combined stream tailings were collected on January 31, 1986. Three moisture content samples were collected for each of the four barrels of samples. The moisture content samples were obtained when the barrels were approximately one quarter, one half and three quarters full. The results of the moisture content analyses were forwarded to the University of Waterloo and are presented in the Appendix.

4.3 PROCESS BRINE SAMPLING

The saturated process brine sample was collected on January 31, 1986 in a 200 litre steel barrel. The sample was obtained from a plant process brine line with a hose being used to fill the barrel.

4.4 PACKAGING AND SHIPMENT OF SAMPLES

Lids were placed on all sample containers immediately upon collection of each sample. All container lids were then subsequently sealed with silicone sealant to prevent any moisture loss of the samples. The plastic pail lids were also secured with tape to prevent the lids from being dislodged.

Four pails of scroll filter and string drum filter samples were each placed in 200 litre steel barrels for shipment. The lids on the steel barrels were secured using a ring and bolt closure and sealed with silicone to ensure no moisture loss of the samples. The inside of the steel barrels were also supplied with epoxy coating to prevent any possible contamination of the bulk samples.

The samples were shipped from the Denison-Potacan Potash Company mine site on February 5, 1986, for use by the University of Waterloo in the backfill research program.

5.0 FACTORS EFFECTING BACKFILL COMPOSITION

There are several factors which could possibly effect the composition of the tailings supplied for underground backfilling. These include changes in the ore, process equipment performance, design changes and the use of different materials for backfilling.

5.1 CHANGES IN THE ORE

Changes in the grade of ore supplied for processing does not effect the composition of the tailings other than a lower feed grade will obvicusly produce a larger quantity of tailings. Based upon present information, there are no indications of any mineralogical changes in the ore which would cause a change in the composition of the tailings.

5.2 PROCESS CHANGES

Changes in mill throughput rates should not cause a change in the tailings composition given normal operating procedures. The performance of the horizontal discharge scroll filters may be effected by changes in mill throughput rates if they are not adjusted prior to the changes. Increased feed on the filter cloth reduces the capability of the filter to remove brine from the filter cake thus increasing the moisture content in the tailings. Proper classification of tailings materials prior to debrining is also important as increased fines content causes single-stage filtration equipment to be blinded thus adversely effecting their performance.

There are no major schedule alterations to the process design or to the process equipment. There are future plans to possibly add an additional slimes filter to the tailings circuit. The choice on the type of filter has not yet been finalized.

5.3 TAILINGS MATERIALS

At present, the process plant tailings are repulped and pumped to surface tailings pond. When mine backfilling operations commence, the waste salt from the surface tailings pond will gradually be reclaimed and placed underground. The reclaimed tailings from the surface tailings pond may possibly have somewhat different characteristics than the tailings obtained directly from the process plant. The characteristics of the reclaimed tailings will have to be fully determined once backfilling operations commence.

There are no plans at present to use any materials other than waste salt tailings from the surface process plant as backfill material.

6.0 CONCLUSIONS

The collection of representative tailings samples from the DPPC surface process plant was successfully completed. The samples were shipped from the mine site to the University of Waterloo for laboratory testing to determine the characteristics and properties of the waste salt tailings as mine backfill.

7.0 LIST OF REFERENCES

1. Mraz Project Consultants Ltd. and University of Waterloo Department of Earth Sciences. "Use of Backfill in New Brunswick Potash Mines Proposal" Volumes 1 and 2, July 17, 1985.

2. Kilborn Limited. "Denison-Potacan Potash Company, Cloverhill Potash Project - Surface Plant Process Procedures and Services, Volume I - Process", Toronto, January, 1985.

3. Kilborn Limited. "Denison-Potacan Potash Company, Cloverhill Potash Project - Surface Plant Process Procedures and Services, Volume II - Ancillary Services, Toronto, January, 1985.

4. Kilborn Limited. "Denison-Potacan Potash Company, Cloverhill Potash Project - Surface Plant Process Procedures and Services, Volume III - Drawings, Toronto, January, 1985.

APPENDIX

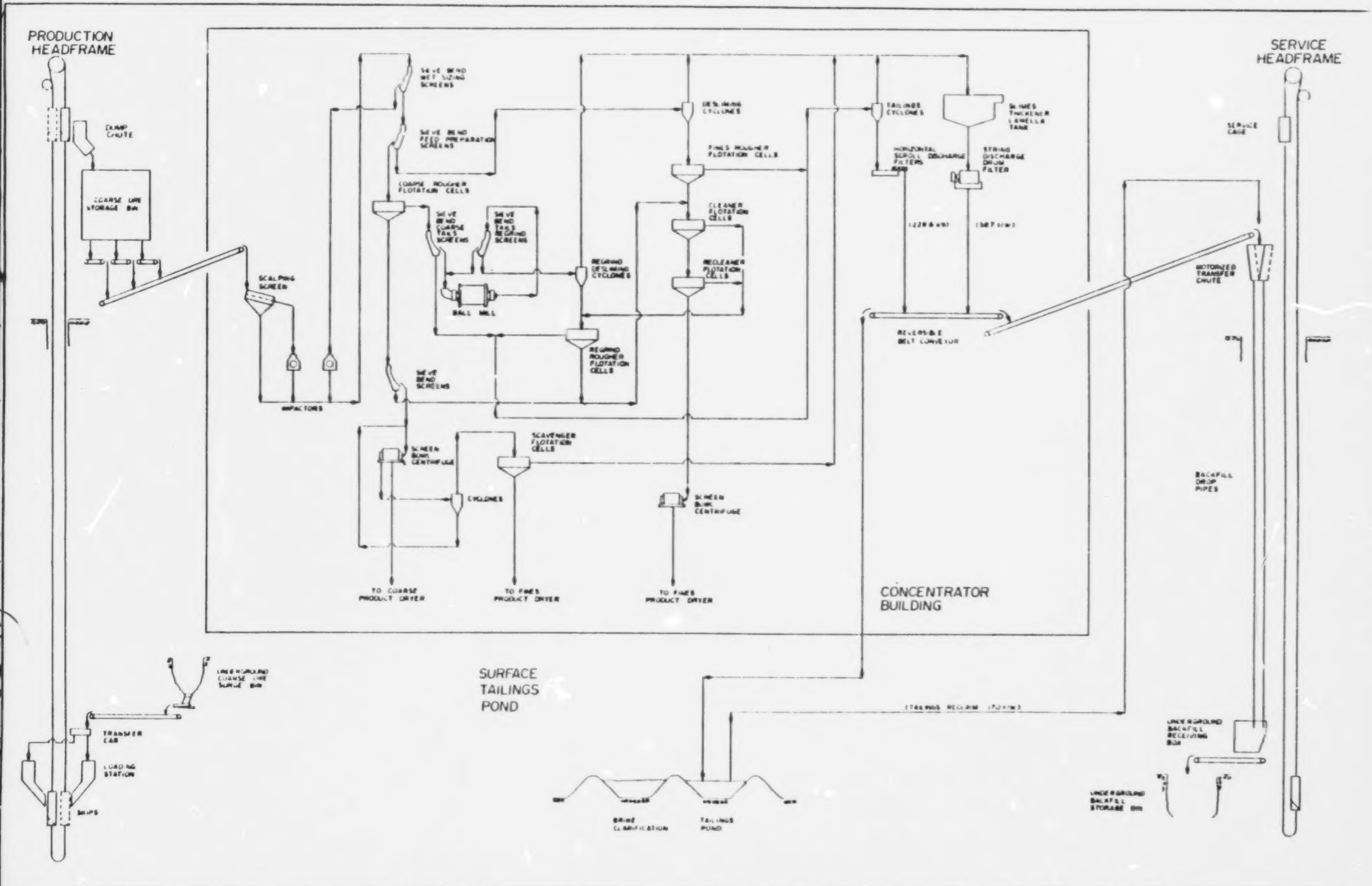
PRODUCTION HEADFRAME
DUMP CHUTE
COARSE ORE STORAGE BIN
SCALPING SCREEN
IMPACTORS
SIEVE BEND WET SIZING SCREENS
SIEVE BEND FEED PREPARATION SCREENS
COARSE ROUGHER FLOTATION CELLS
SIEVE BEND COARSE TAILS SCREENS
SIEVE BEND TAILS REGRIND SCREENS
BALL MILL
REGRIND DESLIMING CYCLONES
REGRIND ROUGHER FLOTATION CELLS
SIEVE BEND SCREENS
SCREEN BOWL CENTRIFUGE
CYCLONES
SCAVENGER FLOTATION CELLS
TO COARSE PRODUCT DRYER
TO FINES PRODUCT DRYER
DESLIMING CYCLONES
FINES ROUGHER FLOTATION CELLS
CLEANER FLOTATION CELLS
RECLEANER FLOTATION CELLS
SCREEN BOWL CENTRIFUGE
TO FINES PRODUCT DRYER
TAILINGS CYCLONES
HORIZONTAL SCROLL DISCHARGE FILTERS
SLIMES THICKENER LAMELLA TANK
STRING DISCHARGE DRUM FILTER
REVERSIBLE BELT CONVEYOR
CONCENTRATOR BUILDING
SURFACE TAILINGS POND
UNDERGROUND COARSE ORE SURGE BIN
TRANSFER CAR
LOADING STATION
SKIPS
BRINE CLARIFICATION
TAILINGS POND
(TAILINGS RECLAIM)
SERVICE HEADFRAME
SERVICE CAGE
MOTORIZED TRANSFER CHUTE
BACKFILL DROP PIPES
UNDERGROUND BACKFILL RECEIVING BOX
UNDERGROUND BACKFILL STORAGE BIN

300-10 B	KILBORN LTD		SCALE NTS		
300-07	KILBORN LTD				

DENISON - POTACAN POTASH COMPANY

BACKFILL PREPARATION FLOWSHEET

268-0010-002

TABLE 1

PRELIMINARY MOISTURE CONTENT ANALYSIS

Sample	% Moisture
Scroll Filter #11	7.23
Scroll Filter #12	7.63
Drum Filter #13	18.08

Note: Sample collection time - 8:45 a.m.

TABLE 2

SCROLL FILTER AND STRING DRUM FILTER MOISTURE CONTENT SAMPLES

Sample (Time)	% Moisture
Scroll Filter #11 (10:38)	8.27
Scroll Filter #12 (10:50)	9.26
Scroll Filter #11 (10:57)	8.33
Scroll Filter #12 (11:08)	9.11
Scroll Filter #11 (11:15)	8.00
Scroll Filter #12 (12:42)	8.05
Drum Filter #13 (11:48)	20.4
Drum Filter #13 (11:55)	18.5
Drum Filter #13 (12:01)	18.3
Drum Filter #13 (12:14)	19.1
Drum Filter #13 (12:35)	19.1

TABLE 3

COMBINED STREAM TAILINGS MOISTURE CONTENT SAMPLES

Sample (Time)	% Moisture
4A (10:51)	6.8
4B (11:07)	7.5
4C (11:13)	6.5
1A (11:23)	6.9
1B (11:38)	7.7
1C (11:47)	8.7
3A (12:48)	7.3
3B (13:02)	7.7
3C (13:15)	8.0
2A (13:23)	8.0
2B (13:37)	7.8
2C (13:51)	7.5

APPENDIX C

DENISON-POTACAN POTASH CO.

SUBJECT: COMPACTED TAILINGS DENSITIES

TO: W. Cusitar - Mraz Project Consultants
D. Mraz - Mraz Project Consultants
C. Fordham - University of Waterloo
C. Benner - Denison-Potacan Potash Co.
A. Ludwig - Denison-Potacan Potash Co.
A. Speed - Denison-Potacan Potash Co.
A. Harasimowicz - Denison-Potacan Potash Co.
S. Munroe - Denison-Potacan Potash Co.

FROM: Mark Frayne

DATE: June 18, 1986

Summary

A total of five compacted tailings samples were collected for density determination from the DPPC tailings pond. All of the samples showed distinctive signs of sedimentation.

Volumes, wet densities, moisture contents, dry densities and true densities were determined for each sample.

The average true density of the compacted tailings was 1.33 g/cc.

Mark Frayne

Mark Frayne

MF/dl

COMPACTED TAILINGS DENSITIES

Introduction

The DPPC tailings pond contains tailings material which has been deposited by two different methods; tailings that have been placed there using dump trucks and tailings that have been pumped in a slurry form. The tailings deposited by the dump trucks does not compact and densify properly while the slurried tailings compacts naturally due to the particle sedimentation. At present all tailings are deposited in a slurried form.

Samples were obtained from the compacted portion of the tailings pond, on May 29, 1986, for density determination. The density values that were obtained will be used for comparison with other compaction methods that will possibly be used on the tailings material. The tailings material will eventually be reclaimed for use as an underground backfill material.

Procedure

To determine the true densities of the material present in the tailings pond, samples that showed distinctive signs of sedimentation were chosen. The deposition of the samples is analogous to the placement of backfill using a hydraulic slurry. The samples were then broken down to a more manageable size and cut into the shape of a cube using a hacksaw.

Due to the nature of the material (ie. crumbling and separating along bedding planes), it was found to be very difficult to obtain shape edges. The edges and corners were rounded which resulted in larger calculated volumes (Table 1) than the actual volumes. This was caused by the method utilized to measure the dimensions and resulted in lower density values. The dimensions were measured using calipers with an accuracy of +0.05 mm. There were three measurements taken for each dimension which were then averaged. The measurements were taken at the top, middle and bottom of each sample. The samples were weighed to an accuracy of 0.1 g.

The volumes and wet densities were then determined (Table 1). The samples were then placed in an oven (100° C) for 24 hours to dry and were then weighed. From the acquired data, the moisture content, dry densities and true densities (according to M.B. Dusseault) were determined (Table 2).

Observations

The placement of the tailings, in the tailings pond, in a hydraulic slurry produces distinctive sedimentary features (ie. bedding planes) in the tailings cake as the brine percolates through the material. It was noted that the material was apparently compacted very firmly but upon handling the compacted tailings lost some of its competency.

The presence of insolubles were noted. They were found to occur in a foamy residue at the boundaries of the tailings pond as well as on the surface as a thin patchy deposit. There was an overall low percentage of insolubles found in the tailings pond.

Conclusions

Samples showing distinctive sedimnetary features were successfully collected and tested.

The average moisture content of the tailings was less than one percent H_2O.

The average true density was found to be 1.33 g/cc.

The following is a typed version of a handwritten draft by M.B. Dusseault:

- Reporting of density data on salt backfill.
- In conventional rock or soil mechanics, where the mineral does not dissolve in the water, it is sufficient to report water content and "as is" density. This is not sufficient for halite backfill, as the fluid has dissolved salt in it at the sacuration point.
- The best way to be consistent is to report the data differently than soils engineers.

I recommend:

a) Water content be expressed as a percentage of the dry mineral weight, as is the case for all soils and rock mechanics.

$$w = \text{water content in \%} = \frac{\text{weight loss on drying}}{\text{weight of dry mineral}}$$

In the lab:

A = Tare + wet material B = Tare + dry material

Weight loss = $A - B$

Dry Mineral = B − Tare$(-w_t)$

$$w = \frac{A-B}{B-\text{Tare}} \cdot 100$$

b) All densities be reported as corrected dry density, wherein the density is corrected for the NaCl which was in solution when the water was in the liquid stage.

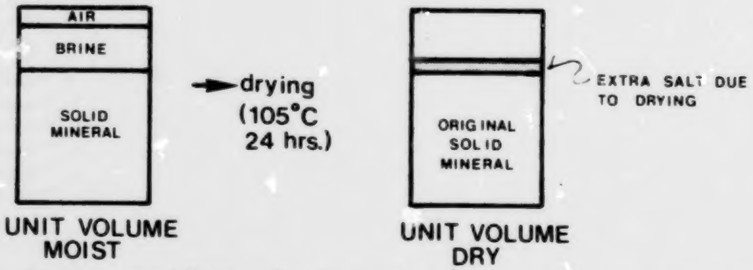
AIR
BRINE
SOLID MINERAL
UNIT VOLUME MOIST
drying
(105°C
24 hrs.)
ORIGINAL SOLID MINERAL
EXTRA SALT DUE TO DRYING
UNIT VOLUME DRY

This "extra" salt is an artifact of drying and does not enter into material behaviour in the in-situ state.

How to calculate corrected dry density:

- In a saturated brine, there are 36 grams NaCl dissolved in each 100 grams H_2O.

W_t = Total weight of dry solids (B - Tare from previous pages)

W_s = True mineral solid (when specimen was moist)

w = Moisture content in % H O of total dry mineral

$\therefore$ $W_s = W_t$ - Weight of salt which was in water

$$W_s = W_t - \frac{0.36 \cdot w \cdot W_t}{100} \qquad (w \text{ in } \%)$$

$$W_s = W_T \left(1 - \frac{0.36}{100} w\right)$$

$\therefore$ True dry density $= \frac{W_s}{\text{Vol}}$

TABLE 1

DENSITY OF COMPACTED TAILINGS

Sample No.	Volume (cm^3)	Wet Weight (g)	Wet Density (g/cc)	Dry Weight (g)	Dry Density (g/cc)
1	583.3	734.6	1.36	727.9	1.35
2	368.5	484.7	1.32	482.3	1.31
3	375.9	510.9	1.36	508.1	1.35
4	222.3	291.1	1.31	290.4	1.31
5	236.3	311.3	1.32	310.6	1.31

TABLE 2

CORRECTED DENSITIES*

Sample No.	Moisture Content (%H_2O of Dry Mat.)	True Mineral Solid (g)	True Dry Density (g/cc)
1	0.92%	725.49	1.35
2	0.50%	481.43	1.31
3	0.55%	507.09	1.35
4	0.24%	290.15	1.31
5	0.23%	310.34	1.31

*According to M. B. Dusseault

APPENDIX D

MECHANICAL PROPERTIES OF HALITE TAILINGS FROM THE DENISON-POTACAN POTASH MINE, SUSSEX, NEW BRUNSWICK

PART I: CHARACTERIZATION OF MATERIALS

By

Chris Fordham, M.Sc.
Maurice Dusseault, Ph.D., P.Eng.

June 1986

1.0 INTRODUCTION

The characterization phase had two purposes:

1: to determine the characteristics of 'normal' tailings for delineation of suitable test conditions.

2: to provide a data base of information to help interpret results obtained from the testing phase of the program

The material characterization consisted of four parts:

1: Moisture Content Determination
2: Grain Size Analysis
3: Mineralogy
4: Scanning Electron Microscopy

Many of the tests performed during this and subsequent phases of the program are standard soils and rock mechanics tests. However, the properties of this material require that certain definitions and modifications be applied to these test procedures.

1.1 Sample Storage

The samples arrived at the University of Waterloo in late February 1986. Three materials were delivered; combined stream tailings (4 x 45 gallon drums), scroll filter tailings (4 x 5 gallon pails), and slimes (4 x 5 gallon pails). One 45 gallon drum of process brine was also delivered.

The combined stream tailings are the end product of the sylvite/halite separation process and contain all waste materials. The scroll filter tailings are the coarse-grained fraction of the tailings. The slimes are the fine-grained tailings. The process brine is used to slurry the tailings during processing. It is a fully saturated brine with respect to NaCl and KCl.

Upon receipt, the combined stream tailings were removed from the 45 gallon steel drums and stored in 5 gallon plastic pails lined with plastic bags. Each plastic pail was labeled as to its origin. This was done to prevent the salt from corroding the steel drums and to maintain as much natural moisture as possible.

The tailings were separated into the plastic pails by putting approximately equal amounts from each depth in the drum into each pail. The moisture content was determined at the top, middle and bottom of each drum. The upper 2/3 of the drum was fairly hard and required a chisel to break it up. It crumbled easily by hand after it had been broken up. The bottom third of the drums was very wet.

2.0 MOISTURE CONTENT DETERMINATION

2.1 Water in Granular Halite

The standard soil mechanics definition of water content is as follows (Craig, 1978);

$$Wc = \frac{Mw}{Ms} \tag{1}$$

where: Wc = Water Content
Mw = Mass of Water
Ms = Mass of Dry Solids

It is usually determined by weighing a soil sample with moisture, drying it in an oven at 105o for 24 hours, and reweighing. The difference in weight is attributed entirely to moisture loss (Mw), and the dry weight is considered to be the total weight of solids (Ms).

The high solubility of salt in water causes any moisture in the tailings to be brine, saturated with respect both NaCl and KCl. When the water is removed by drying, the dissolved salts precipitate. The dry weight then consists of the original solid phase plus the precipitate from the brine. A correction must be applied to the results for correct moisture or liquid content determination. The correction is necessary because the mechanical properties in the field will not be affected by the salt dissolved in the water, only by the density of the solid salt and the amount of water. Therefore, the corrected moisture content leads to a consistent way of reporting bulk field.

$$Ms = Mc + Md \tag{2}$$

where; Ms = Mass of all solids
Mc = Mass of salt crystals
Md = Mass of dissolved salts

The correction factor depends on the amount of dissolved material in the liquid. This can be determined by evaporating a known amount of brine and weighing the precipitate. The amount can be expressed as either a weight of solid per weight of brine or weight of solid per volume of water. The amount of dissolved salt in the process brine is 0.3029 g per gram of brine or .4345 g per ml of water. All future references to brine will refer to process brine unless otherwise stated.

This value can be used to determine the corrected moisture contents as follows:

$$Wct = \frac{Mw}{Ms - [Bc * Mw]} \qquad (3)$$

where; Wct = Corrected moisture content
Mw = Mass of Water
Bc = Saturated brine concentration in mass of dissolved salt per volume of water, ie. grams per millilitre, 0.4345 in this case.

For example, if a sample of wet backfill weighs 202.3 grams before drying and 176.3 grams after drying the corrected moisture content can be determined as follows:

$Mw = 202.3 - 176.3 = 26$ g
$Ms = 176.3$ g
$Bc = 0.4345$ g / ml of water = 0.4345

$$Wct = \frac{26}{176.3 - [0.4345 * 26]}$$

$Wct = 0.1576 = 15.76\%$

To make a tailings sample in the laboratory with a known water content, brine is added to air dried material. The amount of brine added can be determined by the following equation:

$$Mb = \frac{Wc * Mc}{1 - Bd * [1 + Wc]} \qquad (4)$$

where; Mb = Mass of brine to be added
Bd = Saturated brine density in mass of dissolved salt per mass of brine, ie., grams of dissolved salt per gram of brine, 0.3029 in this case.

To calculate a corrected dry density of a material at a known moisture content, both the volume and the corrected dry mass are required.

$$Mc = \frac{Mw - [Bc * Wc] * Mw}{Wc} \qquad (5)$$

and;

$$d = \frac{Mc}{Volume} \qquad (6)$$

where; d = Corrected Dry Unit Weight

Wherever it is not specified all reported values for moisture content and density will be corrected values. Unfortunately, other published data are often inconsistently reported.

2.2 Initial Moisture Content of Tailings Samples

As the combined stream tailings were decanted from the steel drums, samples were taken for moisture content at the top, middle and bottom of the drums. Moisture content determinations were also made for the scroll and slime tailings. The results are listed in Table 1.

Table 1: Initial Moisture Content Determinations

Drum	Location	Wc(%)	Wct(%)
1	top	1.75	1.77
	middle	10.85	11.38
	bottom	19.95	21.85
2	top	2.32	2.34
	middle	5.23	5.35
	bottom	20.61	22.64
3	top	2.54	2.57
	middle	6.06	6.22
	bottom	18.19	19.75
4	top	2.16	2.18
	middle	6.02	6.18
	bottom	21.69	23.94
Scroll	middle	2.89	2.92
Slimes	middle	35.70	42.24 *

* Slimes samples arrived saturated.

3.0 GRAIN SIZE ANALYSIS

Grain size analysis was performed by wet sieving the tailings. Dry sieving was not attempted as the grains tend to clump together when allowed to dry, cemented by the precipitate from the brine. Several sieving fluids were tried including process brine, kerosene, hexane, and acetone. Acetone proved to be the most effective. Microscopic examinations of each sieve fraction showed that only the coarsest fractions showed any clumping and this was such a small portion of the total sample, the effect is considered insignificant. Microscopic examinations also showed no grain surface effects caused by the acetone. All reported grain size curves were obtained using acetone (Figures 1 and 2).

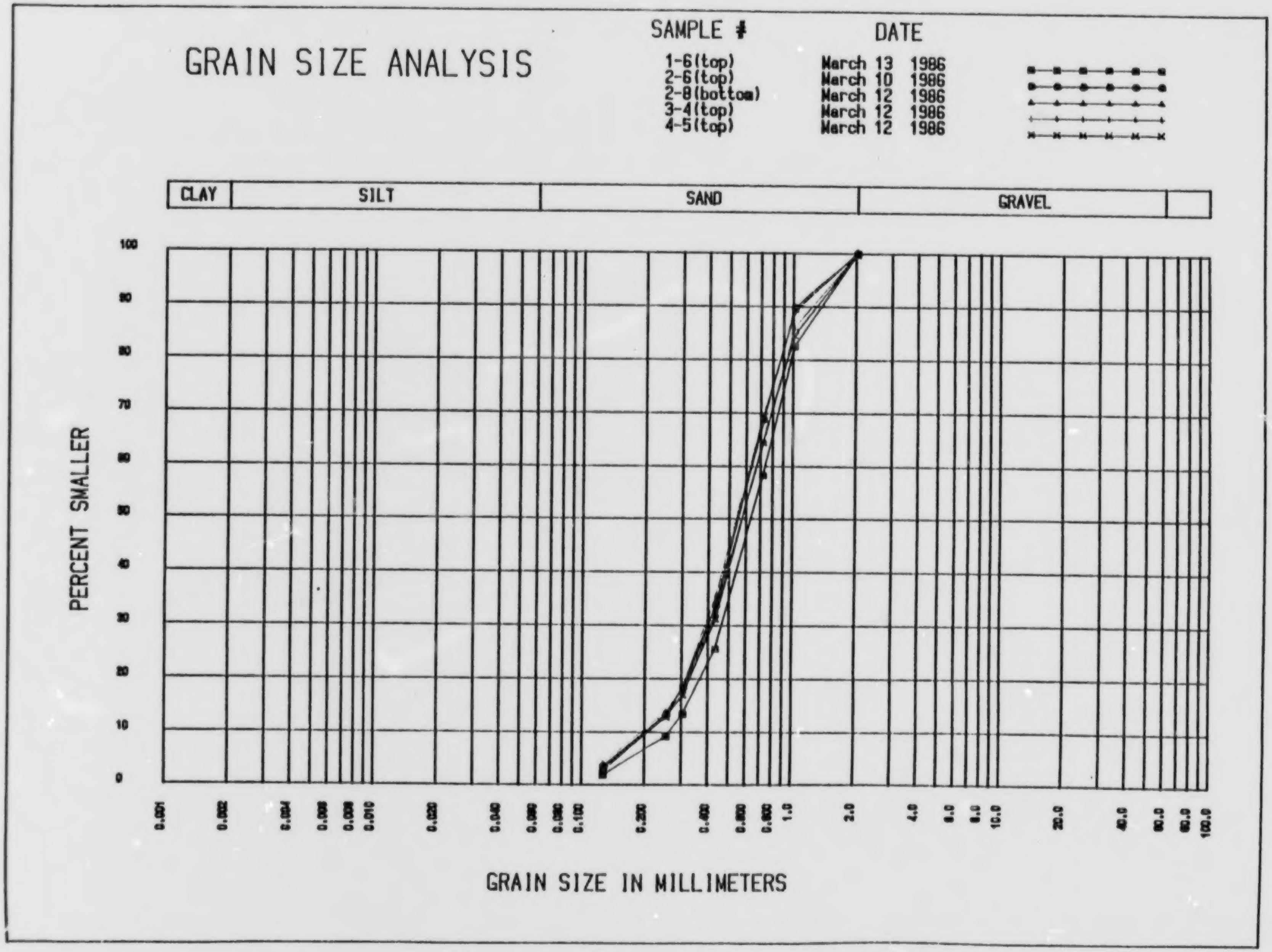

Figure 1: Grain Size Analyses, Bulk Samples

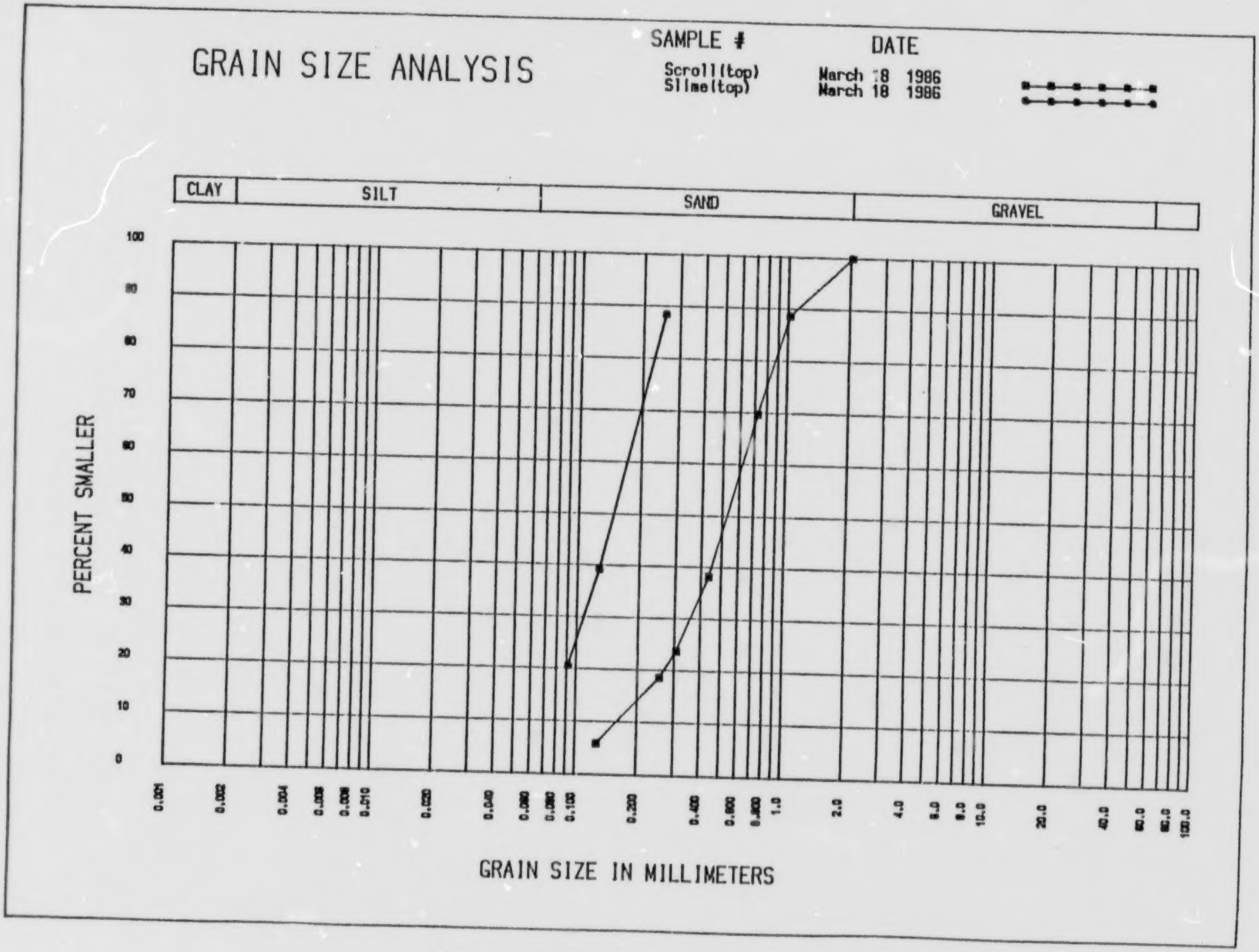

Figure 2: Grain Size Analyses, Scroll and Slimes Tailings

Grain size analysis was performed on one pail from each of the original drums. The samples were taken from the top of each pail. To make sure that no grain size fractionation had occurred during the transfer to the pails, a grainsize analysis of material from the bottom of pail 2-8 was also performed. No grainsize difference was noted between any of the samples (Figure 1).

A grain size analysis was also performed on the scroll and slimes tailings. As expected, there is little overlap between the two samples; the slimes are predominantly (70%) less than 0.2 mm and the scroll filter tailings are predominantly (85%) larger than 0.2 mm (Figure 2).

Grain size analysis indicates the tailings are well graded and have a coefficient of uniformity of (D60/D10) of 3.4. A coefficient of uniformity of less than four represents a very uniformly graded material. Saskatchewan potash tailings have similar uniformity coefficients between 2.3 and 4.0 (Beddoes, 1984; Johnson, 1984), however they appear to have both higher percentages of both larger and smaller grain sizes than the Potacan tailings.

The results of the grain size analysis are summarized below:

1: There is no difference in grain size between any of the combined stream tailings samples

2: Greater than 95% of the combined stream tailings are between 2.0 mm and 0.125 mm in size

3: Most of the fine tailings are found in the slimes while most of the coarse fraction can be found in the scroll filter tailings

4: No traces of insolubles were noted in any samples including the slimes.

3.0 MINERALOGY

The mineralogy of the tailings was studied by two methods; optically using a microscope and by X-ray diffraction. The optical microscope work was performed not only to determine the mineralogy but also to look at crystal shapes and forms of various minerals. X-ray diffraction was performed to determine detailed mineralogy, particularly of any slimes or fines which may not have been clearly visible under the optical microscope.

3.1 Optical Mineralogy

Optical mineralogy was performed on the sieved sample from pail 1-6. Each of the sieve fractions was examined for mineralogy, mineral phases, and particle clumping. The complete descriptions can be found in Appendix I.

Most of the sample is made up of several types of halite; orange, orange/yellow, yellow, and clear. KCl made up less than 5% of material less than 1 mm in diameter. Clumping of smaller grains to form larger grains was only noted in the largest grain sizes, > 2 mm. This grain size range generally made up less than 1% of the total sample. Photographs of sieved material, a bulk sample, scroll and slime tailings can be found in Appendix II.

The grains were also examined for surface effects caused by the acetone. The sieved sample showed no surface etching or other dissolution features. The grains appeared to be very similar to the unsieved bulk sample with the exception that they were somewhat cleaner than fresh grains. This was attributed to the lack of brine precipitate.

3.2 X-Ray Diffraction

X-ray diffraction traces were determined for a bulk sample, a slimes sample, a scroll filter sample, and on material left on each of the eight sieves used in grainsize analysis. The only minerals which appeared on any of the traces were halite and sylvite. The X-ray diffraction traces can be found in Appendix III.

The sylvite contents determined by X-ray diffraction and optically were compared. Approximate sylvite percentages were determined optically by counting the number of sylvite grains in a group of grains. The sylvite content determined from the X-ray diffraction traces was determined using the following formula;

$$KCl\% = \frac{Kp}{(Nap + Kp)} \tag{7}$$

where: KCl% = Percentage KCl
Kp = Combined height of KCl peaks 2, 6, and 10
Nap = Combined height of NaCl peaks 2, 6, and 10

Although this method has not been checked with known halite/sylvite ratios, the results compared well with the optical results (Table 2).

Table 2: Sylvite Percentages Determined Optically and by X-Ray Diffraction

Sieve #	X-Ray (%)	Optical (%)
10	17.9	20.0
18	8.7	2.5
25	8.6	5.0
40	1.5	<1.0
50	0.8	<1.0
60	0.7	<1.0
120	1.0	---

4.0 SCANNING ELECTRON MICROSCOPY

Scanning electron microscopy was performed on a bulk sample, a sample of scroll filter tailings, and a slimes sample. Nothing was done to the samples before they were studied, ie. they had not been washed with acetone during sieving. The bulk, slimes, and scroll samples showed characteristic blocky structure with some smoothing, possibly caused by dissolution. The blotches on some crystal surfaces may be brine precipitate. The scanning electron photographs can be seen in Appendix IV.

5.0 CONCLUSIONS AND RECOMMENDATIONS

The following conclusions have been reached during this phase of the study.

1: Moisture in the tailings is in the form of brine, fully saturated with respect to NaCl and KCl. Moisture content determinations must be corrected to take into account the salt dissolved in the brine, leading to a consistent method of reporting dry bulk density.

2: Ninety five percent of the grain sizes are between 2.0 mm and 0.125 mm.

3: Only the minerals halite and sylvite are present in the tailings.

The following recommendations are suggested for future phases of this study.

1: All moisture contents should be reported as corrected moisture contents; all dry densities as corrected dry densities.

2: The high coefficient of uniformity and the lack of any significant coarse or fine-grained fraction in the tailings suggests that studying the mechanical behavior of various grain size fractions will be of little value. This will be decided after the density testing phase of this program.

3: The small amount of sylvite and lack of any other trace minerals suggests that studying the effects of mineralogy on the mechanical behavior will be of little value.

4: All of the bulk tailings material received for this study show the same basic physical characteristics. This will allow material from any of the four drums to be used for any further testing.

REFERENCES

Beddoes, R.J., 1984. Determination of Engineering Properties of Salt for Backfilling in Underground Potash Mines. Produced by RE/SPEC/ Ltd., Calgary for the Canada Centre for Mineral and Energy Technology, Project No. 310104.

Craig, R.F. 1978. Soil Mechanics. Van Nostrand Reinhold Co. Ltd., Scarborough.

Johnson, R.F., 1984. Investigation of the Physical and Chemical Characteristics of Potash Tailings in Saskatchewan. Produced by Potash Corp. of Saskatchewan for the Canada Centre for Mineral and Energy Technology, Project No. 350204.

APPENDIX I

Optical Microscope Descriptions

Sieve	Description
#10	-40% of particles multigranular -20% KCl -60% orange/yellow NaCl -20% clear NaCl -KCl slightly more pitted
#18	-20% of grains multigranular (small grains about 1mm) -small grains 90% halite -2.5% KCl -10% orange halite -63% yellow halite -25% clear NaCl -frosting on 10% of surfaces
#25	-5% KCl -25% orange NaCl -35% yellow NaCl -35% clear NaCl -20% multigranular (small grains with same characteristic as #18) -sky blue impurities in 1/50 grains
#40	-< 1% KCl -20% orange/yellow NaCl -80% clear NaCl -minor traces of foggy blue halite -< 10% multigranular -orange halite generally planar, clear cubic
#50	-< 1% KCl -20% yellow NaCl -80% clear NaCl -no multigrains -yellow NaCl- transparent and translucent
#60	-< 1% KCl -30% yellow NaCl -70% clear NaCl -more cubic grains
#120	-no visible KCl -20% yellow NaCl -80% clear NaCl
>120	-most common grainsize 0.07 mm -mostly clear NaCl -grains have less regular shape

APPENDIX II: OPTICAL MICROGRAPHS OF DENISON POTACAN TAILNGS

Note: The grid beneath the grains is 1 mm square.

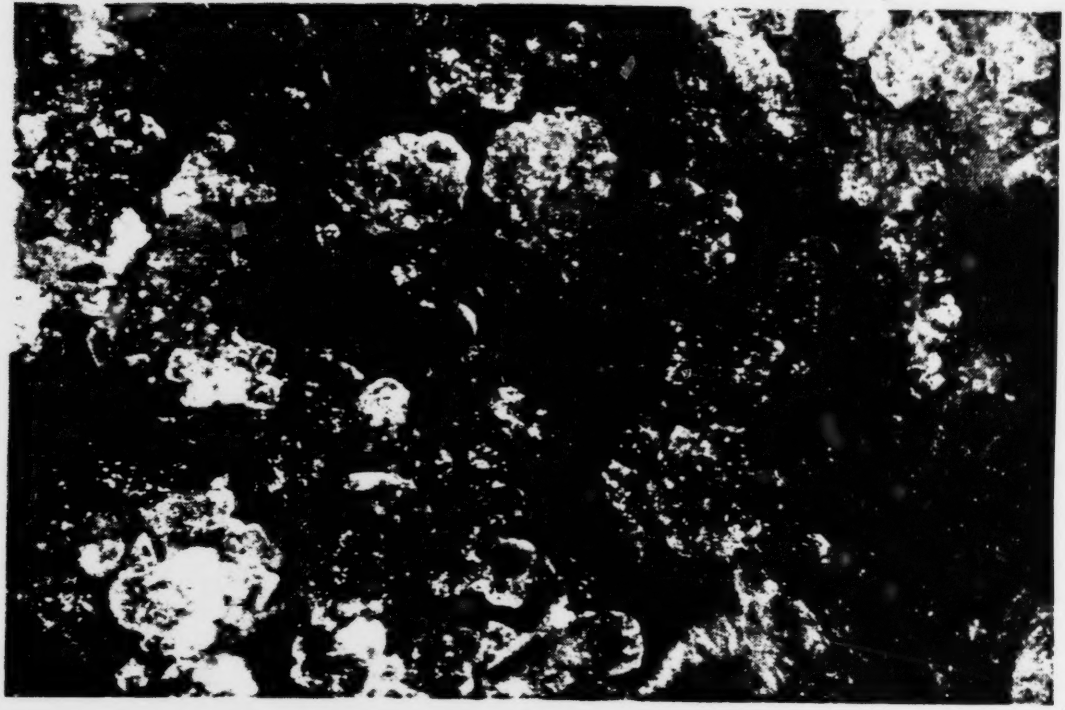

Figure AII.1: Scroll Filter Sample

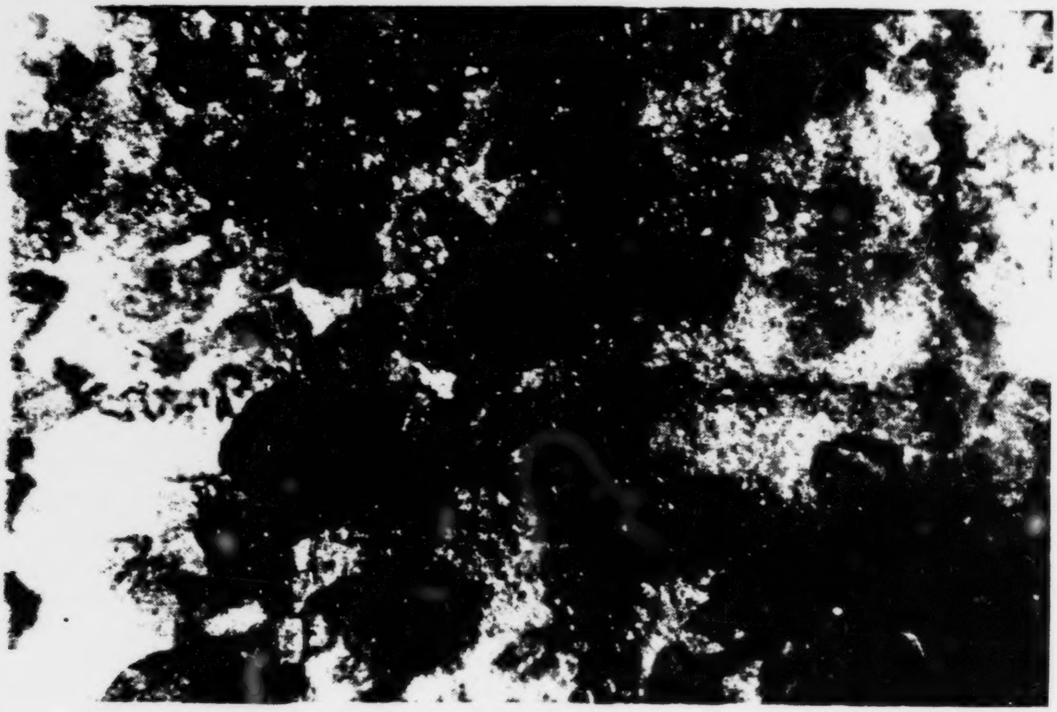

Figure AII.2: Slimes Sample

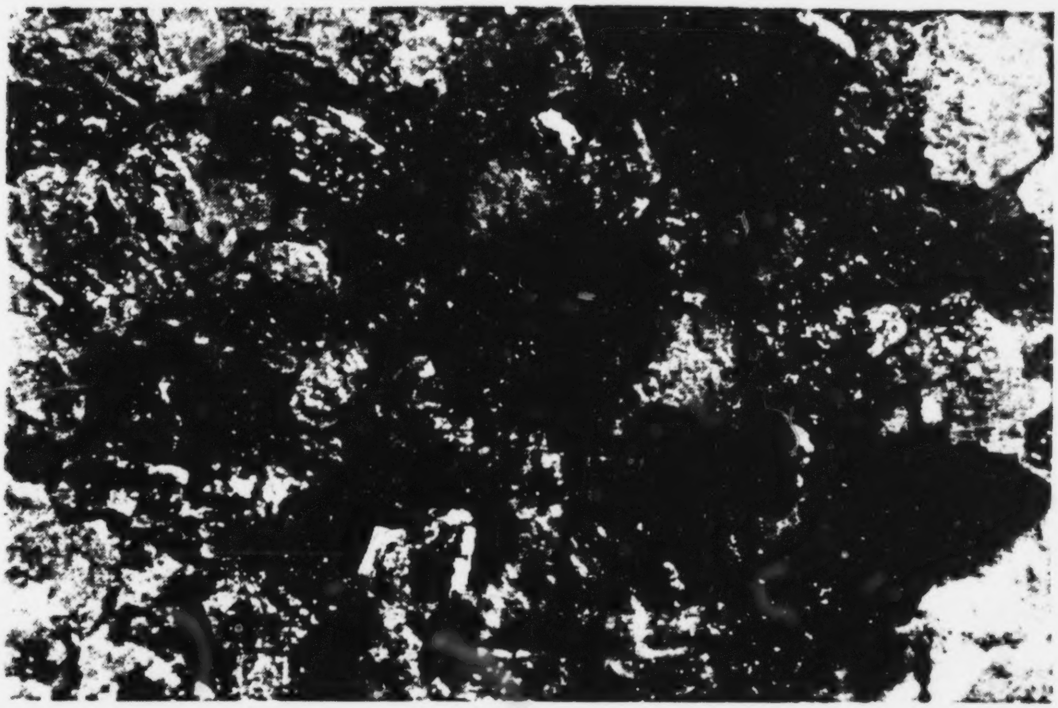

Figure AII.3: Sample 1-6, Bulk Sample

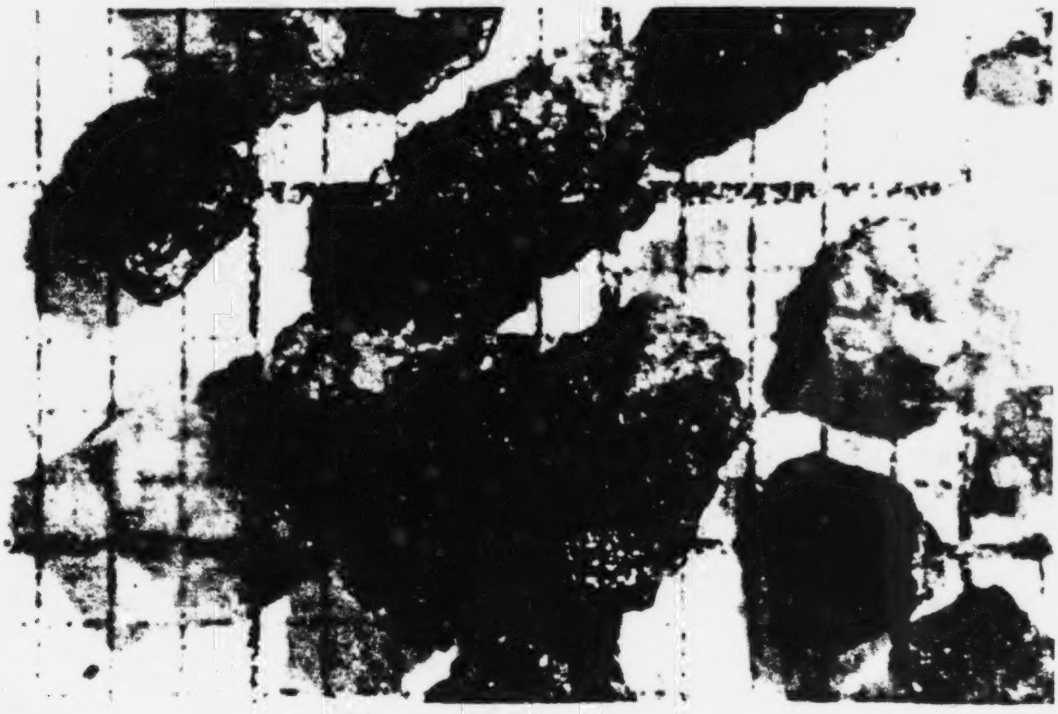

Figure AII.4: Sample 1-6, Sieve #10

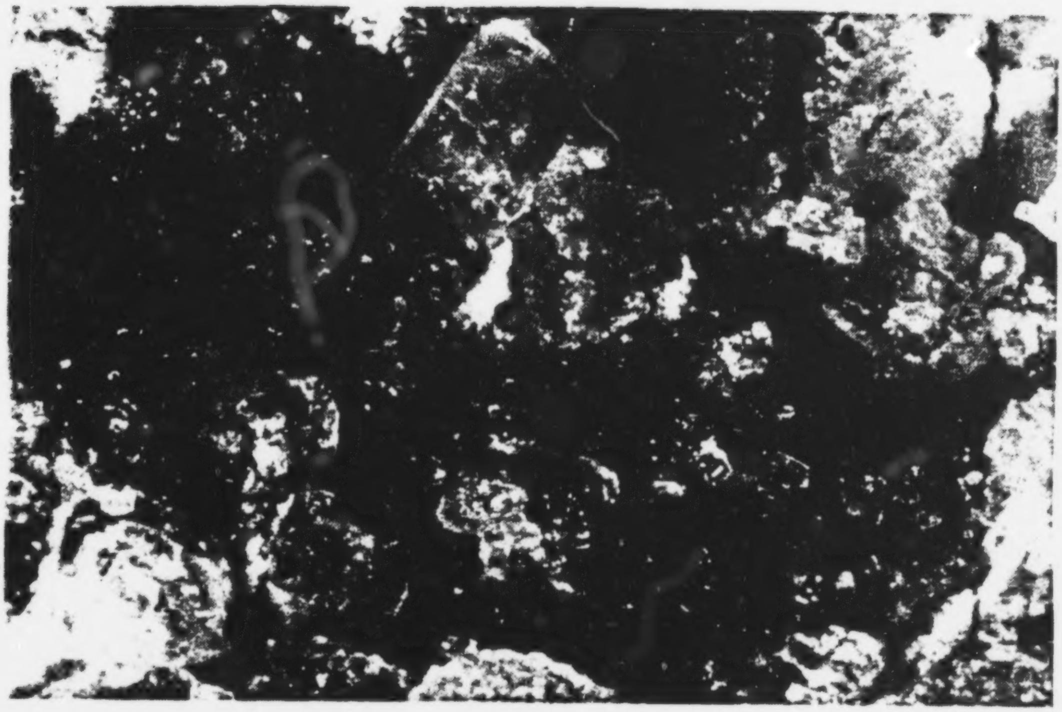

Figure AII.5: Sample 1-6, Sieve #18

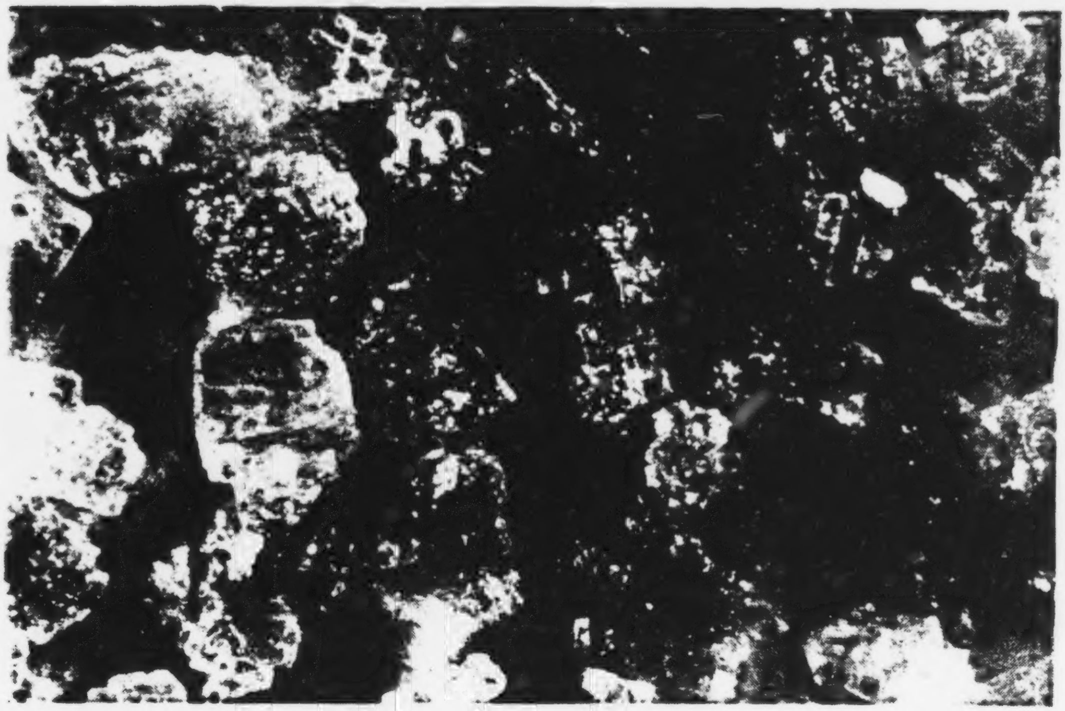

Figure AII.6: Sample 1-6, Sieve #25

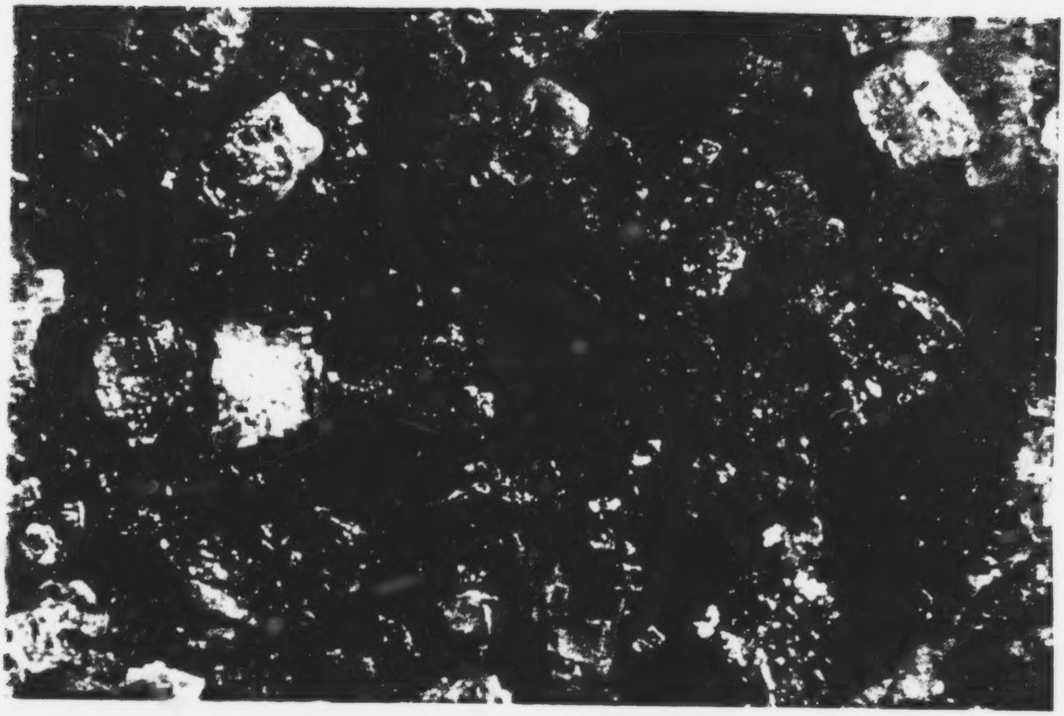

Figure AII.7: Sample 1-6, Sieve #40 (blue filter)

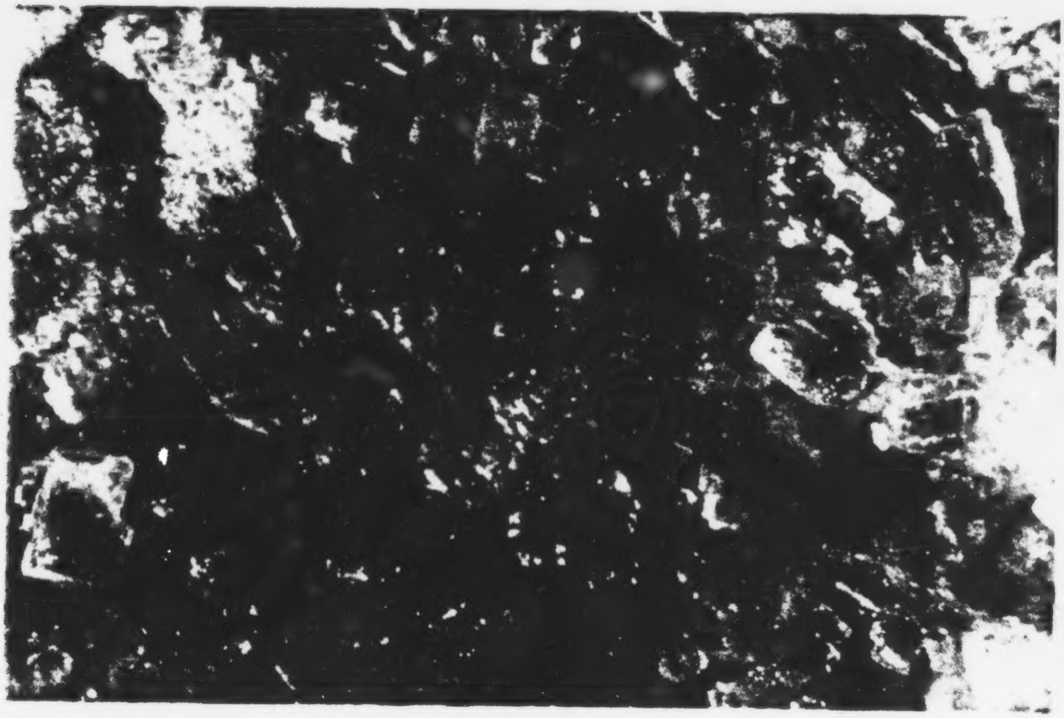

Figure AII.8: Sample 1-6, Sieve #50

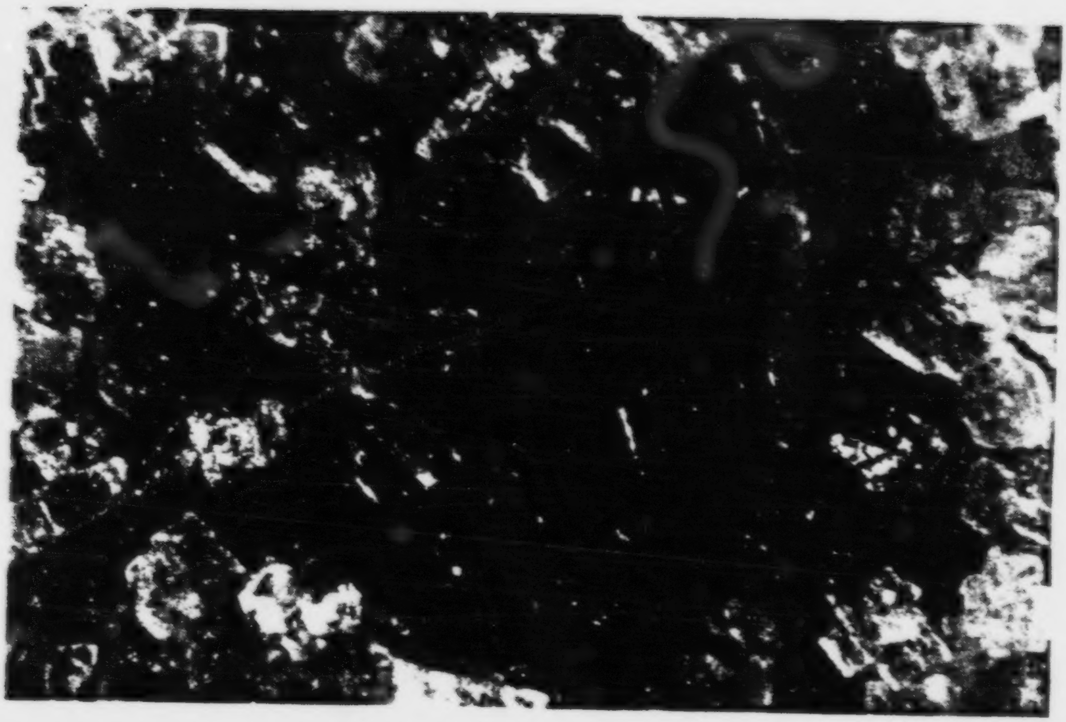

Figure AII.9: Sample 1-6, Sieve #60 (blue filter)

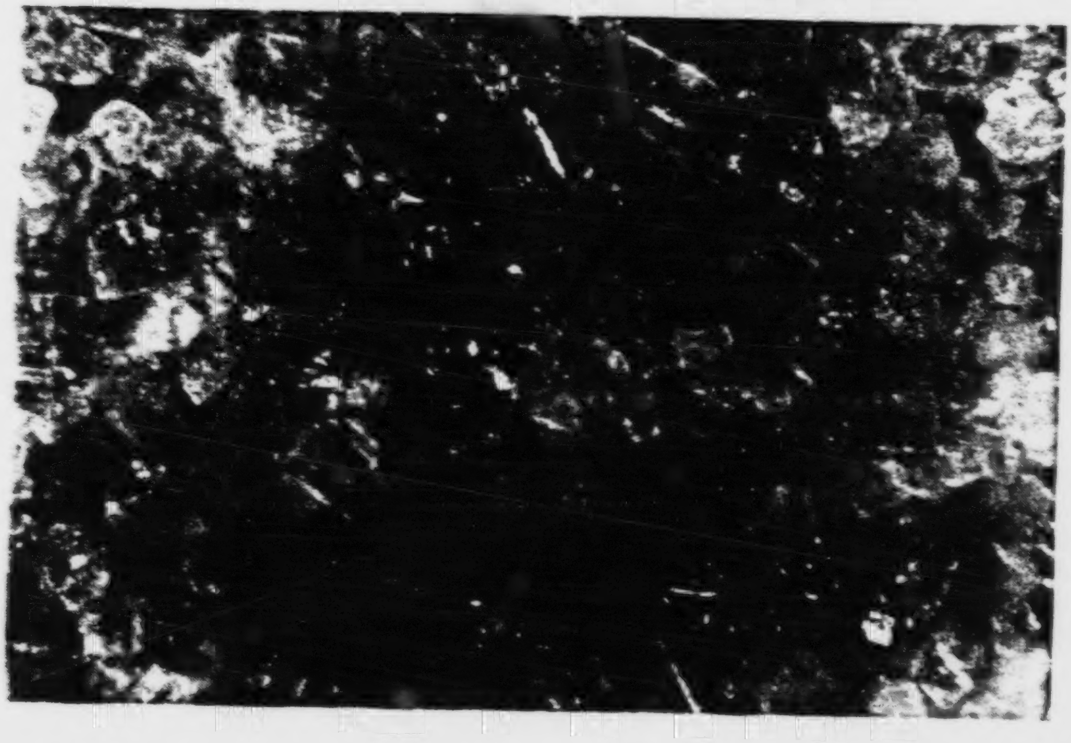

Figure AII.10: Sample 1-6, Sieve #120 (blue filter)

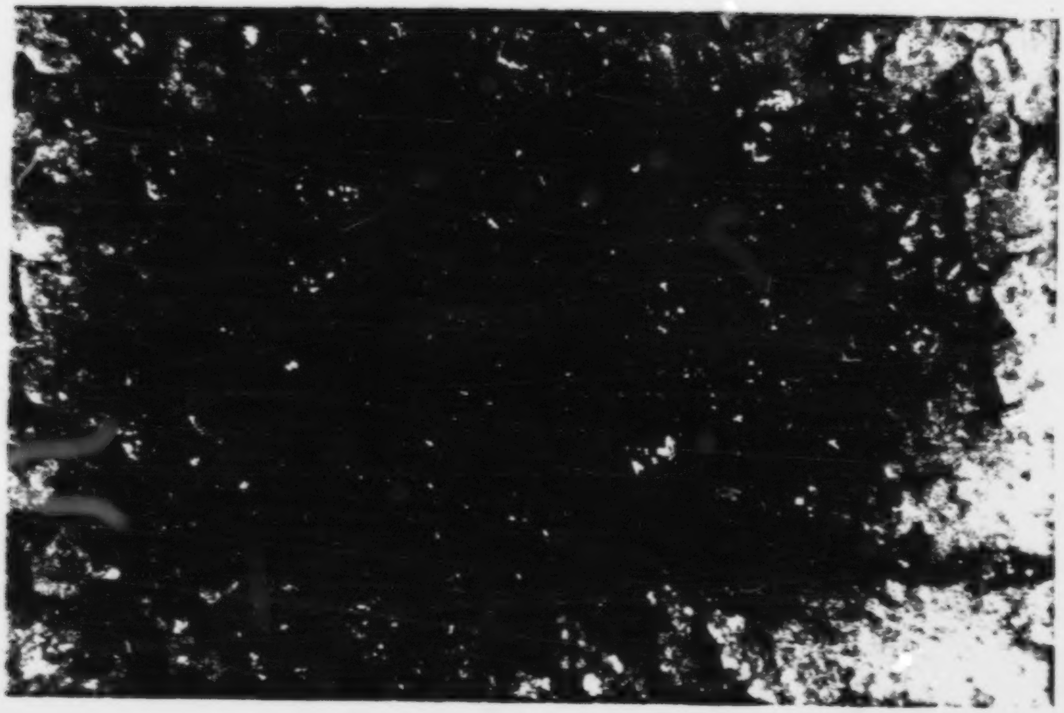

Figure AII.11: Sample 1-6, < Sieve #120

APPENDIX III: X-RAY DIFFRACTION TRACES

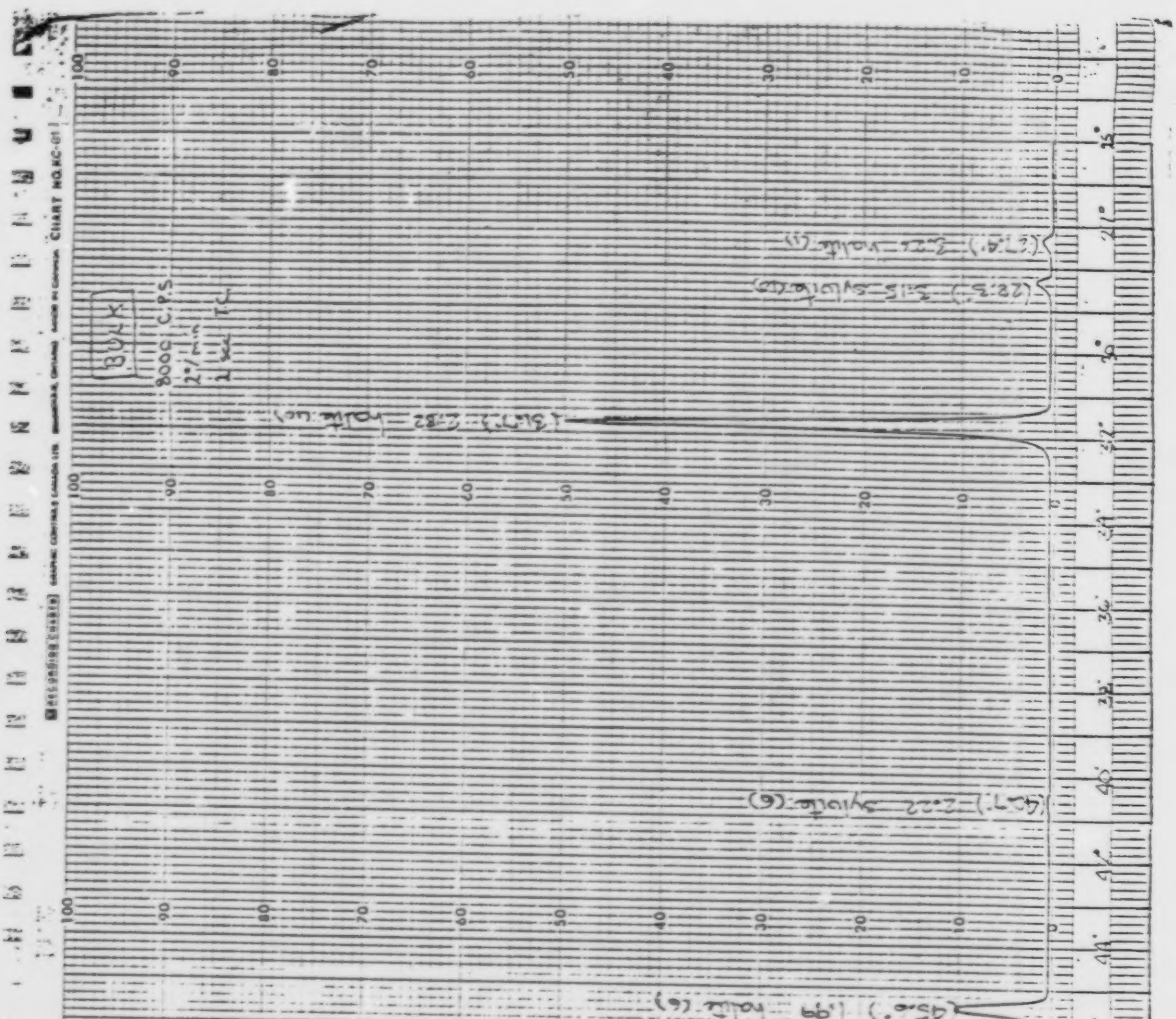
BULK
800C C.P.S.
2°/min
2 sec TC
(27.4°) 3.25 halite (1)
(28.3°) 3.15 sylvite (10)
(31.7°) 2.82 halite (10)
(40.7°) 2.22 sylvite (6)
(45.0°) 1.99 halite (6)
(56.5°) 1.65 halite (2)
0
10
20
30
40
50
60
70
80
90
100
25°
27°
30°
32°
34°
36°
38°
40°
42°
44°
46°
48°
50°
52°
54°
56°
58°
CHART NO.KC-01
MADE IN CANADA

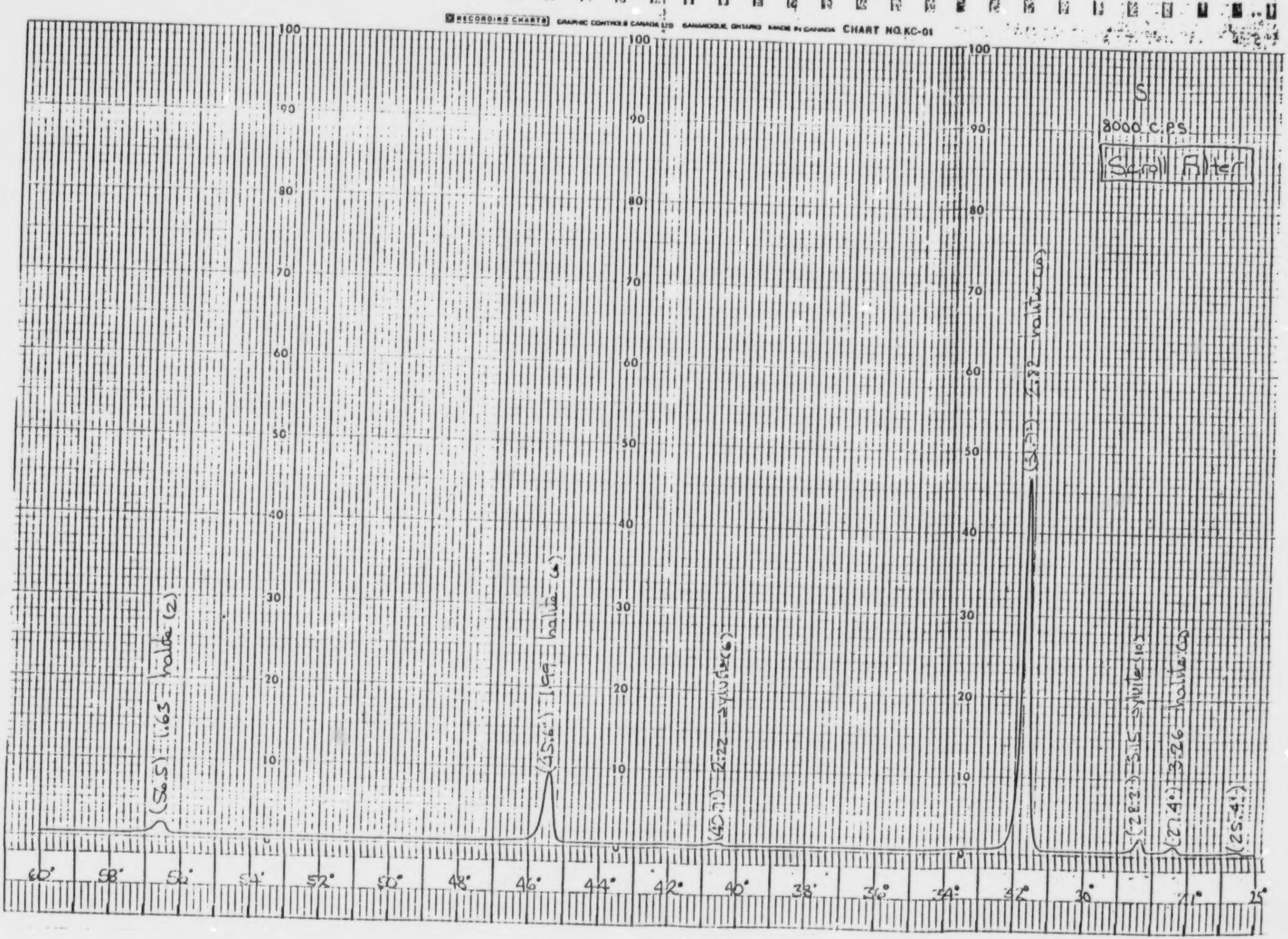
RECORDING CHARTS GRAPHIC CONTROLS CANADA LTD GANANOQUE, ONTARIO MADE IN CANADA CHART NO.KC-01
S
8000 C.P.S.
Scroll Filter
100
90
80
70
60
50
40
30
20
10
0
60°
58°
56°
54°
52°
50°
48°
46°
44°
42°
40°
38°
36°
34°
32°
30°
28°
26°
25°
(56.5) 1.63 halite (2)
(45.6°) 1.99 halite (4)
(40.7°) 2.22 sylvite(6)
(31.7°) 2.82 halite (10)
(28.2°) 3.15 sylvite (10)
(27.4°) 3.26 halite (2)
(25.4°)

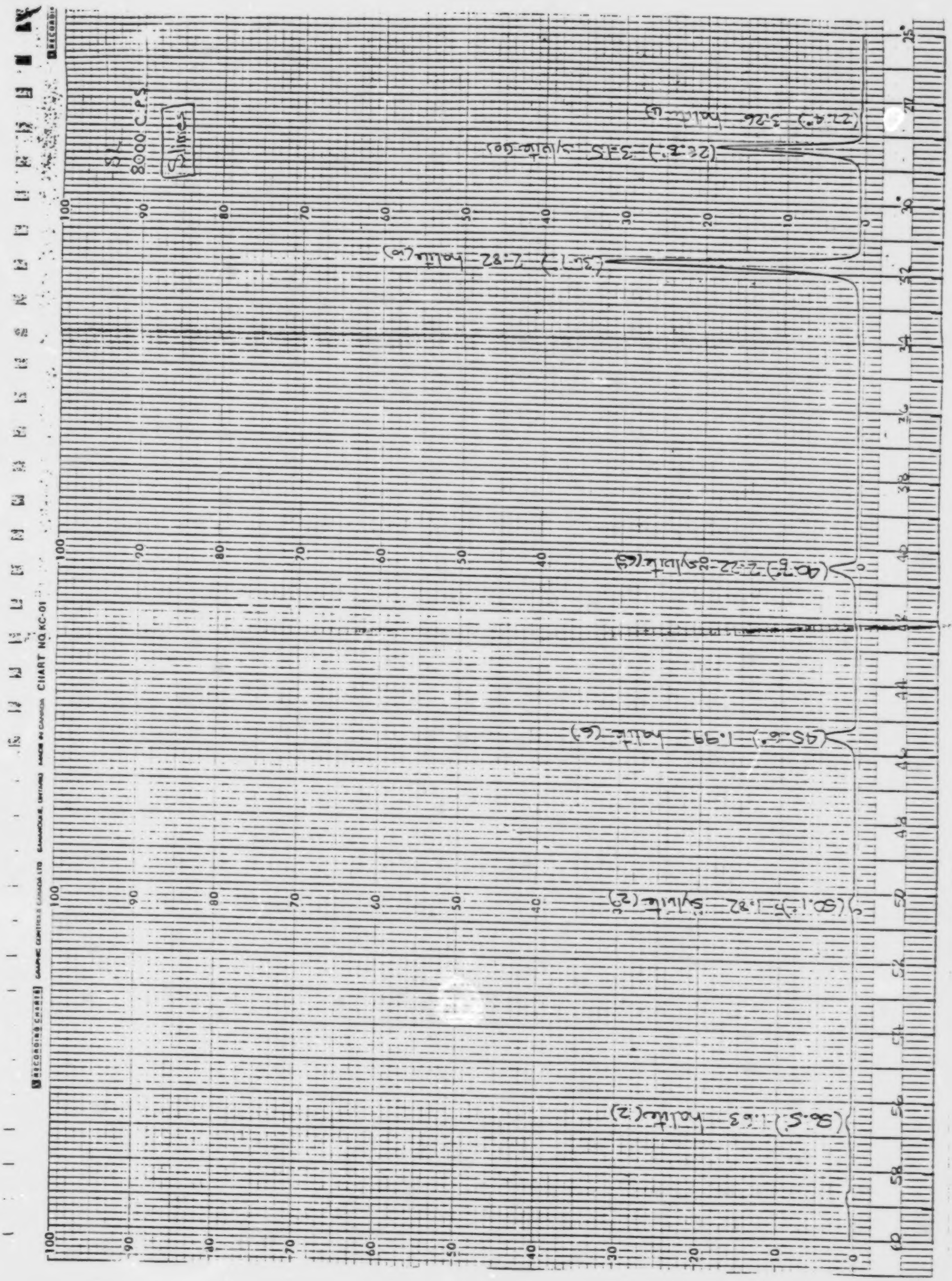
SL
8000 C.P.S
Slimes
(27.4°) 3.26 halite (1)
(28.3°) 3.15 sylvite (100)
(31.7°) 2.82 halite (10)
(40.5°) 2.22 sylvite (6)
(45.6°) 1.99 halite (6)
(50.1°) 1.82 sylvite (2)
(56.5°) 1.63 halite (2)
25°
30°
32
34
36
38
40
44
46
48
50
52
54
56
58
60
0
10
20
30
40
50
60
70
80
90
100
RECORDING CHARTS GRAPHIC CONTROLS CANADA LTD GANANOQUE, ONTARIO MADE IN CANADA CHART NO. KC-01

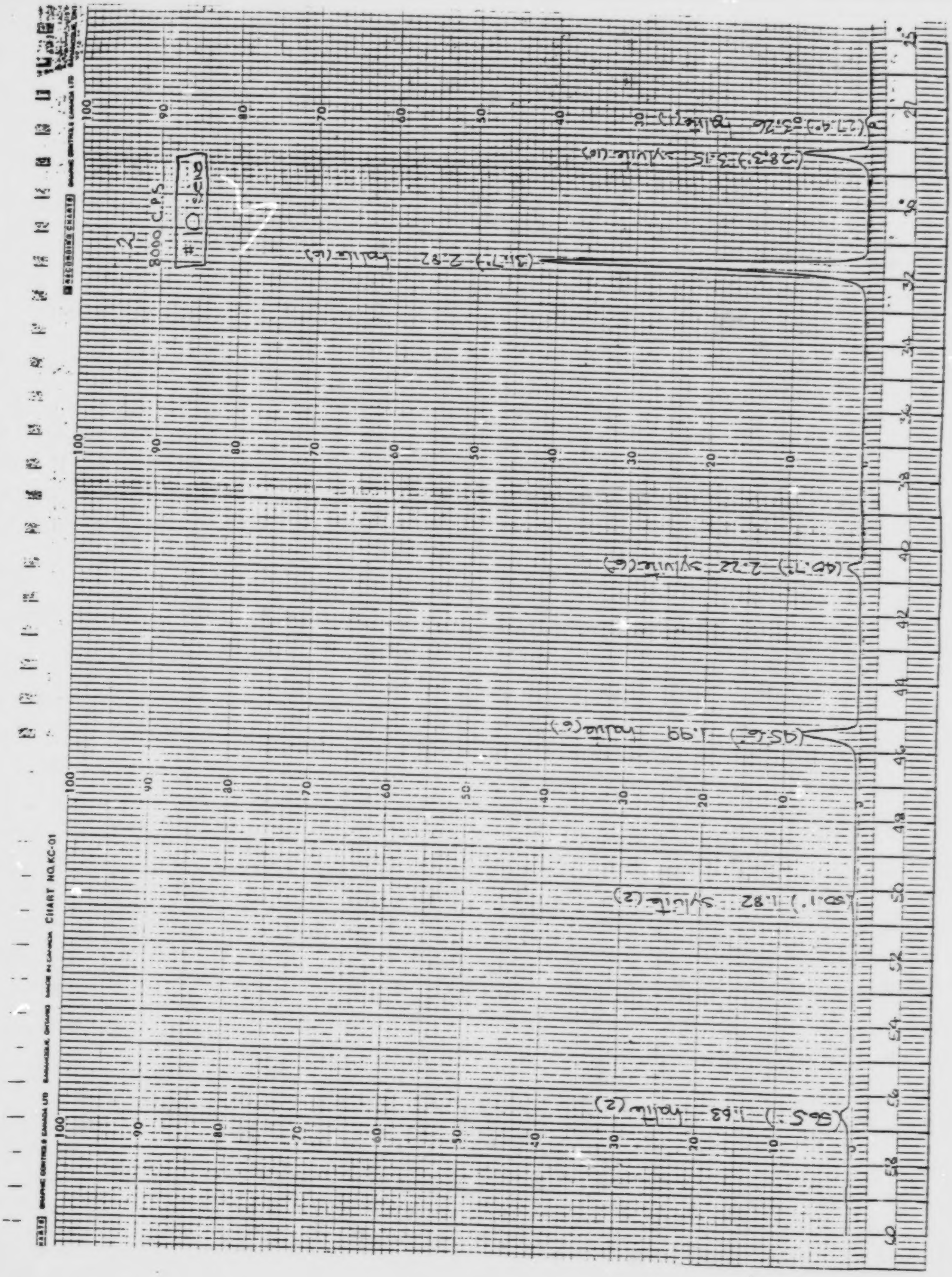
2
8000 C.P.S.
#10 sand
(27.4°) 3.26 halite(1)
(28.3°) 3.15 sylvite(10)
(31.7°) 2.82 halite(10)
(40.7°) 2.22 sylvite(6)
(45.6°) 1.99 halite(6)
(50.1°) 1.82 sylvite(2)
(56.5°) 1.63 halite(2)
25
27
30
32
34
36
38
40
42
44
46
48
50
52
54
56
58
60
100
90
80
70
60
50
40
30
20
10
RECORDING CHARTS
GRAPHIC CONTROLS CANADA LTD
MADE IN CANADA
CHART NO.KC-01

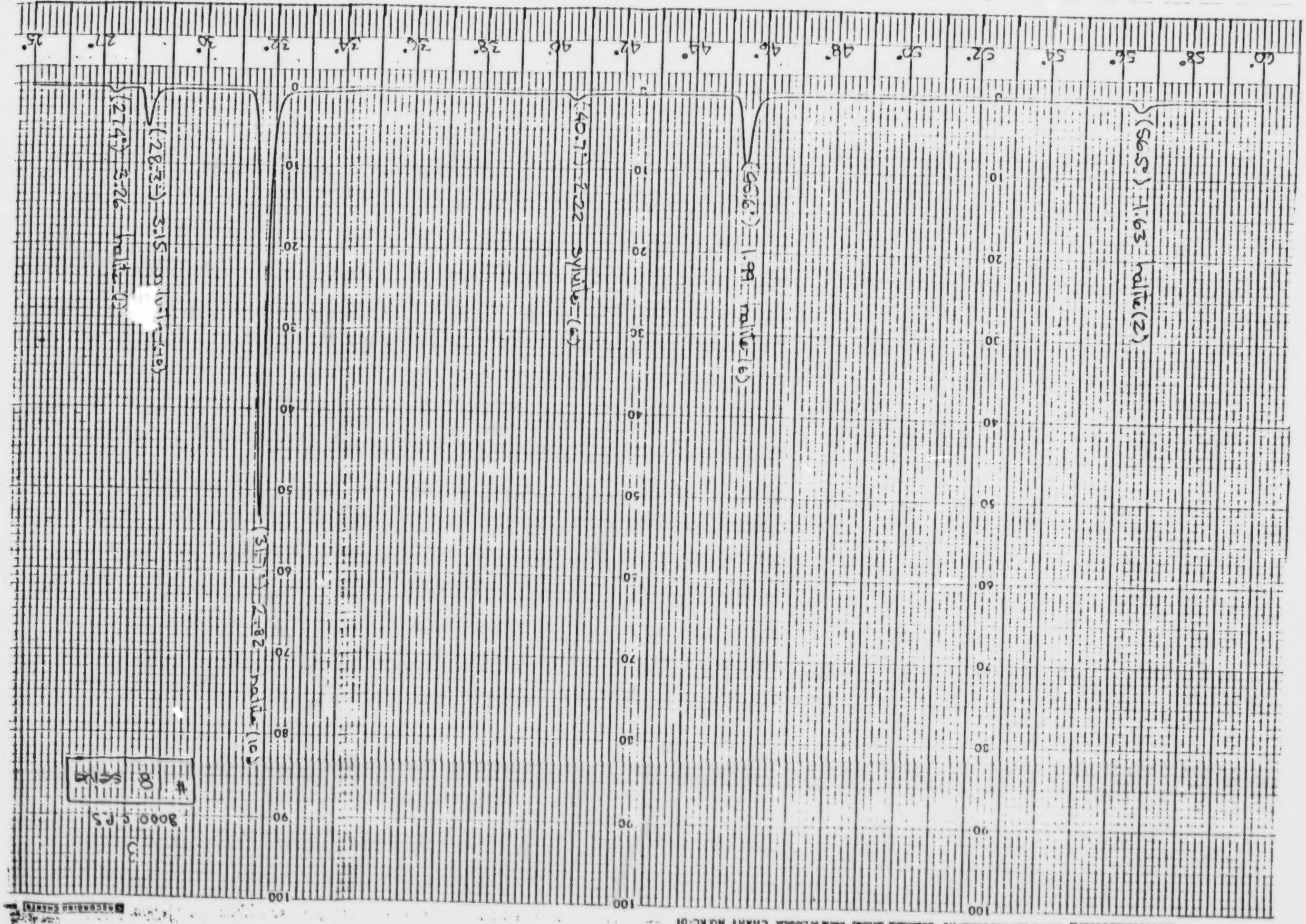
3
8000 c.p.s.
# 8 SPIKE
(27.4°) 3.26 halite (1)
(28.3°) 3.15 sylvite (10)
(31.7°) 2.82 halite (10)
(40.7°) 2.22 sylvite (6)
(45.6°) 1.99 halite (6)
(56.5°) 1.63 halite (2)
25° 27° 30° 32° 34° 36° 38° 40° 42° 44° 46° 48° 50° 52° 54° 56° 58° 60°
0 10 20 30 40 50 60 70 80 90 100
RECORDING CHARTS
GRAPHIC CONTROLS CANADA LTD. GANANOQUE ONTARIO MADE IN CANADA CHART NO. KC-01

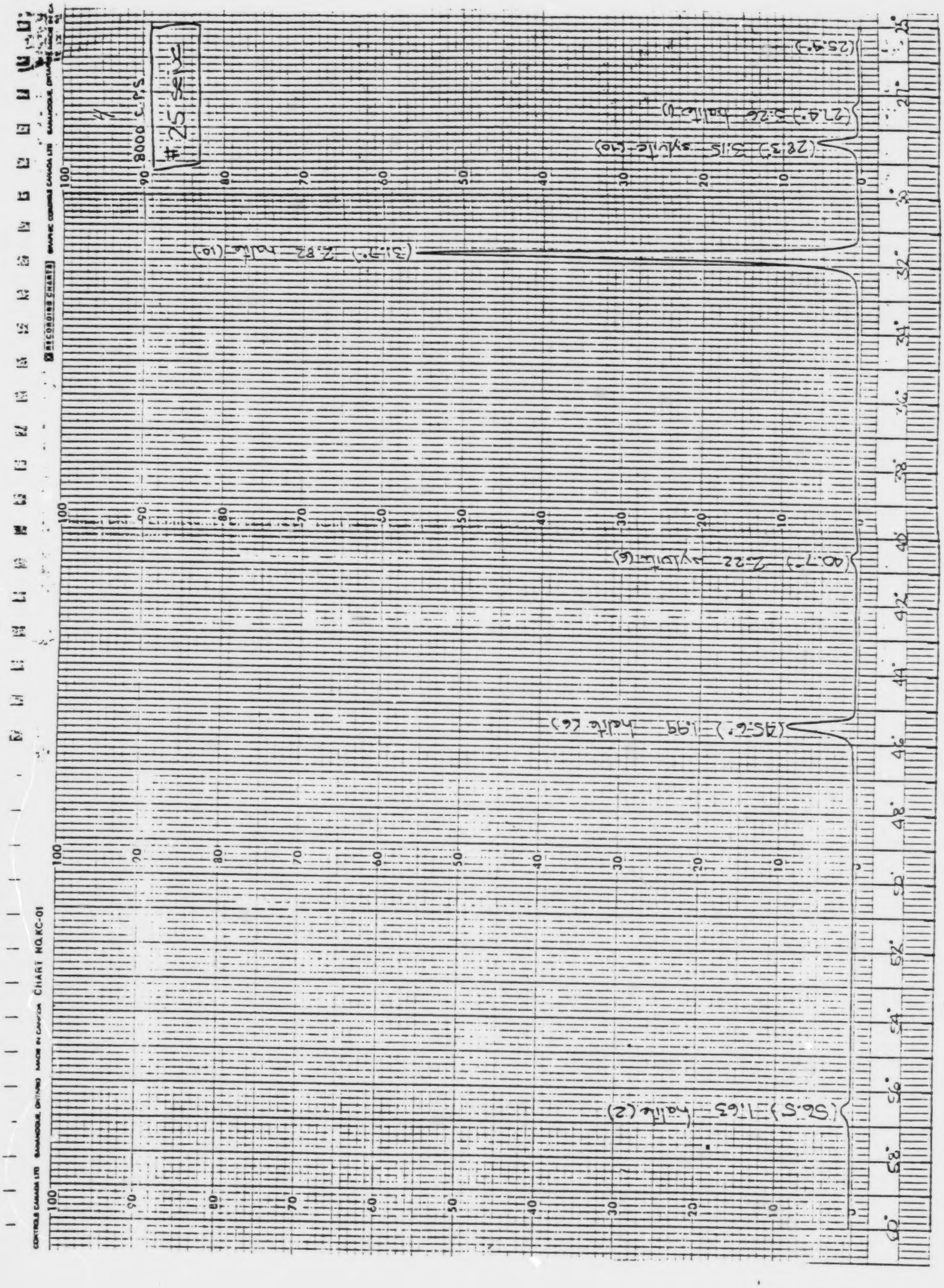

#25 Salt
8000 C.P.S.
(25.4°)
(27.4°) 3.26 halite (1)
(28.3°) 3.15 sylvite (10)
(31.7°) 2.82 halite (10)
(40.7°) 2.22 sylvite (6)
(45.6°) 1.99 halite (6)
(56.5) 1.63 halite (2)
25°
27°
30°
32°
34°
36°
38°
40°
42°
44°
46°
48°
50°
52°
54°
56°
58°
60°
0
10
20
30
40
50
60
70
80
90
100
CONTROLS CANADA LTD. SAMANDOLE, ONTARIO MADE IN CANADA CHART NO.KC-01
RECORDING CHARTS

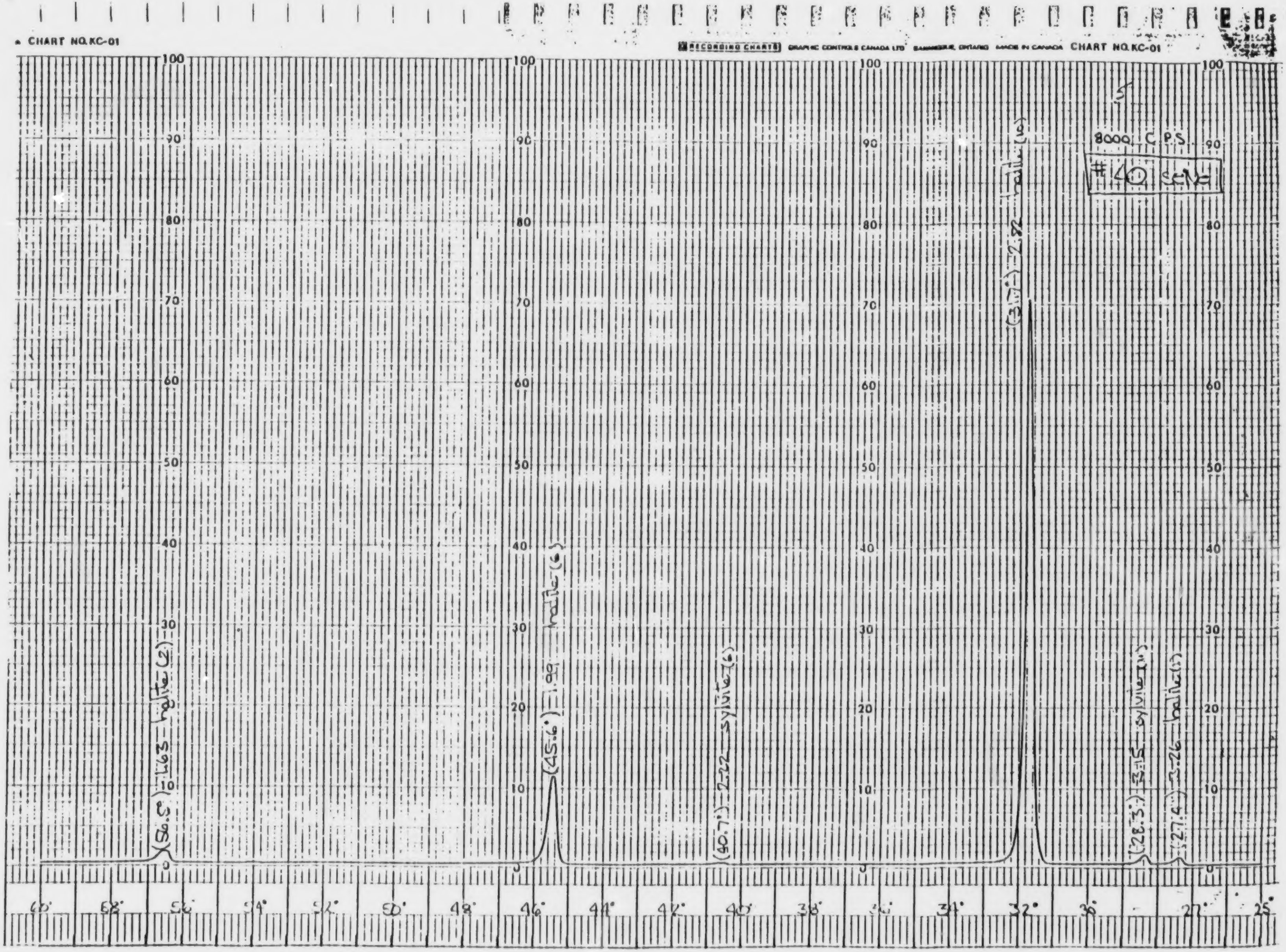
CHART NO. KC-01
RECORDING CHARTS GRAPHIC CONTROLS CANADA LTD. GANANOQUE, ONTARIO MADE IN CANADA CHART NO. KC-01
8000 C.P.S.
#40 Salt
(31.7°) 2.82 halite (10)
(28.3°) 3.15 sylvite (1)
(27.4°) 3.26 halite (1)
(40.7°) 2.22 sylvite (6)
(45.6°) 1.99 halite (6)
(56.5°) 1.63 halite (2)
100
90
80
70
60
50
40
30
20
10
0
60°
58°
56°
54°
52°
50°
48°
46°
44°
42°
40°
38°
36°
34°
32°
30°
27°
25°

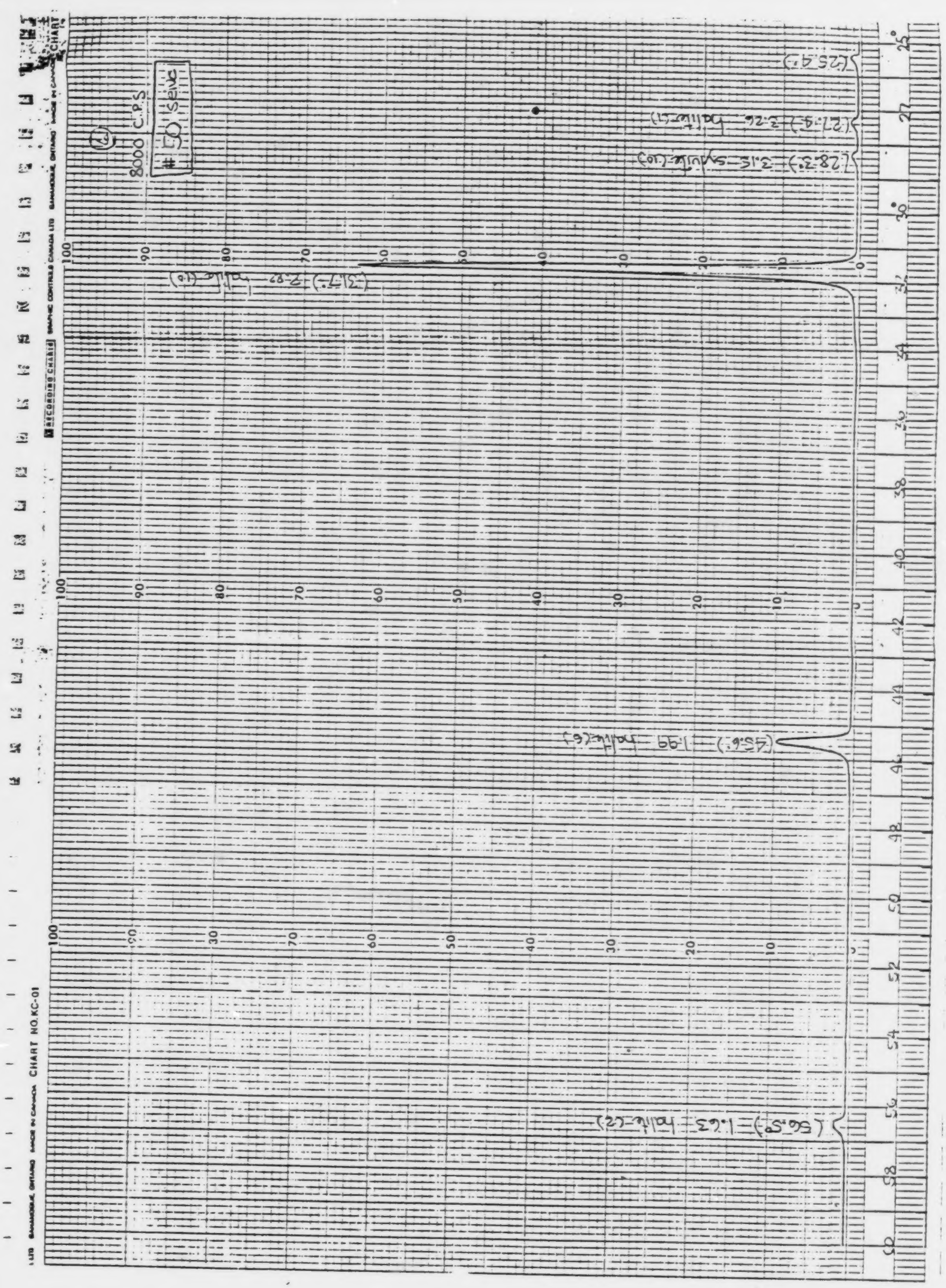
②
8000 C.P.S
# 50 seive
(25.4°)
(27.4°) 3.26 halite (1)
(28.3°) 3.15 sylvite (10)
(31.7°) 2.82 halite (10)
(45.6°) 1.99 halite (6)
(56.5°) 1.63 halite (2)
25°
27
30°
34
36
38
40
42
44
46
48
50
52
54
56
58
60
0
10
20
30
40
50
60
70
80
90
100
RECORDING CHARTS
GRAPHIC CONTROLS CANADA LTD
CHART NO. KC-01

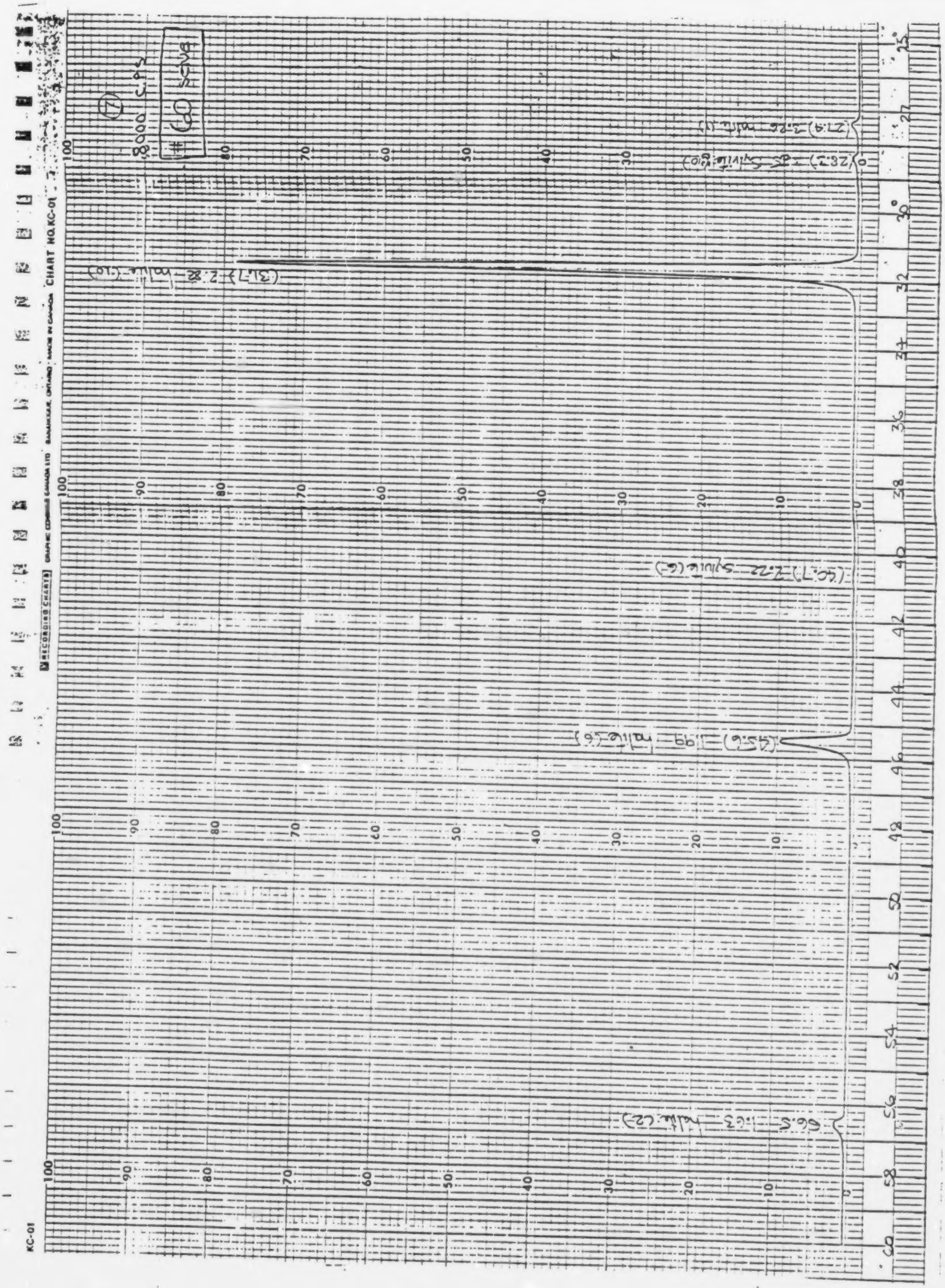
⑦
8000 cps
# 60 seva
(27.4) 3.26 halite (1)
(28.3) 3.15 sylvite (10)
(31.7) 2.82 halite (10)
(40.7) 2.22 sylvite (6)
(45.6) 1.99 halite (6)
56.5 1.63 halite (2)
100
90
80
70
60
50
40
30
20
10
0
25
27
30
32
34
36
38
40
42
44
46
48
50
52
54
56
58
60
RECORDING CHARTS
CHART NO. KC-01
KC-01

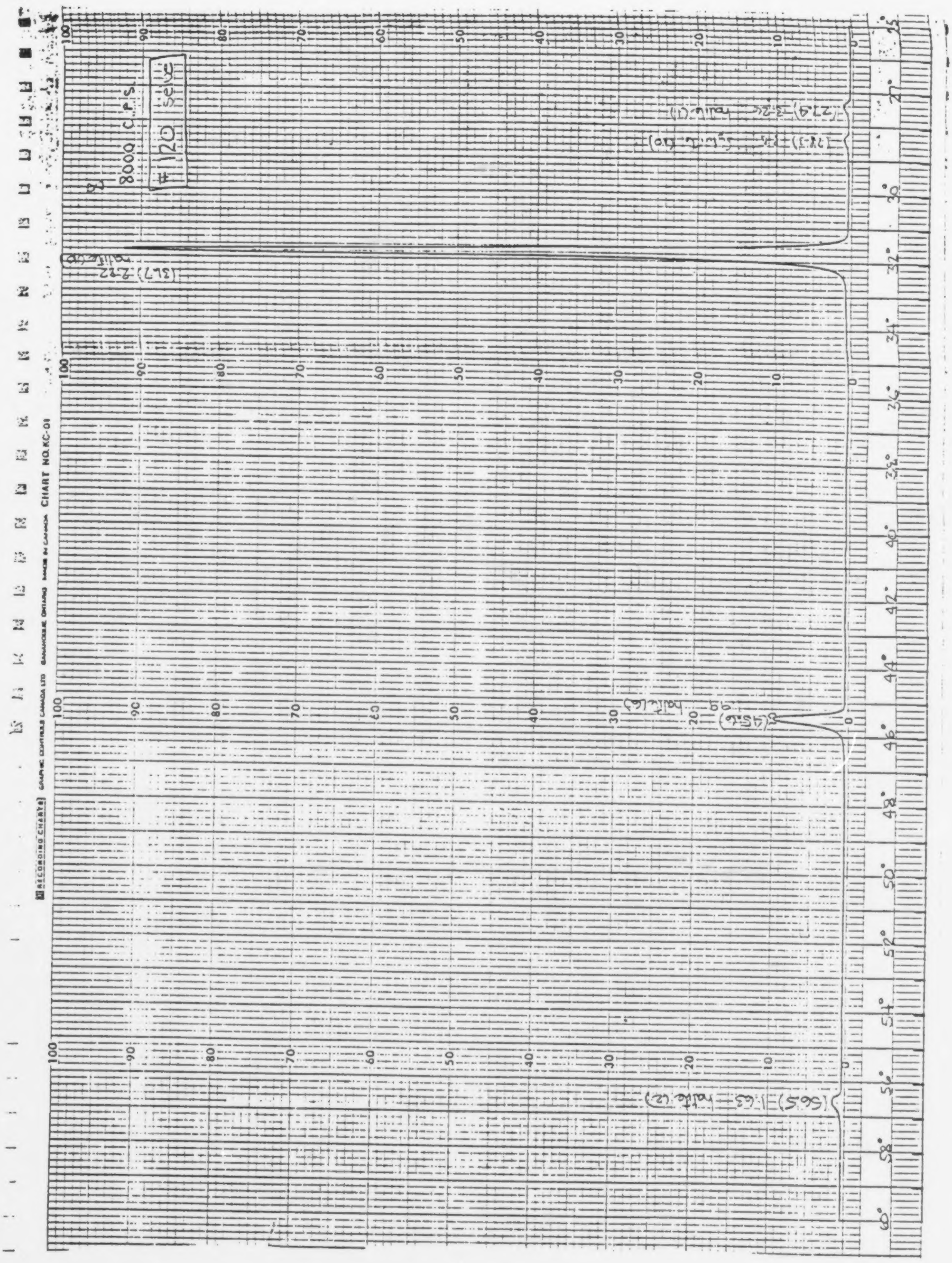
RECORDING CHARTS GRAPHIC CONTROLS CANADA LTD GANANOQUE, ONTARIO MADE IN CANADA CHART NO. KC-01
8000 C.P.S.
#1120 selve
(27.4) 3.26 halite (1)
(28.3) 3.15 sylvite (10)
(31.7) 2.82 halite (10)
(45.6) 1.99 halite (6)
(56.5) 1.63 halite (2)
100
90
80
70
60
50
40
30
20
10
0
25°
27°
30°
32°
34°
36°
38°
40°
42°
44°
46°
48°
50°
52°
54°
56°
58°
60°

APPENDIX IV: SCANNING ELECTRON MICROGRAPHS

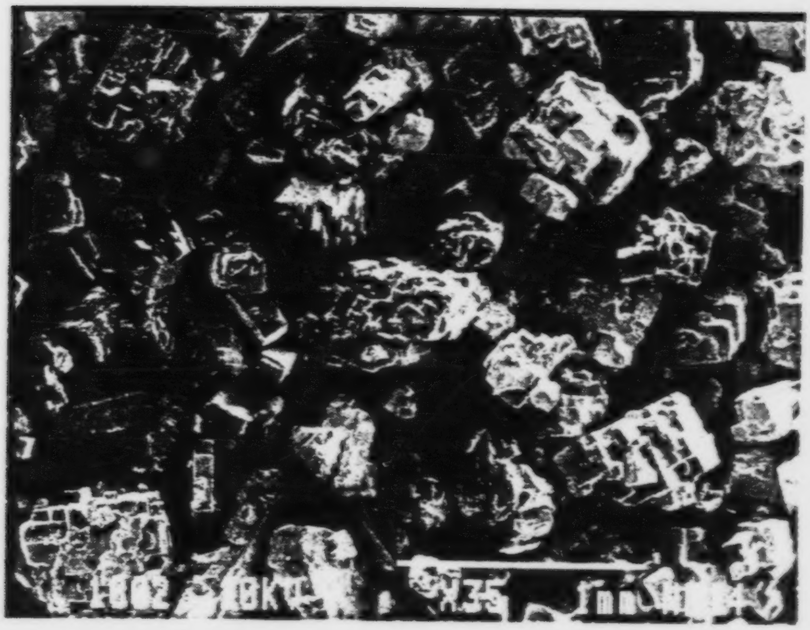
1002
10KV
X35
1mm

Figure AIV.1: Bulk Sample 1-6

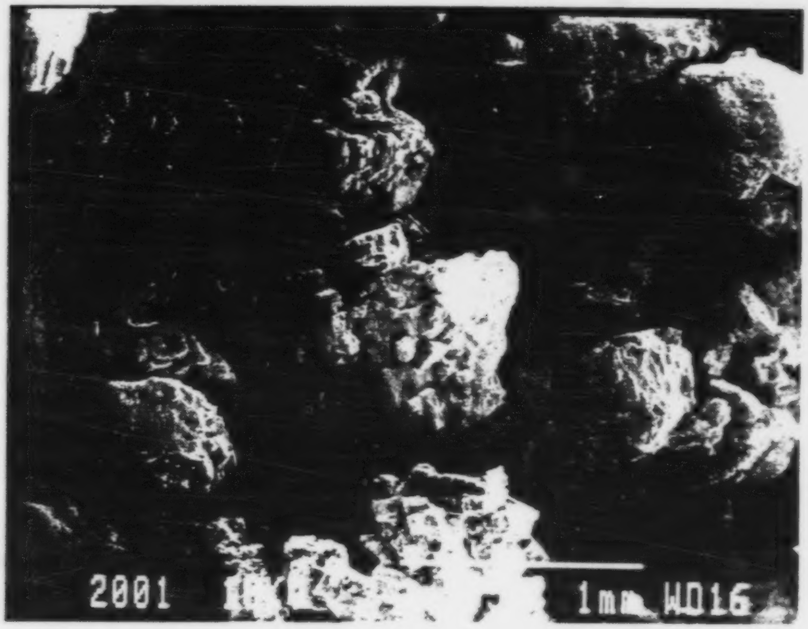
2001
1mm WD16

Figure AIV.2: Scroll Filter Tailings

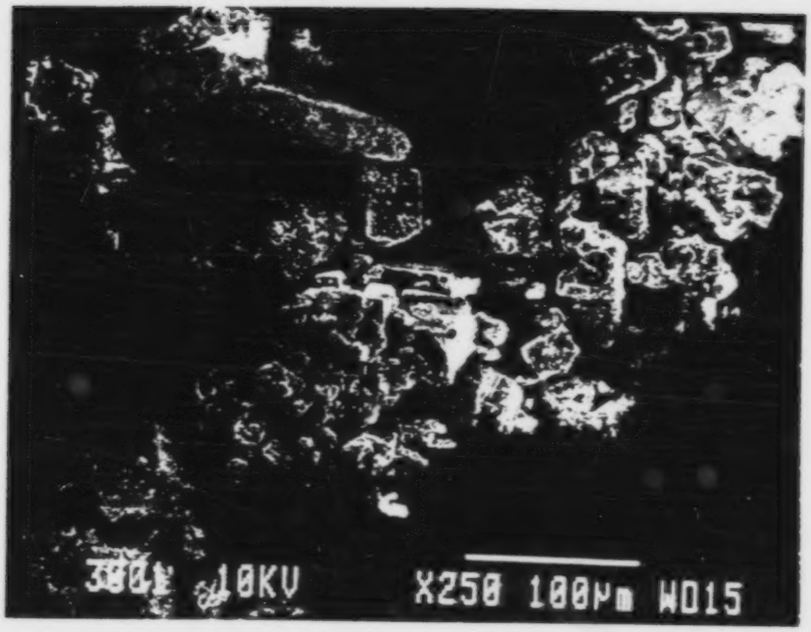
3001 10KV
X250 100µm WD15

Figure AIV.3: Slime Tailings

MECHANICAL PROPERTIES OF HALITE TAILINGS FROM THE DENISON-POTACAN POTASH MINE, SUSSEX, NEW BRUNSWICK

PART II: MOISTURE/DENSITY RELATIONSHIPS

By

Chris Fordham, M.Sc.
Maurice Dusseault, Ph.D., P.Eng.

September 1986

1.0 INTRODUCTION

The placement density of the backfill and its initial moisture content are the most critical variables governing its ultimate behavior. The higher the initial density, the more quickly the backfill will accept load and the lower the amount of total displacement that will occur. The higher the retained moisture content, the sooner the backfill will accept load as well, because the moisture becomes trapped and fills pores. The moisture content also affects the placement density.

This phase of the testing was performed to determine the maximum density/moisture content relationship using a variety of densification techniques. The methods employed were as follows;

1: Standard Proctor Compaction
2: Drop Tests
3: Vibration Compaction
4: Static Load Compaction

All of these tests are measures of the compactability of the backfill. They assume that volume changes are primarily a result of grain reorientation, repacking, and grain contact crushing. Creep processes are considered to have a negligible effect. Each of these tests is a laboratory representation of various field densification techniques but is not a precise simulation. They provide an index of the relative effectiveness of various compaction techniques and are not directly comparable to field conditions. To compare the results, accurate in situ experiments should be undertaken. It is expected that a standard approach that will be applicable to the field will evolve in this program.

The effect of moisture on the densification properties of granular materials has been well documented (Terzaghi and Peck, 1967). It is important to this study because the backfill will contain a certain amount of moisture after processing. Determination of the optimum moisture content/density relationship may lead to better placement conditions. However, the issue of moisture is by no means simple as in the case of classical soil mechanics.

1.2 Previous Work

Particle packing has been studied extensively in the past by petroleum and earthquake engineers, mathematicians, physicists, and biologists. Much of this has been theoretical work on ordered sphere and ellipsoid packings of regular shaped and sized cells. Some work has also been done on polydisperse systems with three or more discrete size distributions (Allen, 1982).

Of more applied interest is the work on polydisperse systems with continuous size distributions and the effect of the mode of deposition on the placement density. This work is primarily concerned with sedimentary processes including drop height and intensity. Kolbuszewski (1948a, 1948b, 1950) noted that high particle velocities can result in dense grain packings. However, as the intensity of falling grains increases, the density of grain packing may decrease.

Compaction of existing and placed cohesionless soils was not studied extensively until the beginning of the twentieth century. The need for information on soil compaction developed from the increased use of automobiles which required a hard road surface to drive on and an increased use of earth-fill dams. In order of effectiveness, the three most common methods available for the compaction of sands and gravels are vibration, watering, and rolling (Terzaghi and Peck, 1967).

Vibration can be applied to a fill or roadbed material by pneumatic vibration tools or simply by the operation of heavy equipment. As an example of the latter, Syncrude Canada Limited uses only bulldozers to blade and compact the sand in their upstream tailings dyke construction, and consistently achieve 90-95% relative density. Compaction of rockfill has been carried out by large rollers equipped with vibrators (Bertram, 1963). By spreading the fill in thin layers and compacting each layer carefully, reasonable compaction has been achieved, with values of 95% relative density easily achieved.

Watering compacts granular materials by breaking down unstable groups of grains and temporarily eliminating capillary forces. For the present case, the lubricating fluid would have to be a fully saturated brine. This method is not nearly as effective as vibration, and has the added problem of introducing large quantities of fluid. It is not likely to be an operationally feasible method.

Rolling provides very little compaction unless the material is almost saturated. It requires the use of large, heavy equipment which may as well be used to pull vibrating equipment capable of considerably more compaction.

1.2 Reporting of Results

The reporting of densities in previous reports has been extremely varied. Some reports have ignored the effects of initial densities (Beddoes, 1984). Others have reported densities but have not qualified the type of density, ie. dry or wet, corrected or uncorrected (Holcomb and Hannum, 1982). Based on the magnitude of previous results, it is the authors' opinion that most results are reported as uncorrected wet densities.

Densities in this report will be reported as corrected dry densities and uncorrected wet densities for comparison. Dry densities are lower than the uncorrected wet densities.

2.0 TEST PROCEDURES

2.1 Specific Gravity of Denison-Potacan Tails

The specific gravity of the Denison-Potacan tails based on the optical and X-Ray diffraction mineralogies is 2.14.

2.2 Sample Preparation

Backfill samples were air dried to remove natural moisture and then rehydrated with process brine to achieve corrected moisture contents of between 0 and 16%. Air drying may have introduced small amounts of new material precipitated from the brine, however, this material is considered to have little effect on the behavior of the backfill.

2.3 Standard Proctor Compaction

Standard Proctor tests were performed to determine the optimum moisture content/dry density relationship of the backfill. This test is used extensively for roadbed and earth filled dam compaction. Test procedures followed those outlined in ASTM D698 Method A.

The Standard Proctor test has been used extensively by previous workers to determine the optimum moisture content/density relationship for halite backfill (Beddoes, 1984; Johnson, 1984; Pufhal and Yoshida, 1982). Its applicability as an index test for halite backfill is unclear, however it is comparable and widely used. The results obtained for halite backfill are quite different than for other materials (Figure 1).

One seeming advantage of using the Standard Proctor is the huge data base of results which already exists. However, the Standard Proctor is almost always used in clayey silty sands, or other similar materials, which are well graded and contain a significant portion of fines. The DPPC tails do not meet these requirements and it is well appreciated that the Standard Proctor is less applicable to sand-type materials. Also, there is the issue that it may fracture the halite grains because the crystals are weaker than typical clastic minerals.

2.4 Drop Tests

Drop tests were performed to simulate the densification achieved by dropping or flinging the backfill into an underground opening. It is understood that if this type of emplacement technique is employed, the material will probably be thrown into the mine horizontally from a mechanical flinger. The drop tests were performed vertically using gravity as the compactive energy source. The results may not be directly comparable; however, the relative effect of various drop heights and moisture contents

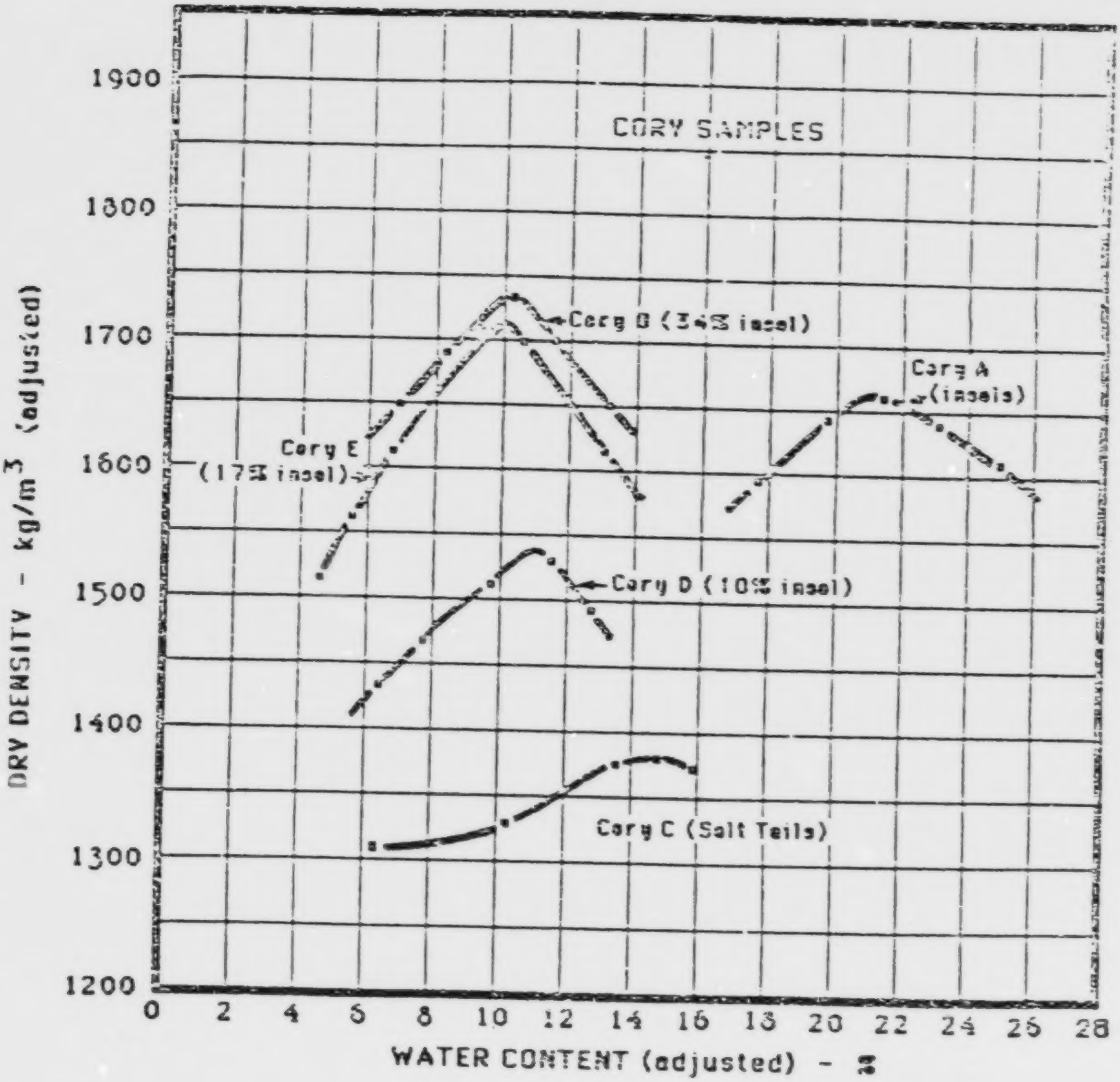

Figure 1: Standard Proctor Compaction test results for salt tails and salt tails with added insoluble material (Johnson, 1984)

give a reasonable approximation of the effectiveness of throwing or dropping the backfill into the mine as opposed to other densification techniques.

The tests were performed by dropping backfill samples down a 5.1 cm diameter drop tube into a volumetrically calibrated measuring cylinder, 6.71 cm in diameter. It is felt that the difference in size between the drop tube and the measuring cylinder allowed for rapid enough air removal to prevent air cushioning. The volume and the mass of the material in the measuring cylinder were calculated to determine the density. The backfill was dropped from four heights; 1, 2, 3, and 6 m. Four corrected moisture contents were used; 0, 4, 8, and 12%. Each material was dropped three times at each height and the results averaged.

2.5 Vibration Testing

Vibration tests were performed to assess the densification achieved by vibrating the backfill while under a normal load. The tests were used to simulate the effect of a vibrating roller or other piece of vibrating heavy equipment on the backfill. The samples were vibrated in a clear plexiglass cylinder 25 cm high and 18.9 cm in diameter on a table vibrating at 60 Hz. The bottom of the cylinder was sealed, therefore we simulated undrained conditions (Figure 2).

Two variables were examined during the testing; moisture content and normal stress. Tests were conducted at moisture contents of 0, 4, 8, and 12%. Weights of 853.1, 1850.5, 9395.0 and 18681.1 g were applied to the surface of the test samples, hence the normal stress applied to the test samples was 335.8, 728.3, 3910.2, and 7357.0 Pa respectively. The first weight of 853.1 g was an aluminum disk 17.8 cm in diameter, slightly smaller than the inside diameter of the test cylinder. This prevented the sides of the cylinder from interfering with the action of the weight on the backfill. All subsequent weights were placed on top of the aluminum disk in the center.

2.6 Static Load Test

A static load test was performed as part of a consolidation test series to determine the necessity of temperature control for long term consolidation testing. The consolidometers allow one dimensional consolidation under a constant stress (Figure 3). The resulting density changes were monitored with time. The test was used to simulate mechanical stowing of the backfill within the mine.

The samples placed in the consolidometers were air dried with no added brine and had an initial dry density of 1.20 g/cc. Density changes within the first four hours were arbitrarily

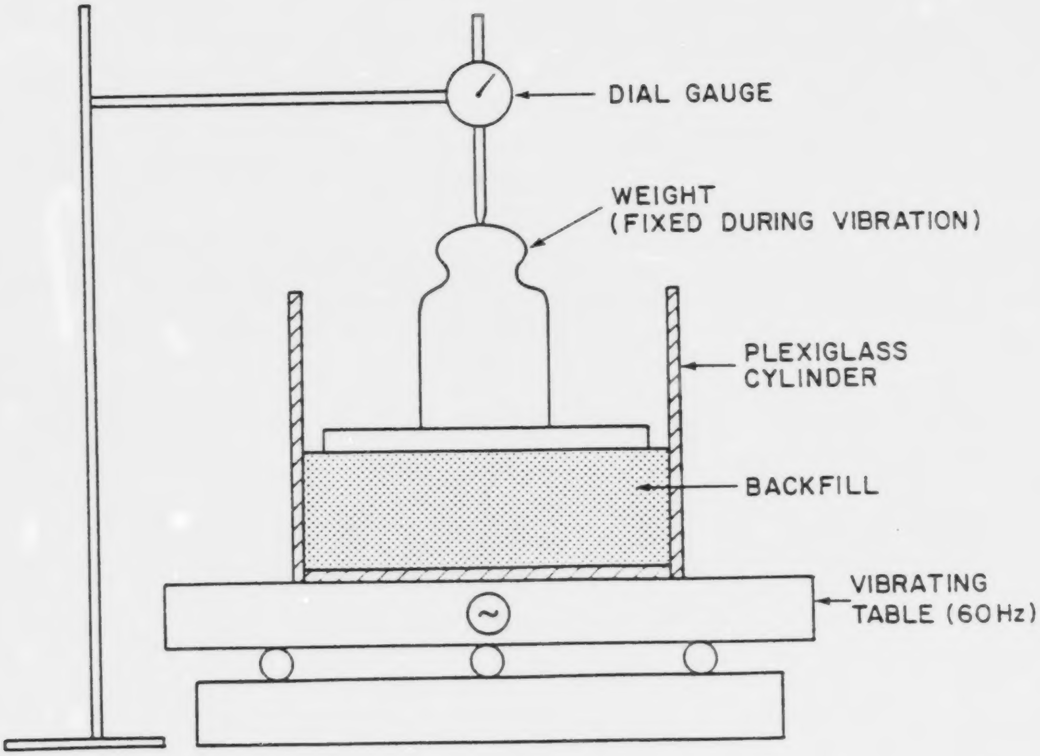
DIAL GAUGE
WEIGHT (FIXED DURING VIBRATION)
PLEXIGLASS CYLINDER
BACKFILL
VIBRATING TABLE (60Hz)

Figure 2: Vibration Test Apparatus

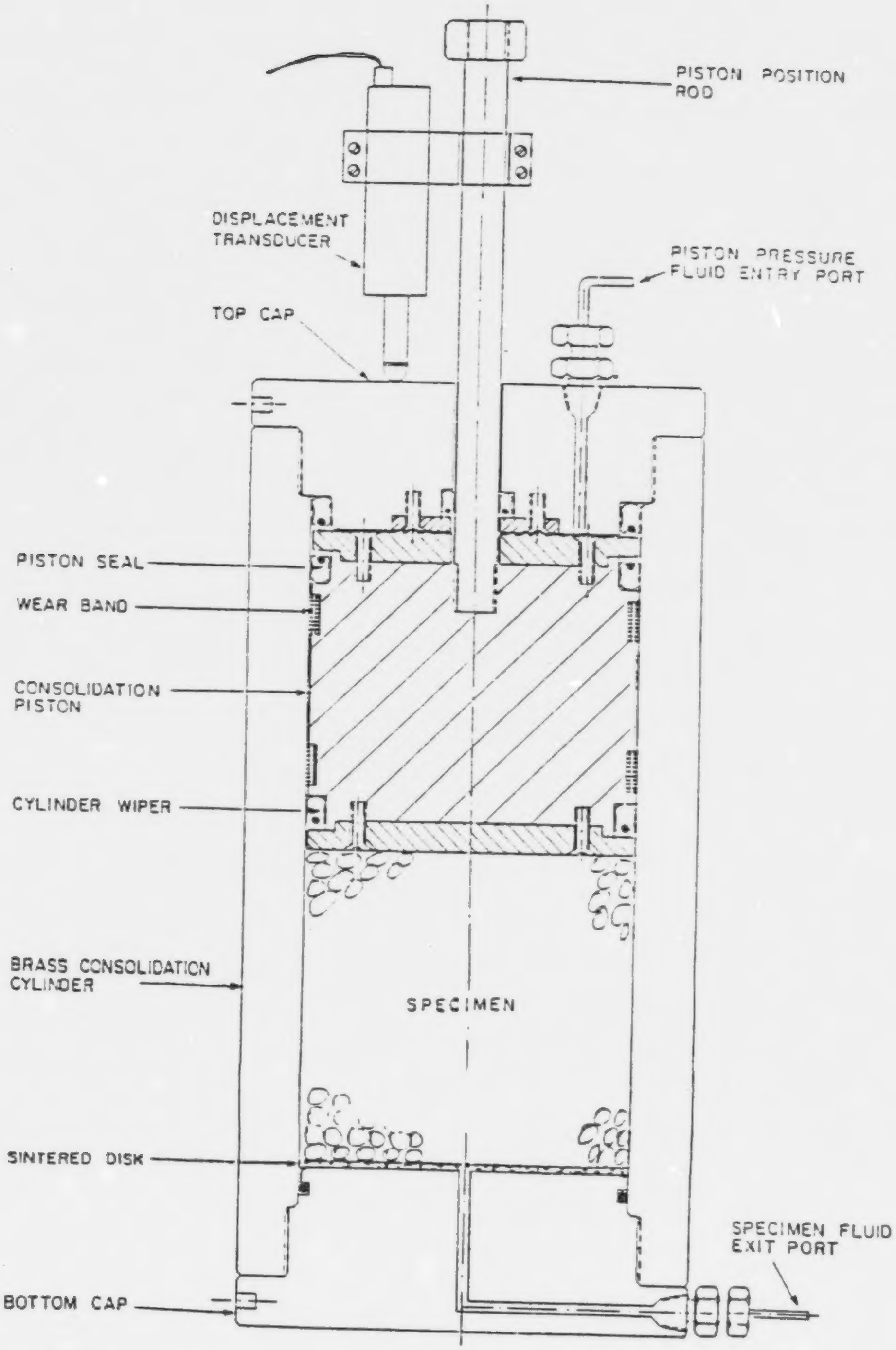
PISTON POSITION ROD
DISPLACEMENT TRANSDUCER
PISTON PRESSURE FLUID ENTRY PORT
TOP CAP
PISTON SEAL
WEAR BAND
CONSOLIDATION PISTON
CYLINDER WIPER
BRASS CONSOLIDATION CYLINDER
SPECIMEN
SINTERED DISK
SPECIMEN FLUID EXIT PORT
BOTTOM CAP

Figure 3: Conslidometer used for Static Load Test

chosen as being primarily due to compaction rather than creep consolidation.

3.0 RESULTS

3.1 Standard Proctor Compaction

The Standard Proctor Compaction test showed that while the wet density of the backfill continues to increase with moisture content up to 16% corrected moisture content, the dry density changes very little but peaks at about 12% corrected moisture content (Table 1; Appendix I).

The maximum increase in dry density with moisture content is only about 4%. The addition or removal of brine from the backfill before it is placed will have little effect and is therefore probably not economic. In addition, it appears that the backfill will drain quickly to about 5-6% moisture and ultimately to about 2-3% (Beddoes, 1984) if full drainage is permitted. Large additions of brine to increase initial density may require pumping systems to remove the brine which will drain from the backfill.

Table 1: Standard Proctor Compaction Results

Moisture Content (%)	Wet Density (g/cc)	Dry Density (g/cc)
0.0	1.33	1.33
4.0	1.42	1.34
8.0	1.52	1.36
12.0	1.63	1.38
16.0	1.68	1.35

3.2 Drop Tests

The drop tests showed that in general, the faster the backfill is dropped or thrown, the greater its initial density. However, the densities achieved are quite low compared to other methods of compaction. The drop heights (1,2,3, and 6 m) were recalculated as velocities as flinger emplacement will be performed at a certain velocity. The velocities calculated from the drop heights are 4.43, 6.262, 7.664, and 10.844 m/s respectively.

Recalculating the drop heights directly as velocities is a somewhat crude approximation. It ignores the effect of tube wall friction, the change in the base height as the material builds up in the measuring cylinder, and wall friction in the measuring cylinder. These factors will decrease the velocity of the particles somewhat. However, the test is still considered a reasonable approximation of flinger type emplacement.

The increase in velocity from 4.43 m/s to 10.84 m/s resulted in a maximum density change of 19.3% at 12% moisture content (Table 2; Appendix II). The dry sample maintained the highest dry density (with the exception of 12% moisture at 10.84 m/s) but had the lowest increase in density with velocity (7.2%).

Table 2: Drop Test Results

Terminal Velocity (m/s)	Moisture Content (%)	Wet Density (g/cc)	Dry Density (g/cc)
4.43	0	1.03	1.03
	4	0.91	0.86
	8	1.00	0.89
	12	1.08	0.92
6.26	0	1.06	1.06
	4	1.00	0.95
	8	1.05	0.94
	12	1.08	0.91
7.66	0	1.06	1.06
	4	1.03	0.98
	8	1.10	0.98
	12	1.17	0.99
10.84	0	1.11	1.11
	4	1.12	1.06
	8	1.20	1.07
	12	1.35	1.14

The drop tests show that compaction will increase with increasing velocity, particularly if the backfill contains some brine. However, the increase in compaction has an upper bound where increases in velocity do not result in further compaction. In fact, extremely high velocities may reduce the density as individual particles may not have time to fill voids as new particles arrive and bounce back occurs.

It is not clear whether the maximum achievable density was reached during these tests. The same density would have to be achieved at at least two successive velocities to determine the maximum achievable density.

3.3 Vibration Tests

Vibration proved to be the most effective method of compacting the backfill. Wet densities of between 1.24 and 1.68 g/cc were achieved after 20 minutes of vibration. The corrected dry densities ranged from 1.19 to 1.42 g/cc. Most of the densification occurred within the first 15 seconds of the test (Table 3; Appendix III).

The stresses applied to the surface of the backfill samples while they were vibrated are considerably less than those that would be applied by a piece of mine equipment driving over placed backfill. It appears that increasing the surface stress may yield greater densities (Figure 4).

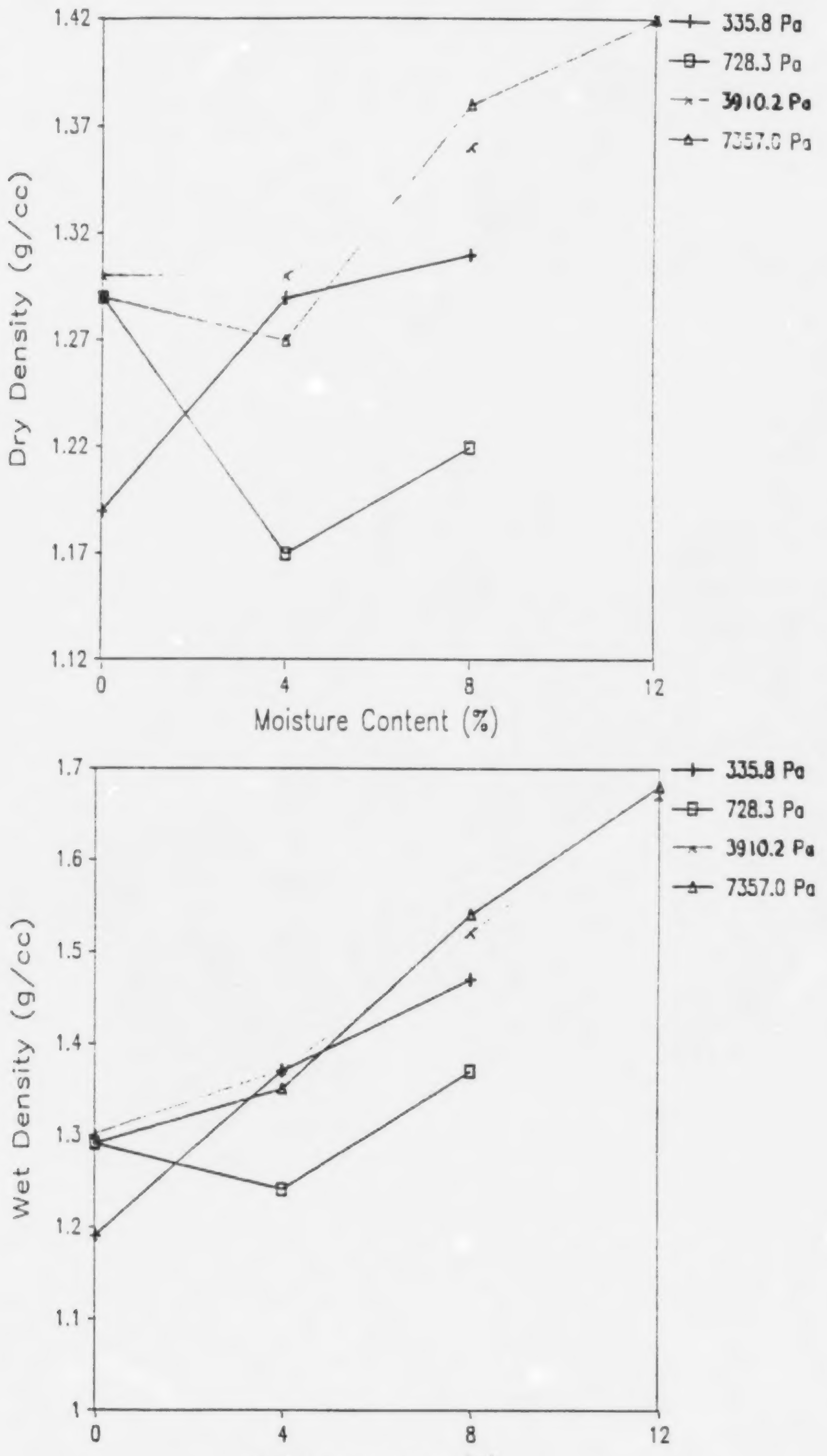

Figure 4: Vibration Test Results

Table 3: Vibration Test Results

Applied Stress (Pa)	Moisture Content (%)	Final Wet Density (g/cc)	Final Dry Density (g/cc)	% of Final Dry Density Achieved After 15 Seconds
335.8	0.0	1.19	1.19	94.1
	4.0	1.37	1.29	92.2
	8.0	1.47	1.31	90.1
728.3	0.0	1.29	1.29	93.0
	4.0	1.24	1.17	92.3
	8.0	1.37	1.22	90.2
3910.2	0.0	1.30	1.30	87.7
	4.0	1.37	1.30	82.4
	8.0	1.52	1.36	80.9
	12.0	1.67	1.42	83.8
7357.0	0.0	1.29	1.29	91.0
	4.0	1.35	1.27	86.6
	8.0	1.54	1.38	84.8
	12.0	1.68	1.42	71.1

The results of the vibration tests show that vibration is the most effective method of densifying or compacting the backfill. Vibration will be used in the preparation of samples for consolidation testing. It will probably be the most effective method of densification in situ. Mine equipment used to emplace the backfill may supply sufficient vibration energy and surface stress to densify it to the point where it will be a viable support material in the required time. If mine vehicles alone do not supply sufficient compactive energy, a vibro-compaction roller may be employed. This will have to be determined in situ.

3.4 Static Load Test

The static load test showed that by applying a static load of 5 MPa to the backfill for 4 hours, the initial dry density of 1.2 g/cc could be increased by about 16-17% to approximately 1.4 g/cc (Table 4; Appendix IV). Five MPa is a considerably higher load than could be applied to the backfill in situ by any type of mechanical stower. However, even under such a high load, the densities achieved after 4 hours of static loading are only about 6-7% higher than those achieved by vibration after 20 minutes and about 20% higher than those achieved by vibration for only 15 seconds. A combination of the two processes, high surface loading and vibration, will probably be the most effective method of densifying the backfill in situ.

Table 4: Static Load Test Results

Time (Hours)	Test 1 Dry Density (g/cc)	Test 2 Dry Density (g/cc)
0	1.200	1.200
0	1.337	1.352 **
1	1.369	1.385
2	1.375	1.393
3	1.379	1.399
4	1.382	1.403

** Instantaneous Volume Change

4.0 CONCLUSIONS AND RECOMMENDATIONS

The following conclusions have been reached during this phase of the study.

1. DPPC tails have a specific gravity of 2.14.
2. The maximum achieved dry density during the current test series was 1.42 g/cc or 1.68 g/cc wet density.
3. The most effective method of densifying the tailings into a usable backfill is by vibro-compaction.
4. The efficiency of any compactive effort diminishes with time. Up to 90% of the final achievable density can be attained within a very short period of time, ie. 15 seconds.
5. Flinger type emplacement and mechanical stowing may be useful during initial placement, however, their use as a densification technique appears unlikely.

The following recommendations are suggested for future phases of this study.

1. An *in situ* vibro-compaction experiment should be undertaken to determine the effectiveness of various placement techniques.
2. Several column experiments will be conducted to determine drained moisture content. Shrinkage will also be examined.
3. Further vibro-compaction tests will be conducted with higher surface loads.

REFERENCES

Allen, J.R.L., 1982. Sedimentary Structures; Their Character and Physical Basis, Volume 1. Elsevier Scientific Publishing Company, New York. 593 pp.

Beddoes, R.J., 1984. Determination of Engineering Properties of Salt for Backfilling in Underground Potash mines. RE/SPEC Ltd., Calgary, for the Canada Center for Mineral and Energy Technology, Project No. 310104.

Bertram, G.E., 1963. Rockfill Compaction by Vibratory Rollers. Panamerican Conf. Soil Mech. Found. Eng., Brazil, vol. 1, pp. 441-455.

Holcomb, D.J., and Hannum, D.W., 1982. Consolidation of Crushed Salt Backfill Under Conditions Appropriate to the WIPP Facility. Sandia National Laboratory Report SAND-82-0630.

Johnson, R.F., 1984. Investigation of the Physical and chemical Characteristics of Potash tailings in Saskatchewan. Potash Corp. of Saskatchewan, Saskatoon, for the Canada Center for Mineral and Energy Technology, Project No. 350204.

Kolbuszewski, J., 1948a. An Experimental Study of the Maximum and Minimum Porosities of Sand. Proc. 2nd Int. Conf. Soil Mech., vol. 1, pp.158-165.

Kolbuszewski, J., 1948b. General Investigation of the Fundamental Factors Controlling Loose Packing of Sands. Proc. 2nd Int. Conf. Soil Mech., vol. 7, pp. 47-49.

Kolbuszewski, J., 1950. Notes on Factors Governing the Porosity of Wind Deposited Sands. Geol. Mag. vol. 87, pp. 433-435.

Pufahl, D.E., and Yoshida, R.T., 1982. A Study of Potash Tailings: Properties and Behavior for Total Extraction Mining. University of Saskatchewan, Saskatoon, for Potash Corp. of Saskatchewan.

Terzaghi, K, and Peck, R.B., 1967. Soil Mechanics in Engineering Practice. John Wiley and Sons, New York. 729 pp.

APPENDIX I: STANDARD PROCTOR COMPACTION RESULTS

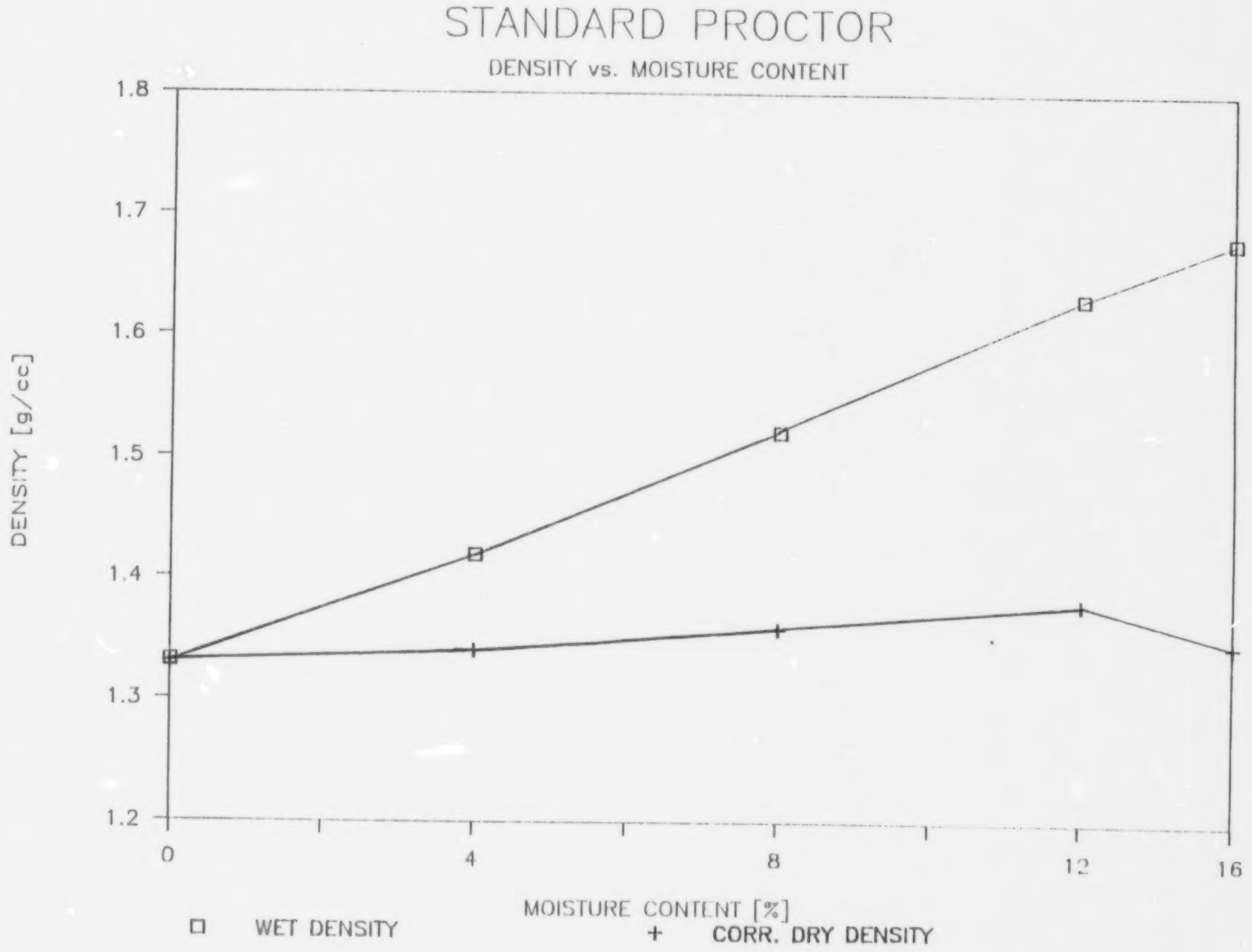
STANDARD PROCTOR
DENSITY vs. MOISTURE CONTENT
DENSITY [g/cc]
1.8
1.7
1.6
1.5
1.4
1.3
1.2
0
4
8
12
16
MOISTURE CONTENT [%]
□ WET DENSITY
+ CORR. DRY DENSITY

APPENDIX II: DROP TEST RESULTS

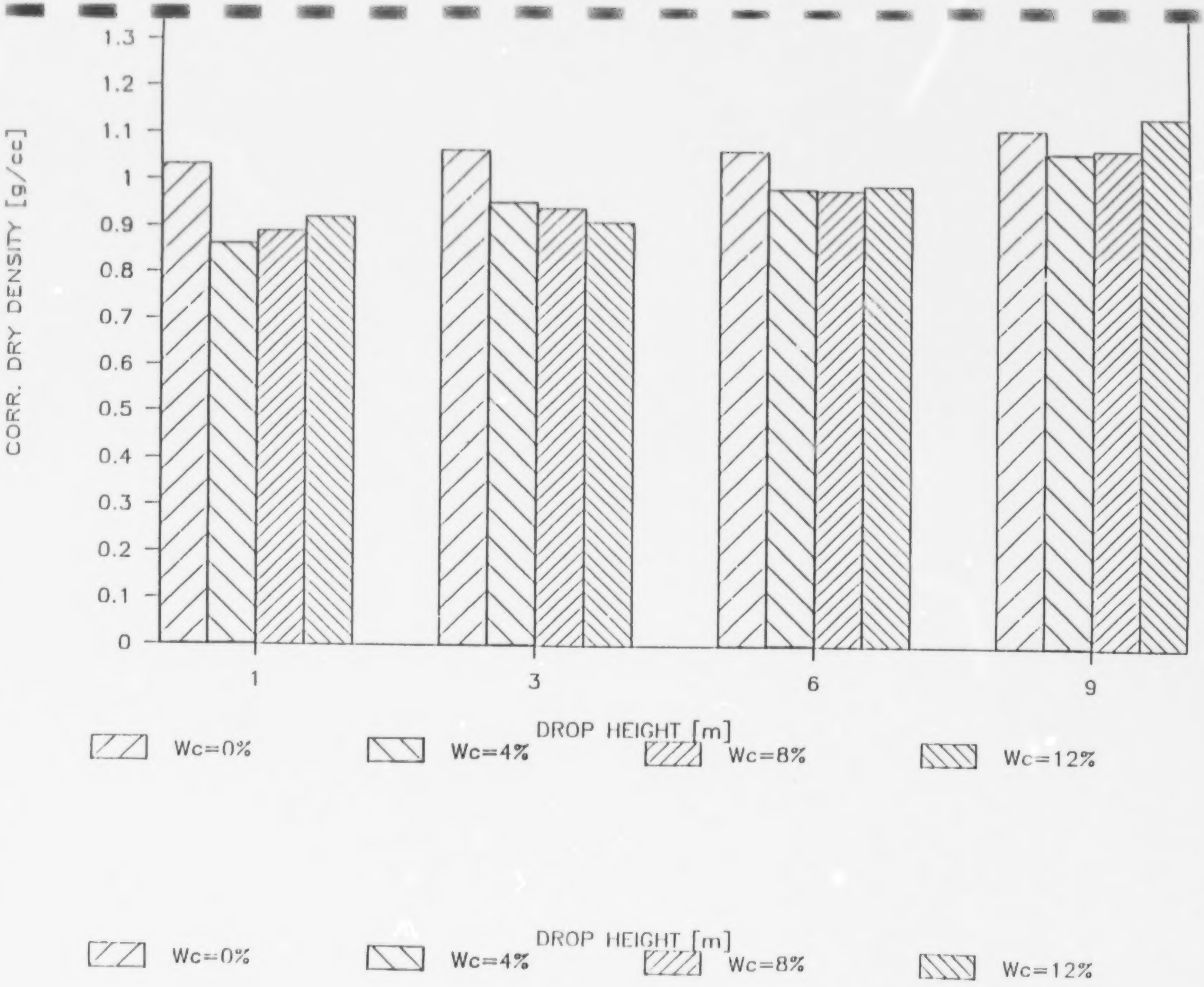
CORR. DRY DENSITY [g/cc]
1.3
1.2
1.1
1
0.9
0.8
0.7
0.6
0.5
0.4
0.3
0.2
0.1
0
1
3
6
9
DROP HEIGHT [m]
Wc=0%
Wc=4%
Wc=8%
Wc=12%
DROP HEIGHT [m]
Wc=0%
Wc=4%
Wc=8%
Wc=12%

APPENDIX III: VIBRATION TEST RESULTS

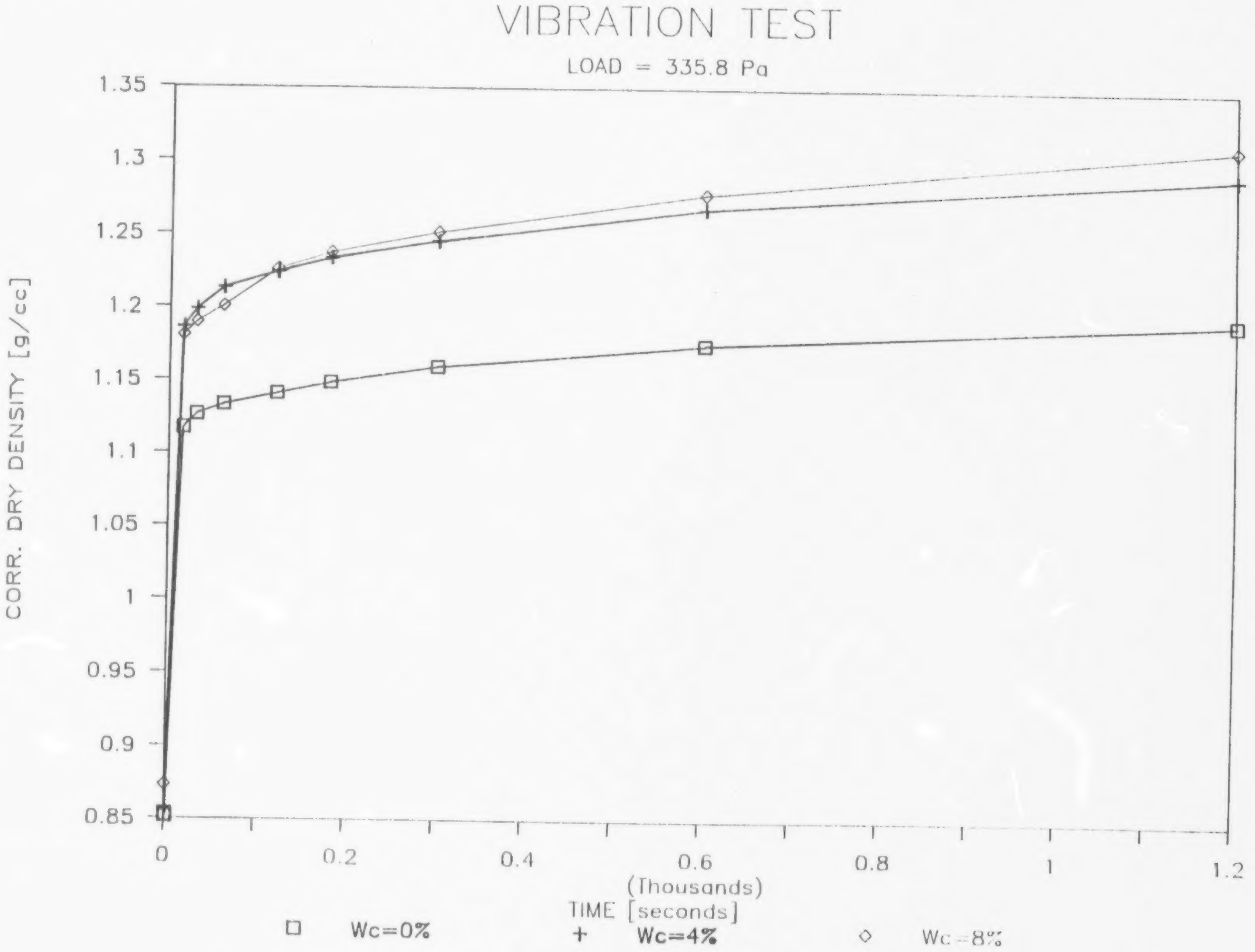
VIBRATION TEST
LOAD = 335.8 Pa
CORR. DRY DENSITY [g/cc]
1.35
1.3
1.25
1.2
1.15
1.1
1.05
1
0.95
0.9
0.85
0
0.2
0.4
0.6
0.8
1
1.2
(Thousands)
TIME [seconds]
□ Wc=0%
+ Wc=4%
◇ Wc=8%

VIBRATION TEST

LOAD = 3.9102 kPa

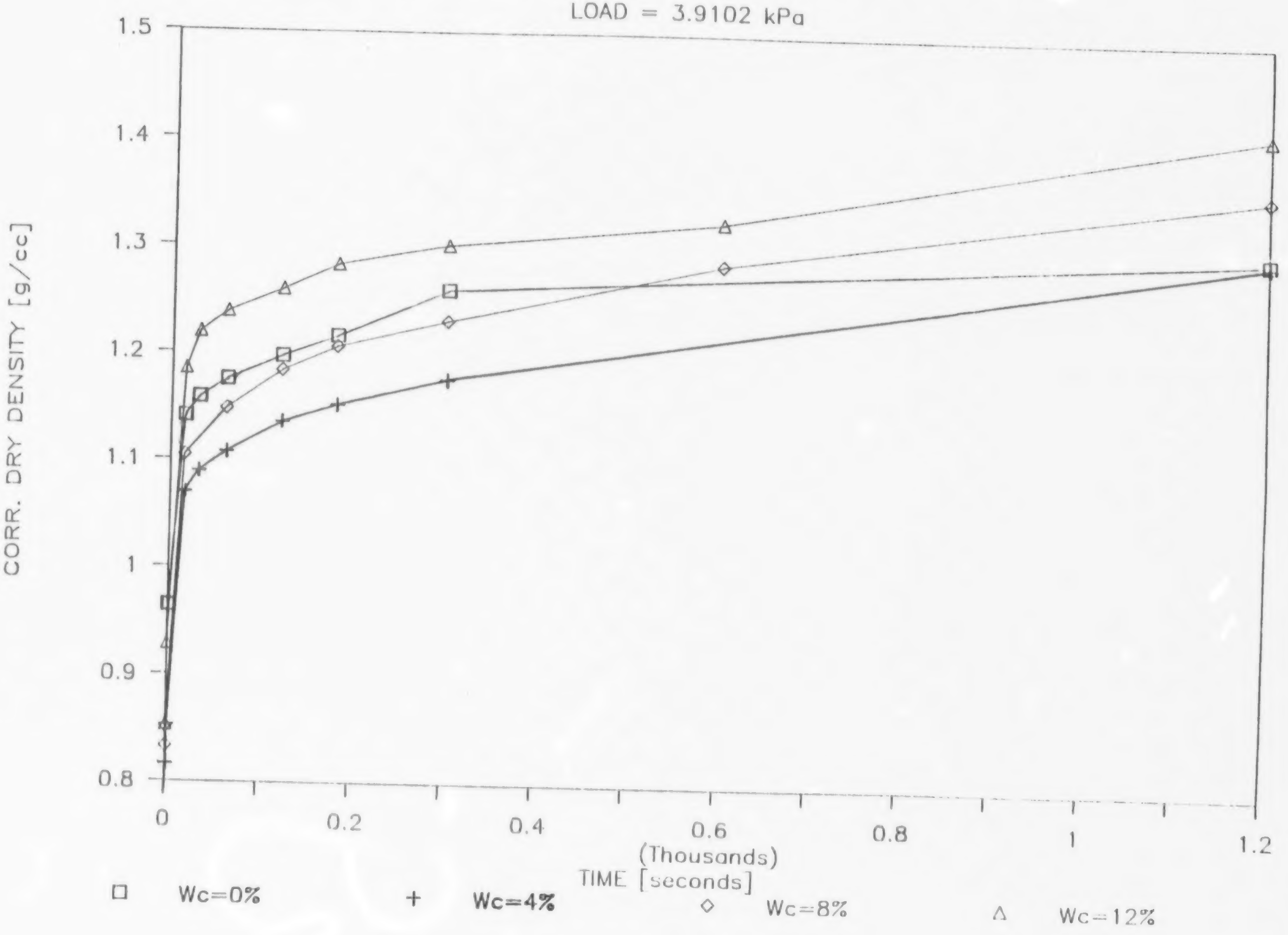

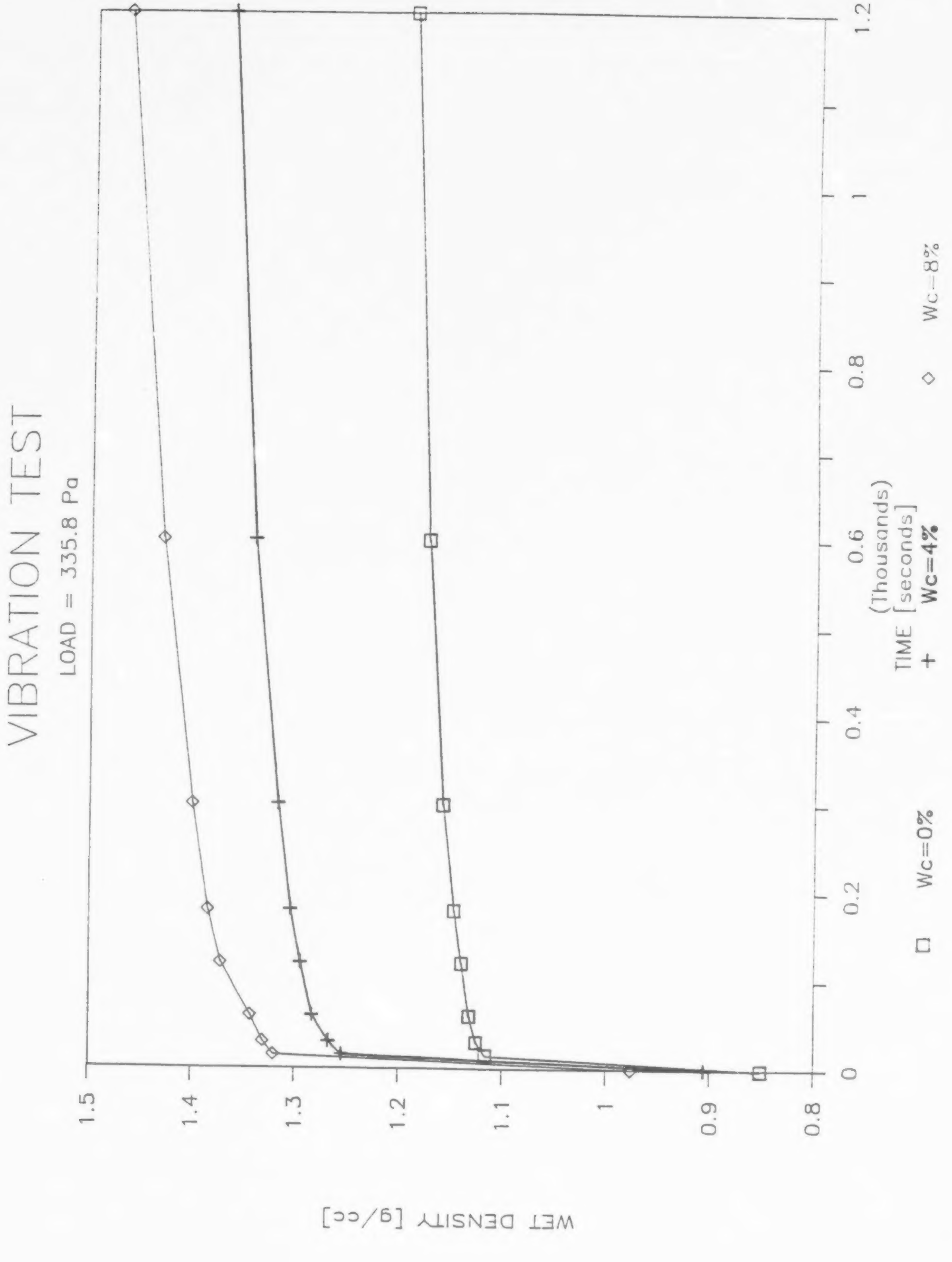

VIBRATION TEST

LOAD = 335.8 Pa

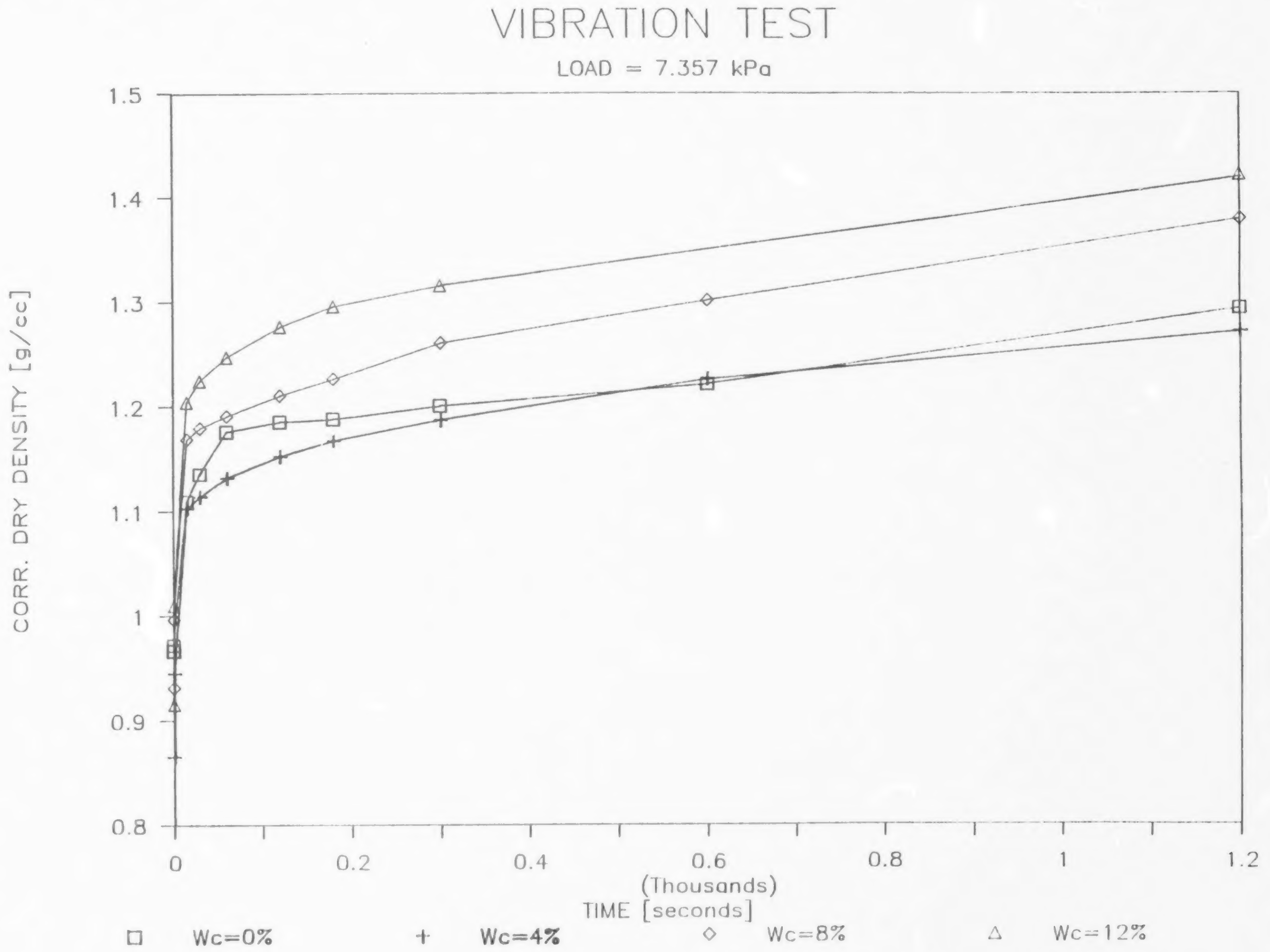
VIBRATION TEST
LOAD = 7.357 kPa
CORR. DRY DENSITY [g/cc]
1.5
1.4
1.3
1.2
1.1
1
0.9
0.8
0
0.2
0.4
0.6
0.8
1
1.2
(Thousands)
TIME [seconds]
□ Wc=0%
+ Wc=4%
◇ Wc=8%
△ Wc=12%

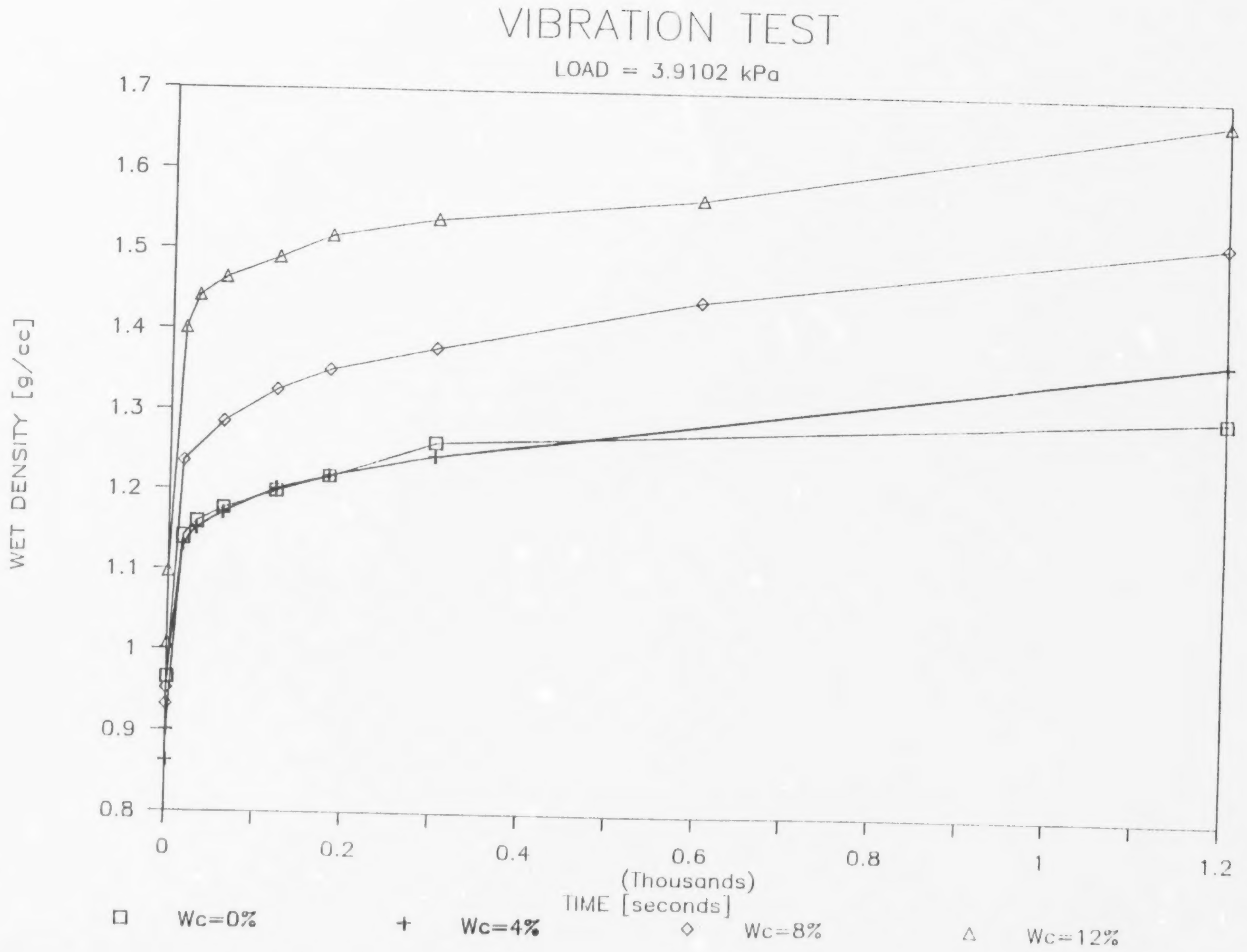
VIBRATION TEST
LOAD = 3.9102 kPa
WET DENSITY [g/cc]
1.7
1.6
1.5
1.4
1.3
1.2
1.1
1
0.9
0.8
0
0.2
0.4
0.6
0.8
1
1.2
(Thousands)
TIME [seconds]
□ Wc=0%
+ Wc=4%
◇ Wc=8%
△ Wc=12%

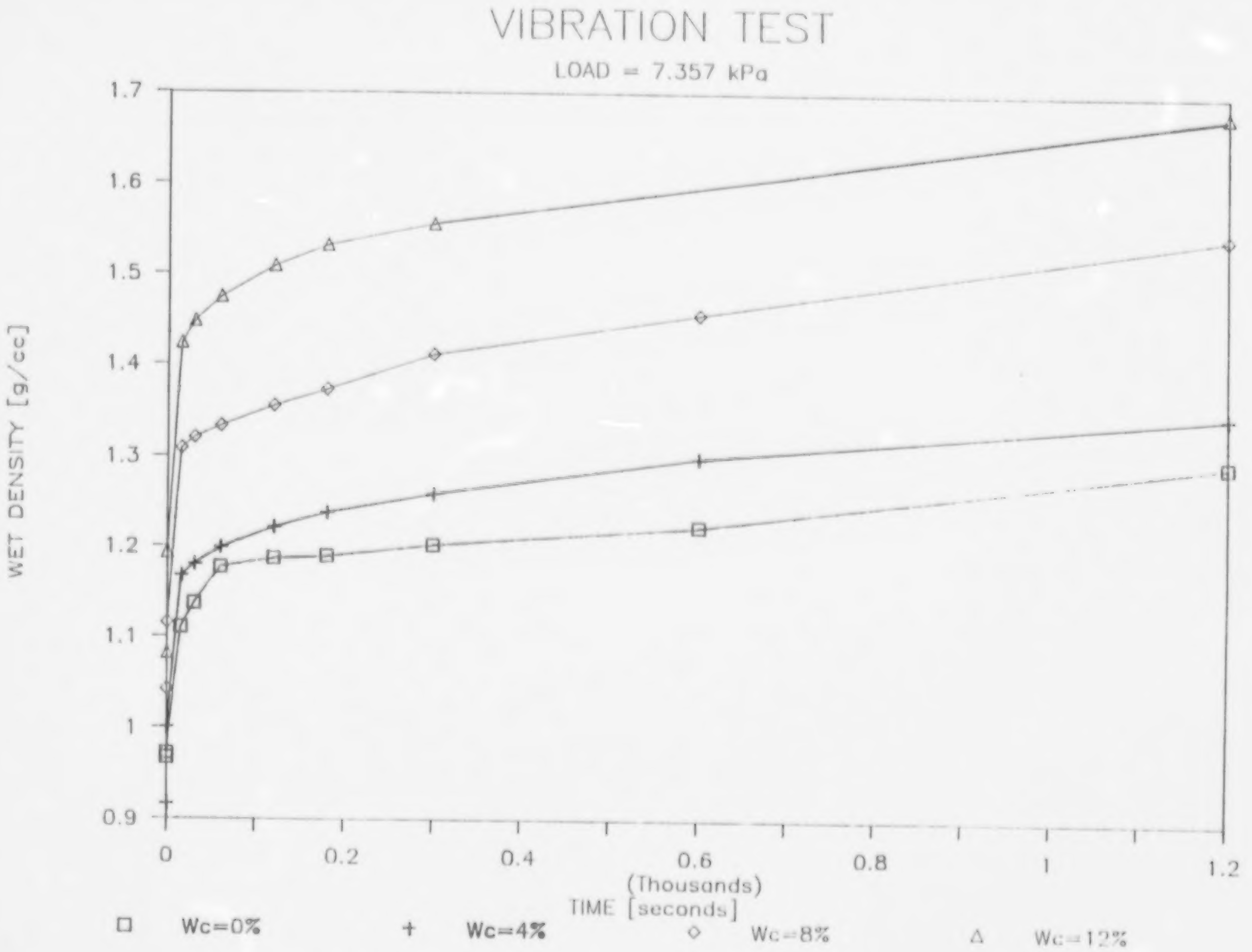
VIBRATION TEST
LOAD = 7.357 kPa
WET DENSITY [g/cc]
1.7
1.6
1.5
1.4
1.3
1.2
1.1
1
0.9
0
0.2
0.4
0.6
0.8
1
1.2
(Thousands)
TIME [seconds]
□ Wc=0%
+ Wc=4%
◇ Wc=8%
△ Wc=12%

APPENDIX IV: STATIC LOAD TEST RESULTS

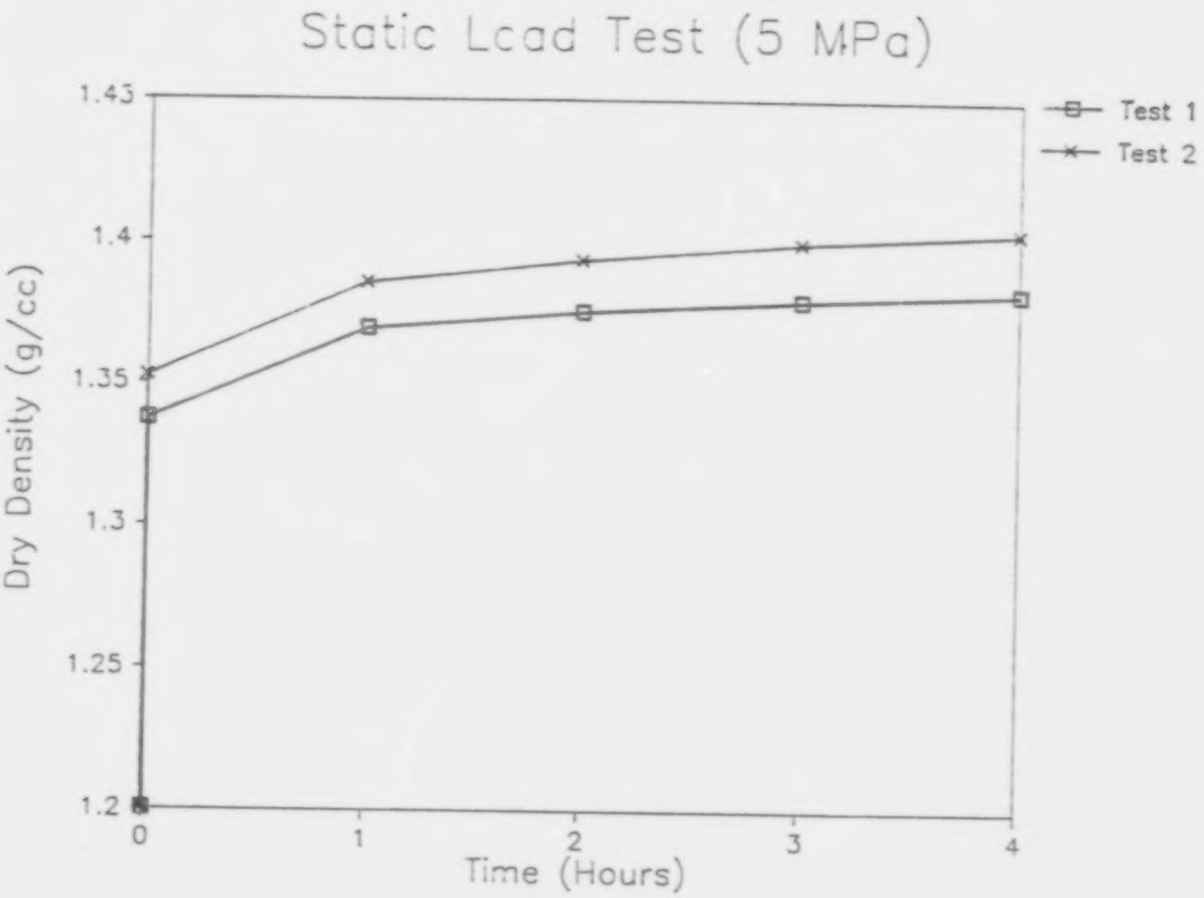
Static Lcad Test (5 MPa)
1.43
1.4
1.35
1.3
1.25
1.2
Dry Density (g/cc)
0
1
2
3
4
Time (Hours)
Test 1
Test 2

APPENDIX E

FIELD DENSITY TESTING
OF BACKFILL MATERIAL AT
DENISON-POTACAN POTASH COMPANY

OCTOBER, 1986

PREPARED FOR:

MRAZ PROJECT CONSULTANTS LIMITED
Saskatoon, Saskatchewan

PREPARED BY:

Shawn Munroe
DENISON-POTACAN POTASH COMPANY
Sussex, New Brunswick

TABLE OF CONTENTS

PAGE

LIST OF FIGURES AND TABLES ii

1. INTRODUCTION 1

2. PROCEDURE 2

3. DENSITY TESTING RESULTS 4

4. OBSERVATIONS 6

5. DISCUSSION 7

6. CONCLUSIONS 8

APPENDIX A: Reporting of Density Data on Salt Backfill 9

APPENDIX B: Sand-Cone Density Testing Procedure 13

APPENDIX C: Field Density Testing Data 17

APPENDIX D: Laboratory Density Testing Results 27

LIST OF FIGURES AND TABLES

List of Figures PAGE

FIGURE 1. Wagner ST-8A Scooptram 3

FIGURE 2. Portable Bomag Vibratory Roller 3

List of Tables

TABLE 1. Summary of Backfill Density Testing Results 5

1. INTRODUCTION

On September 18 - 19, 1986 dewaterd tailings material from the surface concentrator were supplied to the Surface Backfill Storage Building for compaction testing of the backfill material. A Wagner ST-8A scooptram and a portable Bomag vibratory roller were used to compact various size lifts of backfill material. It was originally intended to also use a commercial size vibratory roller to compact backfill material, however, time constraints did not permit this portion of the testing. Density testing was also conducted on tailings material which had been previously deposited in the surface tailings pond. The tailings were deposited in a slurried form and naturally compacted due to particle sedimentation.

The field compaction testing was conducted in an effort to determine the probable densities which may be achieved for the backfill material as it is placed and compacted in the underground workings. The densities which were obtained by the various compaction methods also provided data for comparison purposes with previous backfill compaction testing conducted at the University of Waterloo.

The sand-cone method to determine insitu density was used for the field density trials. All final densities were reported as corrected dry densities as described in Appendix A.

The report briefly describes the various methods of field compaction which were attempted and the subsequent results and observations made during the field density testing.

2. PROCEDURE

Approximately 100 tonnes of tailings material from the surface concentrator were deposited on the floor of the Surface Backfill Storage Building on September 18, 1986.

The backfill was spread into approximately 0.5 m lifts using a Wagner ST-8A scooptram. The backfill was compacted by running the scooptram over the backfill a minimum of ten passes. A lift was considered adequately compacted when no visible gain in compaction was evident under the scooptram's tires. Four 0.5 m lifts of backfill material were spread and compacted using the ST-8A scooptram. The ST-8A scooptram which weighs approximately 30 tonnes is shown in Figure 1.

Density tests were performed in a typical area of a lift after the compaction of the second and fourth lifts. Density tests were also conducted on the next day after initial compaction of the backfill to determine if the drainage of entrapped moisture in the backfill altered its initial compacted density.

A hand shovel was used to spread 75 mm lifts of backfill over a 3 m x 4 m area for compaction with a portable Bomag vibratory roller. The Bomag roller is shown in Figure 2. A minimum of ten passes were made with the vibratory roller for each lift. The first several passes were made without the vibratory action of the roller activated in order to allow the backfill to be slightly compacted prior to being vibrated. A total of five lifts were spread and compacted using the vibratory roller. Density tests were conducted after the compaction of the third and fifth lifts.

Density testing was also conducted on compacted tailings material in the surface tailings pond. The tailings material was deposited in the surface tailings pond in a slurried form where it compacts naturally due to particle sedimentation. The placement of the slurried tailings would be analogous to the hydraulic placement of backfill. Density testing was conducted in a well compacted "dry" area of the tailings pile which had been deposited for approximately four days.

The ASTM Standard Method of Test for "Density of Soil in Place by the Sand-Cone Method" was used for determining the density of the compacted backfill. The procedure used in the sand-cone method of density determination is described in Appendix B. The procedure as outlined was essentially followed with the exception being that representative samples were taken for moisture content analysis rather than drying the entire portion of wet material. This was necessary due to the absence of a portable stove for drying the wet material. The moisture content analyses were conducted at Denison-Potacan Metallurgical Laboratory.

Grade zero silica sand was used in the sand-cone density testing. The density of the silica sand was determined as described in Appendix B. A Mettler PL 6000 electronic balance was used for field mass measurements.

FIGURE - 1

WAGNER ST-8A SCOOPTRAM

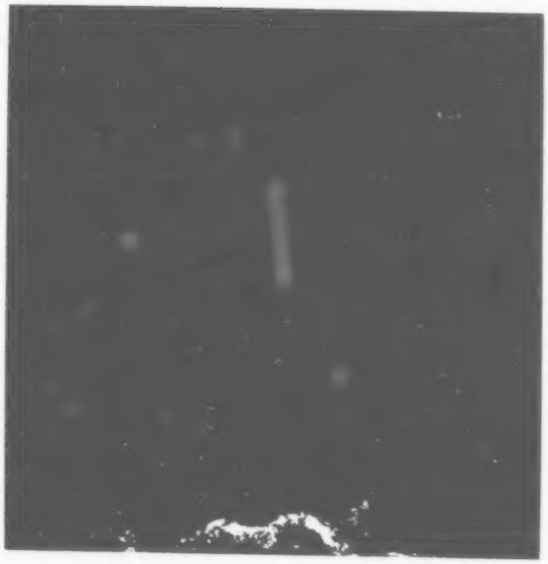

FIGURE - 2

PORTABLE BOMAG VIBRATORY ROLLER

3. DENSITY TESTING RESULTS

A summary of the density testing results are presented in Table 1. The field data and subsequent calculations are included in Appendix C.

Scooptram Compaction

The average density of a 0.45 m lift compacted with the Wagner ST-8A scooptram was 1310 kg/cu. m (1.31 t/cu. m). The density obtained on the day after initial compaction decreased 2.1 % with a 20 % reduction in moisture content.

The average density of a 1.2 m lift compacted with the Wagner ST-8A scooptram was 1448 kg/cu. m (1.448 t/cu. m). The density obtained on the day after initial compaction decreased 3.1 % with a 48 % reduction in moisture content.

Vibratory Roller Compaction

The average density of the lifts compacted with the portable Bomag vibratory roller were 1611 kg/cu. m (1.611 t/cu. m). No density tests were conducted the day after initial compaction of the backfill material with the vibratory roller.

Slurry Sedimentation Compaction

The average density of the tailings pond samples compacted by natural sedimentation processes were 1303 kg/cu. m (1.303 t/cu. m).

TABLE 1.

Summary of Backfill Density Testing Results

Test	Volume (cu. m)	Wet Wt. (g)	Wet Density (kg/cu. m)	Moisture Content *	Dry Wt. (g)	Corr. Dry Wt. (g) **	Dry Density (kg/cu. m)
ST-8A (0.45 m)	0.001475	2132.9	1446	6.6	2000.7	1953.2	1324
ST-8A (1.2 m)	0.001203	1981.2	1647	8.6	1824.7	1768.2	1470
ST-8A (0.45 m[b])	0.001135	1578.8	1391	5.3	1499.9	1471.3	1296
ST-8A (1.2 m[b])	0.001136	1714.4	1509	4.3	1644.1	1618.6	1425
Bomag (0.18 m)	0.001246	2239.0	1797	7.3	2086.7	2031.9	1631
Bomag (0.25 m)	0.001535	2662.9	1735	6.5	2500.5	2442.0	1591
Tailings Pond	0.000841	1173.5	1395	4.8	1119.5	1100.2	1308
Tailings Pond	0.000778	1092.0	1404	5.9	1030.8	1008.9	1297

Notes: [b] - indicates test conducted one day after initial compaction
* - moisture content is based upon dry weight
** - according to Appendix A

4. OBSERVATIONS

The following observations were made during the density testing procedure:

- The angle of repose for the tailings material, supplied to the Surface Backfill Plant from the surface concentrator, was estimated at approximately 35 to 45 degrees.

- The excavation of density testing holes was very easy in the freshly compacted material.

- The excavation of density testing holes on the next day after initial compaction was much more difficult than for the fresh material; a hammer and chisel were required to break through an approximate 2 cm section of hardened crust on the surface of the lift.

- The excavation of density testing holes in the surface tailings pond was extremely difficult; a hammer and chisel were required to break up the entire amount of material which was removed.

- Drainage of entrapped moisture in the backfill material began virtually immediately upon placement as the base of the bottom lift became saturated with brine within several hours of initial placement.

- Approximately 150 litres of brine were estimated to have been liberated from the 100 tonnes of tailings material placed in the Surface Backfill Plant.

- The tailings material as it substantially dried out began to behave much like sand having little or no compactive ability; the material simply crumbled rather than compacting together.

5. DISCUSSION

The density obtained by the use of the ST-8A scooptram to compact the backfill material varied significantly between the 0.45 m and the 1.2 m lifts. It was observed that during compaction of the initial 0.5 m lift that the lift compacted down to a 0.2 m height. This was due to the fact that minimal confinement of the lift was available during compaction. It was felt that the density obtained for the 0.45 m height lift (two - 0.5 m lifts) was less than that obtained for the 1.2 m height lift (four - 0.5 m lifts) due to the fact that a stable base of material had not formed during compaction. The 1.2 m height lift of material had a well developed compacted base thus allowing more compactive effort to be used for compaction rather than lateral displacement of the pile. The density tests for the 0.45 m height lift were conducted more on the edge of the pile rather than in the middle which may also explain the difference in densities which were obtained.

It would appear as though there exists an optimum moisture content for compaction of the backfill material. The three highest densities obtained had moisture contents all greater than 6.5 % while the three lowest obtained densities had moisture contents all less than 6 %. This would suggest that initial compaction of the backfill should take place as soon as possible after placement to avoid a significant drop in moisture content due to brine drainage.

The densities obtained from the field testing program tended to be greater than those obtained from laboratory testing conducted at the University of Waterloo. The density testing results obtained from the University of Waterloo are included in Appendix D. The field vibro-compaction testing averaged 1.611 t/cu. m at approximately seven percent moisture content compared with an average of 1.293 t/cu. m at eight percent moisture content for the laboratory testing. This would suggest that the laboratory vibro-compaction was not nearly as vigorous as that conducted with the portable roller at Denison-Potacan. In general, the density values obtained should be judged on the testing methods and circumstances under which they were conducted.

6. CONCLUSIONS

Field density testing was successfully completed using the sand-cone method of density determination. Vibro-compaction of the backfill material was found to provide the highest corrected dry densities. An average density of 1.611 t/cu. m was obtained using the portable Bomag roller. The average density obtained using a Wagner ST-8A for field compaction was 1.379 t/cu. m while slurry sedimentation compaction in the surface tailings pond averaged 1.303 t/cu. m.

APPENDIX A

Reporting of Density on Salt Backfill

The following is a typed version of a handwritten draft by M.B. Dusseault:

- Reporting of density data on salt backfill.
- In conventional rock or soil mechanics, where the mineral does not dissolve in the water, it is sufficient to report water content and "as is" density. This is not sufficient for halite backfill, as the fluid has dissolved salt in it at the saturation point.
- The best way to be consistent is to report the data differently than soils engineers.

I recommend:

a) Water content be expressed as a percentage of the dry mineral weight, as is the case for all soils and rock mechanics.

$$w = \text{water content in \%} = \frac{\text{weight loss on drying}}{\text{weight of dry mineral}}$$

In the lab:

A = Tare + wet material B = Tare + dry material

Weight loss $= A - B$

Dry Mineral $= B$ − Tare$(-w_t)$

$$w = \frac{A - B}{B - \text{Tare}} \cdot 100$$

b) All densities be reported as corrected dry density, wherein the density is corrected for the NaCl which was in solution when the water was in the liquid stage.

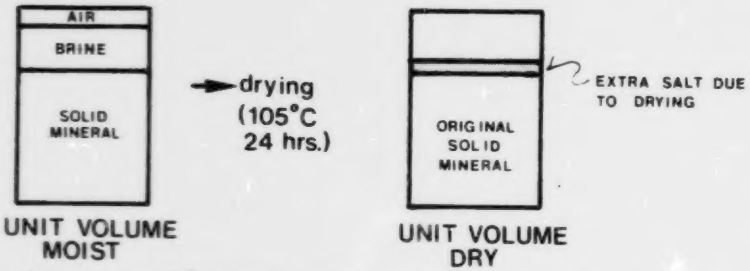
AIR
BRINE
SOLID MINERAL
drying
(105°C
24 hrs.)
ORIGINAL SOLID MINERAL
EXTRA SALT DUE TO DRYING
UNIT VOLUME MOIST
UNIT VOLUME DRY

This "extra" salt is an artifact of drying and does not enter into material behaviour in the in-situ state.

How to calculate corrected dry density:

- In a saturated brine, there are 36 grams NaCl dissolved in each 100 grams H_2O.

W_t = Total weight of dry solids (B - Tare from previous pages)

W_s = True mineral solid (when specimen was moist)

w = Moisture content in % H O of total dry mineral

$\therefore$ $W_s = W_t$ - Weight of salt which was in water

$$W_s = W_t - \frac{0.36 \cdot w \cdot W_t}{100} \qquad (w \text{ in } \%)$$

$$W_s = W_T \left(1 - \frac{0.36}{100} w\right)$$

$\therefore$ True dry density $= \frac{W_s}{Vol}$

APPENDIX B

Sand-Cone Density Testing Procedure

Designation 1556 – 64 (Reapproved 1968)

American National Standard A37.181-1972
Approved June 30, 1972
By American National Standards Institute

Standard Method of Test for

DENSITY OF SOIL IN PLACE BY THE SAND-CONE METHOD[1]

is Standard is issued under the fixed designation D 1556; the number immediately following the designation indicates the ar of original adoption or, in the case of revision, the year of last revision. A number in parentheses indicates the year of t reapproval

Scope

1.1 This method covers the determination of e in-place density of soils. The apparatus scribed herein is restricted to tests in soils ntaining particles not larger than 2 in. (50.8 m) in diameter.

Apparatus

2.1 *Density Apparatus*—The density apparatus shall consist of a 1-gal (4-litre) jar and a tachable appliance consisting of a cylindrical lve with an orifice ½ in. (12.7 mm) in ameter and having a small funnel continuing a standard *G* mason jar top on one end and a rge funnel on the other end. The valve shall ave stops to prevent rotating the valve past e completely open or completely closed posi- ons. The apparatus shall conform to the quirements shown in Fig. 1.

Note 1—The apparatus described here repre- nts a design that has proved satisfactory. Other pparatus of similar proportions will perform ually well so long as the basic principles of the nd volume determination are observed. This appa- atus, when full, can be used with test holes having a olume of approximately 0.1 ft³ (3 dm³). The base late shown in the drawing is optional, its use may ake leveling more difficult but permits test holes of rger diameter and may reduce loss in transferring il from test hole to container as well as afford a ore constant base for tests in soft soils. When the ase plate is used it shall be considered a part of the unnel in the procedures of this test method.

2.2 *Sand*—Any clean, dry, free-flowing, ncemented sand having few, if any, particles assing the No. 200 (75-μm) or retained on the o. 10 (2.00 mm) sieves. In selecting a sand r use several bulk density determinations hould be made using the same representative ample for each determination. To be accepta- le the sand shall not have a variation in bulk density greater than 1 percent.

2.3 *Balances*—A balance or scale of 10-kg capacity accurate to 1.0 g and a balance of 500-g capacity accurate to 0.1 g.

2.4 *Drying Equipment*—Stove or oven or other suitable equipment for drying moisture content samples.

2.5 *Miscellaneous Equipment*—Small pick, chisels, or spoons for digging test hole; 10-in. (254-mm) frying pan or any suitable container for drying moisture samples; buckets with lids, seamless tin cans with lids, canvas sacks or other suitable containers for retaining the density sample, moisture sample or density sand respectively; thermometer for determining the temperature of water, small paint-type brush, slide rule, note book, etc.

3. Procedure

3.1 Determine the volume of the jar and attachment up to and including the volume of the valve orifice as follows (Note 2):

3.1.1 Weigh the assembled apparatus and record.

3.1.2 Place the apparatus upright and open the valve.

3.1.3 Fill the apparatus with water until it appears over the valve.

3.1.4 Close valve and remove excess water.

3.1.5 Weigh the apparatus and water and determine the temperature of the water.

3.1.6 Repeat the procedure described 3.1.1 to 3.1.5 at least twice. Convert the weight of water, in grams, to millilitres by correcting for the temperature as given in 4.1. The volume shall be the average of three determinations with a maximum variation of 3 ml.

Note 2—The volume determined in this procedure is constant as long as the jar and attachment are in the same relative position. If the two are to be separated match marks should be made to permit reassembly to this position.

3.2 Determine the bulk density of the sand to be used in the field test as follows (Notes 3 and 4):

3.2.1 Place the empty apparatus upright on a firm level surface, close the valve, and fill the funnel with sand.

3.2.2 Open the valve and, keeping the funnel at least half full of sand, fill the apparatus. Close the valve sharply and empty excess sand.

3.2.3 Weigh the apparatus with sand and determine the net weight of sand by subtracting the weight of the apparatus.

Note 3—Vibration of the sand during any sand weight-volume determination may increase the bulk density of the sand and decrease the accuracy of the determination. Appreciable time intervals between the bulk density determination of the sand and its use in the field may result in change in the bulk density caused by a change in the moisture content or effective gradation.

Note 4—It is possible to determine the bulk density of the sand in other containers of known volume that dimensionally approximate the largest test hole that will be dug. The general procedure used is that given in 3.4 for determining the volume of the test hole. If this procedure is to be followed it shall be determined that the resulting bulk density equals that given by the jar determination.

3.3 Determine the weight of sand required to fill the funnel as follows (Notes 5 and 6):

3.3.1 Put sand in the apparatus and secure the weight of apparatus and sand.

3.3.2 Seat the inverted apparatus on a clean, level, plane surface.

3.3.3 Open the valve and keep open until after the sand stops running.

3.3.4 Close the valve sharply, weigh the apparatus with remaining sand, and determine the loss of sand. This loss represents the weight of sand required to fill the funnel.

3.3.5 Replace the sand removed in the funnel determination and close the valve.

Note 5—This determination may be omitted if the procedure given in Note 7 is followed. When the base plate is used it shall be considered a part of the funnel.

Note 6—Where test holes of maximum volume are desired it is possible, after the bulk density determination, to settle the sand by vibration and increase the weight of sand in the apparatus. If this procedure is followed, the total weight of sand available shall be determined by weighing.

3.4 Determine the density of the soil in place as follows:

3.4.1 Prepare the surface of the location to be tested so that it is a level plane.

3.4.2 Seat the inverted apparatus on the prepared plane surface and mark the outline of the funnel.

Note 7—In soils such that leveling is not successful a preliminary test shall be run at this point measuring the volume bounded by the funnel and ground surface. This step requires balances at the test site or emptying and refilling the apparatus. After this measurement is completed, carefully brush the sand from the prepared surface.

3.4.3 Dig the test hole inside the funnel mark, being very careful to avoid disturbing the soil that will bound the hole. Soils that are essentially granular require extreme care. Place all loosened soil in a container, being careful to avoid losing any material.

3.4.4 Seat the apparatus in the previously marked position, open the valve, and after the sand has stopped flowing, close the valve (Note 3).

3.4.5 Weigh the apparatus with remaining sand, and determine the weight of sand used in the test.

3.4.6 Weigh the material that was removed from the test hole.

3.4.7 Mix the material thoroughly and secure and weigh a representative sample for moisture determination.

3.4.8 Dry and weigh the moisture sample.

3.5 The minimum test hole volumes suggested in determining the in-place density of soil mixtures are given in Table 1. This table shows the suggested minimum weight of the moisture content sample in relation to the maximum particle size in soil mixtures.

4. Calculations

4.1 Calculate the volume of the density apparatus as follows:

$$V_1 = GT$$

where:

V_1 = volume of the density apparatus, ml,
G = water required to fill the apparatus, g,
T = water temperature volume correction shown in column 3 of Table 2.

4.2 Calculate the bulk density of the sand as follows:

---

[1] This method is under the jurisdiction of ASTM Committee D-18 on Soil and Rock for Engineering Purposes.
Current edition approved Aug. 31, 1964. Originally issued 1958. Replaces D 1556 – 58 T.

$$W_1 = 62.427\,W_2/V_1$$

where:

W_1 = bulk density of the sand, lb/ft³

W_2 = sand required to fill the apparatus (3.2.3) g, and

V_1 = volume of apparatus, (4.1)

4.3 Calculate the moisture content and the dry weight of material removed from the test hole as follows:

$$w = [(W_3 - W_4)/W_4] \times 100$$

$$W_6 = 0.2205\,W_5/(w + 100)$$

where:

w = percentage of moisture, in material from test hole.

W_3 = moist weight of moisture sample, g.

W_4 = dry weight of moisture sample, g.

W_5 = moist weight of the material from the test hole, g, and

W_6 = dry weight of material from test hole, lb.

TABLE 1 Minimum Test Hole Volumes and Minimum Moisture Content Samples Based on Maximum Size of Particle

Maximum Particle Size	Minimum Test Hole Volume, ft³	Minimum Moisture Content Sample, g
No. 4 Sieve (4.75 mm)	0.025	100
½ in (12.5 mm)	0.050	250
1 in (25 mm)	0.075	500
2 in (50 mm)	0.100	1000

4.4 Calculate the in-place dry density of the material tested as follows:

$$V = (W_7 - W_8)/453.6\,W_1$$

$$W = W_6/V$$

where:

V = volume of test hole, ft³

W_7 = sand used, g (3.4.5),

W_8 = sand in funnel (3.3.3) g, and

W = dry density of the tested material, lb/ft³

NOTE 8—It may be desired to express the in-place density as a percentage of some other density, for example, the laboratory maximum density determined in accordance with the Method D 698, Test for Moisture-Density Relations of Soils, Using a 5.5-lb (2.5-kg) Rammer and a 12-in. (304.8-mm) Drop.[6] This relation can be determined by dividing the in-place density by the maximum density and multiplying by 100.

TABLE 2 Volume of Water per Gram Based on Temperature

Temperature		Volume of Water, ml/g
deg C	deg F	
12	53.6	1.00048
14	57.2	1.00073
16	60.8	1.00103
18	64.4	1.00138
20	68.0	1.00177
22	71.6	1.00221
24	75.2	1.00268
26	78.8	1.00320
28	82.4	1.00375
30	86.0	1.00435
32	89.6	1.00497

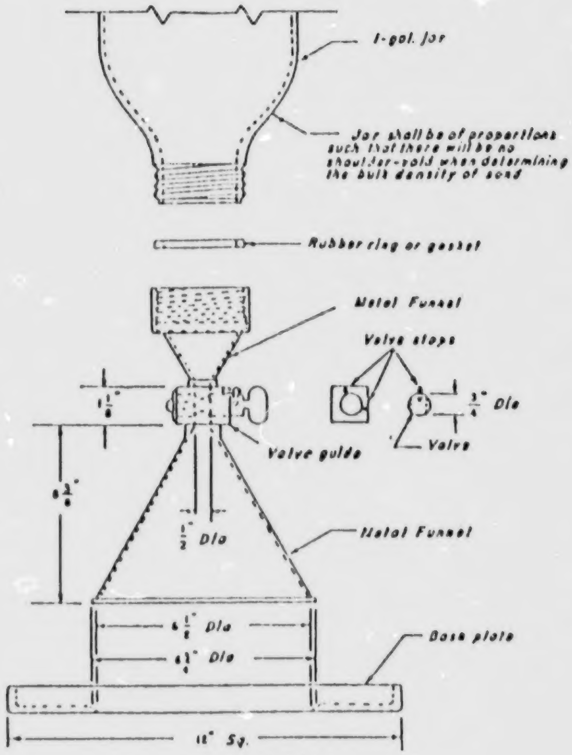
1-gal. jar
Jar shall be of proportions such that there will be no shoulder-void when determining the bulk density of sand
Rubber ring or gasket
Metal Funnel
Valve stops
½" Dia
Valve
1⅜"
Valve guide
6¾"
½" Dia
Metal Funnel
6½" Dia
6¾" Dia
Base plate
12" Sq.

Metric Equivalents

in.	mm	in.	mm
½	12.7	6½	165.1
¾	19.1	6¾	171.5
1⅛	28.6	12	304.8
5⅜	136.5		

FIG. 1 Density Apparatus.

By publication of this standard no position is taken with respect to the validity of any patent rights in connection therewith, and the American Society for Testing and Materials does not undertake to insure anyone utilizing the standard against liability for infringement of any Letters Patent nor assume any such liability.

---

[6] *Annual Book of ASTM Standards*, Part 11.

Part A-Sand Cone Method

PROCEDURE (All the steps except Step 4 are done in the Laboratory)

1. Determine the volume of the density jar as outlined in A.S.T.M. D 1556, Section 3.1 (This may be done at the end.)

2. Determine the bulk density of the sand, to be used in the test, as outlined in A.S.T.M. D 1556 Section 3.2

   Note that:

   - You should allow the sand to flow freely through the cone.
   - You should not tap or shake the jar to make it hold more sand.
   - You should do at least 3 trials and use the average value.

3. Determine the weight of sand required to fill the cone and the groove in the template as outlined in A.S.T.M. D 1556 Section 3.3

   Note that:

   - You should fit the template on the cone before placing the inverted apparatus on a level surface.

4. In the field, do the field density test as outlined in A.S.T.M. D 1556, Section 3.4.

   Note that:

   - You should fill the jar completely before going to the field.
   - You should place the template on the prepared level surface and excavate the hole within the hole in the template.

5. Do the calculations as outlined in A.S.T.M. D1556, Section 4.

APPENDIX C

Field Density Testing Data

Data and Calculations

(1) Volume of the Density Jar

Trial No.	1	2	3
Wt. of (Jar+Cone) (g)	1025.3	1025.4	1025.3
Wt. of (Jar+cone+water to fill Jar) (g)	2017.4	2017.4	2016.7
Wt. of water required to fill Jar, G (g)	992.1	992.0	991.4
Temperature of Water, °C	12°C	12°C	12°C
Corrected Volume of Jar, V_1=GT* (ml) (×1.0003)	992.3	992.2	991.6

* T is the water temperature-volume correction factor. (table 2, D1556)

Average value of Volume of Jar V_1 = 992.0 ml

(2) Bulk Density of the Sand used in the Test

Trial No.	1	2	3
Wt. of (Jar+Cone+Sand to fill Jar) (g)	2346.6	2344.9	2348.3
Wt. of (Jar+Cone) (g)	1025.2	1025.5	1025.5
Wt. of Sand to fill the Jar, W_2 (g)	1321.4	1319.4	1322.8
Bulk Density of Sand, γ =(W2/V1)1000 Kg/M³	1332	1330	1333

Average value of Bulk Density of the Sand, γ_s = Kg/M³ 1332

or γ_s = lb/ft³ 83

(3) Weight of Sand to fill the(Cone+the Groove in the Template), W_c

Trial No.	1	2	3
Wt. of(Jar+Cone+Sand to fill Jar) (g)	3444.1	3285.0	3342.8
Wt. of(Jar+Cone+Sand left in the Jar after filling Cone&Groove) (g)	1938.0	1779.9	1852.7
Wt. of(Sand to fill the Cone+the Groove in the Template). W_c (g)	1506.1	1505.1	1490.1

Average Wt. of(Sand to fill the Cone+the Groove in the

Template = W_c = 1500.4 ± 13 g

(4) Field Test Data and Calculations #1 STB (0.45m)

Wt. of(Jar+Cone+Sand to fill the Jar), A (g)	5959.9
Wt. of(Jar+Cone+Sand after filling the hole), B (g)	2495.1
Wt. of Sand used in the Test = (A-B) (g)	3464.8
Wt. of Sand to fill the Cone+the Groove, W_c (g)	1500.4
Wt. of Sand to fill the hole alone, $W_{sa} = A - B - W_c$ (g)	1964.4
Volume of the Test Hole, $V = \left(\frac{Wsa}{1000}\right) / \gamma_s$ (M^3)	0.001475

(5) Wet Density of the Soil, γ

Wt. of(Container+all the wet soil removed from the Hole 2493.8 g
Wt. of Container .... 360.9 g
Wt. of Wet Soil, W_5 (6.2% MOISTURE) .... 2132.9 g
Wet Density of the Soil, $\gamma = \left(\frac{W_5}{1000}\right)/V$ .... 1446 Kg/M^3

(4) Field Test Data and Calculations #2 ST3 (1.2m)

Wt. of(Jar+Cone+Sand to fill the Jar), A (g)	5960.1
Wt. of(Jar+Cone+Sand after filling the hole), B (g)	2857.8
Wt. of Sand used in the Test = (A-B) (g)	3102.3
Wt. of Sand to fill the Cone+the Groove, W_c (g)	1500.4
Wt. of Sand to fill the hole alone, $W_{sa}=A-B-W_c$ (g)	1601.9
Volume of the Test Hole, $V = \left(\frac{W_{sa}}{1000}\right)/\gamma_s$ (M^3)	0 001203

(5) Wet Density of the Soil, γ

Wt. of(Container+all the wet soil removed from the Hole 2342.1 g

Wt. of Container .... 360.9 g

Wt. of Wet Soil, W_5 (7.9 % MOISTURE) .... 1981.2 g

Wet Density of the Soil, $\gamma = \left(\frac{W_5}{1000}\right)/V$ .... 1647 Kg/M^3

(4) Field Test Data and Calculations # 3 STB (0.45m (b))

Wt. of(Jar+Cone+Sand to fill the Jar), A (g)	6030.8
Wt. of(Jar+Cone+Sand after filling the hole), B (g)	3063.5
Wt. of Sand used in the Test = (A-B) (g)	3012.3
Wt. of Sand to fill the Cone+the Groove, W_c (g)	1500.4
Wt. of Sand to fill the hole alone, $W_{sa}=A-B-W_c$ (g)	1511.9
Volume of the Test Hole, $V = \left(\frac{W_{sa}}{1000}\right)/\gamma_s$ (M^3)	0.001135

(5) Wet Density of the Soil, γ

Wt. of(Container+all the wet soil removed from the Hole 1942.3 g

Wt. of Container .... 363.5 g

Wt. of Wet Soil, W_5 .(5% MOISTURE)................................ 1578.8g

Wet Density of the Soil, $\gamma = \left(\frac{W_5}{1000}\right)/V$ .... 139 Kg/M^3

(4) Field Test Data and Calculations #4 STB (1.2m (b))

Wt. of(Jar+Cone+Sand to fill the Jar), A (g)	5980.0
Wt. of(Jar+Cone+Sand after filling the hole), B (g)	2966.0
Wt. of Sand used in the Test = (A-B) (g)	3014.0
Wt. of Sand to fill the Cone+the Groove, W_c (g)	1500.4
Wt. of Sand to fill the hole alone, $W_{sa} = A-B-W_c$ (g)	1513.6
Volume of the Test Hole, $V = \left(\frac{Wsa}{1000}\right) / \gamma_s$ (M^3)	0.001136

(5) Wet Density of the Soil, γ

Wt. of(Container+all the wet soil removed from the Hole 2077.2g

Wt. of Container 362.8g

Wt. of Wet Soil, W_5 .(4.1% MOISTURE)..................... 1714.4g

Wet Density of the Soil, $\gamma = \left(\frac{W_5}{1000}\right)/V$ .... 1509 Kg/M^3

(4) Field Test Data and Calculations #5 BOMAG (0.180 m)

Wt. of(Jar+Cone+Sand to fill the Jar), A (g)	6018.5
Wt. of(Jar+Cone+Sand after filling the hole), B (g)	2858.8
Wt. of Sand used in the Test = (A-B) (g)	3159.7
Wt. of Sand to fill the Cone+the Groove, W_c (g)	1500.4
Wt. of Sand to fill the hole alone, $W_{sa}=A-B-W_c$ (g)	1659.3
Volume of the Test Hole, $V = \left(\frac{Wsa}{1000}\right)/\gamma_s$ (M^3)	0.001246

(5) Wet Density of the Soil, γ

Wt. of(Container+all the wet soil removed from the Hole 2601.6g

Wt. of Container 362.6g

Wt. of Wet Soil, W_s (6.8% MOISTURE)............... 2239.0g

Wet Density of the Soil, $\gamma = \left(\frac{W_s}{1000}\right)/V$ .... 1797 Kg/M^3

(4) Field Test Data and Calculations #6 BOMAG (0.250 m)

Wt. of(Jar+Cone+Sand to fill the Jar), A (g)	5996.0
Wt. of(Jar+Cone+Sand after filling the hole), B (g)	2450.6
Wt. of Sand used in the Test = (A-B) (g)	3545.4
Wt. of Sand to fill the Cone+the Groove, W_c (g)	1500.4
Wt. of Sand to fill the hole alone, $W_{sa}=A-B-W_c$ (g)	2045.0
Volume of the Test Hole, $V = \left(\frac{Wsa}{1000}\right)/\gamma_s$ (M^3)	0.001535

(5) Wet Density of the Soil, γ

Wt. of(Container+all the wet soil removed from the Hole 3025.7g

Wt. of Container 362.8g

Wt. of Wet Soil, W_5 ..(6.1% MOISTURE)............... 2662.9g

Wet Density of the Soil, $\gamma = \left(\frac{W_5}{1000}\right)/V$ .... 1735 Kg/M^3

(4) Field Test Data and Calculations TAILINGS POND (#7)

Wt. of(Jar+Cone+Sand to fill the Jar), A (g)	5609.8
Wt. of(Jar+Cone+Sand after filling the hole), B (g)	2989.6
Wt. of Sand used in the Test = (A-B) (g)	2620.2
Wt. of Sand to fill the Cone+the Groove, W_c (g)	1500.4
Wt. of Sand to fill the hole alone, $W_{sa}=A-B-W_c$ (g)	1119.8
Volume of the Test Hole, $V = \left(\frac{W_{sa}}{1000}\right)/\gamma_s$ (M^3)	0.000854

(5) Wet Density of the Soil, γ

Wt. of(Container+all the wet soil removed from the Hole 1559.2 g

Wt. of Container .... 365.7 g

Wt. of Wet Soil, W_5 (4.6% MOISTURE) .... 1193.5 g

Wet Density of the Soil, $\gamma = \left(\frac{W_5}{1000}\right)/V$ .... 1395 Kg/M^3

(4) Field Test Data and Calculations TAILINGS POND (#3)

Wt. of(Jar+Cone+Sand to fill the Jar), A (g)	5735.9
Wt. of(Jar+Cone+Sand after filling the hole), B (g)	3199.6
Wt. of Sand used in the Test = (A-B) (g)	2536.3
Wt. of Sand to fill the Cone+the Groove, W_c (g)	1500.4
Wt. of Sand to fill the hole alone, W_{sa}=A-B-W_c (g)	1035.9
Volume of the Test Hole, $V = \left(\frac{W_{sa}}{1000}\right)/\gamma_s$ (M^3)	0.000778

(5) Wet Density of the Soil, γ

Wt. of(Container+all the wet soil removed from the Hole 1457.7 g

Wt. of Container .... 365.7 g

Wt. of Wet Soil, W_5 (5.6% MOISTURE) .... 1092.0 g

Wet Density of the Soil, $\gamma = \left(\frac{W_5}{1000}\right)/V$ .... 1404 Kg/M^3

APPENDIX D

Laboratory Density Testing Results

65.

MATERIAL TEST RESULTS JULY, 1986
DENISON-POTACAN BACKFILL RESEARCH PROJECT
MRAZ PROJECT CONSULTANTS

A. PROCTOR

Water (%)	Wet	Corrected Dry Wt.
4	1.36	1.285
8	1.46	1.305
10	1.49	1.296
12	1.53	1.295
14	1.57	1.295
16	1.64	1.315

B. VIBRO-COMPACTION

Water %	#1 Weight		#2 Weight		#3 Weight	
	Dry (Corr.)	Wet	Dry (Corr.)	Wet	Dry (Corr.)	Wet
0	1.19	1.19	1.29	1.29	1.26	1.26
4	1.29	1.37	1.2	1.27	1.3	1.37
8	1.31	1.47	1.22	1.37	1.35	1.5
12					1.39	1.64

C. DROP TESTS

Moisture	1.0m		2.0m		3.0m		4.0m	
	Corrected		Corrected		Corrected		Corrected	
	Dry	Wet	Dry	Wet	Dry	Wet	Dry	Wet
0	1.03	1.03	1.06	1.06	1.06	1.06	1.11	1.11
4	0.91	0.86	1	0.95	1.03	0.93	1.12	1.06
8	1	0.89	1.05	0.94	1.1	0.98	1.2	1.07
12	1.08	0.92	1.08	0.91	1.17	0.99	1.35	1.14

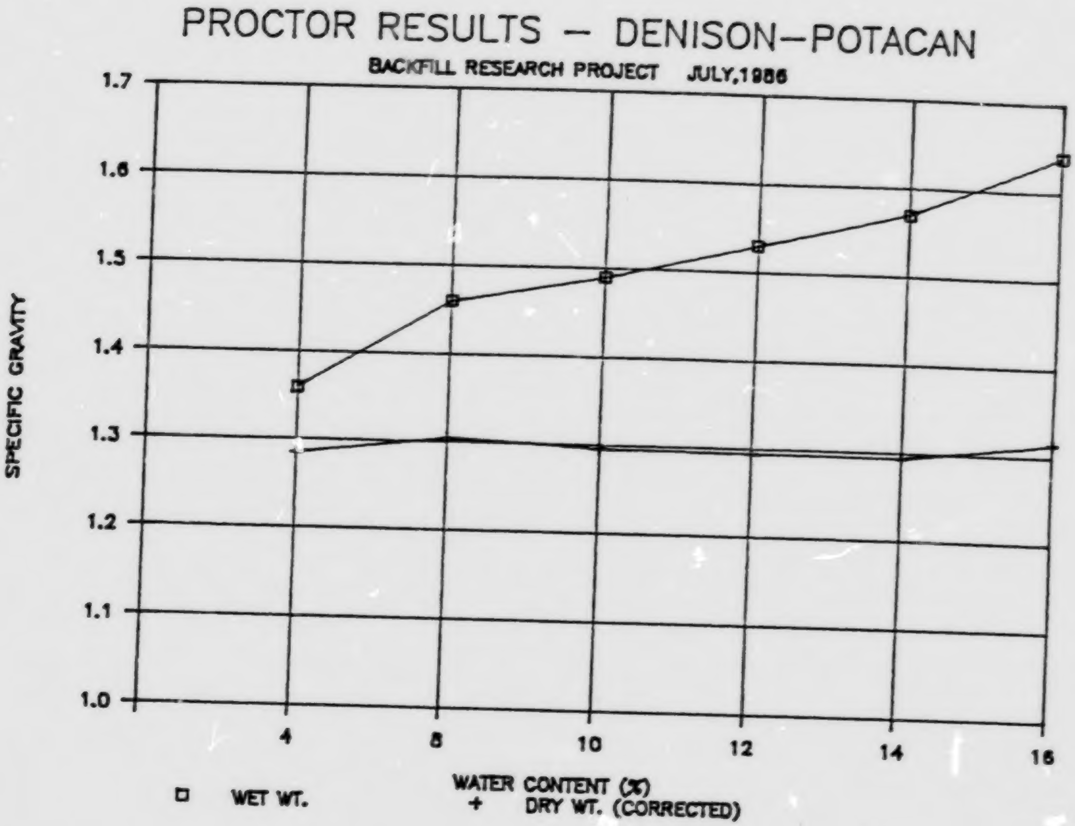
PROCTOR RESULTS – DENISON–POTACAN
BACKFILL RESEARCH PROJECT JULY,1986
SPECIFIC GRAVITY
1.7
1.6
1.5
1.4
1.3
1.2
1.1
1.0
4
8
10
12
14
16
WATER CONTENT (%)
□ WET WT.
+ DRY WT. (CORRECTED)

VIBRO-COMP. (WET) DENISON-POTACAN

BACKFILL RESEARCH PROJECT JULY,1986

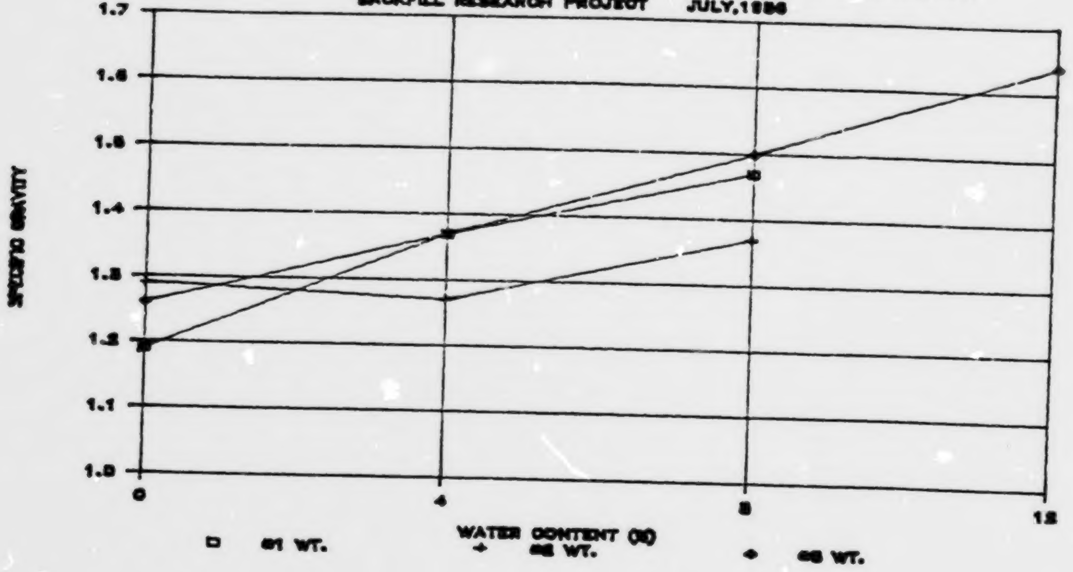

VIBRO-COMP. (DRY) DENISON-POTACAN

BACKFILL RESEARCH PROJECT JULY,1986

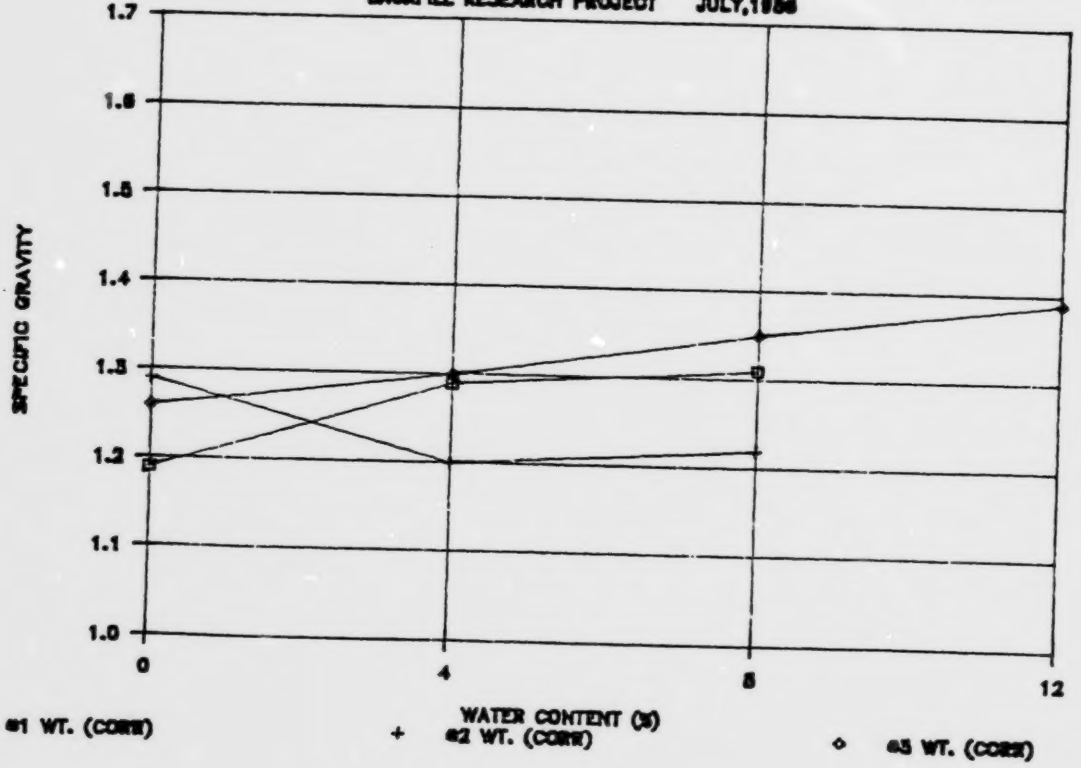

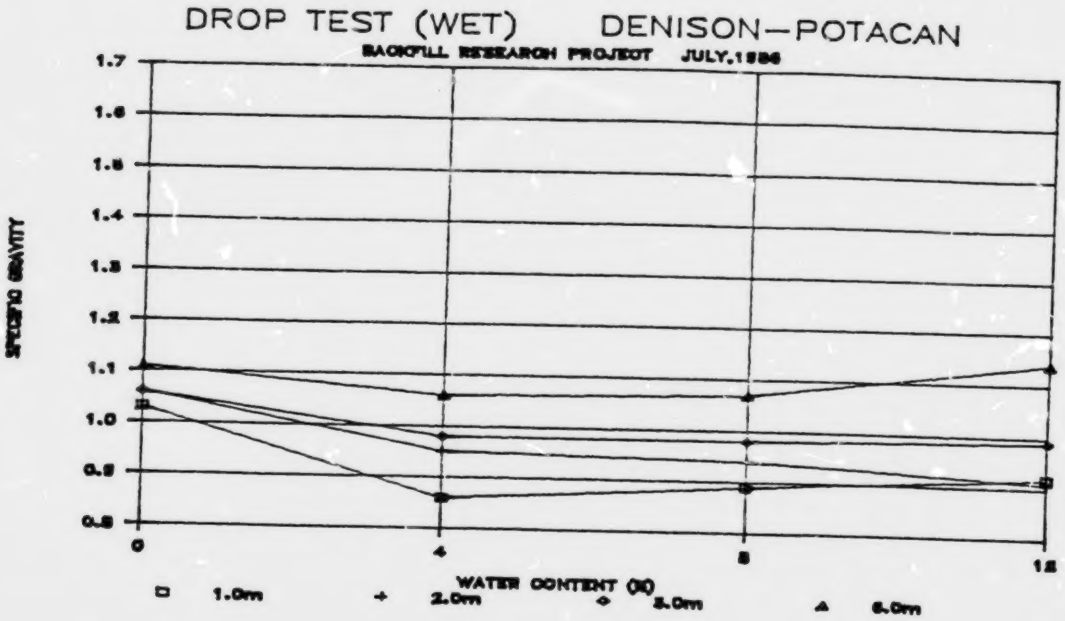

DROP TEST (WET) DENISON—POTACAN

BACKFILL RESEARCH PROJECT JULY,1986

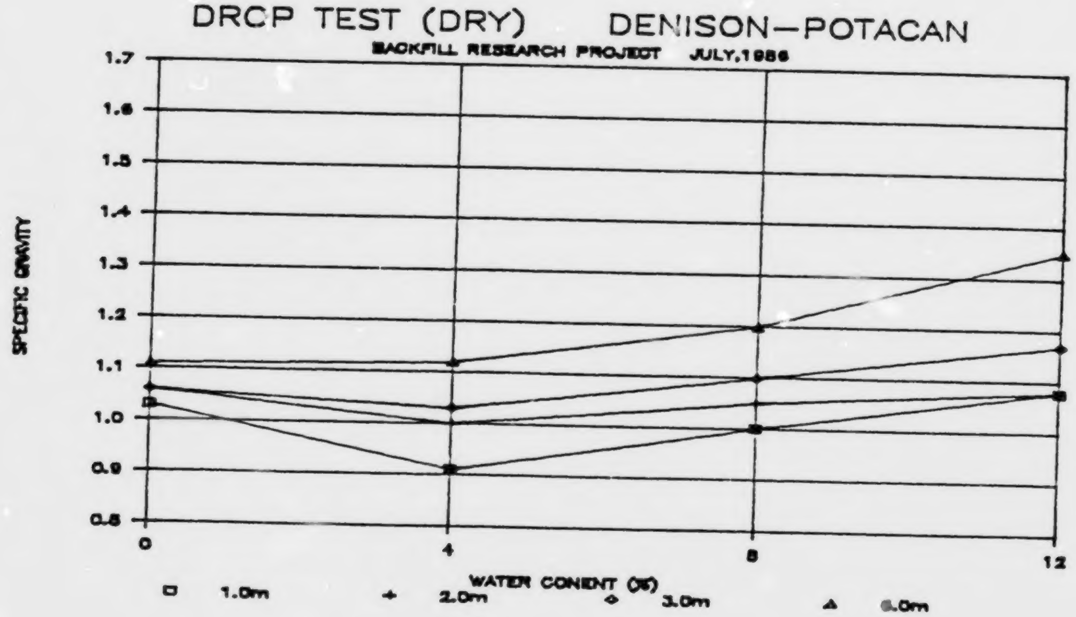

DRCP TEST (DRY) DENISON—POTACAN

BACKFILL RESEARCH PROJECT JULY,1986

Volume
3

Energy, Mines and
Resources Canada

Énergie, Mines et
Ressources Canada

CANMET

Canada Centre
for Mineral
and Energy
Technology

Centre canadien
de la technologie
des minéraux
et de l'énergie

POTASH MINING PROJECT

PROJET D'EXPLOITATION DE LA POTASSE

[illegible] SUR LES MINÉRAUX
[illegible]ERCHE MINIÈRE

USE OF BACKFILL IN NEW BRUNSWICK POTASH MINES

VOLUME 3

IN-SITU TESTING

May, 1987

Final Report By:

DENISON-POTACAN POTASH COMPANY
Sussex, New Brunswick

Prepared by:

MRAZ PROJECT CONSULTANTS LTD
Saskatoon, Saskatchewan

- and -

S. MUNROE
Denison-Potacan Potash Company
Sussex, New Brunswick

Work on the Project was conducted under the auspices of the Canada Centre for Mineral and Energy Technology, Energy, Mines and Resources Canada, funded as part of the Canada/New Brunswick Mineral Development Agreement.

DSS FILE NO: 14SQ.23440-5-9031

DSS CONTRACT SERIAL NO: 0SQ85-00208

CANMET PROJECT NO: 1.4.09.05

CANMET SCIENTIFIC AUTHORITY: Dr. G. Herget

125pp

MICROMEDIA

USE OF BACKFILL IN NEW BRUNSWICK POTASH MINES

VOLUME 3
IN-SITU TESTING

TABLE OF CONTENTS

1.0 SUMMARY

2.0 INTRODUCTION

3.0 ROCK MECHANICS SITES AND RECORD OF IN-SITU DATA

3.1 ROCK MECHANICS STATION

3.2 TEST STOPE

3.3 STOPE 1105

3.4 STOPE 1003

4.0 ROCK MECHANICS INSTRUMENTATION

4.1 MEASUREMENT OF CLOSURE

4.2 MEASUREMENT OF STRAIN

4.3 MEASUREMENT OF STRESS

5.0 100 MM DIAMETER CORE SAMPLING

6.0 SURFACE SUBSIDENCE MONITORING

APPENDIX A

APPENDIX B

APPENDIX C

LIST OF FIGURES

FIGURE 3.0 GENERAL MINE LAYOUT SHOWING ROCK MECHANICS SITES

FIGURE 3.1 ROCK MECHANICS INSTRUMENTATION IN TEST ROOM

FIGURE 3.2 EVALUATION OF ROCK MECHANICS TEST ROOM AS OF JULY 16, 1985

FIGURE 3.3 EVALUATION OF ROCK MECHANICS TEST ROOM AS OF DECEMBER 30, 1986

FIGURE 3.4 ROCK MECHANICS STATION TOTAL VERTICAL CLOSURE (A)

FIGURE 3.5 ROCK MECHANICS STATION TOTAL VERTICAL CLOSURE (B)

FIGURE 3.6 ROCK MECHANICS STATION TOTAL HORIZONTAL CLOSURE (A)

FIGURE 3.7 ROCK MECHANICS STATION TOTAL HORIZONTAL CLOSURE (B)

FIGURE 3.8 ROCK MECHANICS STATION TOTAL DIAGONAL CLOSURE

FIGURE 3.9 TEST STOPE ROCK MECHANICS INSTRUMENTATION

FIGURE 3.10 GENERAL ARRANGEMENT MEASUREMENT OF ABSOLUTE VERTICAL CLOSURE USING WIRE AND PULLEY METHOD IN TEST STOPE

FIGURE 3.11 GENERAL ARRANGEMENT MEASUREMENT OF ABSOLUTE HORIZONTAL CLOSURE USING WIRE AND PULLEY METHOD IN TEST STOPE

FIGURE 3.12 INSTALLATION ARRANGEMENT, RELATIVE CLOSURE STATIONS

FIGURE 3.13 TEST STOPE TOTAL CLOSURE, VERTICAL AND HORIZONTAL

FIGURE 3.14 TEST STOPE VERTICAL RELATIVE CLOSURE

FIGURE 3.15 TEST STOPE (SRC EXTENSOMETER) VERTICAL RELATIVE CLOSURE

FIGURE 3.16 TEST STOPE HORIZONTAL RELATIVE CLOSURE

FIGURE 3.17 TEST STOPE LATERAL PRESSURE CELLS (ROOF)

FIGURE 3.18 TEST STOPE TANGENTIAL PRESSURE CELLS (ROOF)

FIGURE 3.19 TEST STOPE LATERAL PRESSURE CELLS (WALLS)

FIGURE 3.20 TEST STOPE VERTICAL PRESSURE CELLS (WALLS)

FIGURE 3.21 STOPE 1105 ROCK MECHANICS INSTRUMENTATION LAYOUT

FIGURE 3.22 STOPE 1105 VERTICAL RELATIVE CLOSURE

FIGURE 3.23 STOPE 1003 BEARING PILLAR ROCK MECHANICS INSTRUMENTATION

FIGURE 3.24 1988 SUBSIDENCE SURVEY

LIST OF TABLES

TABLE 3.1	ROCK MECHANICS STATION (TEST ROOM)-DETERMINATION OF CLOSURE RATES FOR ROOF AND FLOOR
TABLE 3.2	ROCK MECHANICS STATION (TEST ROOM)-DETERMINATION OF CLOSURE RATES FOR WALLS
TABLE 3.3	ROCK MECHANICS STATION (TEST ROOM)-DETERMINATION OF CLOSURE RATES FOR DIAGONALS
TABLE 3.4	ROCK MECHANICS STATION-VERTICAL TOTAL CLOSURE (A)
TABLE 3.5	ROCK MECHANICS STATION-VERTICAL TOTAL CLOSURE (B)
TABLE 3.6	ROCK MECHANICS STATION-HORIZONTAL TOTAL CLOSURE (A)
TABLE 3.7	ROCK MECHANICS STATION-HORIZONTAL TOTAL CLOSURE (B)
TABLE 3.8	ROCK MECHANICS STATION-DIAGONAL TOTAL CLOSURE
TABLE 3.9	TEST STOPE VERTICAL TOTAL CLOSURE
TABLE 3.10	TEST STOPE-HORIZONTAL TOTAL CLOSURE
TABLE 3.11	TEST STOPE 2.5 M DEEP ANCHOR IN ROOF-RELATIVE CLOSURE
TABLE 3.12	TEST STOPE 5.0 M DEEP ANCHOR IN ROOF-RELATIVE CLOSURE
TABLE 3.13	TEST STOPE 5, 10, 15, 20, 25 AND 30 M DEEP ANCHORS IN ROOF-RELATIVE CLOSURE
TABLE 3.14	TEST STOPE 0.5 M DEEP ANCHOR IN WALL-CLOSURE
TABLE 3.15	TEST STOPE 1.25 M DEEP ANCHOR IN WALL-RELATIVE CLOSURE
TABLE 3.16	TEST STOPE 2.5 M DEEP ANCHOR IN WALL-RELATIVE CLOSURE
TABLE 3.17	TEST STOPE 3.75 M DEEP ANCHOR IN WALL-RELATIVE CLOSURE
TABLE 3.18	TEST STOPE 5.00 M DEEP ANCHOR IN WALL-RELATIVE CLOSURE
TABLE 3.19	TEST STOPE LATERAL PRESSURE CELLS IN ROOF
TABLE 3.20	TEST STOPE TANGENTIAL PRESSURE CELLS IN ROOF
TABLE 3.21	TEST STOPE LATERAL PRESSURE CELLS IN WALL
TABLE 3.22	TEST STOPE VERTICAL PRESSURE CELLS IN WALL
TABLE 3.23	STOPE 1105 - 5, 7.5, 10, 15 AND 20 M DEEP ANCHORS IN ROOF-RELATIVE CLOSURE

LIST OF TABLES
(Continued)

TABLE 5.1 CORE LOG SHEET - HOLE NO. 1

TABLE 5.2 CORE LOG SHEET - HOLE NO. 2

TABLE 5.3 CORE LOG SHEET - HOLE NO. 3

TABLE 5.4 CORE LOG SHEET - HOLE NO. 4

TABLE 5.5 CORE LOG SHEET - HOLE NO. 5

TABLE 6.1 SUBSIDENCE SURVEY RESULTS (1986)

LIST OF APPENDICES

APPENDIX A ROCK MECHANICS INSTRUMENTATION EQUIPMENT

APPENDIX B 100 MM DIAMETER CORE SAMPLING

APPENDIX C SURFACE SUBSIDENCE MONUMENT

SECTION 1.0

1.0 SUMMARY

This volume describes in-situ testing work carried out and the results obtained at the Denison-Potacan mine, both before and during the project conducted under the auspices of CANMET.

A complete record of in-situ rock mechanics data and analysis is provided for stations established as early as February, 1983.

This data, combined with the results of the laboratory testing work previously described in Volume 2, form the basic parameters for both developing and calibrating the numerical model used to analyze mining and backfilling alternatives.

SECTION 2.0

2.0 INTRODUCTION

The significance and value of collecting and analyzing in-situ rock mechanics data was recognized and acted upon by Denison-Potacan as early as 1982, leading to the establishment of the Rock Mechanics Station (Test Room) in February, 1983.

An extensive underground exploration program led to a decision in 1983 to develop the property into a producing mine capable of producing 1.3 million tonnes of product per year. Potash production commenced in July, 1985.

During this time, and to the present day, Denison-Potacan have installed, monitored and analyzed in detail the data from the following sites:

- Rock Mechanics Station Test Room first established February 7, 1983;
- Test Stope Station, first established January 8, 1984;
- Stope 1105 Station, first established August 6, 1986.

These Rock Mechanics Stations were established recognizing that in order to optimize the extraction ratio for the Denison-Potacan deposit the in-situ rock mechanics information was essential.

This included determining the stress-strain distributions around both active mining and test room sites, as well as defining basic material properties. The installation of appropriate rock mechanics instrumentation allowed stress-strain data to be collected.

Basic material properties were determined from the laboratory testing of 100 mm diameter core samples at the University of Waterloo, previously described in Volume 2. The core samples were obtained from the Denison-Potacan mine site to develop and refine material deformation characteristics and their time-related behaviour.

An important component of mining operations at Denison-Potacan is the placement of tailings backfill in the mined out underground workings. The placement of tailings backfill underground allows for an environmentally safe tailings disposal method, as well as the potential of increased recovery of potash resources through secondary pillar recovery.

The collection of the appropriate rock mechanics field data and the determination of basic material properties are the fundamental ingredients or parameters both for developing and calibrating a representative computer analysis (through numerical modelling) of mining and backfilling alternatives.

This volume describes the in-situ data testing program, data collection and analyses used with other research work to evaluate the use of backfill in New Brunswick potash mines.

SECTION 3.0

3.0 ROCK MECHANICS SITES AND RECORD OF IN-SITU DATA

The rock mechanics instrumentation sites used in the 1986 field test program are shown in Figure 3.0. The instrumentation sites include previously excavated rock mechanics test sites (Rock Mechanics Station - Test Room, 1982 and Test Stope, 1983) and present active mining sites (Stope 1105 and Stope 1003). The initial proposed active mining instrumentation site in Stope 1004 had to be abandoned due to delays associated with stope excavation which necessitated choosing Stope 1105 as an alternative active mining instrumentation site.

3.1 ROCK MECHANICS STATION

The test room known as the Rock Mechanics Station (Test Room) was excavated in late 1982 within a 30 m thick vertical limb of the ore body with a Voest Alpine AM50 mining machine. The test room was excavated 4.8 m wide x 4.8 m high.

The Rock Mechanics Station was extensively instrumented with closure stations and unidirectional hydraulic pressure cells to study the steady state behaviour of a "virgin ground" single opening in potash. Unfortunately, due to small strain rates in the test room, the majority of hydraulic pressure cells, which had been confined in the boreholes with compacted sand, failed to produce meaningful results. The original 1983 instrumentation details are shown in Figure 3.1 and the results obtained are presented on the following graphs and tables, as well as the results obtained from the Rock Mechanics Station to date.

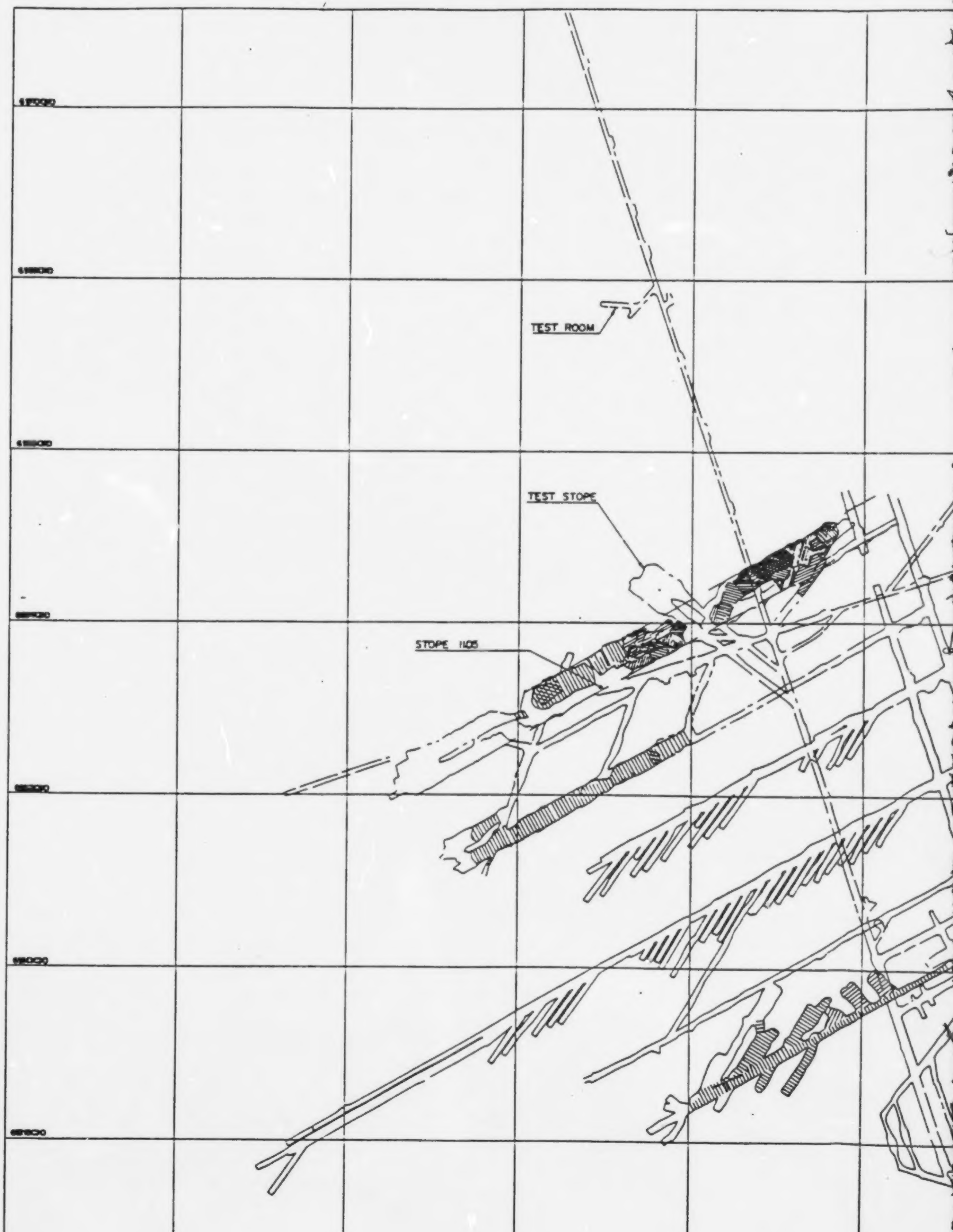
TEST ROOM
TEST STOPE
STOPE 1105
371 400
371 600
371 800
372 000
372 200

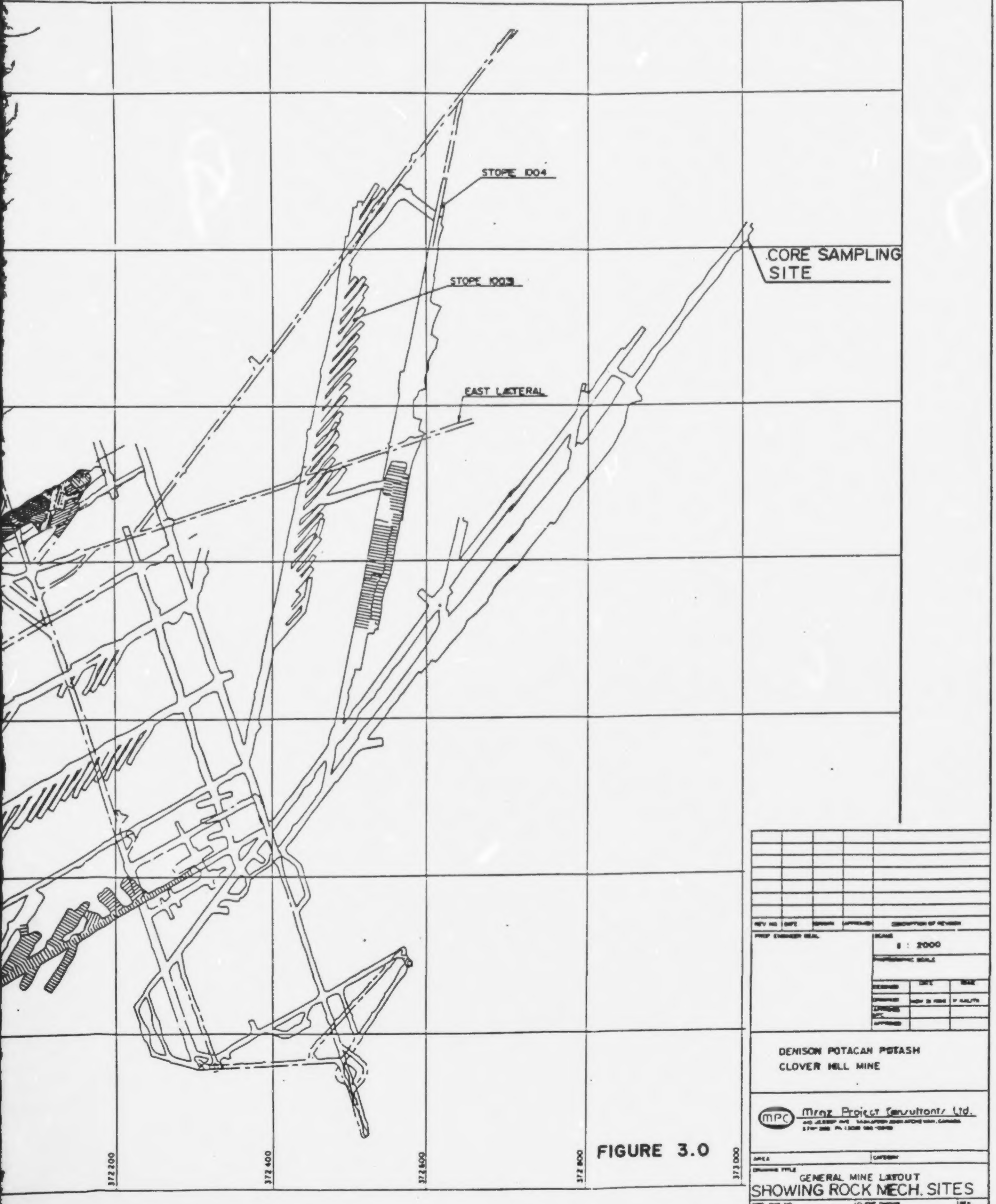
STOPE 1004
CORE SAMPLING SITE
STOPE 1003
EAST LATERAL
372 200
372 400
372 600
372 800
373 000
1 : 2000

FIGURE 3.0

DENISON POTACAN POTASH
CLOVER HILL MINE

Mraz Project Consultants Ltd.

GENERAL MINE LAYOUT
SHOWING ROCK MECH. SITES

DPP 047

10-146

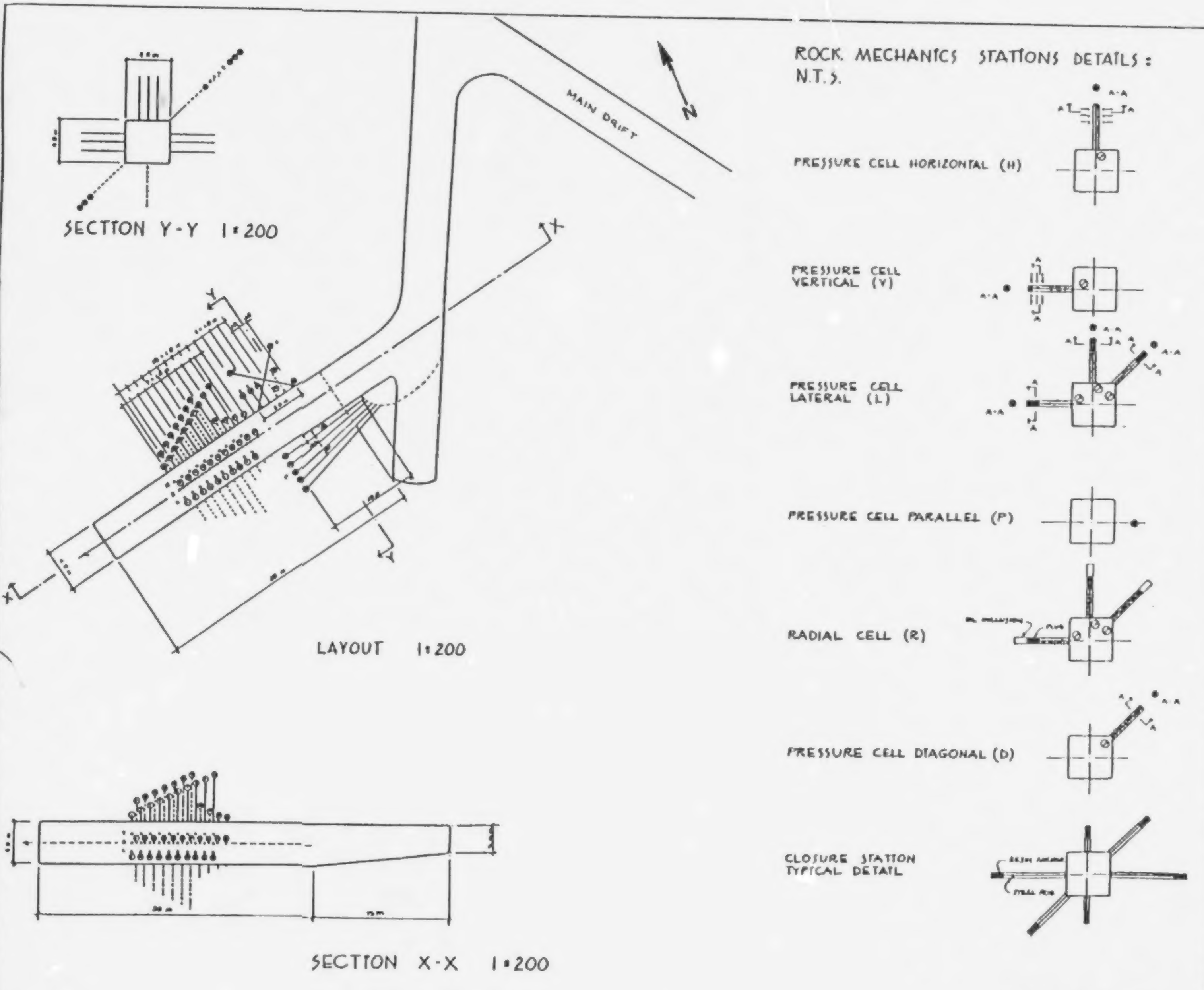
SECTION Y-Y 1:200
MAIN DRIFT
N
X
Y
LAYOUT 1:200
SECTION X-X 1:200
ROCK MECHANICS STATIONS DETAILS:
N.T.S.
PRESSURE CELL HORIZONTAL (H)
PRESSURE CELL VERTICAL (V)
PRESSURE CELL LATERAL (L)
PRESSURE CELL PARALLEL (P)
RADIAL CELL (R)
PRESSURE CELL DIAGONAL (D)
CLOSURE STATION TYPICAL DETAIL
A-A

NOTE:
FOR DESCRIPTION OF ROCK MECHANIC INSTRUMENTATION REFER TO LETTER FROM D MRAZ TO A. LUDWIG OF JAN 7, 1983

FIGURE 3.1

DENISON-POTACAN
POTASH COMPANY
NEW BRUNSWICK
POTASH PROJECT

ROCK MECHANICS INSTRUMENTATION
IN TEST ROOM

10-146

The distribution of closure rates around the Rock Mechanics Station (Test Room) for the period July 22, 1983 to July 16, 1985 is shown in Figure 3.2.

The distribution of closure rates around the Rock Mechanics Station (Test Room) for the period February 28, 1986 to December 30, 1986 are calculated on Tables 3.1 and 3.2 and are shown in Figure 3.3.

In order to determine the value of the Prandtl Strain Rate, the strain rate within the viscoplastic zone should be calculated. The viscoplastic zone is located approximately between the active opening at a depth of about 1.0 m from the walls, roof, and floor on centrelines and its boundary at the point where the shear stress equals the Prandtl Limit, K = 8.8 MPa, as determined in the laboratory, which is at a depth of approximately 4 m.

The average strain rates for the period February 28, 1986 to December 30, 1986 are as follows:

Roof Displacements:

1 m Anchor (mm)	4 m Anchor (mm)	Difference (mm)	$\Delta\dot{u}$ (μm/day)	Interval (m)	$\dot{\epsilon}$ (s^{-1})
4.0	1.8	2.2	7.2	3.0	2.8×10^{-11}
Wall Displacement:					
3.8	1.9	1.9	6.2	3.0	2.4×10^{-11}

Average strain rate ($\dot{\epsilon}$) = 2.6×10^{-11} s^{-1}
The Prandtl Strain Rate will be taken as $\dot{\epsilon}_K \cong 3.0 \times 10^{-11}$ s^{-1}

The results obtained to date from the instrumentation in the Rock Mechanics Station (Test Room) are presented on the following graphs and tables.

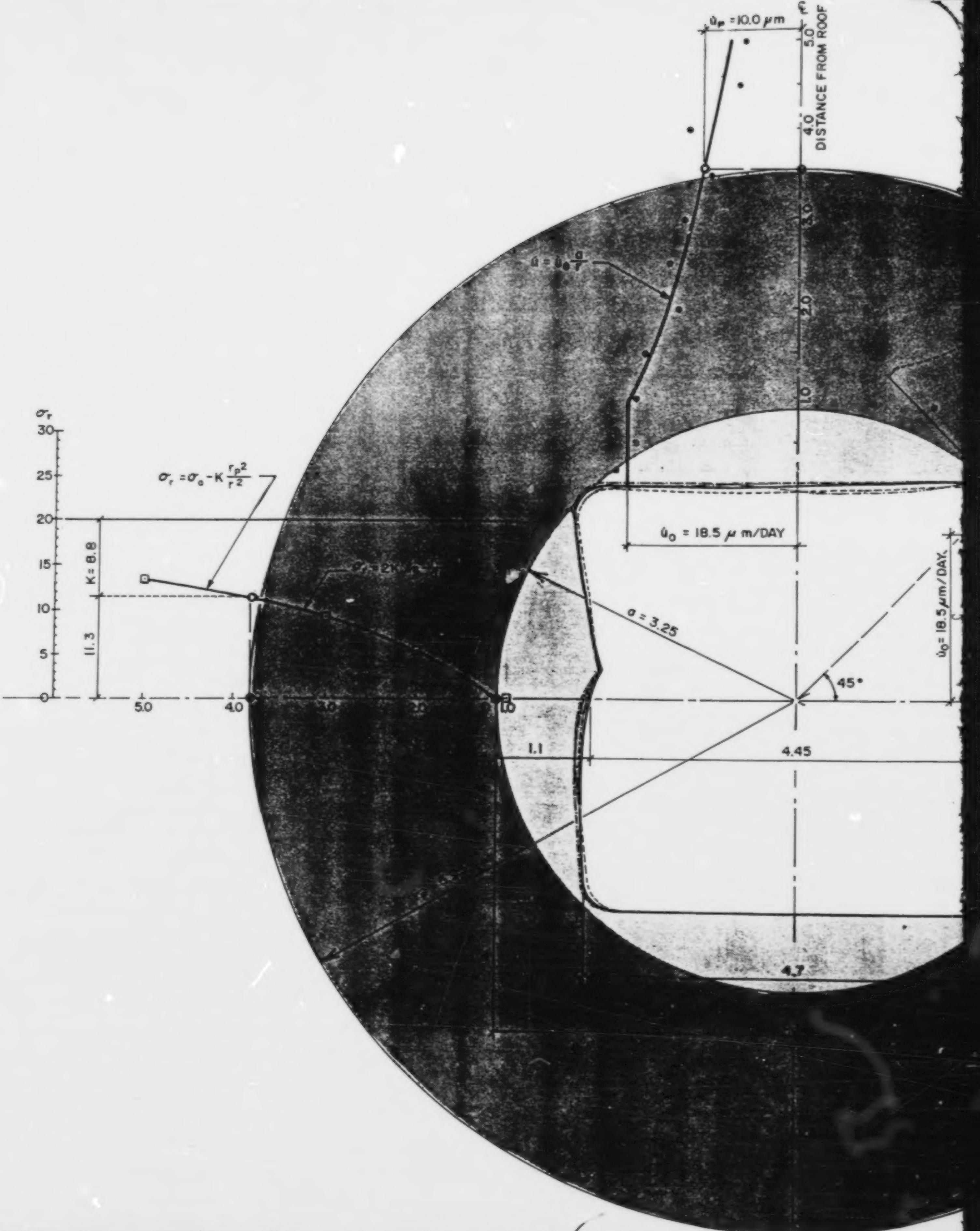

$\dot{u}_P = 10.0\ \mu m$
5.0
4.0
DISTANCE FROM ROOF
3.0
2.0
1.0
$\dot{u} = \dot{u}_0 \frac{a}{r}$
σ_r
30
25
20
15
10
5
0
$\sigma_r = \sigma_0 - K \frac{r_p^2}{r^2}$
K = 8.8
11.3
$\sigma_r = 2K$
5.0
4.0
3.0
2.0
1.0
$\dot{u}_0$ = 18.5 μm/DAY
a = 3.25
$\dot{u}_0$ = 18.5 μm/DAY.
45°
1.1
4.45
4.7

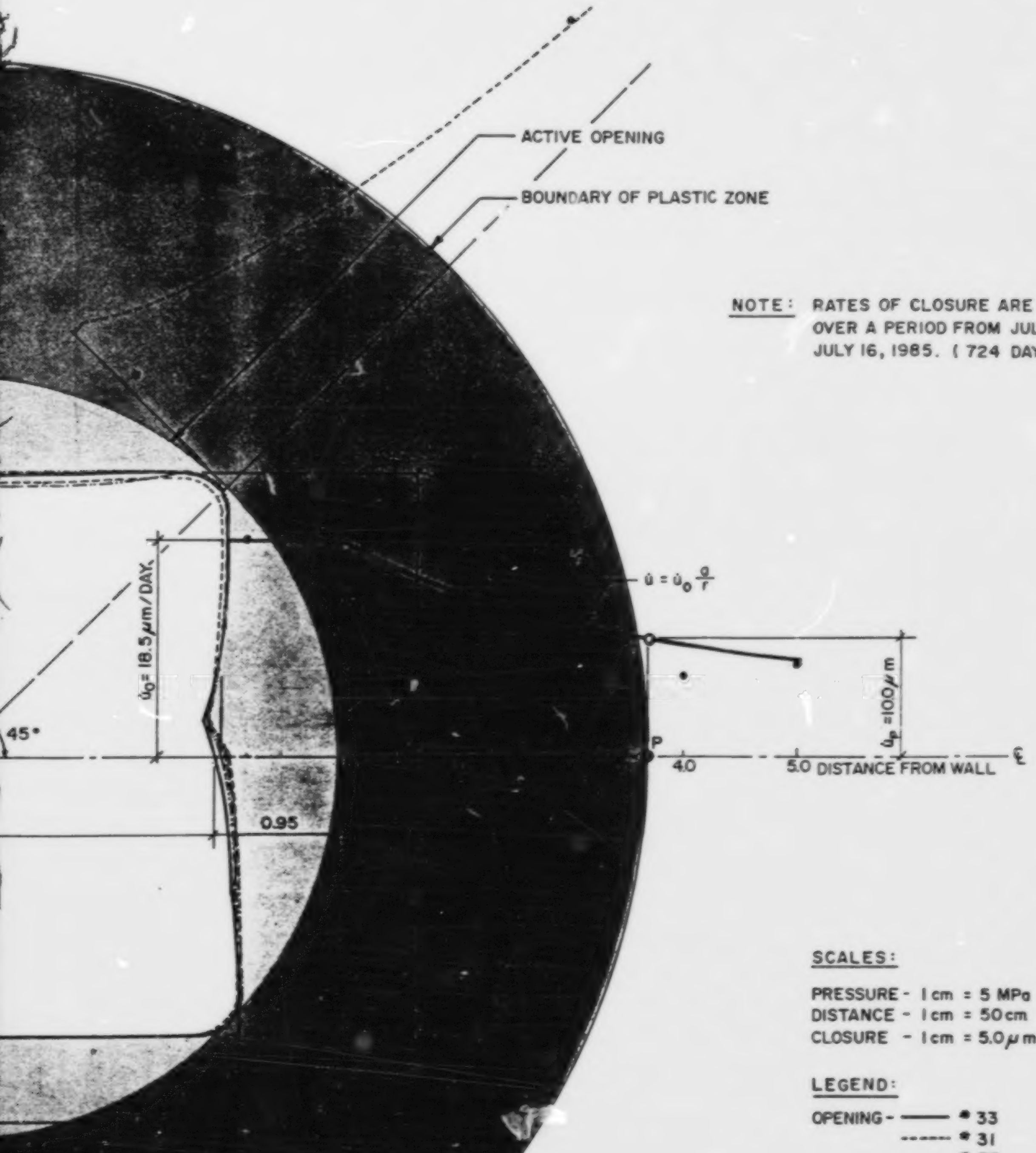
ACTIVE OPENING
BOUNDARY OF PLASTIC ZONE
$\dot{u} = \dot{u}_0 \frac{a}{r}$
$\dot{u}_0$= 18.5 μm/DAY
$\dot{u}_p$ =100μm
45°
0.95
P
4.0
5.0 DISTANCE FROM WALL
℄

NOTE: RATES OF CLOSURE ARE CALCULATED OVER A PERIOD FROM JULY 2, 1983 TO JULY 16, 1985. (724 DAYS)

SCALES:

PRESSURE - 1 cm = 5 MPa
DISTANCE - 1 cm = 50 cm
CLOSURE - 1 cm = 5.0 μm/DAY (micrometer/DAY)

LEGEND:

OPENING - ——— * 33
- - - - - - * 31
— - — - * 37
— - - — * 40

○ ...... MEASURED RADIAL STRESS (MPa)
● ...... MEASURED CREEP RATE (μm/DAY)

DENISON-POTACAN
POTASH COMPANY

EVALUATION OF ROCK MECHANICS
TEST ROOM AS OF JULY 16, 1985

FIG. 3.2

JULY 19/'85

MPC Mraz Project Consultants Ltd.
410 JESSOP AVE., SASKATOON, SASKATCHEWAN, CANADA
S7N 2S5 Ph.(3[illegible]) 933-0240

TABLE 3.1

ROCK MECHANICS STATION (TEST ROOM)

DETERMINATION OF CLOSURE RATES FOR ROOF AND FLOOR

DATA POINT (ANCHOR) (m)	FEB. 28/86 CLOSURE READING (mm)	DEC. 30/86 CLOSURE READING (mm)	DIFFERENCE (mm)	DIFFERENCE AT ROOF OR FLOOR (mm)	DAYS BETWEEN READINGS	CLOSURE RATE (μm/day)
0.2	59.9	69.3	9.4	4.70	305	15.4
0.5	55.5	64.6	9.1	4.55	305	14.9
1.0	52.8	60.8	8.0	4.00	305	13.1
1.5	49.6	56.9	7.3	3.65	305	12.0
2.0	37.7	43.0	5.3	2.65	305	8.7
2.5	42.6	49.4	6.8	3.40	305	11.1
3.0	36.9	43.7	6.8	3.40	305	11.1
3.5	29.3	34.7	5.4	2.70	305	8.9
4.0	24.0	27.6	3.6	1.80	305	5.9
4.5	22.5	26.3	3.8	1.90	305	6.2
5.0	28.3	32.3	4.0	2.00	305	6.6

TABLE 3.2

ROCK MECHANICS STATION (TEST ROOM)

DETERMINATION OF CLOSURE RATES FOR WALLS

DATA POINT (ANCHOR) (m)	FEB. 28/86 CLOSURE READING (mm)	DEC. 30/86 CLOSURE READING (mm)	DIFFERENCE (mm)	DIFFERENCE AT EITHER WALL (mm)	DAYS BETWEEN READINGS	CLOSURE RATE (μm/day)
0.2	59.1	68.6	9.5	4.75	305	15.6
0.5	60.4	68.5	8.1	4.05	305	13.3
1.0	56.8	64.4	7.6	3.80	305	12.5
1.5	54.0	61.7	7.7	3.85	305	12.6
2.0	40.3	46.2	5.9	2.95	305	9.7
2.5	45.5	51.6	6.1	3.05	305	10.0
3.0	28.0	32.6	4.6	2.30	305	7.5
3.5	28.0	32.6	4.6	2.30	305	7.5
4.0	24.2	28.0	3.8	1.90	305	6.2
4.5	28.1	32.4	4.3	2.15	305	7.0
5.0	24.5	28.1	3.6	1.80	305	5.9

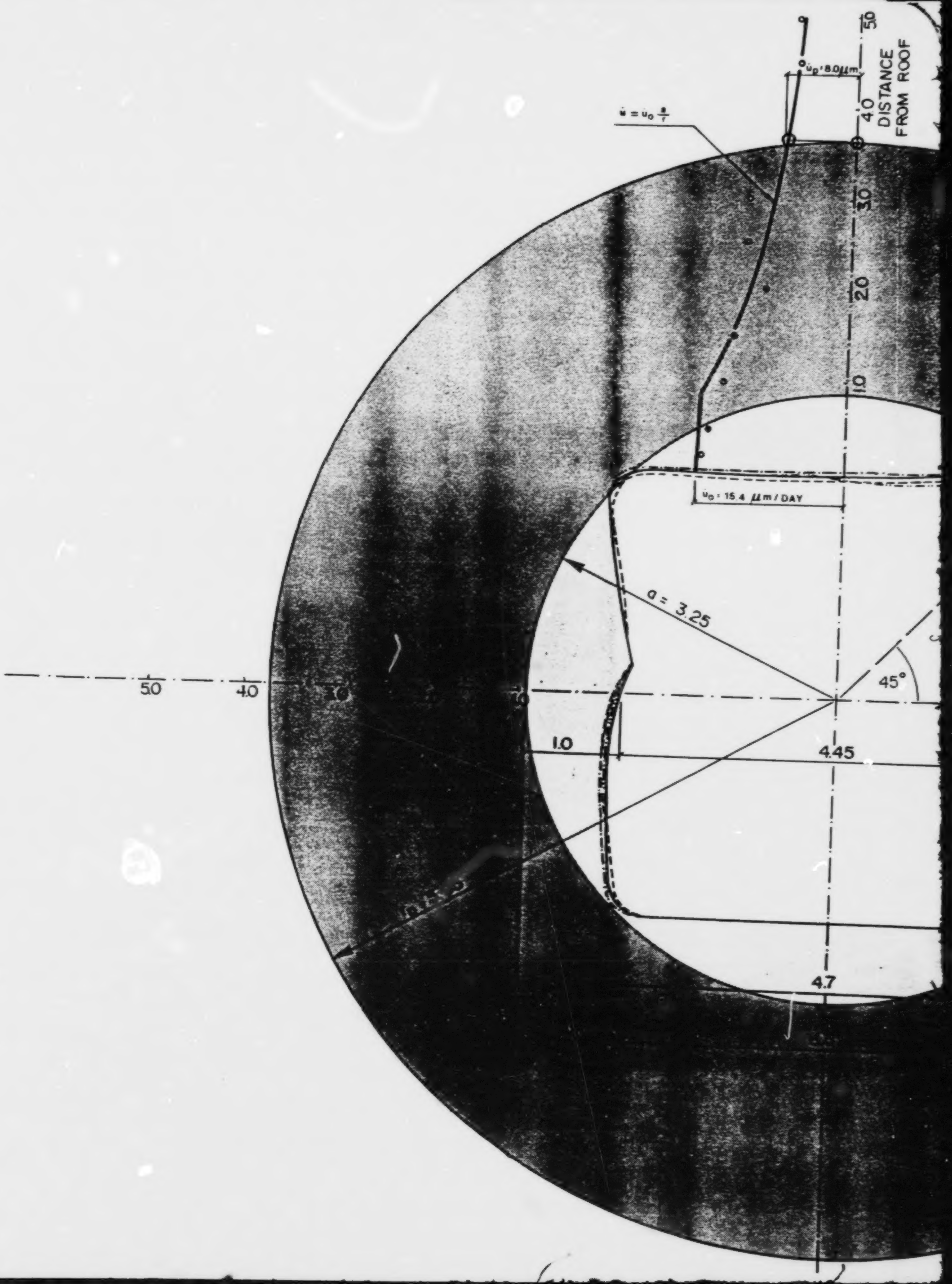
$\dot{u} = \dot{u}_0 \frac{a}{r}$
$\dot{u}_p$: 8.0 μm
5.0
4.0
DISTANCE FROM ROOF
3.0
2.0
1.0
$\dot{u}_0$: 15.4 μm / DAY
a = 3.25
45°
5.0
4.0
3.0
1.0
1.0
4.45
4.7

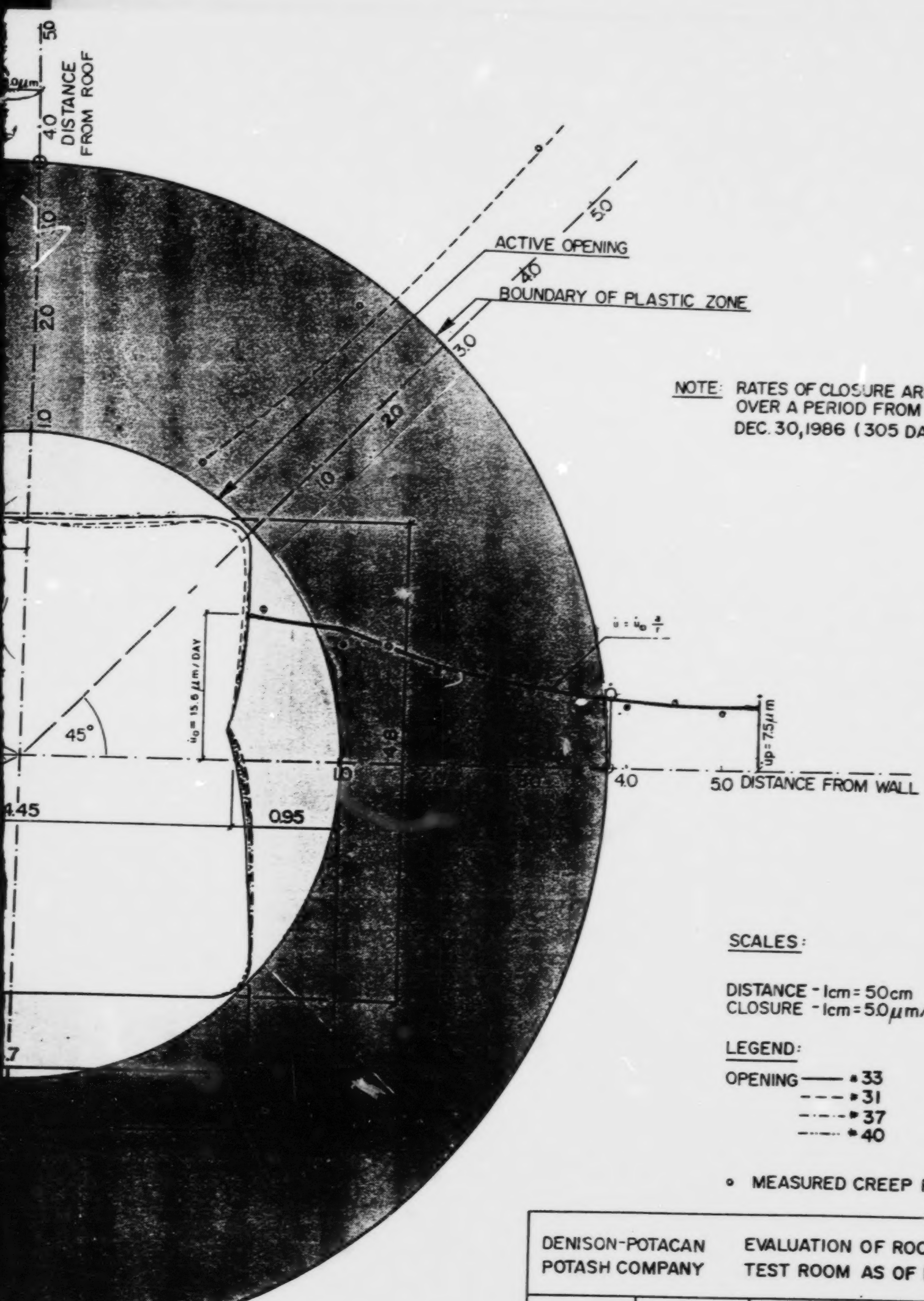
DISTANCE FROM ROOF
5.0
4.0
2.0
1.0
ACTIVE OPENING
BOUNDARY OF PLASTIC ZONE
5.0
4.0
3.0
2.0
1.0
45°
$\dot{u}_0 = 15.6\ \mu m/DAY$
$\dot{u} = \dot{u}_0 \frac{a}{r}$
$\dot{u}_p = 7.5\ \mu m$
1.0
4.0
5.0 DISTANCE FROM WALL
4.45
0.95
4.8
7

NOTE: RATES OF CLOSURE ARE CALCULATED OVER A PERIOD FROM FEB. 28, 1986 TO DEC. 30, 1986 (305 DAYS)

SCALES:

DISTANCE - 1cm = 50cm
CLOSURE - 1cm = 5.0 μm/DAY (micrometer/DAY)

LEGEND:

OPENING —— #33
- - - #31
-·-·- #37
-··- #40

○ MEASURED CREEP RATE (μm / DAY)

DENISON-POTACAN POTASH COMPANY

EVALUATION OF ROCK MECHANICS TEST ROOM AS OF DECEMBER 30. 1986

FIG. 3.3

APR. 12/87

MPC Mraz Project Consultants Ltd.
410 JESSOP AVE. SASKATOON, SASKATCHEWAN, CANADA S7N 2S5 Ph. (306) 955-0240

TABLE 3.3

ROCK MECHANICS STATION (TEST ROOM)

DETERMINATION OF CLOSURE RATES FOR DIAGONALS

DATA POINT (ANCHOR) (m)	FEB. 28/86 CLOSURE READING (mm)	DEC. 30/86 CLOSURE READING (mm)	DIFFERENCE (mm)	DIFFERENCE AT EITHER WALL (mm)	DAYS BETWEEN READINGS	CLOSURE RATE (μm/day)
0.2	40.4	45.9	5.5	2.75	305	9.0
2.5	27.4	33.1	5.7	2.85	305	9.3
5.0	21.1	26.1	5.0	2.50	305	8.2

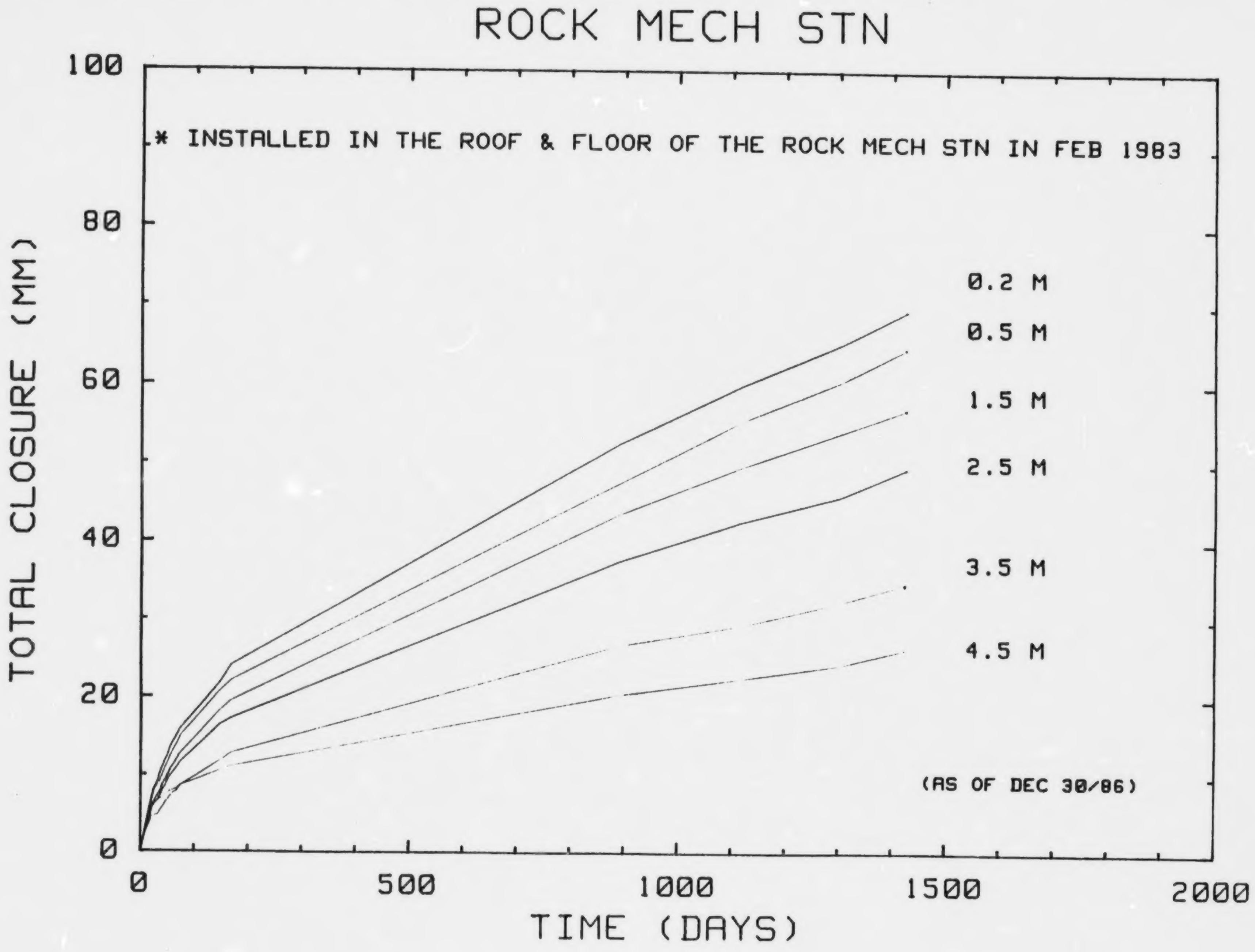
ROCK MECH STN
* INSTALLED IN THE ROOF & FLOOR OF THE ROCK MECH STN IN FEB 1983
TOTAL CLOSURE (MM)
100
80
60
40
20
0
0.2 M
0.5 M
1.5 M
2.5 M
3.5 M
4.5 M
(AS OF DEC 30/86)
0
500
1000
1500
2000
TIME (DAYS)

FIGURE 3.4

TABLE 3.4

STATION : ROCK MECHANICS STATION ROOF AND FLOOR.

MEASUREMENT : TOTAL CLOSURE AT 0.2, 0.5, 1.5, 2.5, 3.5 AND 4.5 M DEPTHS.

DATE	JULIAN CALENDAR DAY	DAYS SINCE FIRST INSTALLATION	0.2 M ANCHOR CUM. CLOSURE (MM)	0.5 M ANCHOR CUM. CLOSURE (MM)	1.5 M ANCHOR CUM. CLOSURE (MM)	2.5 M ANCHOR CUM. CLOSURE (MM)	3.5 M ANCHOR CUM. CLOSURE (MM)	4.5 M ANCHOR CUM. CLOSURE (MM)
FEB. 7/83	38	0						
FEB. 9/83	40	2						
FEB. 10/83	42	3						
FEB. 13/83	44	6						
FEB. 14/83	45	7	2.5	2.5				
FEB. 16/83	47	9	3.3	3.3	2.5	2.5	2.5	2.5
FEB. 22/83	53	15	5.4	5.4	4.3	3.8	3.4	4.7
FEB. 28/83	59	21	7.1	7.2	6.1	5.5	4.6	5.6
MAR. 3/83	62	24	8.2	8.0	6.4	6.1	-	6.0
MAR. 7/83	66	31	9.1	8.7	7.1	6.7	4.7	6.5
MAR. 10/83	69	34	9.9	9.0	-	-	-	-
MAR. 14/83	73	38	10.8	9.8	8.1	7.5	5.6	6.9
MAR. 17/83	76	41	11.1	10.3	8.8	8.1	5.8	7.1
MAR. 21/83	80	45	11.9	10.9	9.2	8.5	6.4	7.3
MAR. 24/83	83	48	12.3	11.4	9.6	9.1	6.6	7.5
MAR. 31/83	90	55	13.7	12.6	10.7	10.0	7.3	7.9
APR. 4/83	94	59	14.2	13.2	11.1	10.2	7.6	8.0
APR. 11/83	101	66	15.0	14.0	11.8	10.9	7.8	8.2
APR. 18/83	108	73	16.0	15.1	12.7	11.6	8.6	8.6
APR. 25/83	115	80	-	-	-	-	-	-
JUNE 7/83	158	123	-	-	-	-	-	-
JUNE 30/83	181	146	21.8	20.8	18.2	16.5	11.8	10.0
JULY 22/83	203	168	24.1	22.1	19.5	17.3	12.9	10.6
JULY 16/85	197	892	52.6	-	43.5	37.5	26.7	20.4
FEB. 28/86	59	1,119	59.9	55.5	49.6	42.6	29.3	22.5
AUG. 29/86	241	1,301	65.1	60.4	-	45.8	32.3	24.3
DEC. 30/86	364	1,424	69.3	64.6	56.9	49.4	34.7	26.3

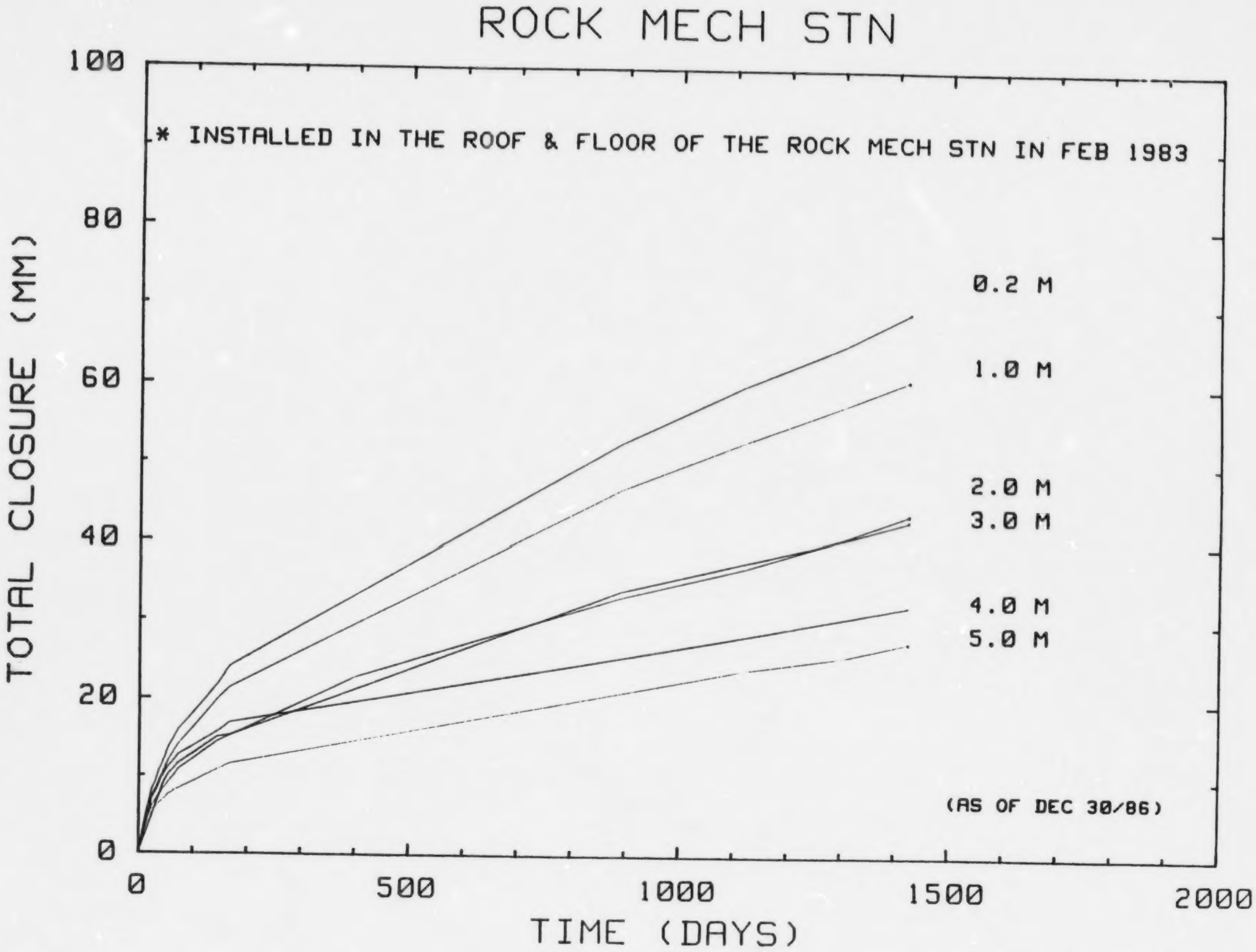
ROCK MECH STN
* INSTALLED IN THE ROOF & FLOOR OF THE ROCK MECH STN IN FEB 1983
TOTAL CLOSURE (MM)
100
80
60
40
20
0
0
500
1000
1500
2000
TIME (DAYS)
0.2 M
1.0 M
2.0 M
3.0 M
4.0 M
5.0 M
(AS OF DEC 30/86)

FIGURE 3.5

TABLE 3.5

STATION : ROCK MECHANICS STATION ROOF AND FLOOR.

MEASUREMENT : TOTAL CLOSURE AT 0.2, 1.0, 2.0, 3.0, 4.0 AND 5.0 M DEPTHS.

DATE	JULIAN CALENDAR DAY	DAYS SINCE FIRST INSTALLATION	0.2 M ANCHOR CUM. CLOSURE (MM)	1.0 M ANCHOR CUM. CLOSURE (MM)	2.0 M ANCHOR CUM. CLOSURE (MM)	3.0 M ANCHOR CUM. CLOSURE (MM)	4.0 M ANCHOR CUM. CLOSURE (MM)	5.0 M ANCHOR CUM. CLOSURE (MM)
FEB. 7/83	38	0						
FEB. 9/83	40	2						
FEB. 10/83	42	3						
FEB. 13/83	44	6						
FEB. 14/83	45	7	2.5	2.5				
FEB. 16/83	47	9	3.3	3.4		2.5	2.5	2.5
FEB. 22/83	53	15	5.4	5.1		4.2	4.1	4.1
FEB. 28/83	59	21	7.1	6.9		5.6	5.4	5.8
MAR. 3/83	62	24	8.2	7.4		6.0	5.6	7.1
MAR. 7/83	66	31	9.1	8.2		6.7	5.8	7.9
MAR. 10/83	69	34	9.9	8.7		-	-	-
MAR. 14/83	73	38	10.8	9.4		7.5	6.4	9.0
MAR. 17/83	76	41	11.1	9.9		7.7	6.6	9.7
MAR. 21/83	80	45	11.9	10.5	8.9	8.3	6.9	10.0
MAR. 24/83	83	48	12.3	10.9	9.3	8.4	7.0	10.5
MAR. 31/83	90	55	13.7	12.1	10.3	9.2	7.6	11.3
APR. 4/83	94	59	14.2	12.5	10.5	9.5	7.7	11.6
APR. 11/83	101	66	15.0	13.3	11.1	10.1	8.1	12.1
APR. 18/83	108	73	16.0	14.1	11.7	10.8	8.3	12.8
APR. 25/83	115	80	-	-	-	-	-	-
JUNE 7/83	158	123	-	-	-	-	-	-
JUNE 30/83	181	146	21.8	19.9	15.1	14.5	10.8	15.0
JULY 22/83	203	168	24.1	21.4	15.3	15.2	11.6	16.0
JULY 16/85	197	892	52.6	46.7	-	33.1	-	25.5
FEB. 28/86	59	1,119	59.9	52.8	37.7	36.9	24.0	28.3
AUG. 29/86	241	1,301	65.1	57.5	40.6	40.7	25.7	-
DEC. 30/86	364	1,424	69.3	60.8	43.0	43.7	27.6	32.3

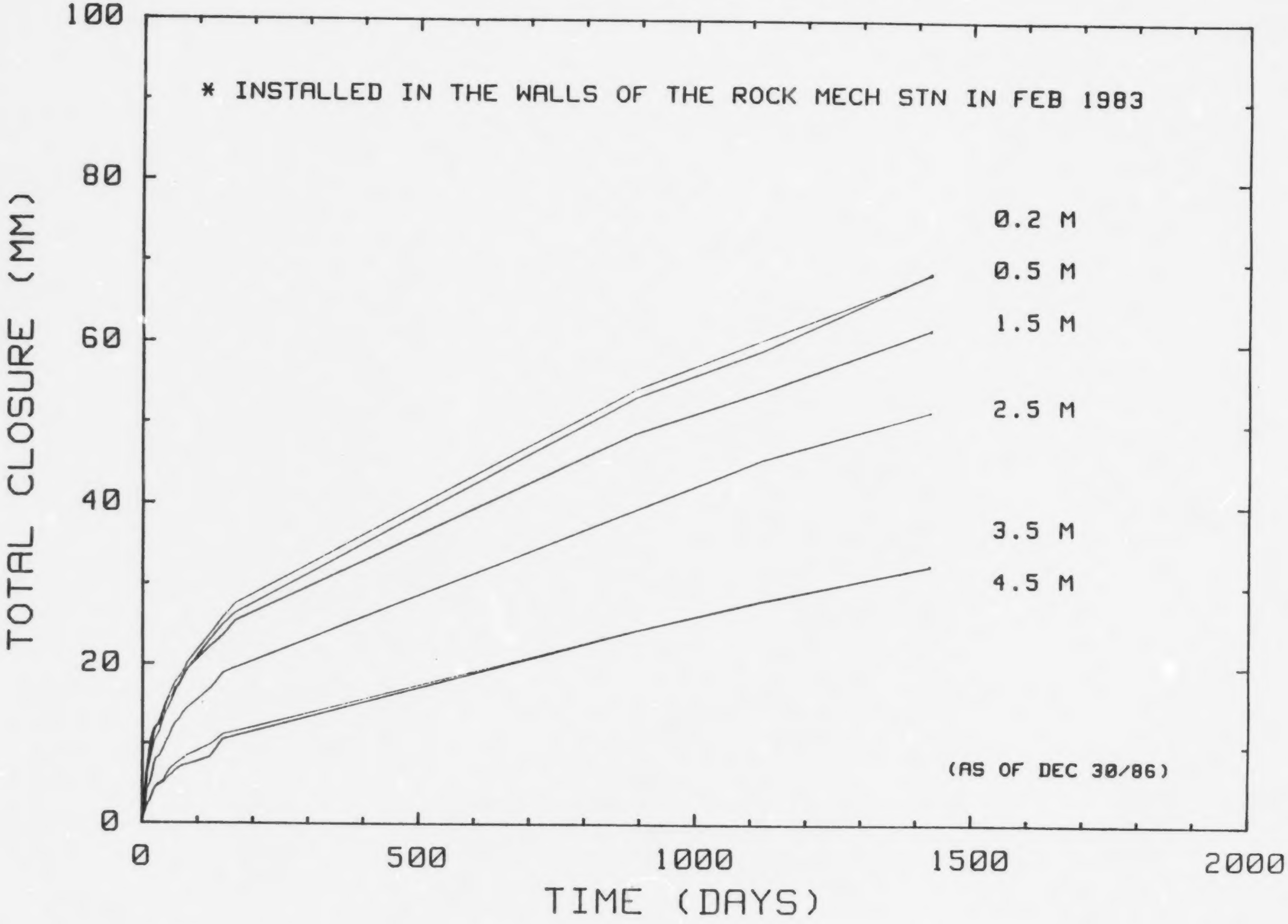
ROCK MECH STN

* INSTALLED IN THE WALLS OF THE ROCK MECH STN IN FEB 1983

(AS OF DEC 30/86)

FIGURE 3.6

TABLE 3.6

STATION : ROCK MECHANICS STATION WALLS.

MEASUREMENT : TOTAL CLOSURE AT 0.2, 0.5, 1.5, 2.5, 3.5 AND 4.5 M DEPTHS.

DATE	JULIAN CALENDAR DAY	DAYS SINCE FIRST INSTALLATION	0.2 M ANCHOR CUM. CLOSURE (MM)	0.5 M ANCHOR CUM. CLOSURE (MM)	1.5 M ANCHOR CUM. CLOSURE (MM)	2.5 M ANCHOR CUM. CLOSURE (MM)	3.5 M ANCHOR CUM. CLOSURE (MM)	4.5 M ANCHOR CUM. CLOSURE (MM)
FEB. 7/83	38	0	0.0	0.0				
FEB. 9/83	40	2	1.7	2.6		1.0		
FEB. 10/83	42	3	2.8	3.3		–		
FEB. 13/83	44	6	4.9	5.5		–		
FEB. 14/83	45	7	5.4	6.3	2.5	3.3	1.8	1.8
FEB. 16/83	47	9	6.4	7.4	6.8	4.2	2.2	2.4
FEB. 22/83	53	15	8.2	9.5	10.2	5.2	3.3	2.7
FEB. 28/83	59	21	10.1	11.5	11.8	7.4	4.3	4.0
MAR. 3/83	62	24	10.6	12.1	12.0	8.1	4.6	4.4
MAR. 7/83	66	31	11.5	13.0	12.3	8.4	5.0	4.8
MAR. 10/83	69	34	12.4	13.5	–	–	–	–
MAR. 14/83	73	38	13.1	14.0	14.0	9.4	5.4	5.0
MAR. 17/83	76	41	13.8	15.0	14.6	10.0	5.9	5.2
MAR. 21/83	80	45	14.3	15.7	15.3	10.5	6.3	5.5
MAR. 24/83	83	48	14.8	16.2	15.7	10.9	6.7	5.8
MAR. 31/83	90	55	15.8	17.3	15.9	12.1	7.1	6.1
APR. 4/83	94	59	16.5	17.8	16.9	12.5	7.4	6.5
APR. 11/83	101	66	17.5	18.3	17.8	13.0	7.7	6.9
APR. 18/83	108	73	18.5	19.1	18.2	13.9	8.1	7.2
APR. 25/83	115	80	19.2	20.1	19.2	14.4	8.5	7.3
JUNE 7/83	158	123	23.1	23.8	22.1	16.9	9.9	8.3
JUNE 30/83	181	146	24.9	25.9	23.5	18.9	11.2	10.0
JULY 22/83	203	168	26.3	27.6	25.3	19.5	11.5	–
JULY 16/85	197	892	53.2	54.3	48.7	–	24.3	24.3
FEB. 28/86	59	1,119	59.1	60.4	54.0	45.5	28.0	28.1
AUG. 29/86	241	1,301	–	–	–	–	–	–
DEC. 30/86	364	1,424	68.6	68.5	61.7	51.6	32.6	32.4

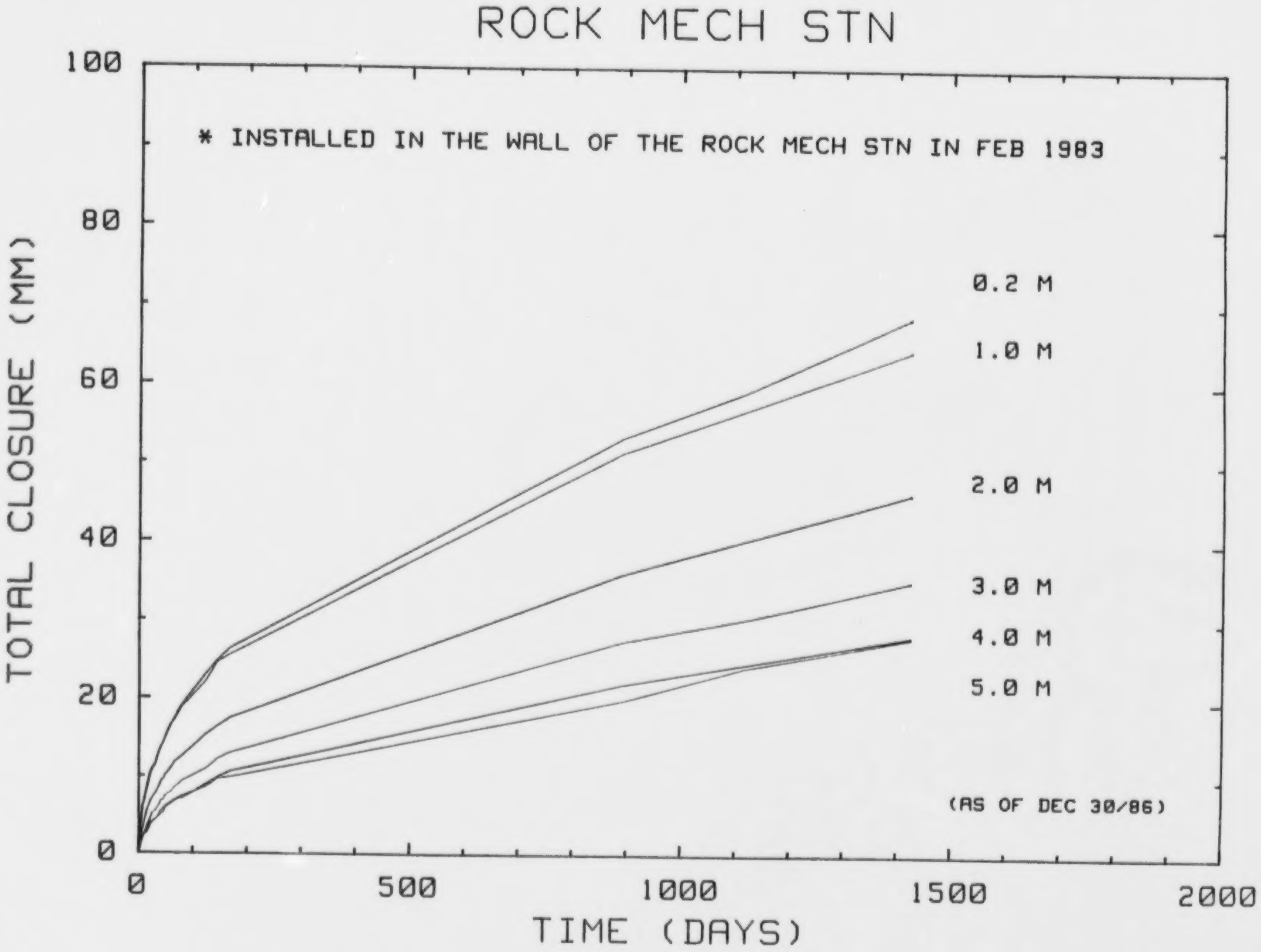
ROCK MECH STN
* INSTALLED IN THE WALL OF THE ROCK MECH STN IN FEB 1983
0.2 M
1.0 M
2.0 M
3.0 M
4.0 M
5.0 M
(AS OF DEC 30/86)
TOTAL CLOSURE (MM)
0
20
40
60
80
100
TIME (DAYS)
0
500
1000
1500
2000

FIGURE 3.7

TABLE 3.7

STATION : ROCK MECHANICS STATION WALLS.

MEASUREMENT : TOTAL CLOSURE AT 0.2, 1.0, 2.0, 3.0, 4.0 AND 5.0 M DEPTHS.

DATE	JULIAN CALENDAR DAY	DAYS SINCE FIRST INSTALLATION	0.2 M ANCHOR CUM. CLOSURE (MM)	1.0 M ANCHOR CUM. CLOSURE (MM)	2.0 M ANCHOR CUM. CLOSURE (MM)	3.0 M ANCHOR CUM. CLOSURE (MM)	4.0 M ANCHOR CUM. CLOSURE (MM)	5.0 M ANCHOR CUM. CLOSURE (MM)
FEB. 7/83	38	0	0.0	0.0				
FEB. 9/83	40	2	1.7	2.5	1.0			
FEB. 10/83	42	3	2.8	3.1	–			
FEB. 13/83	44	6	4.9	5.2	–			
FEB. 14/83	45	7	5.4	5.6	3.2	1.8	1.8	1.8
FEB. 16/83	47	9	6.4	6.5	4.0	2.2	2.4	2.2
FEB. 22/83	53	15	8.2	8.6	5.5	3.5	2.8	2.5
FEB. 28/83	59	21	10.1	10.5	6.8	4.4	3.8	3.5
MAR. 3/83	62	24	10.6	10.9	7.1	5.1	–	3.9
MAR. 7/83	66	31	11.5	11.6	7.8	5.5	4.3	4.3
MAR. 10/83	69	34	12.4	12.4	–	–	–	–
MAR. 14/83	73	38	13.1	13.4	8.8	6.3	4.9	–
MAR. 17/83	76	41	13.8	13.7	9.4	6.9	5.5	5.0
MAR. 21/83	80	45	14.3	14.3	9.6	6.9	5.7	5.2
MAR. 24/83	83	48	14.8	15.0	10.1	7.4	6.0	5.8
MAR. 31/83	90	55	15.8	16.1	10.7	7.8	6.4	6.2
APR. 4/83	94	59	16.5	16.6	11.1	7.9	6.6	6.3
APR. 11/83	101	66	17.5	17.1	11.8	8.6	6.9	6.7
APR. 18/83	108	73	18.5	18.0	12.2	8.9	7.2	7.1
APR. 25/83	115	80	19.2	18.9	12.6	9.4	7.5	7.1
JUNE 7/83	158	123	23.1	22.1	15.3	10.9	8.6	8.9
JUNE 30/83	181	146	24.9	24.6	16.5	12.3	9.8	9.9
JULY 22/83	203	168	26.3	25.5	17.4	13.0	10.0	10.6
JULY 16/85	197	892	53.2	51.3	35.9	27.4	19.9	21.9
FEB. 28/86	59	1,119	59.1	56.8	40.3	28.0	24.2	24.5
AUG. 29/86	241	1,301	–	–	–	–	–	–
DEC. 30/86	364	1,424	68.6	64.4	46.2	32.6	28.0	28.1

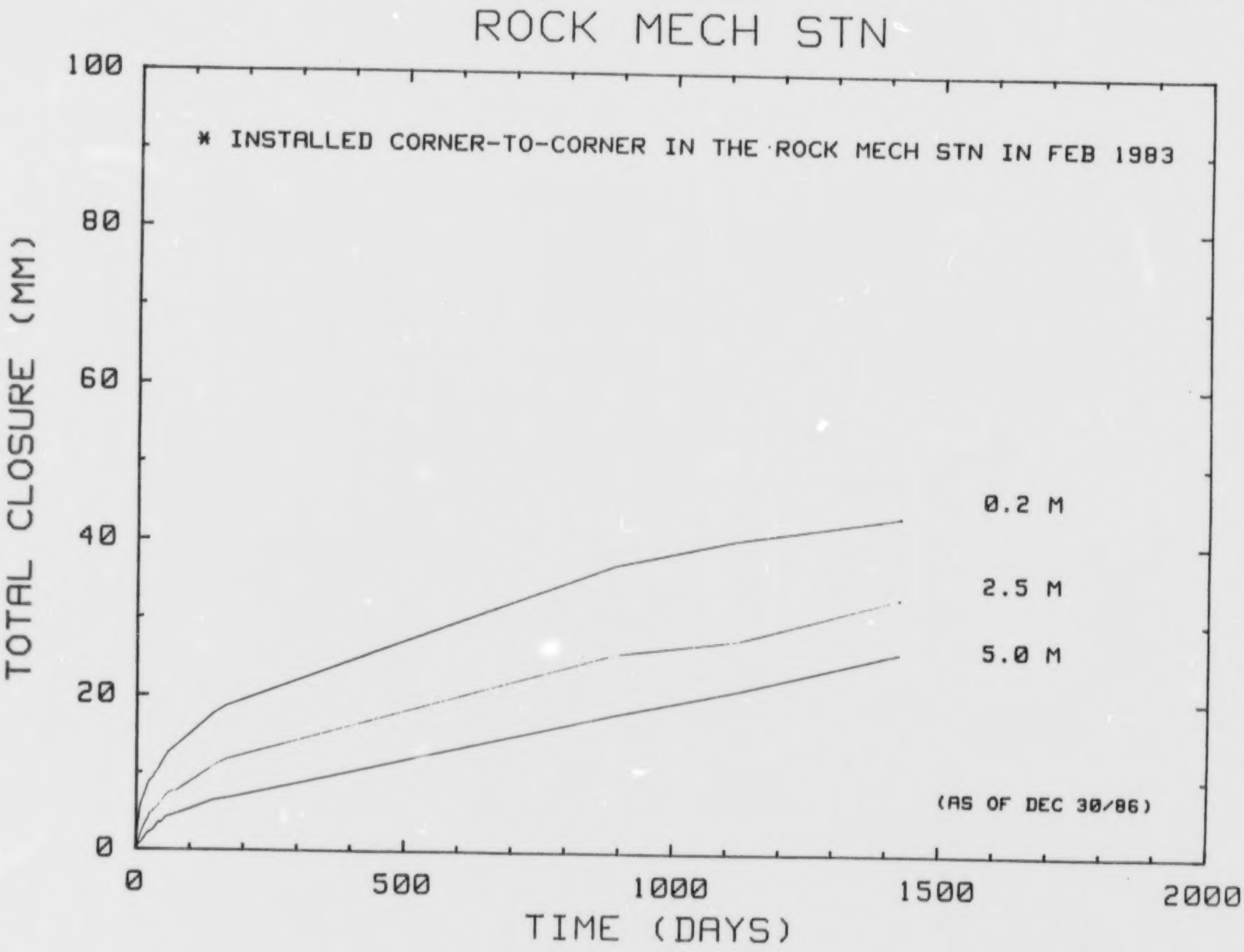
ROCK MECH STN
* INSTALLED CORNER-TO-CORNER IN THE ROCK MECH STN IN FEB 1983
TOTAL CLOSURE (MM)
100
80
60
40
20
0
0
500
1000
1500
2000
TIME (DAYS)
0.2 M
2.5 M
5.0 M
(AS OF DEC 30/86)

FIGURE 3.8

TABLE 3.8

STATION : ROCK MECHANICS STATION CORNER TO CORNER

MEASUREMENT : TOTAL CLOSURE AT 0.2, 2.5 AND 5.0 M DEPTHS.

DATE	JULIAN CALENDAR DAY	DAYS SINCE FIRST INSTALLATION	0.2 M ANCHOR CUM. CLOSURE (MM)	2.5 M ANCHOR CUM. CLOSURE (MM)	5.0 M ANCHOR CUM. CLOSURE (MM)
FEB. 7/83	38	0			
FEB. 9/83	40	2			
FEB. 10/83	42	3			
FEB. 13/83	44	6	0.0		
FEB. 14/83	45	7	5.5	0.0	0.0
FEB. 16/83	47	9	6.0	2.3	0.9
FEB. 22/83	53	15	7.1	3.2	1.4
FEB. 28/83	59	21	8.4	3.9	2.1
MAR. 3/83	62	24	8.9	4.5	2.2
MAR. 7/83	66	31	9.3	5.0	2.5
MAR. 10/83	69	34	9.8	-	-
MAR. 14/83	73	38	10.2	5.5	3.1
MAR. 17/83	76	41	10.4	5.8	3.5
MAR. 21/83	80	45	11.0	6.1	3.6
MAR. 24/83	83	48	11.4	6.5	3.6
MAR. 31/83	90	55	12.2	7.1	4.2
APR. 4/83	94	59	12.6	7.3	4.4
APR. 11/83	101	66	13.0	7.5	4.5
APR. 18/83	108	73	13.4	7.6	4.6
APR. 25/83	115	80	-	-	-
JUNE 7/83	158	123	-	-	-
JUNE 30/83	181	146	17.9	11.1	6.2
JULY 22/83	203	168	18.7	11.8	6.4
JULY 16/85	197	892	37.0	25.6	18.0
FEB. 28/86	59	1,119	40.4	27.4	21.1
AUG. 29/86	241	1,301	-	-	-
DEC. 30/86	364	1,424	45.9	33.1	26.1

3.2 TEST STOPE

The test site known as the Test Stope was excavated in late 1983 with a Voest Alpine AM100 mining machine. The Test Stope was excavated 42 m wide x 4 m high in parallel passes with the AM100.

The Test Stope was originally instrumented in January, 1984, with plate/rebar type relative closure stations in the roof and western pillar at depths of 0.5 m, 2.5 m and 5.0 m. Horizontal and vertical pulley type total closure meters were installed in June, 1984 to provide additional closure data for the Test Stope.

Test Stope rock mechanics instrumentation are installed as shown in Figure 3.9 (Denison-Potacan drawing No. 232-0020-007).

A general arrangement of the measurement of absolute vertical and horizontal closure using the wire and pulley method in the Test Stope is shown in Figures 3.10 and 3.11. The installation arrangement for relative closure stations is shown in Figure 3.12.

In an effort to collect more comprehensive stress and strain data from the Test Stope, hydraulic pressure cells and additional extensometers were installed in 1986 in the western pillar and roof. The results obtained to date from the instrumentation in the Test Stope are presented on the following graphs and tables.

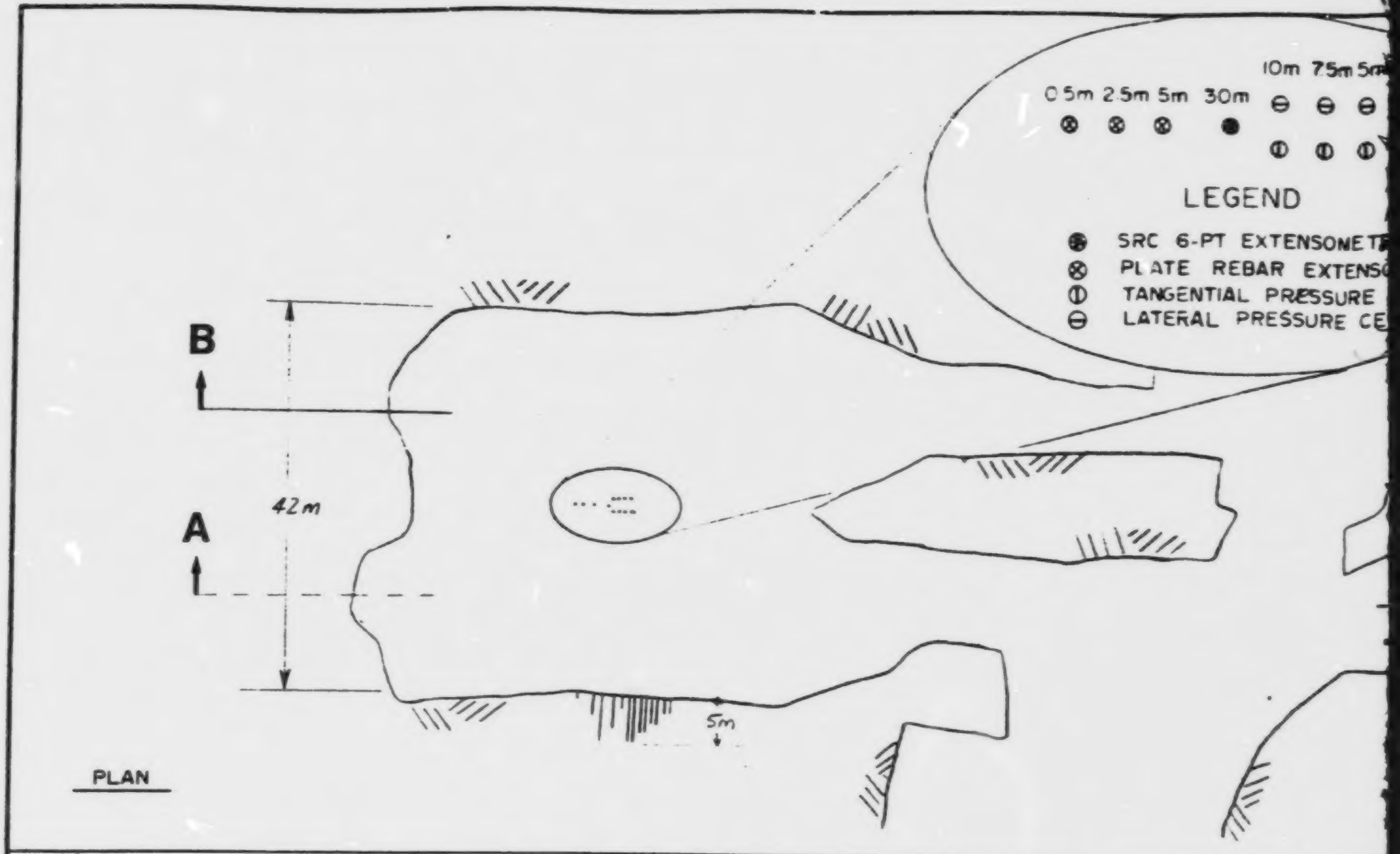
10m 7.5m 5m
0.5m 2.5m 5m 30m
⊗ ⊗ ⊗ ●
⊖ ⊖ ⊖
⦶ ⦶ ⦶
LEGEND
● SRC 6-PT EXTENSOMET
⊗ PLATE REBAR EXTENS
⦶ TANGENTIAL PRESSURE
⊖ LATERAL PRESSURE CE
B
A
42m
5m

PLAN

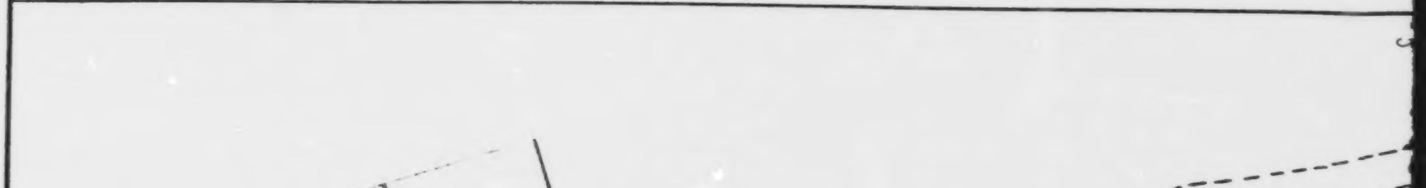
A-A
B-B
30m
10m
0.5m, 2.5m, 5m, 3.75m, 1.25m, 5m, 5m, 4m, 4m, 3m, 3m
⊗ ⊗ ⊗ ⊗ ⊗ ⊖ ⦶ ⊖ ⦶ ⊖ ⦶
LEGEND
⊗ PLATE / REBAR
⊖ VERTICAL PRESS
⦶ LATERAL PRESSU

ELEVATION

	3						SCALE	1:500
	2						DESIGNED BY	
	1						DRAWN BY	S MUNRO
	0						CHECKED BY	
REFERENCE DRAWINGS	NO.	DESCRIPTION OF REVISION	DATE	BY	CHK.	APP.	APPROVED BY	

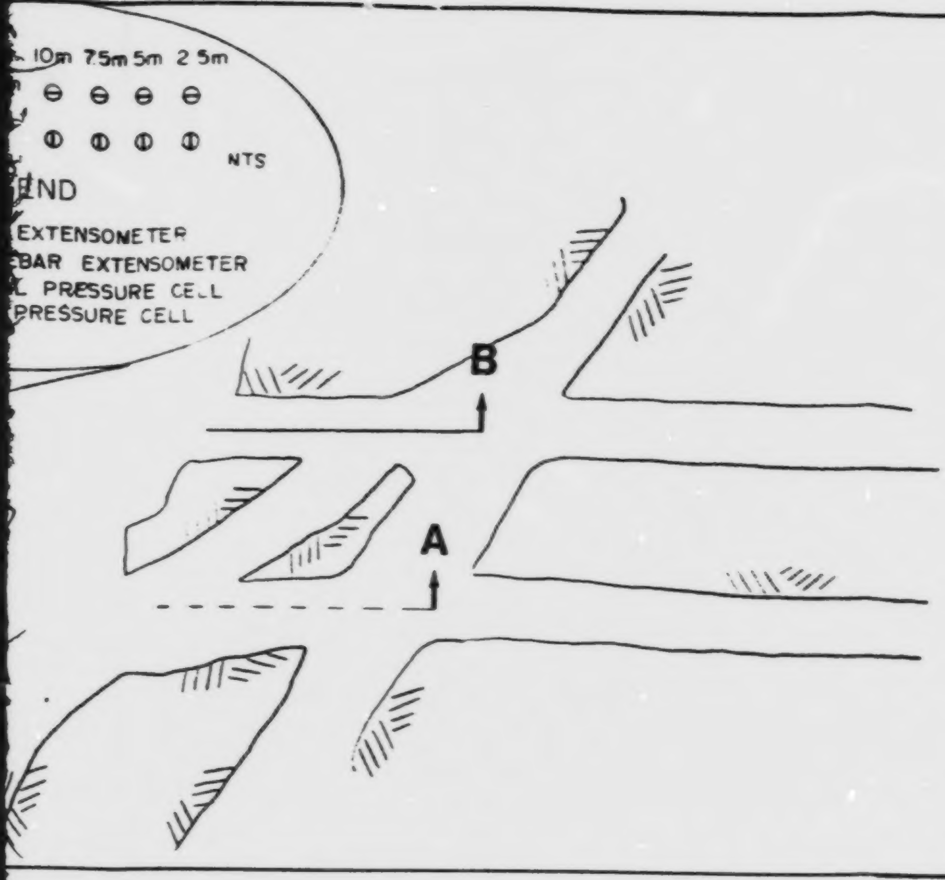
10m 7.5m 5m 2.5m
NTS
END
EXTENSOMETER
BAR EXTENSOMETER
L PRESSURE CELL
PRESSURE CELL
B
A

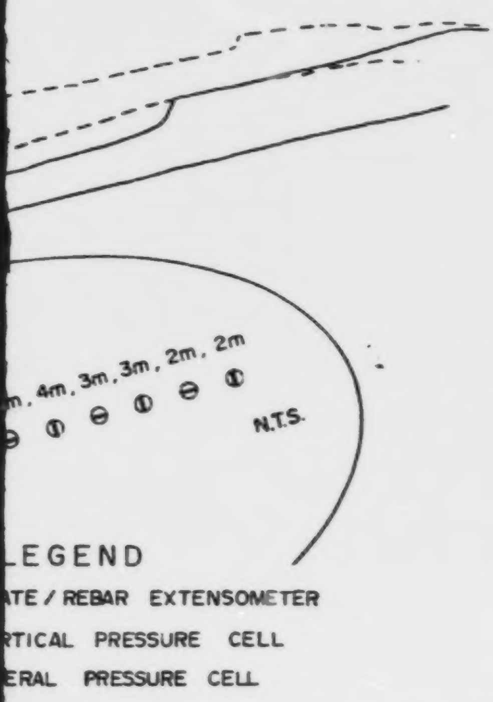
m, 4m, 3m, 3m, 2m, 2m
N.T.S.
LEGEND
ATE / REBAR EXTENSOMETER
RTICAL PRESSURE CELL
ERAL PRESSURE CELL

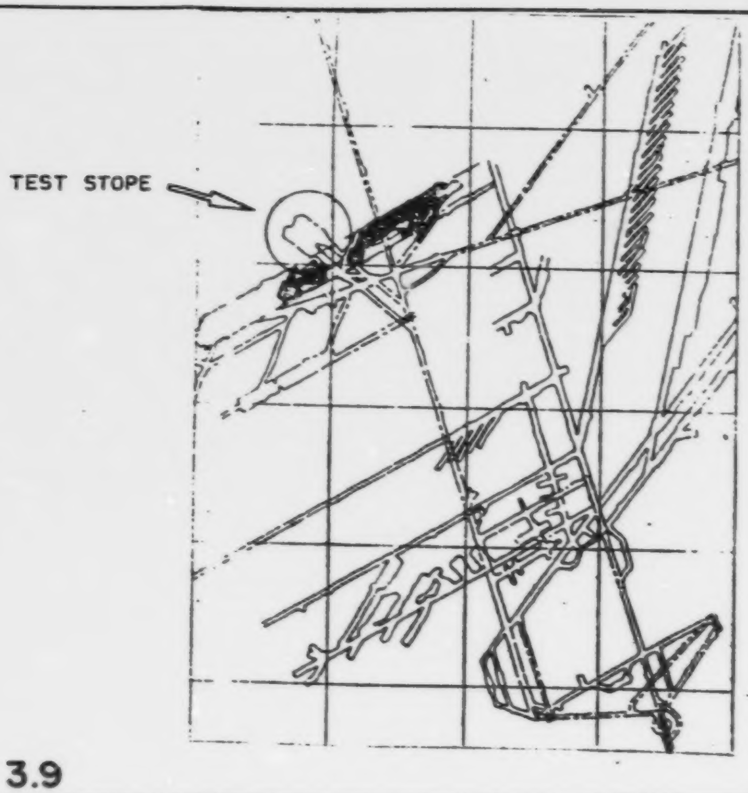

FIGURE 3.9

1:500	DATE	**DENISON - POTACAN POTASH COMPANY** SUSSEX, N.B.	TITLE	TEST STOPE ROCK MECHANICS INSTRUMENTATION
S MUNROE	JULY 1986		DRAWING NO. 232-0020-007	REV.

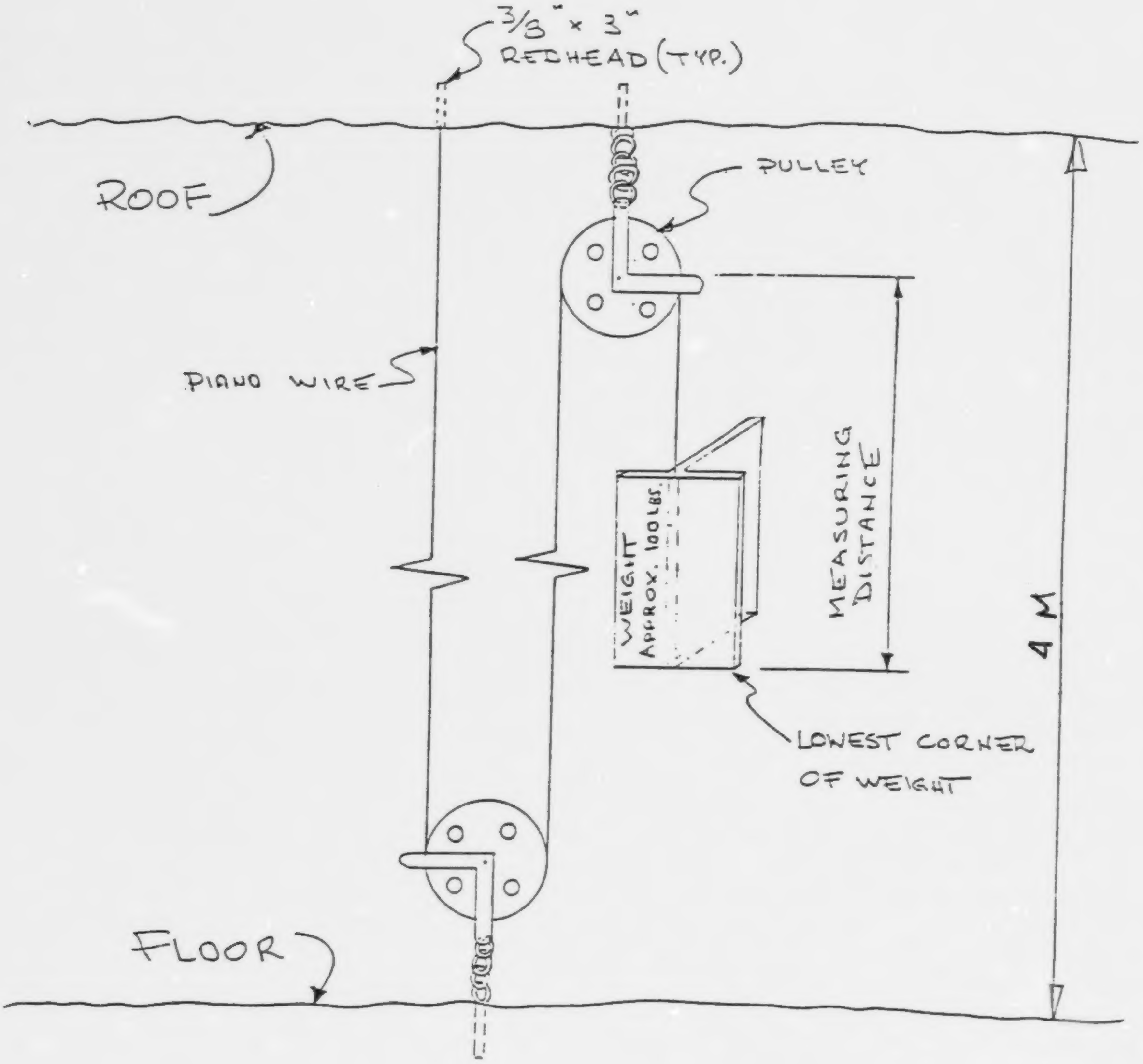
3/8" × 3"
REDHEAD (TYP.)
ROOF
PULLEY
PIANO WIRE
WEIGHT
APPROX. 100 LBS.
MEASURING DISTANCE
4 M
LOWEST CORNER OF WEIGHT
FLOOR

GENERAL ARRANGEMENT

MEASUREMENT OF ABSOLUTE VERTICAL CLOSURE
USING WIRE AND PULLEY METHOD IN TEST STOPE

N.T.S.
MIKE GRAVES
OCT. 29/84

FIGURE 3.10

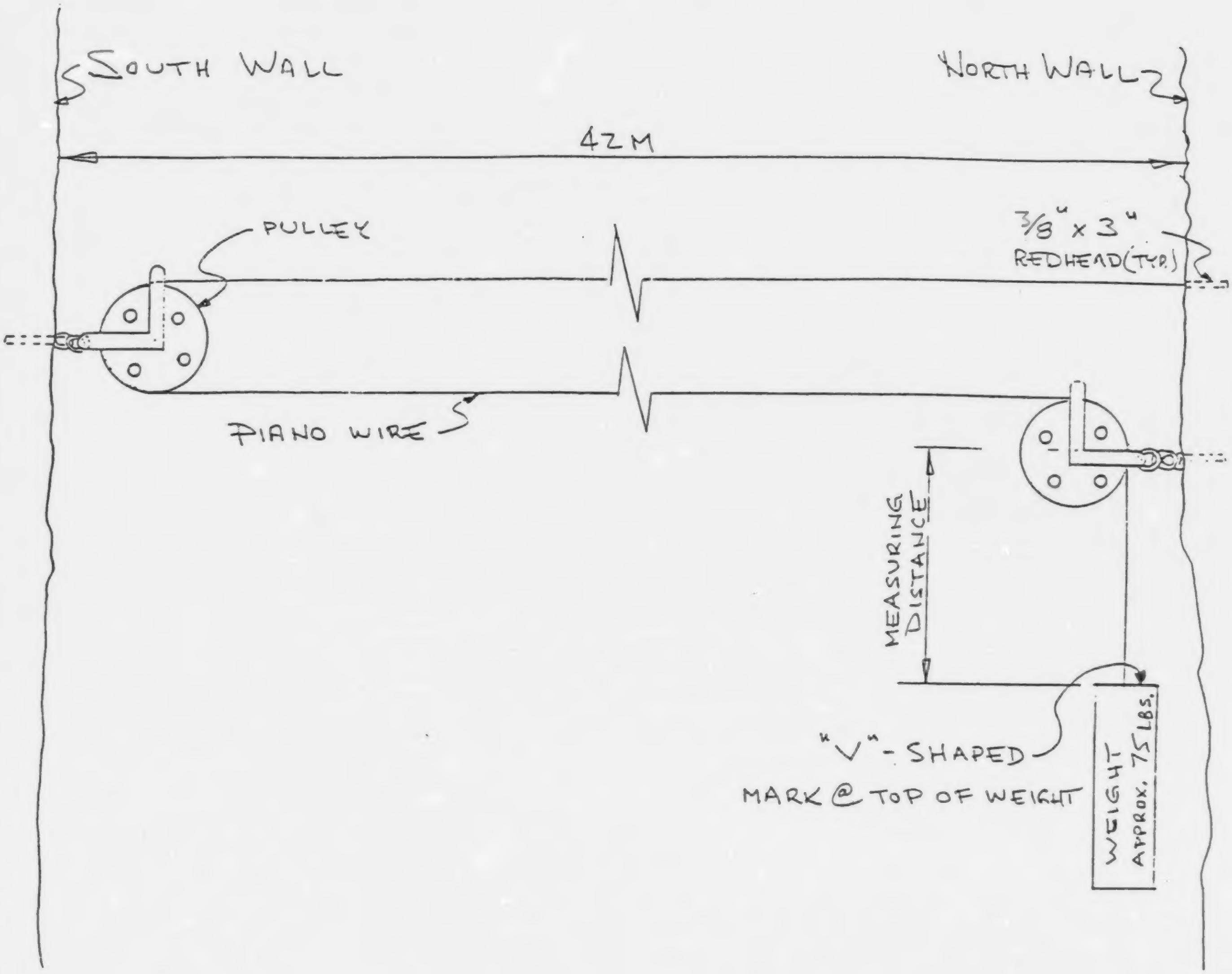

SOUTH WALL
NORTH WALL
42M
PULLEY
3/8" x 3"
REDHEAD (TYP.)
PIANO WIRE
MEASURING DISTANCE
"V"-SHAPED MARK @ TOP OF WEIGHT
WEIGHT
APPROX. 75 LBS.

GENERAL ARRANGEMENT

MEASUREMENT OF ABSOLUTE HORIZONTAL CLOSURE.
USING WIRE AND PULLEY METHOD IN TEST STOPE

N.T.S.
MIKE GRAVES
OCT. 29/84

FIGURE 3.11

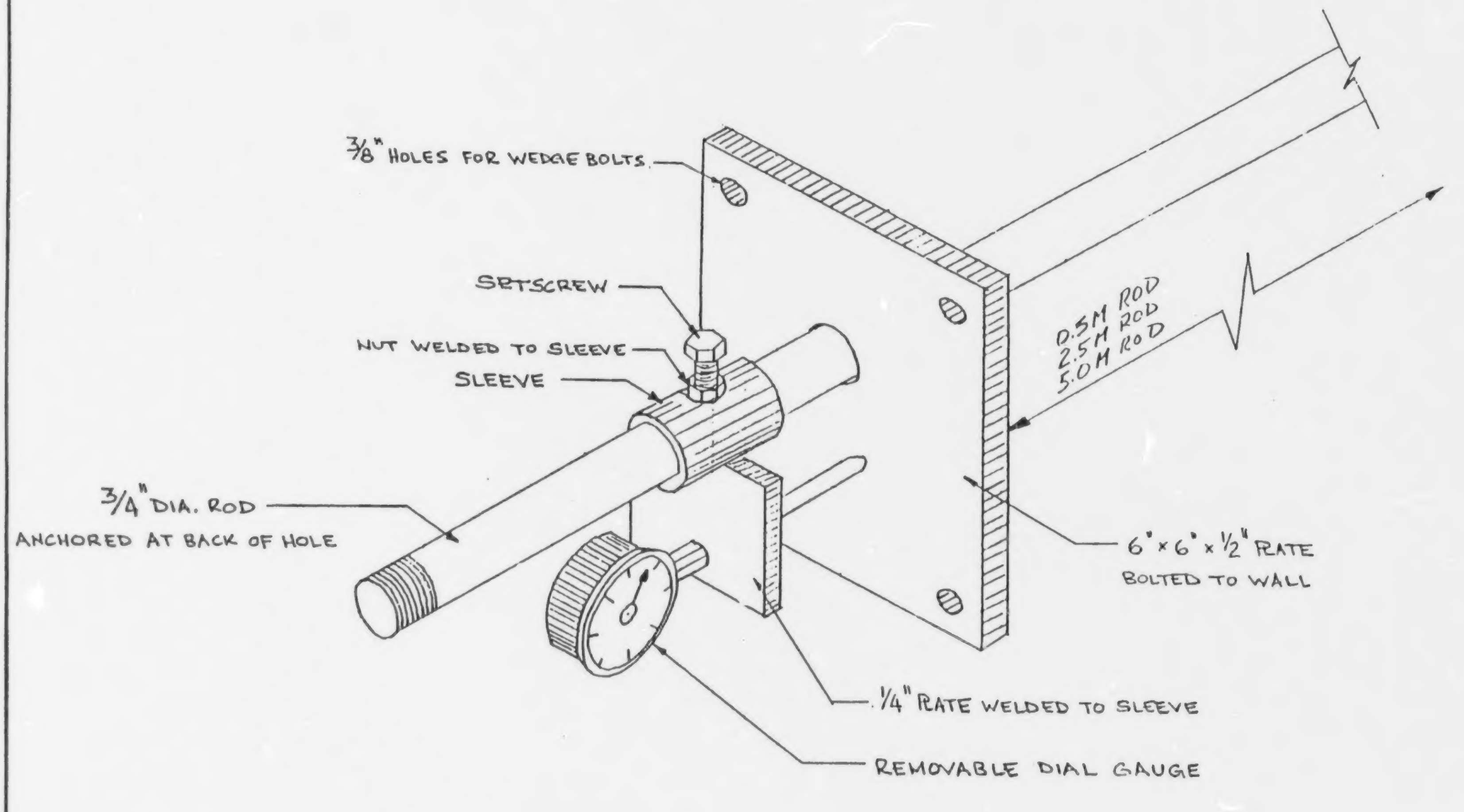
3/8" HOLES FOR WEDGE BOLTS
SETSCREW
NUT WELDED TO SLEEVE
SLEEVE
3/4" DIA. ROD
ANCHORED AT BACK OF HOLE
0.5M ROD
2.5M ROD
5.0M ROD
6" x 6" x 1/2" PLATE
BOLTED TO WALL
1/4" PLATE WELDED TO SLEEVE
REMOVABLE DIAL GAUGE

INSTALLATION ARRANGEMENT
RELATIVE CLOSURE STATIONS

FIGURE 3.12

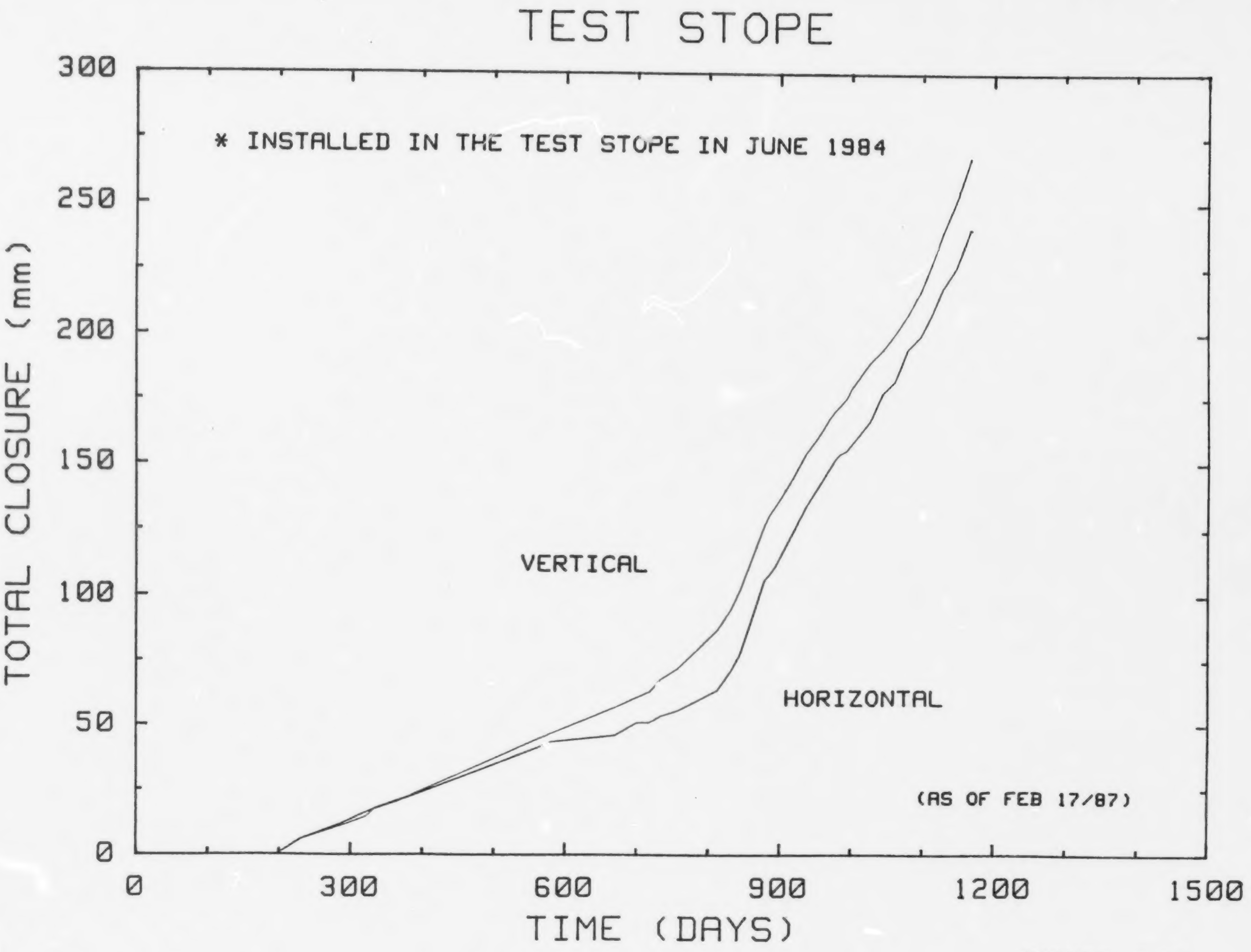
TEST STOPE
* INSTALLED IN THE TEST STOPE IN JUNE 1984
VERTICAL
HORIZONTAL
(AS OF FEB 17/87)
TOTAL CLOSURE (mm)
0
50
100
150
200
250
300
TIME (DAYS)
0
300
600
900
1200
1500

FIGURE 3.13

TABLE 3.9

STATION : TEST STOPE

MEASUREMENT : VERTICAL TOTAL CLOSURE.

MEASUREMENT SYSTEM : WIRE AND PULLEY

DATE	JULIAN CALENDAR DAY	DAYS SINCE EXCAVATION	READING (MM)	CLOSURE (MM)	CUMULATIVE CLOSURE (MM)
JUNE 22/84	174	197	1,179	0.0	0.0
JULY 26/84	208	231	1,236	0.0	0.0
SEPT.18/84	262	285	1,258	11.0	11.0
OCT. 24/84	298	321	1,265	3.5	14.5
NOV. 7/84	312	335	1,272	3.5	18.0
DEC. 19/84	354	377	1,280	4.0	22.0
JUNE 20/85	171	560	1,325	22.5	44.5
JULY 11/85	192	581	1,330	2.5	47.0
OCT. 7/85	280	669	1,350	10.0	57.0
NOV. 8/85	312	701	1,358	4.0	61.0
NOV. 25/85	329	718	1,362	2.0	63.0
DEC. 11/85	345	734	1,372	5.0	68.0
JAN. 3/86	3	757	1,380	4.0	72.0
FEB. 28/86	59	813	1,410	15.0	87.0
MAR. 19/86	78	832	1,426	8.0	95.0
MAR. 31/86	90	844	1,440	7.0	102.0
MAY 5/86	125	879	1,490	25.0	127.0
MAY 12/86	132	886	1,498	4.0	131.0
MAY 21/86	141	895	1,505	3.5	134.5
JUNE 9/86	160	913	1,522	8.5	143.0
JULY 2/86	183	936	1,545	11.5	154.5
JULY 17/86	198	951	1,556	5.5	160.0
AUG. 5/86	217	970	1,573	8.5	168.5
AUG. 12/86	224	978	1,578	2.5	171.0
AUG. 19/86	231	985	1,582	2.0	173.0
AUG. 27/86	239	993	1,587	2.5	175.5
SEPT. 3/86	246	1,000	1,595	4.0	179.5
SEPT.29/86	272	1,026	1,615	10.0	189.5
OCT. 17/86	290	1,044	1,625	5.0	194.5
NOV. 3/86	307	1,061	1,637	6.0	200.5
NOV. 21/86	325	1,079	1,652	7.5	208.0
DEC. 9/86	343	1,097	1,670	9.0	217.0
DEC. 9/86			1,095		
DEC. 24/86	358	1,112	1,116	10.5	227.5
JAN. 9/87	9	1,128	1,140	12.0	239.5
JAN. 28/87	28	1,147	1,165	12.5	252.0
FEB. 17/87	48	1,167	1,181	16.0	268.0

TABLE 3.10

STATION : TEST STOPE

MEASUREMENT : HORIZONTAL TOTAL CLOSURE.

MEASUREMENT SYSTEM : WIRE AND PULLEY

DATE	JULIAN CALENDAR DAY	DAYS SINCE EXCAVATION	READING (MM)	CLOSURE (MM)	CUMULATIVE CLOSURE (MM)
JUNE 22/84	174	197	893	0.0	0.0
JULY 26/84	208	231	905	6.0	6.0
SEPT.18/84	262	285	916	5.5	11.5
OCT. 24/84	298	321	925	4.5	16.0
NOV. 7/84	312	335	928	1.5	17.5
DEC. 19/84	354	377	936	4.0	21.5
JUNE 20/85	171	560	975	19.5	41.0
JULY 11/85	192	581	978	1.5	42.5
OCT. 7/85	280	669	985	3.5	46.0
NOV. 8/85	312	701	995	5.0	51.0
NOV. 25/85	329	718	995	0.0	51.0
DEC. 11/85	345	734	1,000	2.5	53.5
JAN. 3/86	3	757	1,004	2.0	55.5
FEB. 28/86	59	813	1,020	8.0	63.5
MAR. 19/86	78	832	1,035	7.5	71.0
MAR. 31/86	90	844	1,047	6.0	77.0
MAY 5/86	125	879	1,105	29.0	106.0
MAY 12/86	132	886	1,111	3.0	109.0
MAY 21/86	141	895	1,116	2.5	111.5
JULY 2/86	183	937	*	*	134.0
AUG. 5/86	217	971	850	*	*
AUG. 12/86	224	978	849	*	152.0
AUG. 19/86	231	985	853	2.0	154.0
AUG. 27/86	239	993	855	1.0	155.0
SEPT. 3/86	246	1,000	860	2.5	157.5
SEPT.29/86	272	1,026	878	9.0	166.5
OCT. 17/86	290	1,044	896	9.0	175.5
NOV. 3/86	307	1,061	905	4.5	180.0
NOV. 21/86	325	1,079	930	12.5	192.5
DEC. 9/86	343	1,097	940	5.0	197.5
DEC. 24/86	358	1,112	956	8.0	205.5
JAN. 9/87	9	1,128	977	10.5	216.0
JAN. 28/87	28	1,147	993	8.0	224.0
FEB. 17/87	48	1,167	1,009	16.5	240.5

* STATION TAKEN DOWN DUE TO SCOOPTRAM (ST8) TRAFFIC
STATION REINSTALLED ON AUG. 5/86

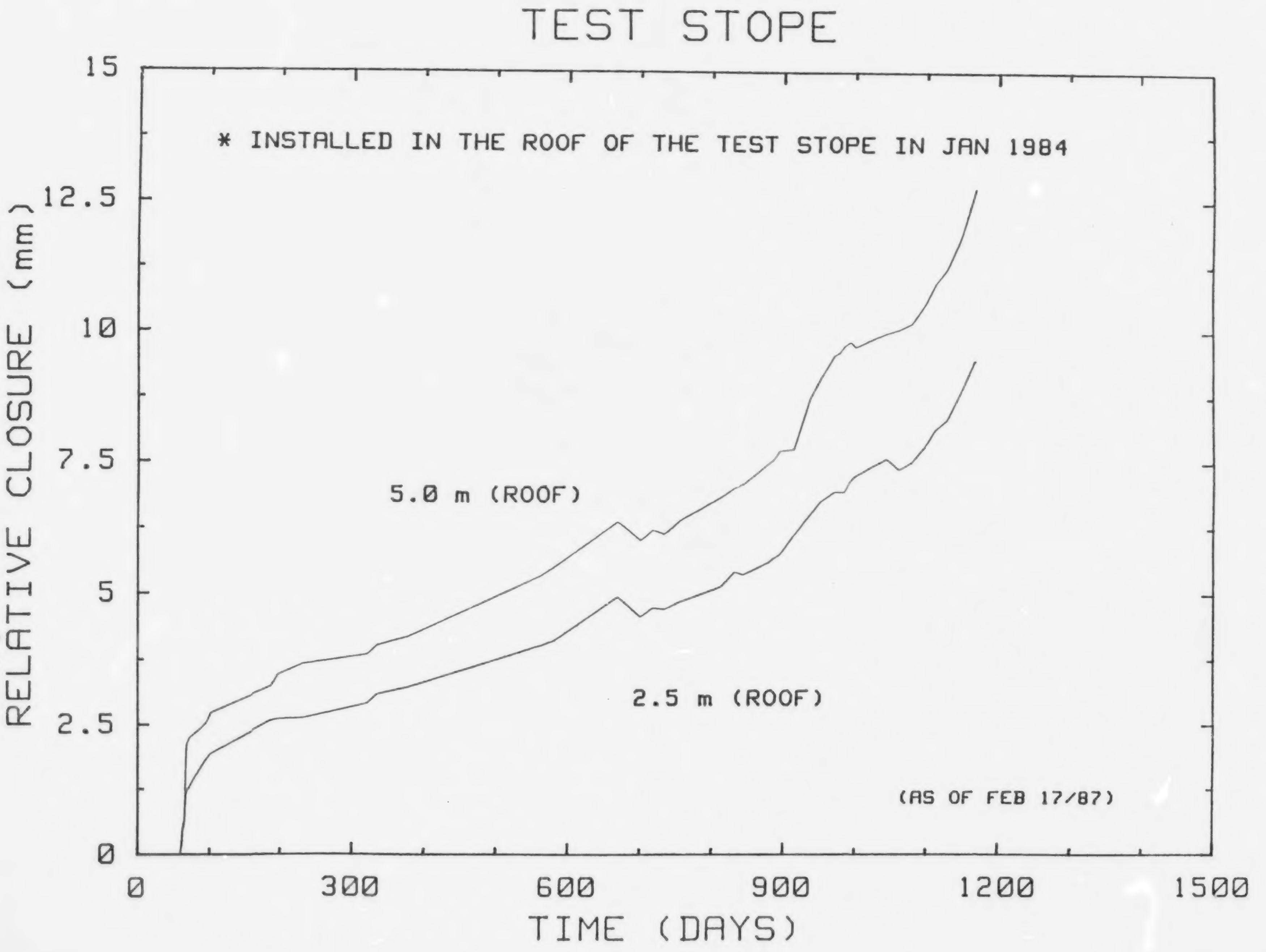
TEST STOPE
* INSTALLED IN THE ROOF OF THE TEST STOPE IN JAN 1984
5.0 m (ROOF)
2.5 m (ROOF)
(AS OF FEB 17/87)
RELATIVE CLOSURE (mm)
15
12.5
10
7.5
5
2.5
0
TIME (DAYS)
0
300
600
900
1200
1500

FIGURE 3.14

TABLE 3.11

STATION : TEST STOPE ROOF.

MEASUREMENT : RELATIVE CLOSURE/ 2.5M DEEP ANCHOR IN ROOF.

MEASUREMENT SYSTEM : RELATIVE CLOSURE STATION.

DATE	JULIAN CALENDAR DAY	DAYS SINCE EXCAVATION	READING (MM)	RELATIVE CUMULATIVE CLOSURE (MM)
FEB 5/84	36	59	6.8	0.0
FEB 8/84	39	62	7.0	0.2
FEB 9/84	40	63	7.2	0.4
FEB 10/84	41	64	7.2	0.4
FEB 11/84	42	65	7.4	0.6
FEB 12/84	43	66	7.7	0.9
FEB 13/84	44	67	7.9	1.1
FEB 14/84	45	68	8.0	1.2
FEB 18/84	49	72	8.0	1.2
FEB 25/84	56	79	8.3	1.5
MAR. 12/84	72	95	8.6	1.8
MAR. 19/84	79	102	8.8	2.0
JUNE 12/84	164	187	9.4	2.6
JUNE 22/84	174	197	9.4	2.6
JULY 27/84	179	232	9.4	2.6
OCT. 24/84	298	321	9.7	2.9
NOV. 7/84	312	335	9.9	3.1
DEC. 19/84	354	377	10.0	3.2
JUNE 20/85	171	560	10.8	4.0
JULY 11/85	192	581	10.9	4.1
OCT. 7/85	280	669	11.8	5.0
NOV. 8/85	312	701	11.4	4.6
NOV. 25/85	329	718	11.6	4.7
DEC. 11/85	345	734	11.5	4.7

TABLE 3.11 (CONT.)

STATION : TEST STOPE ROOF.

MEASUREMENT : RELATIVE CLOSURE/ 2.5M DEEP ANCHOR IN ROOF.

MEASUREMENT SYSTEM : RELATIVE CLOSURE STATION.

DATE	JULIAN CALENDAR DAY	DAYS SINCE EXCAVATION	READING (MM)	RELATIVE CUMULATIVE CLOSURE (MM)
JAN. 3/86	3	757	11.7	4.9
FEB. 28/86	31	813	12.0	5.2
MAR. 19/86	78	832	12.2	5.4
MAR. 31/86	90	844	12.2	5.4
MAY 5/86	125	879	12.4	5.6
MAY 12/86	132	886	12.5	5.7
MAY 21/86	141	895	12.6	5.8
JUNE 9/86	160	914	12.9	6.1
JULY 2/86	183	937	13.3	6.5
JULY 17/86	198	952	13.6	6.8
AUG. 5/86	217	971	13.8	7.0
AUG. 12/86	224	978	13.8	7.0
AUG. 19/86	231	985	13.8	7.0
AUG. 27/86	239	993	14.0	7.2
SEPT. 3/86	246	1,000	14.1	7.3
SEPT. 3/86	-	-	9.2	
SEPT.29/86	272	1,026	9.4	7.5
OCT. 17/86	290	1,044	9.5	7.6
NOV. 3/86	307	1,061	9.3	7.4
NOV. 21/86	325	1,079	9.5	7.5
DEC. 9/86	343	1,097	9.8	7.8
DEC. 24/86	358	1,112	10.1	8.2
JAN. 9/87	9	1,128	10.3	8.3
JAN. 28/87	28	1,147	10.8	8.9
FEB. 17/87	48	1,167	11.4	9.5

TABLE 3.12

STATION : TEST STOPE ROOF.

MEASUREMENT : RELATIVE CLOSURE/ 5.0M DEEP ANCHOR IN ROOF.

MEASUREMENT SYSTEM : RELATIVE CLOSURE STATION.

DATE	JULIAN CALENDAR DAY	DAYS SINCE EXCAVATION	READING (MM)	RELATIVE CUMULATIVE CLOSURE (MM)
FEB 5/84	36	54	0.6	0.0
FEB 8/84	39	46	1.1	0.5
FEB 9/84	40	54	1.2	0.6
FEB 10/84	41	46	1.2	0.6
FEB 11/84	42	54	1.2	0.7
FEB 12/84	43	46	2.0	1.4
FEB 13/84	44	54	2.5	2.0
FEB 14/84	45	46	2.7	2.1
FEB 18/84	49	54	2.8	2.3
FEB 25/84	56	46	2.9	2.3
MAR. 12/84	72	54	3.1	2.5
MAR. 19/84	79	46	3.3	2.7
JUNE 12/84	164	54	3.8	3.3
JUNE 22/84	174	46	4.1	3.5
JULY 27/84	179	54	4.3	3.7
OCT. 24/84	298	46	4.4	3.9
NOV. 7/84	312	54	4.6	4.0
DEC. 19/84	354	46	4.8	4.2
JUNE 20/85	171	560	5.9	5.3
JULY 11/85	192	581	6.1	5.5
OCT. 7/85	280	669	7.0	6.4
NOV. 8/85	312	701	6.6	6.0
NOV. 25/85	329	718	6.8	6.2
DEC. 11/85	345	734	6.7	6.1

TABLE 3.12 (CONT.)

STATION : TEST STOPE ROOF.

MEASUREMENT : RELATIVE CLOSURE/ 5.0M DEEP ANCHOR IN ROOF.

MEASUREMENT SYSTEM : DIAL GAUGE EXTENSOMETER

DATE	JULIAN CALENDAR DAY	DAYS SINCE EXCAVATION	READING (MM)	RELATIVE CUMULATIVE CLOSURE (MM)
JAN. 3/86	3	757	7.0	6.4
FEB. 28/86	31	813	7.4	6.9
MAR. 19/86	78	832	7.6	7.0
MAR. 31/86	90	844	7.7	7.1
MAY 5/86	125	879	8.1	7.5
MAY 12/86	132	886	8.2	7.6
MAY 21/86	141	895	8.3	7.7
JUNE 9/86	160	914	8.7	8.2
JULY 2/86	183	937	9.3	8.8
JULY 17/86	198	952	9.7	9.1
AUG. 5/86	217	971	10.2	9.6
AUG. 12/86	224	978	10.2	9.6
AUG. 19/86	231	985	10.3	9.8
AUG. 27/86	239	993	10.4	9.8
SEPT. 3/86	246	1,000	10.3	9.7
NOV. 3/86	307	1,061	6.0	10.1
NOV. 21/86	325	1,079	6.2	10.2
DEC. 9/86	343	1,097	6.5	10.5
DEC. 24/86	358	1,112	6.9	11.0
JAN. 9/87	9	1,128	7.2	11.2
JAN. 28/87	28	1,147	7.8	11.8
FEB. 17/87	48	1,167	8.8	12.8

TEST STOPE

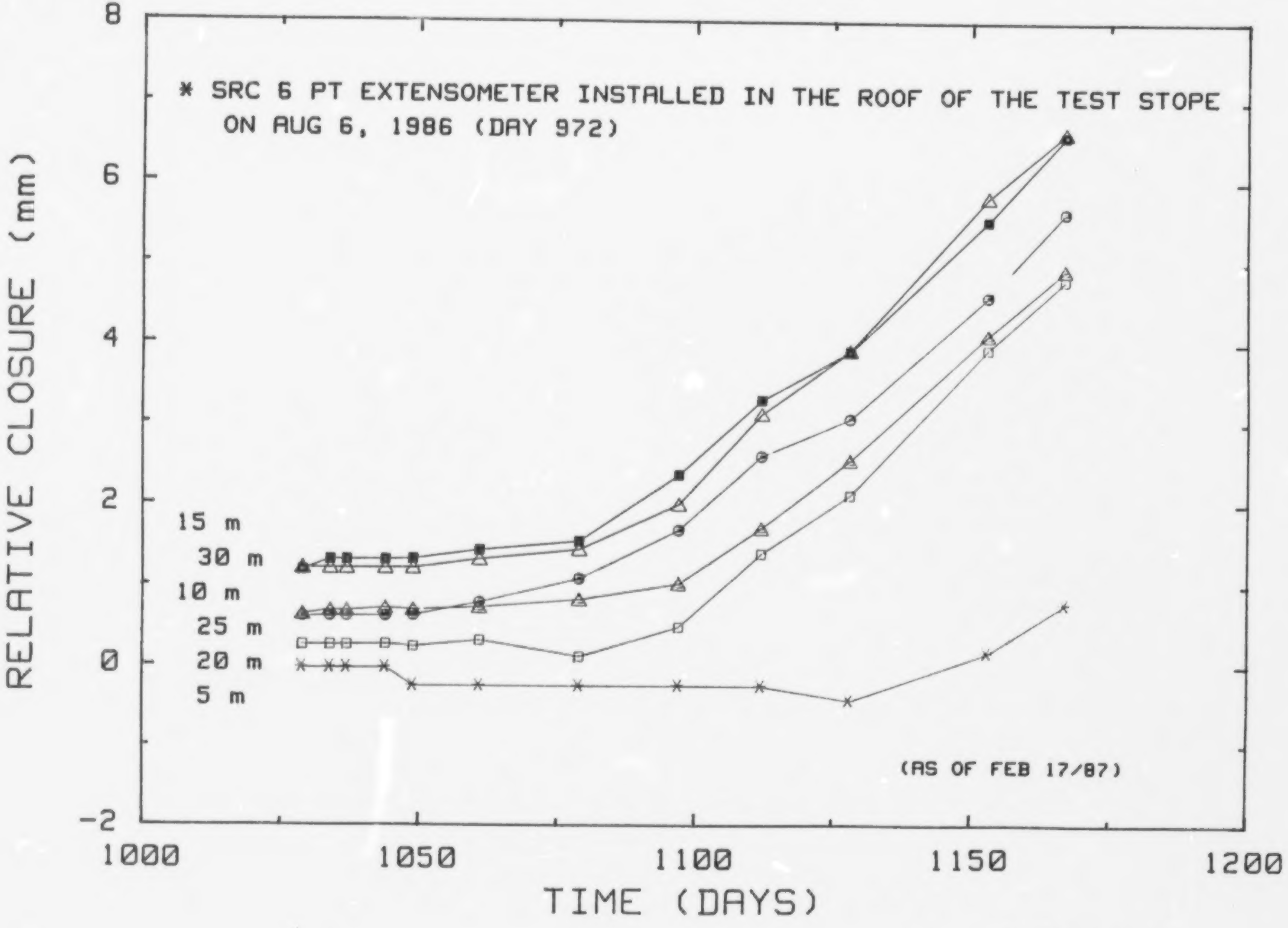

FIGURE 3.15

TABLE 3.13

STATION : TEST STOPE ROOF.

MEASUREMENT : RELATIVE CLOSURE/ 5,10,15,20,25 AND 30 M DEEP ANCHORS IN ROOF.

MEASUREMENT SYSTEM : SRC 6 CHANNEL EXTENSOMETER.

DATE	JULIAN CALENDAR DAY	DAYS SINCE EXCAVATION	5 M ANCHOR CUM. CLOSURE (MM)	10 M ANCHOR CUM. CLOSURE (MM)	15 M ANCHOR CUM. CLOSURE (MM)	20 M ANCHOR CUM. CLOSURE (MM)	25 M ANCHOR CUM. CLOSURE (MM)	30 M ANCHOR CUM. CLOSURE (MM)
AUG. 6/86	218	972						
AUG. 18/86	230	984	0.0	0.0	0.0	0.0	0.0	0.0
OCT. 2/86	275	1,029	0.0	0.6	1.2	0.3	0.6	1.2
OCT. 7/86	280	1,034	0.0	0.6	1.3	0.3	0.7	1.2
OCT. 7/86	RESET							
OCT. 10/86	283	1,037	0.0	0.6	1.3	0.3	0.7	1.2
OCT. 17/86	290	1,044	0.0	0.6	1.3	0.3	0.7	1.2
OCT. 22/86	295	1,049	-0.3	0.6	1.3	0.2	0.7	1.2
NOV. 3/86	307	1,061	-0.3	0.8	1.4	0.3	0.7	1.3
NOV. 21/86	325	1,079	-0.3	1.1	1.5	0.1	0.8	1.4
DEC. 9/86	343	1,097	-0.3	1.7	2.4	0.5	1.0	2.0
DEC. 24/86	358	1,112	-0.3	2.6	3.3	1.4	1.7	3.1
JAN. 9/87	9	1,128	0.4	3.1	3.9	2.1	2.6	3.9
FEB. 17/87	48	1,167	0.8	5.6	6.6	4.8	4.9	6.6

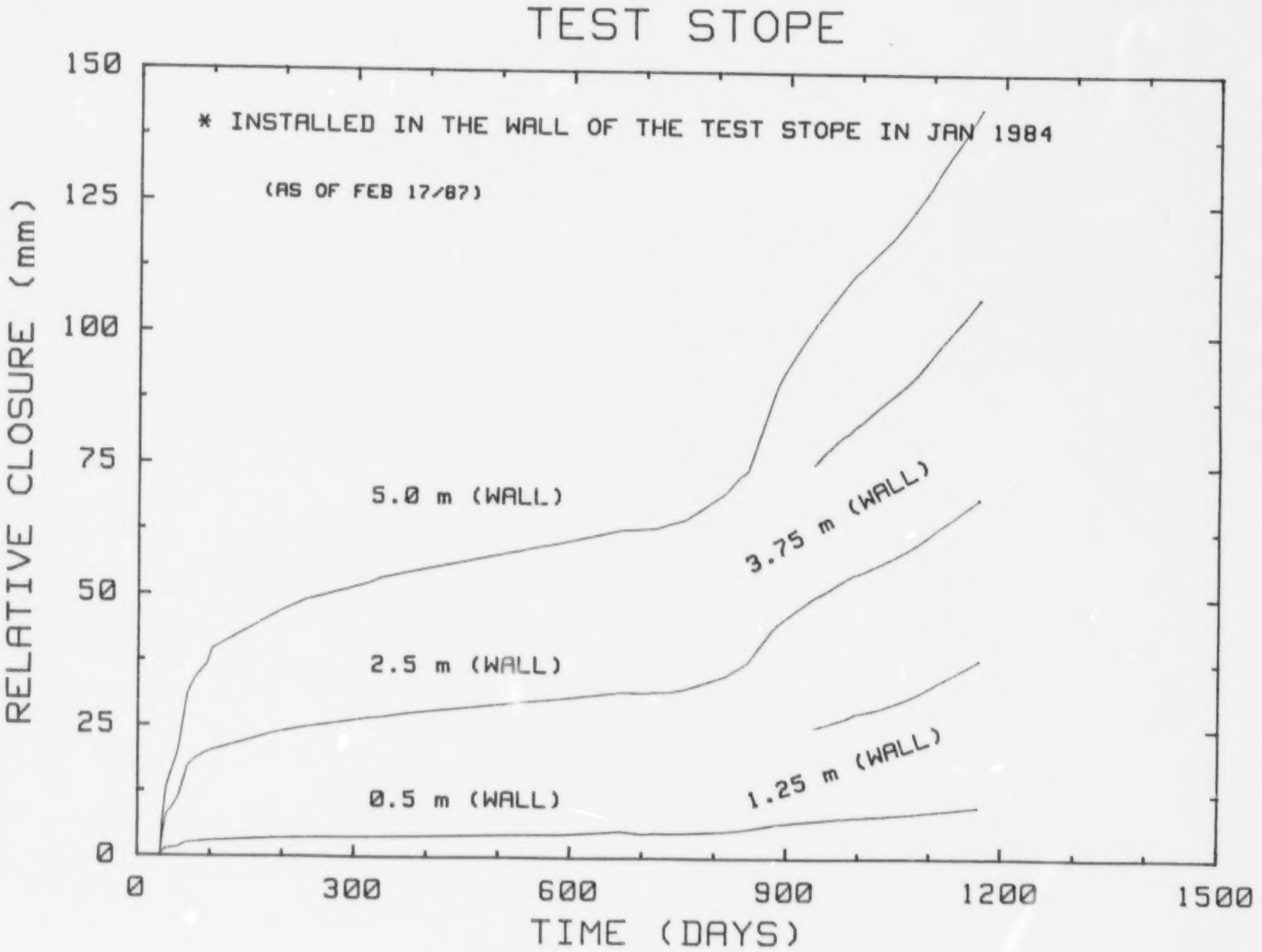
TEST STOPE
* INSTALLED IN THE WALL OF THE TEST STOPE IN JAN 1984
(AS OF FEB 17/87)
5.0 m (WALL)
3.75 m (WALL)
2.5 m (WALL)
1.25 m (WALL)
0.5 m (WALL)
RELATIVE CLOSURE (mm)
150
125
100
75
50
25
0
TIME (DAYS)
0
300
600
900
1200
1500

FIGURE 3.16

TABLE 3.14

STATION : TEST STOPE WEST WALL.

MEASUREMENT : RELATIVE CLOSURE/0.5M DEEP ANCHOR IN WEST WALL.

MEASUREMENT SYSTEM : RELATIVE CLOSURE STATION.

DATE	JULIAN CALENDAR DAY	DAYS SINCE EXCAVATION	READING (MM)	RELATIVE CUMULATIVE CLOSURE (MM)
JAN. 8/84	8	-	4.8	0.0
JAN. 11/84	11	34	5.5	0.8
JAN. 12/84	12	35	5.6	0.9
JAN. 13/84	13	36	5.7	0.9
JAN. 14/84	14	37	5.9	1.1
JAN. 15/84	15	38	6.0	1.2
JAN. 16/84	16	39	6.1	1.3
JAN. 17/84	17	40	6.1	1.3
JAN. 23/84	23	46	6.2	1.5
JAN. 31/84	31	54	6.4	1.6
FEB 3/84	34	57	6.4	1.7
FEB 5/84	36	59	6.7	1.9
FEB 8/84	39	62	6.9	2.1
FEB 9/84	40	63	7.0	2.2
FEB 10/84	41	64	7.0	2.2
FEB 11/84	42	65	7.1	2.3
FEB 12/84	43	66	7.2	2.5
FEB 13/84	44	67	7.2	2.5
FEB 14/84	45	68	7.3	2.5
FEB 18/84	49	72	7.4	2.6
FEB 25/84	56	79	7.5	2.7
MAR. 12/84	72	95	7.7	2.9
MAR. 19/84	79	102	7.8	3.0
JUNE 12/84	164	187	8.2	3.5
JUNE 22/84	174	197	8.3	3.5
JULY 27/84	179	232	8.4	3.6
OCT. 24/84	298	321	8.6	3.8
NOV. 7/84	312	335	8.6	3.9
DEC. 19/84	354	377	8.7	3.9
JUNE 20/85	171	560	9.1	4.4
JULY 11/85	192	581	9.1	4.4
OCT. 7/85	280	669	9.8	5.1
NOV. 8/85	312	701	9.3	4.6
NOV. 25/85	329	718	9.5	4.7
DEC. 11/85	345	734	9.5	4.7

TABLE 3.14 (CONT.)

STATION : TEST STOPE WEST WALL.

MEASUREMENT : RELATIVE CLOSURE/0.5M DEEP ANCHOR IN WEST WALL.

MEASUREMENT SYSTEM : RELATIVE CLOSURE STATION.

DATE	JULIAN CALENDAR DAY	DAYS SINCE EXCAVATION	READING (MM)	RELATIVE CUMULATIVE CLOSURE (MM)
JAN. 3/86	3	757	9.6	4.8
FEB. 28/86	31	813	9.9	5.1
MAR. 19/86	78	832	10.1	5.4
MAR. 31/86	90	844	10.3	5.6
MAY 5/86	125	879	11.1	6.4
MAY 12/86	132	886	11.4	6.6
MAY 21/86	141	895	11.4	6.7
JUNE 9/86	160	914	11.7	6.9
JULY 2/86	183	937	12.0	7.3
JULY 17/86	198	952	12.2	7.4
AUG. 5/86	217	971	12.5	7.7
AUG. 12/86	224	978	12.5	7.7
AUG. 19/86	231	985	12.6	7.8
AUG. 27/86	239	993	12.8	8.0
SEPT. 3/86	246	1,000	12.7	7.9
SEPT. 3/86	-	-	8.0	7.9
SEPT.29/86	272	1,026	8.2	8.1
OCT. 17/86	290	1,044	8.4	8.3
NOV. 3/86	307	1,061	8.5	8.5
NOV. 21/86	325	1,079	8.7	8.6
DEC. 9/86	343	1,097	9.0	8.9
DEC. 24/86	358	1,112	9.2	9.1
JAN. 9/87	9	1,128	9.4	9.3
JAN. 28/87	28	1,147	9.7	9.6
FEB. 17/87	48	1,167	10.0	9.9

TABLE 3.15

STATION : TEST STOPE WEST WALL.

MEASUREMENT : RELATIVE CLOSURE/1.25M DEEP ANCHOR IN WEST WALL.

MEASUREMENT SYSTEM : RELATIVE CLOSURE STATION.

DATE	JULIAN CALENDAR DAY	DAYS SINCE EXCAVATION	READING (MM)	RELATIVE CUMULATIVE CLOSURE (MM)
JULY 2/86	183	937	0.0	25.2
JULY 17/86	198	952	0.5	25.7
AUG. 5/86	217	971	0.9	26.6
AUG. 12/86	224	978	0.3	26.9
AUG. 19/86	231	985	0.4	27.3
AUG. 27/86	239	993	0.6	27.9
SEPT. 3/86	246	1,000	0.2	28.1
SEPT.29/86	272	1,026	0.7	28.8
OCT. 17/86	290	1,044	0.9	29.7
NOV. 3/86	307	1,061	0.9	30.6
NOV. 21/86	325	1,079	1.1	31.7
DEC. 9/86	343	1,097	1.3	33.0
DEC. 24/86	358	1,112	1.1	34.1
JAN. 9/87	9	1,128	1.2	35.3
JAN. 28/87	28	1,147	1.4	36.7
FEB. 17/87	48	1,167	1.5	38.2

TABLE 3.16

STATION : TEST STOPE WEST WALL.

MEASUREMENT : RELATIVE CLOSURE/2.5M DEEP ANCHOR IN WEST WALL.

MEASUREMENT SYSTEM : RELATIVE CLOSURE STATION.

DATE	JULIAN CALENDAR DAY	DAYS SINCE EXCAVATION	READING (MM)	RELATIVE CUMULATIVE CLOSURE (MM)	
JAN. 8/84	8	-	2.4	0.0	
JAN. 11/84	11	34	6.4	4.0	
JAN. 12/84	12	35	7.2	4.7	
JAN. 13/84	13	36	7.7	5.3	
JAN. 14/84	14	37	8.7	6.3	
JAN. 15/84	15	38	9.5	7.1	
JAN. 16/84	16	39	10.2	7.7	
JAN. 17/84	17	40	10.6	8.2	
JAN. 23/84	23	46	11.5	9.1	
JAN. 31/84	31	54	13.3	10.9	
FEB 3/84	34	57	14.3	11.9	
FEB 5/84	36	59	15.1	12.7	RESET
FEB 8/84	39	62	1.9	14.3	
FEB 9/84	40	63	2.2	14.6	
FEB 10/84	41	64	2.7	15.1	
FEB 11/84	42	65	3.2	15.5	
FEB 12/84	43	66	3.6	16.0	
FEB 13/84	44	67	4.2	16.6	
FEB 14/84	45	68	4.7	17.1	
FEB 18/84	49	72	5.4	17.8	
FEB 25/84	56	79	6.4	18.8	
MAR. 12/84	72	95	7.6	20.0	
MAR. 19/84	79	102	8.0	20.4	
JUNE 12/84	164	187	11.4	23.7	
JUNE 22/84	174	197	11.7	24.0	
JULY 27/84	179	232	12.5	24.9	
OCT. 24/84	298	321	14.3	26.7	
NOV. 7/84	312	335	14.4	26.8	
DEC. 19/84	354	377	15.3	27.7	
					RESET
JUNE 20/85	171	560	17.8	30.2	
JULY 11/85	192	581	4.3	30.4	
OCT. 7/85	280	669	5.8	31.8	
NOV. 8/85	312	701	5.7	31.7	
NOV. 25/85	329	718	5.8	31.9	
DEC. 11/85	345	734	5.8	31.9	

TABLE 3.16 (CONT.)

STATION : TEST STOPE WEST WALL.

MEASUREMENT : RELATIVE CLOSURE/ 2.5M DEEP ANCHOR IN WEST WALL.

MEASUREMENT SYSTEM : RELATIVE CLOSURE STATION.

DATE	JULIAN CALENDAR DAY	DAYS SINCE EXCAVATION	READING (MM)	RELATIVE CUMULATIVE CLOSURE (MM)	
JAN. 3/86	3	757	6.4	32.5	
FEB. 28/86	31	813	8.9	35.0	
MAR. 19/86	78	832	10.4	36.5	
MAR. 31/86	90	844	11.5	37.5	
MAY 5/86	125	879	17.8	43.8	
			7.3		RESET
MAY 12/86	132	886	8.3	44.8	
MAY 21/86	141	895	9.3	45.8	
JUNE 9/86	160	914	11.3	47.8	
JULY 2/86	183	937	13.6	50.1	
JULY 17/86	198	952	14.6	51.1	
AUG. 5/86	217	971	16.3	52.8	
AUG. 12/86	224	978	16.9	53.4	
AUG. 19/86	231	985	17.4	53.9	
AUG. 27/86	239	993	18.0	54.5	
SEPT. 3/86	246	1,000	18.2	54.7	
			0.4		
			6.2	54.7	
SEPT.29/86	272	1,026	7.9	56.3	
OCT. 17/86	290	1,044	9.0	57.5	
NOV. 3/86	307	1,061	10.3	58.8	
NOV. 21/86	325	1,079	11.7	60.2	
DEC. 9/86	343	1,097	13.5	61.9	
DEC. 24/86	358	1,112	15.1	63.6	
			11.0		
JAN. 9/87	9	1,128	12.4	65.0	
JAN. 28/87	28	1,147	14.4	67.0	
FEB. 17/87	48	1,167	16.4	69.0	

TABLE 3.17

STATION : TEST STOPE WEST WALL.

MEASUREMENT : RELATIVE CLOSURE/ 3.75M DEEP ANCHOR IN WEST WALL.

MEASUREMENT SYSTEM : RELATIVE CLOSURE STATION.

DATE	JULIAN CALENDAR DAY	DAYS SINCE EXCAVATION	READING (MM)	RELATIVE CUMULATIVE CLOSURE (MM)
JULY 2/86	183	937	0.0	75.4
JULY 17/86	198	952	2.3	77.7
AUG. 5/86	217	971	2.5	80.2
AUG. 12/86	224	978	0.7	80.9
AUG. 19/86	231	985	0.5	81.4
AUG. 27/86	239	993	1.2	82.6
SEPT. 3/86	246	1,000	0.6	83.2
SEPT.29/86	272	1,026	3.1	86.3
OCT. 17/86	290	1,044	2.0	88.3
NOV. 3/86	307	1,061	2.0	90.3
NOV. 21/86	325	1,079	2.3	92.6
DEC. 9/86	343	1,097	3.0	95.6
DEC. 24/86	358	1,112	2.6	98.2
JAN. 9/87	9	1,128	2.4	100.6
JAN. 28/87	28	1,147	3.0	103.6
FEB. 17/87	48	1,167	3.5	107.1

TABLE 3.18

STATION : TEST STOPE WEST WALL.

MEASUREMENT : RELATIVE CLOSURE/ 5.0M DEEP ANCHOR IN WEST WALL.

MEASUREMENT SYSTEM : RELATIVE CLOSURE STATION.

DATE	JULIAN CALENDAR DAY	DAYS SINCE EXCAVATION	READING (MM)	RELATIVE CUMULATIVE CLOSURE (MM)	
JAN. 8/84	8	-	2.2	0.0	
JAN. 11/84	11	34	9.0	6.8	
JAN. 12/84	12	35	10.3	8.2	
JAN. 13/84	13	36	11.5	9.3	
JAN. 14/84	14	37	13.0	10.8	
JAN. 15/84	15	38	14.3	12.1	
JAN. 16/84	16	39	15.3	13.1	
JAN. 17/84	17	40	16.1	13.9	RESET
JAN. 23/84	23	46	5.6	16.3	
JAN. 31/84	31	54	8.8	19.4	
FEB 3/84	34	57	10.7	21.4	
FEB 5/84	36	59	12.4	23.1	RESET
FEB 8/84	39	62	2.8	25.9	
FEB 9/84	40	63	3.5	26.5	
FEB 10/84	41	64	4.3	27.4	
FEB 11/84	42	65	5.4	28.4	
FEB 12/84	43	66	6.1	29.2	
FEB 13/84	44	67	7.0	30.1	
FEB 14/84	45	68	7.8	30.9	
FEB 18/84	49	72	9.2	32.3	
FEB 25/84	56	79	11.1	34.2	
MAR. 12/84	72	95	13.7	36.8	RESET
MAR. 19/84	79	102	5.7	39.7	
JUNE 12/84	164	187	12.2	46.2	
JUNE 22/84	174	197	13.0	47.0	RESET
JULY 27/84	179	232	4.9	49.1	
OCT. 24/84	298	321	8.1	52.4	
NOV. 7/84	312	335	9.0	53.3	
DEC. 19/84	354	377	10.2	54.5	
JUNE 20/85	171	560	15.2	59.5	RESET
JULY 11/85	192	581	4.5	60.0	
OCT. 7/85	280	669	7.2	62.7	
NOV. 8/85	312	701	7.5	62.9	
NOV. 25/85	329	718	7.7	63.1	
DEC. 11/85	345	734	8.2	63.6	

TABLE 3.18 (CONT.)

STATION : TEST STOPE WEST WALL.

MEASUREMENT : RELATIVE CLOSURE/ 5.0M DEEP ANCHOR IN WEST WALL.

MEASUREMENT SYSTEM : RELATIVE CLOSURE STATION.

DATE	JULIAN CALENDAR DAY	DAYS SINCE EXCAVATION	READING (MM)	RELATIVE CUMULATIVE CLOSURE (MM)	
JAN. 3/86	3	757	9.0	64.5	
FEB. 28/86	31	813	14.1	69.6	
MAR. 19/86	78	832	17.2	72.7	
MAR. 31/86	90	844	18.4	73.8	
MAR. 31/86			3.9		RESET
MAY 5/86	125	879	18.0	87.9	
MAY 5/86			7.1		RESET
MAY 12/86	132	886	9.7	90.4	
MAY 21/86	141	895	11.9	92.7	
MAY 21/86			2.2		
JUNE 9/86	160	914	6.5	97.0	
JULY 2/86	183	937	11.1	101.7	
JULY 17/86	198	952	13.9	104.5	
AUG. 5/86	217	971	17.2	107.8	
			0.4		
AUG. 12/86	224	978	10.9	109.1	
AUG. 19/86	231	985	12.2	110.3	
AUG. 27/86	239	993	13.5	111.6	
SEPT. 3/86	246	1,000	14.3	112.4	
SEPT. 3/86	-	-	9.7	112.4	
SEPT.29/86	272	1,026	13.2	116.0	
OCT. 17/86	290	1,044	15.6	118.4	
NOV. 3/86	307	1,061	18.5	121.3	
NOV. 3/86			7.8		RESET
NOV. 21/86	325	1,079	11.1	124.6	
DEC. 9/86	343	1,097	14.6	128.1	
DEC. 24/86	358	1,112	18.1	131.7	
DEC. 24/86			12.2		
JAN. 9/87	9	1,128	15.5	134.9	
JAN. 28/87	28	1,147	19.2	138.6	
JAN. 28/87			4.4		
FEB. 17/87	48	1,167	9.3	143.6	

LATERAL PRESSURE CELLS

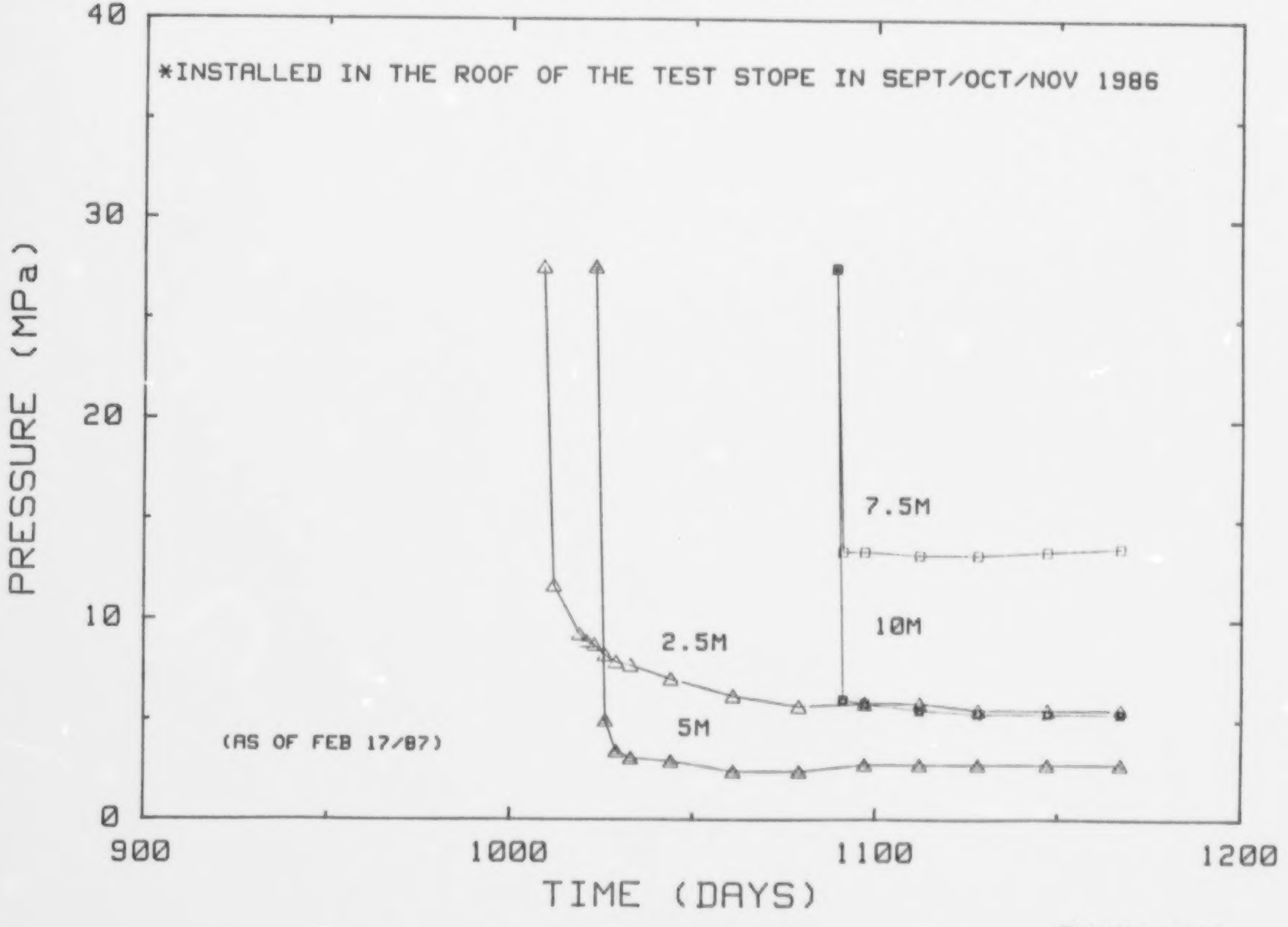

FIGURE 3.17

TABLE 3.19

STATION : TEST STOPE ROOF.

MEASUREMENT : LATERAL PRESSURE AT 2.5,5,7.5 AND 10 M DEPTHS IN ROOF.

MEASUREMENT SYSTEM : SRC UNIDIRECTIONAL PRESSURE CELL.

DATE	JULIAN CALENDAR DAY	DAYS SINCE EXCAVATION	2.5 M PRESSURE CELL - R2.5ML (MPa)	5.0 M PRESSURE CELL - R5ML (MPa)	7.5 M PRESSURE CELL - R7.5ML (MPa)	10 M PRESSURE CELL - R10ML (MPa)
SEPT.12/86	255	1,009	27.58			
SEPT.15/86	258	1,012	11.72			
SEPT.22/86	265	1,019	9.31			
SEPT.24/86	267	1,021	8.96			
SEPT.26/86	269	1,023	8.79	27.58		
SEPT.29/86	272	1,026	8.27	5.00		
OCT. 2/86	275	1,029	7.93	3.45		
OCT. 6/86	279	1,033	7.76	3.10		
OCT. 17/86	290	1,044	7.07	2.93		
NOV. 3/86	307	1,061	6.21	2.41		
NOV. 21/86	325	1,079	5.59	2.41		
DEC. 1/86	335	1,089	-	-	27.58	27.58
DEC. 3/86	337	1,091	-	-	13.45	6.03
DEC. 9/86	343	1,097	5.86	2.76	13.45	5.86
DEC. 24/86	358	1,112	5.86	2.76	13.27	5.52
JAN. 9/87	9	1,128	5.52	2.76	13.27	5.34
FEB. 17/87	48	1,167	5.52	2.76	13.62	5.34

TANGENTIAL PRESSURE CELLS

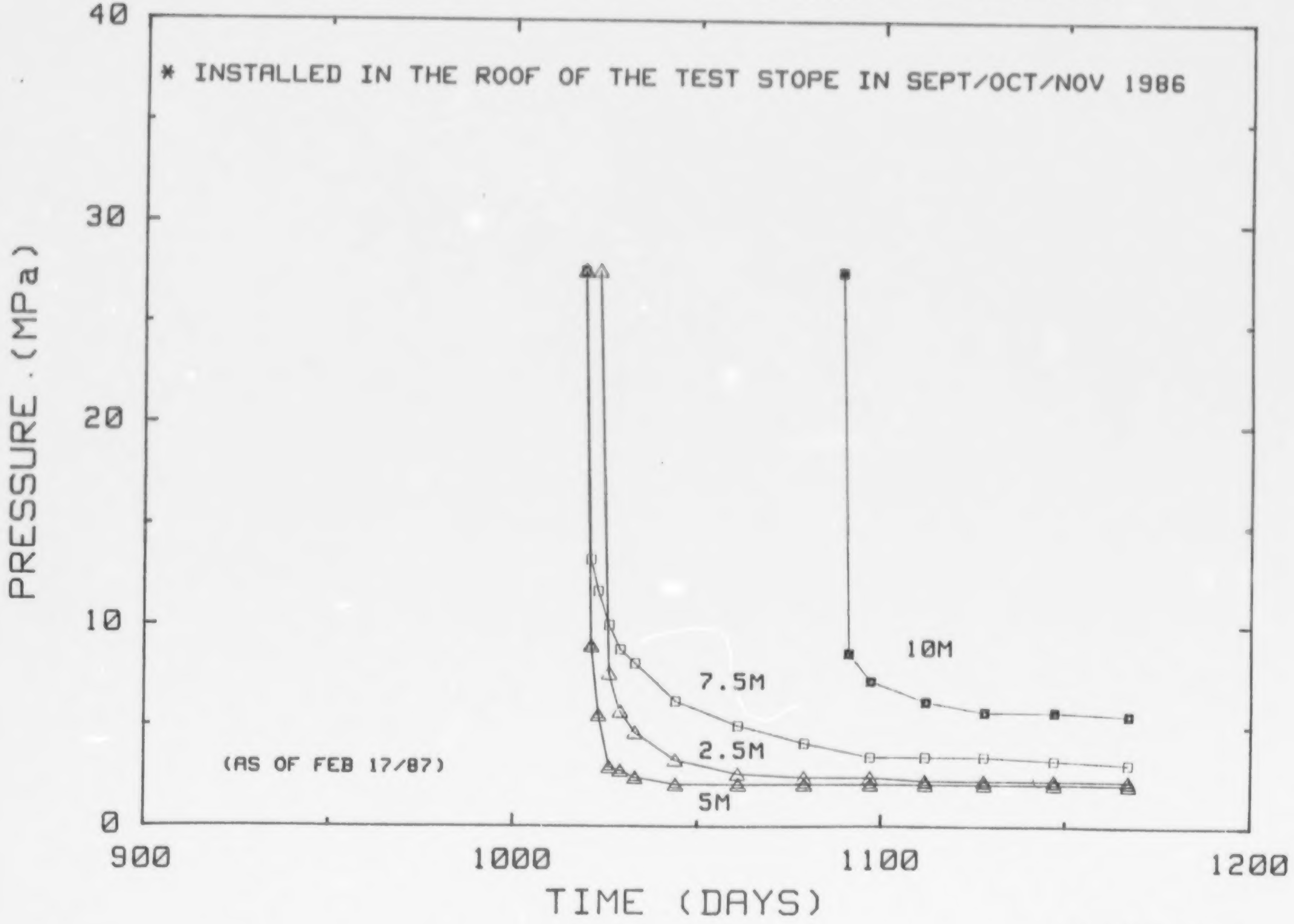

FIGURE 3.18

TABLE 3.20

STATION : TEST STOPE ROOF.

MEASUREMENT : TANGENTIAL PRESSURE AT 2.5,5,7.5 AND 10 M DEPTHS IN ROOF.

MEASUREMENT SYSTEM : SRC UNIDIRECTIONAL PRESSURE CELL.

DATE	JULIAN CALENDAR DAY	DAYS SINCE EXCAVATION	2.5 M PRESSURE CELL - R2.5MT (MPa)	5.0 M PRESSURE CELL - R5MT (MPa)	7.5 M PRESSURE CELL - R7.5MT (MPa)	10 M PRESSURE CELL - R10MT (MPa)
SEPT.22/86	265	1,019		27.58	27.58	
SEPT.24/86	267	1,021		8.96	13.27	
SEPT.26/86	269	1,023	27.58	5.52	11.72	
SEPT.29/86	272	1,026	7.58	2.93	10.00	
OCT. 2/86	275	1,029	5.69	2.76	8.79	
OCT. 6/86	279	1,033	4.65	2.41	8.10	
OCT. 17/86	290	1,044	3.28	2.07	6.21	
NOV. 3/86	307	1,061	2.59	2.07	5.00	
NOV. 21/86	325	1,079	2.41	2.07	4.14	
DEC. 1/86	335	1,089	-	-	-	27.58
DEC. 3/86	337	1,091	-	-	-	8.62
DEC. 9/86	343	1,097	2.41	2.07	3.45	7.24
DEC. 24/86	358	1,112	2.24	2.07	3.45	6.21
JAN. 9/87	9	1,128	2.24	2.07	3.45	5.69
FEB. 17/87	48	1,167	2.24	2.07	3.10	5.52

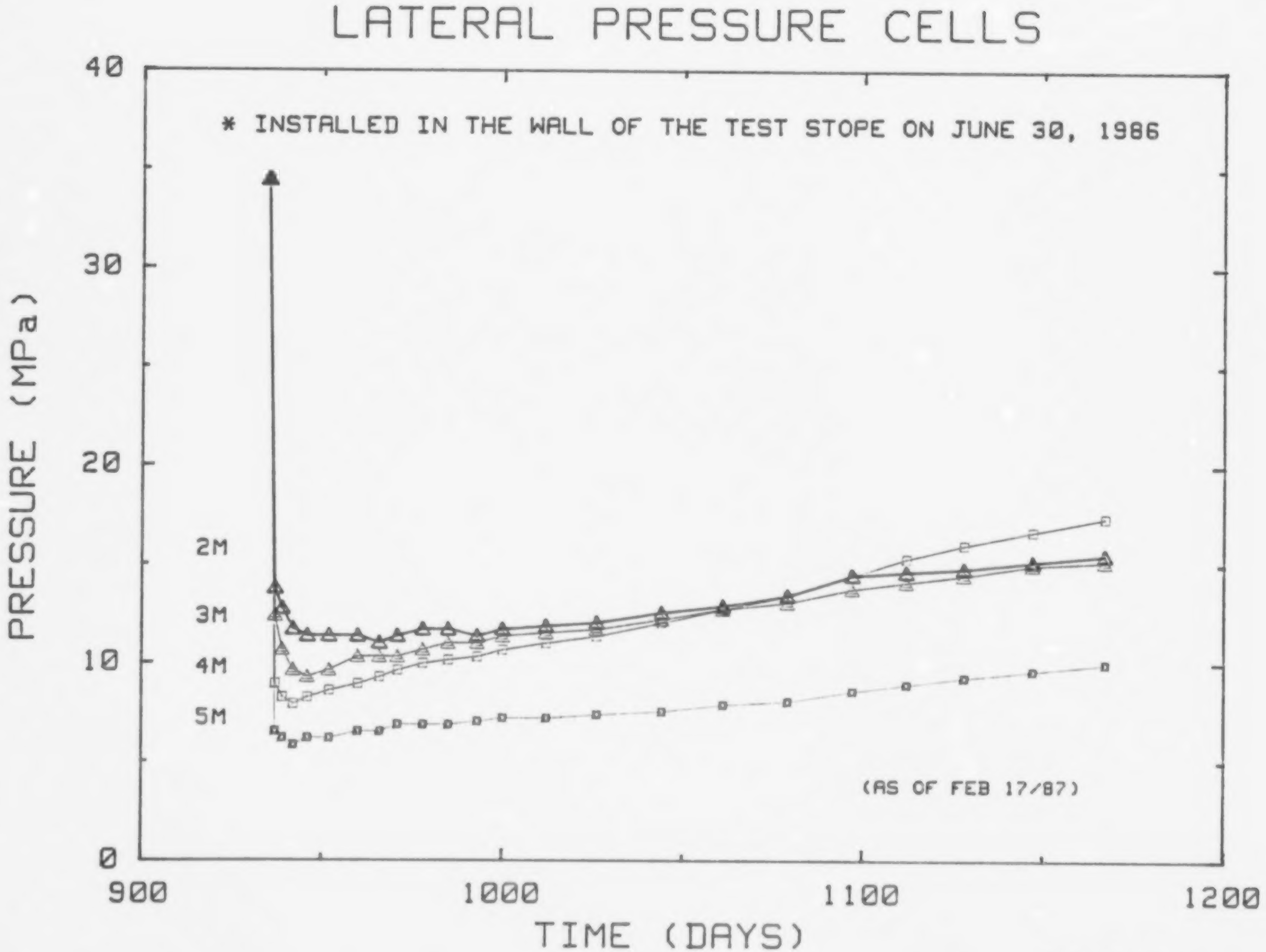
LATERAL PRESSURE CELLS
* INSTALLED IN THE WALL OF THE TEST STOPE ON JUNE 30, 1986
PRESSURE (MPa)
40
30
20
10
0
2M
3M
4M
5M
(AS OF FEB 17/87)
900
1000
1100
1200
TIME (DAYS)

FIGURE 3.19

TABLE 3.21

STATION : TEST STOPE WALL.

MEASUREMENT : LATERAL PRESSURE AT 2,3,4 AND 5 M DEPTHS IN WALL.

MEASUREMENT SYSTEM : SRC UNIDIRECTIONAL PRESSURE CELL

DATE	JULIAN CALENDAR DAY	DAYS SINCE EXCAVATION	2 M PRESSURE CELL - W2ML (MPa)	3 M PRESSURE CELL - W3ML (MPa)	4 M PRESSURE CELL - W4ML (MPa)	5 M PRESSURE CELL - W5ML (MPa)
JUNE 30/86	181	935	34.47	34.47	34.47	34.47
JULY 2/86	183	937	13.79	12.41	8.96	6.55
JULY 4/86	185	939	12.75	10.69	8.27	6.21
JULY 7/86	188	942	11.72	9.65	7.93	5.86
JULY 11/86	192	946	11.38	9.31	8.27	6.21
JULY 17/86	198	952	11.38	9.65	8.62	6.21
JULY 25/86	206	960	11.38	10.34	8.96	6.55
JULY 31/86	212	966	11.03	10.34	9.31	6.55
AUG. 5/86	217	971	11.38	10.34	9.65	6.90
AUG. 12/86	224	978	11.72	10.69	10.00	6.90
AUG. 19/86	231	985	11.72	11.03	10.17	6.90
AUG. 27/86	239	993	11.38	11.03	10.34	7.07
SEPT. 3/86	246	1,000	11.72	11.38	10.69	7.24
SEPT.15/86	258	1,012	11.89	11.55	11.03	7.24
SEPT.29/86	272	1,026	12.07	11.72	11.38	7.41
OCT. 17/86	290	1,044	12.58	12.24	12.07	7.58
NOV. 3/86	307	1,061	12.93	12.76	12.76	7.93
NOV. 21/86	325	1,079	13.45	13.10	13.45	8.10
DEC. 9/86	343	1,097	14.48	13.79	14.48	8.62
DEC. 24/86	358	1,112	14.65	14.13	15.34	8.96
JAN. 9/87	9	1,128	14.82	14.48	16.03	9.31
FEB. 17/87	48	1,167	15.51	17.17	17.41	10.00

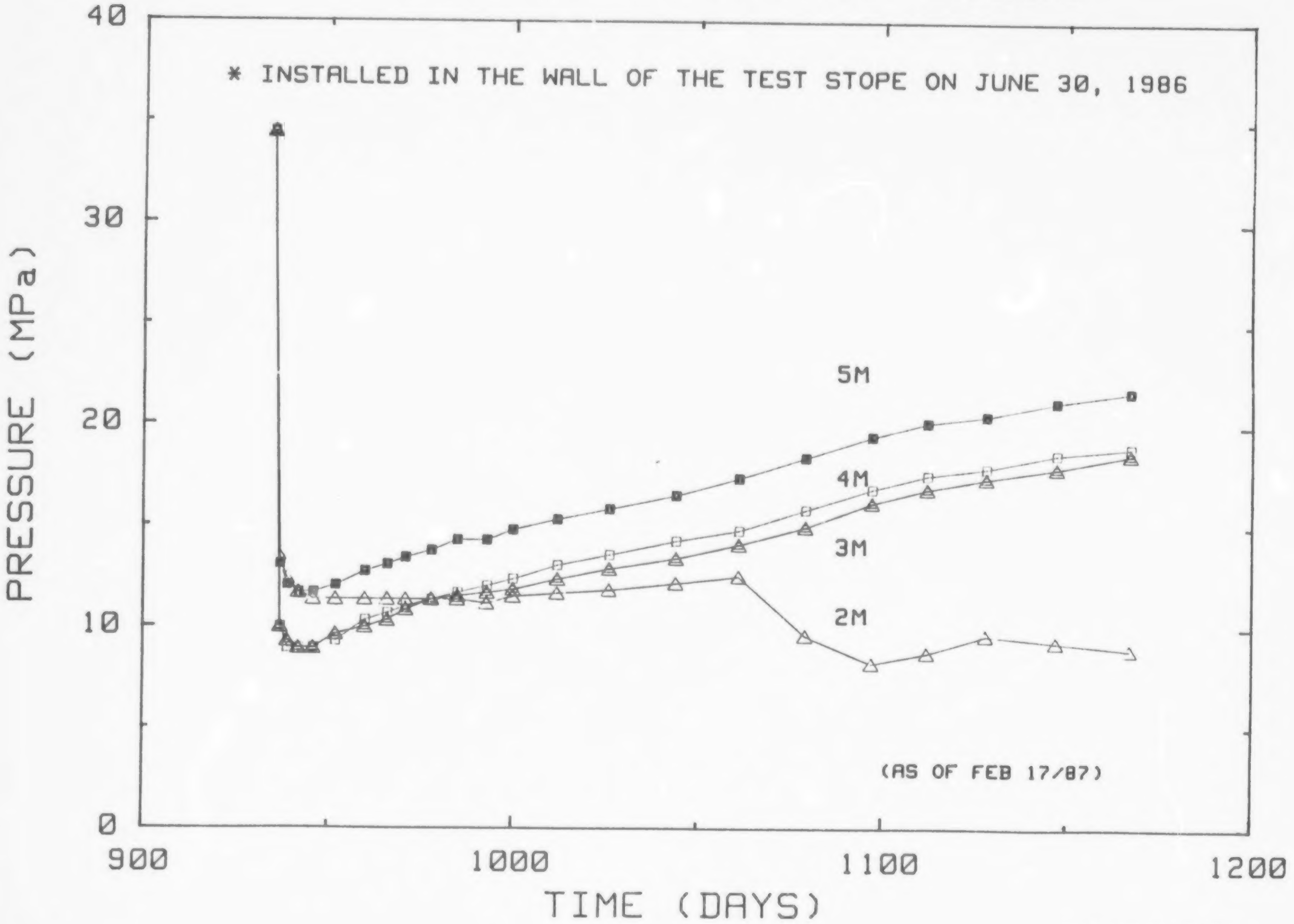

VERTICAL PRESSURE CELLS

FIGURE 3.20

TABLE 3.22

STATION : TEST STOPE WALL.
MEASUREMENT : VERTICAL PRESSURE AT 2,3,4 AND 5 M DEPTHS IN WALL.
MEASUREMENT SYSTEM : SRC UNIDIRECTIONAL PRESSURE CELL

DATE	JULIAN CALENDAR DAY	DAYS SINCE EXCAVATION	2 M PRESSURE CELL - W2MV (MPa)	3 M PRESSURE CELL - W3MV (MPa)	4 M PRESSURE CELL - W4MV (MPa)	5 M PRESSURE CELL - W5MV (MPa)
JUNE 30/86	181	935	34.47	34.47	34.47	34.47
JULY 2/86	183	937	13.44	10.00	10.00	13.10
JULY 4/86	185	939	12.41	9.31	8.96	12.07
JULY 7/86	188	942	11.72	8.96	8.96	11.72
JULY 11/86	192	946	11.38	8.96	8.96	11.72
JULY 17/86	198	952	11.38	9.65	9.31	12.07
JULY 25/86	206	960	11.38	10.00	10.34	12.76
JULY 31/86	212	966	11.38	10.34	10.69	13.10
AUG. 5/86	217	971	11.38	10.86	11.03	13.44
AUG. 12/86	224	978	11.38	11.38	11.38	13.79
AUG. 19/86	231	985	11.38	11.55	11.72	14.31
AUG. 27/86	239	993	11.20	11.72	12.07	14.31
SEPT. 3/86	246	1,000	11.55	11.89	12.41	14.82
SEPT.15/86	258	1,012	11.72	12.41	13.10	15.34
SEPT.29/86	272	1,026	11.89	12.93	13.62	15.86
OCT. 17/86	290	1,044	12.24	13.45	14.31	16.55
NOV. 3/86	307	1,061	12.58	14.13	14.82	17.41
NOV. 21/86	325	1,079	9.65	15.00	15.86	18.44
DEC. 9/86	343	1,097	8.27	16.20	16.89	19.48
DEC. 24/86	358	1,112	8.79	16.89	17.58	20.17
JAN. 9/87	9	1,128	9.65	17.41	17.93	20.51
FEB. 17/87	48	1,167	8.96	18.62	18.96	21.72

3.3 STOPE 1105

Stope 1105 was chosen as an instrumentation site due to its fully excavated mining width (42 m) and an average ore thickness of 12 m to 15 m.

Stope 1105 Rock Mechanics instrumentation are installed and proposed to be installed as shown in Figure 3.21 (Denison-Potacan drawing No. 232-0020-010).

One six-point extensometer was installed in the roof of Stope 1105 in July, 1986 at anchor depths of 2.5 m, 5 m, 7.5 m, 10 m, 15 m and 20 m. Some technical problems occurred with the electronic readout device for the six-point extensometers causing an approximate two month gap in data after the initial readings. There were also some technical problems encountered with the 2.5 m extensometer anchor causing readings to be lost for this depth.

The results obtained to date from the instrumentation in Stope 1105 are presented on the following graphs and tables.

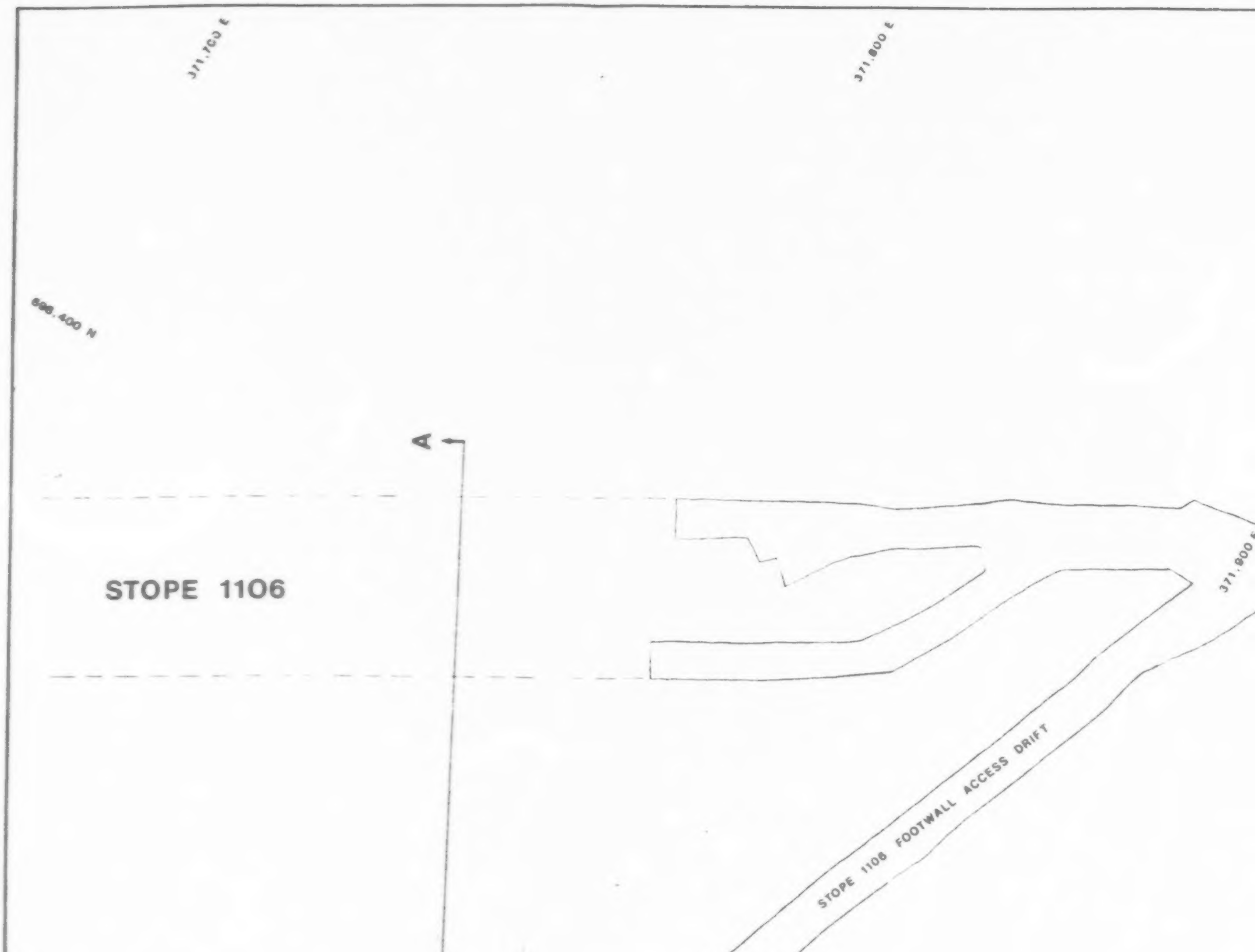
371,700 E
371,800 E
371,900 E
696,400 N
696,300 N
A
STOPE 1106
STOPE 1106 FOOTWALL ACCESS DRIFT
TYPICAL INSTRUMENT CABLE(S) ROUTING
STOPE 1105
A
WEST LATERAL
STOPE 1105 WEST ACCESS DRIFT
PROPOSED REMOTE READOUT CABLE GATHERING LOCATION SITE
READOUT CABLE(S)

		3	
		2	
		1	
		0	
DWG. NO	REFERENCE DRAWINGS	NO	DESCRIPTION OF REVISION

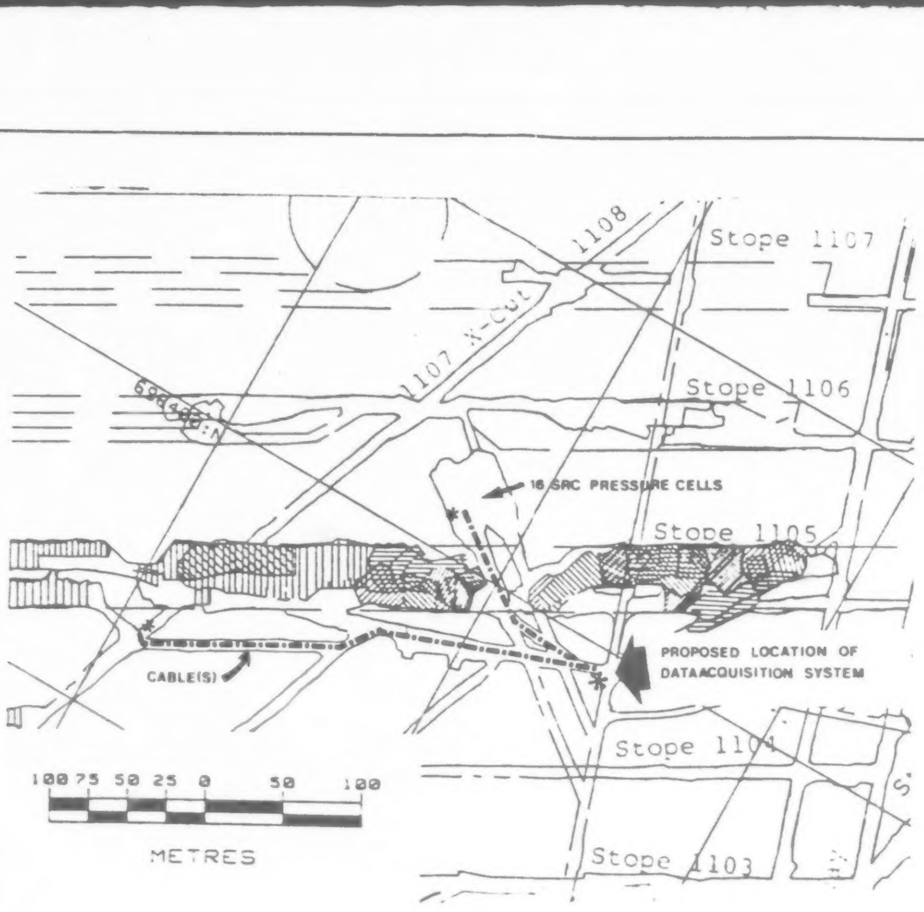
Stope 1107
1108
1107 X-Cut
Stope 1106
16 SRC PRESSURE CELLS
Stope 1105
PROPOSED LOCATION OF DATAACQUISITION SYSTEM
CABLE(S)
Stope 1104
Stope 1103
100 75 50 25 0 50 100
METRES

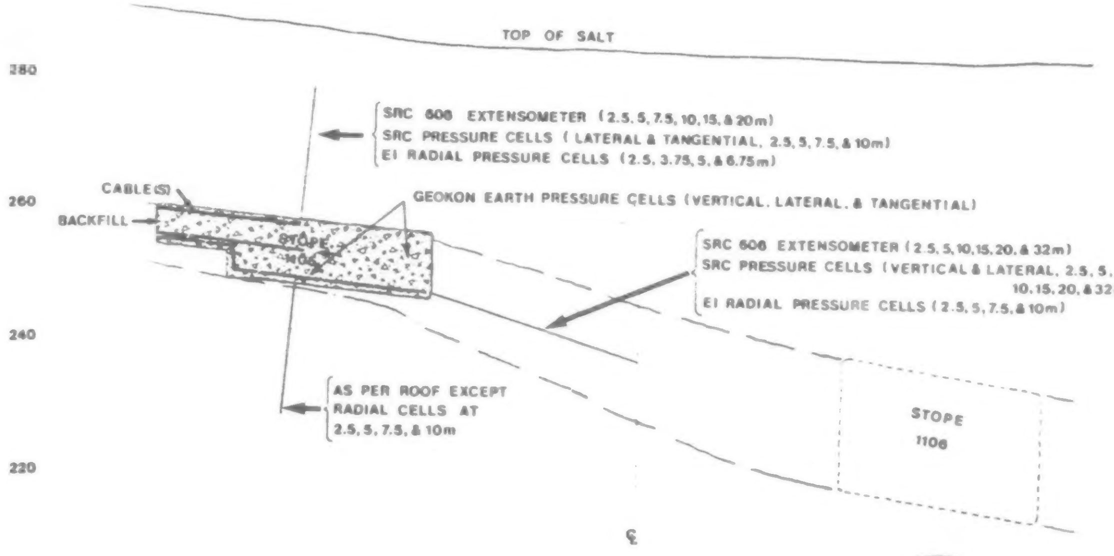
TOP OF SALT
280
260
240
220
SRC 606 EXTENSOMETER (2.5, 5, 7.5, 10, 15, & 20m)
SRC PRESSURE CELLS (LATERAL & TANGENTIAL, 2.5, 5, 7.5, & 10m)
EI RADIAL PRESSURE CELLS (2.5, 3.75, 5, & 6.75m)
CABLE(S)
BACKFILL
STOPE 1105
GEOKON EARTH PRESSURE CELLS (VERTICAL, LATERAL, & TANGENTIAL)
SRC 606 EXTENSOMETER (2.5, 5, 10, 15, 20, & 32m)
SRC PRESSURE CELLS (VERTICAL & LATERAL, 2.5, 5, 10, 15, 20, & 32m)
EI RADIAL PRESSURE CELLS (2.5, 5, 7.5, & 10m)
AS PER ROOF EXCEPT RADIAL CELLS AT 2.5, 5, 7.5, & 10m
STOPE 1106
℄

ISSUED
APR 9 1987
DENISON PO CAN

TYPICAL X-SECTION
A-A

FIGURE 3.21

SCALE 1:500		DATE
DESIGNED BY	MPC Ltd./S.M.	JAN 87
DRAWN BY	S. MUNROE	FEB 87
CHECKED BY		
APPROVED BY		

BY CHK APP

DENISON - POTACAN
POTASH COMPANY

SUSSEX, N.B.

TITLE Stope 1105 Rock Mech. Instrumentation Layout

DRAWING NO 232-0020-010

REV

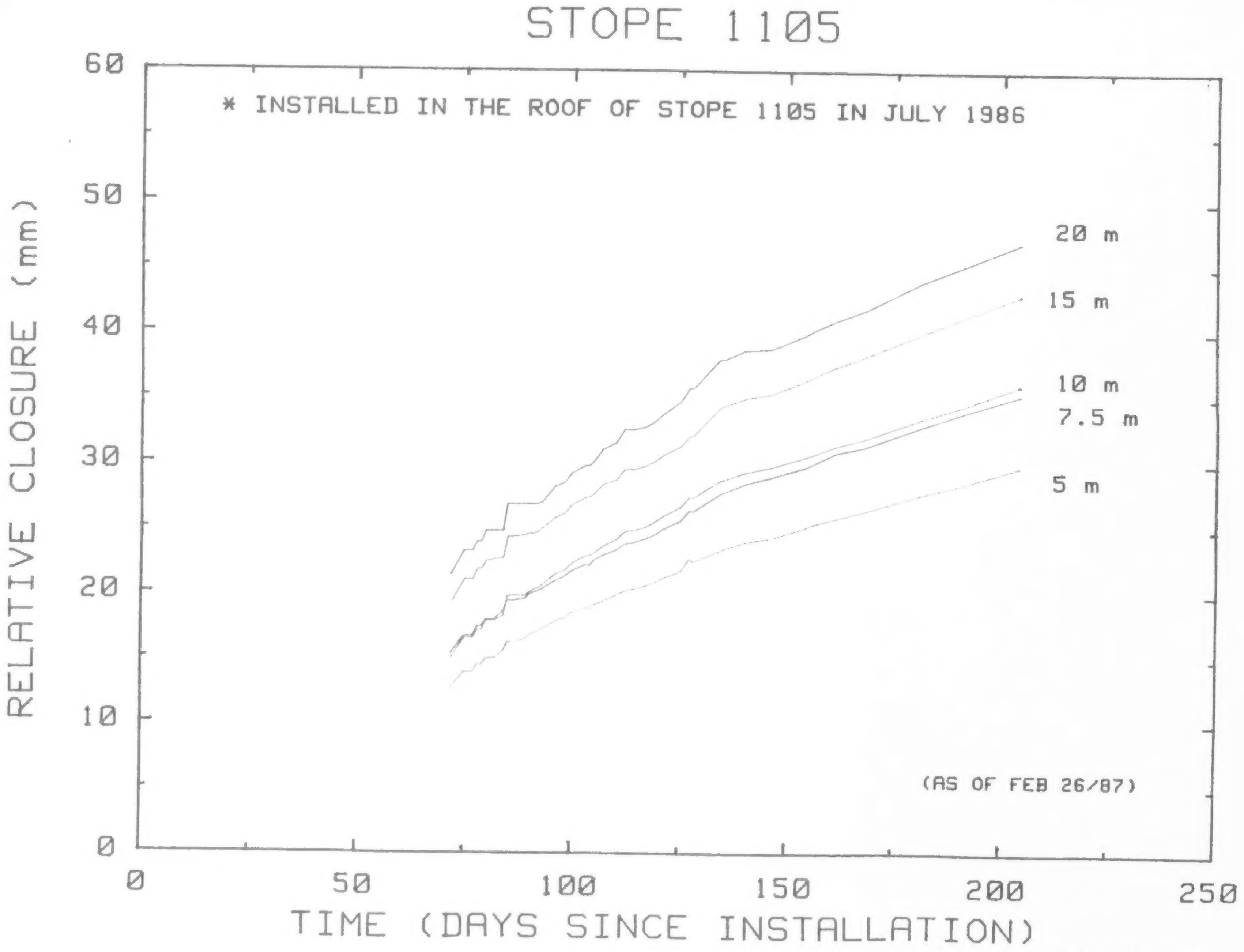
STOPE 1105
* INSTALLED IN THE ROOF OF STOPE 1105 IN JULY 1986
RELATIVE CLOSURE (mm)
0
10
20
30
40
50
60
TIME (DAYS SINCE INSTALLATION)
0
50
100
150
200
250
20 m
15 m
10 m
7.5 m
5 m
(AS OF FEB 26/87)

FIGURE 3.22

TABLE 3.23

STATION : STOPE 1105 ROOF.

MEASUREMENT : RELATIVE CLOSURE AT 5,7.5,10,15 AND 20 M DEPTHS.

DATE	JULIAN CALENDAR DAY	DAYS SINCE FIRST INSTALLATION	5 M ANCHOR CUM. CLOSURE (MM)	7.5 M ANCHOR CUM. CLOSURE (MM)	10 M ANCHOR CUM. CLOSURE (MM)	15 M ANCHOR CUM. CLOSURE (MM)	20 M ANCHOR CUM. CLOSURE (MM)
AUG. 6/86	218	0	0.0	0.0	0.0	0.0	0.0
OCT 17/86	290	72	12.7	15.3	14.9	19.2	21.4
OCT 20/86	293	75	13.8	16.6	16.5	21.0	23.2
OCT 21/86	294	76	13.8	16.6	16.5	21.0	23.2
OCT 22/86	295	77	13.8	16.6	16.5	21.0	23.2
OCT 23/86	296	78	14.4	17.3	17.1	21.8	23.9
OCT 24/86	297	79	14.4	17.4	17.1	21.8	23.9
OCT 25/86	298	80	14.9	17.9	17.8	22.4	24.7
OCT 26/86	299	81	14.9	17.9	17.8	22.4	24.7
OCT 27/86	300	82	14.9	17.9	17.8	22.6	24.7
OCT 29/86	302	84	15.4	18.5	18.2	22.7	24.7
OCT 30/86	303	85	16.1	19.4	19.7	24.3	26.8
OCT 31/86	304	86	16.1	19.4	19.7	24.3	26.8
NOV. 3/86	307	89	16.4	19.5	19.7	24.4	26.8
NOV. 4/86	308	90	16.6	19.9	20.0	24.5	26.8
NOV. 5/86	309	91	16.9	20.0	20.2	24.5	26.8
NOV. 6/86	310	92	17.0	20.1	20.3	24.7	26.8
NOV. 7/86	311	93	17.1	20.3	20.6	24.9	26.9
NOV. 10/86	314	96	17.8	20.9	21.4	25.8	28.1
NOV. 11/86	316	98	18.0	21.2	21.7	26.1	28.4
NOV. 14/86	318	100	18.5	21.7	22.3	26.8	29.2
NOV. 17/86	321	103	18.8	22.1	22.8	27.3	29.8
NOV. 18/86	322	104	18.8	22.1	22.9	27.4	29.8
NOV. 19/86	323	105	19.1	22.5	23.1	27.6	30.1
NOV. 21/86	325	107	19.3	22.9	23.6	28.3	31.0
NOV. 24/86	328	110	19.8	23.3	24.1	28.7	31.5
NOV. 26/86	330	112	20.1	23.7	24.7	29.5	32.5
NOV. 27/86	331	113	20.2	23.9	24.8	29.5	32.5
NOV. 28/86	332	114	20.3	23.9	24.8	29.5	32.5
DEC. 1/86	335	117	20.6	24.2	25.1	29.8	32.7
DEC. 3/86	337	119	20.8	24.5	25.5	30.1	33.1
DEC. 5/86	339	121	21.2	24.9	25.9	30.6	33.7
DEC. 9/86	343	125	21.7	25.6	26.6	31.3	34.6
DEC. 11/86	345	127	22.6	26.3	27.3	32.0	35.7
DEC. 12/86	346	128	22.4	26.3	27.3	32.1	35.7
DEC. 18/86	352	134	23.3	27.6	28.6	34.2	37.9
DEC. 19/86	353	135	23.4	27.7	28.7	34.3	37.9
DEC. 24/86	358	140	23.9	28.4	29.3	34.9	38.6
DEC. 30/86	364	146	24.3	28.9	29.7	35.3	38.7
JAN. 7/87	7	154	25.1	29.7	30.5	36.3	39.8
JAN. 9/87	9	156	25.3	30.0	30.7	36.7	40.2

TABLE 3.23 (CONT.)

STATION : STOPE 1105 ROOF.

MEASUREMENT : RELATIVE CLOSURE AT 5,7.5,10,15 AND 20 M DEPTHS.

DATE	JULIAN CALENDAR DAY	DAYS SINCE FIRST INSTALLATION	5.0 M ANCHOR CUM. CLOSURE (MM)	7.5 M ANCHOR CUM. CLOSURE (MM)	10.0 M ANCHOR CUM. CLOSURE (MM)	15.0 M ANCHOR CUM. CLOSURE (MM)	20.0 M ANCHOR CUM. CLOSURE (MM)
JAN. 14/87	14	161	25.8	30.8	31.3	37.4	40.9
JAN. 21/87	21	168	0.0	31.3	31.9	38.2	41.8
FEB. 3/87	34	181	0.0	32.8	33.4	40.0	43.9
FEB. 13/87	44	191	0.0	33.9	34.4	41.3	45.2
FEB. 26/87	57	204	0.0	35.2	36.0	42.9	46.9

3.4 STOPE 1003

Stope 1003 was chosen as an additional instrumentation site due to delays in installing the instrumentation in Stope 1105. The site chosen in the cross cut between Stope 1003 and Stope 1004 provides immediate unrestricted access to the bearing pillar between the two stopes. Pressure cells will be installed in the bearing pillar, as shown in Figure 3.23 (Denison-Potacan drawing No. 232-020-008).

The pressure cells will be installed in the Stope 1003 half of the bearing pillar due to the fact that only the "top slice" of Stope 1003 has been excavated thus far. This will allow the behaviour of the bearing pillar to be observed as the remainder of Stope 1003 is fully excavated. This will provide additional valuable information to be collected for the Rock Mechanics Test Program.

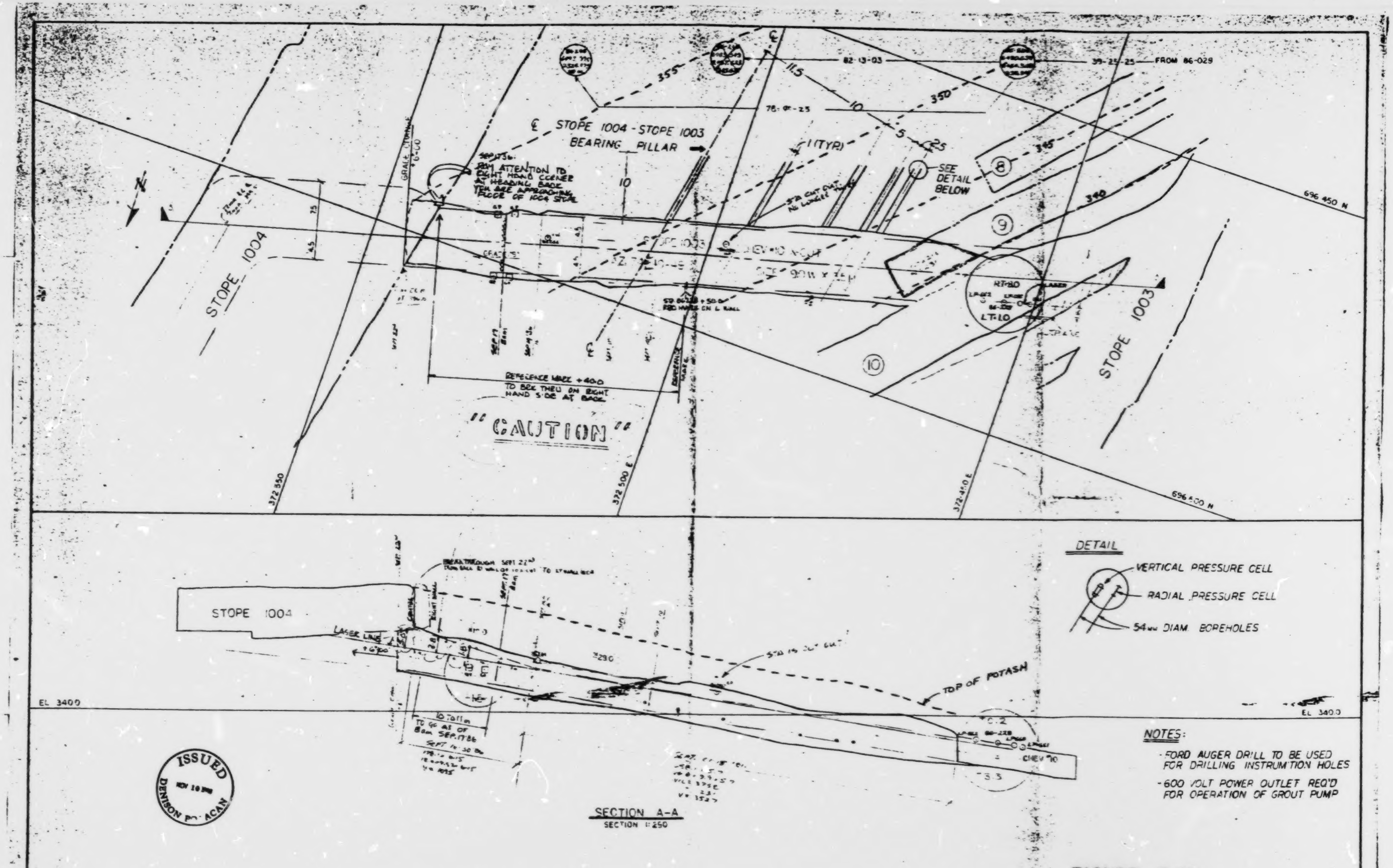
℄ STOPE 1004 - STOPE 1003
BEARING PILLAR
STOPE 1004
STOPE 1003
"CAUTION"
SEE DETAIL BELOW
1 (TYP)
355
350
345
340
115
10
5
25
⑧
⑨
⑩
82-13-03
39-29-25 FROM 86-029
78-01-25
696 450 N
696 400 N
372 350
372 500 E
372 450 E
REFERENCE MARK +40.0 TO BRK THRU ON RIGHT HAND SIDE AT BACK
PAY ATTENTION TO RIGHT HAND CORNER AT HEADING BACK YOU ARE APPROACHING FLOOR OF 1004 STOPE
RT-10
LT-10
SECTION A-A
SECTION 1:250
STOPE 1004
LASER LINE
TOP OF POTASH
EL 340.0
EL 340.0
CHEV 10
DETAIL
VERTICAL PRESSURE CELL
RADIAL PRESSURE CELL
54mm DIAM. BOREHOLES
NOTES:
-FORD AUGER DRILL TO BE USED FOR DRILLING INSTRUMTION HOLES
-600 VOLT POWER OUTLET REQ'D FOR OPERATION OF GROUT PUMP
ISSUED
NOV 10 1986
DENISON POTACAN

FIGURE 3.23

SCALE	1:250
DESIGNED BY	
DRAWN BY	S. MUNROE OCT 86
CHECKED BY	
APPROVED BY	

DENISON - POTACAN
POTASH COMPANY
SUSSEX, N.B.

TITLE STOPE 1003 BEARING PILLAR
ROCK MECH. INSTRUMENTATION

DRAWING No. 232-020-008

SECTION 4.0

4.0 ROCK MECHANICS INSTRUMENTATION

The rock mechanics instrumentation used for the field test program consisted of equipment to measure the closure of mine openings and the stress/strain distributions surrounding mine openings. The equipment ranged from simple inexpensive measurement systems to complex electronic measuring devices.

4.1 MEASUREMENT OF CLOSURE

The closure of mine openings was measured using either an Irad Gage tape extensometer or a homemade wire and pulley style of measurement. The Irad Gage Tape extensometer system is shown in Appendix A.

The tape extensometer was utilized where both measurement reference points were accessible and were not beyond approximately 20 m apart. The tape extensometer allowed measurements to within 0.025 mm (0.001") to be taken.

In areas where the two measurement reference points were not readily accessible or the span to be measured was greater than the length of the tape extensometer, the wire and pulley style of measurement was used. The wire and pulley method, utilizing a steel tape measure, allowed closure measurements to within 0.5 mm to be taken.

4.2 MEASUREMENT OF STRAIN

The strain (relative closure) surrounding mine openings was measured using either a fabricated plate/rebar measurement method or electronic six-point extensometers.

The plate/rebar system of relative closure measurement utilizes a removable dial gauge to measure the travel of an anchored rod relative to a reference plate located on the surface of the opening being monitored. The system is inexpensive and relatively easy to install, however, it has several limitations. These included the fact that a separate hole has to be drilled for each anchor depth and that the weight of the steel rods makes their installation in up holes somewhat cumbersome. The plate/rebar system allowed relative closure measurements to be taken within 0.01 mm.

A model 606 electronic six-point extensometer, manufactured by the Saskatchewan Research Council (SRC), was used to measure relative closure in locations where access was not readily available or where deeper hole depths were to be monitored. Readings to within 0.001 mm were taken utilizing a SRC model 400 electronic readout device. The SRC measurement system is shown in Appendix A.

4.3 MEASUREMENT OF STRESS

The measurement of stress surrounding mine openings was accomplished using unidirectional hydraulic flatjack type pressure cells manufactured by SRC. Various different stress measurements were obtained by altering the position of the pressure cell wafers in the bore hole to suit the desired stress orientations. See the various pressure cell instrumentation details in Appendix A for further details.

The pressure cells were encased in the boreholes utilizing a cementatious grout, rather than the use of encapsulated pressure cell wafers. This allowed for all voids to be immediately filled between the borehole wall and the pressure cell wafer, thus allowing for useful readings to be obtained earlier. Due to the somewhat unique nature of the use of grout to encase the pressure cells, a brief summary of the grouting procedure is presented.

A Moyno 6M4 progressing cavity pump was used to place Sternson M-Bed Superflow grout into the borehole containing the pressure cell wafer. The grouting mixture used was 4.75 l of water per 25 kg bag of M-Bed Superflow. The grout was placed in the borehole through 19 mm (3/4") diameter Type L copper pipe which also served as a pressure cell installation tool. Wooden grout plugs were used to contain the grout in the boreholes and plastic tubing was used as air bleed lines, as well as to monitor grout levels in the boreholes. After completion of grouting, the pressure cells were left for 48 hours at which time they were pressurized.

Various aspects of the pressure cell installations are shown in Appendix A.

SECTION 5.0

5.0 100 MM DIAMETER CORE SAMPLING

The laboratory testing of 100 mm diameter core samples at the University of Waterloo required that core samples be obtained from the Denison-Potacan mine site. Representative Sylvinite, Upper Halite and Lower Gradational Bed core samples were obtained and sent to Waterloo for the laboratory testing program.

An attempt was made to cut 100 mm diameter cores using air flushing for cooling of the core bit and removal of the chips. A tractor drill rig was adapted to drive a 500 mm long thin-walled tube using tungsten carbide inserts at the cutting edge.

Penetration rates in a down-hole were very slow with very fine chip size. The drilling site was relocated and an up-hole was attempted using an auxiliary air flushing hook-up from a portable compressor. Penetration rates were better; about 200 mm depth in ten minutes.

The bit was withdrawn at this point, and it was discovered that two of the carbides had broken off, probably due to excessive heat generation. The section of core inside was severely fractured into a series of discs, between 10 mm and 15 mm thick.

It was decided, as a result of this trial, to abandon the attempt to drill dry cores. Subsequent core drilling would be attempted using Denison-Potacan's geological exploration drill, which uses brine flushing and conventional coring tools.

The Model 200 Superdrill coring drill rig was used with a Craelius T6S 131 mm x 1500 mm core barrel, part no. 8392027903. A Craelius Corborit tungsten carbide bit was used with the T6S core barrel. The T6S core barrel, Corborit core bit and the Model 200 Superdrill are shown in Appendix B.

The usage of the Model 200 Superdrill made the sites for obtaining the core samples dependent upon the location of the current exploration drilling program. The location of the Superdrill at the time of the 100 mm diameter coring was in Panel 10 Back Entry. The coring location is shown in Figure 3.0.

Coring was conducted during the week of July 7 to 11, 1986 to obtain the representative roof, ore and floor samples. Three holes, 6 m in length, were drilled with a total of 15 Upper Halite (roof) samples being obtained. Two holes, one 13.5 m and one 15 m in length, were drilled to obtain 14 Sylvinite Ore and 12 Lower Gradational Bed (floor) samples.

An attempt was made to obtain core samples perpendicular to the bedding planes to eliminate the adverse effects of these features on consistent laboratory testing. The holes which were drilled were within 5 degrees of perpendicular at the hole collar. It was impossible to obtain the cores exactly perpendicular to the bedding due to roof height limitations in the Back Entry.

The cores were taken from the core barrel and placed in specially designed core boxes for the 100 mm diameter cores. The cores were logged and suitable samples were placed in separate core boxes for shipping (see Appendix B). Core samples were considered suitable for shipment if their length to width ratio was greater than two and if no cracks and fractures were visible in the sample. The first 1.5 m section for each hole was discarded to avoid the possible presence of stress relief cracks and microfractures associated with the excavation of the opening.

The core log sheets for all core samples taken follow on Tables 5.1 to 5.5.

TABLE 5.1

CORE LOG SHEET

1/1

HOLE NO. : #1
LOCATION : Panel 10 Back Entry
POSITION : Roof
ANGLE : +35 degrees
START : 1.5m - 6.0m
DATE : July 9, 1986

SECTION	COMMENT
1.5 m - 3.0 m	- Upper Halite (U.H.) - fine grained, pink to dark pink colour. - very small amount of clay present. - bedding at offset of 5 degrees. - Sample #7: 1.9 m - 2.4 m (U.H.) - Sample #8: 2.7 m - 3.0 m (U.H.)
3.0 m - 4.5 m	- UH; fine grained, % clay increasing, abundant clay seams at 3.4 - 3.8 m; dirty pink colour; bedding. - some large halite crystals (1 cm) associated with clay seams. - small amount of sylvite associated with clay seams. - Sample #9: 3.1 m - 3.4 m (U.H.) - Sample #10: 3.4 m - 3.75 m (U.H.) - Sample #11: 3.75 m - 4.0 m (U.H)
4.5 m - 6.0 m	- U.H.; fine grained, dirty pink colour; abundant clay seams and inclusions; - boracite and sylvite associated with large clay seams. - Boracite inclusions begin at 5.2 m . - % clay increases. - Sample #12: 4.75 m - 5.1 m (U.H.) - Sample #13: 5.1 m - 5.4 m (U.H.) - Sample #14: 5.4 m - 5.65 m (U.H.)

TABLE 5.2

CORE LOG SHEET

1/1

HOLE NO. : #2
LOCATION : Panel 10 Back Entry
POSITION : Roof

ANGLE : + 35 degrees
START : 1.5 m - 6.0 m
DATE : July 9, 1986

SECTION	COMMENT
1.5 m - 5.0 m	- Upper Halite (U.H.) - dirty pink colour, fine grained. - small amount of clay inclusions. - bedding present at an angle of approx. 5% from the vertical. - No samples obtained.
5.0 m - 6.0 m	- U.H.; dirty pink colour; fine grained clay inclusions as well as clay seams are present; boracite and sylvite inclusions associated with clay seams. - bedding present at offset of approx. 5 degrees from vertical. - Sample #4: 5.0 m - 5.25 m (U.H.) - Sample #5: 5.4 m - 5.7 m (U.H.) - Sample #6: 5.7 m - 6.0 m (U.H.)

TABLE 5.3

CORE LOG SHEET

1/1

HOLE NO. : #3	ANGLE : + 35 degrees
LOCATION : Panel 10 Back Entry	START : 1.5 m - 7.5 m
POSITION : Roof	DATE : July 9, 1986

SECTION	COMMENT
1.5 m - 4.5 m	- Upper Halite (U.H.) - fine grained, dirty pink, small amount of clay inclusions. - bedding present at an angle of approx. 5 degrees from the vertical - Sample #1: 2.55 m - 2.77 m (U.H.)
4.5 m - 4.75 m	- U.H.; large percent of clay present, abundant seams; core highly friable, pinkish green colour; fine grained.
4.75 m - 6.0 m	- fine grained U.H., dirty pink colour, abundant clay present occurring in seams, boracite inclusions are associated with the clay seams. - bedding at 5 degrees off perpendicular. - Sample #2: 4.75 m - 5.0 m (U.H.) - Sample #3: 5.1 m - 5.4 m (U.H.)
6.0 m - 7.5 m	- Same as previous section; clay seams are not as abundant.

TABLE 5.4

CORE LOG SHEET

1/2

HOLE NO. : #4
LOCATION : Panel 10 Back Entry
POSITION : Floor
ANGLE : - 35 degrees
START : 1.5 m - 7.5 m
DATE : July 15, 1986

SECTION	COMMENT
1.5 m - 2.1 m	- C/B Zone; high grade ore (20 - 30% KCL) - fine grained; red colour - abundant slickensides with very fine blue halite crystals associated. - small amount of clay - Sample #33: 1.75 m - 2.1 m (C/B Zone) - sides etched due to jamming of core barrel
2.1 m - 3.0 m	- low grade zone becoming a Barren Zone. - low % KCL decreasing to zero. - sylvite occurs in stringers. - blue halite, clay and slickensides associated with stringers. - fine grained; red colour to dirty pink. - some large halite crystals(1 cm). - Sample #34: 2.45 m - 2.85 m - low grade to barren (transitional)
3.0 m - 6.8 m	- Barren Zone (BZ); very little KCL. - some KCl present associated with clay seams. - fine grained, dirty pink. - % clay increased. - medium sized halite crystals. - Sample #35: 5.0 m - 5.35 m (BZ) - Sample #36: 5.35 m - 5.6 m (BZ) - Sample #37: 5.6 m - 5.85 m (BZ) - Sample #38: 6.1 m - 6.4 m (BZ)
6.8 m - 7.5 m	- Transitional Zone; Barren Zone to A Zone - % KCl increasing; small amount of clay. - fine grained; a few large halite crystals present (approx. 1 cm). - minor amount of blue halite crystals - crystals have a schistose appearance. - light red colour. - Sample #39: 6.8 m - 7.5 m (transitional Zone)
7.5 m - 11 m	- A Zone; (20-25 % KCl) - fine grained, red colour. - schistose pattern; large halite crystals present. - small amount of clay. - a few slickensides but not as many as most of the ore.

TABLE 5.4 (Cont'd)

CORE LOG SHEET

2/2

HOLE NO. : #4
LOCATION : Panel 10 Back Entry
POSITION : Floor
ANGLE : - 35 degrees
START : 7.5 m - 13.5 m (end)
DATE : July 15, 1986

SECTION	COMMENT
7.5 m - 11 m (Cont'd)	- Sample #40: 7.5 m - 8.05 m (A Zone) - Sample #41: 8.05 m - 8.4 m (A Zone) - Sample #42: 8.45 m - 8.75 m (A Zone) - Sample #43: 8.75 m - 9.0 m (A Zone) - Sample #44: 10 m - 10.25 m (A Zone) - normal C/B Zone appear - darker red probably because richer in KCl and clay. - Sample #45: 10.5 m - 10.7 m (A Zone) - lighter colour - % KCl is decreased
11.0 m - 13.5 m	- Lower Gradational Bed (LGB); fine to med grained halite. - dirty pink colour - abundant clay seams with a small amount of KCl associated. - Sample #46: 11.3 m - 11.55 m (LGB) - Sample #47: 12.15 m - 12.6 m (LGB) - Sample #48: 12.7 m - 13.05 m (LGB)

TABLE 5.5

CORE LOG SHEET

1/2

HOLE NO. : #5
LOCATION : Panel 10 Back Entry
POSITION : Floor
ANGLE : - 35 degrees
START : 1.5 m - 10.5 m
DATE : July 14, 1986

SECTION	COMMENT
1.5 m - 2.0 m	- C/B Zone; approx. 30% KCl. - red colour; fine grained - slickensides are very abundant throughout this zone. - very fine crystals of blue halite present throughout zone; more abundant around slickensides. - no clay apparent.
2.0 m - 2.6 m *Note: Barren Zone between C/B Zone is not typical	- low grade zone (approx. 5 % KCl) marking the beginning of a Barren Zone. (BZ) - % KCl decreasing, clay content increasing - clay occurs as seams - blue halite and slickensides disappear. - grain size increasing from fine to medium, dirty pink colour. - similar to Lower Gradational Bed (LGB) - Sample #15: 2.2 m - 2.45 m (LG) - Sample #16: 2.5 m - 2.8 m (BZ) - transition between low grade (LG) and Barren Zone.
2.6 m - 6.2 m	- Barren Zone (less than 1% KCl) - medium grained; dirty pink colour - abundant clay seams with a low % of KCl associated. - similar to LGB. - Sample #17: 3.5 m - 3.9 m (BZ) - Sample #18: 5.95 m - 6.2 m (BZ)
6.2 m - 6.6 m	- low grade zone (approx. 5% KCl) - transition between Barren and A Zone. (A Zone to ore zone; 10 - 30% KCl) - fine grained, reddish colour. - % clay decreasing; % KCl increasing - Sample #19: 6.2 m - 6.6 m (LG)
6.6 m - 10.5 m	- A Zone, approx. 20% KCl - fine grained, red colour - large halite crystals (1 cm) present throughout zone. - small amount of clay occurring in seams. - no slickensides; very small amount of fine blue halite crystals. - Sample #20: 6.75 m - 7.0 m (A Zone) - Sample #21: 7.0 m - 7.25 m (A Zone) - Sample #22: 7.6 m - 7.85 m (A Zone) - Sample #23: 8.2 m - 8.6 m (A Zone) - Sample #24: 10.1 m - 10.35 m (A Zone)

TABLE 5.5 (Cont'd)

CORE LOG SHEET

2/2

HOLE NO. : #5
LOCATION : Panel 10 Back Entry
POSITION : Floor
ANGLE : - 35 degrees
START : 10.5 m - 15.0 m
DATE : July 14, 1986

SECTION	COMMENT
10.5 m - 12.0 m	- transition from low grade A Zone to LGB - fine grained to medium grained - reddish to dirty pink colour - small amount of clay - KCl occurring in stringers. - Sample #25: 10.6 m - 10.85 m (A Zone) - Sample #26: 10.85 m - 11.15 m - transition (A Zone to LGB) - Sample #27: 11.6 m - 11.95 m (LGB)
12.0 m - 15.0 ,	- LGB; very low KCl content (approx. 1% KCl) - KCl occurs in stringer; fine grained to medium grained halite - clay associated with the KCl seams - dirty pink colour. - Sample #28: 12.4 m - 12.7 m (LGB) - Sample #29: 12.9 m - 13.25 m (LGB) - Sample #30: 13.65 m - 14.05 m (LGB) - Sample #31: 14.05 m - 14.25 m (LGB) - Sample #32: 14.25 m - 14.6 m (LGB)

SECTION 6.0

6.0 SURFACE SUBSIDENCE MONITORING

The installation and monitoring of surface subsidence monuments was considered an essential component of the field test program. The rate of mining induced subsidence will provide valuable insight into both the closure of the mined out workings and of the load bearing response of the main bearing pillars and backfilled stopes.

A total of 17 surface subsidence monuments were installed over Panel 10 workings in the summer of 1985. The monuments and their installed locations are shown in Figure 3.24 (Denison-Potacan drawing No. 232-0030-001). The initial subsidence survey was conducted in September, 1985.

It should be noted that at the time of installation of thes subsidence monuments, the majority of mining activity was scheduled to occur in Panel 10. Due to a combination of mining and geological factors, the mining emphasis has shifted from Panel 10 to Panel 11. For this reason, an attempt will be made to install additional surface subsidence monuments over Panel 11 workings in 1987.

The subsidence survey results for 1986 are presented on Table 6.1

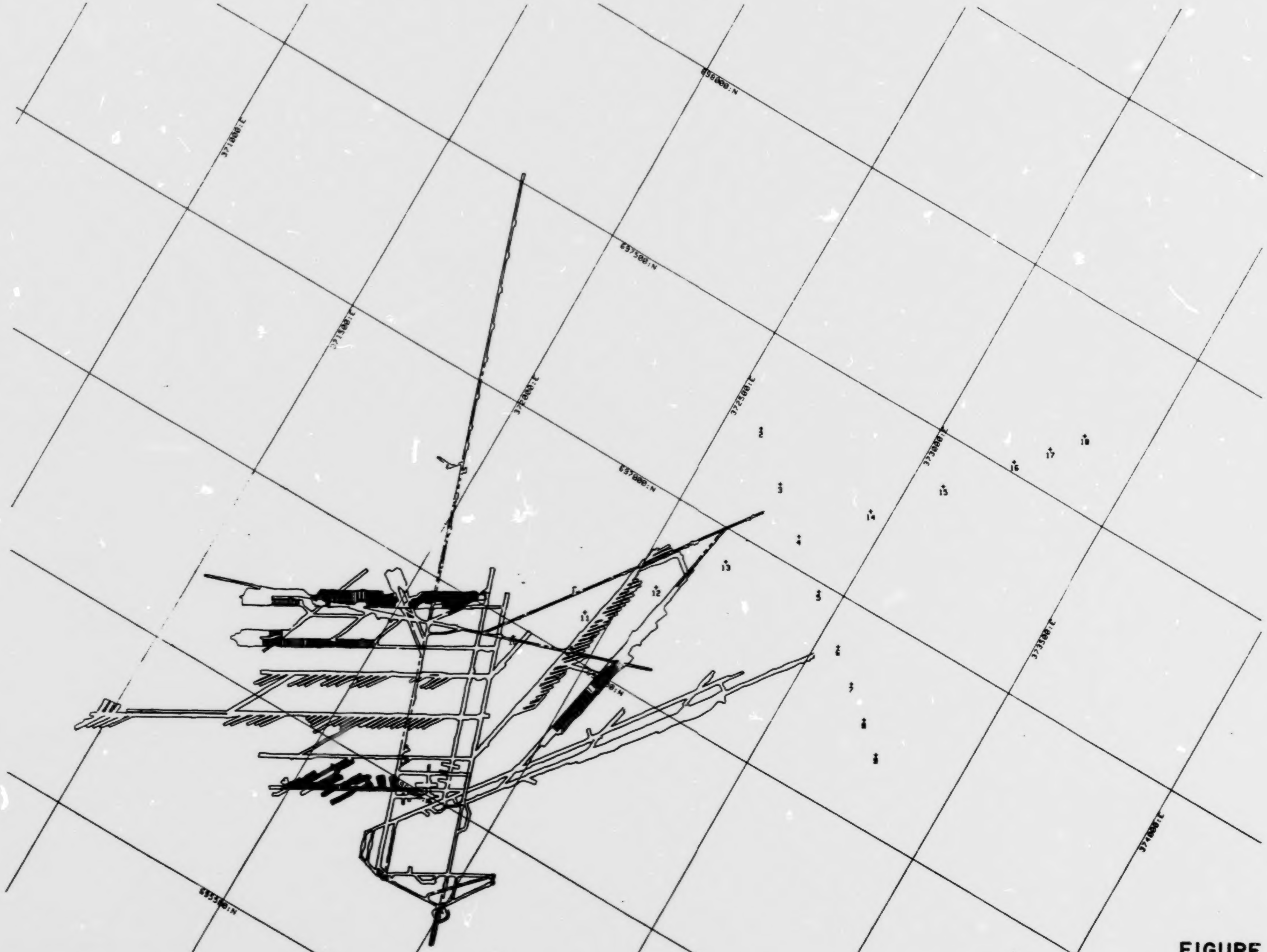
658000:N
657500:N
657000:N
656500:N
655500:N
371000:E
371500:E
372000:E
372500:E
373000:E
373500:E
374000:E
2
3
4
5
6
7
8
9
11
12
13
14
15
16
17
18

FIGURE 3.24

NOTES: MINE PLAN SHOWN AS OF NOV 3, 1986

		3						SCALE	1:5000	DATE
		2						DESIGNED BY		
		1						DRAWN BY	S. MUNROE	MAY 1987
		0						CHECKED BY		
		NO.	DESCRIPTION OF REVISION	DATE	BY	CHK.	APP.	APPROVED BY		

DENISON - POTACAN
POTASH COMPANY
SUSSEX, N.B.

TITLE
1986 SUBSIDENCE SURVEY

DRAWING NO.
232-0030-001
REV.

TABLE 6.1

SUBSIDENCE SURVEY RESULTS (1986)

STATION	1986 ELEVATION (m)	1985 ELEVATION (m)	CHANGE IN ELEVATION (m)
2	67.84300	67.83519	+0.00781
3	64.99161	64.98401	+0.00760
4	52.58114	53.57561	+0.00553
5	47.71823	47.71331	+0.00492
6	39.87404	39.87124	+0.00280
7	33.50381	33.49994	+0.00387
8	31.04022	31.03380	+0.00642
9	24.70450	24.63701	+0.06749
10	47.99010	48.00228	-0.01218
11	43.88534	43.89312	-0.00778
12	45.08492	44.98328	+0.10164
13	51.56058	51.50108	+0.05950
14	55.67990	55.67072	+0.00918
15	58.50398	58.49383	+0.01015
16	53.53155	53.52329	+0.00826
17	51.60466	51.59414	+0.01052
18	48.86193	48.85140	+0.01053

APPENDIX A

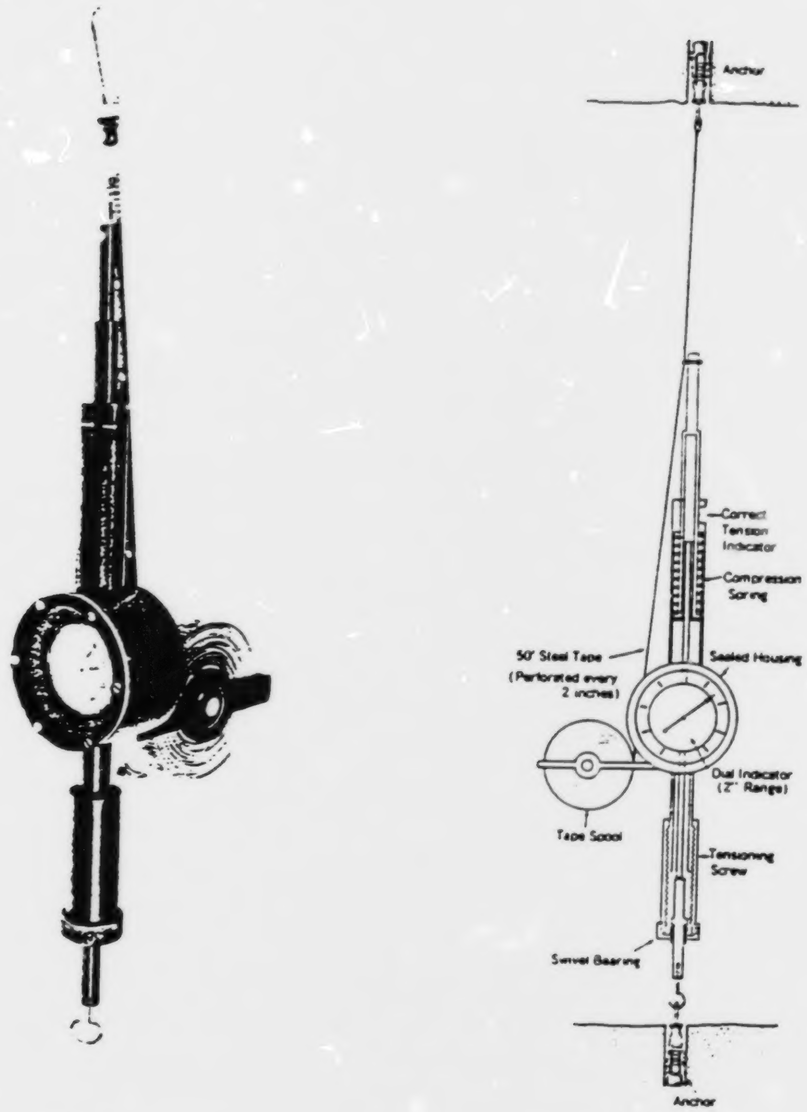
Anchor
Correct Tension Indicator
Compression Spring
50' Steel Tape (Perforated every 2 inches)
Sealed Housing
Dial Indicator (2" Range)
Tape Spool
Tensioning Screw
Swivel Bearing
Anchor

(a) Tape Extensometer

(b) Design details

Figure A1

Irad Gage Tape Extensometer

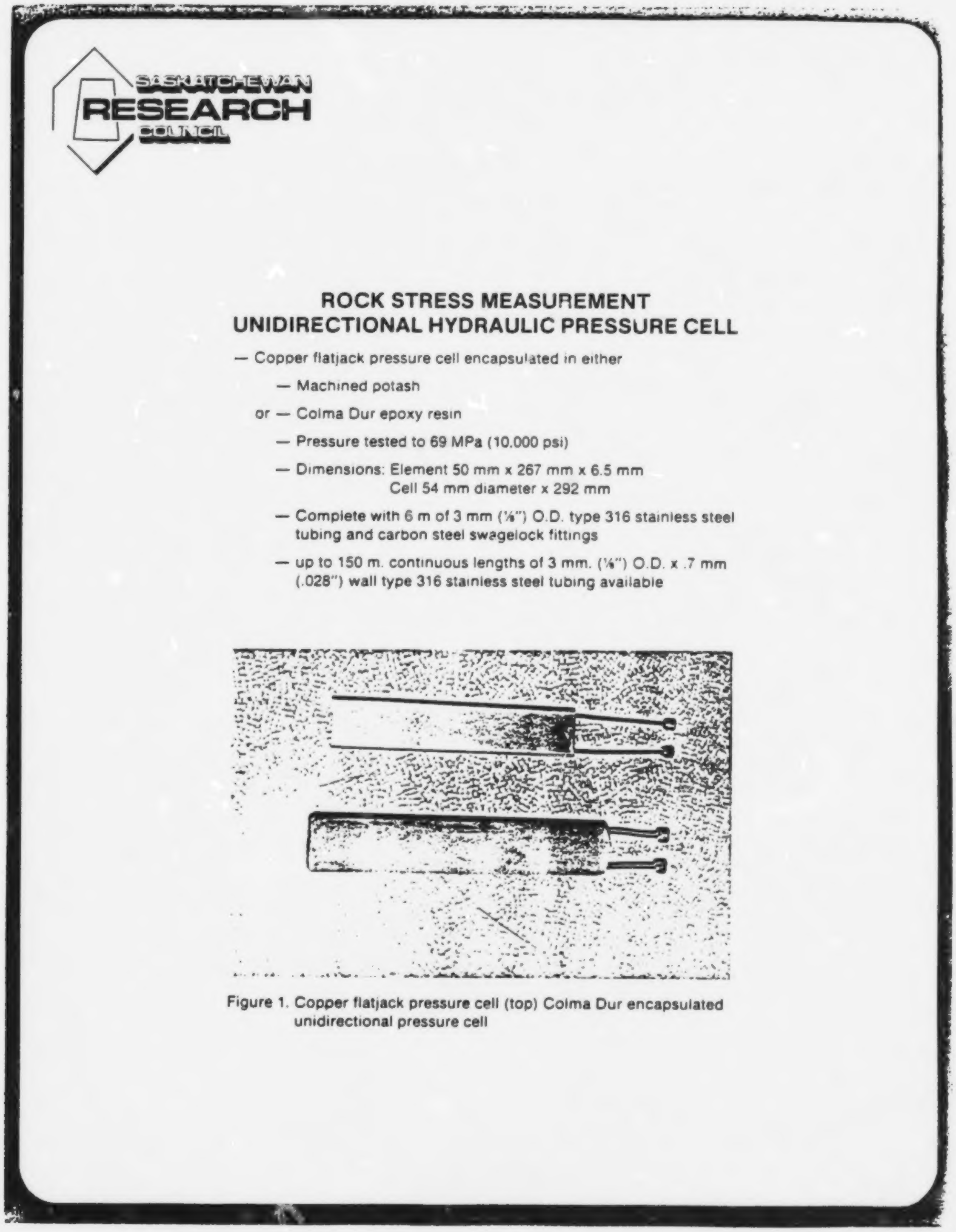

SASKATCHEWAN
RESEARCH
COUNCIL

ROCK STRESS MEASUREMENT UNIDIRECTIONAL HYDRAULIC PRESSURE CELL

- Copper flatjack pressure cell encapsulated in either
  - Machined potash
- or — Colma Dur epoxy resin
  - Pressure tested to 69 MPa (10,000 psi)
  - Dimensions: Element 50 mm x 267 mm x 6.5 mm
    Cell 54 mm diameter x 292 mm
  - Complete with 6 m of 3 mm (⅛") O.D. type 316 stainless steel tubing and carbon steel swagelock fittings
  - up to 150 m. continuous lengths of 3 mm. (⅛") O.D. x .7 mm (.028") wall type 316 stainless steel tubing available

Figure 1. Copper flatjack pressure cell (top) Colma Dur encapsulated unidirectional pressure cell

Figure A2

SRC Unidirectional Hydraulic Pressure Cell

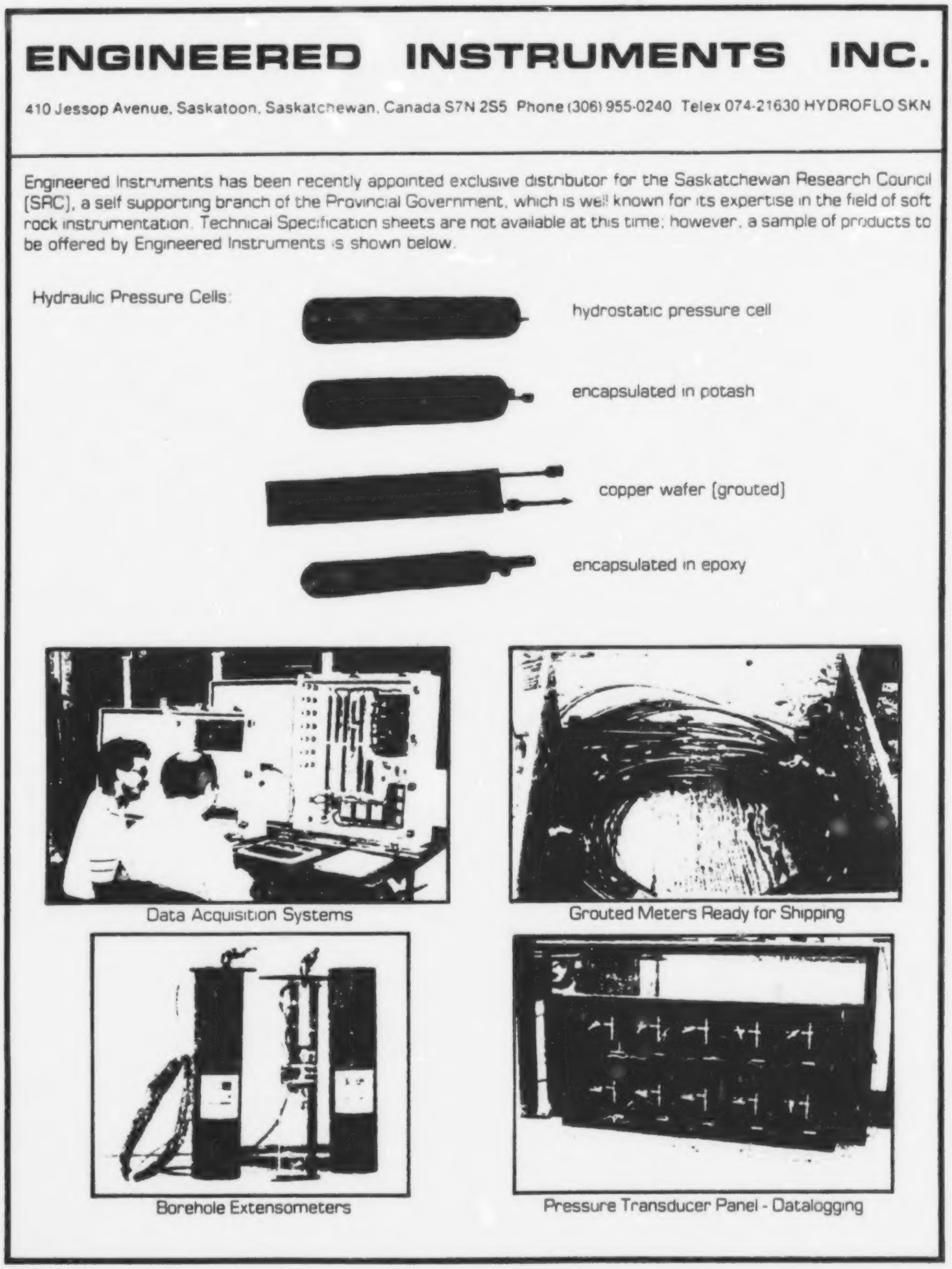

ENGINEERED INSTRUMENTS INC.

410 Jessop Avenue, Saskatoon, Saskatchewan, Canada S7N 2S5 Phone (306) 955-0240 Telex 074-21630 HYDROFLO SKN

Engineered Instruments has been recently appointed exclusive distributor for the Saskatchewan Research Council (SRC), a self supporting branch of the Provincial Government, which is well known for its expertise in the field of soft rock instrumentation. Technical Specification sheets are not available at this time; however, a sample of products to be offered by Engineered Instruments is shown below.

Hydraulic Pressure Cells:

hydrostatic pressure cell

encapsulated in potash

copper wafer (grouted)

encapsulated in epoxy

Data Acquisition Systems

Grouted Meters Ready for Shipping

Borehole Extensometers

Pressure Transducer Panel - Datalogging

Figure A3

SRC Rock Mechanics Instrumentation

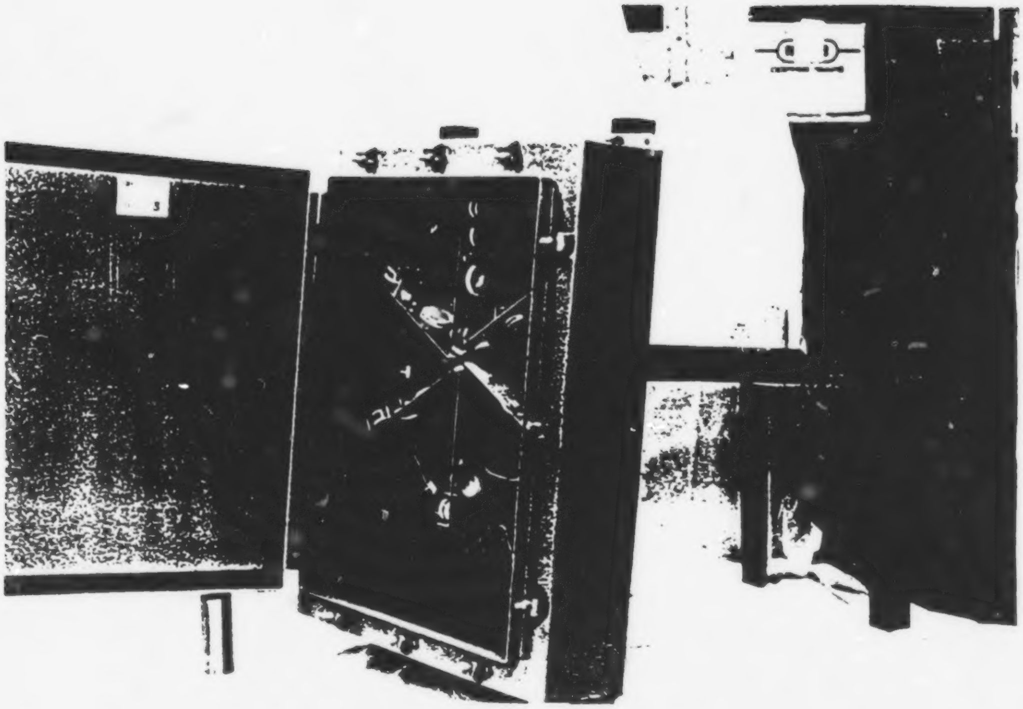

Figure A4

SRC Model 606 Six-point Extensometer

Figure A5

SRC Titanium Rock Anchor
(pins extended)

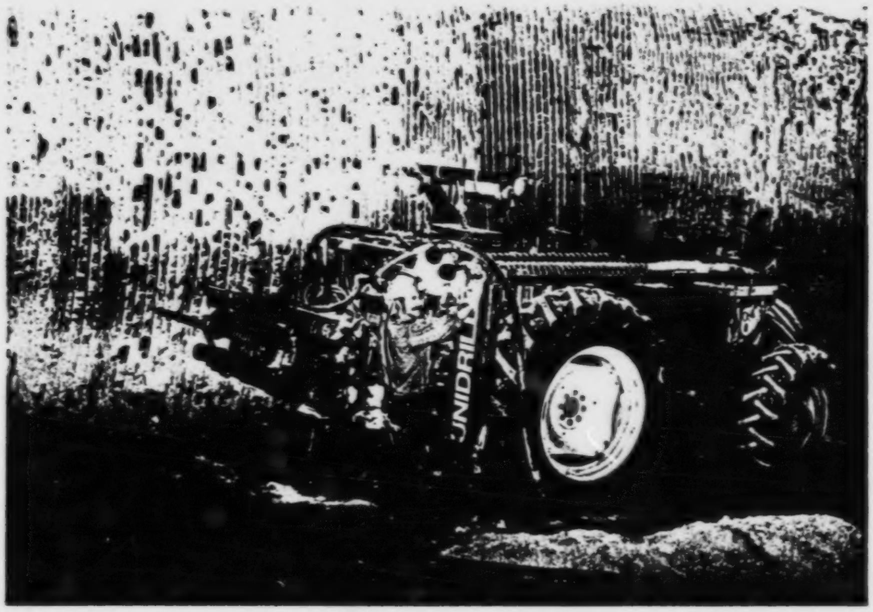

Figure A6

Tractor Mounted Unidrill

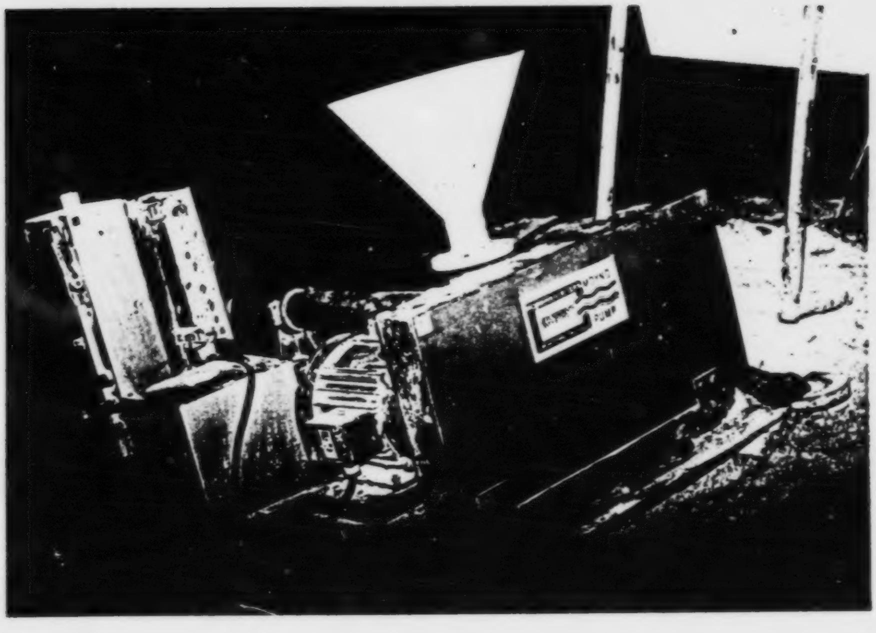

Figure A7

Moyno 6M4 Progressing Cavity Pump

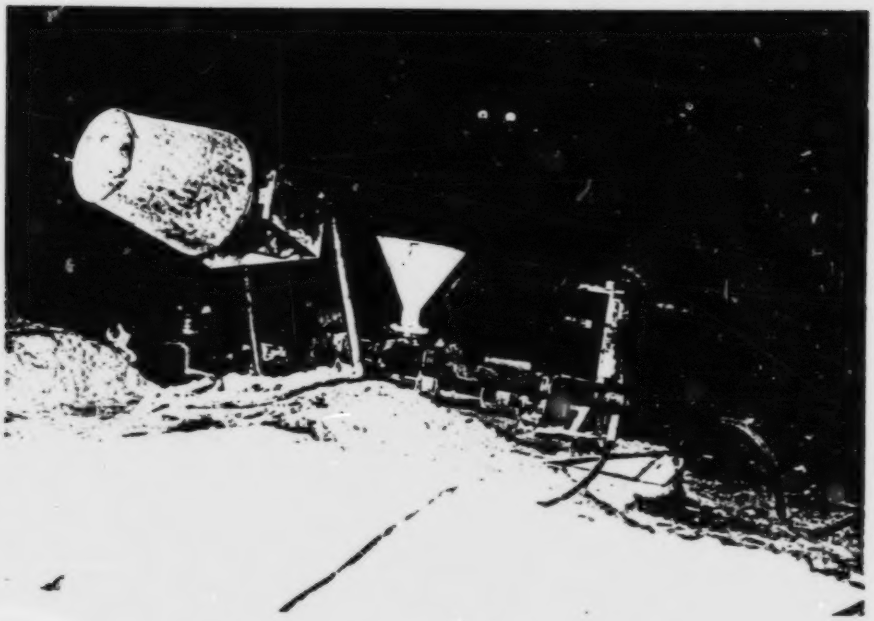

Figure A8

Pressure Cell Grouting Configuration

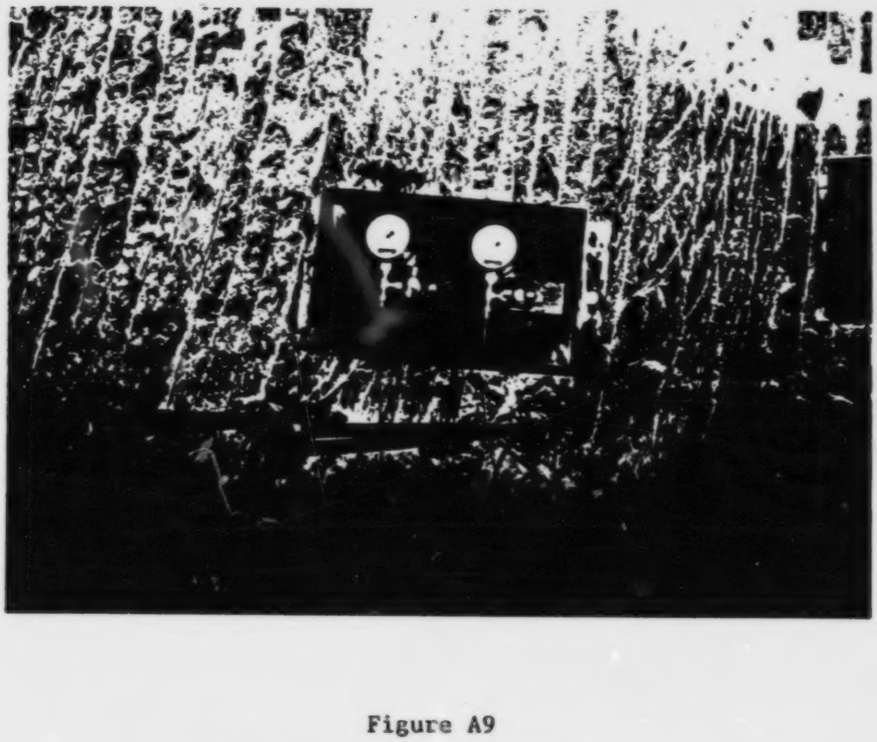

Figure A9

Pressure Cell Gauge Panel

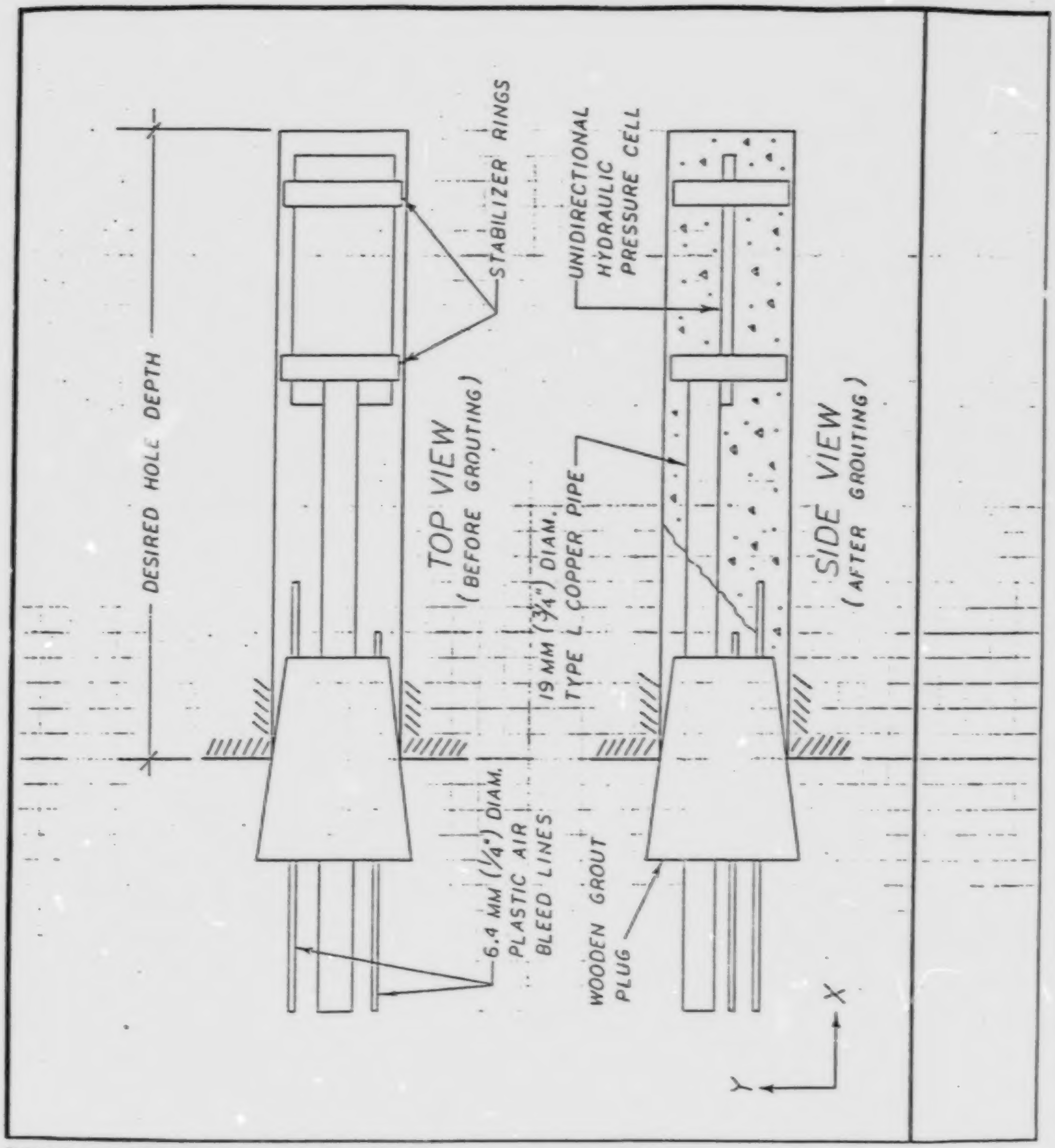
DESIRED HOLE DEPTH
STABILIZER RINGS
TOP VIEW
(BEFORE GROUTING)
UNIDIRECTIONAL
HYDRAULIC
PRESSURE CELL
19 MM (3/4") DIAM.
TYPE L COPPER PIPE
SIDE VIEW
(AFTER GROUTING)
6.4 MM (1/4") DIAM.
PLASTIC AIR
BLEED LINES
WOODEN GROUT
PLUG
X
Y

DENISON-POTACAN POTASH COMPANY Figure A10

SUBJECT PRESSURE CELL HORIZONTAL GROUTING CONFIGURATION
DATE 14-11-86
PROJECT USE OF BACKFILL IN NB POTASH MINES
SHEET 1 OF 1
DEPT. ENGINEERING
PROJECT NO.
NOTE : NOT DRAWN TO SCALE
BY S. MUNROE
DPPC ENG 002

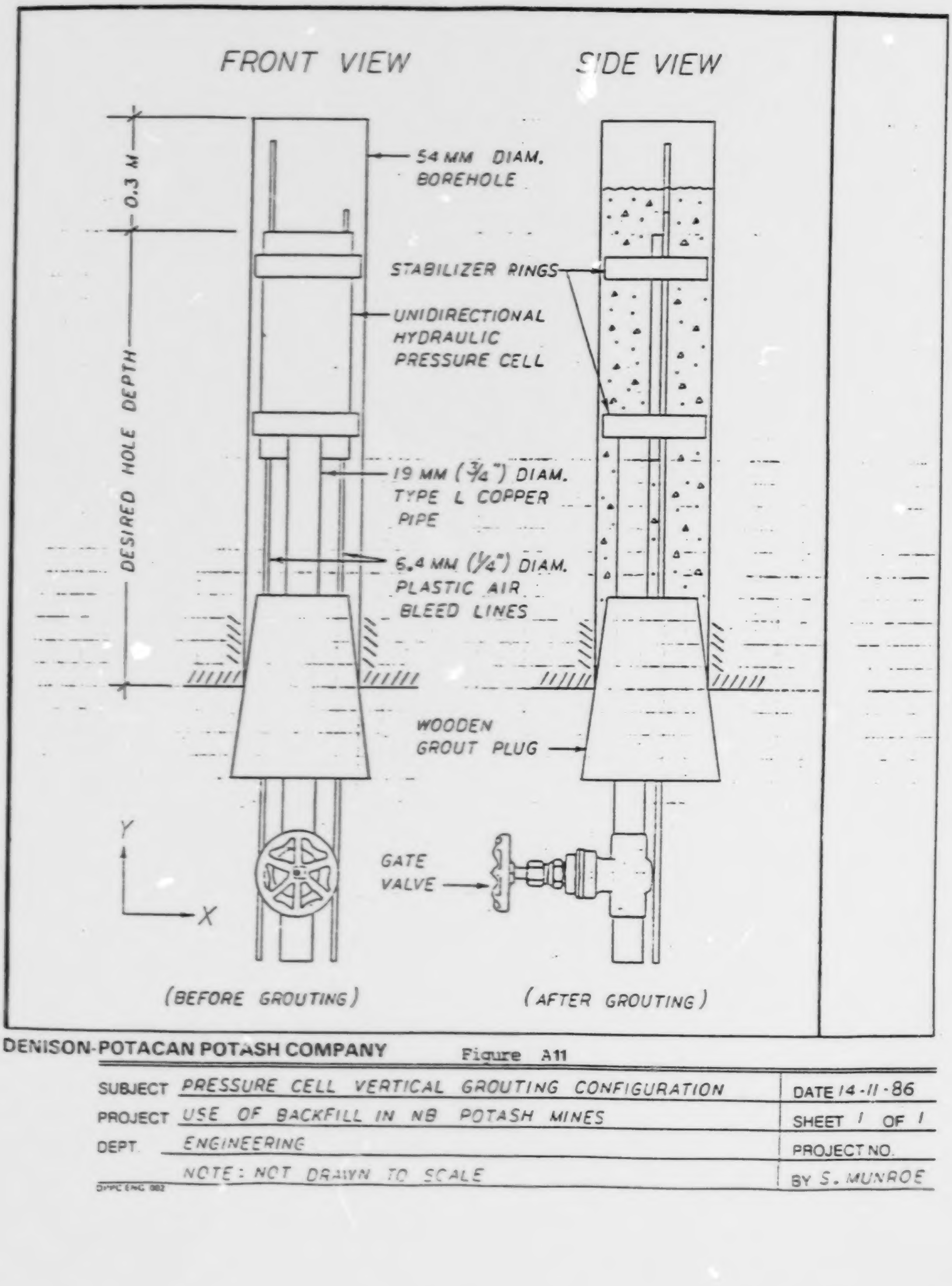
FRONT VIEW
SIDE VIEW
0.3 M
DESIRED HOLE DEPTH
54 MM DIAM. BOREHOLE
STABILIZER RINGS
UNIDIRECTIONAL HYDRAULIC PRESSURE CELL
19 MM (3/4") DIAM. TYPE L COPPER PIPE
6.4 MM (1/4") DIAM. PLASTIC AIR BLEED LINES
WOODEN GROUT PLUG
GATE VALVE
Y
X
(BEFORE GROUTING)
(AFTER GROUTING)

DENISON-POTACAN POTASH COMPANY

Figure A11

SUBJECT PRESSURE CELL VERTICAL GROUTING CONFIGURATION	DATE 14-11-86
PROJECT USE OF BACKFILL IN NB POTASH MINES	SHEET 1 OF 1
DEPT. ENGINEERING	PROJECT NO.
NOTE: NOT DRAWN TO SCALE	BY S. MUNROE

DPPC ENG 002

M-BED SUPERFLOW

DESCRIPTION

M-BED SUPERFLOW is a premixed, non-metallic, shrinkage compensating grout, composed of portland cements, flow agents, and graded siliceous sand. This dry grout requires only the addition of water for use at consistencies ranging from dry pack to fluid.

FEATURES

Volume Stability

M-BED SUPERFLOW contains special cements that produce a regulated expansion during their hydration. The rate of expansion has been designed to offset shrinkage, due to plastic settlement and drying, in both the plastic and hardened states.

M-BED SUPERFLOW produces an overall expansion of 0.4%, elimating the need for total restraint to acheive design strengths.

Range of Placing Consistencies

Flowability agents provide the mechanism which allows M-BED SUPERFLOW to be placed at consistencies ranging from dry pack to fluid without segregation and still maintaining low water-cement ratios.

Conversion: 1.0 KSI = 1000 psi
1.0 MPa = 1 N/mm^2
145 psi = 1 MPa

PROPERTIES

Compressive Strength vs Time (days)

A.S.T.M. C-109-77

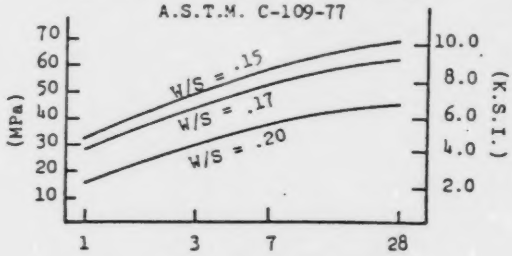

Flexural Strength vs Time (days)

A.S.T.M. C-348-72

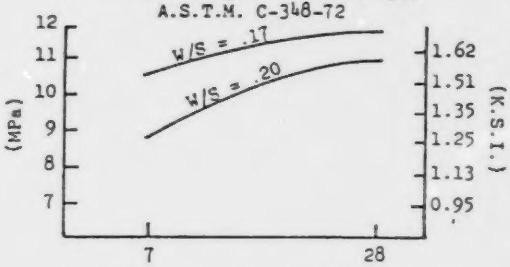

Compression vs Time (days)

A.S.T.M. C-109-77

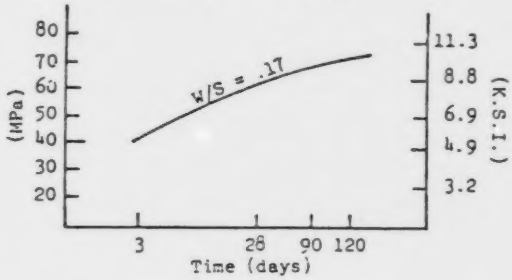

NOTE: W/S = Water:Solids Ratio.

Cont'd ....

[illegible]

CONSISTENCY	WATER: SOLIDS	WATER PER 25 kg BAG (litres)	YIELD PER 25 kg BAG (litres)	YIELD PER 25 kg BAG (cu.ft.)	WET DENSITY (kg/m^3)	TEMP.	WORK LIFE (Hr.)	INIT. SET (Hr.)	FINAL SET (Hr.)
FLOWABLE	.15	3.75	12.3	0.43	2270	10°C	1.25	7.5	8.50
						22°C	1.00	4.5	5.00
						45°C	.70	3.0	3.25
POURABLE	.17	4.25	12.8	0.45	2260	10°C	1.50	7.5	9.00
						22°C	1.00	6.5	7.00
						45°C	.50	3.5	4.00
FLUID	.20	5.00	13.3	0.47	2240	10°C	1.60	8.0	9.50
						22°C	1.00	7.0	7.50
						45°C	.50	3.5	4.00

CONSISTENCY	FLOW(%)	FLOW(SEC.)	W:S	TESTING SPECIFICATION
FLOWABLE	150%+ @ 25 drops		.15	A.S.T.M. C109-77, U.S. CORPS CRD-C227
POURABLE	135% @ 5 drops	85	.17	A.S.T.M. C109-77, U.S. CORPS CRD-C79
FLUID		25 - 30	.20	U.S. CORPS CRD-C79

PROPERTY	W/S	AGE	RESULTS	TESTING SPECIFICATION
EXPANSION	.20	28day	Less than 0.4%	U.S. CORPS OF ENG. CRD-C588-79
FLOW	.20		20-30 sec.	U.S. CORPS OF ENG. CRD-C79
BLEEDING	.20		None visible	U.S. CORPS OF ENG. CRD-C9, A.S.T.M. C-232
COMPRESSION	.15	3 days	48 MPa	U.S. CORPS OF ENG. CRD-C227, A.S.T.M. - C109
	.17	3 days	43 MPa	U.S. CORPS OF ENG. CRD-C227, A.S.T.M. - C109
	.20	3 days	27 MPa	U.S. CORPS OF ENG. CRD-C227, A.S.T.M. - C109

M-BED SUPERFLOW

Strength Development

The rate of strength development, both in compression and tensile, provides for early loading, specifically when used at the drier consistencies. The rate of strength development can be seen from the graphs provided.

In-Service Conditions

The ability of M-BED SUPERFLOW to be used at a fluid consistency allows placement in constrained areas with as little as 13mm clearance.

M-BED SUPERFLOW may be exposed to in-service temperatures ranging from sub-zero to 176°C without significant variations in strength.

The absence of metallic aggregate makes it suitable for use in most conditions encountered in exterior exposure such as wet-dry cycling and continuous wet.

There are no chlorides present in M-BED SUPERFLOW, therefore placement in conjunction with prestressing steel cables or reinforcing bar is not a constraint.

AREAS OF USE

General

M-BED SUPERFLOW is an economical, general purpose, non-shrink grout that can be used for the installation of anchor bolts, heavy machinery base plates, column sole plates etc..... For more specific information refer to the Structural Grout Selection Chart and Flow Table.

M-BED SUPERFLOW should not be used in areas of extremely high vibration; where service temperatures will exceed 176°C; or where contact is likely with acids or alkalis.

DIRECTIONS FOR USE

Surface Preparation

The concrete substrate should be flooded with clean, non-saline water 24 hours prior to grouting. All excess water is to be removed so the substrate will be in a saturated, surface damp condition at the time of grouting.

All surfaces that will be in contact with the grout should be clean and free of grease, oil, standing water, laitance, loose material or any other contaminant that could impair the placing or in-service performance of the structural grout.

MIXING

Mixing should be done mechanically (slow speed) to ensure even consistency. The water must be added to the mixer prior to the addition of the dry grout; water content not exceeding a maximum dosage of 5.0 litres per 25 kg bag of dry grout. The initial mixing period before placement will depend on the efficiency of the mixer. Therefore, mixing should continue until an even consistency is achieved before actual placing of the grout. The fresh grout may be remixed for a period of 1 hour after the initial mixing, after which time the grout should then be discarded.

Placing Consistencies:

Dry-Pack

M-BED SUPERFLOW must be firmly pressed or rammed into place. Use metal or hardwood tamping tools and mason's trowel. Consistency should be such that pressuring into a firm hand ball shows no evidence of cracking or excessive surface moisture.

Plastic

M-BED SUPERFLOW may be rodded into place or trowel handled in areas where freedom of movement is available. Consistency can range from slightly dry to that of wet masonry mortar.

Fluid

M-BED SUPERFLOW may be used with low pressure cement grouting equipment or may be poured into place.

All joints in form work should be caulked with a suitable caulking material such as Sternson's Acryflex.

NOTE:
High points must be adequately vented to allow entrapped air to escape; the exposed grout need not be restrained to achieve design strengths.

Curing

The placed grout should be moist cured for a minimum of 24 - 36 hours at which time a suitable curing and sealing compound should be applied such as Sternson's Florseal. This will ensure sufficient moisture for intended strength development.

Cleanup

Cleanup of the still unset grout can be done with water.

NOTE: For further information see "Instructions For Use" supplied with each unit.

CAUTION:
M-BED SUPERFLOW contains portland cement as do most normal concretes. It therefore has similar effects when prolonged exposure to the skin occurs.

ADDITIONAL DATA

Packaging

M-BED SUPERFLOW is packaged in multi-walled, heavy-duty paper bags containing a polyethylene liner to guard against breakage and moisture contamination. Each unit contains 25 kg of dry, premixed M-BED SUPERFLOW grout.

Storage

M-BED SUPERFLOW should be stored in a dry area within a temperature range of 15 - 25° C for best results. For exterior storage, precautions should be taken to keep the grout dry as possible such as covering with a tarpaulin.

Shelf Life

1 year plus, properly stored.

Availability - M-BED SUPERFLOW is available across Canada and around the world through local distributors. For further information regarding distribution, contact STERNSON LIMITED, HEAD OFFICE IN BRANTFORD, ONTARIO, CANADA.

MAY/80

APPENDIX B

Craelius T6 and T6S

Thin-walled core barrels for coring in medium hard, soft and friable formations, metric and American hole sizes.

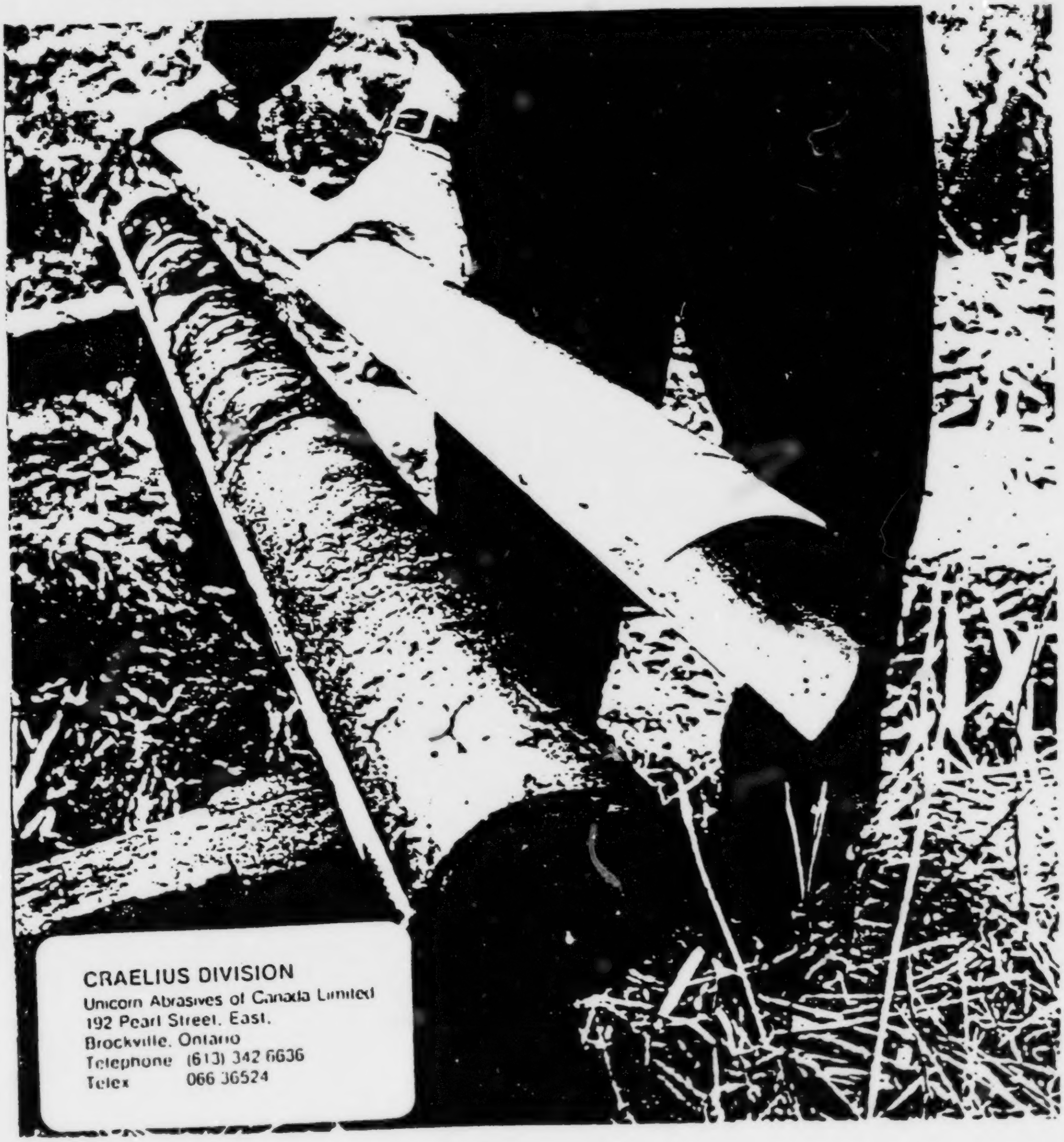

CRAELIUS DIVISION
Unicorn Abrasives of Canada Limited
192 Pearl Street, East,
Brockville, Ontario
Telephone (613) 342 6636
Telex 066 36524

Figure B1

Craelius T6S Core Barrel

CORBORIT

Design

CORBORIT® is a registered trademark for CRAELIUS tungsten carbide drill bits. The cutting edges comprise of crushed cemented carbide grains (2–5 mm in size) brazed to the drill blank. The type of drill bit governs the grain size in the tungsten carbide insert.

CORBORIT® during drilling has a considerably larger number of cutting edges in contact with the rock formation than a drill bit with inserts. This reduces vibration – producing a better quality core sample – and allows the drill bit to be used at higher rotation speeds than drill bits with inserts. A suitable rotation speed is governed by the rock formation and other factors during drilling. Normally the peripheral speed can vary between 0.5 – 2 m/sec. (Recommended peripheral speed, approx. 1 m/sec.)

Area of application

CORBORIT® drill bits are better suited for harder rock formations (hardness group 1–4) than drill bits with inserts. CORBORIT® drill bits are mainly intended for drilling in soft formations and are therefore primarily used in conjunction with core barrels T6, T6S and SK6L.

CORBORIT® drill bits are also well suited for cleaning drill holes, eg. removal of foreign bodies, burned bits etc.

CORBORIT® drill bits can in certain applications replace the more expensive diamond drill bits, eg. when drilling soft formations where diamonds with a size of 8–15 spc are normally used.

Another advantage with CORBORIT®, when using air as the flushing medium, is the design of the cutting edges which provide more effective cooling and heat dissipation.

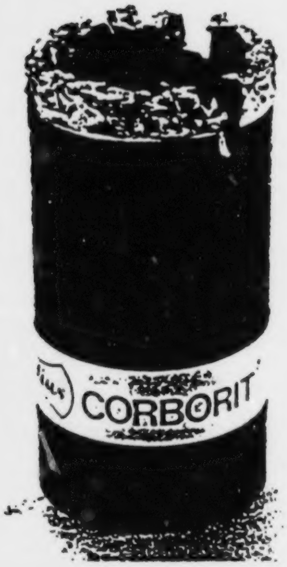

CORBORIT® drill bit. Tungsten carbide drill bit with crushed cemented carbide cutting edges.

Figure B2

Craelius Corborit Drill Bit

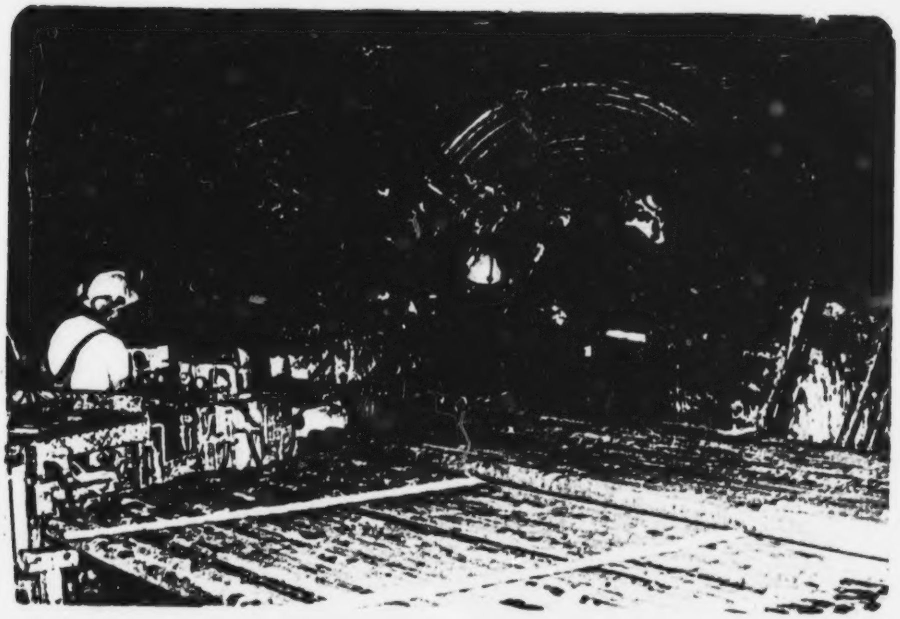

Figure B3

Model 200 Superdrill

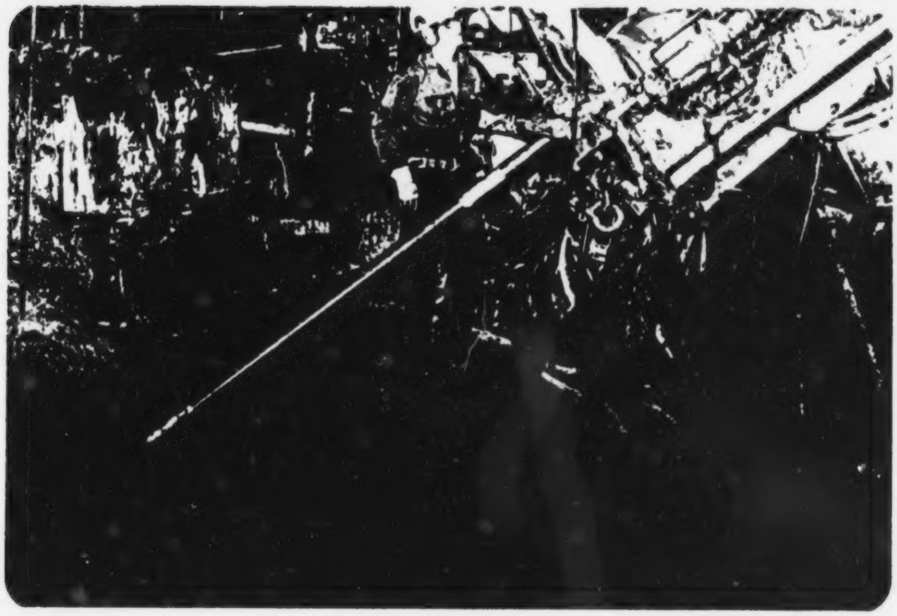

Figure B4

Model 200 Superdrill
(drilling down-hole)

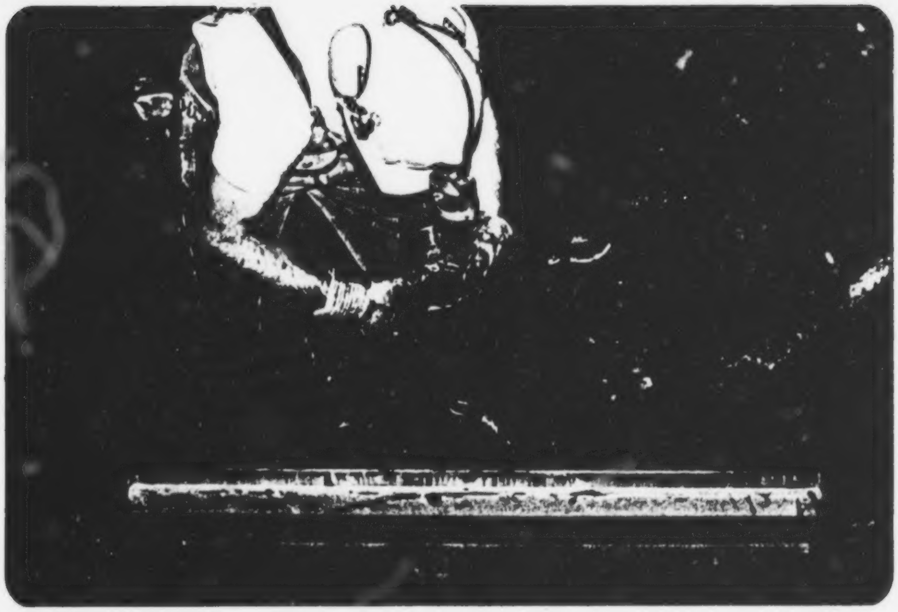

Figure B5

Removal of Core Samples From
T6S Core Barrel

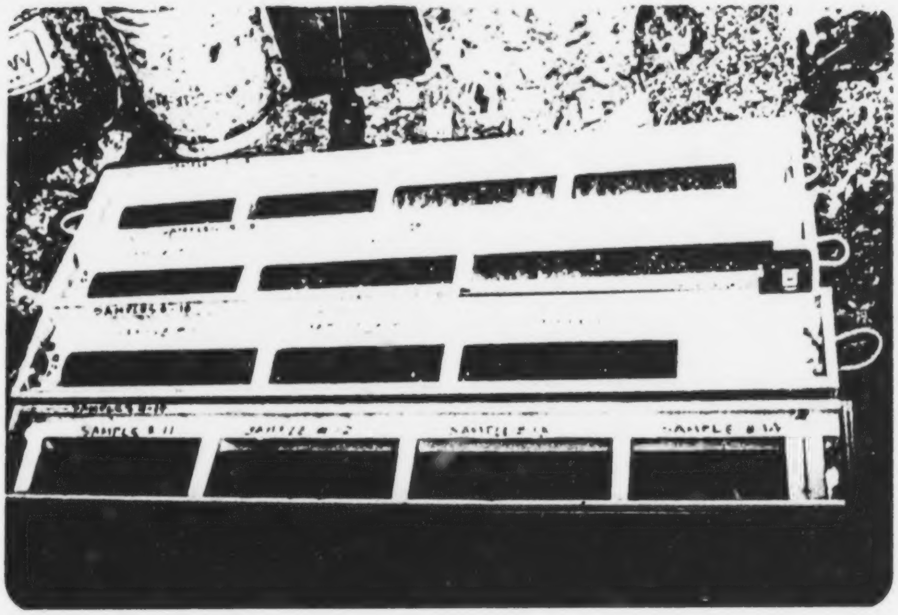

Figure B6

Core Samples Packed for Shipment

APPENDIX C

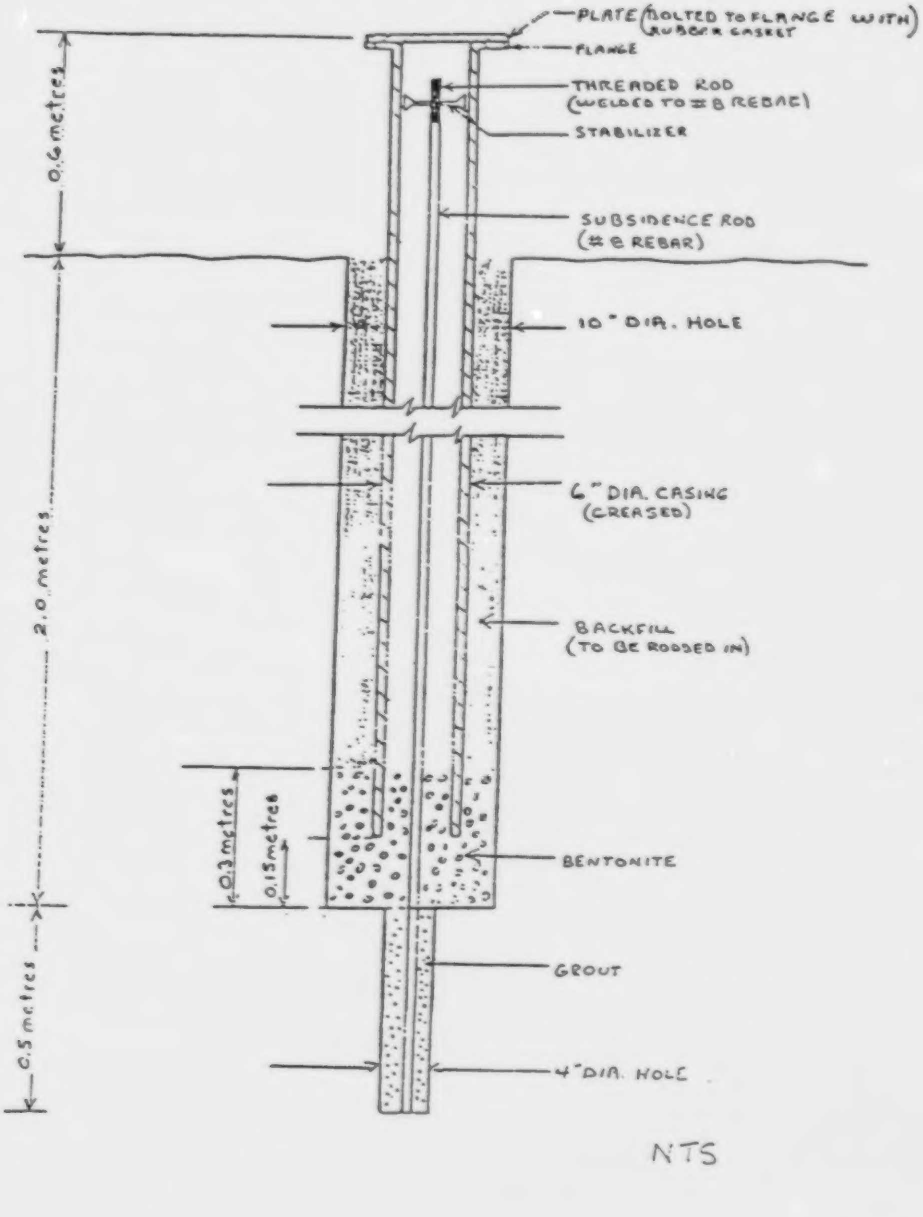
PLATE (BOLTED TO FLANGE WITH RUBBER GASKET)
FLANGE
THREADED ROD (WELDED TO #8 REBAR)
STABILIZER
SUBSIDENCE ROD (#8 REBAR)
10" DIA. HOLE
6" DIA. CASING (GREASED)
BACKFILL (TO BE RODDED IN)
BENTONITE
GROUT
4" DIA. HOLE
0.6 metres
2.0 metres
0.3 metres
0.15 metres
0.5 metres
NTS

Figure C1

Surface Subsidence Monument

Volume
4

Energy, Mines and Resources Canada
Énergie, Mines et Ressources Canada

CANMET

Canada Centre for Mineral and Energy Technology
Centre canadien de la technologie des minéraux et de l'énergie

POTASH MINING PROJECT

PROJET D'EXPLOITATION DE LA POTASSE

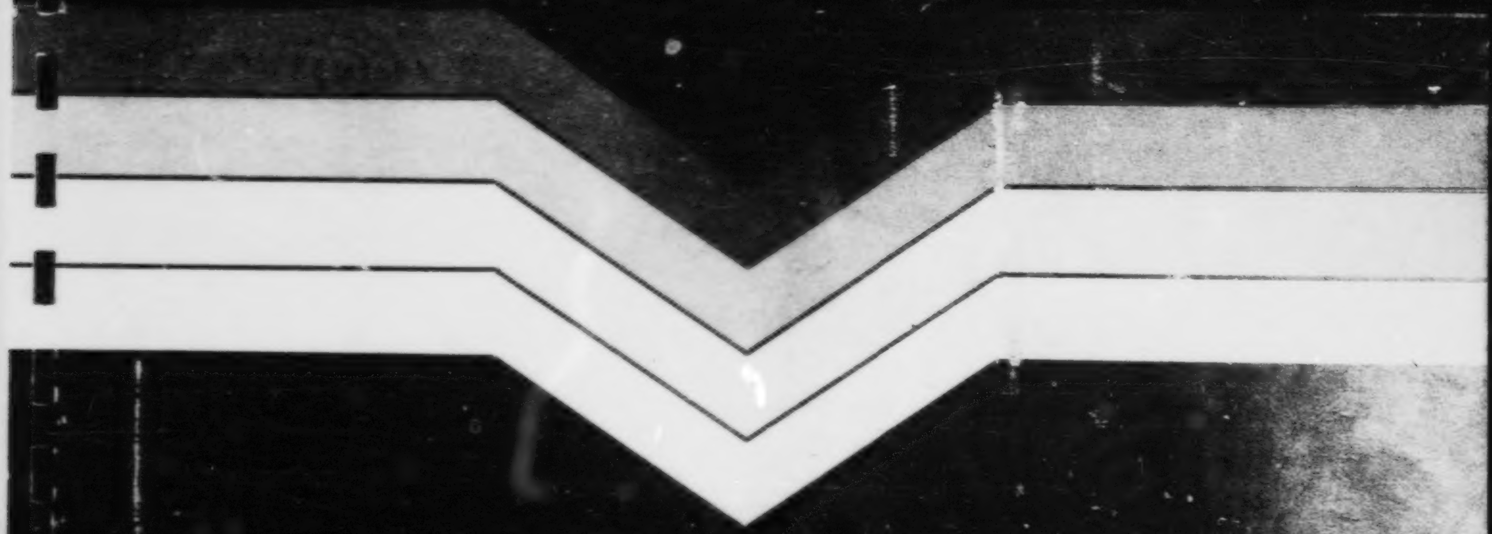

USE OF BACKFILL IN NEW BRUNSWICK POTASH MINES

VOLUME 4

INTACT MATERIAL BEHAVIOURAL MODEL

May, 1987

Final Report By:

DENISON-POTACAN POTASH COMPANY
Sussex, New Brunswick

Prepared by:

MRAZ PROJECT CONSULTANTS LTD
Saskatoon, Saskatchewan

- and -

M.B. DUSSEAULT
Dept. of Earth Sciences, University of Waterloo
Waterloo, Ontario

Work on the Project was conducted under the auspices of the Canada Centre for Mineral and Energy Technology, Energy, Mines and Resources Canada, funded as part of the Canada/New Brunswick Mineral Development Agreement.

DSS FILE NO: 14SQ.23440-5-9031

DSS CONTRACT SERIAL NO: 0SQ85-00208

CANMET PROJECT NO: 1.4.09.05

CANMET SCIENTIFIC AUTHORITY: Dr. G. Herget

MICROMEDIA

168pp

USE OF BACKFILL IN NEW BRUNSWICK POTASH MINES

VOLUME 4

INTACT MATERIAL BEHAVIOURAL MODEL

TABLE OF CONTENTS

1.0 SUMMARY

2.0 INTRODUCTION

3.0 THE INTEGRATED OBSERVATIONAL APPROACH

4.0 CONCEPTS, BEHAVIOURAL MODELS AND CONSTITUTIVE LAWS

4.1 INTRODUCTION
4.2 PLASTIC AND VISCOUS BEHAVIOUR
4.3 FAILURE, RUPTURE, YIELD, STRENGTH AND STRAIN WEAKENING

5.0 THE PROPOSED BEHAVIOURAL MODEL FOR SALTROCKS

5.1 INTRODUCTION AND BRIEF HISTORY
5.2 THE ISSUE OF MODEL VALIDITY
5.3 ATOMIC PROCESSES
5.4 THE BEHAVIOURAL MODEL
5.5 THE LOWER LIMIT FOR INITIATION OF FLOW
5.6 PRANDTL LIMIT
5.7 STRAIN RATE AT THE PRANDTL LIMIT
5.8 THE MOHR-COULOMB RUPTURE LIMIT
5.9 THE VISCOUS LAW BELOW THE PRANDTL LIMIT
5.10 THE VISCOUS LAW ABOVE THE PRANDTL LIMIT, BELOW RUPTURE
5.11 THE ISSUE OF PRIMARY OR TRANSIENT CREEP
5.12 THE ISSUE OF ELASTIC PROPERTIES

6.0 REFERENCES

APPENDIX A
APPENDIX B
APPENDIX C

LIST OF FIGURES

FIGURE 1.1 RANGES OF BEHAVIOUR FOR A SALTROCK OPENING

FIGURE 4.1 TYPES OF YIELD

FIGURE 4.2 FAILURE AND STRAINING PHENOMENA

FIGURE 5.1 BEHAVIOURAL ZONES AND STRESS DISTRIBUTION ADJACENT TO A SINGLE MINE OPENING

FIGURE 5.2 DEFINITION OF THE PRANDTL LIMIT

FIGURE 5.3 THE EFFECT OF NORMAL STRESS ON CREEP RATE

FIGURE 5.4 CREEP LAW USED IN MODELLING

LIST OF APPENDICES

APPENDIX A DEFINITIONS OF TERMS FOR SALTROCK MECHANICS

APPENDIX B THE DESIGN OF OPENINGS IN SALTROCK USING A MULTIPLE MECHANISM VISCOPLASTIC LAW

APPENDIX C EFFECTS OF GEOMETRY ON THE BEARING CAPACITY OF PILLARS IN SALTROCK

SECTION 1.0

1.0 SUMMARY

This volume describes the development of the behavioural model used in the numerical modelling carried out to simulate the behaviour of the openings which Denison-Potacan have excavated and instrumented.

The behavioural model approach used is justified with reference to the literature on crystal physics and examples given of how the model corresponds to the actual behaviour in the field.

The material model used has the following major elements:

a) Below a specific activation shear stress (Prandtl Limit), deformation processes are diffusion controlled and the relationship between the effective plastic stress and the rate of strain is through a power law of exponent 1.0.

b) The turning point in the behavioural law is specified by two parameters; the Prandtl Limit and the Prandtl Strain Rate, both of which were measured or estimated in the laboratory and in the field through use of a test room.

c) The behavioural law above the Prandtl Limit, but below the rupture criterion, is assumed to be a simple relationship for analytic simplicity. However, the actual function relating strain rate and plastic stress is a complex one which includes effects of the normal stress and the non-linear rate at which dislocations are generated in a medium experiencing cracking and crack healing. For the present, a simple power law is assumed with an exponent between 4.5 and 6.0. Future refinements are expected in this formulation. This portion of the behavioural law is best developed through laboratory testing.

d) The upper limit to the steady state creep regime is the Mohr-Coulomb rupture criterion which is a conventional strain weakening behaviour evidenced when laboratory saltrock specimens are strained at a sufficiently rapid rate and under a sufficiently low confining stress as to exhibit rupture.

All of the regimes and the parameters have been explained in terms of reasonable physical mechanisms which have been documented in the crystal physics and materials science literature.

The ranges of behaviour are shown in Figure 1.1.

Where:

σ ... normal stress

τ ... shear stress

K ... Prandtl Limit (activation shear stress required to activate crack growth/healing creep mechanism)

UCS ... uniaxial compressive strength

Y ... brittle yield criterium

r ... radial distance

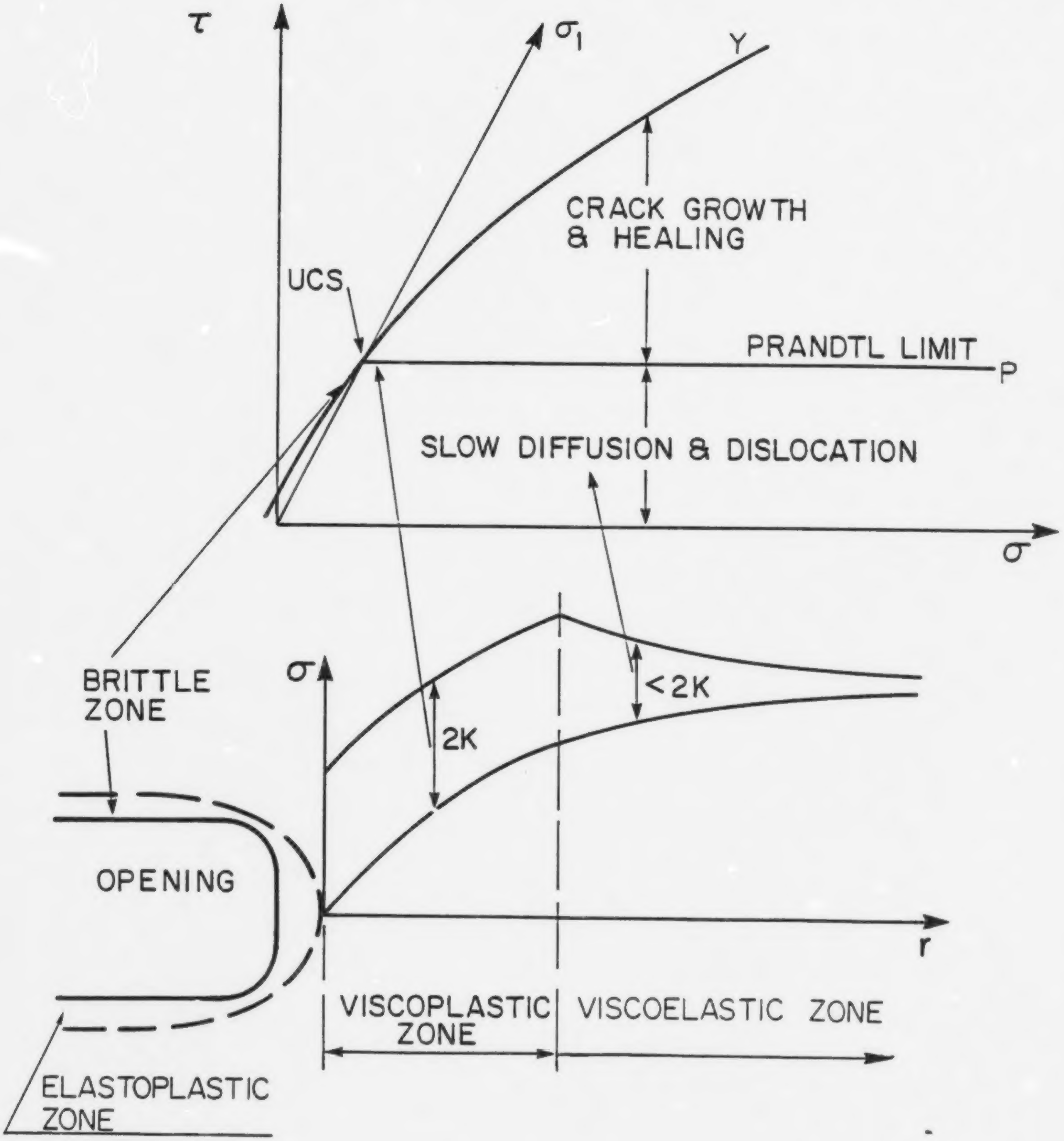

τ
σ1
Y
CRACK GROWTH
& HEALING
UCS
PRANDTL LIMIT
P
SLOW DIFFUSION & DISLOCATION
σ
BRITTLE
ZONE
σ
2K
< 2K
OPENING
r
VISCOPLASTIC
ZONE
VISCOELASTIC ZONE
ELASTOPLASTIC
ZONE

RANGES OF BEHAVIOUR FOR A SALTROCK OPENING

FIGURE 1.1

SECTION 2.0

2.0 INTRODUCTION

The Denison-Potacan backfill study required that numerical modelling be carried out to simulate the behaviour of the openings which Denison-Potacan constructed and instrumented (Mraz and Dusseault, 1986). The goal of this modelling is to develop appropriate numerical approaches which can eventually be used to evaluate the time dependent behaviour of multiple openings and multiple openings filled with backfill. More specifically, the eventual goal is to be able to predict the time required before the backfill is maintaining a sufficient amount of the overburden load so that the second stage mining can be effected at the Denison-Potacan site. If this goal can be reached, a great deal of confidence in the understanding of material behaviour and the application of modelling to real mining situations can be expected. This does not directly solve the problem of transferring the capability into the mining industry, as the whole package is exceedingly complex, but if the goals are successful, it will be demonstrated that the integrated approach of testing, modelling, instrumentation and careful design can be more rigorously implemented in the potash mining industry. This will result in greater economy of production.

The major components of a numerical model are:

a) The set of numerical algorithms which solve the differential equations of stress and strain, as well as, viscous flow and an appropriate method of simulating the boundary conditions of stress, displacement, time and tractions.

b) Detailed knowledge of the geometry of the structure to be modelled, including the variations of the geometry with time (excavation stages) and the precise placement of the different lithologic units.

c) Correct material constitutive laws for the various lithologies to be encountered.

The first of these is not too serious an issue; adequate two-dimensional viscoplastic programs exist, or can be developed from public domain codings with some effort to handle the time dependent behaviour issue. This is not intended to trivialize the difficulty in carrying out high quality modelling. It is not a task for a novice, nor for someone who only does it occasionally. It requires the services of someone who has expertise, as well as, experience with the particular model and an appreciation of the practical application. Also, few models in existence are capable of handling the input/output aspects adequately for all problems, i.e. post-processing has to be designed carefully for the particular application. This means that a great investment in time to generate good results, correctly presented graphically, is necessary and that problems with data management of the huge modelling data files will develop. Nevertheless, the statement that adequate two-dimensional elastoviscoplastic models exist is correct, despite the fact that they require experts to use.

The second issue is usually solved by the detailed site investigation that accompanies mine exploration and development. The major lithologies are clearly identified, the boundaries between units are defined to within a few centimeters, the room dimensions and sequence of excavations are available, etc. Under normal rock mechanics circumstances, detailed geometrical information would also be required about the joints and fissures, but for the case of saltrocks, taking into account the existence of the active opening, the mass can be assumed to behave as a continuum. This means that detailed fabric data is not necessary for macroscopic modelling. (More detailed data may, however, be required if the effect of clay seams or anhydrite beds are present in particular areas.)

The third is, without a doubt, the most critical one to the backfill project. This is also the case for most rock mechanics modelling; our ability to model geometrically complex problems is not really limited by the numerical methods or the hardware. It is, however, limited very seriously by the lack of a sufficiently exact behavioural law for the rock materials. This is the case even for elastic/brittle rocks, as we in general know remarkably little about the behaviour of the rock mass when subjected to the unloading and plane strain stress paths usually found in mining situations. Almost all material behavioural laws are developed from laboratory data which are derived from conditions of pure compressive loading (rather than unloading) and cylindrically symmetrical geometry with radial loading and no confinement (as opposed to the confinement associated with plane strain).

This issue of an inadequate or insufficiently detailed constitutive model is not trivial; it is one of the major reasons that even today almost all mines in all types of rock are designed essentially empirically, and adjusted operationally to address behavioural issues as they arise. In the last few years, better understanding of the behaviour of saltrocks has evolved, and a behavioural model has been developed which makes sense from a physics point of view and which yields reasonable results in case history analysis. This model is applicable to salt rocks, but not to "conventional" hard rocks, although it may, with modifications, also be applicable to coal. It is a model for a material that behaves as a continuum, not a jointed set of blocks and contains some element of novelty. The behavioural model is not accepted by all professionals in the area as the appropriate model; some strong arguments have been brought to bear on it. However, it has withstood these criticisms and is currently providing some of the best matches to field behaviour that have ever been attained (Dusseault, et al., 1987). If the model of behaviour that has evolved can be implemented in an observational manner in the field, it will have a considerable effect on mine design in saltrocks.

The purpose of this volume is to develop the behavioural model in considerable detail from a phenomenological point of view, justify the approach by reference to the literature on crystal physics and then give examples of how the model really corresponds to the actual behaviour in the field.

The exposition will hopefully be quite rigorous, but a serious attempt is made to bring the understanding of the model within the purview of the non-expert who is familiar with the basics of material behaviour. Consequently, great use is made of simple models of behaviour, diagrams and field examples. This is intended to aid in the process of technology transfer, as an appreciation of the material behaviour will go a long way to helping aid the implementation of these methods in the industry.

Section 3.0 deals with the integrated observational approach to the solution of complex design problems in mine geomechanics, as it was that method which led to the current understanding. Section 4.0 presents a series of simple "theoretical" behavioural models, as in order to understand the implications of the behavioural model developed for the isothermal behaviour of saltrock, the conventional, ideal material models should be examined in some detail. Section 5.0 develops the model from the field data and the laboratory data and shows how it explains many phenomena quite well.

SECTION 3.0

3.0 THE INTEGRATED OBSERVATIONAL APPROACH

The observational approach to design in earth materials is a technique which was laid down formally in the 1960's. Basically, the method is simple with a logical approach to design in earth materials, which are inhomogeneous, non-isotropic, and which can exhibit significant non-linearity of properties with time, stress and temperature. All the degrees of variability cannot be rigorously quantified in the laboratory and certainly not in the field; the time and cost would be prohibitive. Therefore, a dynamic learning approach is taken, as listed below:

a) Problem definition;
b) Selection of analytic tools;
c) Delineation of physical properties;
d) Preliminary design;
e) Initial behavioural prediction;
f) Monitoring approach definition;
g) Prototype construction and confirmation or denial or predictions, iterating back to steps (b) and (c) as required;
h) Operational design refinement, includes provision for more testing and modelling to improve economics or safety;
i) Periodic reassessment of project, iterating as required to previous steps, particularly if conditions change.

An integrated and observational approach to mine design problems would seem to be a superior, but as yet, is little practiced. Until the last few decades, mining was carried out with minimum rigorous geomechanics input. Mine design relied only on the experience of the engineers who designed and operated the mine, and perhaps even more on the experienced crews who worked at the face. This experience was, and continues to be, extremely valuable, but now can be enhanced by the modelling, laboratory and monitoring methods developed in the last two decades. This enhancement can only occur within the observational approach outlined above.

SECTION 4.0

4.0 CONCEPTS, BEHAVIOURAL MODELS AND CONSTITUTIVE LAWS

4.1 INTRODUCTION

The writers have observed that words are often used differently by different people, particularly in situations where a continuum mechanics terminology is used to fit phenomena of rock mechanics, or by people with considerable expertise in conventional rock mechanics who simply use the same terminology, hence, the same concepts when dealing with saltrocks. A glossary of terms commonly encountered in saltrock geomechanics is included as Appendix A in this material behaviour section. To avoid misunderstanding, some of the concepts are highlighted below.

In order to design in rock, it is necessary to have a model of material behaviour which can be used to relate directly to the conditions under which the prototype will perform. The engineer must know which models are reasonable representations of reality under a given set of conditions. In addition to a model of behaviour, the engineer must know certain hard facts about a particular rock; these facts, expressed in a manner which is a function of the model used, are the constitutive law.

A constitutive law is a particular set of parameters for a specific rock which defines its behaviour within the limitations (bounds) set down by a particular behavioural model. For example, if the chosen model is linear elastic with no failure, then only two unique parameters need to be evaluated to provide the constitutive law for a given material. More complex behavioural models will require more complex constitutive laws to fully describe the rock behaviour under the appropriate conditions.

4.2 PLASTIC AND VISCOUS BEHAVIOUR

The term "plastic" deformation implies irrecoverable deformation, nothing else. Saying that a material behaves plastically is often interpreted incorrectly to mean that it undergoes time dependent behaviour, or that it deforms according to some specific rule of flow. The latter may be true, but it is incidental to plastic behaviour.

The time dependent deformation of saltrocks is plastic; deformations are not recovered when stresses are returned to their initial values. Permanent deformation can be purely volumetric, as for example, when a sand or a clay is subjected to a change in all-around stress, with water being expelled. In the case of an increasing shear stress, such as is encountered in saltrock in the vicinity of an underground opening, dilatent materials will undergo volumetric increase which is permanent. Materials which are of almost zero porosity and can yield in a viscous manner will undergo plastic shear distortion, but will exhibit no change in volume if the rate of shear strain is slow, and if the principal stresses are maintained constant.

Time dependency in earth materials can be of several types. Time dependent behaviour referred to as viscous is the type where the rate of development of shear strain is a function of the magnitude of the shear stress:

strain rate = f (shear stress)

The nature of the viscous relationship is not specified; it is only known that a relationship exists. Other factors may affect the strain rate, for example:

strain rate = g (shear stress, normal stress, temperature
moisture content, crystal size, etc.)

4.3 FAILURE, RUPTURE, YIELD, STRENGTH AND STRAIN WEAKENING

"Failure" is the loss of capacity to perform the stipulated function for which a structure was designed. The term does not refer to load carrying capacity exclusively; it can refer to other functions, such as the ability to retain water, as in the case of a dam or a pressure tunnel. Misuse of the term "failure" leads to confusion. For example, excavations remain stable and serviceable in spite of the development of ruptured zones in the roof or wall rock. Broken (ruptured) zones can be retained by surrounding rock and support systems and continue to carry a portion of the load. When "failure" is used in such a situation, it can incorrectly be taken to imply failure of the entire excavation and support system. In general, in a salt mining situation, the term "failure" has little global meaning. It is recommended that the term not be used in any engineering context, unless it is clear that the ability to carry out the function is removed or seriously impaired.

"Rupture" is the breakage or fracturing that occurs when rock is stressed to its strength limit. If the ability to carry stress decreases, the term "strain weakening" is preferred as more descriptive. The term "failure" must not be used to mean "rupture". A specimen of saltrock subjected to a sudden tensile or compressive stress of sufficient magnitude will rupture.

"Strength" refers to the stress state at which a rock specimen, or rock mass element, ruptures. Equivalent terms to "strength" are peak strength, maximum (peak) shearing resistance, shear strength, maximum devitoric stress, etc. Some of these terms have subtly different meanings and clarification is necessary if misunderstanding could occur. "Residual strength" is the stress state that can be carried by the specimen or element after large strain. It is usually much lower than the peak strength, but may be greater if the rock continues to "strain harden" after a yield point is surpassed. In the case of saltrocks, the terms strength and residual strength should be used with greater caution, as there are time effects in saltrocks and stipulation of strain rate may be necessary in some circumstances.

The use of "residual strength" may lead to confusion. In granular materials (soil mechanics), it refers to a basic material parameter considered independent of peak strength and the stress path or strain rate used to reach that point. The residual strength of rock is not a fundamental parameter because of the increased damage associated with higher strain rates and because of the effect of different minerals partially fragmented in the rupture plane. Many rock engineers prefer the term "ultimate strength", but the former will be used to conform to more general current practice. In saltrocks, the concept of ultimate or residual strength is not of great value. In analyses of underground openings in salt, it is fully justified to assume that the ruptured material within the active opening has no residual strength at all, because continued viscous straining moves this material around and causes it to become completely detached after some time. As a result of this strain incompatibility, even though some short term support is expected, long term support cannot be relied on for the ruptured materials.

"Yield" occurs when rock is stressed beyond its "elastic limit" and is characterized by a "permanent set" developing beyond a particular stress state. Yield leads to a measureable "residual strain" remaining when the rock is unloaded. Stress levels sufficient to cause yield may be equal to, but are generally less than, those that cause rupture. Yield is, therefore, associated with macroscopic plastic behaviour and reflects a significant change in the microstructure or in the internal crystal relationships which in general cannot be reversed. Yield does not necessarily imply rupture or surpassing of peak strength. Figure 4.1 gives simple stress and strain curves for axially loaded specimens of different materials showing "yield" behaviour. The different types of yield curves again imply that it is desirable to draw a diagram or be very careful in using the word yield. At the very least, the word should be qualified, as in:

- perfectly plastic yield,
- strain weakening (or work softening, strain softening) yield,
- work hardening yield,
- viscoplastic yield.

To try and eliminate problems of semantics, this discussion reserves the term "failure" for the rock structure and the term "yield" as a sudden decrease in the rate at which a rock element can carry more load. "Strength" is used to refer to the maximum current load carrying capacity of a rock element. More specifically, at any instant in the stress and strain life of an element of saltrock, that element has an instantaneous (very short term) strength at the current confining stress and a potential for long term strength capacity, both of which are functions of the strain rate the material has experienced to that point.

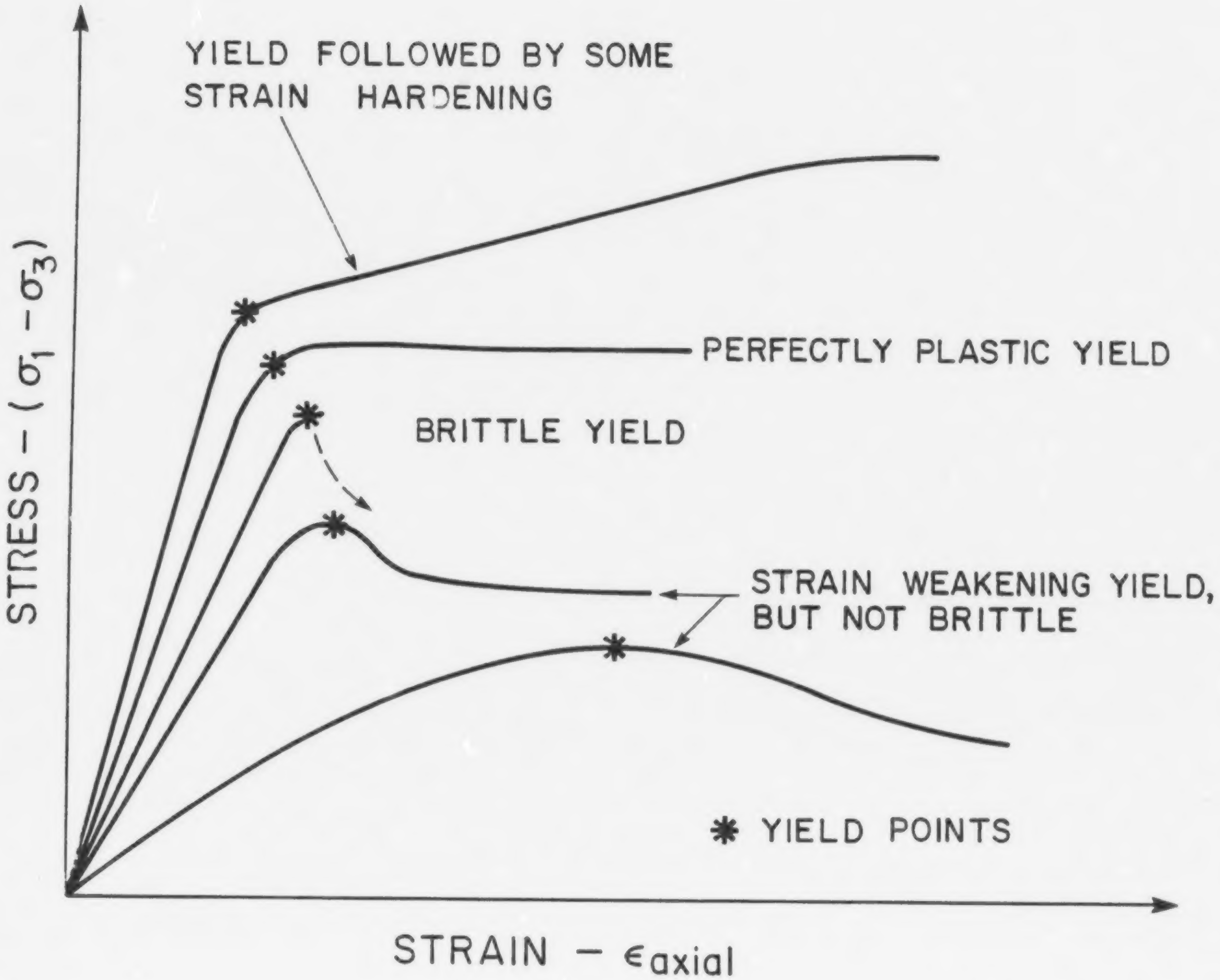
YIELD FOLLOWED BY SOME STRAIN HARDENING
PERFECTLY PLASTIC YIELD
BRITTLE YIELD
STRAIN WEAKENING YIELD, BUT NOT BRITTLE
✱ YIELD POINTS
STRESS – ($\sigma_1 - \sigma_3$)
STRAIN – ϵ_{axial}

TYPES OF YIELD

FIGURE 4.1

The term strain weakening is used in preference to the term strain softening. The term strain softening is a product of the classical continuum mechanics approach to materials, such as metals, which display a sudden decrease in the shear modulus at a certain point, or which become less rigid gradually as strain is increased, particularly tensile strain. These concepts are explained more fully in Figure 4.2, which shows a number of stress and strain curves for real materials and for idealizations of real material. Saltrocks subjected to sudden large deviatoric loads (high shear stress level) will fail in a brittle, sudden fashion, displaying a considerable amount of strain weakening. However, if the loads are applied gradually, or if the confining stresses are high, the whole concept of "yield" has to be carefully defined.

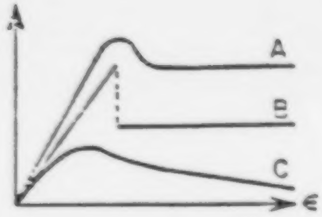

STRAIN WEAKENING **BEHAVIOUR**
(LOSS OF STRENGTH)

A-NORMAL DENSE SAND

B-LINEAR-ELASTIC/STRAIN-WEAKENING/PERFECTLY-PLASTIC

C-CONTINUED WEAKENING (FABRIC DESTRUCTION)

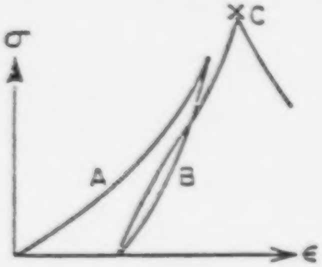

STRAIN STIFFENING **BEHAVIOUR**
(GAIN IN RIGIDITY)

A-LOADING

B-UNLOAD-RELOAD CYCLE

C-YIELD (RUPTURE) POINT LEADING TO STRAIN WEAKENING

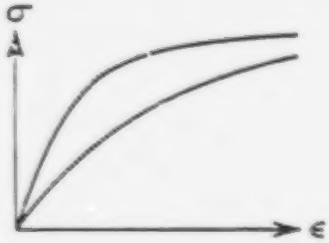

STRAIN SOFTENING **BEHAVIOUR**
(YIELD NOT MENTIONED)

SOFT CLAYS AND LOOSE SANDS

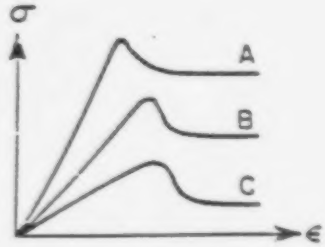

STRESS STIFFENING **BEHAVIOUR**

A-HIGH CONFINING STRESS

B-INTERMEDIATE CONFINING STRESS

C-LOW CONFINING STRESS

FAILURE AND STRAINING PHENOMENA

FIGURE 4.2

SECTION 5.0

5.0 THE PROPOSED BEHAVIOURAL MODEL FOR SALTROCKS

5.1 INTRODUCTION AND BRIEF HISTORY

The history of the development of an appropriate material model for saltrocks has been characterized by parallel monologues, that of the pure scientist based on physical arguments and laboratory experiments, and that of the mining engineer based on empirical observations and experience. Both approaches have their strengths, but both also have limitations. For example, a considerable amount has been written on the behaviour of single pure crystals of halite without the necessity of relating the single crystal behaviour to that of a polycrystalline mass. This is fundamental to materials science, but has not led to useful generalizations applicable to mine design. On the other hand, purely observational approaches can be in serious error without an appreciation of the behavioural law, or with inadequate information. This is often the case with mining knowledge which is empirical, hence, limited in its generality. This report will attempt to develop a behavioural model which is based on physical reality, but which also generates a material macroscopic law appropriate for numerical modelling of saltrocks for engineering purposes.

There have been a few attempts to apply rigorous continuum mechanics approaches to the case of saltrock mining or solution cavities. These approaches have been to a considerable degree unsatisfactory because the behavioural laws have been ignored in favour of a purely empirical approach using parameters which have no physical meaning and are only used for "curve fitting". The classic equation used to simulate the behaviour of model pillars in the laboratory environment is a good example. The form used was a multiple power law:

$$\dot{e} = A \times t^{l} \times T^{m} \times s^{n} \qquad (1)$$

Where:

$\dot{e}$ ..... strain rate
A ..... empirical constant
t ..... time in consistent units
T ..... temperature in degrees Kelvin
s ..... vertical average stress on model pillar

The three exponents are purely curve fitting numbers which have no fundamental science behind them and the multiplicative constant is a very strange number with time units of 1/l, stress units of 1/n, etc. Because n can have a value of 3.0 in one case, 4.5 in another, the constant A cannot be compared for different materials, geometries, and has no physical meaning.

This approach has many other flaws. Using a power law relationship for time is quite incorrect, as any exponent less than 1.0 gives a continually decreasing strain rate, something which does not correspond to the reality evidenced by salt glaciers or salt domes, which clearly demonstrate steady state flow. This is because the empirical curve fit cannot account for the geometric transient component, as well as the microstructural transient component rigorously in a single equation. Steady state creep is a real behaviour, but room closure rates decrease with time. This is not evidence of strain hardening, it is evidence of changing geometries; pillars get fatter and room volumes become less.

This section will present the behavioural model which has been developed by Mraz and Dusseault. The details of the model for the behaviour of intact saltrock is not yet complete in detail. It awaits continued test results and more attempts to match field behaviour through numerical modelling. However, all the major elements are in place and preliminary modelling results indicate that there is reasonable certainty that the model is correct in its major aspects.

5.2 THE ISSUE OF MODEL VALIDITY

A material behavioural model is not necessarily correct just because it can be used to "fit" the behaviour of a particular structure underground. There are cases where a model was derived to fit laboratory data, then extrapolated to pressures and temperatures well beyond the laboratory range and the model simply was inappropriate. The major elements of what constitutes validity of a material behavioural model for rock mechanics are important to remember.

- It must not contravene laws of physics.
- It must be applicable to realistic situations; that is, some macroscopic predictive capacity must exist.
- It must be developed for the conditions for which it is to be applied, or else the ability to extrapolate the model must be unquestionably sound (this has been a major problem in salt rock mechanics).
- It must include all major physical processes, otherwise it is not representative of reality.

- It must be reasonable, yet sufficiently concise as to be useful. Excessively complex formulations, such as a multi-parameter law can be adjusted ad infinitum to "fit" particular situations.
- It must have predictive capacity at some reasonable level of accuracy. At the very least, the predictive capacity can be qualitative, rather than quantitative, but it still must exist. In this case, a model may only be useful for comparative analysis ("sensitivity" analysis).
- Its behavioural constants or parameters must have some physical significance. The "A" parameter in the power law above is an example of a parameter which has no physical significance.

These are not trivial issues. For example, many researchers have argued at great length about the strain hardening behaviour of salt. Their major contention is that all laboratory tests show it, therefore, it is a mechanism which must be incorporated into descriptions of material behaviour for field applications. The first part of this is valid, the second is not; the existence of salt glaciers, salt domes, and mines which continue to close after decades suggest steady state processes are dominant, not strain hardening processes.

Another major issue, alluded to above, is the laboratory testing of saltrocks in the strain rate region of 10^{-2} to 10^{-8} s^{-1} (Carter and Heard, 1970; Arieli et al., 1982) and then extrapolating those data in a linear manner to strain rates often three orders of magnitude lower. There has not been, to the writer's knowledge, a comprehensive set of laboratory tests of saltrock at the strain rates observed in mining.

5.3 ATOMIC PROCESSES

To make the very important point that the derivation of a behavioural law is not necessarily a trivial endeavour, a listing of reasonable creep processes are listed here, each of which can give rise to deformation behaviour, potentially with some viscous component. The list is developed from one in Frost and Ashby (1982).

a) Rupture or ideal elastoplastic behaviour, characterized by flow when the strength criterion is exceeded and, for most rock materials and for saltrocks at high strain rates and low stresses, evidencing frictional behaviour. The latter component means that there is a direct relationship between the magnitude of the mean normal stress and the rupture criterion.

b) Low temperature plasticity by dislocation glide. The rate of glide and the stress at which this glide can be allowed is related to basic crystal lattice restraints, giving rise to a discrete stress (Peierls' stress) below which dislocation glide will not occur. The fundamental lattice resistance has to do with the energy required to glide a row of atoms opposite another row of atoms, rupturing and re-establishing bonds. This type of deformation terminates for single crystals at grain boundaries, where the dislocations "daylight" or disappear. In the case of a macroscopic polycrystalline mass, the dislocations will not daylight; a number of the "flaws" will accumulate on the intercrystalline boundary to generate a small volume flaw where there is a large stress concentration.

Eventually, this will focus a strain dislocation onto the adjacent crystal, causing the flaw to propagate across it, albeit in another orientation. The process moves from crystal to crystal in a "steady state" macroscopic process, although microscopic processes are definitely not continuous. This type of behaviour, integrated over an "infinite" number of crystals, leads to steady state behaviour as long as there is no permanent rupture along the glide planes.

c) As a subset of the above, power law creep is evidenced from the dislocation glide and can also be evidenced from dislocation glide plus dislocation climb.

d) Diffusional processes, including lattice diffusion (Nabarro-Heering), which is the migration of lattice vacancies, grain boundary diffusion in liquid films (Coble creep), or interface reaction controlled diffusional flow, which is the growth of one crystal at the expense of another by mass transfer across the boundary. Included here should be fluid inclusion migration under a differential stress field.

We will discuss another mechanism which we refer to as stable crack growth. This is really a case of localized plastic flow (item a, above), but with simultaneous crack blunting and other processes, particularly dislocaton climb/glide. In a polycrystalline material with flaws, the conditions of deviatoric and normal pressure are not identical throughout, particularly at the tips of cracks where extremely high shear and normal stresses can be generated. Also, crystals of more than one mineral are present and the elastic properties of the individual crystals may not be the same in all lattice directions. Processes different than those in the rest of the polycrystalline mass can occur locally, and these must somehow be expressed as a macroscopic law which can be used in a deterministic analysis.

5.4 THE BEHAVIOURAL MODEL

The behavioural model will be presented, then the five major elements will be discussed individually. Three of the elements are explicitly yield points, two of the elements are the viscous flow laws for the regions of stress space bounded by the yield points (surfaces in the case of a three-dimensional stress representation).

Field verification would appear to exist for three explicit yield levels which are important for saltrock behaviour understanding.

The first of these yield levels is the shear stress level required to initiate flow. This is the shear stress that is required to trigger true plastic viscosity, that is to say, time dependent behaviour that is not recoverable upon stress relaxation. There is general agreement among researchers that saltrocks display time dependent behaviour at shear stresses down as low as 1 to 3 MPa and perhaps as low as 0 MPa.

It is desirable to discuss the third limit before returning to the second yield limit. The third limit corresponds to a classical Mohr-Coulomb (Navier-Coulomb) rupture criterion. It is evidenced when a specimen of saltrock in the field or in the laboratory is subjected to a high enough stress level at a rapid enough strain rate to achieve brittle rupture. The criterion is not as simple as for perfectly brittle silicate rocks; it requires a statement of time because it can be shown that with a very high confining stress, it is impossible to achieve strain weakening failure in saltrocks at the displacement rates achievable on a press (2 mm/s), and the Mohr-Coulomb criterion becomes very flat. At low confining stresses, the stress at which a saltrock ruptures is somewhat dependent on the strain rate. If the deviatoric stress level is just above the Mohr-Coulomb criterion, the saltrock will fail, perhaps in minutes or hours. If a much faster strain rate is imposed, a higher shear stress and lower strain to brittle rupture is evidenced. These "different" behaviours actually correspond to the concepts of tertiary and secondary creep as originally conceived in the creep literature.

We do not, in the case of mining engineering, have to be concerned about the behaviour of the material above the lowermost Mohr-Coulomb line, nor do we have to be concerned at the macroscopic scale with the onset of tertiary creep or with the "perfectly plastic" behaviour associated with very high confining stresses and shear stresses. We simply never get into that regime, nor does any saltrock material in nature over the long term. Stresses are macroscopically redistributed to eliminate these high stress conditions.

The second yield point, the one referred to as K or the Prandtl Limit, is the major element in this behavioural model. It is not used by others in the mining industry, but is clearly a real parameter of fundamental importance which has been well documented in the scientific literature (Figures 3. 5 and 4.13 in Poirier, 1985; Figure 10.2 in Frost and Ashby, 1982; Skrotzki and Haasen, 1984; others). As a specimen is subjected to higher shear stresses, it will exhibit ever more rapid time dependent behaviour. Below a certain limit, very slow diffusion rate controlled mechanisms dominate creep. When a certain activation shear stress level is reached, however, dislocation glide and microcrack formation processes begin. These microcrack formation and dislocation glide processes do not destroy the material, however, because of the capability of saltrock to heal itself through local flow at the extremely high stressed tips of microcracks.

The Prandtl Limit divides the generalized stress field into two regions:

1. Low stress processes: These are probably diffusion controlled processes described in Section 4.3 d. They depend on stress with a different relationship than those processes above the Prandtl Limit.

2. High stress processes: These are associated with dislocation glide and climb, concentration of stresses at the tips of these dislocations and rapid flow to heal flaws generated by the dislocations. Steady state creep still happens in this region.

5.5 THE LOWER LIMIT FOR INITIATION OF FLOW

The mechanisms for creep at very low shear stresses have been documented in the physics literature (Poirier, 1985; Frost and Ashby, 1982; see Section 5.3). Pure vacancy diffusion is so slow as to be irrelevent in the mining time frame. Saltrocks have thin liquid films along grain boundaries and liquid inclusions. Ions can migrate fairly rapidly along these thin films. The presence of this moisture has some effect, but it is not yet fully understood, particularly at very low stresses and strain rates (Speirs et al., 1986; Urai et al., 1986). These diffusive processes can occur seemingly at any shear stress level.

This lower limit in the plastic behaviour of salt would be a true Bingham yield limit. Below it, there would be no movement of a time dependent nature, above it, viscous movement would take place. Does such a limit exist? It seems to be a reasonable concept for metallic bonds, for covalent bonds, or for materials that have a discrete "cohesion" at the molecular level that has to be overcome to allow flow. In the case of saltrocks with a small moisture content, the mechanisms of slow grain recrystallization and diffusional creep as the result of the channelling of ions along the thin liquid films seem to have no lower stress limit, so that the value of this limit would approach 0 MPa, for all practical purposes. It will be assumed to be zero, as this can lead to no detectable error in the mining engineering frame.

5.6 PRANDTL LIMIT

Measurements of stresses in pillars in potash mines in Saskatchewan led to the observation that the difference between the maximum (vertical) and the minimum (radial horizontal) stresses tended to stabilize at a particular value (Mraz, 1980, 1984). The results were not unequivocal, but clearly pointed to a mechanism which tended to equilibrate the shear stresses by some type of differential flow mechanism. Results of laboratory tests clearly show that the concept of a "yield limit for the onset of more rapid plastic flow" is a reasonable one (Dusseault et al., 1987).

The postulation of such a limit is not entirely novel; what has been done is to use the criterion specified or implied by others as the stress trigger for a particular mechanism at about 20 MPa (Langer, 1984; Berest and Minh, 1984). This applies viscoplastically at steady state if in a saltrock mass, enough material is available to redistribute the stress so that a "viscoelastic" zone exists. The attached Figure 5.1 shows how this is achieved in the case of a virgin ground opening, where:

$\sigma_\theta(\sigma_1)$ ... tangential (major) principal stress
$\sigma_r(\sigma_3)$ ... radial (minor) principal stress
K ... Prandtl Limit
r ... radial distance

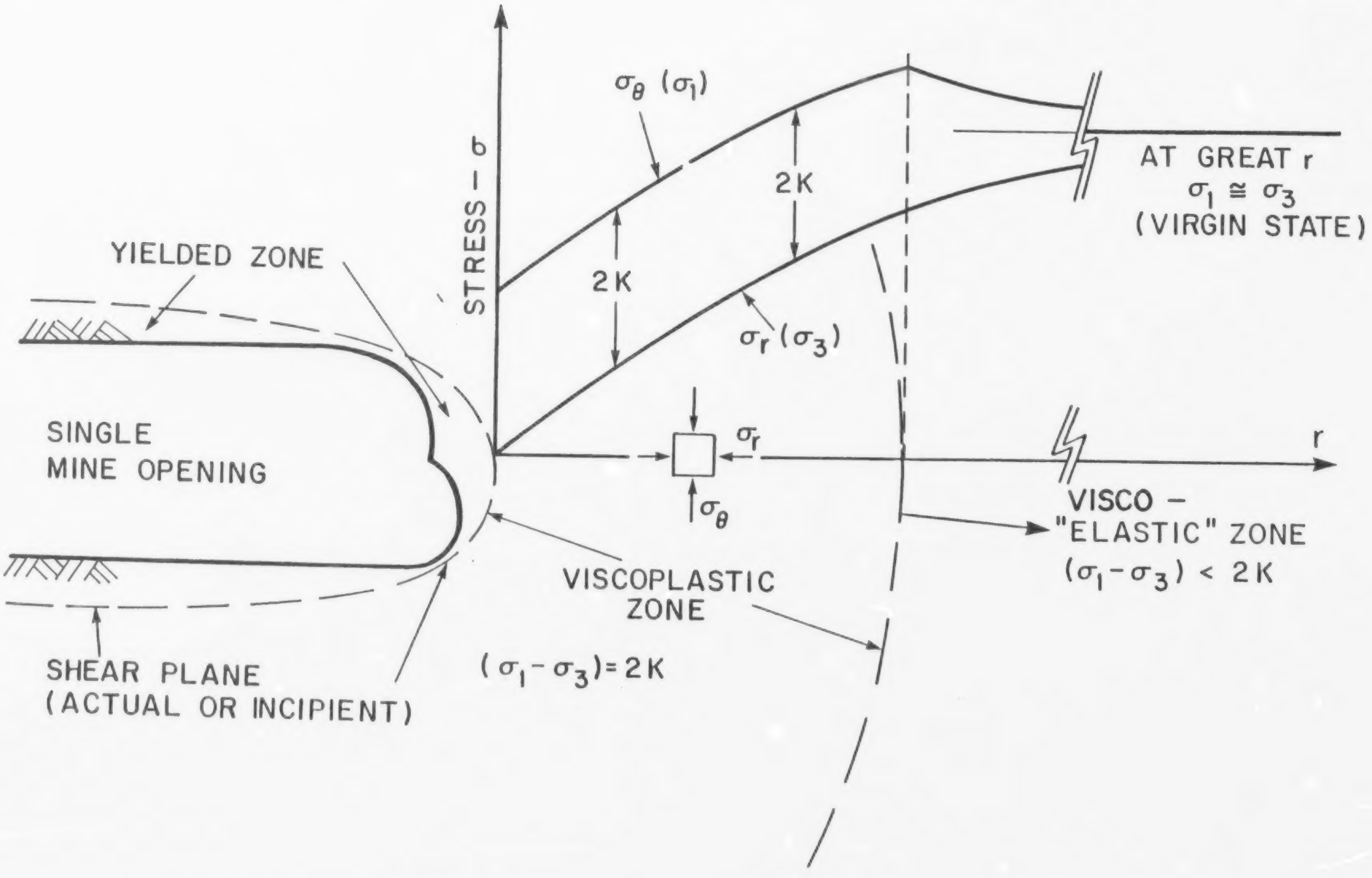
STRESS – σ
σ_θ (σ_1)
2K
2K
σ_r (σ_3)
AT GREAT r
$\sigma_1 \cong \sigma_3$
(VIRGIN STATE)
YIELDED ZONE
SINGLE
MINE OPENING
σ_r
σ_θ
r
VISCO –
"ELASTIC" ZONE
$(\sigma_1 - \sigma_3) < 2K$
VISCOPLASTIC
ZONE
$(\sigma_1 - \sigma_3) = 2K$
SHEAR PLANE
(ACTUAL OR INCIPIENT)

BEHAVIORAL ZONES AND STRESS DISTRIBUTION ADJACENT TO A SINGLE MINE OPENING

FIGURE 5.1

What is the Prandtl Limit, in a physical mechanisms sense? It is the explicit boundary between two different viscous regimes, and is the shear stress required to trigger a set of deformation mechanisms which are associated with dislocation climb/glide and crack growth/healing. In all cases, the value of the Prandtl Limit can be determined by laboratory tests or by careful instrumentation in the field, and the use of both methods is advocated if detailed predictive modelling is to be carried out. This double confirmation is the most convincing argument that the Prandtl Limit is a real parameter describing a real phenomenon, not simply a figment of plotting data in a different manner.

The physical meaning of the K parameter is quite clear. It is the turning point of a constitutive law that plots as two straight lines on a log-log plot of shear stress (or plastic effective stress) and strain rate. In Figure 5.2, the law is simplified by drawing the intersection point as a sudden angle. In reality, there is probably a transition zone and some curvature of the "heel" of the relationship. This curved heel is more typical of reality, as the mechanisms in polycrystalline saltrock materials, paricularly rocks with at least two minerals, cannot be expected to be triggered at a single value of macroscopic stress.

Some factors associated with the Prandtl Limit should be summarized:

a) Below the Limit, material flows without the possibility of structural damage as long as it is in general compression.

b) Above the Limit, if the confining stress is zero (corresponding to unconfined compression test conditions), damage can occur, leading to strain weakening behaviour.

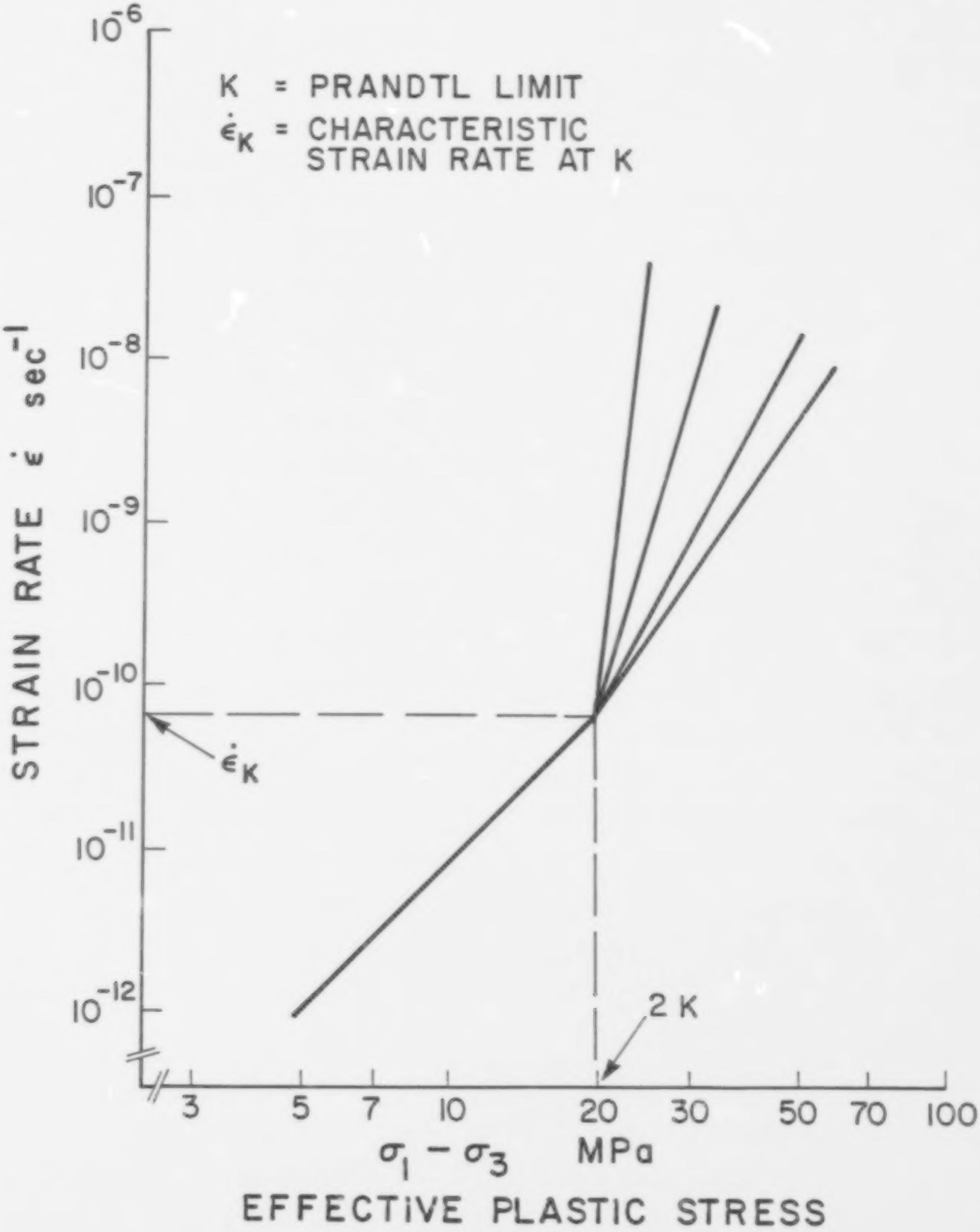

DEFINITION OF THE PRANDTL LIMIT

FIGURE 5.2

c) The value of the Limit is unaffected by the normal stress level, therefore, it corresponds to a classical Tresca Yield Limit (not necessarily a rupture limit).

d) The Limit is not a rupture criterion, nor is it a classical Bingham flow initiation criterion, nor is it a plastic flow criterion; it is a criterion for the initiation of a new set of deformational mechanisms which have different relationships to the shear stress.

e) The Limit can be determined independently in the laboratory or in the field, and it is different for different materials, a function of mineralogy in particular.

f) In the field, if enough material is available, the differential stresses will stabilize at the value of the Prandtl Limit. (Hence, the use of the term "limit", as it defines a very important limiting state in the equilibrium analysis of saltrocks.)

5.7 STRAIN RATE AT THE PRANDTL LIMIT

Another fundamental premise of the behavioural approach advocated herein is that the Prandtl Limit is characterized by a unique strain rate for a particular material. This is called the Prandtl Strain Rate, and it is claimed that a particular value for one material must be independently determined for different materials. A log-log plot of shear stress versus strain rate has a discrete kink associated with the Prandtl Limit. The other parameter which delineates that kink is the strain rate.

The Prandtl Strain Rate cannot be determined easily in the laboratory for most materials because it is typically on the order of 5 x $10^{-11}s^{-1}$ or less. This strain rate could be achieved in the laboratory, but tests at this strain rate would have to be carried out for the better part of a year under one condition of stress in order to be acceptable. The lowest reasonable strain rate which can be easily achieved in the laboratory for mine design purposes is in the range of 5 to 10 x $10^{-10}s^{-1}$. Longer tests require a research environment of great stability.

How is the Prandtl Strain Rate to be determined? If a virgin ground opening at sufficient depth is established with full instrumentation, the Prandtl Strain Rate is the strain rate calculated at the boundary of the viscoplastic/viscoelastic boundary. The averaging effect of the huge mass of saltrock gives a very reasonable averaged value of this parameter. This is the case at Denison-Potacan where the square opening Test Room and the Test Stope were both established in virgin ground and the value of the Prandtl Strain Rate determined from the square opening. When this data point is applied to the Test Stope, it gives very reasonable predictions.

It is desirable to obtain the Prandtl Strain Rate in the field for another important reason. It is believed that the value is sensitive to moisture content (Speirs et al., 1986), and in the field situation, there is absolutely no change in moisture in the viscoplastic and viscoelastic regimes. The "averaging" effect, and the certainty that the value is representative of true field conditions are extremely important aspects of the numerical and analytical modelling being carried out on the Denison-Potacan approach. Tying the constitutive law firmly to macroscopic behaviour is an important element of the approach recommended in this discussion.

In summary, the stipulation of the "kink" in the behavioural law curve requires that two parameters be determined; the Prandtl Limit and its characteristic Prandtl Strain Rate. These are different for different materials and can be determined in-situ or in the laboratory.

5.8 THE MOHR-COULOMB RUPTURE LIMIT

At the level of shear and normal stresses that are important to mine design and specifically the stresses that develop around the openings, the brittle behaviour of saltrock is important for the initial development of the active opening (the elastoplastic portion of the behavioural field around an opening, Mraz and Dusseault, 1987). In fact, the brittle behaviour of saltrock, in combination with the virgin stress state, is "responsible" for the existence of the active opening. The outer boundary of the active opening is the last point at which the saltrock has experienced Mohr-Coulomb brittle rupture and seems to stabilize quite soon after an opening is created.

The brittle rupture criterion cannot be determined in the field. It is determined in much the same manner as for a brittle elastic rock, except that two conditions are different and care must be taken so that these conditions are not abused, leading to incorrect or misleading test results.

First, the strength is clearly a function of strain rate; not so much in the case of uniaxial compression or extension, but definitely so in the case of triaxial confinement. Therefore, strength is defined as the "lowest axial stress at which strain weakening rupture will develop for a given value of confining stress, given as much time as possible, and before 10% or 15% strain". This condition is necessary for a consistent strength definition. Carrying out laboratory tests beyond 15% strain is not recommended because the platen punching, barrelling and non-uniform stress conditions in the specimen invalidate results beyond that point. Also, in the field, materials simply do not experience that amount of strain before rupturing, if they rupture at all. Because of the processes involved in saltrock, the whole concept of creep rupture, as outlined by Carter and Hansen (1983), should be carefully re-examined. There is probably no chance of genuine rupture at constant stress conditions in the laboratory or the field, as long as that stress is below the Mohr-Coulomb lower most rupture limit.

The second condition is that the confining stress is below some value (on the order of 15 to 20 MPa for halite), otherwise it is impossible to rupture the specimen; it simply yields in a classical plastic manner up to the limit of the strain rate of the testing machine. It bears mentioning that the stresses and strain rates evidenced at these conditions are never encountered in actual mining conditions, hence, the mechanisms are quite irrelevant to design aspects.

What is the mechanism responsible for the Mohr-Coulomb rupture limit? The rupture limit can be looked on as the boundary between stable crack growth (leading to steady state) and unstable crack growth (leading to tertiary creep). Because the process of crack extension is sensitive to normal stress, the criterion is steeply inclined. Unstable crack growth means that new rupture surfaces are being created at a rate faster than they are being healed.

5.9 THE VISCOUS LAW BELOW THE PRANDTL LIMIT

The inclination of the strain rate versus effective plastic stress on a log-log plot should be a straight line if the processes are rate controlled, as diffusive processes are.

Probably the relationship between the effective plastic stress and the creep rate is by an exponent of from 1 to 3, based on robust physical arguments (e.g. Poirier, 1985). It is also quite reasonable to postulate that these processes are not significantly affected by the normal stress level because they are not dilational movement processes, which dislocation climb and glide are. Hence:

$$\dot{\epsilon}_{ss} = A \times (s_1 - s_3)^m \quad \text{for } (s_1 - s_3) < 2K \tag{2}$$

$\dot{\epsilon}_{ss}$ ... steady state strain rate

The exponent is assigned symbol "m", rather than "n", to emphasize its value below 2K being different from its value above 2K.

Or, in its more correct form, wherein we choose to normalize the equation with respect to the Prandtl Limit and the Prandtl Strain Rate for the particular model:

$$\frac{\dot{\epsilon}_{ss}}{\dot{\epsilon}_{K}} = \left[\frac{s_1 - s_3}{2K} \right]^{m} \text{for } (s_1 - s_3) < 2K \qquad (3)$$

The benefit of the normalization procedure is that all the material constants are in perfectly consistent units and have a distinct physical meaning.

Authors that do not recognize the existence of the change in the behavioural law do not agree on an exponent and also usually extend the "law" into ranges far beyond that for which it was determined in the laboratory. In particular, they take the behaviour above the Prandtl Limit and extend it down to stress regions where it simply does not apply. This results in serious under prediction of the strain rates of virgin ground openings (Munson and Fossum, 1986).

The numerical modelling undertaken for this project shows that an exponent of 1.0 is reasonable for the process below 2K. This is acceptable as an assumption in the modelling being carried out, but is not unequivocal proof that the value of the exponent is exactly 1.0. There is not wholesale agreement that such a generalization can be made at present; the physics are not entirely clear. However, for the simple reason that the predictions clearly match the measurements in the virgin ground openings where the behaviour is dominated by the flow of materials below the Prandtl Limit, this assumption will be used in the modelling for the material outside the viscoplastic zone.

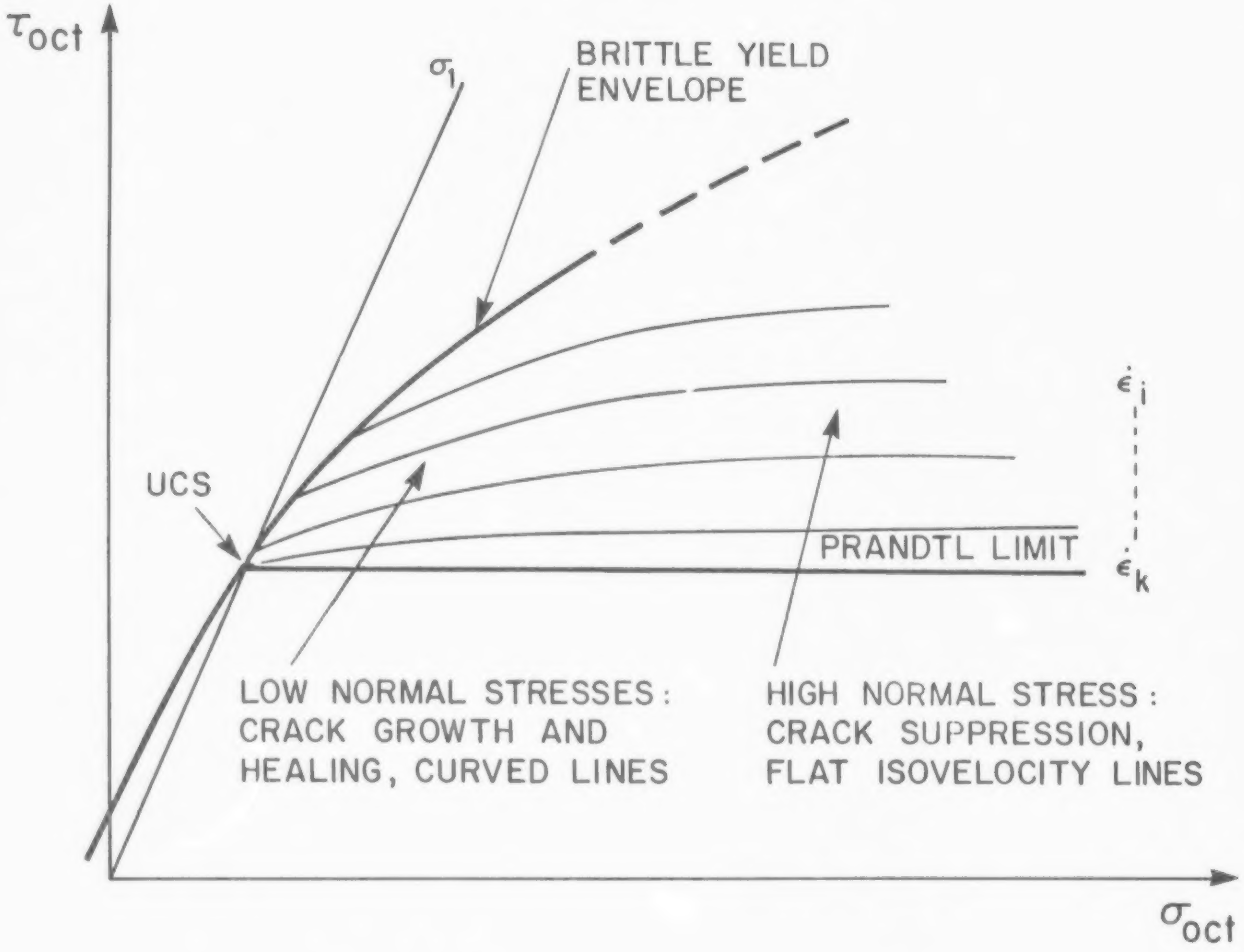

τ_{oct}
σ_1
BRITTLE YIELD ENVELOPE
UCS
$\dot{\epsilon}_i$
PRANDTL LIMIT
$\dot{\epsilon}_k$
LOW NORMAL STRESSES: CRACK GROWTH AND HEALING, CURVED LINES
HIGH NORMAL STRESS: CRACK SUPPRESSION, FLAT ISOVELOCITY LINES
σ_{oct}

THE EFFECT OF NORMAL STRESS ON CREEP RATE

FIGURE 5.3

5.10 THE VISCOUS LAW ABOVE THE PRANDTL LIMIT, BELOW RUPTURE

Above the activation shear stress (above 2K), the relationship between shear stress and the strain rate takes on a much different form, with the "average" exponent being greater, it seems, than 4.5. There is some evidence that the exponent is much greater than 4.5, if the confinement is extremely low as in the case of an uniaxial creep test. Above the 2K limit, the strain rate also is weakly dependent on the normal stress level or the degree of confinement. This makes a great deal of sense. In fact, in some more rigorous formulations of creep laws, the normal stress dependency is explicitly included for this class of mechanisms. Why it is often excluded by numerical modellers in salt rock geomechanics is not clear. However, it is not that important an effect, because it occurs above the 2K value of shear stress and a well designed mine will not have the bearing elements above 2K when full overburden load is reimposed and redistributed. Also, the strain rates at shear stresses appreciably above 2K are much higher than those evidenced in mines.

Dislocation climb/glide can be looked on as the movement of a dilational centre in a medium and, as pointed out by many (Frost and Ashby, 1982; Poirier, 1985), is a normal stress sensitive process. If it is a normal stress sensitive process, lines of equal velocity should be inclined in a stress space plot and they certainly are for sylvinite and salt. This normal stress dependency has been ignored by others, or the amount of testing was insufficient to detect it. In fact, the inclination of the constant strain rate lines is an important part of the method of determining the Prandtl Limit in the laboratory (Figure 5.3).

At very high normal stresses, the isocreep lines become gradually horizontal in an octahedral stress/normal stress plot (parallel to the Prandtl Limit). This is because as the normal stress increases, the dilational aspects of the mechanism and the creating and healing of microcracks are suppressed by direct compression of the crystalline lattice. In these conditions, only dislocation glide remains a real viable mechanism.

A process of dilation centre migration can lead to steady state creep because of the mechanism suggested earlier; accumulation of defects at a grain boundary until the stress concentration is large enough to cause the dilational centre to propagate into the adjacent grain.

For the region above the Prandtl Limit, the strain rate law is not simple because of the existence of the Mohr-Coulomb failure criterion and because the processes are sensitive to normal stresses. If we take the data from an extensive series of tests at the same mean normal stress (octahedral stress), the line relating strain rate and effective plastic stress is not straight in a log-log space. This is not a new idea, Skrotzki and Hansen (1984) have pointed it out and the concept is alluded to in Frost and Ashby (1982) and Poirier (1985).

Interestingly, in a real mining situation, the behaviour of the material above the 2K value is not as important as might be expected. This is because the "kink" in the behavioural law acts as a "state attractor" and all material experiencing stresses higher than 2K will re-adjust internal velocities to equal 2K, providing of course that there is enough material available in which to redistribute stresses. The behavioural law above 2K is critical to understanding transient behaviour and also to the modelling of backfill consolidation if the pillars are split, placing stresses firmly in the region above 2K, leading to accelerated closure. In these cases, we must have good information about the strain rates in the stress region above 2K by about 5 MPa.

The lower limiting line for the various "constant creep rate curves" above the 2K limit is expected to have an exponent of 3.0. This is the so-called "natural" stress dependance for a process which depends on a density of dislocation centres in a crystalline medium. It can be derived from first principles and relatively robust assumptions (Weertman, 1972; Brown and Ashby, 1980). At lower confining stresses, the value is greater than 3.0, as non-linear dilational processes are dominant.

Now the reader can appreciate why the debate rages as to the "correct" value of the exponent on the power law formulation. First, the power law formulation breaks down at plastic stresses greater than the Prandtl Limit (Skrotzkiand Hansen, 1984). Second, the data are collected over a relatively rapid strain rate and are simply "fit" to a single power law equation, forcing the material to conform to the behavioural model imposed by the assumptions inherent in that approach. Third, tests are carried out at ranges of confining stress and the average of the strain rates leads to a value generally between 4.5 and 6.0. Clearly, the latter were, on average, carried out at somewhat lower confining stresses, but higher shear stresses than the former.

We have chosen, for the economic modelling of the material at Denison-Potacan a statistical fit to a range of creep test data yielding an exponent of approximately 6.0 (Figure 5.4). It is recognized that this univalued approach does not fully correspond to the actual behaviour. An equation which more closely fits the data is given in Dusseault et al. (1987), but this equation has not yet been incorporated into modelling and more experimental data are required to refine the actual values of the parameters.

5.11 THE ISSUE OF PRIMARY OR TRANSIENT CREEP

The current model does not specifically include the issue of transient creep. This is reasonable in mining situations where the stresses equilibrate in from two to six months. Transient creep, it is believed, is not a fundamental process. If a specimen of salt is mounted in a triaxial creep frame and immediately subjected to a relatively high shear stress, the transient phase will be relatively long. However, if the specimen is subjected for a few days to a hydrostatic stress at the depth of burial, then tested, the transient phase is much shorter. Furthermore, in stage creep tests, the transient creep phase length is much less for the third and fourth steps than it is for the first step, whether or not the stress path is one of step stress increases or decreases. If the nature of transient creep is so variable in the laboratory, what does it mean in-situ? This means that we cannot yet use it in the field and that the degree of specimen damage directly affects it, therefore, it is flaw related rather than material related.

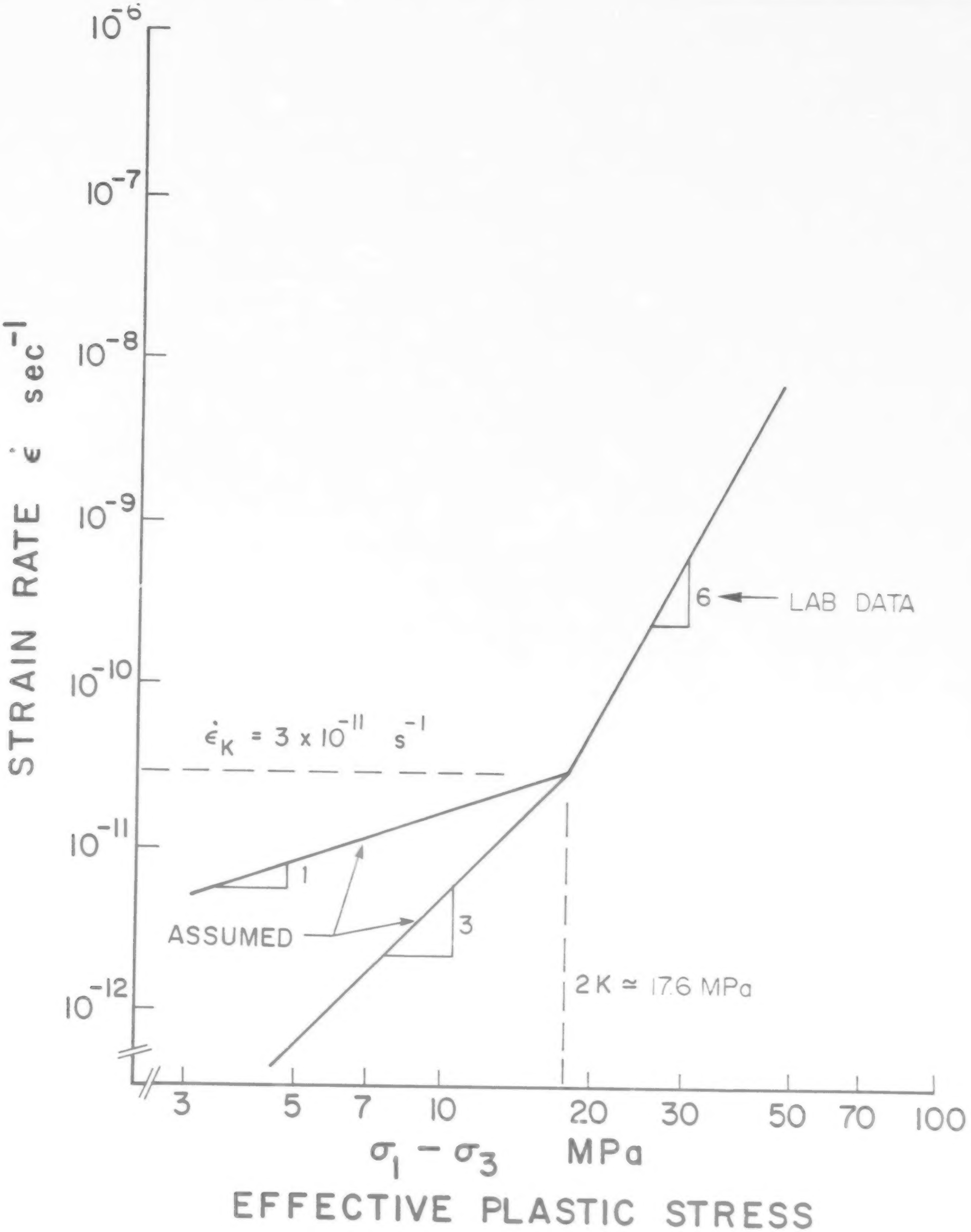

CREEP LAW USED IN MODELLING

FIGURE 5.4

There is another aspect of transient creep which occurs in-situ, which is in no way analagous to the laboratory transient creep. This is the macroscopic change in closure rate which occurs in the first two to six months after excavation of a room. This is the result of the stresses equilibrating at a uniform stress difference of 2K within the viscoplastic zone and the stabilizing of the elastoplastic/viscoplastic boundary. It has nothing to do with the microstructural stress redistribution which occurs in a specimen in the laboratory. The latter is an internal reallocation of the stresses between the various polycrystals so that a uniform strain rate is evidenced. When the load is placed on an assumed unflawed specimen in the laboratory, there is some crystal that experiences a higher stress than all others, and this crystal strains rapidly, reallocating stress to adjacent crystals, which in turn cast off excess stress to the next adjacent crystals. This process continues as transient creep until no significant stress concentrations exist and the external strain rate is the integrated internal crystal strain rates, with no further allocations. To compare this process with the macroscopic reallocation of stresses in-situ is not warranted. Also, the stress path followed in the field (unloading) is rarely simulated in the laboratory, where monotonic loading is usually the rule.

Another aspect of transient behaviour, which the writer contends is incorrectly addressed, is the lack of clear differentiation between material "strain hardening" and geometrically based slow reduction in creep rates. The latter have their source in the slow closure of rooms and the "fattening" and "shortening" of pillars as creep continues. This must result in diminution of closure rates, but is not prima facie evidence of a strain hardening mechanism in-situ.

The treatment of transient creep in Carter and Hansen (1983) shows how the empirical approach is unsatisfactory. As yet, a suitable example or model for transient laboratory creep has not been formulated. This model assumes that it is not a dominant process in mining engineering, the steady state is much more critical. Also, the modelling under this project shows that a significant amount of the field transient creep can be correctly simulated using the bilinear behavioural law suggested herein. We believe that when elastoplastic behaviour is rigorously incorporated and when a useable law for the stress and strain rate relationship above 2K is determined, a closer match will be evidenced.

5.12 THE ISSUE OF ELASTIC PROPERTIES

In rocks exhibiting primarily elastic behaviour, Young's modulus and Poisson's ratio uniquely govern the distribution of stresses, strains and displacements. In saltrocks, the elastic component of behaviour is of minor importance. In numerical modelling of the time dependent behaviour of saltrocks, stiffness of the elastic component governs only the initial stress and strain distributions at time equal zero, thereafter, viscous component takes over, causing stress redistribution through creep. It can be shown that even substantial variations in elastic stiffness will affect only slightly the transient creep, and will not affect at all the long term behaviour. However, true transient creep cannot be successfully modelled with reasonable effort. Usually, the numerical models "excavate" entire underground cavities instantaneously, whereas the actual mining activities take place gradually (mechanical excavations) or in small increments (drill and blast). The effect of this discrepancy is considerable and it obscures any variations in elastic stiffness. Thus, unless the modeller is prepared to simulate excavation of a room or a mine in hundreds or thousands of excavation steps and a correspondingly greater number of time steps, the effect of the "true" elastic properties of saltrock is negligible. Actually, back calculating the "elastic properties" to match the actual transient behaviour would give a better simulation of reality. Obviously, these would become phenomenological parameters rather than true material properties.

In this research project, the transient (short term) behaviour of underground cavities is not important. Rather, the long term behaviour under the conditions of full load equilibrium will govern the behaviour of stopes. Thus, the calibration runs of the Test Room and the Test Stope are considered accurate because the "steady state" (long term) behaviour was matched very well. The error resulting from inaccurate modelling of transient creep will be negligible, amounting to less than 1% of total displacement in the long term.

In order to avoid controversy, the authors have determined "elastic" properties of modelled salt rocks by unload/reload method. Their use in modelling, however, must be perceived in the context of the above discussion.

SECTION 6.0

6.0 REFERENCES

Arieli, A., Heard, H.C. and Mukherjee, A.K., 1982. Deformation modelling in sodium chloride at intermediate and elevated temperatures. In "Mechanical Testing for Deformation Model Development, ASTM STP 756", eds. Rhode, R. W. and Swearengen, J.C., pp 342-365.

Baar, C.A., 1977. Applied Salt Rock Mechanics 1. The in-situ behaviour of salt rocks. Developments in Geotechnical Engineering 16A. Elsevier Scientific Publishing Co., Amsterdam, 294 pages.

Baleshta, J.R. and Dusseault, M.B., 1986. Triaxial testing of intact salt rocks: pressure control, pressure systems, cell and frame design. In "ASTM Specialty Conference on Triaxial Testing", Louisville, Kentucky, proceedings in press.

Berest, P. and Minh, D.N., 1984. Deep Underground Storage Caverns in Rock Salt: Interpretation of In-Situ Data from French and Foreign Sites. "Proceedings of the First Conference on the Mechanical Behaviour of Salt", eds: Hardy, H.R. and Langer, M., Trans Tech Publications, pp 555-572.

Brady, B.H.G. and Brown, E.T., 1985. "Rock Mechanics for Underground Mining." George Allen and Unwin, London, 527 pages.

Brown, A.M. and Ashby, M.F., 1980. On the power law creep equation. "Scripta Metallurgica, 14," pp 1297-1302.

Carter, N.L. and Heard, H.C., 1970. Temperature and rate dependent deformation of halite. "American Journal of Science, Vol. 269", pp 193-249.

Carter, N.L. and Hansen, F.D., 1983. Creep of Rock salt. "Tectonophysics", 92, pp 275-333.

Daemen, J.J.K., 1975. "Tunnel Support Loading Caused by Rock Failure." PhD Thesis, Civil Engineering, University of Minnesota.

Dusseault, M.B. and Mraz, D., 1983. Salt rock constitutive behavior. "Proceedings of Potash '83", editor, R.M. McKercher, Saskatoon, Saskatchewan, pp 311-320.

Dusseault, M.B., Mraz, D., Unrau, J. and Fordham, C., 1985. Test procedures for salt rock. In "Research and Engineering Applications in Rock Masses, Proceedings 26th US Symposium on Rock Mechanics", pp 313-319.

Dusseault, M.B., Mraz, D.Z. and Rothenburg, L., 1987. The design of openings in salt rock using a viscoplasticity/viscoelasticity criterion. Accepted for presentation and publication in the 27th US Rock Mechanics Symposium.

Fordham, C.J., Dusseault, M.B., and Mraz, D.Z., 1986. Triaxial Testing of Creep and Yield Behaviour of Intact Salt Rock. In "ASTM Specialty Conference on Triaxial Testing", Louisville, Kentucky.

Frost, H.J. and Ashby, M.F., 1982. "Deformation-Mechanism Maps; The Plasticity and Creep of Metals and Ceramics." Pergamon Press, Toronto, 1982.

Heard, H.C., 1972. Steady-state flow in polycrystalline halite at pressure of 2 kilobars. In "Flow and Fracture of Rocks, Geophysical Monograph 16", American Geophysical Union, Washington, D.C., pp 191-209.

Horseman, S. and Passaris, E., 1984. Creep Tests for Storage Cavity Closure Prediction. "Proceedings of the First Conference on the Mechanical Behavior of Salt", eds: Hardy, H.R. and Langer, M., Trans Tech Publications, pp 119-157.

Kaiser, P.K., 1977. "Time-Dependent Behavior of Tunnels in Jointed Rock Masses." PhD Thesis, Department of Civil Engineering, University of Alberta, Edmonton, Alberta, Canada, 395 pages.

Kovari, K., 1977. Micromechanics model of progressive failure in rock and rock-like material. "International Symposium on Geomechanics of Structurally Complex Formations", Capri, Italy, Vol 1, pp 307-316.

Langer, M., 1984. The Rheological Behaviour of Rock Salt. "Proceedings of the First Conference on the Mechanical Behaviour of Salt", eds: Hardy, H.R. and Langer, M., Trans Tech Publications, pp 201-240.

Mirza, U.A., 1984. Predictions of Creep Deformations in Rock Salt Pillars. "Proceedings of the First Conference on the Mechanical Behavior of Salt", eds: Hardy, H.R. and Langer, M., Trans Tech Publications, pp 310-337.

Mraz, D.Z., 1984. Solutions to pillar designs in plastically behaving rocks. "CIM Bullti , Vol 77", 868, pp 55-62.

Mraz, D.Z. and Dusseault, M.B., 1986. Long Term Behavior of a Test Room in Potash. In "Rock Mechanics: Key To Energy Production, Proceedings of the 27th US Rock Mechanics Symposium", pp 405-414.

Mraz, D.Z. and Dusseault, M.B., 1987. Effects of Geometry on the Bearing Capacity of Pillars in Saltrock. To be published in the CIM Bulletin. Presented at the 1986 CIM Rock Mechanics and Strata Control Committee Workshop, Saskatoon, Saskatchewan, November, 1986. Preprint included.

Munson, D.E. and Fossum, A.F., 1986. Comparison between Predicted and Measures South Drift Closures at the WIPP Using a Transient Creep Model for Salt. In "Rock Mechanics: Key to Energy Production, Proceedings of the 27th US Rock Mechanics Symposium", pp 931-939.

Munson, D.E., Torres, T.M. and Blankenship, D.A., 1986. Early Results from the Thermal/Structural In Situ Test Series at the WIPP. In "Rock Mechanics: Key to Energy Production, Proceedings of the 27th US Rock Mechanics Symposium, 923-930.

Poirier, J.P., 1985. "Creep of Crystals (High Temperature deformation processes in metals, ceramics and minerals)". Cambridge Earth Science Series, Cambridge University Press, Cambridge, 260 pages.

Preece, D.S., 1986. Three Dimension Modelling of the Wedge Pillar Portion of the WIPP Geomechanical Evaluation (Room G) In Situ Experiment. In "Rock Mechanics: Key to Energy Production, Proceedings of the 27th US Rock Mechanics Sympoisum", pp 917-922.

Serata, S., 1982. Stress Control Methods: Quantitative Approach to Stabilizing Mine Openings in Weak Ground, Proc. "First International Conference on Stability in Underground Mining", pp 52-98.

Spiers, C.J., Urai, J.L., Lister, G.S., Boland, J.N. and Zwart, H.J., 1986. "The influence of fluid-rock interaction on the rheology of salt rock." Final Report of Research for the Commission of the European Communities, Nuclear Science and Technology Report EUR 10399 EN. 131 pages.

Urai, J.L, Spiers, C.J., Zwart, H.J. and Lister, G.S., 1986. Weakening of rock salt by water during long-term creep. "Nature, Vol 324" (December), pp 554-557 (also editorial commentary by M.K. Jenyon, pp 515-16, same issue).

Wallner, M., 1983. Stability calculations concerning a room and pillar design in rock salt. "Proceedings of the 5th International Congress on Rock Mechanics, Melbourne, Australia", pp D9-D16.

Wallner, M., 1984. Analysis of Thermomechanical Problems Related to the Storage of Heat Producing Radioactive Waste in Rock Salt. "Proceedings of the First Conference on the Mechanical Behavior of Salt", eds: Hardy, H.R. and Langer, M., Trans Tech Publications, pp 740-763.

Weetman, J., 1972. High temperature creep produced by dislocation motion. In "J.E. Dorn Memorial Symposium", Cleveland, Ohio.

APPENDIX A

DEFINITIONS OF TERMS FOR SALT ROCK GEOMECHANICS

by

Maurice B. Dusseault, P.Eng.
Professor and Chairman, Geological Engineering Programme
The University of Waterloo
Waterloo, Ontario, CANADA, N2L 3G1

Dennis Z. Mraz, P.Eng.
President, Mraz Project Consultants Ltd.
410 Jessop Ave.
Saskatoon, Saskatchewan, CANADA, S7L 2S5

and

Douglas Hambley, P.Eng.
Research Officer, Argonne National Laboratory
9700 South Cass Avenue
Argonne Illinois, 60439, USA

Draft date
87/05/01

PREAMBLE

There can be considerable confusion as to the precise meanings of terms when they are generated in one field of endeavor, then applied in another. This is the case with salt rock geomechanics in that the casual use of terms adopted from classical continuum mechanics and hardrock mining can lead to significant misunderstanding. One of the better examples is the term "yield", variously interpreted as "plastic behavior", "onset of flow", "post-elastic straining", "failure", "viscoplastic onset", and so on. The intent of this document is to generate a consistent vocabulary by precisely defining terms commonly encountered in the theory and practice associated with saltrock geomechanics.

Not everyone will agree with these definitions, as usage varies from person to person and from company to company. In a very few cases (e.g. replacing strain-softening with strain-weakening), a departure from conventional practice is recommended because the term in common usage was borrowed directly from elsewhere and can be misleading. In several cases (e.g. failure), persistent misuse or excessive use has necessitated semantic limitation to a specific set of conditions more restrictive than those normally assumed. Where a written definition does not suffice, a diagram has been used. Consistent use of a glossary such as this will help eliminate misunderstanding and error. Eventually, though this will take some years, a widely-accepted consistent usage will develop, as is the case with the area of Geology, which uses the American Geological Institute (AGI) Glossary of Geology as a reference for semantic decisions.

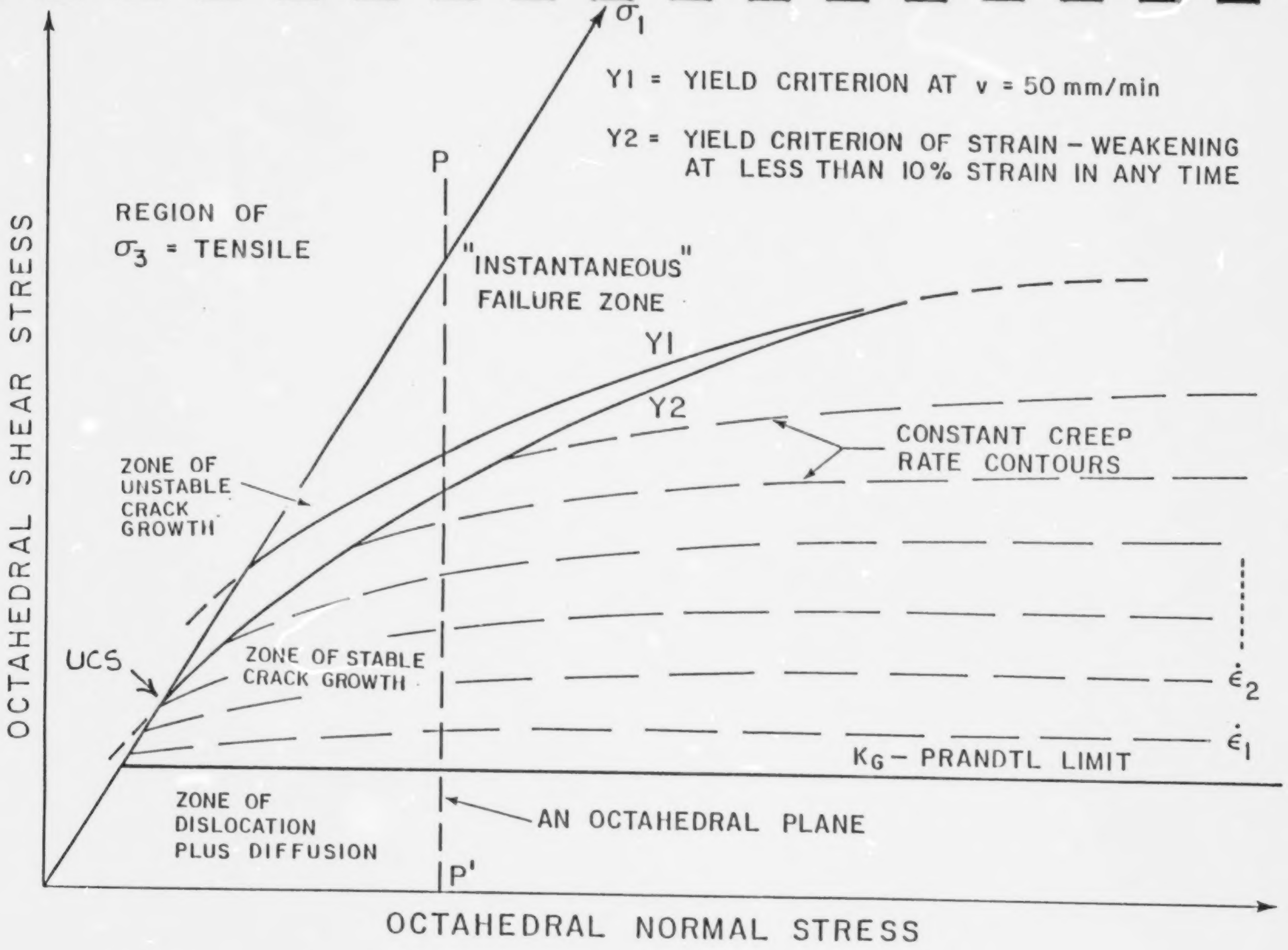
Y1 = YIELD CRITERION AT v = 50 mm/min
Y2 = YIELD CRITERION OF STRAIN - WEAKENING AT LESS THAN 10% STRAIN IN ANY TIME
σ1
P
REGION OF σ3 = TENSILE
"INSTANTANEOUS" FAILURE ZONE
Y1
Y2
CONSTANT CREEP RATE CONTOURS
ZONE OF UNSTABLE CRACK GROWTH
UCS
ZONE OF STABLE CRACK GROWTH
ε̇2
ε̇1
KG - PRANDTL LIMIT
ZONE OF DISLOCATION PLUS DIFFUSION
AN OCTAHEDRAL PLANE
P'
OCTAHEDRAL SHEAR STRESS
OCTAHEDRAL NORMAL STRESS

FIGURE 1a. PROCESSES FOR SALTROCK CREEP, OCTAHEDRAL COMPRESSIVE PLANE

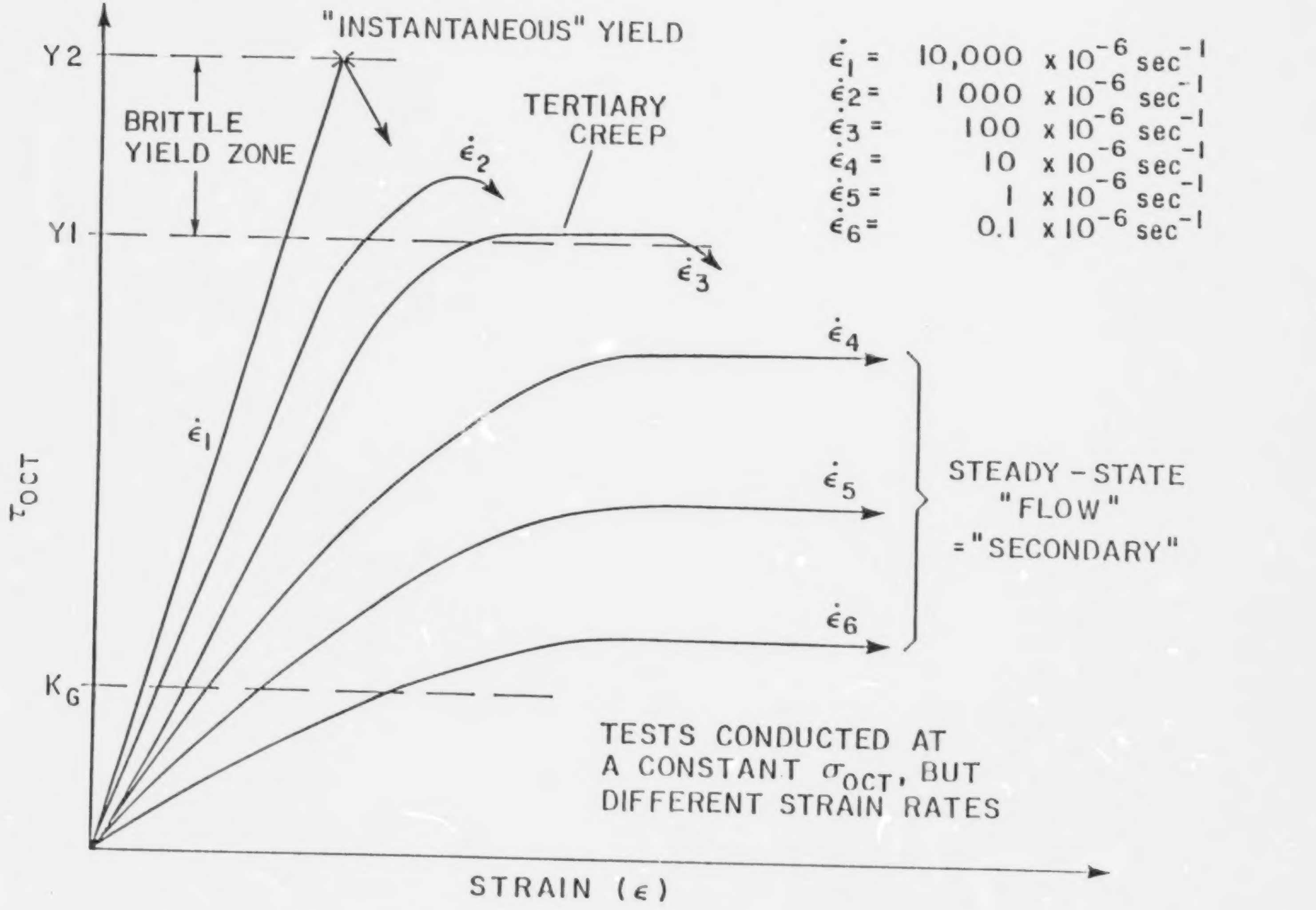

TIME- DEPENDENCY OF THE FAILURE STRESS, AND THE STRAIN RATES ASSOCIATED WITH VARIOUS EQUILIBRATED STRESS LEVELS

FIGURE 1b RELATIONSHIP OF STRAIN RATE TESTS OF STRESS SPACE

GLOSSARY

ACCELERATING CREEP: A condition where the rate of change of creep strain is increasing with time. In this state, if the stress state remains constant, the material will eventually reach a condition of brittle yield or strain-weakening. The term is considered synonymous with tertiary creep.

ACTIVE OPENING: This term is synonymous to the term "equivalent opening. It is related directly to the usage "elastoplastic zone" to describe the region where saltrocks have experienced strain-weakening, or brittle rupture.

ANALYTIC METHOD: A way of obtaining a solution to a complex design problem by applying analytic equations which have been derived for that class of problems. The solution to a problem obtained in such a manner is commonly referred to as a "closed-form solution". The term is contrasted with "empirical" and "numerical" design methods.

ATTENUATING CREEP: Creep that is decelerating and that will eventually cease. The term is synonymous with terminating creep, but is not the same as primary creep or transitional creep (refer to those terms).

AXIAL STRAIN (AND AXIAL STRESS): The strain (or stress) in the axial direction of a triaxial cell, often called the stress (or strain) in the "z" direction. The term has meaning only for a cylindrical specimen or for a circular or equant mine element (as in the axial stress distribution in a pillar or in the axial direction of a tunnel).

BEARING PILLAR: In a mining system with pillars of different sizes, the bearing pillars are the ones designed to carry the overburden load, in contrast to the yield pillars.

BOUNDARY ELEMENT METHOD: A numerical technique in which the boundaries of openings in a continuum, rather than the whole continuum, are subdivided into discrete elements. The solution for the stresses at a particular point in the medium is achieved by applying the appropriate influence function to elements along the boundary. These influence functions are derived from closed-form analytic solutions of simpler problems (e.g. Kelvin, Boussinesq, Cerrutti, Mindlin, Westergaard solutions), usually within the assumptions associated with ideal elasticity or ideal viscous behavior. The method is of particular use in linear elastic rock mechanics, or in linear, isotropic, viscoelastic media. One requirement is that the entire medium have the same properties, that is, it must be homogeneous, and this may be an excessive restraint in realistic situations.

BRITTLE YIELD (OR BRITTLE FAILURE): A condition when rock undergoes a sudden reduction in strength at relatively small strains (less than 10%). By definition, all brittle yield is also strain-weakening yield, but the reverse does not hold. Brittle yield is exhibited by all hard rocks over the range of engineering stresses. Figure 2 shows various types

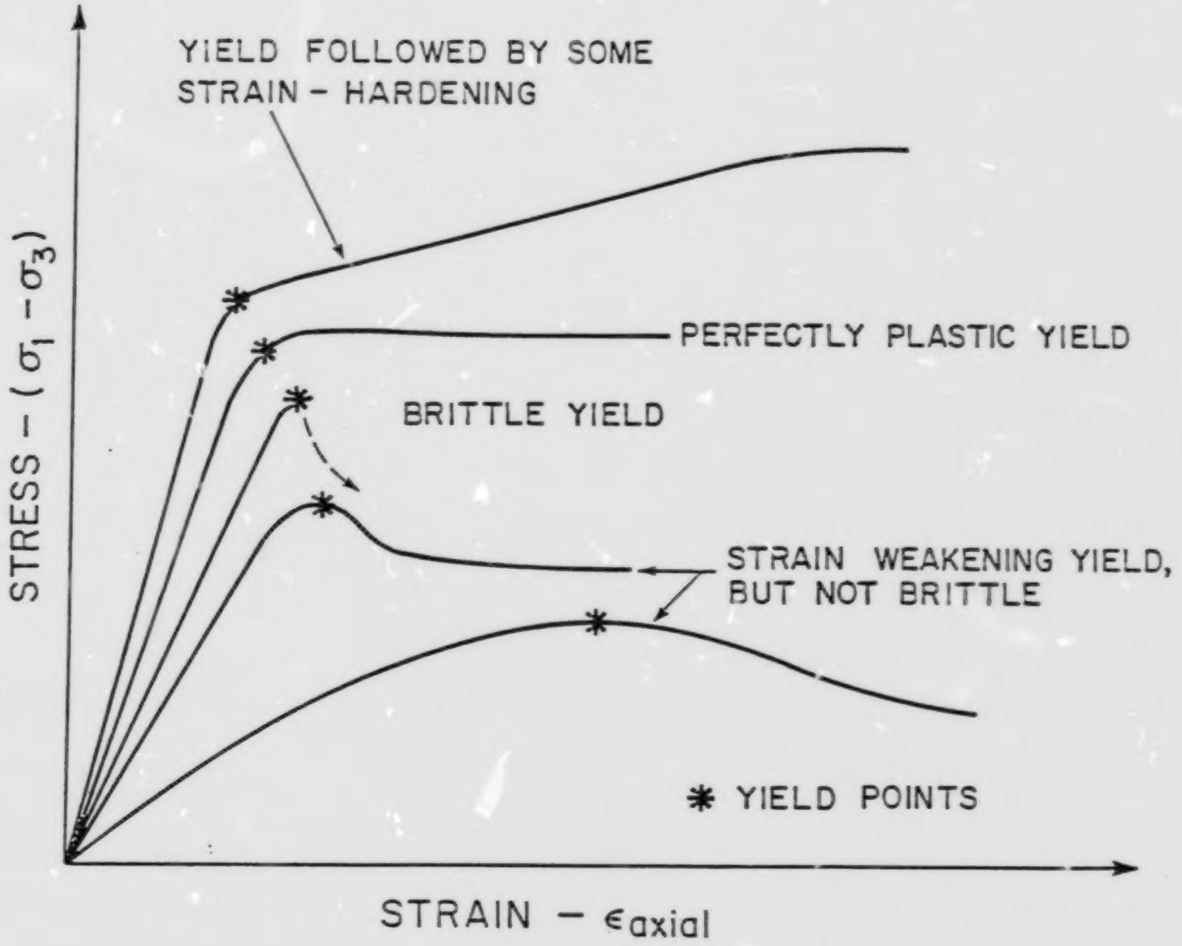

FIGURE 2 . TYPES OF YIELD

of yield. In the case of viscoplastic rocks there is an additional complexity in that time may have to be included in a brittle yield criterion.

BULK MODULUS: A measure of how much a unit volume of a material compresses under a unit increase in stress. Also, the slope of a plot of the mean triaxial compressive stress (the three principal stresses are not necessarily equal) versus volumetric strain (Figure 3). The bulk modulus is generally taken to be the inverse of the compressibility.

CLOSURE: The amount that an underground opening has closed (decreased in height or width) in a given time (closure rate), or since the room was opened (total closure), measured between opposite points (e.g. roof to floor, wall to wall, or diagonal closure). If unqualified, the term is usually assumed to mean vertical closure. In most hardrock, continued closure implies that the rock around the opening is continuing to dilate; that is, microcracks are extending, joints are loosening, or bed separation is taking place. Closure in saltrock openings does not imply deterioration of the mass because of the capacity for viscous deformation without strain-induced material deterioration (constant volume deformation).

COMPRESSIBILITY: A measure of the volumetric strain of a unit volume of a material due to a unit change in stress, defined as:

Compressibility = 1. Change in volume

$$\text{BULK MODULUS} = B = \frac{V \cdot \Delta\sigma}{\Delta V}$$

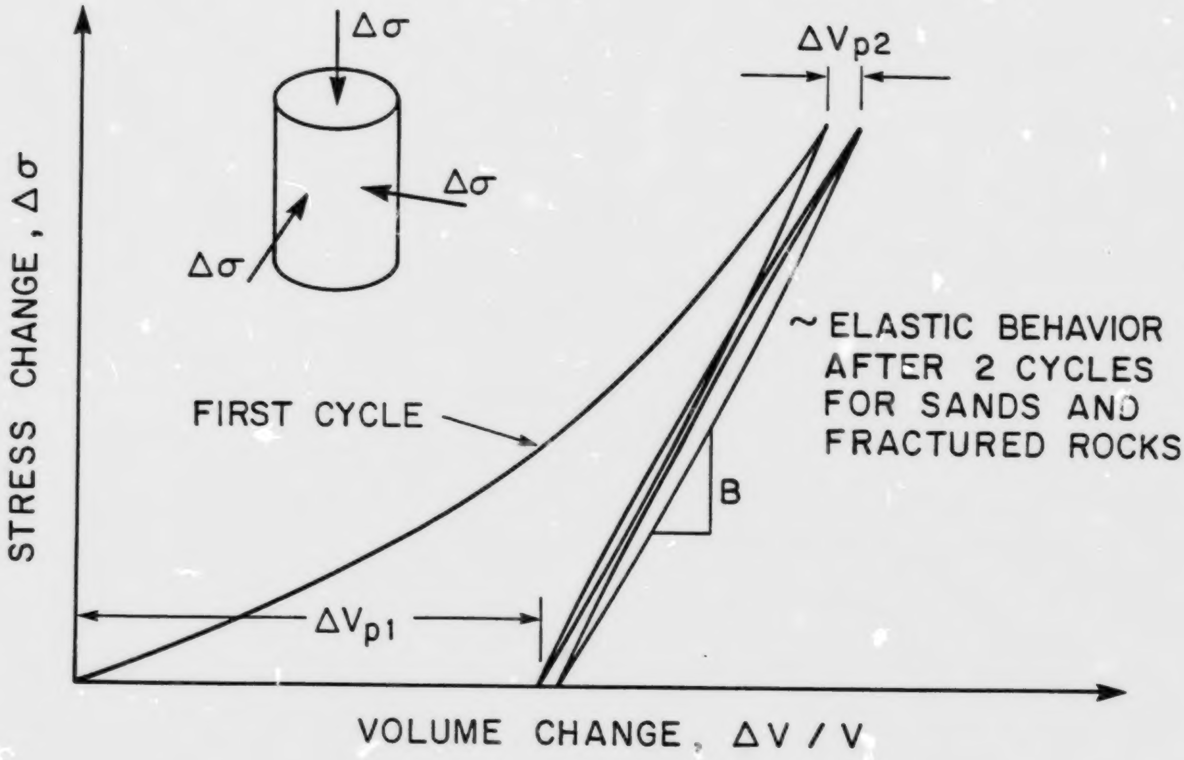
Δσ
Δσ
Δσ
ΔV$_{p2}$
~ ELASTIC BEHAVIOR AFTER 2 CYCLES FOR SANDS AND FRACTURED ROCKS
FIRST CYCLE
B
ΔV$_{p1}$
STRESS CHANGE, Δσ
VOLUME CHANGE, ΔV / V

ΔV_p = PLASTIC DEFORMATION

Fig. 3 VOLUMETRIC PLASTIC DEFORMATION

V Unit change in stress

The compressibility is fundamental measure of the deformability of a material and plays an important role in analysis and modelling. If the vertical strain per unit vertical stress change is measured, a "uniaxial compressibility" can be derived and used, as in the case of a no-lateral-yield cell to measure the load-deformation behavior of a granular medium. If all stresses are changed equally and the volumetric strain measured, it is the "volumetric compressibility" and is equal to the inverse of the bulk modulus.

CONSTITUTIVE LAW: The relationship defining the structural response of a material to changes in stress state, temperature, time, as well as other variables which can affect its mechanical state. Some type of constitutive law is required to carry out design involving stress changes. For conventional rock, the constitutive law relates stress, strain, and shearing resistance. For saltrocks, a more complex law is required because of the dominance of the time factor and the sensitivity to temperature. The octahedral plane diagram for a specific saltrock (Figure 1) is a partial constitutive law. The constitutive law for a given material must be determined by testing, although reasonable estimates can be made if sufficient experience is available. Also, there are many "constitutive laws" expressed as idealizations as people generally try to express phenomena in terms of familiar behavior. The behavior of saltrocks in general cannot be conveniently expressed in "familiar" terms, but must include a time component explicitly. This is why, time and again, even highly experienced engineers ask "What is the strength of saltrock?" The question makes sense for a hardrock, but for a saltrock, it is an ill-posed question, and the real issues of time-dependency of properties can be overlooked.

CREEP: Continued non-recoverable deformation at a constant stress. Creep occurs in most engineering materials upon an increase in shear stress beyond some particular "yield threshold" which may be a function of the material, temperature, stress, moisture content, and so on. For most rock engineering, creep strains are small and terminating; consequently, most rock engineering design methods appropriately ignore creep. However, in saltrocks, design is predicated by creep behavior as high creep rates can be encountered within the normal range of engineering stresses.

CREEP LAW: A relationship expressing the rate of deformation of a material in terms of other factors such as temperature, shear stress, time, etc. A creep law can be an extremely simple relationship, a complex equation, a set of numbers in a table, or lines on a graph. Most creep laws generally used are in equation form and are approximations to laboratory or field data.

DELAYED DEFORMATION: The deformation that a creeping material displays some time after the stresses are imposed, in contrast to instantaneous deformation.

DEVIATORIC STRESS: The amount by which a given stress deviates from the hydrostatic (or spherical) stress. Therefore if s(x) is stress in the x direction, its deviatoric component can be written as:

$$s(x)_{dev} = s(x) - \frac{s(1)+s(2)+s(3)}{3} ,$$

where s(i) [i=1,2,3] are principal stresses. For tests carried out in standard triaxial cells where s(2)=s(3) (compression test) or s(1)=s(2) (extension test), the term "deviatoric" stress is taken to be the difference between the axial and the lateral stress, s(1)-s(3). It is a reasonable assumption that for a zero porosity continuum, volumetric changes are caused by changes in the hydrostatic stress, and shear distortion and creep are caused by the deviatoric stresses.

DIFFUSION CREEP: Processes of time-dependent deformation wherein the mechanism of deformation is controlled by a concentration gradient, which may be the gradient of stress, ionic concentration, or other process for which a version of Fick's Law may be written as:

velocity = constant x (gradient)

(e.g. v = ki for porous flow or dT/dt = D dT/dx for heat flow.) Gradients control the movement of ions along grain boundaries or through fluid inclusions, diffusion of vacancies, or creep processes governed by defect concentration per unit volume. Vacancy diffusion can occur at shear stresses approaching zero (albeit at vanishingly small rates). These processes are of little concern in conventional hardrock engineering, but are of some interest in saltrock design. Diffusion creep processes are slow in terms of engineering design in saltrock, but over geologic time, are responsible for vast diapiric structures and the isotropic, lithostatic stress condition found as the virgin stress state in practically all salt deposits. This raises the point that in a saltrock there is no "truly equilibrated" stress condition except the isotropic lithostatic one. Pure diffusion creep processes which do not depend on the existence of crystal lattice defects (dislocations) are generally thought to be related to shear stress in a linear manner (exponent of 1.0):

$$\dot{e} = A\ (s1-s3)^{1}$$

where strain rate is related to the stress difference through a constant "A", which is some kind of a normalized creep rate.

DILATION: Expansion during increasing shear stress through the generation of microfissures and grain rotation. In order to undergo strain-weakening or brittle yield, saltrocks will dilate. This does not occur during steady-state creep (viscoplastic) deformation or in perfectly plastic yield.

DISLOCATION CREEP: A mechanism for the time-dependent behavior of a material which involves planes of atoms moving past one another inside individual crystals. Some people assume that some types of dislocation creep require a particular activation shear stress (energy level) to occur, and that this activation shear stress is independent of the mean normal stress. Others contend that there is no lower limit for dislocation-driven creep, onlt that is becomes vanishingly small at reduced shear stresses. Theory shows, relatively conclusively and borne out by experiments at high temperatures, that a power law can express the rate to be expected from dislocation processes. The rate depends on the density of dislocations in the crystalline mass, and leads to:

$$\dot{e} = B\ (s1-s3)^{3}$$

where "B" is a normalized constant relating the strain rate to the stress difference raies to a high power. This type of equation breaks down at stress levels above the Prandtl Limit. Dislocation theory is extremely complex, as are the mathematics associated with these processes.

ELASTIC: Behavior corresponding to a particular idealized material behavioral model consisting of the following assumptions: deformations are uniquely associated with the stress level, all deformations are recovered when stress is removed, the material does not fail, no time-dependent behavior is possible, and the relationship between stress and strain uses unvarying material parameters (elastic constants). Within these assumptions, no viscoplastic behavior or yielding behavior is possible. Purely elastic assumptions can be reasonable approximations for hardrock, but are of little value for design in creeping materials.

For hardrock, it is usual to use an "elastic/rupture" assumption where stresses and strains are assumed elastic until a specific brittle yield limit is surpassed, at which point the rock "immediately" loses most of its lad carrying capacity. Elastic behavior is of some interest to viscoplastic materials such as salt and potash in that it gives the "instantaneous" deformation upon excavation. However, after a very small time, the viscous deformations totally dominate the strain history of these materials.

ELASTICITY (THEORY OF): A body of relationships relating stresses and displacements in materials for various geometries and boundary load or strain conditions. The great majority of the solutions assume linear relations between stress and strain, as such conditions are analytically tractable. The assumptions inherent in the theory are very stringent, and limit the classes of design problems which can be approached this way. The simplicity of elastic solutions, hence their ease of use, has tended to blind practitioners to the limiting assumptions of the theory when applied to highly plastic or creeping rocks.

ELASTIC ROCK: Rock in which there is an appoximately linear relationship between stress and strain when under load, with the original condition being recovered when the load is removed. By extension, rock in which design can be carried out with reasonable precision using assumptions of elastic behavior. Elastic-brittle behavior refers to approximately elastic deformation followed by major and sudden strain-weakening.

"ELASTIC" ZONE: The zone beyond the viscoplastic region where the *in situ* shear stress is less than the plastic limit. The word elastic is placed in quotes because the region is not truly elastic, but does exhibit very slow creep, as evidenced by the isotropic *in situ* stress conditions found in virgin deposits. The term is inappropriate because the very slow deformations in this region are no truly reversible, and they are also viscous in nature. It is recommended that the term "viscoelastic" zone be used instead, particularly to differentiate it from the zones referred to as elastoplastic or viscoplastic. The term "elastic", wherever possible, should be used only to refer to truly stable equilibrium zones (no straining at an equilibrated stress).

ELASTOPLASTIC: A behavioral model for materials implying a stress range where deformations are elastic and fully recoverable, limited by a yield stress beyond which any additional deformation is totally non-recoverable. The idealized version of elastoplasticity models has use in saltrock engineering, but a viscosity relationship is also required in general. The term elastoplastic is applied for convenience to the zone of ruptured material within the active opening, although this material has no real capacity to bear load as it is completely unconfined. (A more correct term would be "elastic - strain-weakening - plastic" behavior.)

EMPIRICAL METHODS: Approaches to the solution of design problems based on experience and case histories. Engineers always use empirical judgement in design, but realize that analysis and theory are extremely powerful tools. The long-term trend in engineering has always been to more rigorous quantification and less empiricism, since empirical knowledge is only valid for the conditions under which it was obtained. Therefore extrapolation to different conditions has limited validity. Because of the viscoplastic deformation mechanisms in saltrock, a purely empirical approach relating hardrock experience to saltrock design problems may result in serious errors. However, all design efforts must also be examined carefully based on actual field behavior and experience in similar materials.

EQUIVALENT OPENING: Around an opening in rock there is usually a region of material which has undergone brittle yield and can carry little to no load. As a suitably conservative design assumption, this material is included as part of the opening to give the "equivalent" opening. The boundary of the equivalent opening therefore separates intact (minimally damaged) rock from yielded rock. For a saltrock, the equivalent opening boundary is the surface which separates the viscoplastic zone from the elastoplastic zone where the salt has experienced brittle rupture (Figure 4). The geometry of the equivalent opening in a saltrock can be affected significantly by discontinuities or by the presence

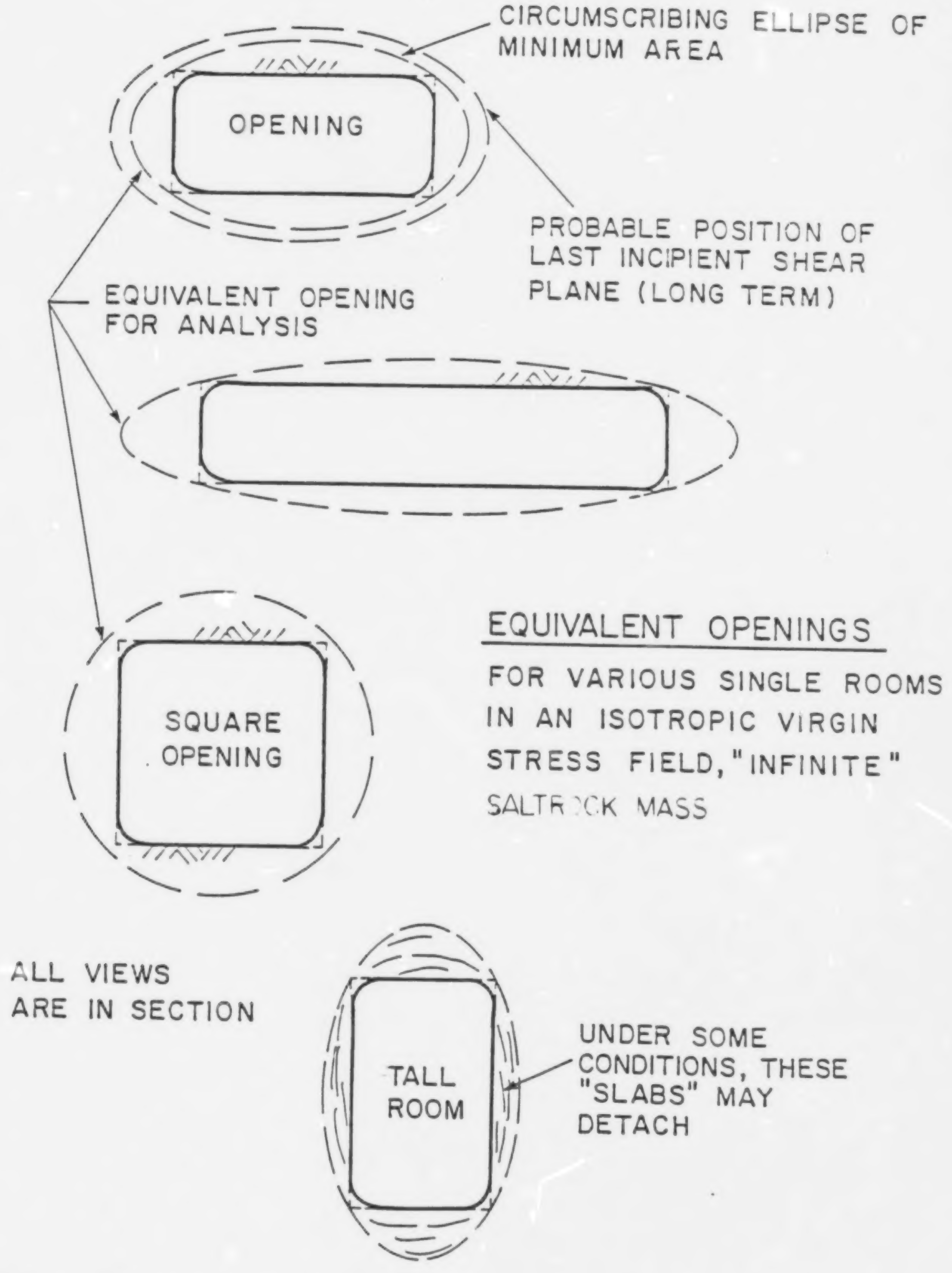
CIRCUMSCRIBING ELLIPSE OF MINIMUM AREA
OPENING
PROBABLE POSITION OF LAST INCIPIENT SHEAR PLANE (LONG TERM)
EQUIVALENT OPENING FOR ANALYSIS
EQUIVALENT OPENINGS
FOR VARIOUS SINGLE ROOMS IN AN ISOTROPIC VIRGIN STRESS FIELD, "INFINITE" SALTROCK MASS
SQUARE OPENING
ALL VIEWS ARE IN SECTION
TALL ROOM
UNDER SOME CONDITIONS, THESE "SLABS" MAY DETACH

FIGURE 4. EQUIVALENT OR ACTIVE OPENING CONCEPT

of adjacent elastic rock. Figure 5 shows typical equivalent openings around openings of various shapes, assuming a homogeneous saltrock medium at sufficient depth to allow the equivalent opening to develop fully. At shallower depths where the overburden stress is lower, a full circumscribing elliptical shape cannot develop, and the equivalent opening is smaller than implied in Figure 5.

EVAPORITE: A mineral formed as the result of evaporation of the water in which the mineral was dissolved. In addition to all saltrocks, evaporites also include gypsum, anhydrite, and calcite (under certain conditions). In a salt lake such as the Dead Sea in Israel, salt crystals, as well as minute amounts of gypsum and calcite, are currently being deposited by evaporation.

FAILURE: Failure is difficult to define rigorously, as the term is used differently by many people, and because failure of an element is not synonymous with failure of the assembly. For example, a pillar may have a strain-weakened zone near the periphery (i.e. a "failed" zone), but the pillar itself may be sound and well-designed. When a test specimen surpasses its peak shearing resistance, it is often said to have "failed" (many people say yielded or strain-weakened); however, the specimen can still carry some load, so that "failure" is not complete. Another way of defining failure is as loss of design function. For example, if a pillar is designed to withstand two million Newtons (450,000 pounds)

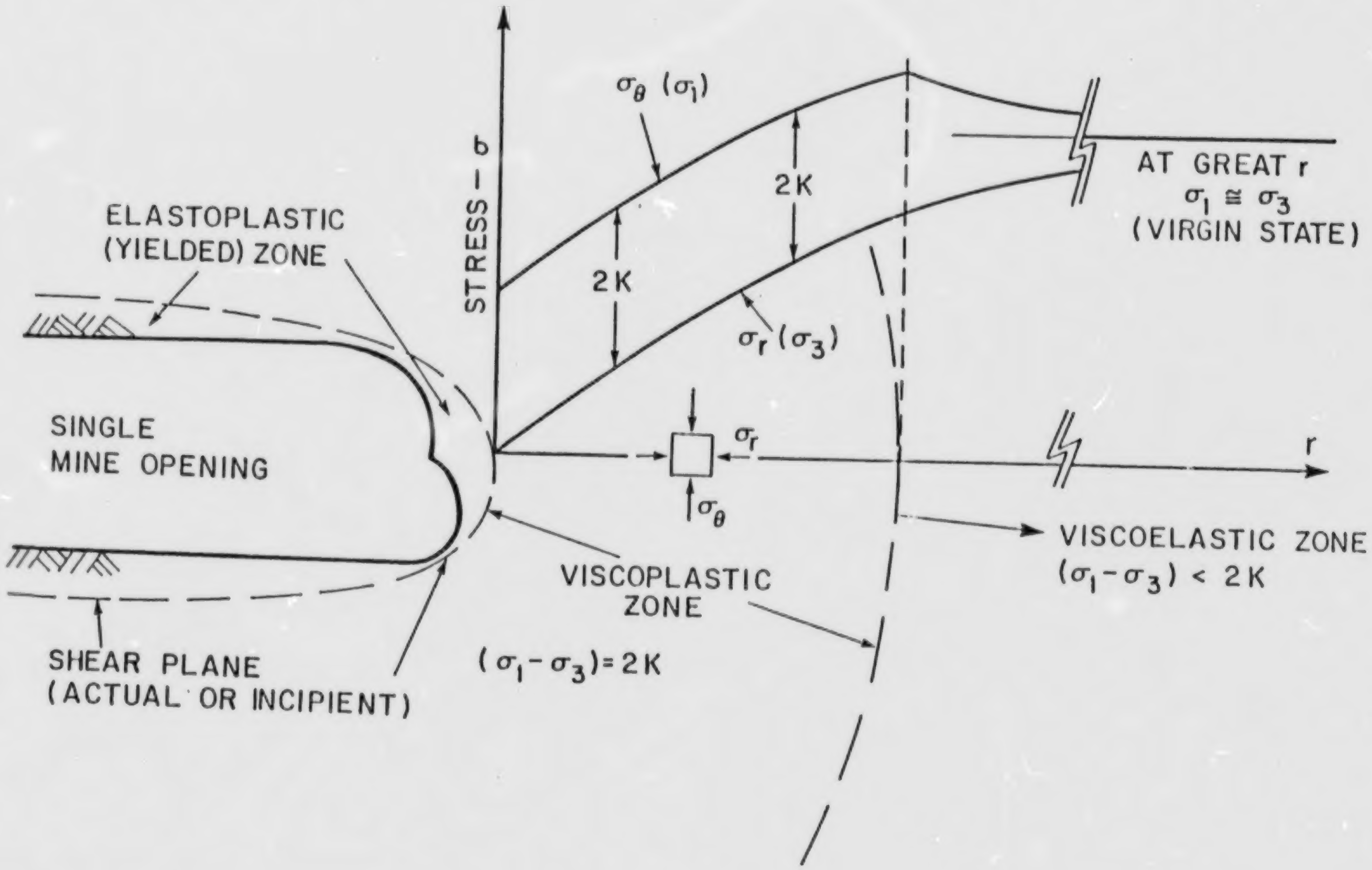
$\sigma_\theta\ (\sigma_1)$
STRESS – σ
2K
2K
$\sigma_r\ (\sigma_3)$
AT GREAT r
$\sigma_1 \cong \sigma_3$
(VIRGIN STATE)
ELASTOPLASTIC
(YIELDED) ZONE
SINGLE
MINE OPENING
σ_r
σ_θ
r
VISCOELASTIC ZONE
$(\sigma_1 - \sigma_3) < 2K$
VISCOPLASTIC
ZONE
$(\sigma_1 - \sigma_3) = 2K$
SHEAR PLANE
(ACTUAL OR INCIPIENT)

FIGURE 5a. BEHAVIOURAL ZONES AND STRESS DISTRIBUTION ADJACENT TO A SINGLE MINE OPENING, STEADY STATE CONDITIONS

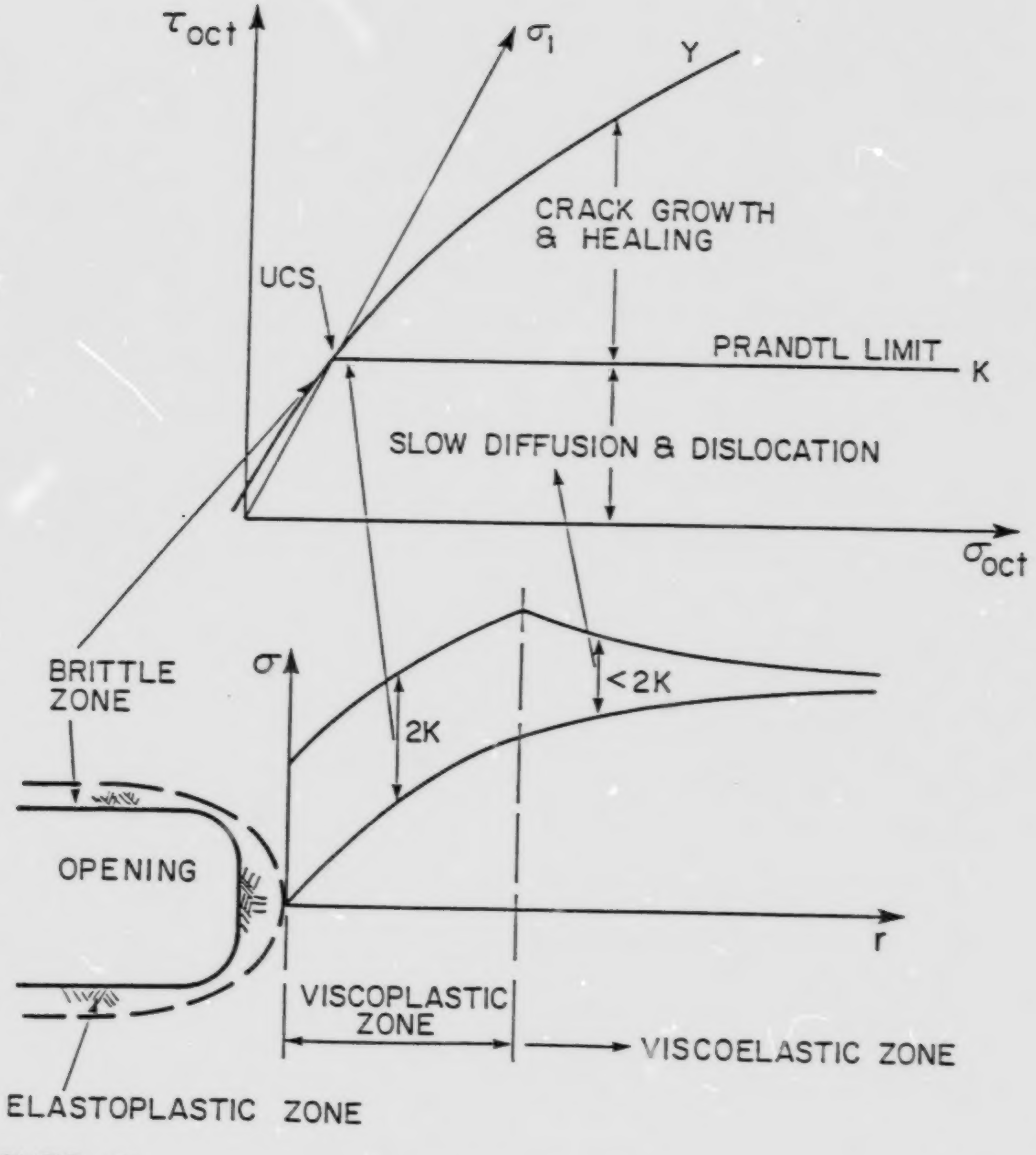
τ_{oct}
σ_1
Y
CRACK GROWTH & HEALING
UCS
PRANDTL LIMIT
K
SLOW DIFFUSION & DISLOCATION
σ_{oct}
BRITTLE ZONE
σ
2K
<2K
OPENING
r
VISCOPLASTIC ZONE
VISCOELASTIC ZONE
ELASTOPLASTIC ZONE

FIGURE 5b
RANGES OF BEHAVIOUR FOR A SALTROCK OPENING, RELATED TO A STRESS-PROCESS DIAGRAM

without strain-weakening, but is unable to because of a decline in load-bearing capacity, then it has failed, but it may still be carrying some load. Since the word failure has negative connotations and is widely misunderstood, it must be used with extreme caution, and only when loss of design function has occurred.

FAILURE CRITERION: The rule stipulating the maximum stress conditions that a rock element can withstand. This term is the most common one, but "peak strength criterion", "yield criterion", or "maximum stress criterion" are more precise. Referring to Figure 6, all stress states below the peak strength (or failure) criterion are stable before rupture, and any attempt to generate a stress condition above the line will prove impossible: the material ruptures before those stress conditions can be attained. Once failed, the rock is weaker, therefore it has a new, lower criterion, the lower line in Figure 6. In reality, the peak strength criterion for saltrocks is a zone, not a single surface, because of time-dependent effects (Figure 1). In a three-dimensional stress representation, it is a region bounded by two concentric curved conical surfaces which have a cross-sectional shape determined empirically. Purely theoretically derived criteria may be of use in rock mechanics, but materials must be tested to determine the numerical value of the parameters involved. Because there are different mechanisms involved at different stresses in saltrock, a single theoretical approach to a failure criterion may be inade-

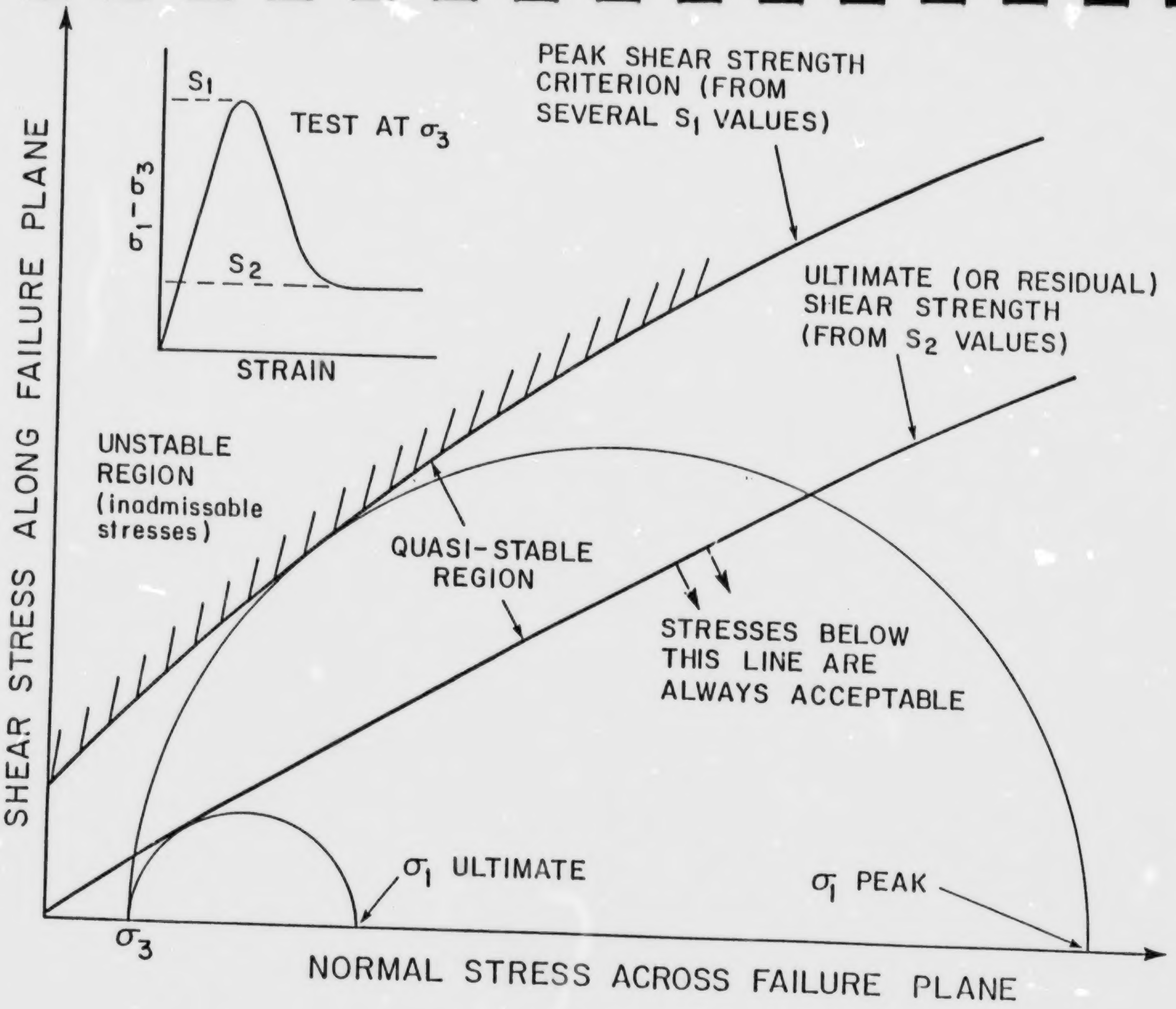
PEAK SHEAR STRENGTH CRITERION (FROM SEVERAL S_1 VALUES)
ULTIMATE (OR RESIDUAL) SHEAR STRENGTH (FROM S_2 VALUES)
S_1
S_2
TEST AT σ_3
$\sigma_1 - \sigma_3$
STRAIN
UNSTABLE REGION (inadmissable stresses)
QUASI-STABLE REGION
STRESSES BELOW THIS LINE ARE ALWAYS ACCEPTABLE
σ_1 ULTIMATE
σ_1 PEAK
σ_3
SHEAR STRESS ALONG FAILURE PLANE
NORMAL STRESS ACROSS FAILURE PLANE

FIGURE 6. CONVENTIONAL STRENGTH CRITERIA

quate; time may have to be stipulated. (Refer to Mohr-Coulomb behavior

FINITE ELEMENT MODELLING (METHOD): A numerical procedure involving dividing up a structure into small blocks, stipulating the way these blocks are joined, specifying rigorously how the block will deform (with stress time or temperature changes for example), defining the block properties, and then applying the forces on the structure. One then solves the equations for the internal displacements and stresses, as functions of time if necessary. For geometrically complex problems it is without a doubt the strongest and potentially the most realistic numerical method available to the engineer. It is not limited to a particular type of material (such as elastic), and can accept any well-posed constitutive law. However, as with any numerical method, input must be realistic as poor behavioral assumptions may lead to significant error, particularly for time-dependent problems where the solution is carried out in many small "time-steps". The requirements for use are a realistic constitutive law, geometry that can be reasonably approximated, and a knowledge of the load and time history the structure will experience. For viscous media, a time rate viscous law linking stresses and strains and time is a requirement for finite element modelling.

FLOW: Continued displacement under shearing stress, a fundamental property of fluids. The measure of the ability of a material to resist flow is called the viscosity. Because saltrocks flow over time, albeit slowly as compared to liquids, they can be looked upon as extremely viscous liquids, although their viscosity does not have to be constant as in the case of ideal or Newtonian fluids. Truly elastic materials can be considered to have an infinite viscosity.

FRACTURE: A small- to medium-sized, natural or man-made discontinuity in a material as in "a blasting-induced fracture". The term is also used to describe processes associated with strain-weakening or brittle failure as in: "the rock is developing a fracture network leading to a permanent reduction in strength".

HALITE: The naturally occurring evaporitic mineral comprised almost exclusively of sodium chloride, often referred to as rock salt. In addition to being the major (and often only) constituent of tabular and domal salt deposits, halite is usually a major component of all potash ores.

HARDROCK: Rocks of high strength which can often be modelled as elastic materials exhibiting brittle and sudden rupture. Because the rocks themselves are so strong, it is usually found that the behavior of structures in hardrock is dominated by natural discontinuities (joints, bedding planes). Examples of typical hardrocks are granite, quartzite, gabbro, diorite, basalt, syenite, gneiss, etc. Metamorphic rocks such as schist, shales, slate are usually classified as hardrock, and low porosity limestones, sandstones and dolomites may also be so classified from a behavioral viewpoint. Normally, sedimentary rocks such as mudstones, marl, siltstones, coal, oolitic limestone, etc., can be considered as hardrocks only if highly indurated, whereas igneous and metamorphic rocks are almost always classified as hardrocks. The difference between hardrock and softrock is based on a strength measure, but there is no absolute agreement on what strength value to use. In general, hardrocks must have a high uniaxial compressive strength, a high modulus of elasticity, and must not display appreciable viscous behavior under normal engineering conditions.

HYDROSTATIC STRESSES: This term is used differently by different people. Some use it to refer to the all-around equal pressure applied by a column of water, others use it to mean any equal all-around stress condition, often equal to the entire lithostatic stress. Still others use it to refer to the spherical component of the stress tensor; that is, the octahedral normal stress, or the mean normal stress. If a rock is in an hydrostatic stress condition, there can be no shear stresses on any plane.

INTACT ROCK: Rock which has not been fractured or strain-weakened by the excavation process, or has not been excessively weathered or altered so that discontinuities exist everywhere at a small scale. For example, beyond the elastoplastic zone around an opening in saltrock or hardrock, "intact rock" can be found. For intact salt, we assume no fissures or significant fractures are present. For hardrocks, natural fracture systems can be found in material referred to as "intact rock". intact It may nevertheless be fissured and jointed.

ISOTROPIC: Equal in all directions. An isotropic material is one which has the same properties in all directions. An isotropic virgin stress state is one where all the principal stresses are equal, and therefore no shear stresses can be present. Saltrocks are usually very close to isotropic in their geomechanical properties.

INSTANTANEOUS STRESS OR RESPONSE: More of a concept than a reality except when dealing with blast loading of strong brittle rock, the term is used to refer to the conditions under theoretical, very rapid action. For example, some engineers refer to the stress condition in a pillar after "instantaneous" excavation. The concept is of considerable use in analysis and numerical modelling, as it represents a limiting case, and very complex sequential excavation can be represented by instantaneous excavation of one segment at a time. The conclusions drawn from modelling of this type are usually somewhat conservative, therefore they are of considerable use in design.

INSTANTANEOUS DEFORMATION: In the semantics of time-dependent behavior, when a stress is applied to a creeping material, the instantaneous deformation is that deformation which occurs immediately upon application of the stress; all other deformation is delayed (or time-dependent). It is the deformation that precedes primary creep, and it is directly related to the elastic parameters of the rock.

ISOTROPIC LITHOSTATIC STRESS CONDITION (ASSOCIATED WITH VIRGIN STRESSES): The normal virgin stress condition in saltrock deposits, characterized by all stresses equal to each other and equal to the overburden total stress. The mechanism responsible for the isotropic stress condition is diffusion creep which acts slowly with respect to engineering works, but has a major effect over geologic time.

LITHOSTATIC: Pressure (stress) equal to the weight of the entire overburden of rock. The pre-mining stress in any rock mass in the vertical direction usually approximates lithostatic, but the horizontal stresses may be greater or less, depending on the stress history of the rock mass. In saltrocks, if there is no ongoing tectonic deformation, the vertical and horizontal stresses are equal and hydrostatic.

MOHR-COULOMB MATERIAL: A material which behaves in failure as a frictional material, so that the yield criterion can be expressed as a function between shear stress and normal stress. In weak soils, intergranular friction dominates yield; in rock, crack propagation and growth processes control yield. In an "idealized" Mohr-Coulomb material, the intermediate principal stress has no bearing on failure,

$$\sigma_1, \sigma_2 = \frac{\sigma_x + \sigma_y}{2} \pm \sqrt{\tau_{xy}^2 + \left(\frac{\sigma_x - \sigma_y}{2}\right)^2}$$

$$\theta = \tan^{-1}\left[\frac{2 \cdot \tau_{xy}}{(\sigma_x - \sigma_y)}\right]$$

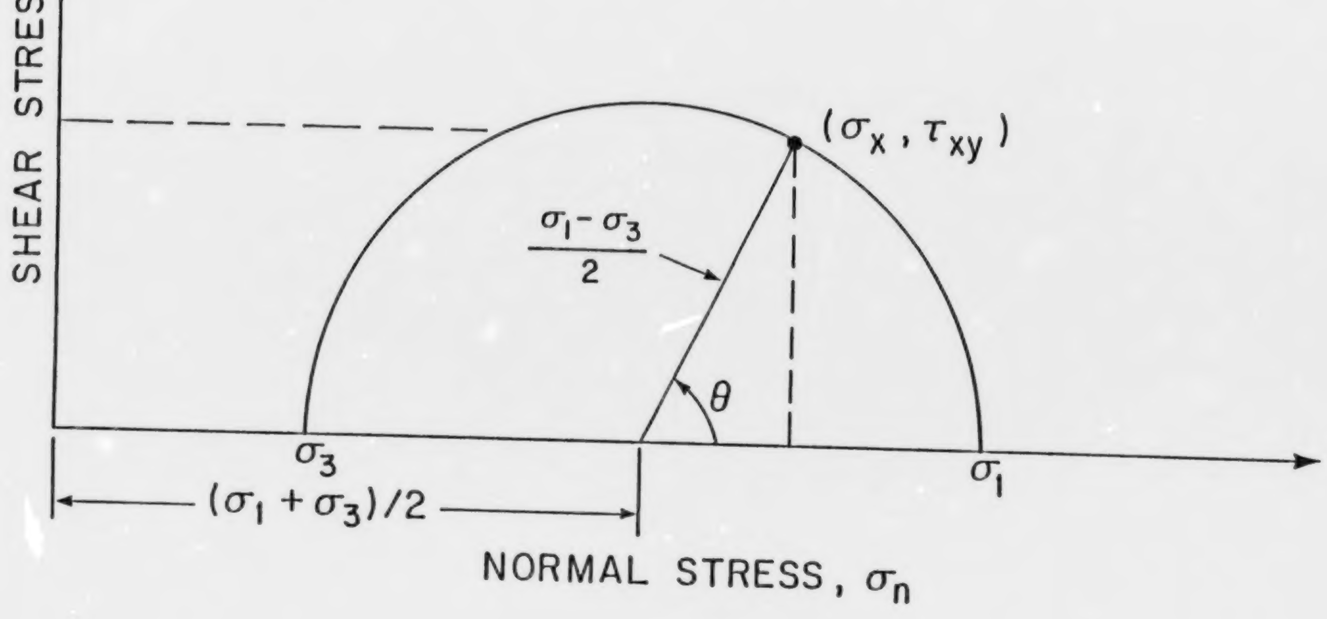
SHEAR STRESS, τ
(σ_x , τ_{xy})
$\frac{\sigma_1 - \sigma_3}{2}$
θ
σ_3
σ_1
$(\sigma_1 + \sigma_3)/2$
NORMAL STRESS, σ_n

FIGURE 7a. SOLVING FOR STRESSES USING THE GEOMETRIC RELATIONSHIPS ON A MOHR'S CONSTRUCTION

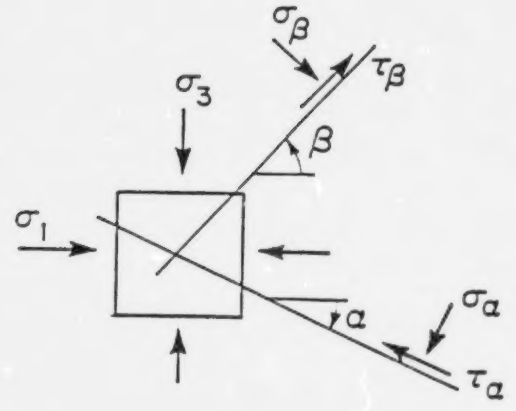
σ_β
τ_β
σ_3
β
σ_1
α
σ_α
τ_α

ELEMENTAL REPRESENTATION OF STRESSES AT A POINT, TWO DIMENSIONS

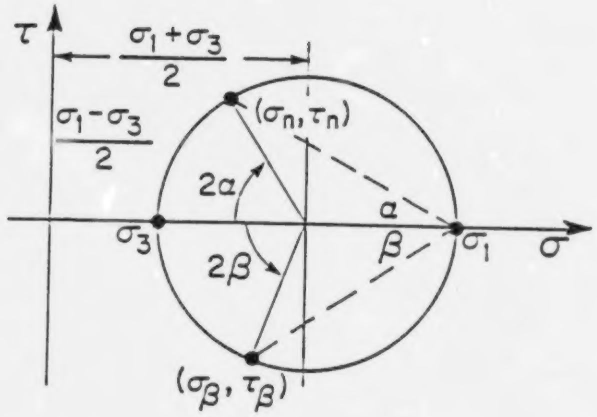
τ
$\frac{\sigma_1+\sigma_3}{2}$
$\frac{\sigma_1-\sigma_3}{2}$
(σ_n, τ_n)
2α
α
σ_3
β
σ_1
σ
2β
$(\sigma_\beta, \tau_\beta)$

MOHR'S CONSTRUCTION TO GRAPHICALLY COMPUTE STRESSES ON A PLANE

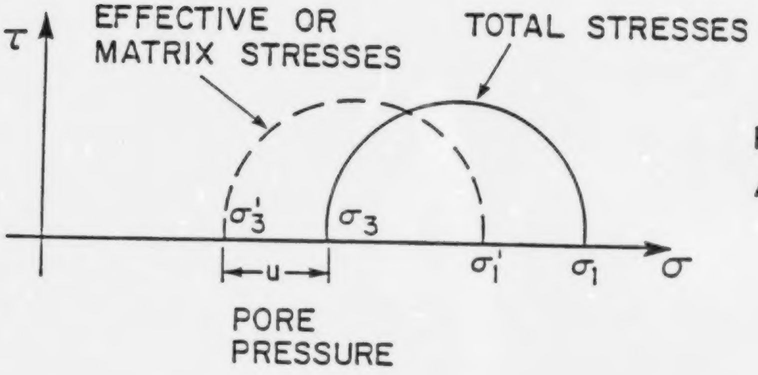
τ
EFFECTIVE OR MATRIX STRESSES
TOTAL STRESSES
σ_3'
σ_3
u
σ_1'
σ_1
σ
PORE PRESSURE

PORE PRESSURE ON A MOHR'S DIAGRAM

FIGURE 7b MOHR'S DIAGRAM FOR STRESSES (2-D)

only the minor and major principal stresses. Soils and other granular materials, rocks, sugar, and so on are often treated as "ideal" Mohr-Coulomb materials. A Mohr-Coulomb strength criterion is plotted in Figure 6 for a compressive condition. It it were assumed that the material followed another behavioral rule, the criterion might look like the three-dimensional surface shown in Figure 8a. The octahedral plane cross section of this would be a circle and would actually be a modified "Von Mises" yield criterion. In cross section, the ideal Mohr-Coulomb rupture criterion looks like a deformed hexagon (Figure 8b). This figure also shows data for geomaterials indicating that ignoring intermediate stress effects is a reasonable and slightly conservative assumption for all geomaterials. Insufficient data exists as yet for saltrocks to decide which model of behavior is most appropriate for strain-weakening yield, but we are fairly certain it is a Mohr-Coulomb shape, as it is governed by the same cracking processes as that of hard rock or other geomaterials, and shows considerable normal stress dependency. Note that the classification of a material as a Mohr-Coulomb material implies nothing about deformation, time-dependency, or behavior other than the shear stress-normal stress relationship in yield. In soils, it is common to assume the relationship between normal and shear stress as linear; in rock, a parabolic assumption may be more reasonable, depending on the stress level of interest, but both are Mohr-Coulomb material assumptions.

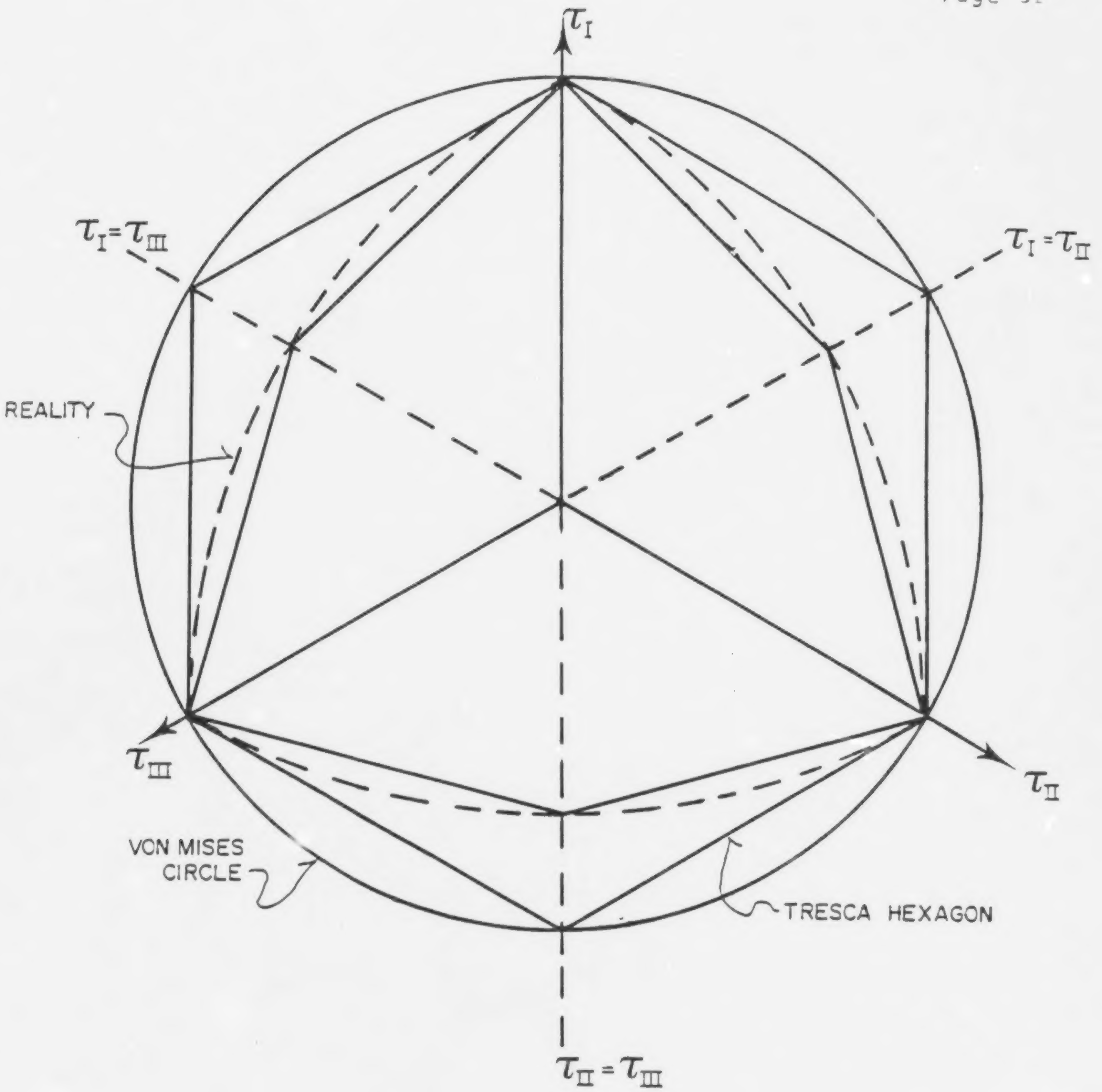
τ_I
$\tau_I = \tau_{III}$
$\tau_I = \tau_{II}$
REALITY
τ_{III}
τ_{II}
VON MISES CIRCLE
TRESCA HEXAGON
$\tau_{II} = \tau_{III}$

SHAPES OF DIFFERENT YIELD CRITERIA
SHOWING WHY MOHR-COULOMB IS A
CONSERVATIVE APPROXIMATION
OF REALITY

FIGURE 8a

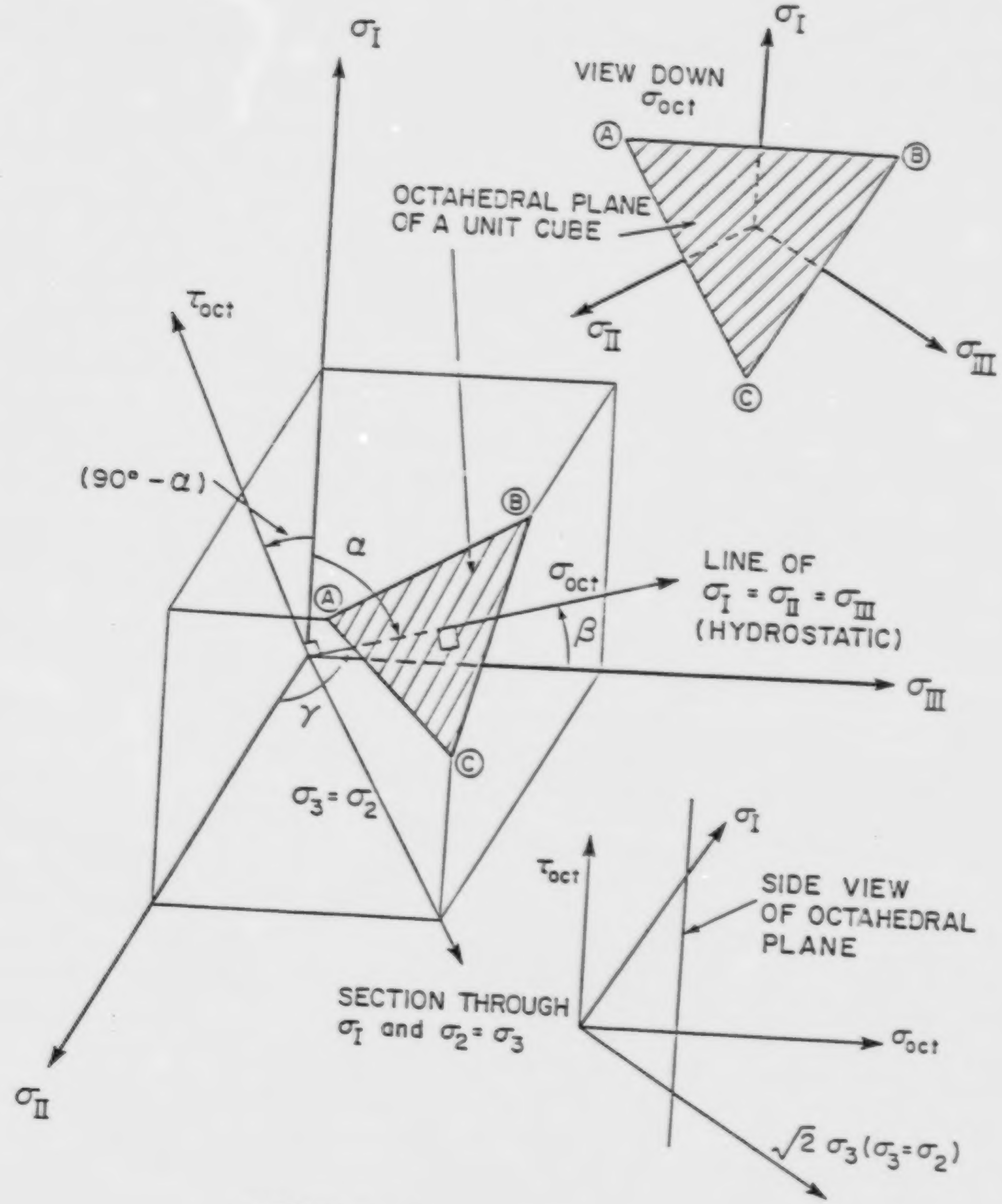
σ_I
τ_{oct}
$(90° - \alpha)$
α
Ⓐ
Ⓑ
Ⓒ
γ
β
σ_{oct}
OCTAHEDRAL PLANE OF A UNIT CUBE
LINE OF $\sigma_I = \sigma_{II} = \sigma_{III}$ (HYDROSTATIC)
σ_{III}
$\sigma_3 = \sigma_2$
SECTION THROUGH σ_I and $\sigma_2 = \sigma_3$
σ_{II}
VIEW DOWN σ_{oct}
σ_I
σ_{II}
σ_{III}
SIDE VIEW OF OCTAHEDRAL PLANE
τ_{oct}
σ_{oct}
$\sqrt{2}\,\sigma_3 (\sigma_3 = \sigma_2)$

FIGURE 8b

GEOMETRY OF STRESS SPACE AND DEFINITION OF THE OCTAHEDRAL PLANE

NON-LINEAR BEHAVIOR: Behavior which cannot be described by first-order equations with constant parameters. In reality, all natural materials are "non-linear", as their properties change with stress, strain rate, temperature, and so on. However, a linear assumption often suffices for design. By definition, if the yield function or failure criterion of a material is stress-path dependent or stress-history dependent, it is non-linear; that is, it deviates from linear elastic (constant parameter) assumptions.

NORMAL STRESS: The component of stress which is normal (perpendicular) to a given plane in a material. All planes in a rock mass have a normal stress component which can be calculated if the complete stress state is known.

NORMAL STRESS (MEAN): The average of the three principal normal stresses at a point in a stressed rock mass. It is related to the value of the first stress invariant "I1". By definition, I1 = s1+s2+s3, and s_{mean} = (s1+s2+s3)/3.

NUMERICAL METHOD: A method of solving problems by the simultaneous solution of sets of equations which each describe the conditions over a small region of the structure, the individual equations being coupled together by some method. Almost all realistic problems in rock (particularly time-dependent problems) must be approached by numerical methods. Among the common methods are displacement discontinuity, boundary element, boundary integral, finite difference, and finite element methods. The latter is the most powerful for geometrically complex stress-strain-strength problems which are non-linear.

NUMERICAL MODEL: A representation of a physical problem achieved in a numerical scheme after making attendant assumptions and necessary simplifications, is called a numerical model. This contrasts with a physical scale model, an analytic model (closed-form solution), or an empirical model.

OCTAHEDRAL PLANE: The plane in stress space (viz) which contains a principal stress axis plus the octahedral line which is equidistant from the three axes in the (+,+,+) octant. The three most used octahedral planes are the octahedral compressional plane, the extensional plane, and the plane corresponding to plane strain conditions. Figure 1 is an octahedral plane diagram for compressional triaxial cell stress conditions: i.e. s1 = s(axial) > s2 = s3 = s(radial). The extensional plane would be for the condition s1 = s2 = s(radial), with the axial stress as s3.

OCTANT: Any set of three orthogonal coordinate axes divide up the plotted space into eight open sectors, each called an octant. If the origin is the (0,0,0) point, then the octants can be labelled as (+,+,+), (+,+,-), (+,-,+), (-,+,+), (+,-,-), (-,+,-), (-,-,+), and (-,-,-). If the three axes correspond to the principal stresses and compression is positive, almost all constitutive information will be found in the (+,+,+) octant, as rocks and soils are weak in tension, and every other octant has at least one of the stresses tensile (negative).

PLASTIC: A description of permanent (irrecoverable) deformation, or a process dominated by permanent deformation. The term is contrasted with elastic (recoverable) deformation. The term does not imply a time-dependent component, although time-dependent deformations are usually plastic. Hence, viscoplastic, elastoplastic, elastic-ideally plastic, and so on, are terms used to refer to models of material behavior comprising several types of deformation. Viscous behavior is plastic, but plastic is not necessarily viscous. Elastic and plastic are in a sense opposites, because if a deformation is not one, it must be the other, but both occur simultaneously in most deformation problems involving geomaterials.

PLASTICITY (THEORY OF): A body of theory involving the prediction of deformations of a plastic nature. What is required to solve a plasticity problem is a "flow" rule (not to be confused with a viscous law) relating plastic strain increments and stress increments and accompanying stress redistribution, which is in turn a function of the elastic and plastic deformation parameters.

POLYCRYSTALLINE MATERIAL: Materials such as salt or granite that are comprised of an assemblage of individual crystals. The term is used to imply that the material is not a glass, a clastic material (e.g. sand or clay), a monocrystal, or a ceramic.

POTASH: In the fertilizer industry, potassium oxide. The evaporitic potassium minerals mined to obtain potassium are referred to as potash ores or simply "potash". All evaporitic potash ores, however, are dominantly potassium chloride (sylvite) and also contain considerable quantities of halite. Potash ore is invariably found enclosed in bedded salt deposits, rarely true domal salts, although domal salt can contain small amounts of evaporitic potassium minerals. The term potash is loosely used, as it originally was used to refer to the potassium carbonate residue from lixiviated wood ashes.

PLASTIC LIMIT: The shear stress level required for initiation of a particular plastic deformation mechanism. Below the plastic limit, strains are elastic; above, they are non-recoverable. A yield criterion is not necessarily synonomous with a plastic limit. Because deformation after strain-weakening yield is largely plastic, some refer to the peak strength as a plastic criterion, but this is not strictly correct. In fact, some plastic deformation probably took place before peak strength.

PRIMARY CREEP: Creep characterized by a decelerating creep rate. In Figure 9, which is a conventional and inadequate way of looking at the creep of a saltrock, the curved initial portion is referred to as primary creep. In fact, saltrocks _in situ_ do not move from a condition of steady-state creep to tertiary creep, as implied by the diagram. See secondary

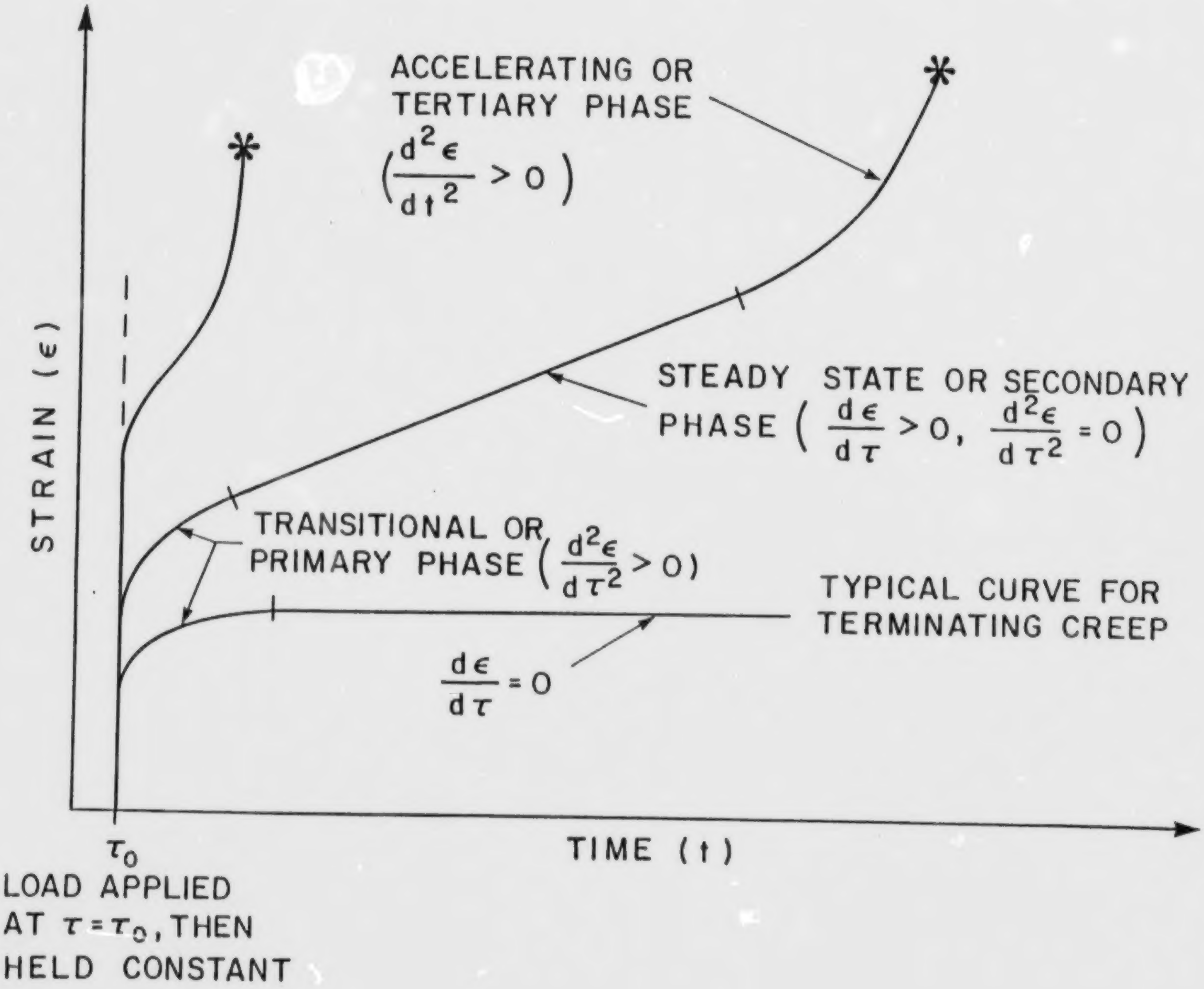
ACCELERATING OR TERTIARY PHASE $\left(\frac{d^2\epsilon}{dt^2} > 0\right)$
STEADY STATE OR SECONDARY PHASE $\left(\frac{d\epsilon}{d\tau} > 0,\ \frac{d^2\epsilon}{d\tau^2} = 0\right)$
TRANSITIONAL OR PRIMARY PHASE $\left(\frac{d^2\epsilon}{d\tau^2} > 0\right)$
TYPICAL CURVE FOR TERMINATING CREEP
$\frac{d\epsilon}{d\tau} = 0$
STRAIN (ϵ)
TIME (t)
τ_0
- LOAD APPLIED AT $\tau = \tau_0$, THEN HELD CONSTANT

FIGURE 9 CONVENTIONAL CREEP CONCEPTS

and tertiary creep.

PRINCIPAL STRESS: One of the mutually perpendicular stresses which are associated with those faces in a material which have no shear stresses on them. It can be proven that for every stress condition where the three principal stresses (s1, s2, s3) are unequal, shear stresses exist on all planes except the principal planes. Reference to the Mohr-Coulomb diagram, Figure 7, will demonstrate this. Generally, it is the major and minor principal stresses which have the most dramatic effect on strength behavior; see Mohr-Coulomb material.

RHEID: A body that has the property of being able to flow. Hence, rheological modeling describes systems that flow.

RHEOLOGY: The study of the flow and deformational properties of materials exhibiting large time-dependent deformability and viscous behavior.

SAFETY FACTOR: The ratio of resisting forces divided by driving forces (resisting over activating). The concept derives from civil engineering and is often used in mining engineering pillar or stope design to provide some assurance that the openings will be stable for the requisite time. In general, the selection of a appropriate safety factor is a matter of experience backed up by analysis. The design safety factor is empirically adjusted depending on the desired life span of the mine element, a situation that requires implicit recognition of the limitations of elasticity-based design procedures. The use of a safety factor approach is contentious in situations where a univalued strength cannot be defined, as is the case with saltrocks. An observational approach is preferable, whereby one carefully observes to see if deformations are accelerating or if rock conditions are deteriorating rapidly. The degree of acceptable deterioration is determined by the length of service required from the mine element considered and the decisions for mine element design in saltrocks are more complex than simple safety factor considerations. Simplistic approaches useful in other areas cannot be applied directly to saltrock mechanics.

SALTROCK: Minerals belonging to the metallic halide group, including halite, sylvite, bischoffite, carnallite, and kieserite. All saltrocks are evaporites, but the reverse is not true; for instance, gypsum and anhydrite are evaporites but not saltrocks.

SECONDARY CREEP: Time-dependent displacement characterized by a constant strain rate at a constant stress difference (shear stress). See Figure 9 and tertiary and primary creep.

SHEAR STRESS: The stress difference that tends to displace adjacent particles of a material on opposite sides of a plane in opposite directions. Shear stresses on a specified plane are easily computed from principal stress values and directions. Creep rates are strongly dependent on the shear stress levels. Most earth materials tend to fail in shear rather than in other modes such as crushing. Because the particular shear stress at which failure occurs is a function of the normal stress, analysis of the displacement rates and the resistance of mine elements requires estimation of the actual shear and normal stresses acting upon stipulated planes.

SHEAR STRESS (OCTAHEDRAL): A generalized measure of the level of shear stress in three dimensions acting at a point in a stressed rock. It is taken to be the orthogonal distance from the octahedral line (the line normal to the (1,1,1), or octahedral planes). The distance is the square root of the sum of the squares of the deviatoric stresses, and can be written as:

$$\text{octahedral shear stress} = \frac{1}{3}\sqrt{(s1-s2)^2 + (s2-s3)^2 + (s3-s1)^2}$$

where s1, s2, s3 are the principal stresses. The equation allows the average shear stress within the sample to be estimated and used in equations. For a saltrock, the higher the octahedral shear stress level, the higher the strain rate. Expressed in terms of principal stress space, the higher the value of octahedral shear stress, the farther away is the stress condition from a pure spherical stress state (isotropic, s1=s2=s3). Accordingly, the actual stress state is farther away from the space diagonal normal to the octahedral planes, as the space diagonal represents hydrostatic (spherical) stress conditions. An attempt to show this can be found in the diagrams.

SHEARING RESISTANCE: In its simplest form, the ability of a material to withstand shear stresses on a plane. The ability of rocks to withstand shear stresses is also observed to be a function of the normal stress across the plane, and is usually expressed by a yield criterion relating shear to normal stresses:

$$S = C + N \tan \phi$$

where S = shear stress along the failure plane
C = cohesion (intercept on the shear stress axis of a Mohr-Coulomb diagram)
N = normal stress across the failure plane
ϕ = angle of shearing resistance.

This of course is the Mohr-Coulomb criterion that has been shown to be inadequate for saltrocks, because the ability to withstand shear stress in viscous polycrystalline materials is also a function of strain rate.

SOFT ROCK: Rock of low compressive strength, low deformation modulus, and usually of sedimentary origin. Typical examples are mudstone, clay shale, most sandstones, oolitic limestone, anhydrite, coal, etc. Saltrocks are often classified as softrocks, but should be considered as a separate class: viscous rocks.

STABLE CRACK GROWTH: The condition whereby new internal area is created in a material under stress (i.e. crack development), but that the rate is stably declining, or the cracks are being healed by some mechanism as fast as they are being created. This process is associated with stresses below the long-term strain-weakening strength criterion. The phenomena of stable and unstable crack growth are reasonable physical processes which aid in explaining material behavior, but rigorous quantification of the processes has proven very difficult in the laboratory, and extension to field conditions has as yet not been accomplished with any degree of success. The conceptual value is important.

STEADY-STATE CONDITIONS (usually steady-state creep): Conditions where the stresses are not changing with time, nor are the displacement rates, therefore there is neither accelerating nor decelerating displacement.

STRAIN HARDENING: A term that has its origin in fracture mechanics and metals plasticity, but that can be quite misleading to those those not totally familiar with its meaning in that context. It originally referred to iron, which has a yield point (boundary between elastic and perfectly plastic yield at constant stress) at about 0.2% strain, deforms almost as a perfectly plastic material for some strain beyond that level, then begins to be able to take more stress for a period before rupture (Figure 10). The confusion arises with the use of the term "hardening" as this refers to a metallurgical/chemical effect in metals and a type of plasticity quite different from what is observed in rocks. A more appropriate term would be strain-strengthening, but the phenomenon is not observed in rocks in the field under normal strain rates. There is increasing evidence that the

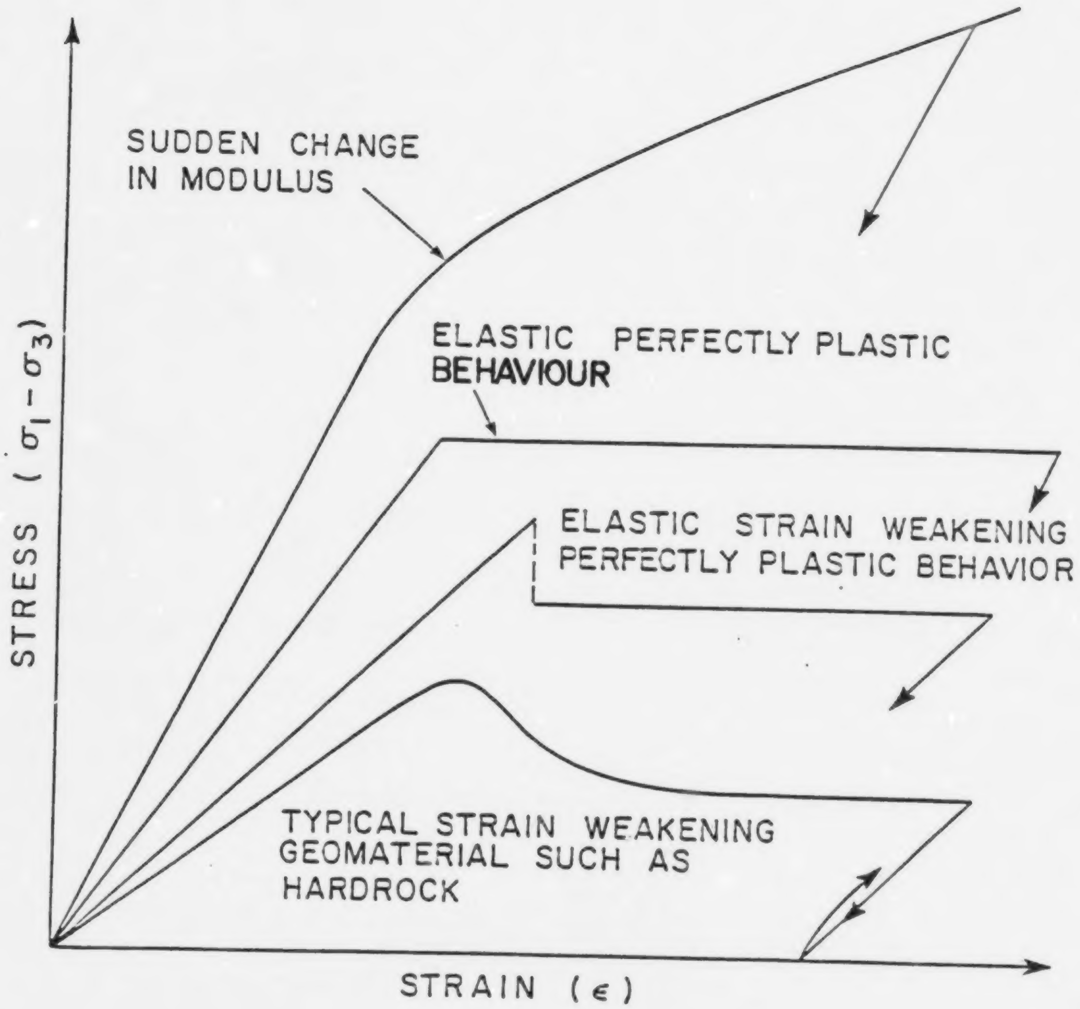
SUDDEN CHANGE IN MODULUS
ELASTIC PERFECTLY PLASTIC BEHAVIOUR
ELASTIC STRAIN WEAKENING PERFECTLY PLASTIC BEHAVIOR
TYPICAL STRAIN WEAKENING GEOMATERIAL SUCH AS HARDROCK
STRESS ($\sigma_1 - \sigma_3$)
STRAIN (ϵ)

FIGURE 10a

DIFFERENT TYPES OF YIELD, "ELASTIC" MATERIAL phenomenon of strain-hardening applied to salt is a function of laboratory or borehole scale effects, and does not extend to the salt mass.

STRAIN RATE: The strain exhibited in a certain time interval divided by the time, usually in seconds. Hence, the units of strain rate are in $(\text{seconds})^{-1}$ because strains themselves are unitless (L/L). To give an idea of the magnitude of strain rates, if a 60 foot tall pillar is shortening by one foot per year, the average strain rate at the central cross-section is :

$$de/dt = \frac{(1/60)}{365 \times 24 \times 60 \times 60} = 0.000000000528$$

$$= 5.3 \times 10^{-10} \ \text{sec}^{-1}$$

This is such a slow rate that it is difficult to systematically measure in the laboratory, even on 200 mm specimens, without special equipment. Nevertheless, this would be considered quite a rapid rate in a mining situation. This points out a fundamental difficulty in laboratory creep testing: the strain rates available in the laboratory are the upper range of those encountered in the field, and the realm of geological strain rates ($<10^{-12}$) are not accessable to laboratory technique.

STRAIN SOFTENING: The opposite of strain hardening; that is, a loss of strength with increasing strain. For those unfamiliar with the term, the use of "softening" instead of "weakening" can be confusing. In this glossary, the term

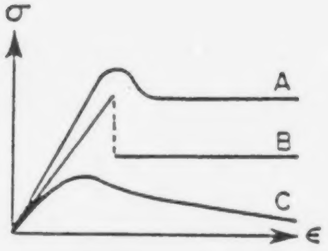

STRAIN WEAKENING BEHAVIOR
(LOSS OF STRENGTH)

A - NORMAL DENSE SAND
B - LINEAR-ELASTIC/STRAIN-WEAKENING/PERFECTLY-PLASTIC
C - CONTINUED WEAKENING (FABRIC DESTRUCTION)

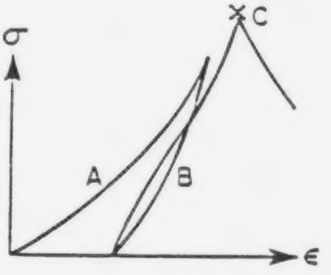

STRAIN STIFFENING BEHAVIOR
(GAIN IN RIGIDITY)

A - LOADING
B - UNLOAD - RELOAD CYCLE
C - YIELD (RUPTURE) POINT LEADING TO STRAIN-WEAKENING

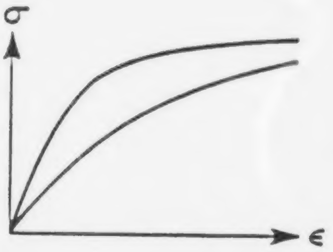

STRAIN SOFTENING BEHAVIOR
(YIELD NOT MENTIONED)

SOFT CLAYS AND LOOSE SANDS

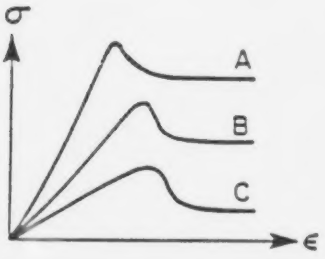

STRESS STIFFENING BEHAVIOR (WITH INCREASING CONFINING STRESS)

A - HIGH CONFINING STRESS
B - INTERMEDIATE CONFINING STRESS
C - LOW CONFINING STRESS
- EACH ALSO SHOWS STRAIN - WEAKENING

FIGURE 10b FAILURE AND STRAINING PHENOMENA

"strain-weakening" is preferred because its meaning is more precise; however, the reader must be aware that the term "strain-softening" is more commonly used. See below for more details.

STRAIN WEAKENING: Loss of strength (ability to withstand shear stress) as strain increases. All materials at some shear stress level eventually cease to be able to carry more load. If there is an associated and appreciable drop in that capacity, the term strain-weakening applies. All hard rocks under normal temperatures and engineering level stresses are strain-weakening. If saltrocks are placed at stresses below the lowermost yield line (Y2 in Figure 1), they will not exhibit strain-weakening. Also, if the confining stress in a triaxial test is greater than about 12-15 MPa, saltrock specimens do not show strain-weakening behavior even under extremely rapid strain rates (.001 to .01 /sec).

STRENGTH: The ability to withstand load. The term has no real meaning in rock mechanics unless specified more precisely as in shear strength, compressive strength, and tensile strength. For saltrocks, the use of the term strength can be extremely misleading, and is of little use. Specification of a particular confining stress and strain rate is required before the term can have meaning.

STRESS ARCH: The development of a region of reduced vertical stress above (and below) an opening in the earth. The vertical stress which was carried by the material in the

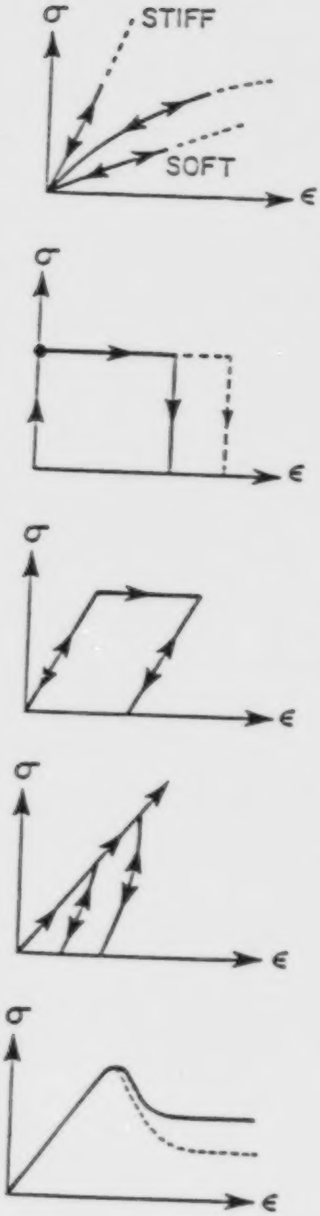

ELASTIC BEHAVIOR: FULLY RECOVERABLE STRAINS
(STRAIGHT LINES ARE LINEAR-ELASTIC BEHAVIOR)

IDEALLY PLASTIC BEHAVIOR (OR RIGID-PLASTIC):
FULLY -NON RECOVERABLE STRAINS

LINEAR ELASTIC / PERFECTLY PLASTIC BEHAVIOR

PARTIALLY PLASTIC BEHAVIOR

ACTUAL MATERIAL BEHAVIOR

FIGURE 10c ELASTICITY AND PLASTICITY

opening prior to excavation is redistributed away from the opening. In a viscous saltrock, the concept of a zone of reduced vertical stress (a stress-relief zone as it is commonly called) is used to create openings which have reduced deformation rates due to the reduced deviatoric stresses in the region of lower vertical stress. Arching is aided greatly by the tendency of saltrocks to flow more rapidly with increased stress: if more stress is applied to a single pillar for whatever reason, accelerated flow relieves the stress, the stress arch is enhanced, distributed more widely, and so maintained. Figure 11 shows the sequential development of a stress arch in a multiple entry system.

STRESS INVARIANT: Continuum mechanics analysis of the stresses at any point in a medium (six independent values) will show that there are three separate combinations of those stresses which are invariant no matter what the choice of axis system orientation. These three invariants can also be looked on as the three roots of a cubic equation, that is, the three eigenvalues of a three-dimensional stress tensor. The three invariants are:

$$I1 = s1 + s2 + s3$$

$$(4 \times I2^2)/3 = (s1-s2)^2 + (s2-s3)^2 + (s3-s1)^2$$

$$I3 = s1 \times s2 \times s3$$

Because these functions are invariant at a given point in space, there is a strong incentive to try and describe the material behavior (yield functions, deformation laws, creep

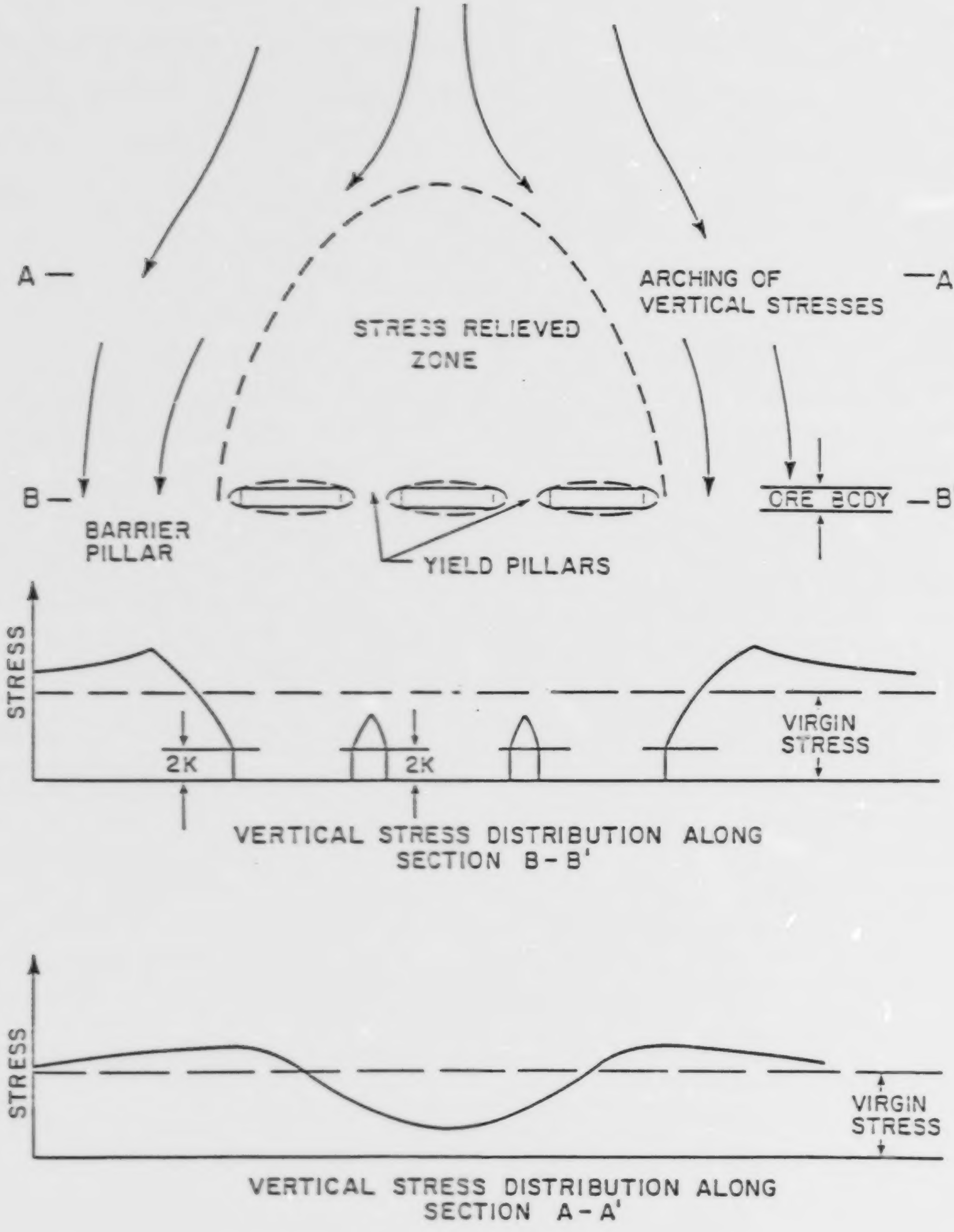
A
A'
B
B'
ARCHING OF VERTICAL STRESSES
STRESS RELIEVED ZONE
BARRIER PILLAR
YIELD PILLARS
ORE BODY
STRESS
2K
2K
VIRGIN STRESS
VERTICAL STRESS DISTRIBUTION ALONG SECTION B-B'
STRESS
VIRGIN STRESS
VERTICAL STRESS DISTRIBUTION ALONG SECTION A-A'

FIGURE 11

DEVELOPMENT OF A STRESS ARCH IN A MULTIPLE ENTRY SYSTEM AT STEADY STATE laws) in terms of these invariants, as they are independent of direction. There are also deviatoric stress invariants which refer to the deviation of the stress invariats from the hydrostatic (spherical) stress state:

$$J1 = 0$$

$$J2 = 3 \times (I1)^{2} - I2$$

$$J3 = I3 - (I2 \times I1) + (2 \times I1^{3})$$

Similar strain invariants can be derived if strains are analysed in the same manner.

STRESS PATH: The path through stress space that a specimen follows during a laboratory test, or that a material point follows in the field as stresses change. It is considered important that the material in the laboratory simulate the stress path (and stress change rate) in the field, as closely as economy permits. Because we now understand that almost all geomaterials have material properties which are functions of the stress history, the prediction of future behavior depends on the stress path history, including strain rate. As a simple example, if in its history a hardrock has ever experienced yield, its currently available shearing resistance is greatly reduced.

STRESS RELIEF METHOD: A variation of room-and-pillar mining developed in British coal mines in the 1940's, in East German salt mines in the early 1950's, and brought to the Canadian potash industry for Saskatchewan potash mines in the 1960's and 1970's. From there it is gradually spreading to all salt rock operations, both in tabular and in domal operations. The method explicitly recognizes the beneficial effect of confining stress on the ability of saltrock material to withstand stress, the development of a stress arch, and the development of an equivalent opening. The system consists of extremely wide bearing pillars with good confinement, separated by multiple mining entries (usually three to five), which are in the stress relief zone, and require only relatively thin yield pillars to carry the local roof load.

STRESS RELIEF ZONE: See stress arch and stress relief method.

STRESS SPACE: A plot of the three principal stresses along three mutually perpendicular (orthogonal) axes, giving a three-dimensional representation of the stress condition. Any stress state possible can be plotted in such a coordinate system because all stress states can be expressed as three principal stresses. A stress state plot (Figure 12) has eight sectors (octants), the (+,+,+) sector being the most important for rock mechanics (compression positive by convention) because rocks are relatively weak in tension compared to compression. Figure 1 is a plane in stress space which contains the octahedral line (isotropic lithostatic conditions) and one major axis. The flat (planar) surfaces orthogonal to the octahedral line are called octahedral planes. The farther away a point is from the octahedral line, the greater the shear stress in the body. In the most general possible representation of intact isotropic

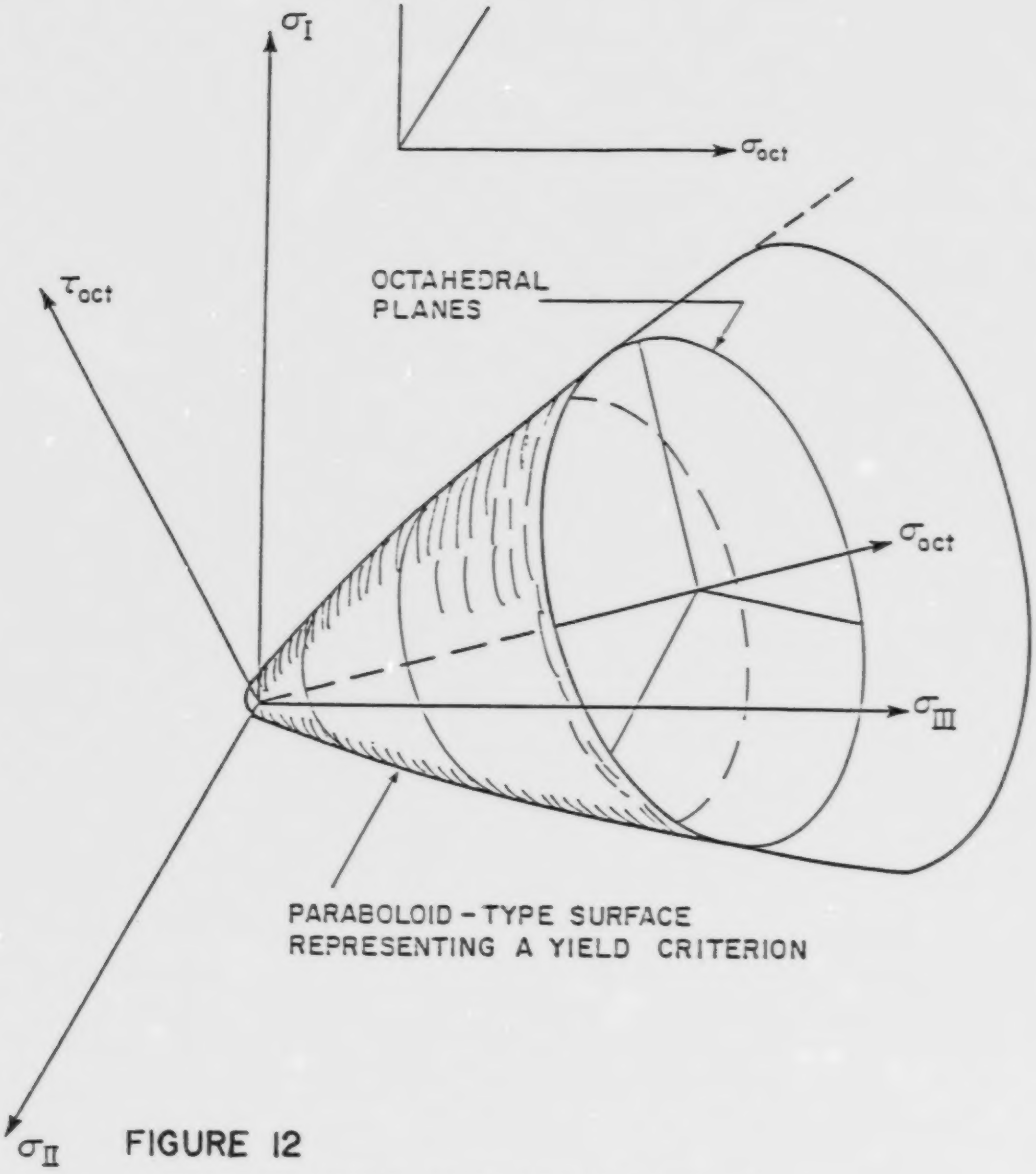
σ_I
σ_{oct}
τ_{oct}
OCTAHEDRAL PLANES
σ_{oct}
σ_{III}
PARABOLOID - TYPE SURFACE REPRESENTING A YIELD CRITERION
σ_{II}

FIGURE 12

A SINGLE YIELD SURFACE PLOTTED IN STRESS SPACE

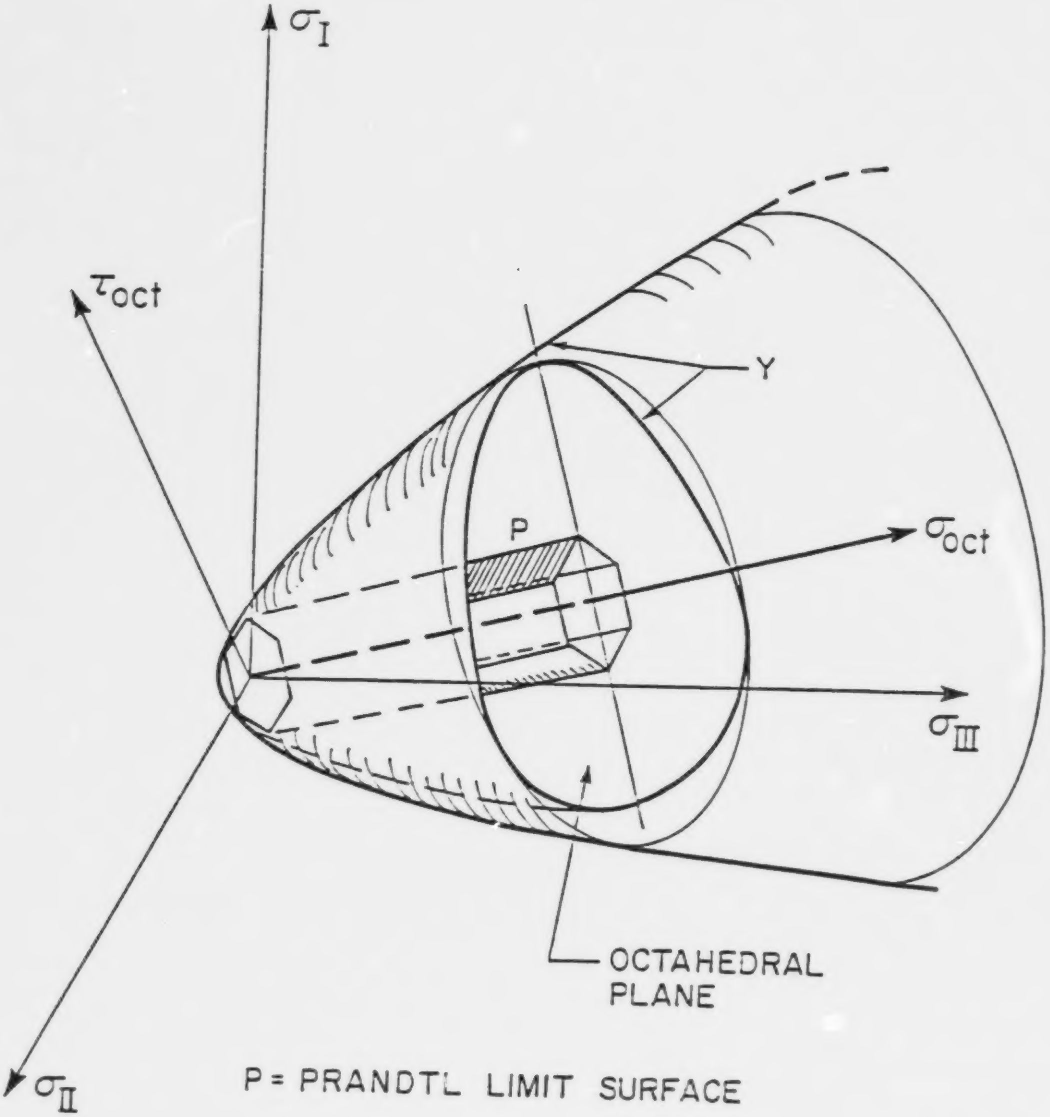
σ_I
τ_{oct}
Y
P
σ_{oct}
σ_{III}
OCTAHEDRAL PLANE
σ_{II}

P = PRANDTL LIMIT SURFACE

FIGURE 13
THREE - DIMENSIONAL CONSTITUTIVE SURFACES

characterized by a continued deceleration. This is a characteristic of all conventional hardrocks and softrocks stressed to levels below their long-term strength, but the concept of terminating creep is of little merit in saltrock geomechanics as even at stresses well below the plastic limit, extremely slow but steady creep continues, as evidenced by the isotropic lithostatic virgin stress state in situ. The similarity to primary creep is noted, but the two terms are not necessarily synonomous: primary creep is not necessarily terminating, but all terminating creep is primary by definition.

TRANSITIONAL CREEP: When an element of a saltrock is subjected to a sudden increase or decrease in deviatoric stress, it undergoes a period of rapid movement, transitional creep, before settling into a stable creep movement. This can be demonstrated for laboratory specimens, and it is also shown in pillars and ribs subjected to stress changes, although the two processes are the result of very different mechanisms: internal redistribution of load to individual polycrystal faces for the laboratory specimen, and development of the equivalent opening for the field case, whereby the viscoplastic zone grows until full stress redistribution of shear stresses at the plastic limit or equilibrium shear stress occurs.

TRIAXIAL CELL: A laboratory device which is used to test cylindrical specimens of rock. Figures 14a and 14b give several examples of triaxial cells. The first is a simple

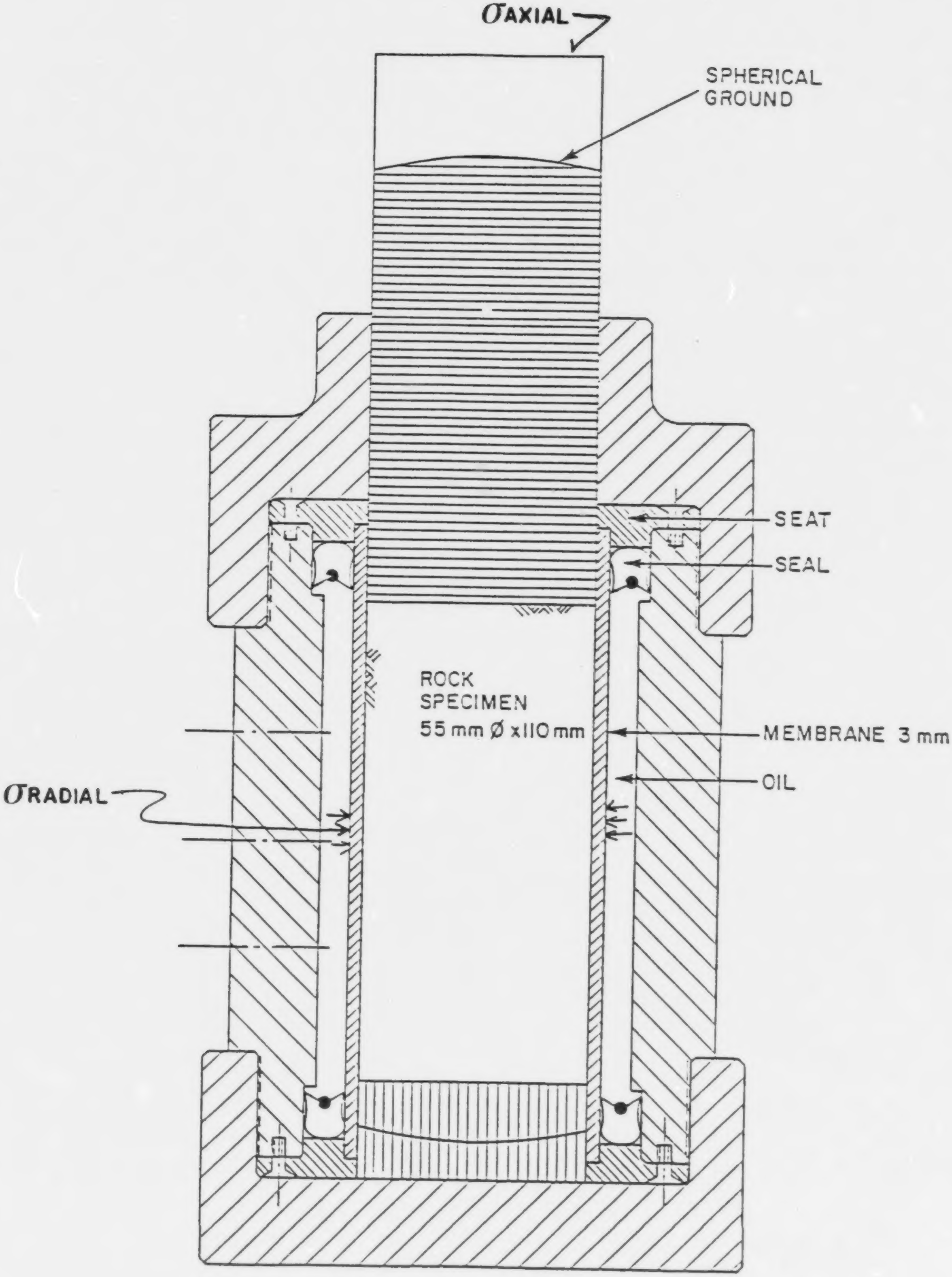
σAXIAL
SPHERICAL GROUND
SEAT
SEAL
ROCK SPECIMEN 55 mm Ø x110 mm
MEMBRANE 3 mm
OIL
σRADIAL

FIGURE 14a. CONVENTIONAL TRIAXIAL ROCK CELL

one requiring an external reaction frame, actuator, and measurement device; the second is a self-contained design. The confining stress is applied as oil pressure acting on the flexible membrane and this acts against the specimen as a pure radial stress. The axial load, either compressional or extensional, is applied through a ram whose load is either altered by a constant displacement (constant strain-rate test) or maintained at a constant stress level (constant stress test). The latter is more useful for creep testing; the former is more useful for conventional rock mechanics testing. It is only possible to have two different stresses in the triaxial cell because either s2=s3 (triaxial compression) or s1=s2 (triaxial extension). The name triaxial has remained, though the stress state is not truly triaxial. In the stress space diagram, compressional and extensional triaxial cell conditions plot on major planes, but all possible stress states cannot be tested in the triaxial cell.

TRIAXIAL STRESS STATE: The general stress state in the ground where the three principal (and orthogonal) stresses are unequal.

TRIAXIAL TEST: A test carried out using a triaxial cell with a frame around it to apply loads.

UNIAXIAL COMPRESSION TEST: A compression test carried out on a specimen without lateral confining stress, s2=s3=0, s1= axial stress. As can be seen on Figure 1, this condition

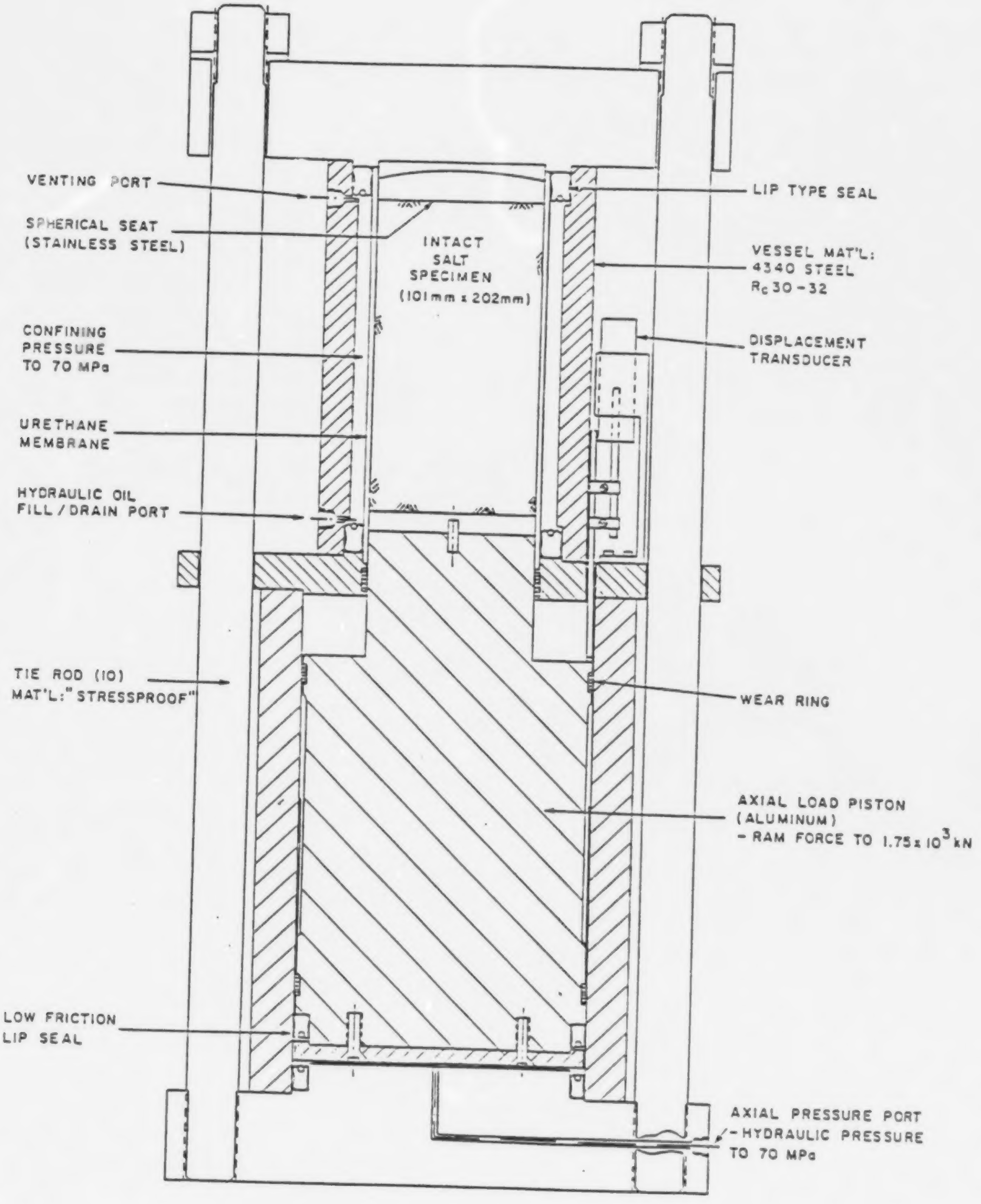
VENTING PORT
SPHERICAL SEAT (STAINLESS STEEL)
INTACT SALT SPECIMEN (101mm x 202mm)
CONFINING PRESSURE TO 70 MPa
URETHANE MEMBRANE
HYDRAULIC OIL FILL / DRAIN PORT
TIE ROD (10) MAT'L: "STRESSPROOF"
LOW FRICTION LIP SEAL
LIP TYPE SEAL
VESSEL MAT'L: 4340 STEEL Rc 30 - 32
DISPLACEMENT TRANSDUCER
WEAR RING
AXIAL LOAD PISTON (ALUMINUM) - RAM FORCE TO 1.75 x 10³ kN
AXIAL PRESSURE PORT - HYDRAULIC PRESSURE TO 70 MPa

FIGURE 14b INTERNALLY ACTUATED TRIAXIAL CELL (WATSALT DESIGN)

only represents one point on the generalized stress-behavior diagram, and it is difficult or impossible to extrapolate to other general stress conditions. Even in hardrocks, the test is no longer considered to be anything but an indicator of behavior, and is rarely used alone in design. In saltrock opening design, it has a use, but a more general approach to the stess/strain/time/strength behavior is warrented.

UNSTABLE CRACK GROWTH: The condition found in the region between the lower and upper bounds of failure (Y1 and Y2) where the rate of growth of cracks exceeds the ability of the saltrock to heal the cracks internally by rapid flow. See stable crack growth.

VIRGIN STRESS STATE: The initial stress state in the ground before any openings have been created. This is a very important factor in rock mechanics design. In saltrocks, the virgin stress condition usually is very close to an isotropic lithostatic stress.

VISCOPLASTIC ZONE: The zone where shear stresses are equal to or slightly greater than those predicated by the plastic limit, and where the saltrock is undergoing viscous deformation that is also permanent (plastic). Within the viscoplastic zone, the stress difference (s1-s3) is equal, although the magnitudes of the stresses are not.

VISCOELASTIC ZONE: The region beyond the outermost bound of the viscoplastic zone where viscous processes still occur, but at a very slow rate. The difference between the stresses is not constant as in the viscoplastic zone, but decreases gradually away from the opening as the stresses approach the virgin state at great distances (Figure 5). The term elastic in this case is to imply that the stress distribution is assumed to be pertaining to an elastic assumption rather than an ideally plastic assumption. Whether this is fully justified in practice is not known, but the magnitude of associated error cannot be large for viscous-dominated processes.

VISCOSITY: The measure of the resistance of a fluid to flow. Materials of high viscosity move more slowly than materials of low viscosity at the same shear stress level. Saltrocks, mantle materials (rocks under high temperature and pressure), and ice all have viscosities.

VISCOUS: Having the property of viscosity. That is, materials which display a dependency between the shear stress level and the rate of shear displacement.

YIELD: A sudden change in curvature of the stress-strain curve (Figure 2). Generally, in metals, the yield point is taken to be the onset of plastic deformation. In hard rocks this may be a reasonable assumption if the yield point is about 80% of the peak strength. In saltrocks, the term brittle yield is used for the sudden drop in ability to carry more load (strain-weakening), which only occurs under rapid loading and low confining stresses. At higher confining stresses, saltrock will display something approaching perfectly plastic yield (at high strain rates). The Prandtl Limit can be considered a yield point in the conventional sense because it is a sudden change in curvature of the strain rate - shear stress curve (Figure 15), indicating that the material has begun to exhibit viscoplastic phenomena due to cracking mechanisms rather than diffusion-dislocation ones. Great care must be exercised in the use of the term "yield" when discussing saltrocks. Misuse of the term has led to considerable confusion.

YIELDED ZONE: The zone of material within the equivalent opening. This material has been sheared and is no longer intact, therefore it has a low load-carrying capacity, and will tend to slab off under continued deformation of the opening. See Figures 4 and 5. It is also an elastoplastic zone.

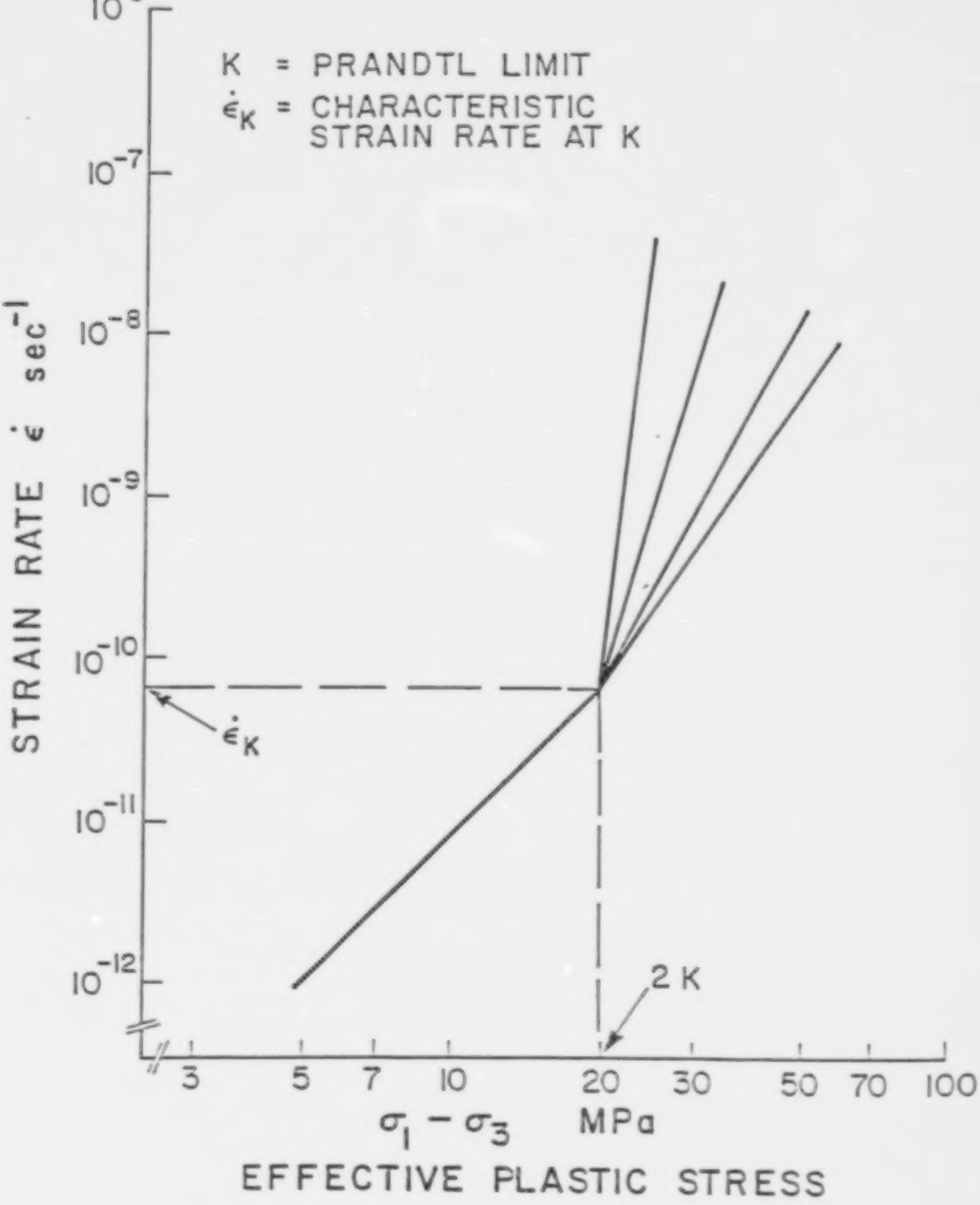

· DEFINITION OF THE PRANDTL LIMIT

FIGURE 15 CHANGE IN CREEP RATE AT A PLASTIC LIMIT

LIST OF FIGURES

FIGURE 1A	PROCESSES FOR SALTROCK CREEP, OCTAHEDRAL COMPRESSIVE PLANE
FIGURE 1B	RELATIONSHIP OF STRAIN RATE TESTS TO STRESS SPACE
FIGURE 2	TYPES OF YIELD
FIGURE 3	VOLUMETRIC PLASTIC DEFORMATION
FIGURE 4	EQUIVALENT OR ACTIVE OPENING CONCEPT
FIGURE 5A	BEHAVIOURAL ZONES AND STRESS DISTRIBUTION ADJACENT TO A SINGLE MINE OPENING, STEADY STATE CONDITIONS
FIGURE 5B	RANGES OF BEHAVIOUR FOR A SALTROCK OPENING, RELATED TO A STRESS - PROCESS DIAGRAM
FIGURE 6	CONVENTIONAL STRENGTH CRITERIA
FIGURE 7A	SOLVING FOR STRESSES USING THE GEOMETRIC RELATIONSHIPS ON A MOHR'S CONSTRUCTION
FIGURE 7B	MOHR'S DIAGRAM FOR STRESSES (2-D)
FIGURE 8A	SHAPES OF DIFFERENT YIELD CRITERIA SHOWING WHY MOHR-COULOMB IS A CONSERVATIVE APPROXIMATION OF REALITY
FIGURE 8B	GEOMETRY OF STRESS SPACE AND DEFINITION OF THE OCTAHEDRAL PLANE
FIGURE 9	CONVENTIONAL CREEP CONCEPTS
FIGURE 10A	DIFFERENT TYPES OF YIELD, "ELASTIC" MATERIAL
FIGURE 10B	FAILURE AND STRAINING PHENOMENA
FIGURE 11	DEVELOPMENT OF A STRESS ARCH IN A MULTIPLE ENTRY SYSTEM AT STEADY STATE
FIGURE 12	A SINGLE YIELD SURFACE PLOTTED IN STRESS SPACE
FIGURE 13	THREE-DIMENSIONAL CONSTITUTIVE SURFACES
FIGURE 14A	CONVENTIONAL TRIAXIAL ROCK CELL
FIGURE 14B	INTERNALLY ACTUATED TRIAXIAL CELL (WATSALT DESIGN)
FIGURE 15	CHANGE IN CREEP RATE AT A PLASTIC LIMIT

APPENDIX B

The design of openings in saltrock using a multiple mechanism viscoplastic law

Maurice B. Dusseault, P.Eng.
University of Waterloo, Waterloo, Ontario, CANADA, N2L 3G1

Dennis Z. Mraz, P.Eng.
Mraz Project Consultants, Saskatoon, Saskatchewan, CANADA, S7N 2S5

Leo Rothenburg, P.Eng.
University of Waterloo, Waterloo, Ontario, CANADA, N2L 3G1

1 ABSTRACT

A design approach using isothermal intact saltrock steady-state creep behavior has developed from laboratory testing, field monitoring, and numerical modelling. Creep data at various stress states can be contoured with respect to strain rate on a stress space plot. The contours flatten towards a viscoplastic criterion (not a brittle or Bingham limit), which we call the Prandtl Limit. It is not practical to test at the low strain rates below the limit, but instrumented virgin ground openings allow in situ confirmation of the Prandtl Limit and measurement of the Prandtl Strain Rate, both fundamental parameters.

Brittle failure tests give a classical Mohr-Coulomb failure envelope up to confining stress of about 15 MPa, then failure becomes difficult to define, as strain rates are very fast, and strain weakening is not evidenced below 25% strain. The constitutive model has an outer parabolic surface corresponding to peak strength, and an inner cylindrical surface, the Prandtl Limit, which is an activation shear stress. Below the Prandtl Limit, slow deformation processes dominate; above it, strain rate is dependent on normal stress, indicating processes of dilational dislocation movement, crack generation and healing.

2 INTRODUCTION

Time-dependent deformation of saltrocks is the result of a number of mechanisms, different ones dominating behavior at different stress levels. For example, saltrocks display steady-state creep with no volume change at low shear stresses; at elevated stresses, they behave as Mohr-Coulomb materials, with deformation behavior dominated by crack growth. It is not reasonable that a single formulation would lead to an acceptable constitutive model for salt behavior at all stress levels, and a slightly different approach has been developed with some success in practice. Although field measurements are not unequivocal proof of the approach, they give support to the model within the time frames, stress ranges, and temperature ranges encountered in mining.

On the scale of mine openings, saltrocks are considered true steady-state materials because mechanisms exist for the ionic lattice which permit constant deformation rates (Skrotzki and Haasen, 1984), in contrast to silicates, oxides, sulfides and other covalently bonded minerals at normal temperatures and pressures. Difficulty in predictions of field creep rates and magnitudes purely from current laboratory test approaches suggests that current creep law forms are incomplete (Munson and Fossum, 1986). To rectify this, a different, field-based approach is suggested, using a combination of field and laboratory data. It is not radically different from previously published approaches (Wallner, 1984, Langer, 1984), but there are differences in the approach to quantifying the behavioral parameters.

3 STEADY-STATE CREEP BEHAVIOR

Laboratory creep tests: Isothermal constant stress and structure tests are carried out using a stage-loading method, not allowing strain to exceed 7.5-10%. This limit is because of specimen barreling and platen penetration, and because in mining situations, it is rare that an element of saltrock experiences strains larger than 10%. It is essential that comparable processes are studied on one material, not another altered by having undergone excessive deformation and defect annealing. The strain-time curve approaches a constant deformation rate, and for practical purposes, a tangent to the creep curve at three weeks is taken as steady-state (Figure 1), recognizing that "true steady state" may not have been reached. Statistical and conceptual arguments as to strain hardening and what constitutes true steady state are available in the literature (Wawersik, 1985). Well-known mechanisms exist which must lead to steady state in the field, otherwise salt domes and glaciers would not exist. We are studying mechanisms at strain rates pertinent to mining, solution cavity design, and waste isolation.

In the field, there are an "infinite" number of crystals, hence the laboratory artifact of strain-hardening is not relevant. Care is required in deciding on specimen size, crystal size, data acceptance, and the use to which it is put. Quasi-static creep tests are not acceptable for determination of steady-state parameters, as increasing stress continually does not allow stabilization of the intercrystalline stress distribution, hence steady state cannot be evidenced.

Test results are presented as a plot of strain rate versus plastic effective stress (Figure 2). The scatter of data is not atypical of creep testing, and tests conducted at various normal stresses will show different inclinations. If at various octahedral normal stresses a conventional power law is fit to the few points, a trend of higher exponents with lower normal stresses is found. This is supported by others (Skrotzki and Haasen, 1984) who show that power law fits break down above a certain limit. Because above that limit creep processes are dominated by the movement of dilation centers through the ionic lattice (cross-slip, glide, etc.), it is only logical that there is a normal stress effect. Also, movement of dilation centers does not lead to volume change if the rate of generation of the defects is the same as the rate of annealing, as is the case in the "infinite" mine.

Laboratory estimation of the Prandtl Limit: Results over a range of stress states are plotted on the compressive octahedral plane, and steady-state strain rates are contoured (Figure 3). A shear stress limit is clearly approached for the inclination of the isocreep lines.

This limit appears to be a horizontal line, unaffected by normal stress. We call it the Prandtl Limit, and it is different for different materials. It delineates the boundary between regions of stress space dominated by different deformation mechanisms, and is a valid criterion for design. It is not a classical Tresca, Mohr-Coulomb, or Bingham criterion. It is the shear stress level at which new mechanisms can be initiated, leading to a stronger dependency of the strain rate on the stress. Figure 3.4 in Poirier (1985) is particularly instructive: the lower corner point corresponds to our Prandtl Limit, the upper one the brittle yield. For a particular saltrock there is a unique deformation rate asso-ciated with the Prandtl Limit; this value is very low ($< 10^{-10}\ s^{-1}$), and cannot be easily determined in the laboratory. It will be determined in situ.

Field measurement of the Prandtl Limit and Prandtl Strain Rate: Laboratory strain rates are usually in excess of field strain rates, and it is not feasible to carry out tests at low strain rates, particularly if several materials are being tested for design purposes. Also, small variations in moisture content or crystal size between seemingly identical specimens can give a great deal of scatter at extremely low strain rates. For any significant project such as a mine, a square test room in virgin ground should be instrumented, excavated, and monitored for a long period. The benefits of field monitoring are that variations in material behavior are averaged volumetrically, and issues of sample treatment and laboratory methodology do not arise. A saltrock bed of thickness four or five times the room diagonal is preferred, and thick beds of strong elastic rock should be avoided. Pressure cells in tangential and radial directions are installed on at least one radius out a distance at least twice the room diagonal length, and multipoint extensometers are installed horizontally, vertically, and diagonally, and monitored periodically (Mraz and Dusseault, 1986).

Monitoring will show many things. First, the active opening boundary will be determined, and the circumferential shear planes (debonding) will be demonstrated, providing the opening is deep enough (> 500 m). Once steady state is approximated, usually within a year, the visco-plastic zone boundary, the uniform shear stress in that zone, and the strain rate at the zone boundary can be calculated (Mraz, 1984). It will be found that for a virgin ground opening at sufficient depth the active opening is a circumscribing circle, the viscoplastic zone shear stress is equal to the Prandtl Limit from the lab tests, and the strain rate in that zone is equal to the Prandtl Strain Rate.

Strain rates below the Prandtl Limit and modelling a case history: To predict the closure rate of a single test opening, knowledge of behavior below the Prandtl Limit is necessary as the entire rock mass is below that limit except for a small zone around the room. For a large mine, this is not the case: all pillars and significant zones in the abutments are near or at the Prandtl Limit (Fig. 4), so the effect of low shear stresses is minimized, and closure rates are due only to the strain rates of material near the Prandtl Limit. The nature of processes which dominate below the Prandtl Limit leads to a power-law equation with the strain rate independent of normal stress, but the exponent has been variously argued to be anywhere from 1 to 4.5 (Poirier, 1985). Field data are of great value, as experimental exponent determination would require a series of creep tests lasting many years because of extremely slow strain rates and data scatter.

Four years of virgin ground opening strains and stresses were available to model (Mraz and Dusseault, 1986). The creep law used in the finite element model was a compound "dogleg" power law, using a Prandtl Limit value of 8.8 MPa as the turning point, and a exponent of 6.0 above the limit, based on laboratory data (Fig. 5). The same form of law was employed below the dogleg, but with several values of exponent. An exponent of 1.0 seems to give an excellent match to the magnitude, distribution, and rate of strain. The value of the Prandtl Strain Rate used was 3.0×10^{-11}, determined from the extensometer data *in situ*. The opening geometry is given elsewhere (Mraz and Dusseault, 1986); a typical simulation result is shown in Figure 6.

These results are not "cooked": the Prandtl Limit and upper exponent were determined *a priori* in the laboratory, the Prandtl Strain Rate was determined directly *in situ*, and a low exponent has many advocates (Spiers *et al.*, 1986). *This "history match" in no way proves that the exponent is precisely 1.0, or even that it is a constant.* It is known that at shear stresses below the Prandtl Limit there are several processes acting (Langer, 1984) including solid vacancy diffusion, ionic diffusion along grain boundaries, liquid crystal mass transfer processes, recrystallization processes (lateral grain boundary migration) and perhaps others. To suppose that variations in these factors have no effect is nonsense. However, if none of them are dilational processes, it is conceivable that the value of the exponent remains the same, but that for different materials, the values of the Prandtl Limit and the Prandtl Strain Rate are changed, leading to different strain rates, but at the same exponent value. More instrumented rooms in different materials are required to address this contention.

Stated rigorously, de/dt being the strain rate:

$$de/dt = C_1 \, (\sigma_1 - \sigma_3)^m \; ; \; m \text{ probably} < 3.0 \quad \text{for } 2K < \sigma_1 - \sigma_3 \qquad \text{eq. 1A}$$

or, in the preferred normalized form:

$$\dot{e} / \dot{e}_K = [(\sigma_1 - \sigma_3)/2K]^m \qquad \text{equation 1B}$$

At the Prandtl Limit ($K = (\sigma_1 - \sigma_3)/2$), for pure polycrystalline halite and several potash ores of different mineralogy, the strain rate at the Prandtl Limit has been estimated as:

$$(de/dt)_K = 2 \times 10^{-11} \text{ to } 2 \times 10^{-10} \; ; \quad @ \; \sigma_1 - \sigma_3 = 2K \qquad \text{eq. 2}$$

$\sigma_1 - \sigma_3$ is the viscoplastic effective stress for triaxial compression, and K is the Prandtl Limit. Because *viscoplastic processes act at any shear stress level in saltrock*, there is no "threshold shear stress" required for steady state creep (Langer, 1984).

Creep mechanisms above the Prandtl Limit: At shear stresses above K (constant normal stress), ever higher (but still steady-state) strain rates are observed. The value of the exponent, *if* a power law is appropriate, is different for different materials. At intermediate confining stresses the data are difficult to correlate because of material differences, and large amounts of data are required. If a simple equation such as equation 1 is used, the exponent is variable and is quite large for unconfined conditions, where cracking is permitted with no normal stress promoting healing and suppressing dilational defect migration processes. High confining stress will suppress crack processes, and the exponent converges on some value, 3 to 4.5 being the expected range. An expression which fits the data better than others, and implicitly recognizes the multiple mechanisms is:

$$\dot{e} = \dot{e}_K \left| \frac{T}{K} \right|^m + \frac{T - K}{u} \left| \left(\frac{T}{N}\right) \right|^{\frac{nK}{N}} \qquad \text{for } T > K \qquad \text{equation 3}$$

where T is octahedral shear stress, N is octahedral normal stress, u is a normalized Bingham viscosity, K is the Prandtl Limit, n is an experimental constant, and the Prandtl Strain Rate is estimated as explained. Note that the processes below the Prandtl Limit are still acting, but at any significant shear stress, are totally overshadowed by the new processes triggered at 2K.

4 RUPTURE CRITERION

Brittle yield criterion: If a series of conventional strain-rate controlled uniaxial and triaxial tests are carried out over a range of strain rates and stress conditions, a lower bound brittle yield envelope is found. Because it is strain rate dependent, a reasonable definition must be stipulated: we define it as the locus of all points where strain-weakening rupture is achieved in a finite time before 10% strain is evidenced. Because strain weakening is evidence of coalescing crack processes, the curve is a conventional "failure criterion" of classical rock mechanics, and is expressed as follows:

$$\sigma_1 = (\sigma_c/2)\left[(1-mr) + \sqrt{(1+mr)^2 + 4m(\sigma_3/\sigma_t)}\,\right] \qquad \text{equation 4}$$

where r is the ratio of the tensile to unconfined short term strengths (subscripts t and c), and m is an empirical factor.

At high confining stresses, the brittle yield criterion becomes indefinable because strain-weakening cannot be achieved even at strain rates of 10^{-2} s^{-1} or faster. For example, this condition is reached at 15 MPa for a potash ore consisting of 50/50 sylvite and halite. The material behaves as a classic elastoplastic material, but the strain rates are extremely rapid at high confining and shear stresses. The strain rates associated with brittle yield are so high as to never be encountered in situ except shortly after room excavation, and in fact that is the reason for the rapid development of the active opening. The two limits, the Mohr-Coulomb Yield Limit and the Prandtl Limit, must not be confused; they are fundamentally different.

A comment on crack processes is appropriate. The brittle criterion approaches the Prandtl Limit very closely when there is no confining stress. We now understand that a saltrock begins to experience crack propagation phenomena and dilational dislocation movement when the Prandtl Limit is exceeded. However, providing there is some normal stress, the rheid behavior of saltrocks allows the cracks to heal, blunt, rotate, leading to steady state creep. The proof in part can be seen by the small amount of normal stress dependency of the strain rate, evidenced by the curvature of the isocreep lines in Figure 3. Because K is the lower limit of crack processes, it is a straight line with no normal stress dependency. The convergence of the Y and 2K criteria at the $\sigma_2=\sigma_3$ = 0.0 axis is not coincidental; if there is no confining stress, cracks have insufficient capability to heal. The meeting of the criteria is therefore rational. The ability to heal cracks at normal engineering stresses is the major difference between salt and silicate rocks. It is a major reason why we have proposed this new approach to a constitutive law for saltrocks.

The relationship of the conventional creep regimes to our proposed constitutive isothermal picture is now clearer: referring to Figure 7, primary or decelerating creep is not on the diagram because all data relate only to steady state or brittle yield; secondary creep (steady state) is characteristic of all stress states below the brittle yield line; and above that line, tertiary creep processes leading to strain-weakening rupture are possible. Primary creep we believe to be the internal stress reallocation of a stress change, and should be largely explainable by using the multiple mechanism law on a micromechanics model: we are currently attempting this numerically.

5 CONSTITUTIVE LAW PLOTTED IN STRESS SPACE

The specific equation form of the laws are as yet somewhat unclear, but the general relationship of the pertinent critical surfaces in three-dimensional stress axes is shown in Figure 8. These plots are in reference to steady state isothermal behavior only. Currently, the Prandtl Limit is plotted as a Von Mises rather than a Tresca criterion. A more detailed diagram (Fig. 9) of the triaxial compressive plane of Figure 8 contains information as to the behavioral regimes. This is no longer a conceptual plot: major aspects have been identified by laboratory tests and field monitoring.

6 SUMMARY

Evidence exists that an explicit multiple mechanism creep law is correct for saltrocks. The following approach is advocated:

1. Creep occurs at all shear stress levels, leading to geological time processes, but mined openings trigger different processes;
2. The Prandtl Limit and Prandtl Strain Rate are fundamental material parameters representing a change in creep mechanisms, hence they constitute the shear stress and viscosity parameters of a Tresca shape viscoplastic flow criterion, and a multiple mechanism law is required;
3. The Prandtl Limit (K) is the activation shear stress necessary to trigger processes of dilational dislocation movement and crack growth, which are both affected by normal stress levels;
4. Below 2K, a power law with a low exponent (1 to 3) seems best; above 2K, it is not yet clear how to represent the range of strain rates observed;
5. 2K can be determined in the laboratory and confirmed in the field; processes above 2K can be tested in the laboratory easily; processes below 2K are so slow that field determination is recommended; and,
6. The rupture criterion is a classical curved Mohr-Coulomb surface, typical of processes of crack generation and crack coalescence.

7 ACKNOWLEDGMENTS

Denison Mines and CANMET have supported parts of this work. MBD and LR specifically thank the Natural Sciences and Engineering Research Council of Canada for their unflagging support of academic endeavor. Special thanks to Steve Marcus, without whose help the learning process would have been much slower. Jim Baleshta, John Unrau, Mike Souliere, and Chris Fordham have all helped greatly.

Langer, M. 1984. The Rheological Behavior of Rock Salt. Proceedings of the First Conference on the Mechanical Behavior of Salt, eds: Hardy, H.R. and Langer, M., Trans Tech Publications, pp 201-240.

Mraz, D.Z. 1984. Solutions to pillar designs in plastically behaving rocks. CIM Bulletin, V. 77, 868, pp 55-62.

Mraz, D.Z. and Dusseault, M.B. 1986. Long Term Behavior of a Test Room in Potash. In: Rock Mechanics: Key to Energy Production, Proceedings of the 27th US Rock Mechanics Symposium, pp 405-414.

Munson, D.E. and Fossum, A.F. 1986. Comparison between Predicted and Measures South Drift Closures at the WIPP Using a Transient Creep Model for Salt. In: Rock Mechanics: Key to Energy Production, Proceedings of the 27th US Rock Mechanics Symposium, pp 931-939.

Poirier, J.-P. 1985. Creep of Crystals (High temperature deformation processes in metals, ceramics and minerals). Cambridge Earth Science Series, Cambridge University Press, Cambridge, 260 pages.

Skrotzki W. and Haasen, P. 1984. The role of cross-slip in the steady-state creep of salt. 2d Conf on the Mechanical Behavior of Salt, Hannover, preprint.

Spiers, C.J., Urai, J.L., Lister, G.S., Boland, J.N. and Zwart, H.J. 1986. The influence of fluid-rock interaction on the rheology of salt rock. Report of Research for the Commission of the European Communities, Nuclear Sci. and Tech. Rept. EUR 10399 EN. 131 pages.

Wallner, M. 1984. Analysis of Thermomechanical Problems Related to the Storage of Heat Producing Radioactive Waste in Rock Salt. Proceedings of the First Conference on the Mechanical Behavior of Salt, eds: Hardy, H.R. and Langer, M., Trans Tech Publications, pp 740-763.

Wawersik, W.R. 1985. Determination of Steady State Creep Rates and Activation Parameters for Rock Salt. In Measurement of Rock Properties at Elevated Pressures and Temperatures, Special Technical Publication 869, ASTM, Philadelphia, pp 72-92.

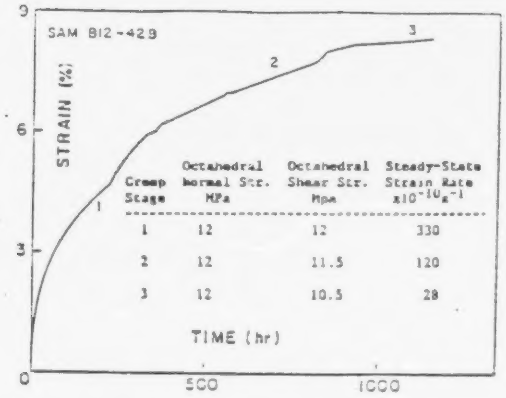

Creep Stage	Octahedral Normal Str. MPa	Octahedral Shear Str. Mpa	Steady-State Strain Rate $x10^{-10}s^{-1}$
1	12	12	330
2	12	11.5	120
3	12	10.5	28

FIG. 1 STAGE CREEP TESTS

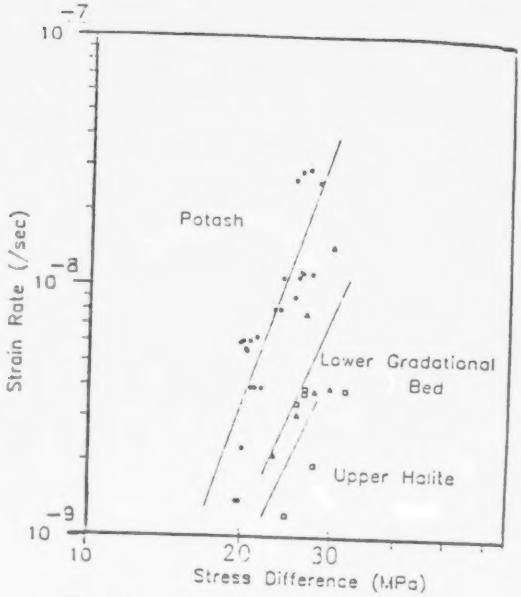

FIG. 2 STRESS DIFFERENCE vs. STRAIN RATE

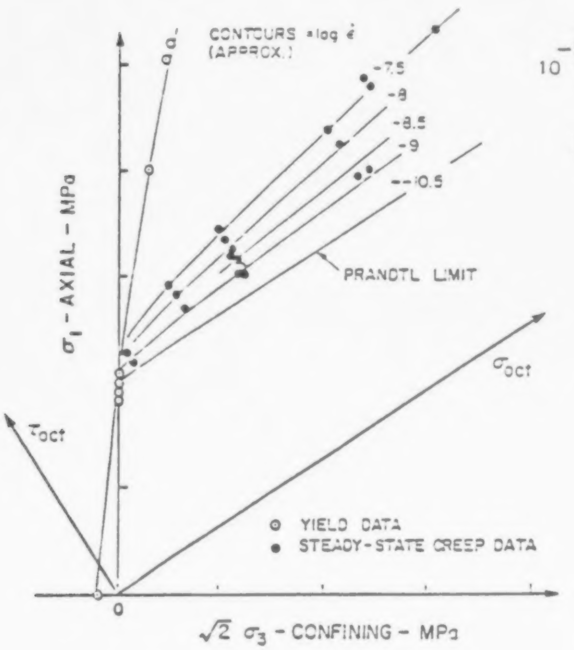

FIG. 3 YIELD AND CREEP DATA, DOMAL HALITE

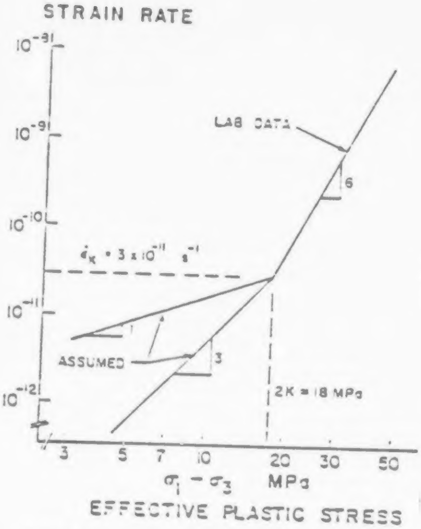

FIG. 5 CREEP LAW USED IN MODELLING

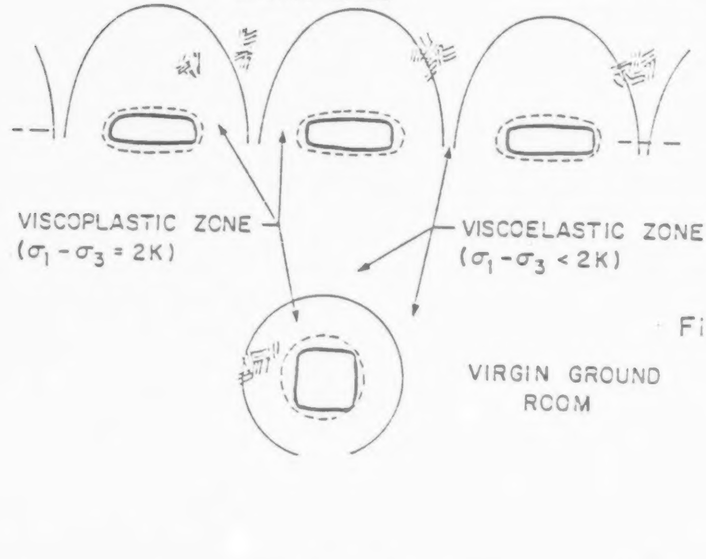
MINING CASE
VISCOPLASTIC ZONE ($\sigma_1 - \sigma_3 = 2K$)
VISCOELASTIC ZONE ($\sigma_1 - \sigma_3 < 2K$)
VIRGIN GROUND ROOM

FIG. 4 MINING AND VIRGIN CONDITIONS

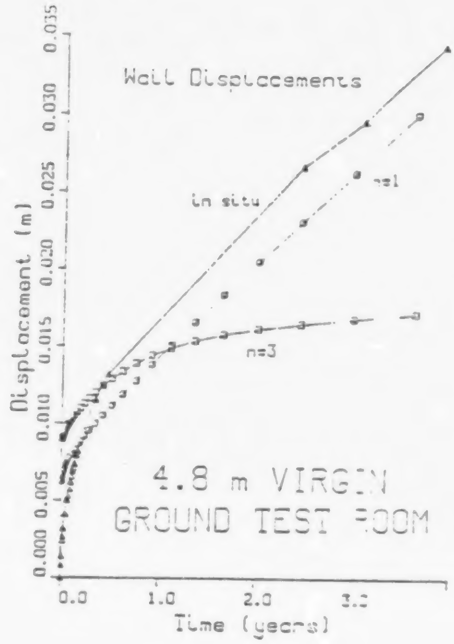

FIG. 6 NUMERICAL SIMULATION RESULTS

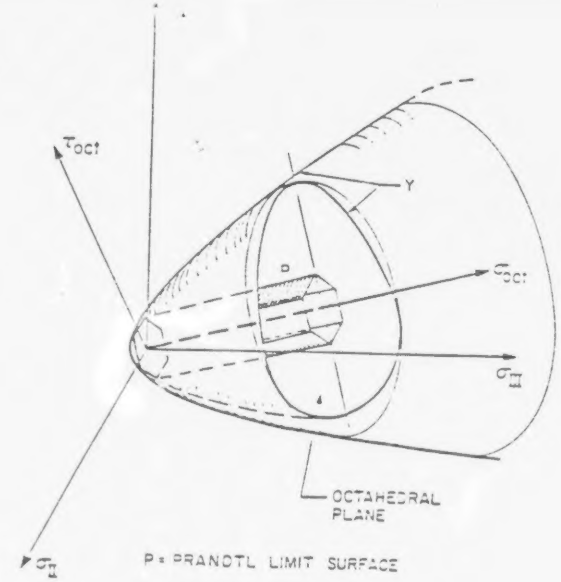
τ_{oct}
Y
P
σ_{oct}
σ_{II}
OCTAHEDRAL PLANE
σ_{II}
P = PRANDTL LIMIT SURFACE

FIG. 8 THREE - DIMENSIONAL SURFACES

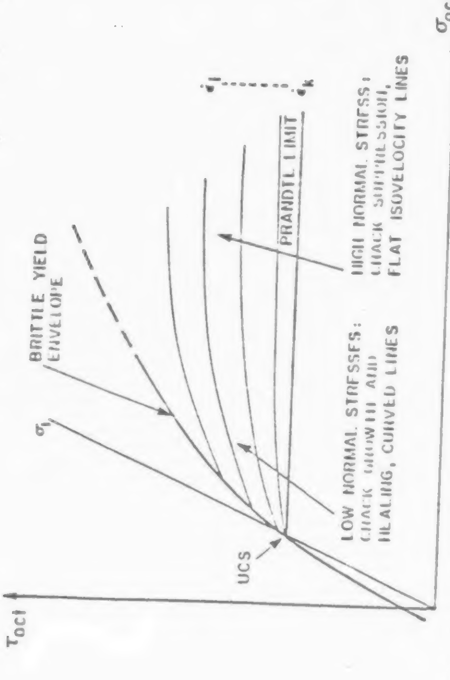
τ_{oct}
σ_{oct}
σ_1
BRITTLE YIELD ENVELOPE
UCS
LOW NORMAL STRESSES: CRACK GROWTH AND HEALING, CURVED LINES
HIGH NORMAL STRESS: CRACK SUPPRESSION, FLAT ISOVELOCITY LINES
PRANDTL LIMIT
K

FIG 7 THE EFFECT OF NORMAL STRESS ON CREEP RATE

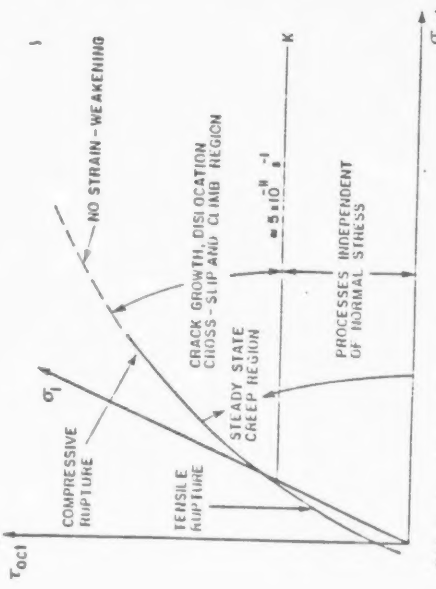
τ_{oct}
σ_{oct}
σ_1
NO STRAIN-WEAKENING
CRACK GROWTH, DISLOCATION CROSS-SLIP AND CLIMB REGION
$\approx 5\times10^{-8}\ s^{-1}$
PROCESSES INDEPENDENT OF NORMAL STRESS
STEADY STATE CREEP REGION
COMPRESSIVE RUPTURE
TENSILE RUPTURE
K

FIG 9 PROCESS REGIONS

APPENDIX C

MPC Mraz Project Consultants Ltd.
410 Jessop Avenue, Saskatoon, Saskatchewan Canada, S7N 2S5 Phone (306)955-0240

EFFECTS OF GEOMETRY ON THE BEARING CAPACITY OF PILLARS IN SALTROCK

By:

Dennis Z. Mraz, P. Eng.
Mraz Project Consultants Ltd
Saskatoon, Saskatchewan

And:

Maurice B. Dusseault
University of Waterloo
Waterloo, Ontario

Presented At

CIM RMSCC Workshop
Saskatoon, Saskatchewan
November, 1986

EFFECTS OF GEOMETRY ON THE BEARING CAPACITY OF PILLARS IN SALTROCK

BY

Dennis Z. Mraz, P.Eng.
Mraz Project Consultants Limited
Saskatoon, Saskatchewan, CANADA, S7N 2S5

and

Maurice B. Dusseault, P.Eng.
Departments of Earth Sciences and Civil Engineering
University of Waterloo
Waterloo, Ontario, CANADA, N2L 3G1

ABSTRACT

Excavations in saltrocks will exhibit continuous modification of shape due to a combination of time-dependent deformation and yield mechanisms. The rapidity of the change and the geometrical shape of the modified mine opening ("active opening" as we call it) depend on rock properties, virgin stress level, extraction ratio, and mining sequence. In turn, the shape of the active opening has a substantial effect on the stress distribution in mine pillars. Processes leading to the development of the active opening and its role in pillar load capacity are described and a pillar evaluation procedure is proposed. This new approach is based on continuum mechanics as dictated by _in situ_ measurements.

There are three important cases to consider in active opening development: the case of high initial stress, the case of low initial stress, and the intermediate condition where initially the salt rock is not exposed to stresses much beyond failure, but will be at a later stage in the mine life.

CASE I

The major principal stress near the opening at the time of excavation can substantially exceed the limiting strength criterion. This typically occurs in two cases: excavation in virgin areas of deep mines where stresses have not been relieved; and, in excavations in abutment pillars or bearing pillars which are supporting transferred loads from previously mined areas.

The following limiting strength criterion is employed (Figure 1):

$$\sigma_1 = \frac{1}{2}\sigma_C\left[(1-sr) + \sqrt{(1+sr)^2 + 4s\,\frac{\sigma_3}{\sigma_C}}\right] \qquad (1)$$

$$r = \frac{\sigma_T}{\sigma_C}$$

σ_1 ... major principal stress,
σ_3 ... minor principal stress,
σ_C ... uniaxial compressive strength at long time,
σ_T ... tensile strength, and,
s ... an empirical factor.

This criterion has been developed from actual test data by Rothenburg (1986), and corresponds to a parabolic shape. Note that there is no reduction factor included to account for the degree of jointing of the rock; intact salt rock is unjointed, therefore no strength reduction factor for "brokenness" is required. This is an important and fundamental difference between saltrock and hard rock: the former is amenable to continuum analysis, the latter requires assessment of a blocky or discontinuous mass.

Upon excavation, this failure criterion is immediately exceeded around the opening, but the damage is limited to the active opening, provided that the loads can be effectively transferred to other intact areas of the mine such as confined pillars and abutments. As a rule, shear fracture occurs along segments which are approximately circular (Figure 2), where

$$a_v = \frac{1}{\sqrt{2}} h \tag{2}$$

$$a_h = \frac{1}{\sqrt{2}} v \tag{3}$$

The initial dimensions of the active opening depend on the height (v) and width (h) of the actual opening at the time of excavation. If the shape of the actual opening is not subsequently altered, the horizontal and vertical dimensions of the active opening will be:

$$2d = h + (\sqrt{2} - 1)\, v \tag{4}$$

$$2b = v + (\sqrt{2} - 1)\, h \tag{5}$$

Material outside the active opening is in a state of general compression and differential stress, and it will creep uniformly (viscously) from all directions if the following conditions are met: the stress is fully redistributed (steady state); the salt mass is homogeneous, isotropic and large with respect to the opening; and, the segments within the active opening are fully detached. The last two conditions are rarely fully met, therefore minor variations are to be expected. The assumption of full detachment leads to conservative design, as partial attachment will provide a small extra support component. In any case, these conditions are reasonably approximated in many cases.

As the general creep continues, the dimensions of the active opening are modified as follows (Figure 3):

$$2d_1 = (h-C) + (\sqrt{2} - 1)(v-C) \tag{6}$$

$$2b_1 = (v-C) + (\sqrt{2} - 1)(h-C) \tag{7}$$

C ... total closure since excavation

CASE II

In very shallow excavations in saltrock, the major principal stresses at the time of excavation are well below the limiting strength criterion (Equation 1). Initially there is no failure and no inwards curvature of the walls of the opening. However, very slow creep movement occurs nonetheless because saltrocks can creep at any differential stress level. Because the shape of openings is in general incompatable with zero volume change creep, which is an ideally viscous process, stress concentrations will develop in corners, resulting in gradual development of fractures as the opening surfaces develop inwards curvature (Figure 4). The severity of the fracturing depends on the stress level and closure rate. For large closures, which may take considerable times under these low stress conditions, the material within the active opening may fail in tension, as slabs of unconfined material will tend to buckle. However, the original pillar remains intact, as the fracture only occurs within the material which has moved into the original actual opening. Yield in this case is governed by the differences in confinement rather than overstress.

Assuming the wall curvature can be approximated by a circular arc:

$$(a - \frac{C}{2})^2 + (\frac{v}{2} - \frac{C}{2})^2 = a^2 \tag{8}$$

hence,

$$a_h = \frac{v^2}{4C} - \frac{v-C}{2} \tag{9}$$

and similarly,

$$a_v = \frac{h^2}{4C} - \frac{h-C}{2} \tag{10}$$

CASE III

The intermediate case is the one where the stresses at time of excavation are close to the yield point, causing incompletely developed or latent fractures, which may become fully detached at a later time. This can occur in intermediate virgin ground depth excavations, or in excavations in partially stress relieved zones using multiple entry systems. In these circumstances, the excavation sequence of adjacent rooms and the consequences of load transfer can result in the full development of the fractured zone, and in the normal conservative approach to engineering design, it is appropriate to assume that the active opening takes the shape of an ellipse with conjugate diameters equal to the diagonals of the mine opening (Mraz, 1984):

$$b = \frac{1}{\sqrt{2}} v \tag{11}$$

$$d = \frac{1}{\sqrt{2}} h \tag{12}$$

$$b_1 = \frac{1}{\sqrt{2}} (v-C) \tag{13}$$

$$d_1 = \frac{1}{\sqrt{2}} (h-C) \tag{14}$$

This case does not differ appreciably from the case of the high initial stresses and the analysis for that case can be applied. The analysis should consider the maximum stresses to be expected when full overburden load is re-established on the pillars.

STRESS DISTRIBUTIONS IN PILLARS

Analytic stress solutions for the two limiting cases will now be developed. Analytic solutions are only possible for simple geometries, and the derivations will be for the case of very long pillars which approach plane strain conditions. Previous experience has shown this to be the most efficient geometry if designed correctly, more efficient than circular or square pillars due to increased confinement at the pillar core.

For an analysis of pillar stresses, a behavioral law is required for the stress distribution at steady state. This law is to be combined with the geometry and virgin stress information to give the pillar stress distribution. Two behavioral laws for plasticity are analytically convenient and are sufficient approximations of reality (Mraz, 1984); the ideally plastic substance and the generalized plastic substance. For the latter:

$$\tau = K + \sigma(F) \qquad (15)$$

τ ... shear stress,
σ ... normal stress,
K ... activation shear stress (Prandtl Limit),
F ... constant describing the effect of normal stress on the plastic yield shear stress.

(The latter constant was formerly called the tangent of internal plastic friction angle by Mraz and Dusseault, 1983.)

In the case of an ideally plastic substance, the yield point is defined not by a curve as above, but by a single yield parameter related to the shear stress level. If it is a Tresca criterion, it is the maximum shear stress that governs. If it is a Von Mises criterion, the mean shear stress governs.

$$\tau = \kappa \qquad (16)$$

τ ... shear stress in the body,
κ ... ideally plastic shear stress

THE VISCOPLASTIC PILLAR

The criteria stated in equations 15 and 16 are identical at low normal stress ($K = \kappa$), but the latter is more conservative for engineering design if $\tau = \kappa$ is stipulated because it assumes that the yield level does not increase with normal stress but remains constant and approximately equal to the limiting strength criterion at boundary. Assuming the radius of curvature of the active opening boundary (a) in the horizontal direction controls the stress distribution in that direction:

$$\sigma_1 = \sigma_v = 2\kappa(1+ln(\frac{r}{a})) \qquad (17)$$

$$\sigma_3 = \sigma_h = 2\kappa(ln(\frac{r}{a})) \qquad (18)$$

σ_v ... vertical stress across horizontal plane,
σ_h ... radial stress along horizontal plane.

At steady state (equilibrium), the load per unit width carried by the pillar is the sum of the stresses, hence:

$$L_M = \int_0^p \sigma_v dr = 2\int_a^{r_q} \sigma_v dr + 2\int_{r_q}^{q+r_q} \sigma_v dr \qquad (19)$$

If the pillar is very thick, there is a "viscoelastic" core within which the shear stresses are less than the plastic yield limit. An approximation has been made for simplicity to account for the component of vertical stress in the viscoelastic core.

The integral in equation 19, when applied to this general case, gives the following result for the ideally plastic substance:

$$L_M = 4K\,[q + (r_q + q)\ ln \frac{r_q}{a}] \qquad (20)$$

where all the relevant geometries are defined in Figure 5.

The maximum long-term load that a pillar will ever bear in a real situation is the full overburden load; that is, the virgin lithostatic tributary load:

$$L_o = \sigma_o p \qquad (21)$$

And, equating 20 and 21 for equilibrium conditions:

$$\frac{\sigma_o}{2K} = \frac{2}{p}\,[q + (r_q + q)\ ln \frac{r_q}{a}\ ] \qquad (22)$$

If the following relationships are defined:

$M = \frac{m}{v}$ ... pillar width-to-height ratio, (23)

$R_o = \frac{\sigma_o}{2K}$ ... virgin stress ratio, (24)

$E = 1 - \frac{m}{p}$ ... extraction ratio, and, (25)

$Q = \frac{2q}{p}$ ... elastic core to spacing ratio, (26)

and substituted into equation 22, noting that (Figure 2):

$$r_q = \frac{m + v}{2} - q \qquad (27)$$

we obtain:

$$R_o = Q + \left[\frac{(M+1)(1-E)}{M}\right] \ln\left[\frac{1}{\sqrt{2}} + \frac{M}{\sqrt{2}}\left(1 - \frac{Q}{1-E}\right)\right] \qquad (28)$$

This expression is an explicit solution for the required width-to-height ratio of a salt rock pillar defined in terms of virgin stress ratio (initial overburden divided by the plastic yield stress limit), radius of curvature of the active opening, and all relevant geometry including extraction ratio and room height. It is solved and presented in Figure 6. The effect of width-to-height ratio on the size of the viscoelastic core can be easily evaluated.

If the width of the central viscoelastic zone is zero (i.e.: 2q = 0), then the pillar is fully in a viscoplastic state and the actual shear stress throughout the pillar is greater than K:

$$\frac{\sigma_n}{2\kappa} = \frac{2\, r_a}{p} \ln \frac{r_n}{a} = \frac{(M+1)(1-E)}{M} \ln \frac{M+1}{\sqrt{2}} \tag{29}$$

Pillars must be sized with these principles, keeping in mind that ignoring them may lead to excessively rapid closure which can result in extensive damage and poor safety conditions. The effect of geometry is all-important in saltrock pillar and room design. In this derivation, the explicit inclusion of full geometry, the inclusion of stress state, and the introduction of a critical and fundamental material parameter in one equation which gives reasonable results is to our knowledge novel.

THE FULLY VISCOELASTIC PILLAR

If the actual shear stress at the pillar edge is less than the Prandtl Limit, the whole pillar is in a viscoelastic state. At zero confining stress, the Prandtl Limit is approximately equal to the long-term unconfined compressive strength, therefore no portion of the pillar can possibly exceed the limiting strength. However, as slow creep continues, tensile fractures may develop, particularly if the stress difference is close to the plastic yield limit (2K). Substituting 9 and 10 into the equilibrium statement (22) gives:

$$\kappa = \frac{\sigma_o p}{\left[\frac{v^2}{C} + 2(m+C-v)\right] \ln\left(1 + \frac{m}{\frac{v^2}{2C} - v + C}\right)} \tag{30}$$

Defining the following ratios

$$\bar{\varepsilon} = \frac{C}{v} \quad \text{... average pillar strain, and} \tag{31}$$

$$R_K = \frac{\kappa}{K} \quad \text{... shear stress ratio } (< 1.0), \tag{32}$$

and substituting these and equations 23 to 26 into 30 gives:

$$R_K = \frac{2MR_o}{(1-E)\left[\frac{1}{\varepsilon} + 2(M + \bar{\varepsilon} - 1)\right] \ln\left(\frac{2M\bar{\varepsilon}}{2\bar{\varepsilon}(\bar{\varepsilon} - 1) + 1} + 1\right)} \tag{33}$$

This equation is solved and presented in Figure 7 for a number of reasonable cases. It shows that the load bearing capacity of a pillar in a situation where the stresses in it are everywhere less than the Prandtl Limit will clearly increase as strain increases. This results in ever-slowing closure rates because the pillar width-to-height ratio increases with time. Although the closure rates decrease with time, it is clear that this is a geometric effect, not a fundamental strain-hardening or time-hardening characteristic of the salt. This observation is general: decreases in closure rates in the field are due to increases in pillar width to height ratio as the result of viscous flow.

DISCUSSION

To this point the significance of the parameter K has not been discussed. Figure 8 shows a schematic diagram with the principal stresses along the axes of what is referred to as "stress space". There is a central cylinder and an exterior paraboloid which is slightly triangular in shape, but both are centered around the line which represents the "hydrostatic" stress condition. The paraboloid is the three-dimensional equivalent of equation 1: it is a limiting strength criterion for the condition of brittle rupture. The inner cylinder represents the Prandtl Limit, which is the surface below which only viscoelastic creep occurs, and which can be considered as a classical Von Mises criterion for initiation of viscoplastic behavior. It is the three-dimensional equivalent of eq. 16 at $\kappa = K$. If the stresses in the pillar are on or slightly above this surface, creep processes are more rapid, and are classified as viscoplastic.

Reference to the Prandtl Limit as an activation stress has been made (equation 15) because it is the shear stress level required to activate a new set of creep mechanisms which result in much more rapid deformation. In order for the pillar to remain in kinematic equilibrium, stresses in the pillar must redistribute themselves at that activation shear stress level. This redistribution is what we observe as the initial rapid deformation in mine pillars. It is the essential mechanical response required to establish viscous flow compatiblity in the pillar. The initial rapid movements in laboratory specimens (primary creep) as well as in the field are not evidence of different mechanisms than those controlling steady state creep: they are simply internal structural responses required to distribute load equally to the polycrystalline mass. Once load is shared equitably, steady state ensues.

If there is no viscoelastic core and the pillar stress difference exceeds 2K, the stresses must stabilize at some value higher than 2K to carry the load, and more rapid deformation ensues. The stress distribution within the pillar will exactly correspond to that required to achieve kinematic compatability, given the more rapid creep rates due to elevated shear stresses. Of course, this assumes that there are no adjacent pillars onto which excess load can be shed, which is never the case. In mine situations, there are other mine elements onto which loads are shed, and stress redistribution is effected through complex interaction of pillars, roof, floor, and abutments.

The design conditions presented herein are realistic for plane-strain pillars at steady-state once overburden loads are fully reimposed. This is because of the robustness of the assumptions which have been confirmed by in situ measurements of stresses and displacements. Also, since the equilibrium analysis is of the critical cross-section of the pillar, there is no worse case. Nevertheless, the analysis cannot include the effect of pillar interaction with overlying and underlying viscoplastic, viscoelastic, or elastic strata. This requires a full three-dimensional numerical solution of a viscoplastic assembly; a challenging but entirely feasible task with current computing tools.

CONCLUSIONS

Various cases of opening geometries encountered in saltrock mines have been outlined in this paper. The differing geometries depend largely on virgin stress states and the interaction of room and pillar geometry. The plane strain analytic solutions presented apply to an equilibrated steady-state condition when the overburden loads are all returned to the pillars. This is the required case to study to assure long-term mine health. Similar analytic approaches can be developed for other simple pillar geometries, but the very long pillar is by far the most efficient geometry in actual mine conditions, and must be used whenever possible to maximize extraction ratio and mine safety.

REFERENCES

Mraz, D.Z. 1984. Solutions to pillar design in plastically behaving rocks, Bulletin of the CIM, 77, 868, 55-62.

Mraz, D.Z. and Dusseault, M.B. 1983. Method of Correlation of Laboratory Tests with In Situ Conditions, Proceedings of the Sixth International Symposium on Salt, Toronto, Vol. 2, 259-268.

Rothenburg, Leo 1986. Personal communication, University of Waterloo, Waterloo, Ontario.

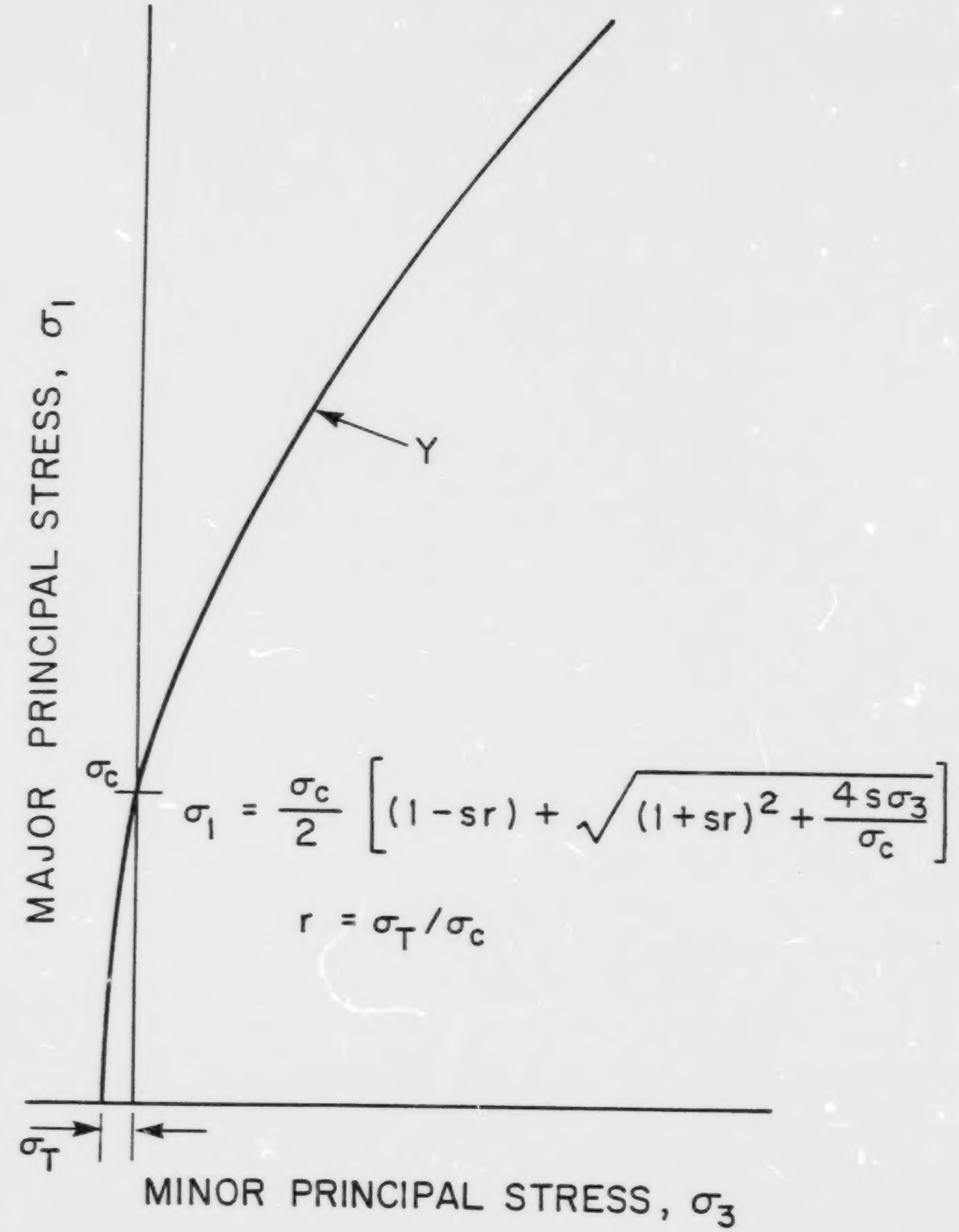

FIG. 1 LIMITING STRENGTH CRITERION

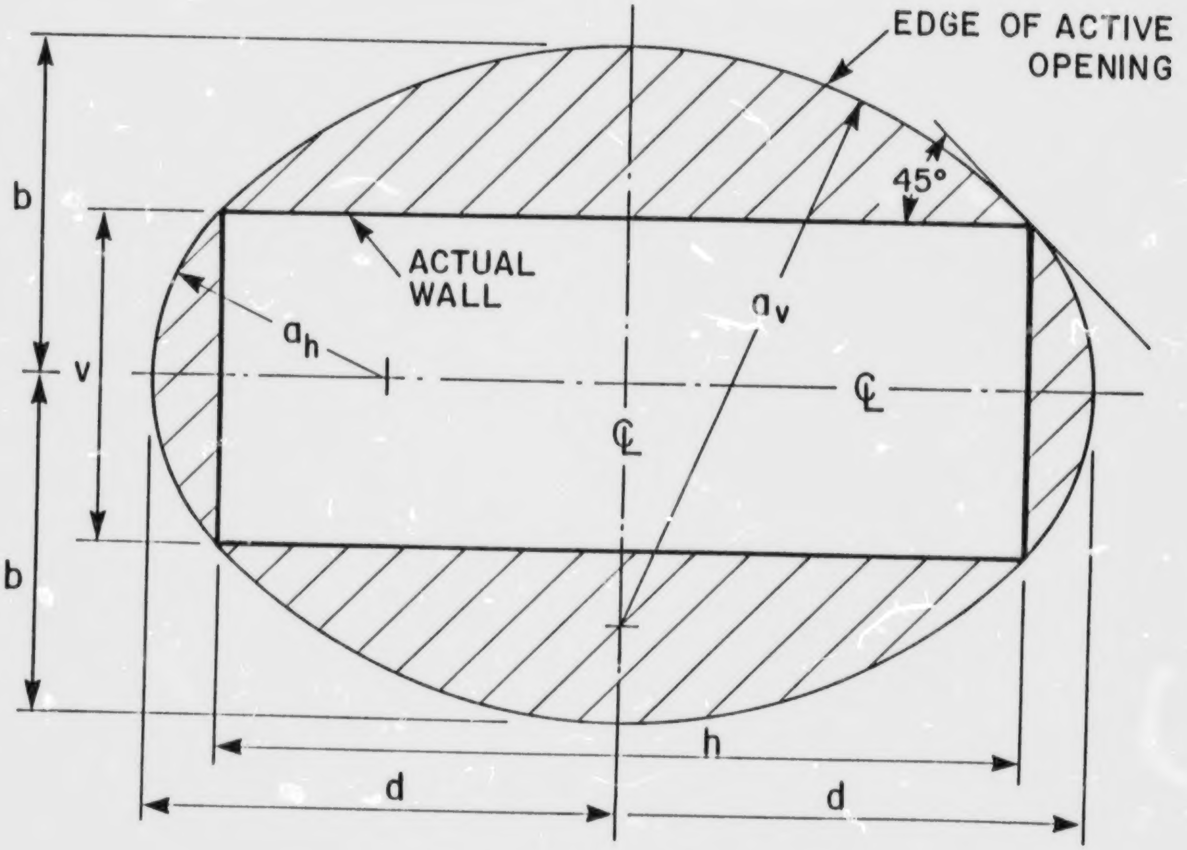
EDGE OF ACTIVE OPENING
45°
ACTUAL WALL
a_v
a_h
b
v
b
℄
℄
h
d
d

FIG. 2 ACTIVE OPENING GEOMETRY DUE TO OVERSTRESS -CASE I

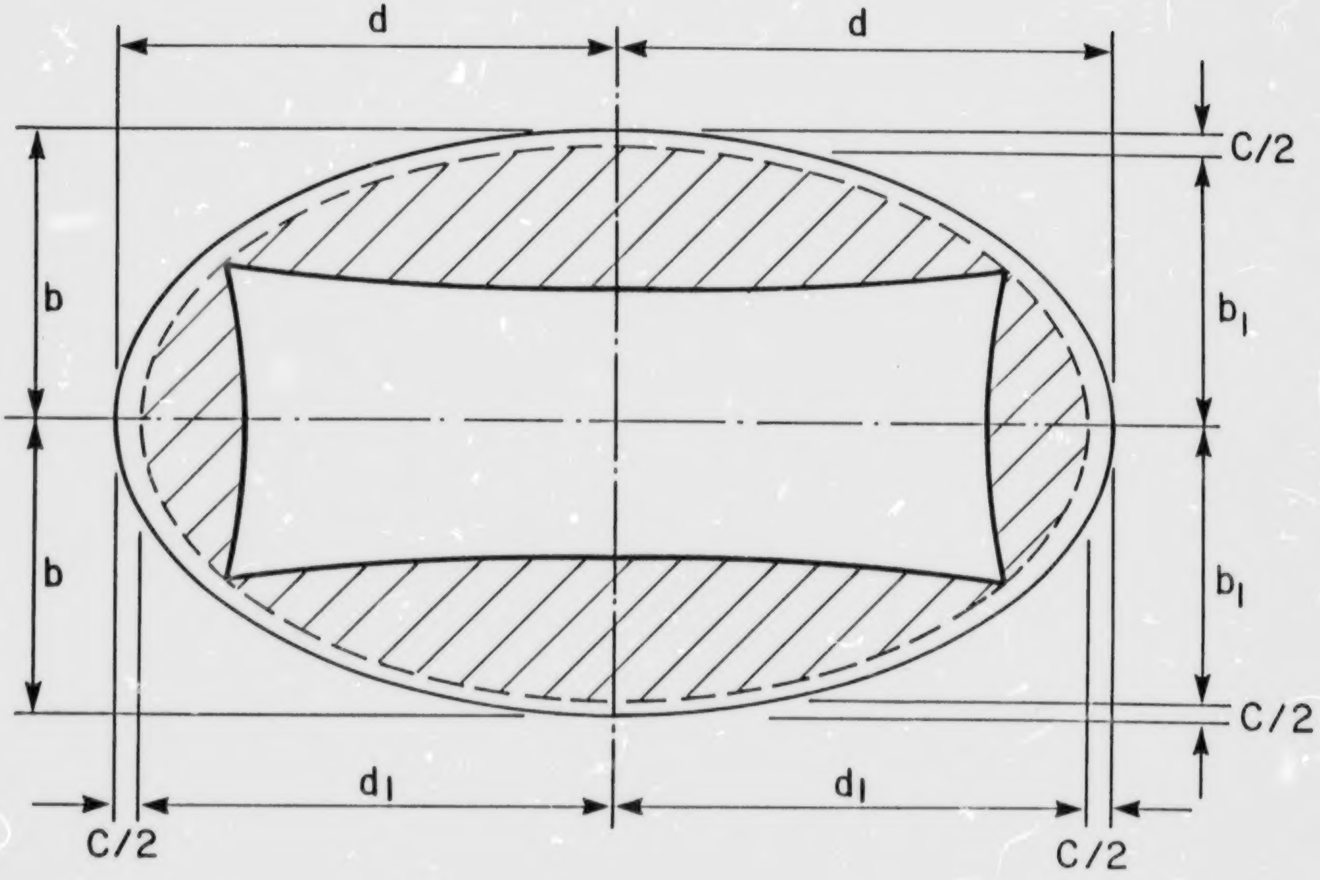
d
d
b
b
b_1
b_1
C/2
C/2
d_1
d_1
C/2
C/2

FIG.3 ACTIVE OPENING GEOMETRY AFTER CLOSURE – CASE I

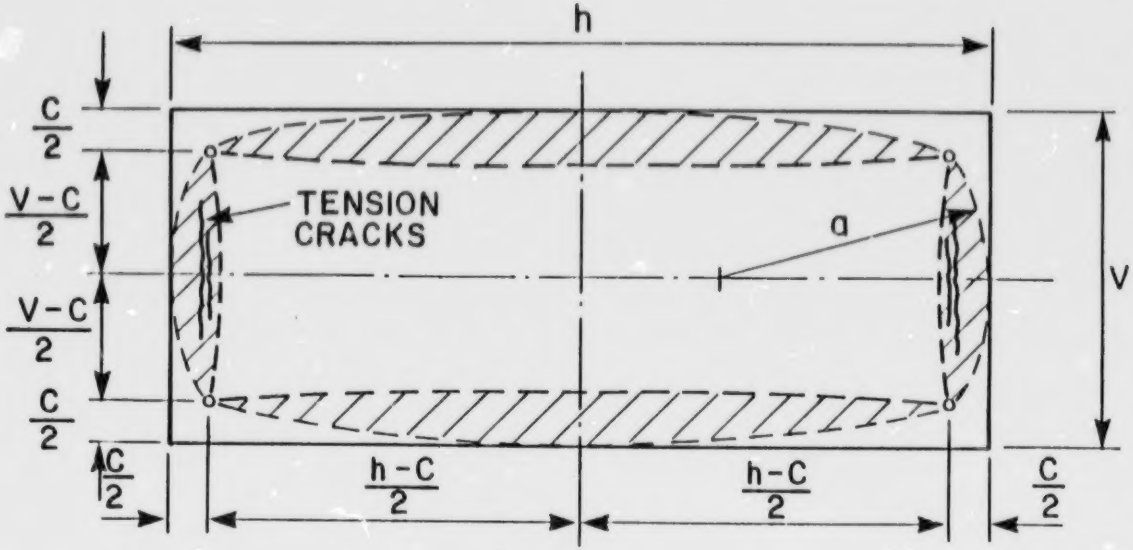

h
C/2
V-C/2
V-C/2
C/2
C/2
TENSION CRACKS
a
V
h-C/2
h-C/2
C/2

FIG. 4 ACTIVE OPENING GEOMETRY DUE TO SLOW CLOSURE AT LOW STRESS - CASE II

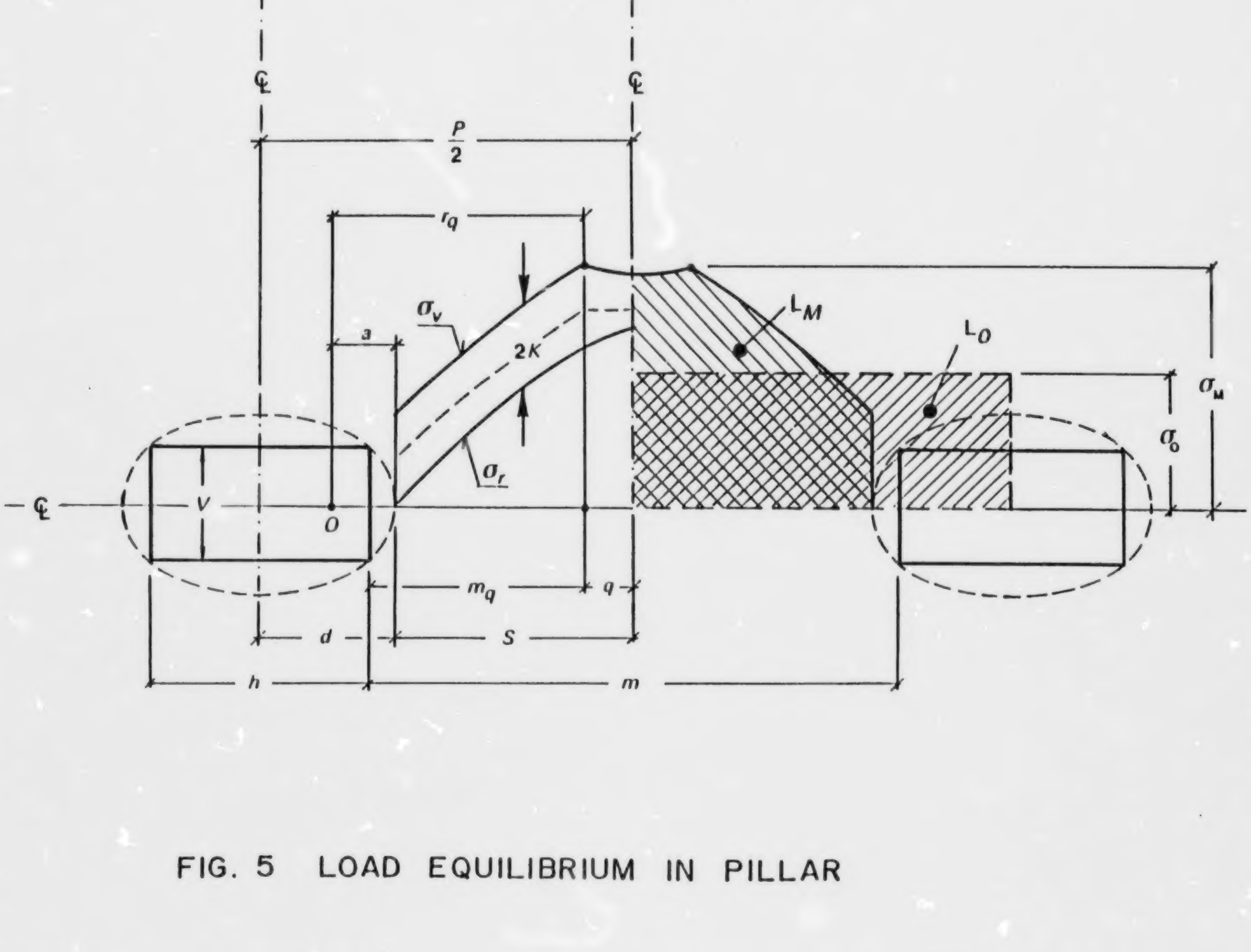
℄
℄
P/2
r_q
σ_v
2K
a
L_M
L_O
σ_M
σ_o
σ_r
— ℄
V
O
m_q
q
d
S
h
m

FIG. 5 LOAD EQUILIBRIUM IN PILLAR

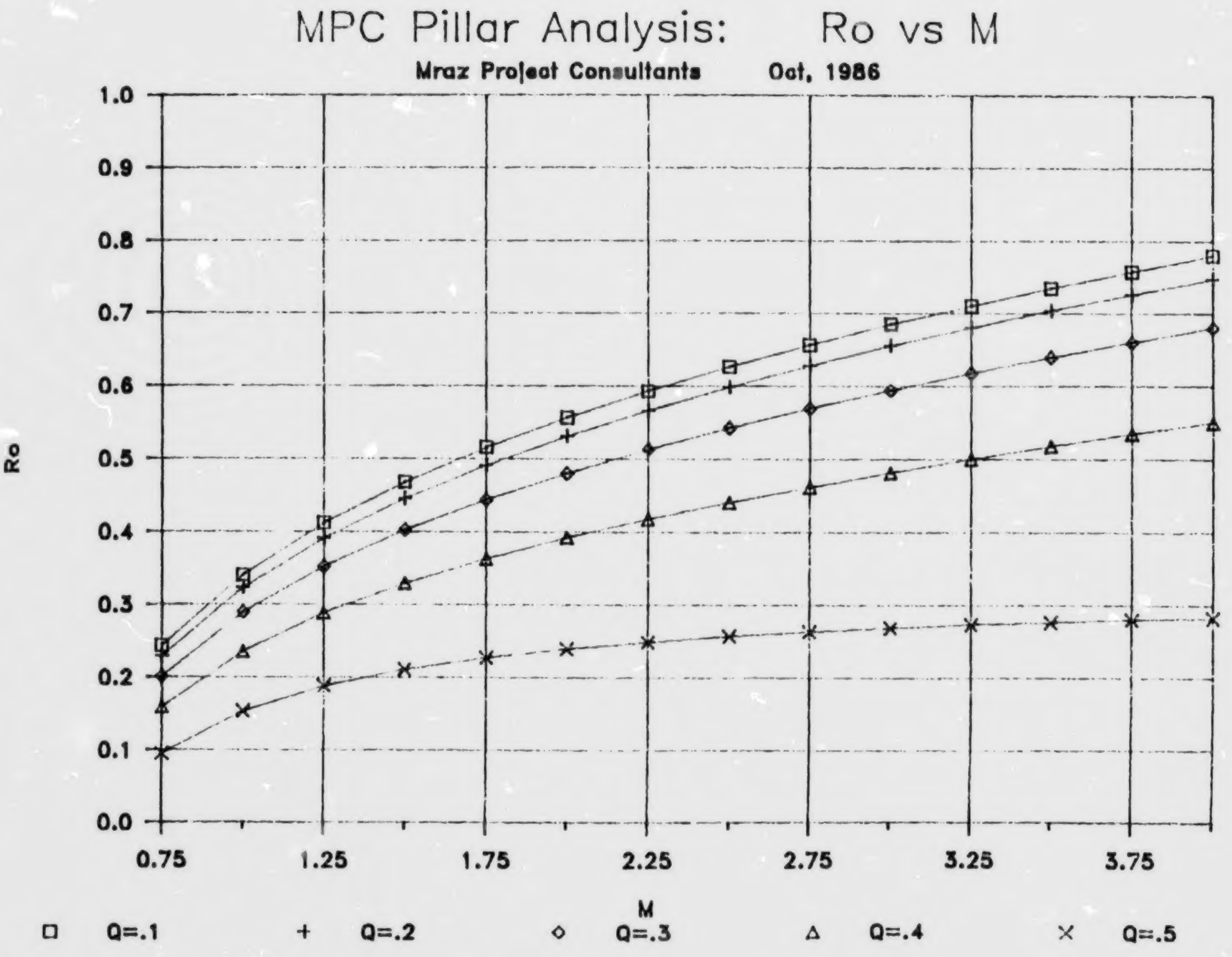
MPC Pillar Analysis: Ro vs M
Mraz Project Consultants Oct, 1986
Ro
1.0
0.9
0.8
0.7
0.6
0.5
0.4
0.3
0.2
0.1
0.0
0.75
1.25
1.75
2.25
2.75
3.25
3.75
M
□ Q=.1
+ Q=.2
◇ Q=.3
△ Q=.4
× Q=.5

FIGURE 6

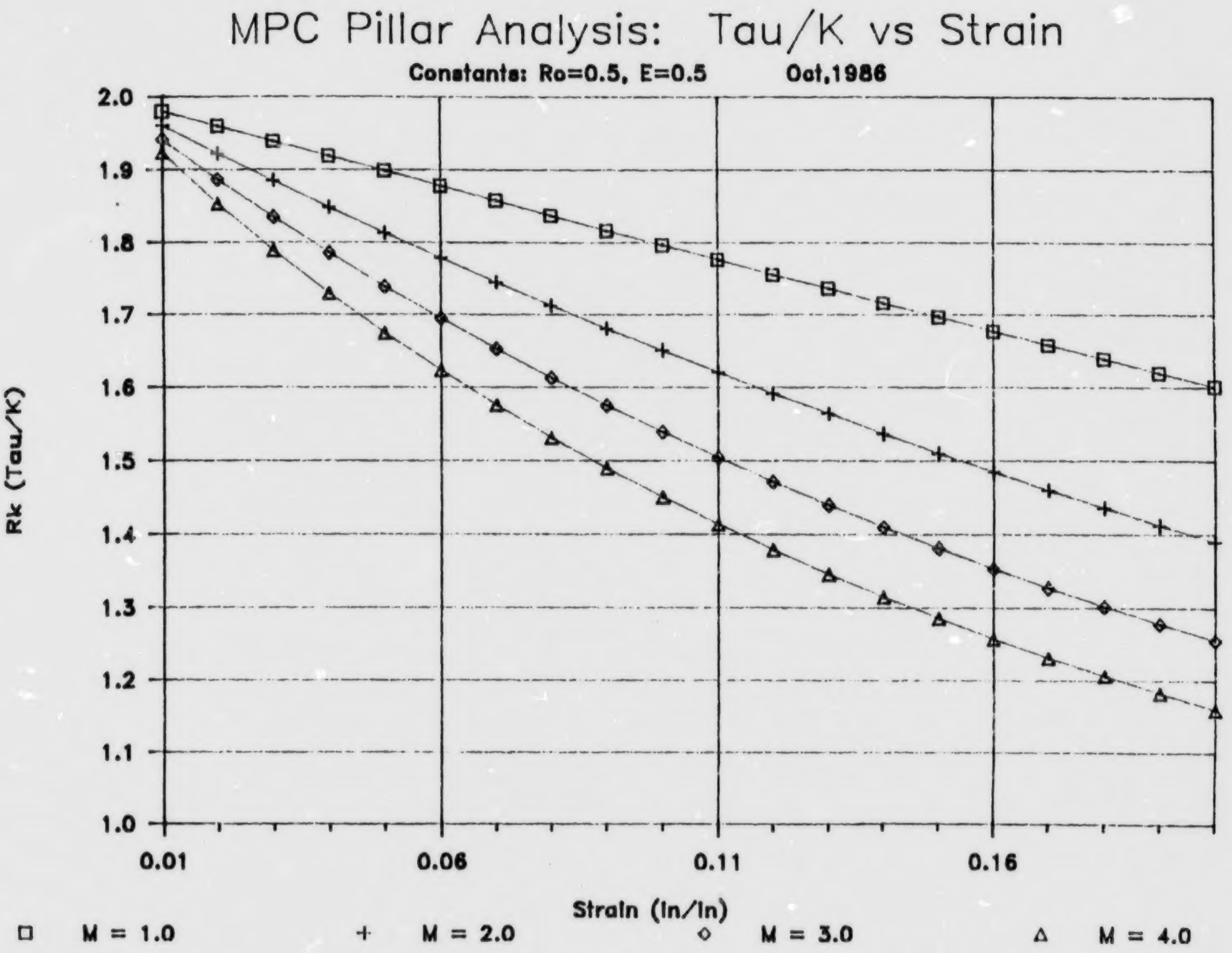
MPC Pillar Analysis: Tau/K vs Strain
Constants: Ro=0.5, E=0.5
Oct,1986
Rk (Tau/K)
2.0
1.9
1.8
1.7
1.6
1.5
1.4
1.3
1.2
1.1
1.0
0.01
0.06
0.11
0.16
Strain (In/In)
□ M = 1.0
+ M = 2.0
◇ M = 3.0
△ M = 4.0

FIGURE 7

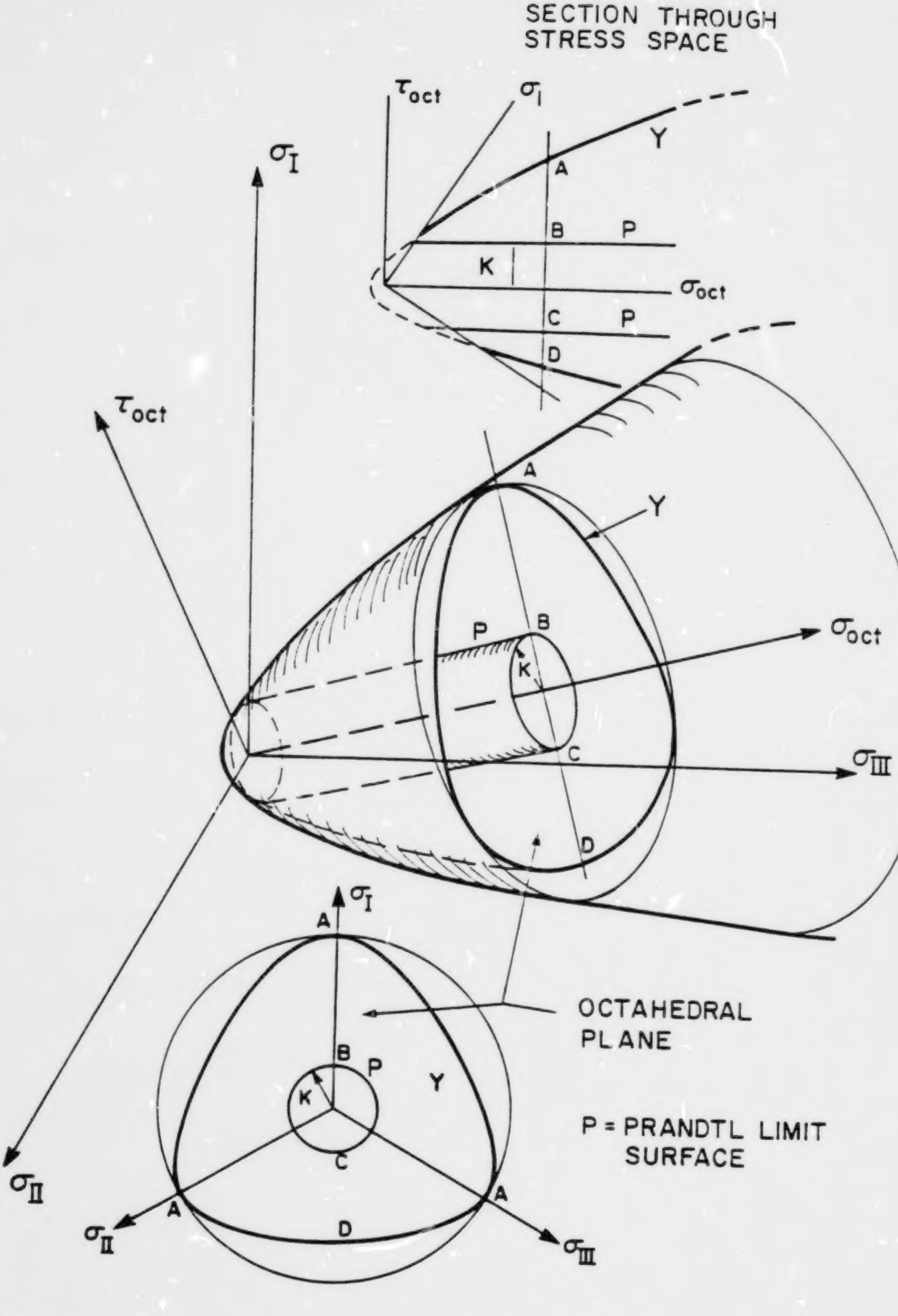
SECTION THROUGH
STRESS SPACE
τ_{oct}
σ_I
Y
A
B
P
K
σ_{oct}
C
P
D
σ_I
τ_{oct}
A
Y
P
B
K
σ_{oct}
C
σ_{III}
D
σ_I
A
OCTAHEDRAL
PLANE
B
P
Y
K
C
P = PRANDTL LIMIT
SURFACE
σ_{II}
A
A
σ_{II}
D
σ_{III}

FIG. 8 SHAPE OF Y AND PRANDTL LIMIT SURFACES IN STRESS SPACE.

Volume

5

Energy, Mines and Resources Canada
Énergie, Mines et Ressources Canada

CANMET
Canada Centre for Mineral and Energy Technology
Centre canadien de la technologie des minéraux et de l'énergie

POTASH MINING PROJECT

PROJET D'EXPLOITATION DE LA POTASSE

PROGRAMME DE [illegible]
LABORATOIRE [illegible]

MINIER [illegible]

[illegible]

USE OF BACKFILL IN NEW BRUNSWICK POTASH MINES

VOLUME 5

PREDICTION OF LONG TERM RESPONSE OF DENISON-POTACAN STOPES

May, 1987

Final Report By:

DENISON-POTACAN POTASH COMPANY
Sussex, New Brunswick

Prepared by:

MRAZ PROJECT CONSULTANTS LTD
Saskatoon, Saskatchewan

- And -

DEPT. OF EARTH SCIENCES, UNIVERSITY OF WATERLOO
Waterloo, Ontario

Work on the Project was conducted under the auspices of the Canada Centre for Mineral and Energy Technology, Energy, Mines and Resources Canada, funded as part of the Canada/New Brunswick Mineral Development Agreement.

DSS FILE NO: 14SQ.23440-5-9031

DSS CONTRACT SERIAL NO: 0SQ85-C0208

CANMET PROJECT NO: 1.4.09.05

CANMET SCIENTIFIC AUTHORITY: Dr. G. Herget

232 pp

MICROMEDIA

USE OF BACKFILL IN NEW BRUNSWICK POTASH MINES

VOLUME 5
PREDICTION OF LONG TERM RESPONSE OF DENISON-POTACAN STOPES

TABLE OF CONTENTS

1.0 SUMMARY

2.0 INTRODUCTION

3.0 NUMERICAL ANALYSIS
3.1 THE PROGRAM VISCOT
3.2 CHARACTERISTICS OF VISCOT
3.3 VISCOT MODIFICATIONS

4.0 VERIFICATION AND CALIBRATION OF VISCOT

5.0 NUMERICAL MODELLING ANALYSES
5.1 PREDICTION OF 12.5 M AND 30 M STOPE BEHAVIOUR
5.2 MULTIPLE ROOMS AND BACKFILL
5.3 PREDICTION OF LONG TERM RESPONSE OF DENISON-POTACAN STOPES

6.0 DENISON-POTACAN 4.8 M x 4.8 M VIRGIN GROUND OPENING ANALYSES
6.1 ROOF DISPLACEMENTS
6.2 WALL DISPLACEMENTS
6.3 SHEAR STRESS IN WALLS
6.4 MAJOR PRINCIPAL STRESS IN WALLS
6.5 MINOR PRINCIPAL STRESS IN WALLS
6.6 DISPLACEMENT RATE DISTRIBUTION
6.7 STRAIN RATE DISTRIBUTION
6.8 SHEAR STRESS DISTRIBUTION
6.9 MAJOR PRINCIPAL STRESS DISTRIBUTION
6.10 MINOR PRINCIPAL STRESS DISTRIBUTION

7.0 DENISON-POTACAN 4 M X 42 M TEST STOPE, VIRGIN GROUND
7.1 ROOF DISPLACEMENTS
7.2 WALL DISPLACEMENTS
7.3 STRAIN RATE DISTRIBUTION
7.4 SHEAR STRESS DISTRIBUTION
7.5 MAJOR PRINCIPAL STRESS DISTRIBUTION
7.6 MINOR PRINCIPAL STRESS DISTRIBUTION

VOLUME 5
TABLE OF CONTENTS (Continued)

8.0 DENISON-POTACAN 4 M X 42 M STOPE
8.1 ROOF DISPLACEMENTS
8.2 WALL DISPLACEMENTS
8.3 MINOR PRINCIPAL STRESS IN WALLS
8.4 STRAIN RATE DISTRIBUTION
8.5 SHEAR STRESS DISTRIBUTION
8.6 MAJOR PRINCIPAL STRESS DISTRIBUTION
8.7 MINOR PRINCIPAL STRESS DISTRIBUTION

9.0 DENISON-POTACAN 12.5 M X 42 M STOPE
9.1 ROOF DISPLACEMENTS
9.2 WALL DISPLACEMENTS
9.3 MINOR PRINCIPAL STRESS IN WALLS
9.4 STRAIN RATE DISTRIBUTION
9.5 SHEAR STRESS DISTRIBUTION
9.6 MAJOR PRINCIPAL STRESS DISTRIBUTION
9.7 MINOR PRINCIPAL STRESS DISTRIBUTION

10.0 DENISON-POTACAN 30 M X 42 M STOPE
10.1 ROOF DISPLACEMENTS
10.2 WALL DISPLACEMENTS
10.3 MINOR PRINCIPAL STRESS IN WALLS
10.4 STRAIN RATE DISTRIBUTION
10.5 SHEAR STRESS DISTRIBUTION
10.6 MAJOR PRINCIPAL STRESS DISTRIBUTION
10.7 MINOR PRINCIPAL STRESS DISTRIBUTION

11.0 APPROXIMATE CLOSED FORM SOLUTION ANALYSIS
11.1 ANALYTICAL MODEL
11.2 GEOMETRY OF ACTIVE OPENING
11.3 VIRGIN GROUND CLOSURE RATES
11.4 CLOSURE RATES IN MINING STOPES WITHOUT BACKFILL
11.4.1 CLOSURE RATES AT AVERAGE SHEAR STRESS EQUAL TO K
11.4.2 CLOSURE RATES AT AVERAGE SHEAR STRESS GREATER THAN K
11.4.3 COMPARISON WITH NUMERICAL ANALYSIS

LIST OF FIGURES

FIGURE 4.1 DPPC 4.8 M X 4.8 M VIRGIN GROUND TEST ROOM

FIGURE 4.2 DPPC 4.8 M X 4.8 M VIRGIN GROUND TEST ROOM-ROOF DISPLACEMENTS

FIGURE 4.3 DPPC 4.8 M X 4.8 M VIRGIN GROUND TEST ROOM-WALL DISPLACEMENTS

FIGURE 4.4 DPPC 4.8 M X 4.8 M TEST STOPE-WALL DISPLACEMENTS

FIGURE 4.5 DPPC 4.8 M X 3.8 M VIRGIN GROUND TEST ROOM-DISPLACEMENT RATES IN PILLAR

FIGURE 4.6 DPPC 4.8 M X 4.8 M VIRGIN GROUND TEST ROOM-DISPLACEMENT RATES IN ROOF

FIGURE 4.7 DPPC 4 M X 42 M TEST STOPE

FIGURE 4.8 DPPC 4 M X 42 M TEST STOPE, VIRGIN GROUND-ROOF DISPLACEMENTS

FIGURE 4.9 DPPC 4 M X 42 M TEST STOPE, VIRGIN GROUND-WALL DISPLACEMENTS

FIGURE 5.1 DPPC 12.5 M X 42 M STOPE

FIGURE 5.2 DPPC 30 M X 42 M STOPE

FIGURE 5.3 DPPC 42 M WIDE STOPES-ROOF DISPLACEMENTS

FIUGRE 5.4 DPPC 42 M WIDE STOPES-WALL DISPLACEMENTS

FIGURE 5.5 DPPC 4 M X 42 M STOPE-ROOF DISPLACEMENTS

FIGURE 5.6 DPPC 4 M X 42 M STOPE-WALL DISPLACEMENTS

FIGURE 5.7 DPPC 12 M X 42 M STOPE-ROOF DISPLACEMENTS

FIGURE 5.8 DPPC 12 M X 42 M STOPE-WALL DISPLACEMENTS

FIGURE 5.9 DPPC 30 M X 42 M STOPE-ROOF DISPLACEMENTS

FIGURE 5.10 DPPC 30 M X 42 M STOPE-WALL DISPLACEMENTS

FIGURE 5.11 STOPE BACKFILL INTERACTION PREDICTION DPPC BACKFILL DENSITY VS. TIME

LIST OF FIGURES (Continued)

DPPC 4.8 M X 4.8 M VIRGIN GROUND TEST ROOM

FIGURE 6.1 ROOF DISPLACEMENTS

FIGURE 6.2 WALL DISPLACEMENTS

FIGURE 6.3 SHEAR STRESS, YEARS 0.00 TO 1.68 X 10^{-2}

FIGURE 6.4 SHEAR STRESS, YEARS 2.52 X 10^{-2} TO 9.08 X 10^{-1}

FIGURE 6.5 SHEAR STRESS, YEARS 1.35 X 10^{0} TO 5.09 X 10^{0}

FIGURE 6.6 MAXIMUM PRINCIPAL STRESS, YEARS 0.00 TO 1.68 X 10^{-2}

FIGURE 6.7 MAXIMUM PRINCIPAL STRESS, YEARS 2.52 X 10^{-2} TO 9.08 X 10^{-1}

FIGURE 6.8 MAXIMUM PRINCIPAL STRESS, YEARS 1.35 X 10^{0} TO 5.09 X 10^{0}

FIGURE 6.9 MINIMUM PRINCIPAL STRESS, YEARS 0.00 TO 1.68 X 10^{-2}

FIGURE 6.10 MINIMUM PRINCIPAL STRESS, YEARS 2.52 X 10^{-2} TO 9.08 X 10^{-1}

FIGURE 6.11 MINIMUM PRINCIPAL STRESS, YEARS 1.35 X 10^{0} TO 5.09 X 10^{0}

DPPC 4.8 M X 4.8 M VIRGIN GROUND OPENING

FIGURE 6.12 DISPLACEMENT RATES, TIME 0.00 YEARS

FIGURE 6.13 DISPLACEMENT RATES, TIME 1.68 X 10^{-2} YEARS

FIGURE 6.14 DISPLACEMENT RATES, TIME 9.08 X 10^{-1} YEARS

FIGURE 6.15 DISPLACEMENT RATES, TIME 4.71 X 10^{0} YEARS

FIGURE 6.16 STRAIN RATES, TIME 0.00 YEARS

FIGURE 6.17 STRAIN RATES, TIME 1.68 X 10^{-2} YEARS

FIGURE 6.18 STRAIN RATES, TIME 9.08 X 10^{-1} YEARS

FIGURE 6.19 STRAIN RATES, TIME 4.71 X 10^{0} YEARS

LIST OF FIGURES (Continued)

DPPC 4.8 M X 4.8 M VIRGIN GROUND OPENING (Continued)

FIGURE 6.20 SHEAR STRESS, TIME 0.00 YEARS

FIGURE 6.21 SHEAR STRESS, TIME 2.06 X 10^{-2} YEARS

FIGURE 6.22 SHEAR STRESS, TIME 1.11 X 10^{0} YEARS

FIGURE 6.23 SHEAR STRESS, TIME 5.09 X 10^{0} YEARS

FIGURE 6.24 MAJOR PRINCIPAL STRESS, TIME 0.00 YEARS

FIGURE 6.25 MAJOR PRINCIPAL STRESS, TIME 2.06 X 10^{-2} YEARS

FIGURE 6.26 MAJOR PRINCIPAL STRESS, TIME 1.11 X 10^{0} YEARS

FIGURE 6.27 MAJOR PRINCIPAL STRESS, TIME 5.09 X 10^{0} YEARS

FIGURE 6.28 MINOR PRINCIPAL STRESS, TIME 0.00 YEARS

FIGURE 6.29 MINOR PRINCIPAL STRESS, TIME 2.06 X 10^{-2} YEARS

FIGURE 6.30 MINOR PRINCIPAL STRESS, TIME 1.11 X 10^{0} YEARS

FIGURE 6.31 MINOR PRINCIPAL STRESS, TIME 5.09 X 10^{0} YEARS

DPPC 4 M X 42 M TEST STOPE, VIRGIN GROUND

FIGURE 7.1 ROOF DISPLACEMENTS

FIGURE 7.2 WALL DISPLACEMENTS

FIGURE 7.3 STRAIN RATES, TIME 0.00 YEARS

FIGURE 7.4 STRAIN RATES, TIME 1.68 X 10^{-2} YEARS

FIGURE 7.5 STRAIN RATES, TIME 9.08 X 10^{-1} YEARS

FIGURE 7.6 STRAIN RATES, TIME 1.73 X 10^{1} YEARS

FIGURE 7.7 SHEAR STRESS, TIME 0.00 YEARS

FIGURE 7.8 SHEAR STRESS, TIME 2.06 X 10^{-2} YEARS

FIGURE 7.9 SHEAR STRESS, TIME 9.08 X 10^{-1} YEARS

LIST OF FIGURES (Continued)

DPPC 4 M X 42 M TEST STOPE, VIRGIN GROUND (Continued)

FIGURE 7.10 SHEAR STRESS, TIME 1.84 X 10^{1} YEARS

FIGURE 7.11 MAJOR PRINCIPAL STRESS, TIME 0.00 YEARS

FIGURE 7.12 MAJOR PRINCIPAL STRESS, TIME 2.06 X 10^{-2} YEARS

FIGURE 7.13 MAJOR PRINCIPAL STRESS, TIME 9.08 X 10^{-1} YEARS

FIGURE 7.14 MAJOR PRINCIPAL STRESS, TIME 1.84 X 10^{1} YEARS

FIGURE 7.15 MINOR PRINCIPAL STRESS, TIME 0.00 YEARS

FIGURE 7.16 MINOR PRINCIPAL STRESS, 2.06 X 10^{-2} YEARS

FIGURE 7.17 MINOR PRINCIPAL STRESS, 9.08 X 10^{-1} YEARS

FIGURE 7.18 MINOR PRINCIPAL STRESS, TIME 1.84 X 10^{1} YEARS

DPPC 4 M X 42 M TEST STOPE

FIGURE 8.1 ROOF DISPLACEMENTS

FIGURE 8.2 WALL DISPLACEMENTS

FIGURE 8.3 WITH BACKFILL, MINIMUM PRINCIPAL STRESS, YEARS 0.00 TO 1.68 X 10^{-2}

FIGURE 8.4 WITH BACKFILL, MINIMUM PRINCIPAL STRESS, YEARS 2.52 X 10^{-2} TO 9.08 X 10^{-1}

FIGURE 8.5 WITH BACKFILL, MINIMUM PRINCIPAL STRESS, YEARS 1.35 X 10^{0} TO 3.21 X 10^{1}

FIGURE 8.6 STRAIN RATES, TIME 0.00 YEARS

FIGURE 8.7 STRAIN RATES, TIME 1.41 X 10^{-2} YEARS

FIGURE 8.8 STRAIN RATES, TIME 1.13 X 10^{0} YEARS

FIGURE 8.9 STRAIN RATES, TIME 8.66 X 10^{0} YEARS

LIST OF FIGURES (Continued)

DPPC 4 M X 42 M TEST STOPE (Continued)

FIGURE 8.10 SHEAR STRESS, TIME 0.00 YEARS

FIGURE 8.11 SHEAR STRESS, TIME 1.73 X 10^{-2} YEARS

FIGURE 8.12 SHEAR STRESS, TIME 1.13 X 10^{0} YEARS

FIGURE 8.13 SHEAR STRESS, TIME 9.23 X 10^{0} YEARS

FIGURE 8.14 MAJOR PRINCIPAL STRESS, TIME 0.00 YEARS

FIGURE 8.15 MAJOR PRINCIPAL STRESS, TIME 1.73 X 10^{-2} YEARS

FIGURE 8.16 MAJOR PRINCIPAL STRESS, TIME 1.13 X 10^{0} YEARS

FIGURE 8.17 MAJOR PRINCIPL STRESS, TIME 9.23 X 10^{0} YEARS

FIGURE 8.18 MINOR PRINCIPAL STRESS, TIME 0.00 YEARS

FIGURE 8.19 MINOR PRINCIPAL STRESS, TIME 1.73 X 10^{-2} YEARS

FIGURE 8.20 MINOR PRINCIPAL STRESS, TIME 1.13 X 10^{0} YEARS

FIGURE 8.21 MINOR PRINCIPAL STRESS, TIME 9.23 X 10^{0} YEARS

DPPC 12 M X 42 M STOPE

FIGURE 9.1 ROOF DISPLACEMENTS

FIGURE 9.2 WALL DISPLACEMENTS

FIGURE 9.3 WITH BACKFILL, MINIMUM PRINCIPAL STRESS, YEARS 0.00 TO 8.41 X 10^{-2}

FIGURE 9.4 WITH BACKFILL, MINIMUM PRINCIPAL STRESS, YEARS 1.26 X 10^{-1} TO 4.54 X 10^{0}

FIGURE 9.5 WITH BACKFILL, MINIMUM PRINCIPAL STRESS, YEARS 6.25 X 10^{0} TO 3.29 X 10^{1}

FIGURE 9.6 STRAIN RATES, TIME 0.00 YEARS

FIGURE 9.7 STRAIN RATES, TIME 2.22 X 10^{-2}

FIGURE 9.8 STRAIN RATES, TIME 1.13 X 10^{0}

FIGURE 9.9 STRAIN RATES, TIME 1.41 X 10^{1}

LIST OF FIGURES (Continued)

DPPC 12 M X 42 STOPE (Continued)

FIGURE 9.10 SHEAR STRESS, TIME 0.00 YEARS

FIGURE 9.11 SHEAR STRESS, TIME 2.22 X 10^{-2}

FIGURE 9.12 SHEAR STRESS, TIME 1.13 X 10^{0}

FIGURE 9.13 SHEAR STRESS, TIME 1.54 X 10^{1}

FIGURE 9.14 MAJOR PRINCIPAL STRESS, TIME 0.00 YEARS

FIGURE 9.15 MAJOR PRINCIPAL STRESS, TIME 2.22 X 10^{-2}

FIGURE 9.16 MAJOR PRINCIPAL STRESS, TIME 1.13 X 10^{0}

FIGURE 9.17 MAJOR PRINCIPAL STRESS, TIME 1.54 X 10^{1}

FIGURE 9.18 MINOR PRINCIPAL STRESS, TIME 0.00 YEARS

FIGURE 9.19 MINOR PRINCIPAL STRESS, 2.22 X 10^{-2} YEARS

FIGURE 9.20 MINOR PRINCIPAL STRESS, 1.13 X 10^{0} YEARS

FIGURE 9.21 MINOR PRINCIPAL STRESS, 1.54 X 10^{1} YEARS

DPPC 30 M X 42 M STOPE

FIGURE 10.1 ROOF DISPLACEMENTS

FIGURE 10.2 WALL DISPLACEMENTS

FIGURE 10.3 WITH BACKFILL, MINIMUM PRINCIPAL STRESS, YEARS 0.00 TO 8.41 X 10^{-2}

FIGURE 10.4 WITH BACKFILL, MINIMUM PRINCIPAL STRESS, YEARS 1.26 X 10^{-1} TO 4.37 X 10^{0}

FIGURE 10.5 WITH BACKFILL, MINIMUM PRINCIPAL STRESS, YEARS 5.88 X 10^{0} TO 3.01 X 10^{1}

FIGURE 10.6 STRAIN RATES, TIME 0.00 YEARS

FIGURE 10.7 STRAIN RATES, TIME 2.22 X 10^{-2} YEARS

FIGURE 10.8 STRAIN RATES, TIME 1.13 X 10^{0} YEARS

FIGURE 10.9 STRAIN RATES, TIME 1.27 X 10^{1} YEARS

LIST OF FIGURES (Continued)

DPPC 30 M X 42 M STOPE

FIGURE 10.10 STRAIN RATES, TIME 0.00 YEARS

FIGURE 10.11 STRAIN RATES, TIME 2.22 X 10^{-2} YEARS

FIGURE 10.12 STRAIN RATES, TIME 1.13 X 10^{0} YEARS

FIGURE 10.13 STRAIN RATES, TIME 1.38 X 10^{1} YEARS

FIGURE 10.14 MAJOR PRINCIPAL STRESS, TIME 0.00 YEARS

FIGURE 10.15 MAJOR PRINCIPAL STRESS, TIME 2.22 X 10^{-2} YEARS

FIGURE 10.16 MAJOR PRINCIPAL STRESS, TIME 1.13 X 10^{0} YEARS

FIGURE 10.17 MAJOR PRINCIPAL STRESS, TIME 1.38 X 10^{1} YEARS

FIGURE 10.18 MINOR PRINCIPAL STRESS, TIME 0.00 YEARS

FIGURE 10.19 MINOR PRINCIPAL STRESS, TIME 2.22 X 10^{-2} YEARS

FIGURE 10.20 MINOR PRINCIPAL STRESS, TIME 1.13 X 10^{0} YEARS

FIGURE 10.21 MINOR PRINCIPAL STRESS, TIME 1.38 X 10^{1} YEARS

FIGURE 11.1 STRESS DISTRIBUTION MODELS: GENERALLY AND IDEALLY PLASTIC SUBSTANCES

FIGURE 11.2 LOAD EQUILIBRIUM IN PILLAR

LIST OF TABLES

TABLE 4.1 MATERIAL PROPERTIES USED IN NUMERICAL MODELLING OF DENISON-POTACAN SALT AND BACKFILL

TABLE 5.1 VIRGIN GROUND OPENING - DISPLACEMENT RATES

TABLE 5.2 DENISON-POTACAN 4 M X 42 M STOPE, BACKFILL DENSITY VS. TIME

TABLE 5.3 DENISON-POTACAN STOPE, BACKFILL DENSITY VS. TIME

TABLE 5.4 DENISON-POTACAN 30 M X 42 M STOPE, BACKFILL DENSITY VS. TIME

TABLE 11.1 COMPARISON OF ANALYTICAL AND NUMERICAL PREDICTIONS OF STEADY STATE DISPLACEMENT RATES AT WALL

SECTION 1.0

1.0 SUMMARY

This volume describes the numerical modelling work and results obtained at the University of Waterloo using the computer program VISCOT. The program VISCOT is described as to its characteristics and modifications that have been made (prior to this research project) to increase efficiency and speed of data analysis.

The procedure in using VISCOT is described and the property criteria used for numerical modelling are summarized.

Verification and calibration of the VISCOT model with in-situ data is described.

The numerical modelling analyses and predictions of closure and interaction of the backfill are presented graphically over the mine project life and an analyses made of changes in the backfill density with time for stope geometries examined.

Numerical modelling predictive results as to roof/floor and wall displacements are presented in combination with the associated strain rates, shear stresses, major principal stresses and minor principal stresses that are presented in detail for the stope geometries examined.

SECTION 2.0

2.0 INTRODUCTION

Numerical modelling was performed using the computer code or program known as VISCOT at the University of Waterloo, Ontario.

Using property criteria derived, both from laboratory and in-situ testing, this numerical modelling program was used to simulate and predict mining induced stresses and room closure both with and without tailings backfill.

This volume describes the analyses used, and predictions arrived at, for the long term behaviour of mining stopes with and without backfill.

SECTION 3.0

3.0 NUMERICAL ANALYSIS

3.1 THE PROGRAM VISCOT

The program used in the numerical analysis of Denison-Potacan mine openings is known as VISCOT. This public program was written by INTERA consultants for the Office of Nuclear Waste Isolation in the United States. In this application, the program was used to model a single staged excavation in potash followed by backfill emplacement. The model was used to predict stress redistribution and displacement rates around the mine opening before and after backfilling.

3.2 CHARACTERISTICS OF VISCOT

VISCOT has the following major features:

- Axisymmetric and two-dimensional plane strain and plane stress options.
- Four, eight or nine node elements.
- Viscoelastic and elastoviscoplastic options (i.e. elastic, viscous and yield options), but not simultaneously.
- Non-linear elastic assumption for backfill material.
- Stresses solved by a finite element Galerkin procedure, strain stepping in discrete time steps by an Eulerian finite difference formulation.
- The ability to accommodate thermally induced stress changes by incorporating volume changes defined by a constant coefficient of thermal expansion (requires parallel use of heat flow finite element, or finite difference program geometrically coupled).
- A viscous behaviour law defined by closed form equation.

3.3 VISCOT MODIFICATIONS

Modifications were made to the program in order to make it more efficient and to speed up the data analysis:

- A simple mesh generator was introduced which allowed direct input of all mesh geometries, initial stresses, displacements and material properties. Existing meshes can also be edited.

- Full graphics output (on screen and hard copy) of stresses, strain rates and displacements in all, or a series, of defined elements.

SECTION 4.0

4.0 VERIFICATION AND CALIBRATION OF VISCOT

Whereas both laboratory and in-situ data have provided the criteria for the VISCOT numerical model, the actual in-situ responses in the Test Room and the Test Stope provide the most meaningful results with which to verify and calibrate the model.

The Test Room at Denison-Potacan represents the first step in calibrating the model. It is in virgin ground, its boundary conditions are easily understood and, most importantly, it has been monitored since 1982. With these features in mind, a finite element grid was prepared to model the in-situ stresses and displacements (Figure 4.1). The following criteria was used to develop the mesh:

1) Two lines of symmetry were available; vertically through the centre of the roof and horizontally through the centre of the pillar. This allowed only one-quarter of the full room geometry to be analyzed, reducing the number of elements and allowing greater element density around the opening.

2) One material, Sylvinite Bed, was used throughout the mesh. Material properties for all materials used in numerical modelling are shown in Table 4.1.

DPPC 4.8 m VIRGIN GROUND TEST ROOM

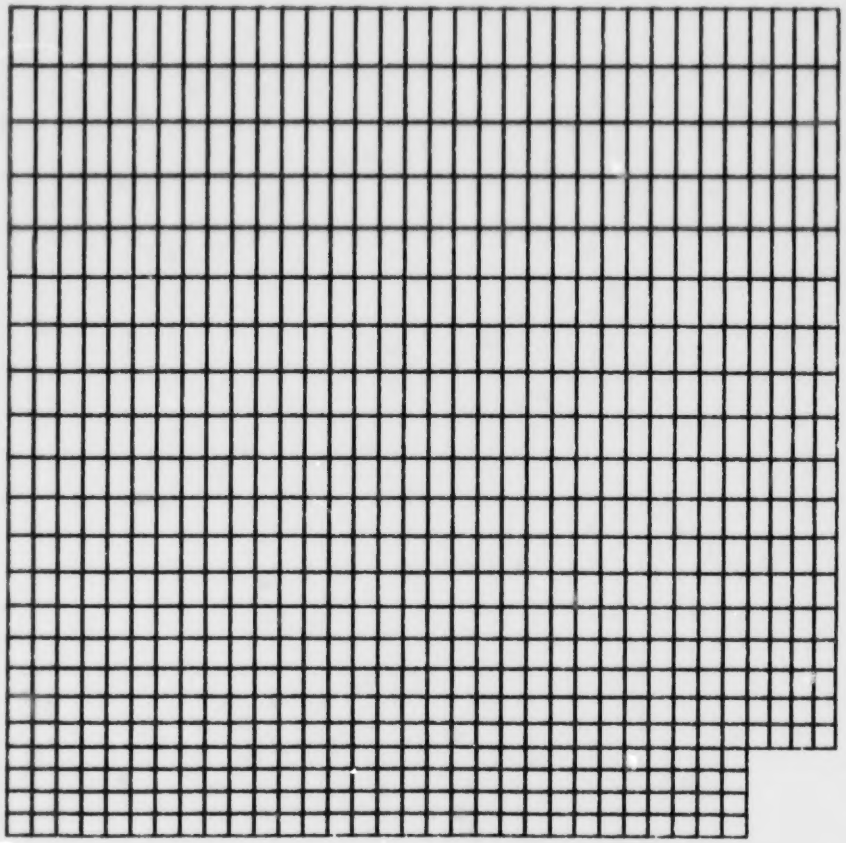

FIGURE 4.1

TABLE 4.1

MATERIAL PROPERTIES USED IN NUMERICAL MODELLING OF DENISON-POTACAN SALT AND BACKFILL

Sylvinite Bed:

Modulus of Elasticity	5462 GPa
Poisson's Ratio	0.33
2K	17.6 MPa
ϵ_K	$3 \times 10^{-11} s^{-1}$
n	5.96
m	1.0

Upper Halite:

Modulus of Elasticity	10210 GPa
Poisson's Ratio	0.33
2K	20.0 MPa
ϵ_K	$3 \times 10^{-11} s^{-1}$
n	4.5
m	1.0

Lower Gradational Bed:

Modulus of Elasticity	6908 GPa
Poisson's Ratio	0.33
2K	18.8 MPa
ϵ_K	$3 \times 10^{-11} s^{-1}$
n	4.8
m	1.0

Anhydrite Breccia (Elastic):

Modulus of Elasticity	5000 GPa
Poisson's Ratio	0.24

Backfill:

Initial Modulus of Elasticity	60 MPa
Rate of change of modulus of elasticity with stress	60 MPa
Moisture Content	2.5%

Material properties, which ultimately govern the way a numerical model behaves, were derived from several sources; laboratory tests, in-situ measurements and scientific literature. Six parameters are required to adequately model a single material:

a) A modulus of elasticity. This is determined from the unload/reload portion of a stress and strain during a brittle yield test. This procedure is described in detail in Volume 3. This parameter governs distribution of elastic stresses and strains.

b) Poisson's Ratio which governs the lateral distribution of an imposed stress. This parameter was obtained from the scientific literature.

c) The Prandtl Limit, K (discussed in Volume 4). Twice this value (2K) is the shear stress required to initiate crack growth and other phenomena which cause significant increases in creep rates with small increases in shear stress. Below this level of stress, diffusion and dislocation phenomenon dominate with much lower strain rates. It can be determined from laboratory tests, or measured in-situ. Both methods were used to determine the Prandtl Limit for this research project. It may also be approximated by half of the unconfined compressive strength.

d) The strain rate that a material will undergo while at a shear stress level of 2K. This parameter can be measured in-situ or calculated from laboratory data. Because this strain rate is extremely slow, it is difficult to measure accurately in the laboratory, so in-situ measurements are considered to be the most accurate way of determining this value.

e) The creep law exponent above a shear stress level of 2K, n. This parameter is determined primarily from laboratory data.

f) The creep law exponent below a shear stress level of 2K, m. This parameter was determined by comparing the in-situ measurements to numerical modelling results.

3) The overburden stress was assumed to be 20 MPa. This value has been determined from the in-situ measurements and overcoring in anhydrite formation adjacent to the salt. As well, 20 MPa was applied horizontally to the mesh as the Test Room is under virgin ground conditions where the far field stresses are hydrostatic.

The results of the initial run showed horizontal and vertical steady state creep rates that matched the values measured in-situ very closely, as shown in Figures 4.2, 4.3, 4.4, 4.5 and 4.6. The calibration of the m exponent, the exponent of the creep law below the 2K shear stress limit, was done by varying its value between 1 and 3. This range was determined based on literature reviews and physical principles of viscoelasticity.

The goal of the modelling approach taken during this work was the prediction of steady state closures with time as these ultimately govern the rate at which a room will close onto backfill. Transient phase displacements make up a small portion of the total closure a room undergoes. The in-situ transient phase displacements were not available as instrumentation could not be installed immediately after the excavation. It

DPPC 4.8m VIRGIN GROUND TEST ROOM

Roof Displacements

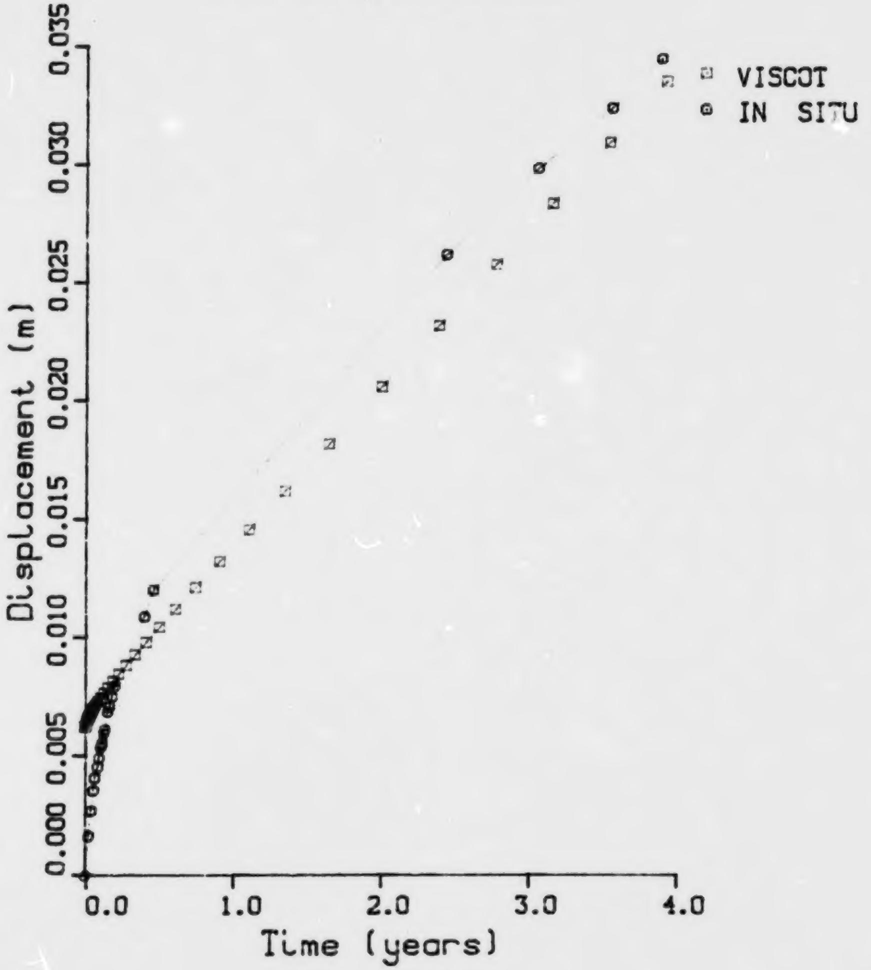

FIGURE 4.2

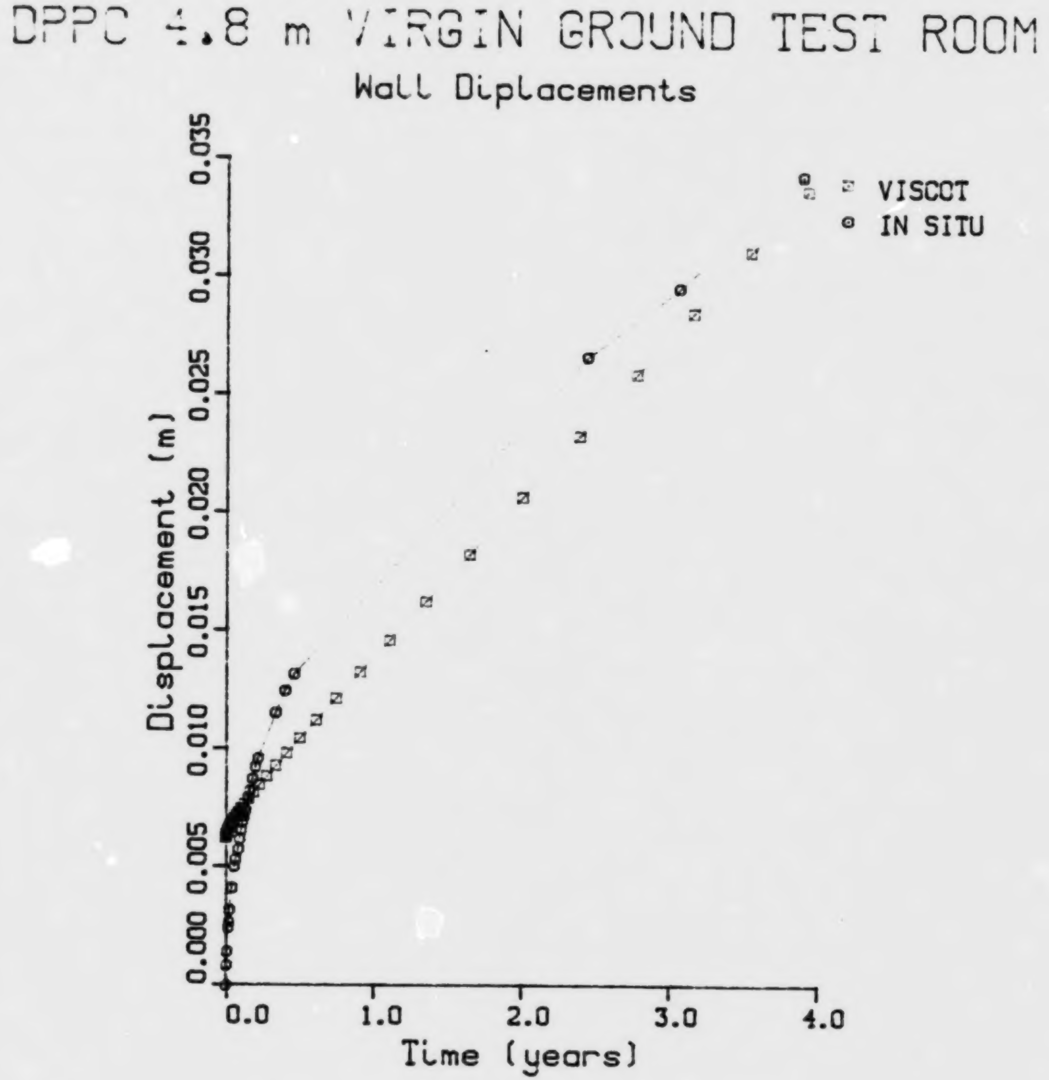
DPPC 4.8 m VIRGIN GROUND TEST ROOM
Wall Diplacements
VISCOT
IN SITU
Displacement (m)
0.000
0.005
0.010
0.015
0.020
0.025
0.030
0.035
Time (years)
0.0
1.0
2.0
3.0
4.0

FIGURE 4.3

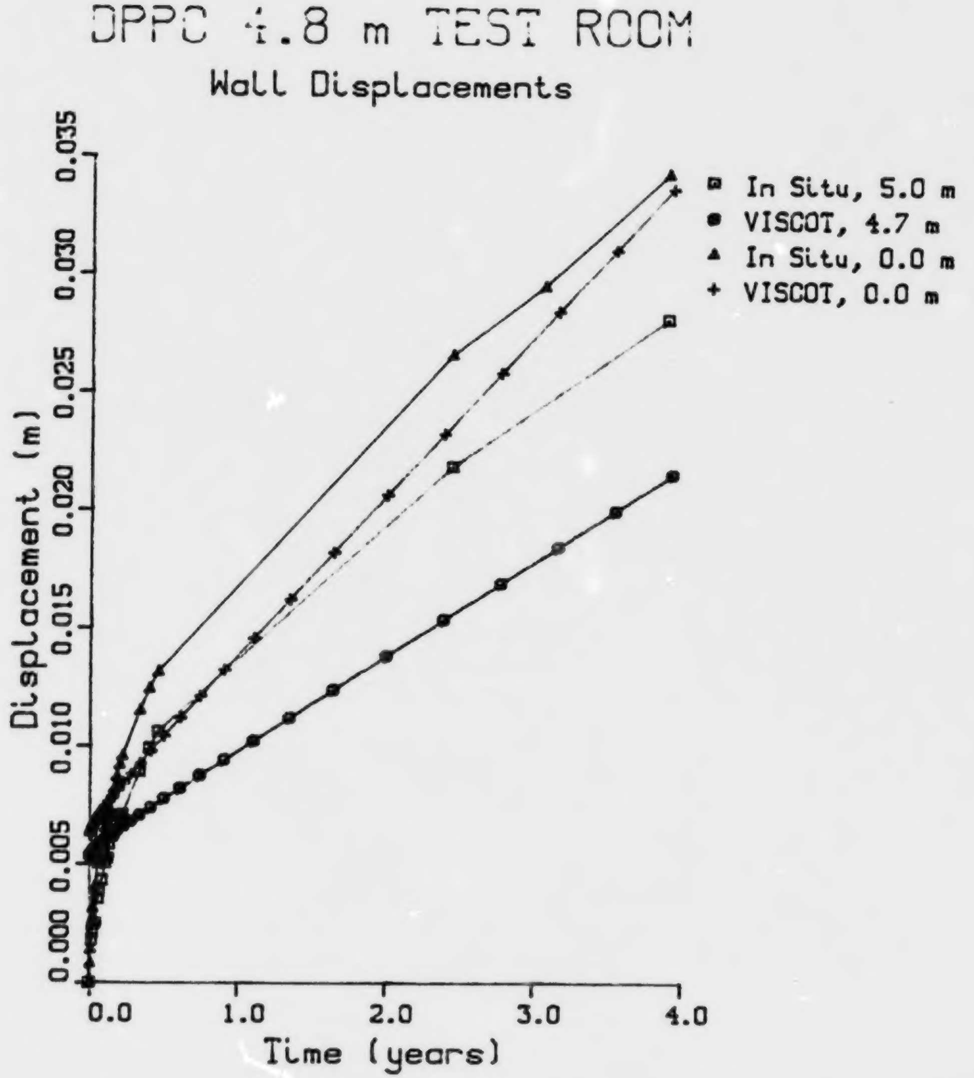
DPPC 4.8 m TEST ROOM
Wall Displacements
Displacement (m)
0.000
0.005
0.010
0.015
0.020
0.025
0.030
0.035
Time (years)
0.0
1.0
2.0
3.0
4.0
▫ In Situ, 5.0 m
● VISCOT, 4.7 m
▲ In Situ, 0.0 m
+ VISCOT, 0.0 m

FIGURE 4.4

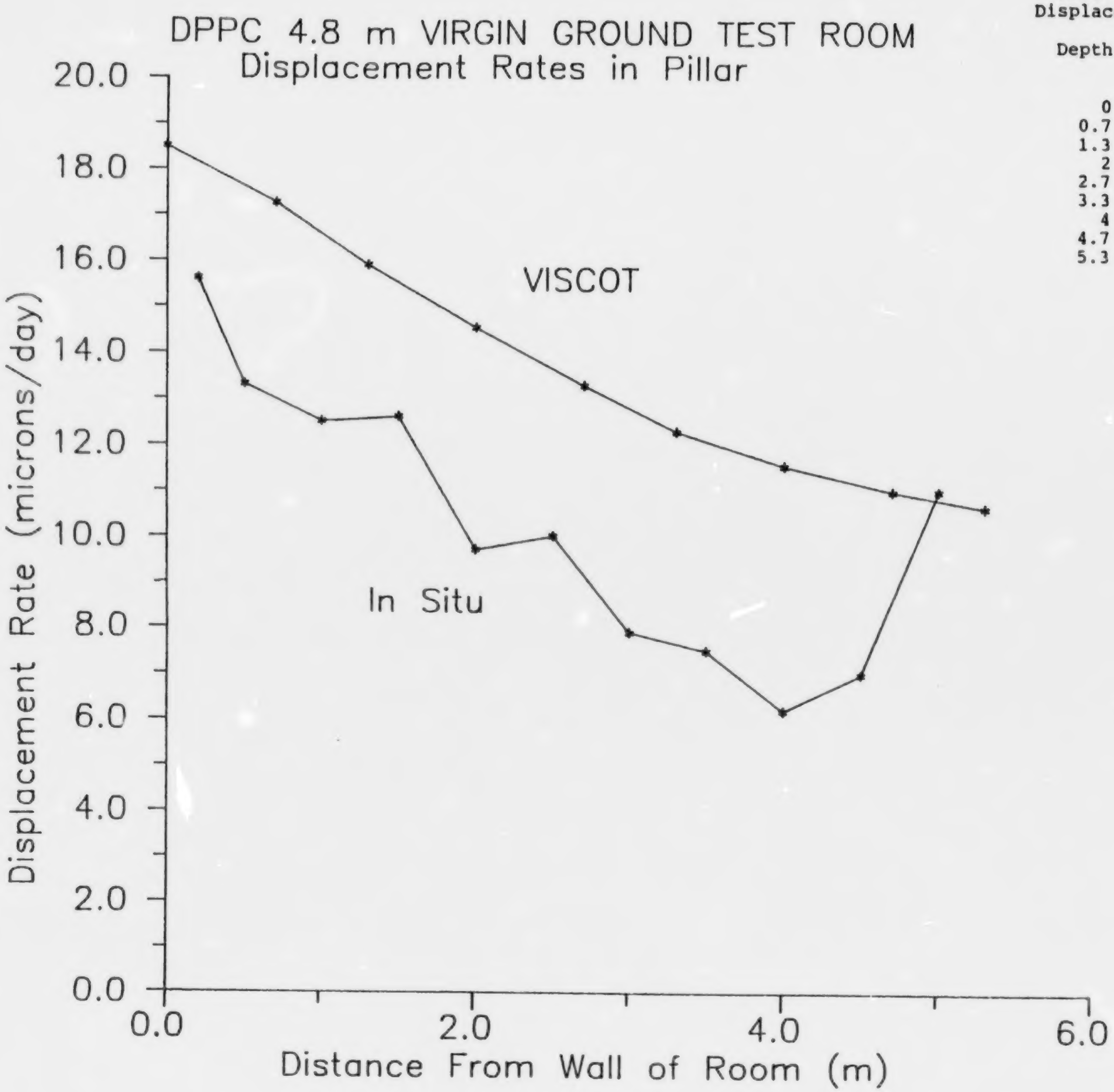
DPPC 4.8 m VIRGIN GROUND TEST ROOM
Displacement Rates in Pillar

DPPC 4.8 m VIRGIN GROUND OPENING
Displacement Rates in Pillar (VISCOT)

Depth (m)	Displacement Rate (microns/day)
0	18.49315
0.7	17.26027
1.3	15.89041
2	14.52054
2.7	13.26027
3.3	12.27397
4	11.53424
4.7	10.98630
5.3	10.63013

FIGURE 4.5

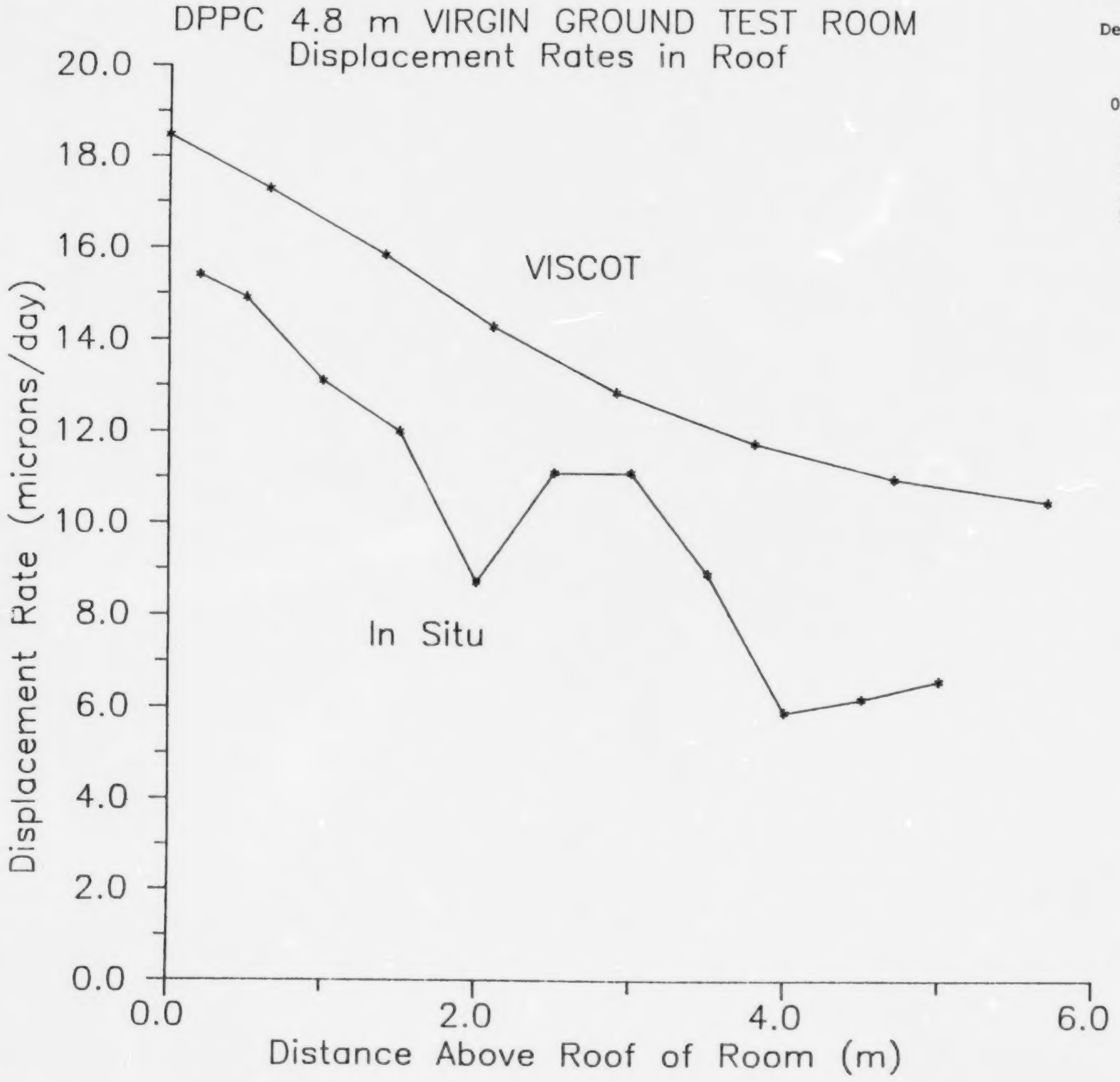

DPPC 4.8 m VIRGIN GROUND OPENING
Displacement Rates in Roof (VISCOT)

Depth (m)	Displacement Rate (microns/day)
0	18.46575
0.65	17.28767
1.4	15.83561
2.1	14.27397
2.9	12.84931
3.8	11.75342
4.7	10.98630
5.7	10.49315

FIGURE 4.6

is clear, however, that in order to model these correctly, a much more detailed approach is required as actual excavation may take several weeks or months where the model assumes instantaneous excavation.

The next case to be analyzed was more complex; a 4 m x 42 m Stope under both virgin ground and mining conditions. The finite element grid is shown in Figure 4.7. Here again, in-situ data was available from a Test Stope at Denison-Potacan to calibrate the model and confirm some of the basic assumptions. More complexity was added to the geometry and materials involved to increase its capacity as a predictive tool for future runs where no field measurements exist. The following conditions were employed for the numerical modelling runs on the Test Stope under virgin ground conditions:

1. Two axes of symmetry were available through the centre of the roof and the centre of the pillar.

2. Three materials were used; Sylvinite Bed within the pillar, Upper Halite for 50 m above the roof of the opening and 90 m of elastic overburden material, an anhydrite breccia. All material properties can be seen in Table 4.1.

3. The overburden stress was again assumed to be 20 MPa. The correlation between the in-situ results and the numerical modelling results for the Test Room showed this to be a reasonable assumption. A horizontal stress of 20 MPa was also added to the mesh for the same reasons outlined above.

DPPC 4×42 m TEST STOPE

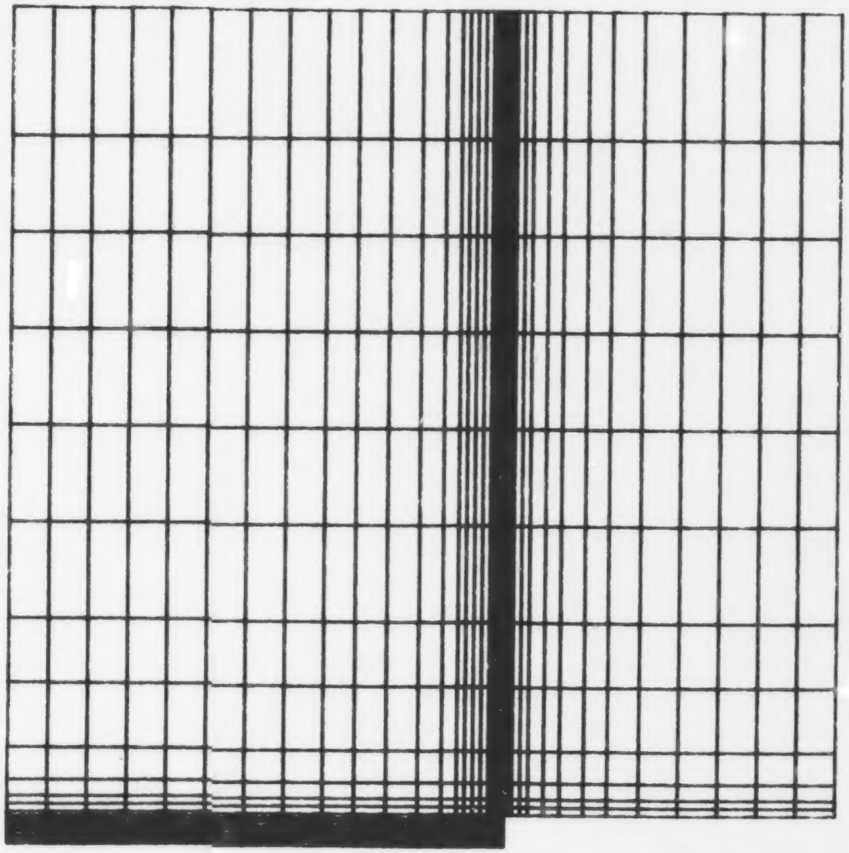

FIGURE 4.7

In-situ, the Test Stope was monitored for about 2.5 years under virgin ground conditions and then under mining conditions. Use of this room for calibration purposes was complicated, however, by the presence of adjacent openings, some of which were located perpendicular to the Test Stope. This meant that for modelling purposes, the room was not in true plane strain or plane stress conditions, but somewhere between.

Under plane strain conditions, the continuum is considered infinite in the lateral direction (perpendicular to the plane of the mesh) and is therefore allowed lateral stresses, but no lateral strains. This is an extremely good approximation to a long stope geometry. Under plane stress conditions, the continuum is considered to be very thin perpendicular to the plane of the mesh and can strain in the lateral direction, but lateral stresses remain at zero or at some fixed constant value.

VISCOT is designed to analyze plane strain and plane stress conditions. To analyze the Test Stope, plane strain conditions were chosen because lateral stresses were known to be greater than zero. However, the initial lateral stresses were allowed to be low, but build with time. This type of analysis proved to be the most appropriate based on a comparison to in-situ data and the in-situ measurements were matched very well, as shown in Figures 4.8 and 4.9.

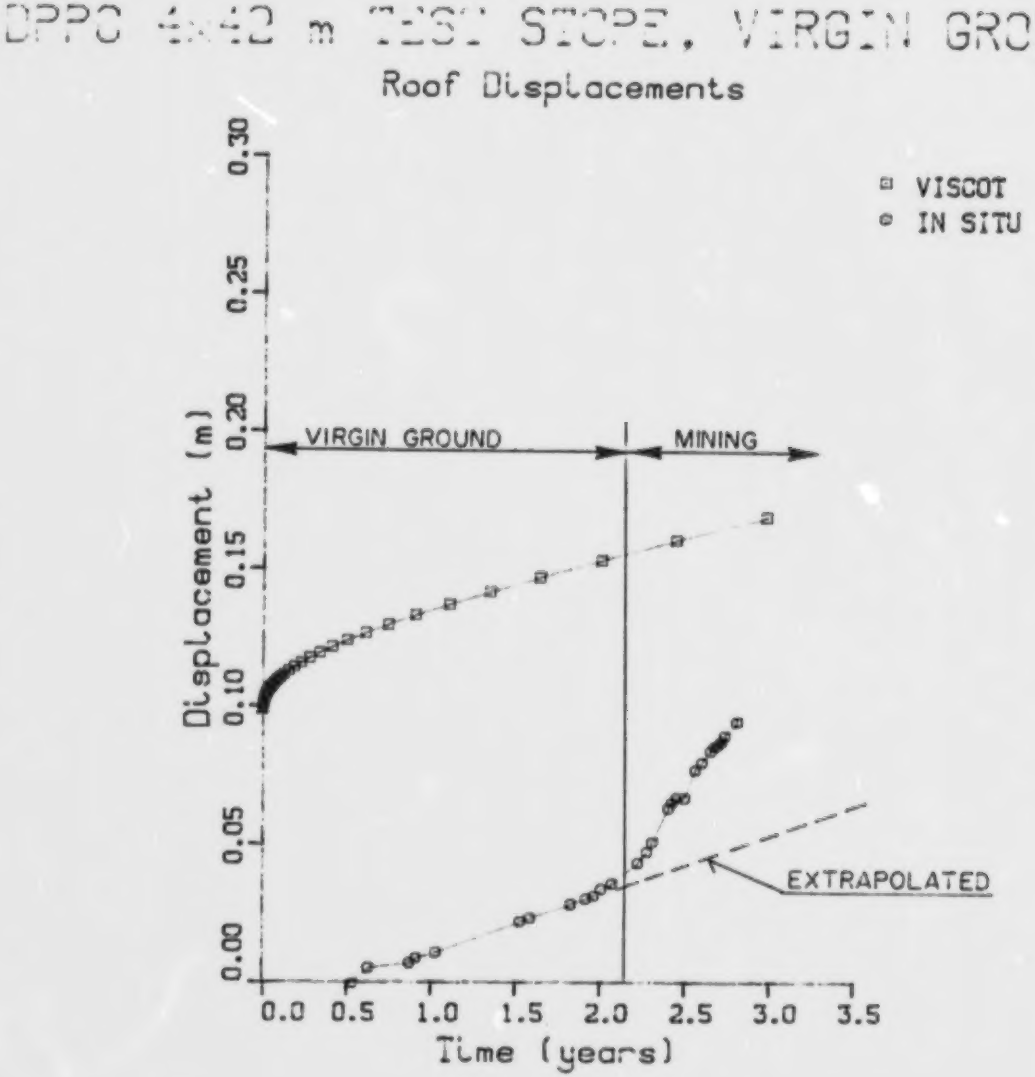
DPPC 4x42 m TEST STOPE, VIRGIN GROUND
Roof Displacements
VISCOT
IN SITU
VIRGIN GROUND
MINING
EXTRAPOLATED
Displacement (m)
0.00
0.05
0.10
0.15
0.20
0.25
0.30
0.0
0.5
1.0
1.5
2.0
2.5
3.0
3.5
Time (years)

FIGURE 4.8

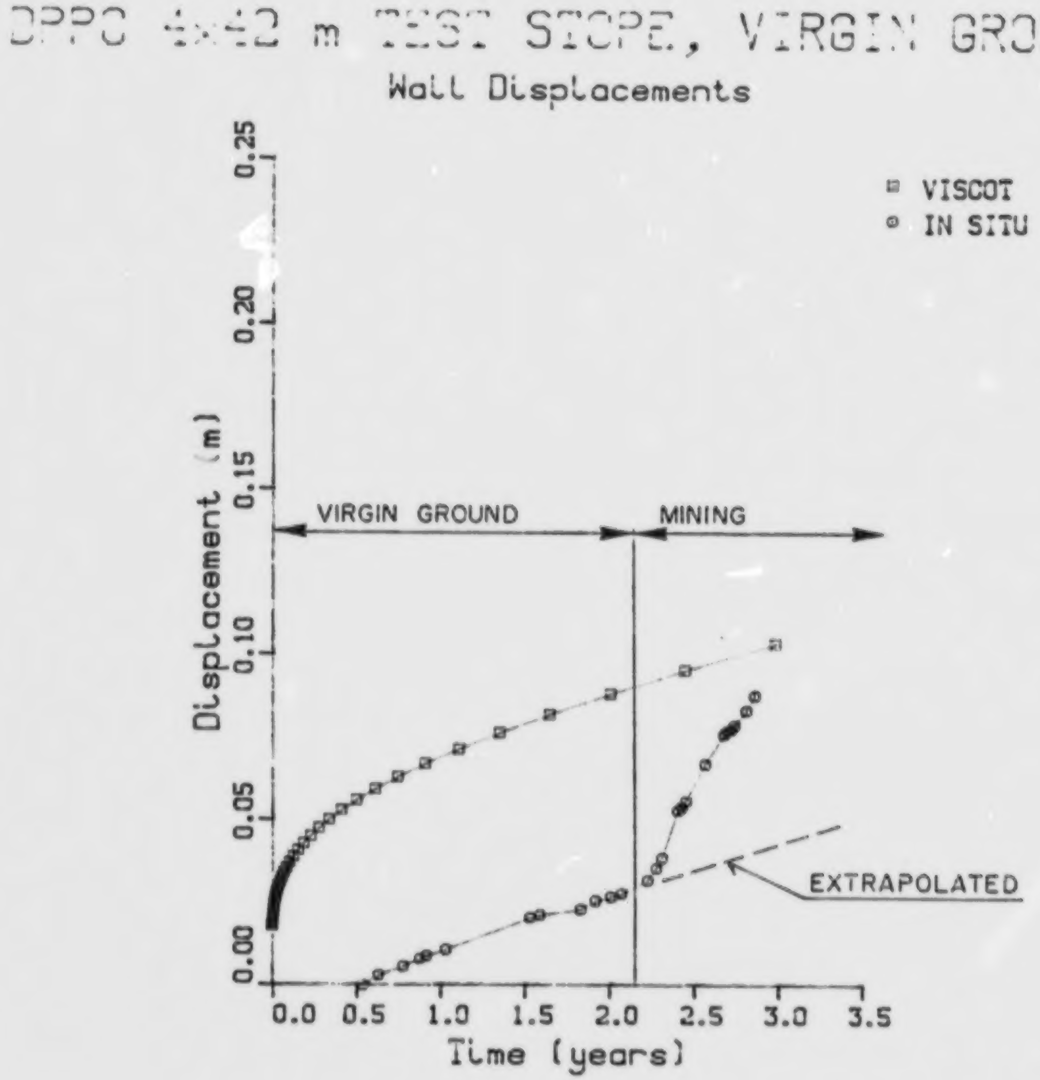
DPPC 4x42 m TEST STOPE, VIRGIN GROUND
Wall Displacements
VISCOT
IN SITU
VIRGIN GROUND
MINING
EXTRAPOLATED
Displacement (m)
0.00
0.05
0.10
0.15
0.20
0.25
Time (years)
0.0
0.5
1.0
1.5
2.0
2.5
3.0
3.5

FIGURE 4.9

SECTION 5.0

5.0 NUMERICAL MODELLING ANALYSES

When in-situ results had been matched successfully for the Test Stope under virgin ground conditions, a new mesh was created for the same 4 m x 42 m room under mining conditions. The new mesh included half of a 63 m wide pillar, three salt materials and no elastic overburden. It was found that an elastic roof beam was unnecessary for modelling of the test stope so it was omitted in favour of greater element density around the opening. The following parameters were used to model the Test Stope under mining conditions:

1. Three axes of symmetry, two through the roof and pillar centres, as above, and a third vertically through the pillar forming the left side of the mesh.

2. Three materials were employed; Sylvinite Bed within the pillar, 2 m of Lower Gradational Bed, and 48 m of Upper Halite. Lower Gradational Bed material properties were employed for the transition zone between the Sylvinite Bed and the Upper Halite.

3. The overburden stress was again assumed to be 20 MPa. No horizontal stress was applied to the mesh, as the left and right boundaries of the mesh are axes of symmetry and are only allowed movement in the vertical direction (rollers).

5.1 PREDICTION OF 12.5 M AND 30 M STOPE BEHAVIOUR

Two new meshes were created to model the 12.5 m and 30 m high by 42 m wide stopes (Figures 5.1 and 5.2). These geometries were chosen to represent the average room at Denison-Potacan (12.5 m x 42 m) and the highest proposed room (30 m x 42 m). Both rooms were modelled as single rooms in a panel of multiple parallel rooms. The conditions employed are as follows:

1. Three axes of symmetry; one through the centre of the roof and two through the pillar, horizontally and vertically.

2. Three materials; Sylvinite Bed in the pillar, 2 m of Lower Gradational Bed and 48 m of Upper Halite.

3. An overburden stress of 20 MPa. No horizontal stresses were applied to the mesh.

Since no field data was available to compare to the numerical results, the numerical results had to be judged based on the previous runs, as shown in Figures 5.3 and 5.4. Both the 12.5 m and 30 m high rooms showed a faster closure rate than the 4.0 m high room. As well, as the room got closer to square (30 m x 42 m), the roof and wall displacement rates got closer. They should be approximately equal for a square room, a feature noted in the in-situ measurements and the numerical results for the Test Room.

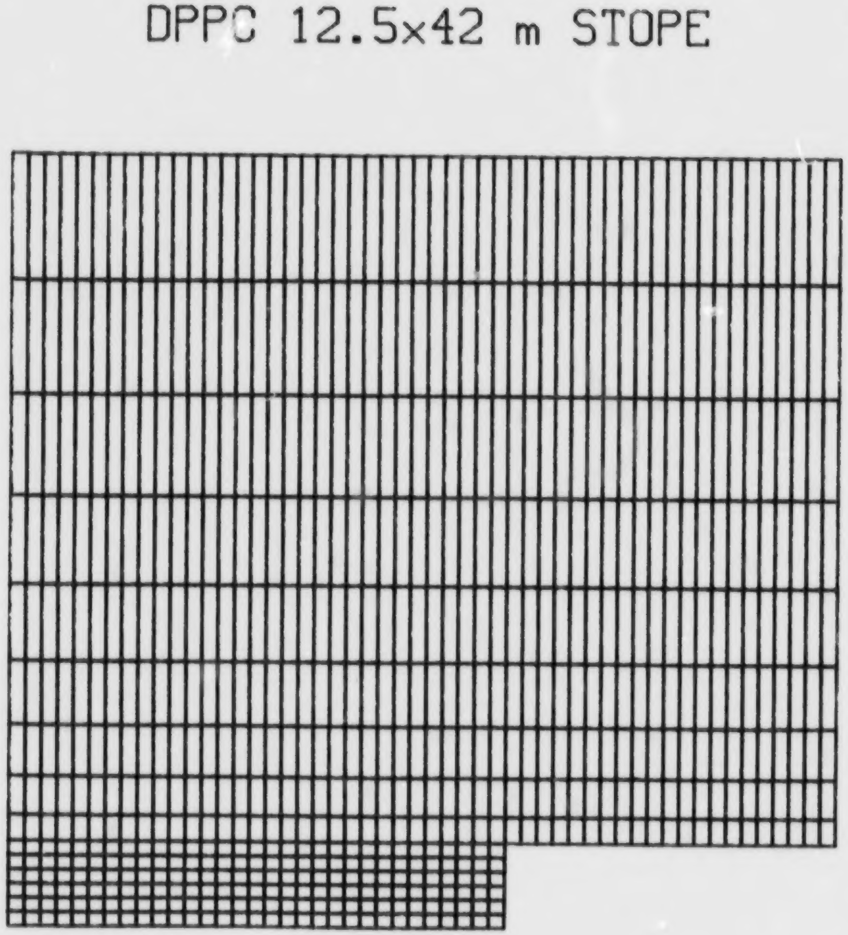

DPPC 12.5×42 m STOPE

FIGURE 5.1

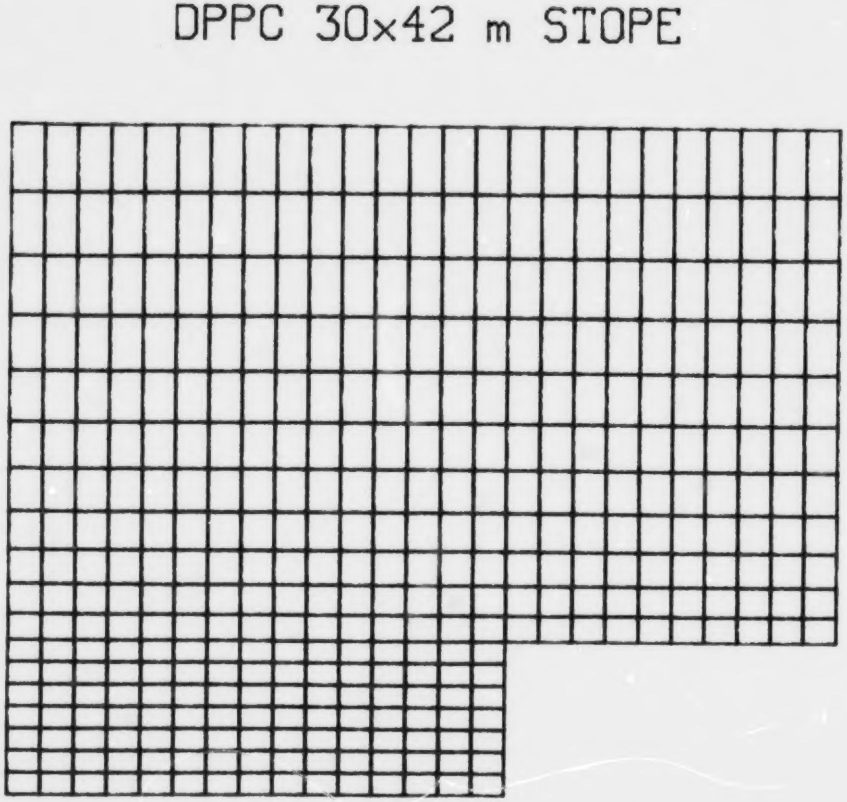
DPPC 30×42 m STOPE

FIGURE 5.2

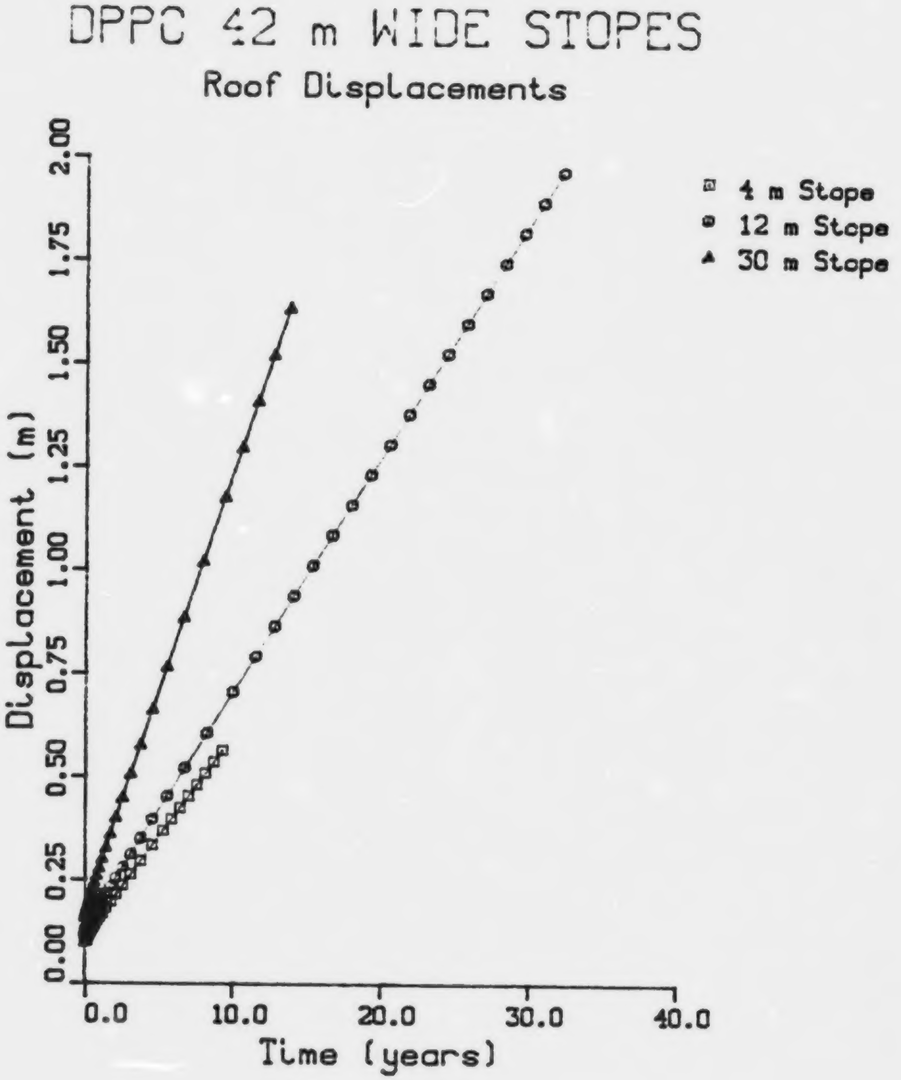
DPPC 42 m WIDE STOPES
Roof Displacements
Displacement (m)
0.00
0.25
0.50
0.75
1.00
1.25
1.50
1.75
2.00
Time (years)
0.0
10.0
20.0
30.0
40.0
□ 4 m Stope
○ 12 m Stope
▲ 30 m Stope

FIGURE 5.3

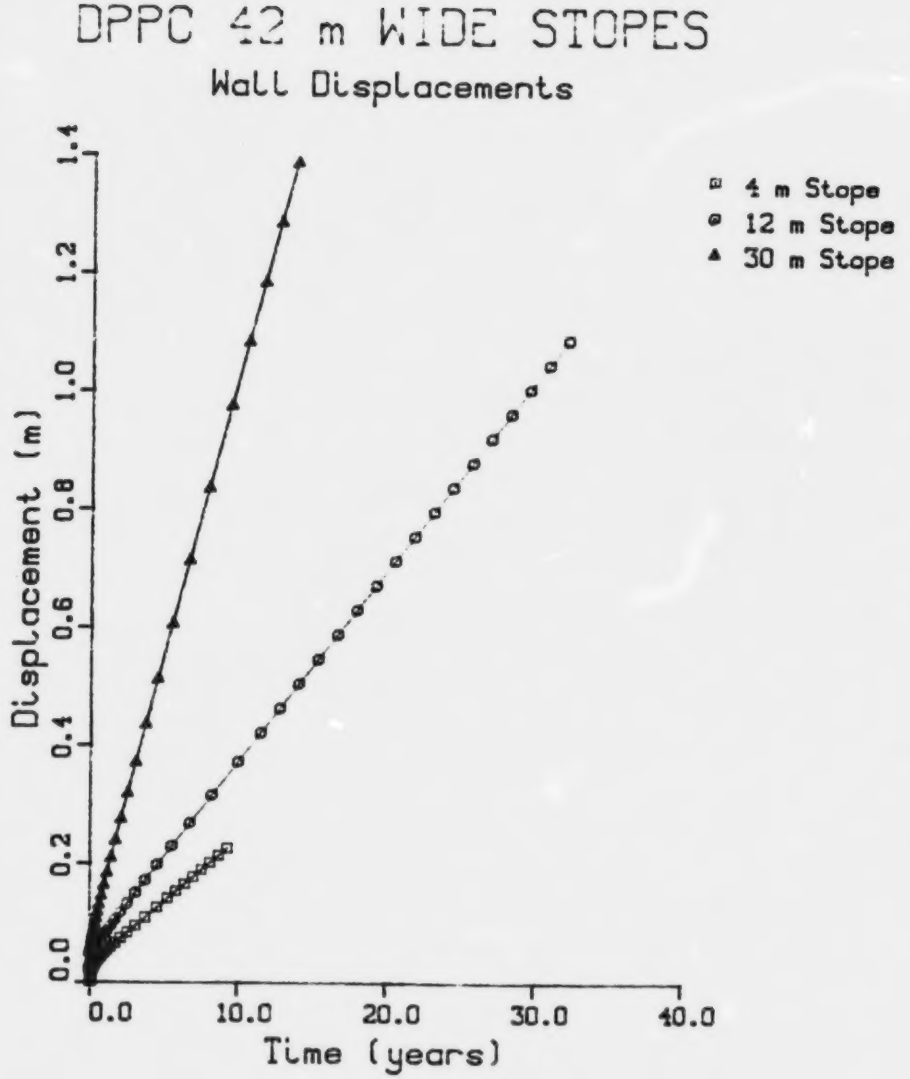
DPPC 42 m WIDE STOPES
Wall Displacements
Displacement (m)
0.0
0.2
0.4
0.6
0.8
1.0
1.2
1.4
Time (years)
0.0
10.0
20.0
30.0
40.0
4 m Stope
12 m Stope
30 m Stope

FIGURE 5.4

5.2 MULTIPLE ROOMS AND BACKFILL

Three rooms were chosen for backfill studies; the 4 m, 12.5 m and 30 m x 42 m rooms. All boundary conditions were the same for each mesh:

1. Three axes of symmetry; one through the centre of the roof and two through the pillar, one vertically and one horizontally.

2. Three materials; Sylvinite Bed in the pillar, 2 m of Lower Gradational Bed and about 48 m of Upper Halite. As well, a backfill material was placed within the opening.

3. Overburden stress of 20 MPa.

Three new meshes were generated to model the salt and backfill interaction. Each had the exact geometry of the empty room meshes, but elements were placed within the opening and backfill material properties were given to these elements.

The backfill material model within VISCOT assumes it to behave in a non-linear elastic fashion. This behavioural approach assumes that the modulus of elasticity of the material increases as the stress increases; essentially the material gets stiffer as with increased stress. This assumption is reasonable for initial estimates of the effect of backfill on room closure; as the roof closes on the backfill, the stress on the backfill will increase and the backfill will densify and become stiffer. The drawback to this approach is that it does not allow the backfill to creep; under a constant stress, the model would predict that the backfill will not move. This is obviously not correct, however, as the roof closes on the backfill, the stress on the backfill will change allowing the backfill to "creep" or densify by small elastic strains. In reality, inelastic time dependent strains also exist.

Two parameters are required to model the backfill and initial modulus of elasticity and a rate of change of that modulus with stress (Table 5.1). These values were determined from the initial strains and the stress/strain/time relationships observed during the consolidation tests (Volume 3). To calculate these values, tests must be performed under known backfill parameters, i.e. density, moisture content, etc. To model for different backfill parameters, further tests need to be performed under the desired conditions to obtain new non-linear elastic parameters. The drawbacks of this approach are outlined below:

1. The non-linear elastic moduli require tests at various conditions, i.e. density, moisture content, etc.
2. Comparing non-linear elastic moduli to measurements available in-situ (density) is difficult without extensive laboratory analyses.
3. The non-linear elastic assumption will not allow creep.

TABLE 5.1
DENISON-POTACAN 4.8 M VIRGIN GROUND OPENING DISPLACEMENT RATES IN PILLAR (VISCOT)

DEPTH (m)	DISPLACEMENT RATE (μ/day)
0	18.49315
0.7	17.26027
1.3	15.89041
2.0	14.52054
2.7	13.26027
3.3	12.27397
4.0	11.53424
4.7	10.98630
5.3	10.63013

DENISON-POTACAN 4.8 M VIRGIN GROUND OPENING DISPLACEMENT RATES IN ROOF (VISCOT)

DEPTH (m)	DISPLACEMENT RATE (μ/day)
0	18.46575
0.65	17.28767
1.4	15.83561
2.1	14.27397
2.9	12.84931
3.8	11.75342
4.7	10.98630
5.7	10.49315

Initially, it was proposed to include a gap between the backfill and the roof by reducing the modelled placement density to incorporate the gap, i.e. for a 1 m gap in a 4 m x 42 m room with an initial density of 1,400 kg/cubic metre, the modelled initial density would have to be reduced to 1,050 kg/cubic metres. To simplify the analysis, no gap was employed between the backfill and the roof of the rooms as the backfill parameters were obtained for backfill which is less dense than expected placement densities. The non-linear elastic moduli used to model the Denison-Potacan backfill were determined for backfill with an initial density of 1.2 g/cc. Any greater initial density will decrease the time required for the backfill to act as a reasonable support for the roof of the opening. The predictions show that the backfill's ability to support the roof and slow room closures is quite dramatic, even at an extremely low placement density. This is encouraging as placement densities are currently about 1.5 g/cc.

The predictions of backfill performance can only be used as a guide to the salt and backfill interaction. Unlike the empty stope behaviour, no in-situ measurements are available to verify the approach or the results. Until such time as data are available, modelling of salt and backfill interactions can only be used as a sensitivity analysis for various geometries and backfill properties.

Figures 5.3 to 5.10 show predictions of roof/floor and wall displacements for stopes 12.5 m and 30 m high by 42 m wide with and without backfill. Note that displacements are for a single surface and must be doubled to represent total closure.

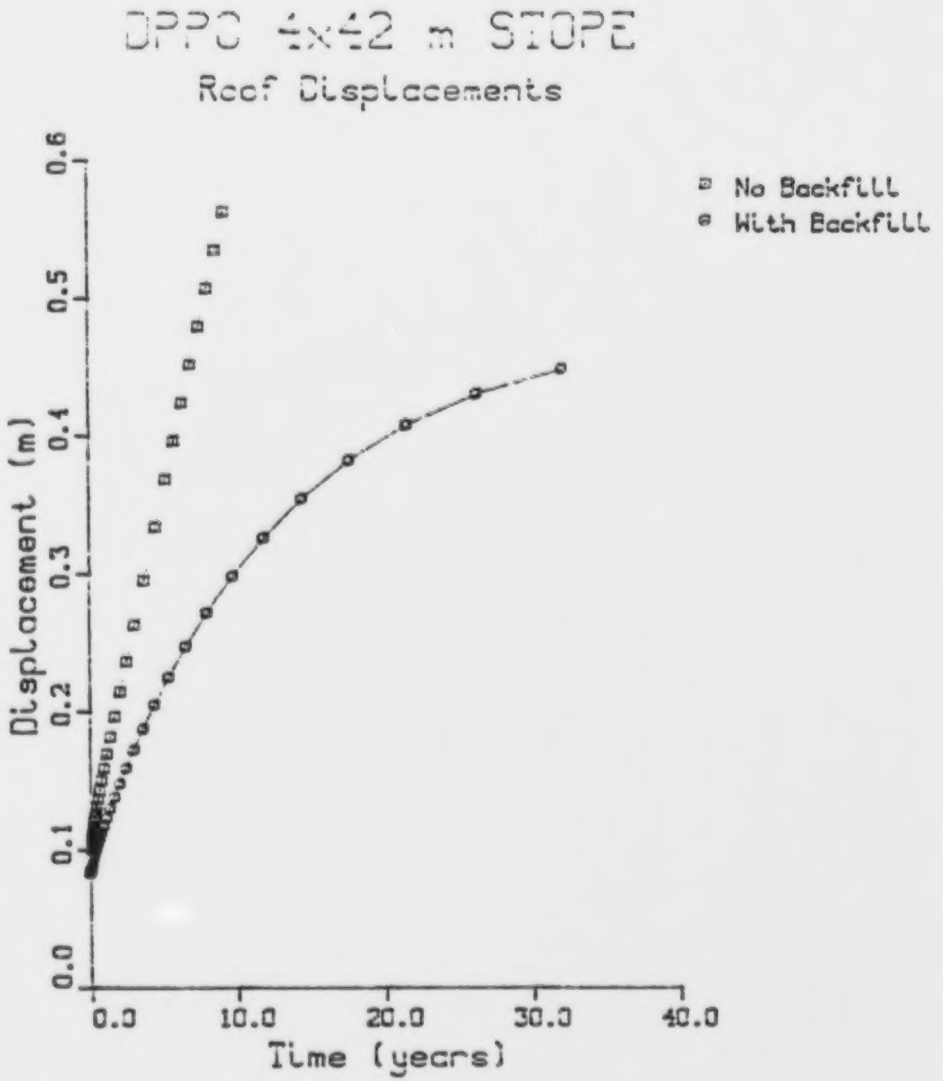
DPPC 4x42 m STOPE
Roof Displacements
No Backfill
With Backfill
Displacement (m)
0.0
0.1
0.2
0.3
0.4
0.5
0.6
Time (years)
0.0
10.0
20.0
30.0
40.0

FIGURE 5.5

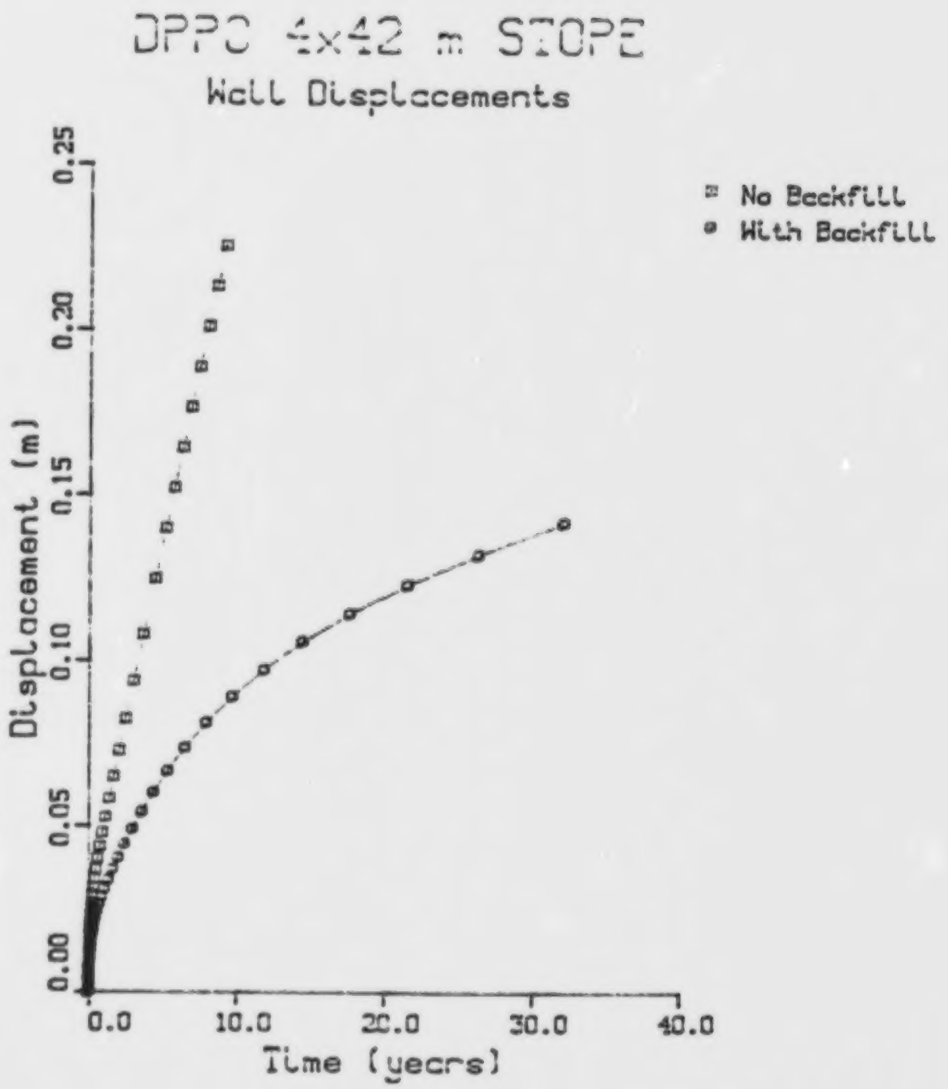
DPPC 4x42 m STOPE
Wall Displacements
No Backfill
With Backfill
Displacement (m)
0.00
0.05
0.10
0.15
0.20
0.25
Time (years)
0.0
10.0
20.0
30.0
40.0

FIGURE 5.6

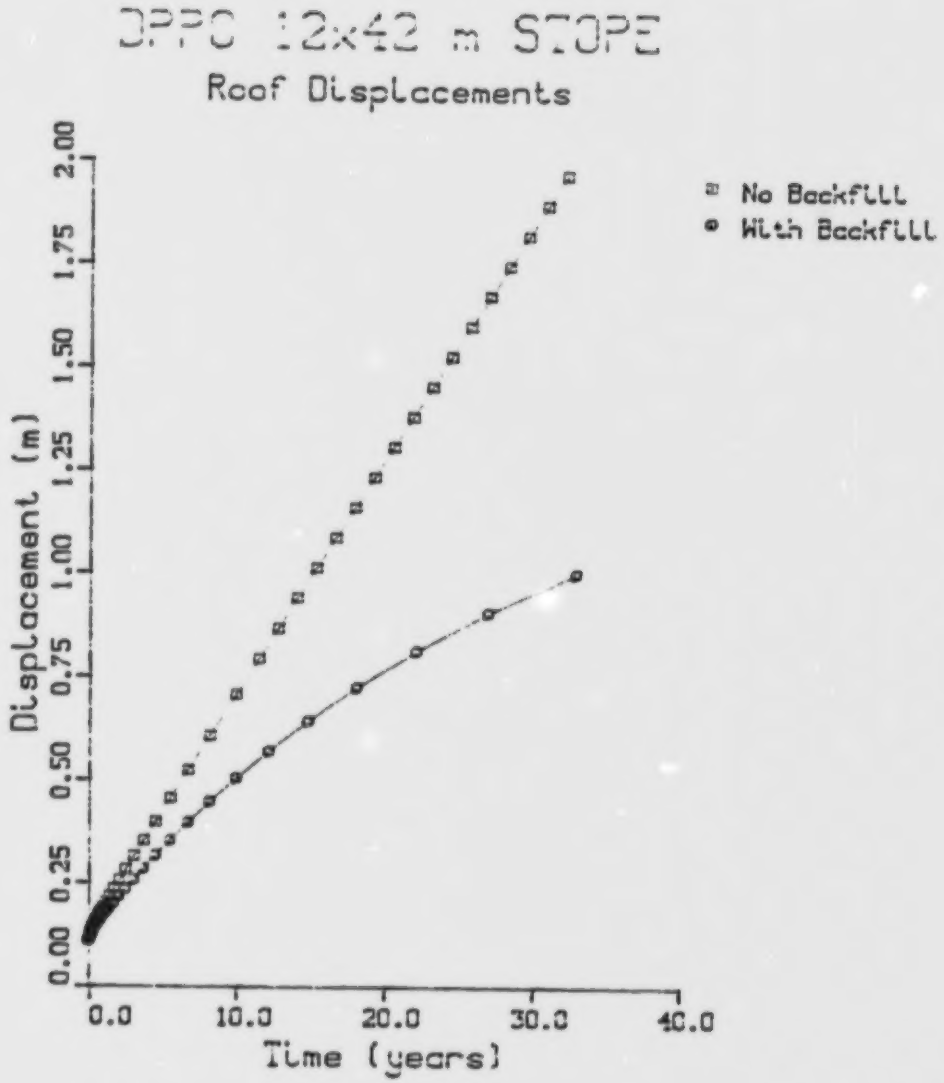
DPPC 12x42 m STOPE
Roof Displacements
Displacement (m)
0.00
0.25
0.50
0.75
1.00
1.25
1.50
1.75
2.00
0.0
10.0
20.0
30.0
40.0
Time (years)
▫ No Backfill
● With Backfill

FIGURE 5.7

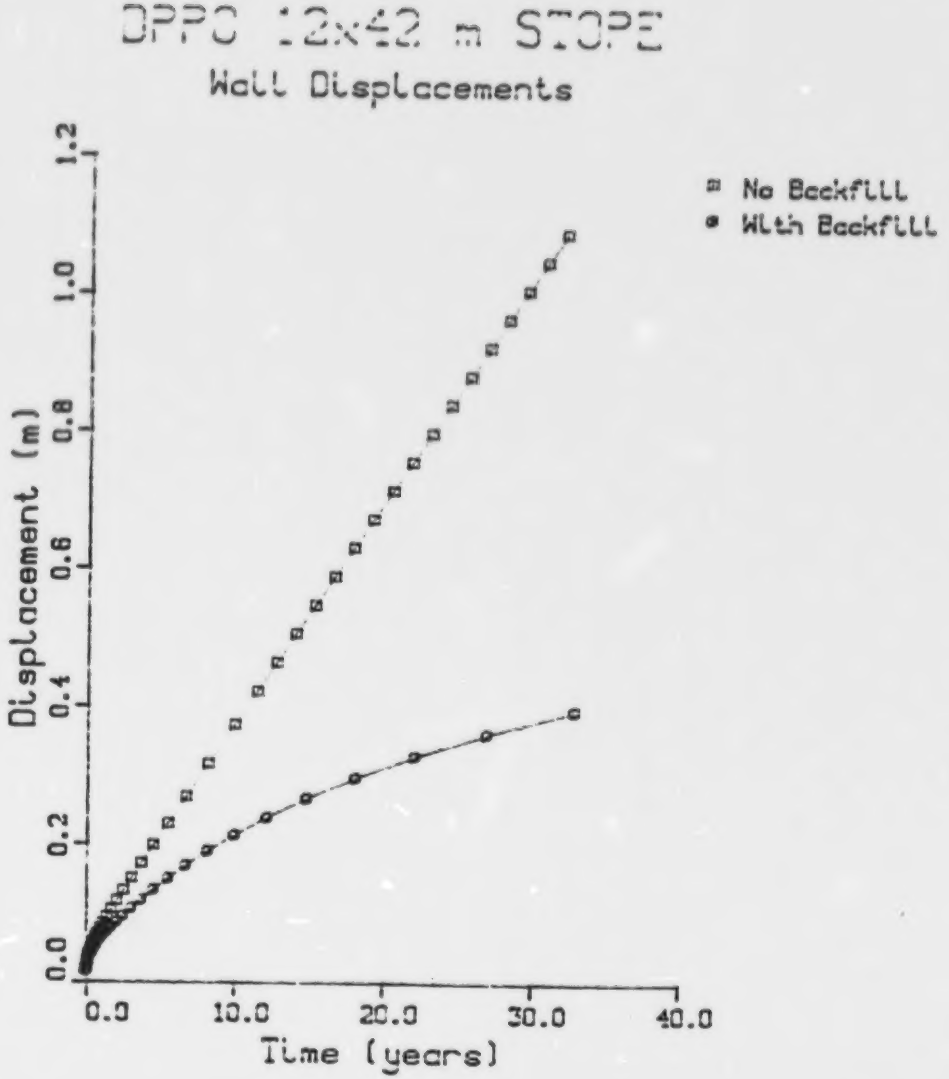
DPPC 12x42 m STOPE
Wall Displacements
Displacement (m)
0.0
0.2
0.4
0.6
0.8
1.0
1.2
0.0
10.0
20.0
30.0
40.0
Time (years)
No Backfill
With Backfill

FIGURE 5.8

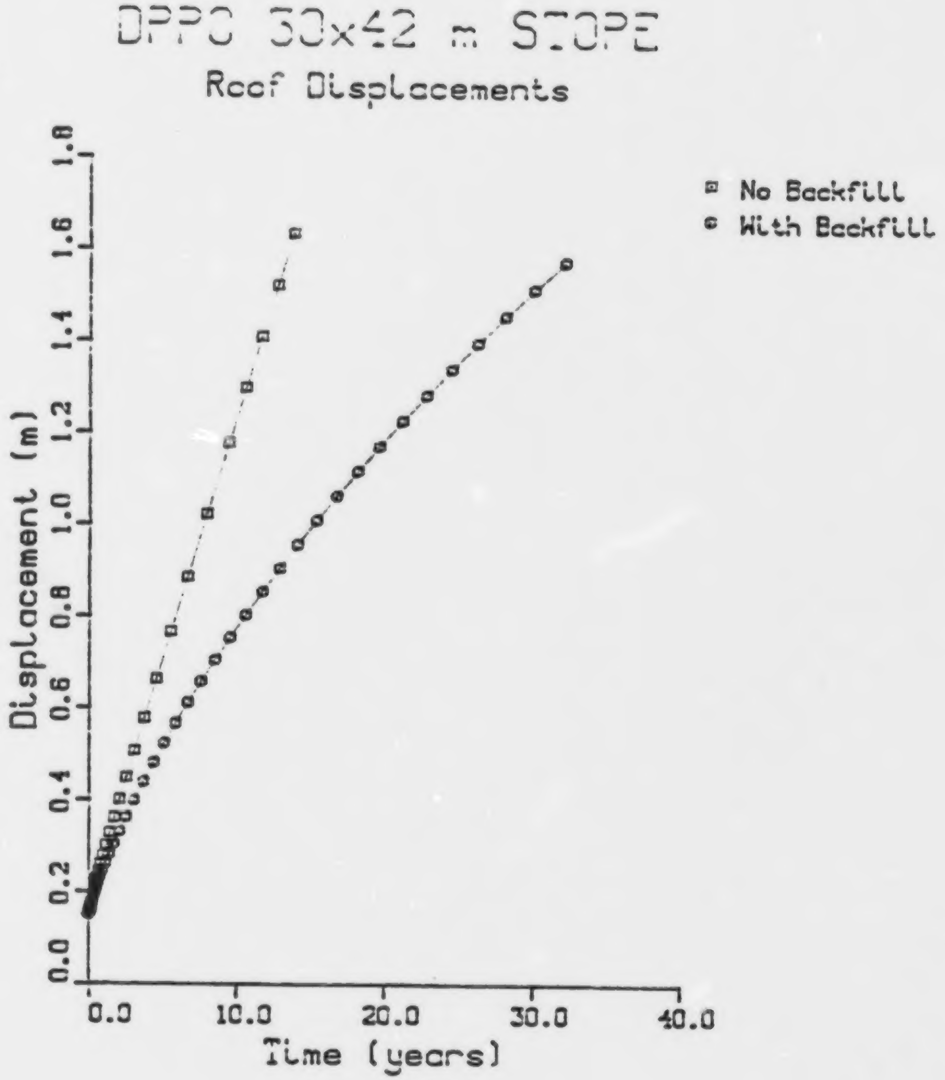
DPPC 30x42 m STOPE
Roof Displacements
Displacement (m)
0.0
0.2
0.4
0.6
0.8
1.0
1.2
1.4
1.6
1.8
0.0
10.0
20.0
30.0
40.0
Time (years)
No Backfill
With Backfill

FIGURE 5.9

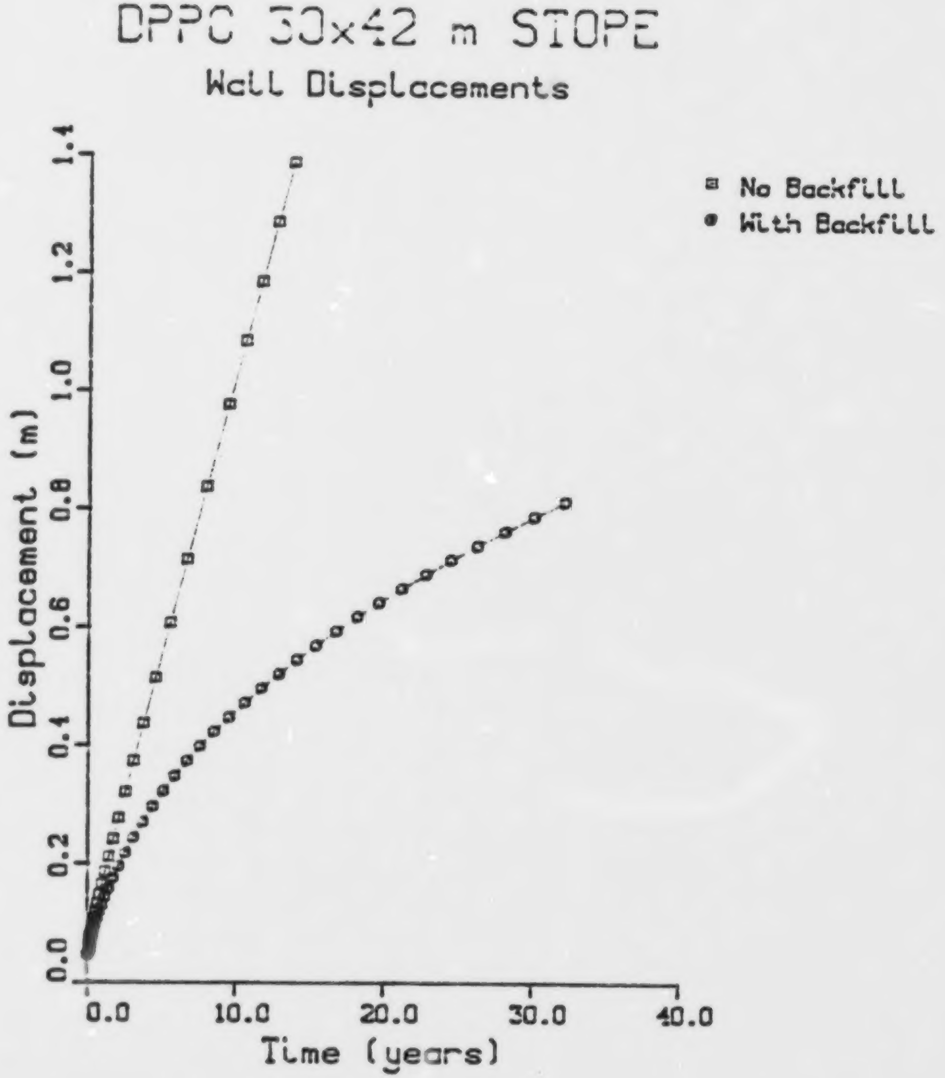
DPPC 30x42 m STOPE
Wall Displacements
Displacement (m)
0.0
0.2
0.4
0.6
0.8
1.0
1.2
1.4
Time (years)
0.0
10.0
20.0
30.0
40.0
□ No Backfill
● With Backfill

FIGURE 5.10

5.3 PREDICTION OF LONG TERM RESPONSE OF DENISON-POTACAN STOPES

It was not anticipated that the backfill would substantially slow down the convergence of the stopes. However, as can be seen in the previous sections, the computer runs do indicate that there will be a substantial slow down in convergence that might aggravate, to some extent, the problem associated with delayed compaction and, hence, the ability (or suitability) of the backfill to support the overburden.

Based on the above predictions, the following Tables 5.2, 5.3 and 5.4 have been developed to calculate the changes in emplaced backfill as stope closure occurs.

The assumptions used are:

- Top 0.5 m of stope is filled at 1.0 S.G.
- Next 1.5 m of stope is filled at 1.4 S.G.
- Balance of stope is filled at 1.6 S.G.

The use of different specific gravities reflects the different methods of backfilling that may be utilized.

Based on these calculations, the changes in backfill density have been plotted against time, as shown in Figure 5.11.

TABLE 5.2

DENISON-POTACAN 4 M X 42 M STOPE
BACKFILL DENSITY VS. TIME

YEAR	ROOF TO FLOOR CLOSURE (M)	WALL TO WALL CLOSURE (M)	NEW ROOF/FLOOR DIMENSION (M)	NEW WALL/WALL DIMENSION (M)	STOPE X-SECT. AREA (M^2)	BACKFILL X-SECT. AREA .5M @ 1.0 DENSITY (M^2)	BACKFILL X-SECT. AREA 1.5M @ 1.4 DENSITY (M^2)	BACKFILL X-SECT. AREA 2.0M @ 1.6 DENSITY (M^2)	TOTAL BACKFILL AREA (M^2)	BACKFILL IN-SITU MASS (000'S KG)	AVERAGE BACKFILL DENSITY (G/C.C)
STOPE AT TIME OF BACKFILLING			4.00	42.00	168	21	63	84	168	244	1.45
0	0.17	0.00	3.83	42.00	161				161	244	1.52
5	0.44	0.12	3.56	41.88	149				149	244	1.64
10	0.60	0.18	3.40	41.82	142				142	244	1.72
15	0.72	0.22	3.28	41.78	137				137	244	1.78
20	0.80	0.24	3.20	41.76	134				134	244	1.82
25	0.86	0.26	3.14	41.74	131				131	244	1.86
30	0.88	0.28	3.12	41.72	130				130	244	1.88
35	0.90	0.29	3.10	41.71	129				129	244	1.89

TABLE 5.3

DENISON-POTACAN 12.5 M X 42 M STOPE
BACKFILL DENSITY VS. TIME

YEAR	ROOF TO FLOOR CLOSURE (M)	WALL TO WALL CLOSURE (M)	NEW ROOF/FLOOR DIMENSION (M)	NEW WALL/WALL DIMENSION (M)	STOPE X-SECT. AREA (M^2)	BACKFILL X-SECT. AREA .5M @ 1.0 DENSITY (M^2)	BACKFILL X-SECT. AREA 1.5M @ 1.4 DENSITY (M^2)	BACKFILL X-SECT. AREA 10.5 M @ 1.6 DENSITY (M^2)	TOTAL BACKFILL AREA (M^2)	BACKFILL IN-SITU MASS (000'S KG)	AVERAGE BACKFILL DENSITY (G/C.C)
STOPE AT TIME OF BACKFILLING			12.50	42.00	525	21	63	441	525	815	1.55
0	0.20	0.02	12.30	41.98	516				516	815	1.58
5	0.66	0.28	11.84	41.72	494				494	815	1.65
10	1.04	0.43	11.46	41.57	476				476	815	1.71
15	1.30	0.54	11.20	41.46	464				464	815	1.76
20	1.54	0.63	10.96	41.37	453				453	815	1.80
25	1.74	0.70	10.76	41.30	444				444	815	1.84
30	1.90	0.75	10.60	41.25	437				437	815	1.86
35	2.10	0.81	10.40	41.19	428				428	815	1.90

TABLE 5.4

DENISON-POTACAN 30 M X 42 M STOPE
BACKFILL DENSITY VS. TIME

YEAR	ROOF TO FLOOR CLOSURE (M)	WALL TO WALL CLOSURE (M)	NEW ROOF/FLOOR DIMENSION (M)	NEW WALL/WALL DIMENSION (M)	STOPE X-SECT. AREA (M^2)	BACKFILL X-SECT. AREA .5M @ 1.0 DENSITY (M^2)	BACKFILL X-SECT. AREA 1.5M @ 1.4 DENSITY (M^2)	BACKFILL X-SECT. AREA 28.0 M @ 1.6 DENSITY (M^2)	TOTAL BACKFILL AREA (M^2)	BACKFILL IN-SITU MASS (000'S KG)	AVERAGE BACKFILL DENSITY (G/C.C)
STOPE AT TIME OF BACKFILLING			30.00	42.00	1,260	21	63	1,176	1,260	1,991	1.58
0	0.30	0.08	29.70	41.92	1,245				1,245	1,991	1.60
5	1.04	0.64	28.96	41.36	1,198				1,198	1,991	1.66
10	1.54	0.90	28.46	41.10	1,170				1,170	1,991	1.70
15	2.00	1.12	28.00	40.88	1,145				1,145	1,991	1.74
20	2.36	1.30	27.64	40.70	1,125				1,125	1,991	1.77
25	2.70	1.44	27.30	40.56	1,107				1,107	1,991	1.80
30	3.04	1.56	26.96	40.44	1,090				1,090	1,991	1.83
35	3.32	1.68	26.68	40.32	1,076				1,076	1,991	1.85

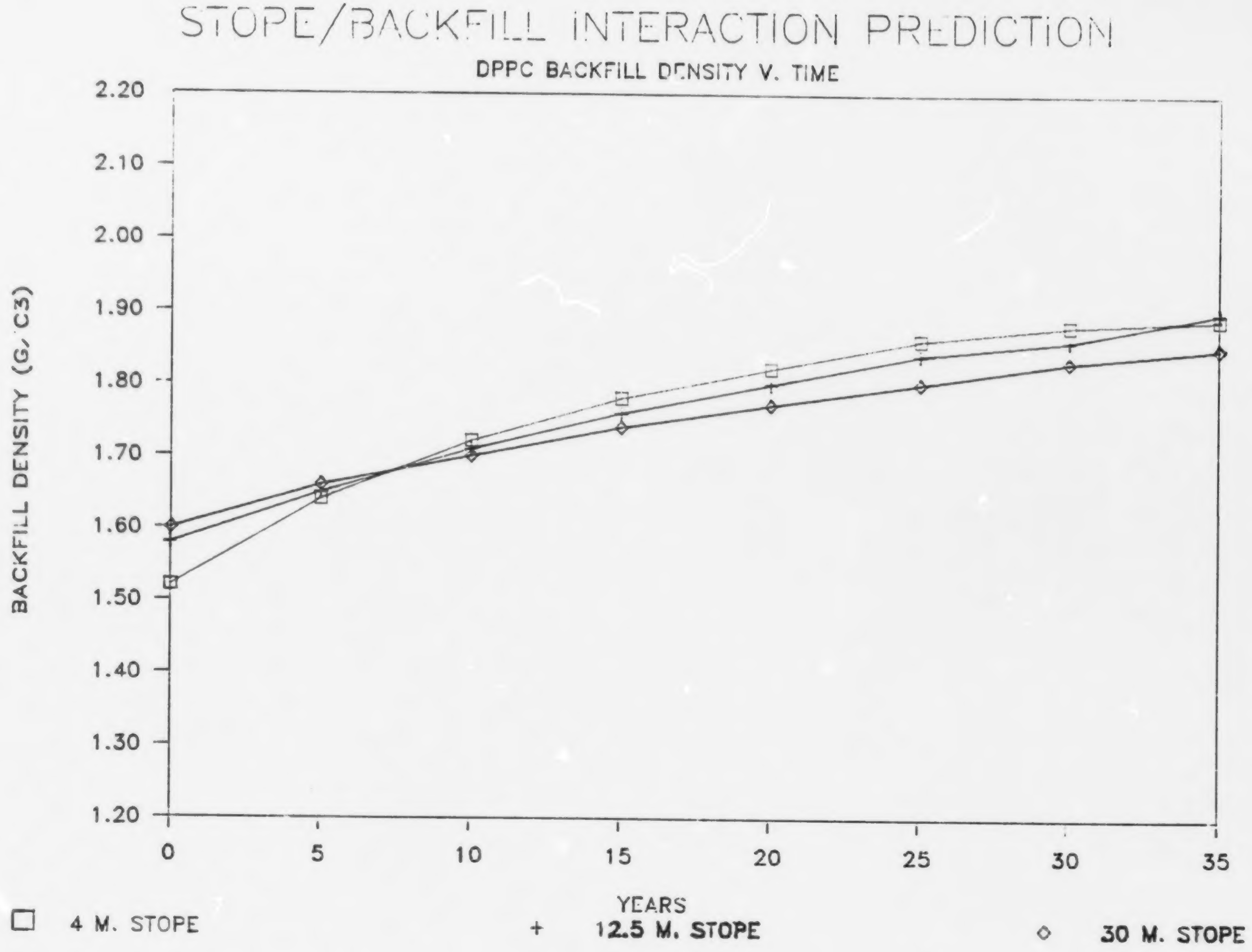
STOPE/BACKFILL INTERACTION PREDICTION
DPPC BACKFILL DENSITY V. TIME
BACKFILL DENSITY (G/C3)
2.20
2.10
2.00
1.90
1.80
1.70
1.60
1.50
1.40
1.30
1.20
0
5
10
15
20
25
30
35
YEARS
□ 4 M. STOPE
+ 12.5 M. STOPE
◇ 30 M. STOPE

FIGURE 5.11

Since a target of ten years has been set from the time of complete backfilling of two adjacent stopes to the time that second stage mining takes place in the intervening pillar, then it would appear that the process of backfill consolidation is too slow, and other measures must be taken to improve consolidation and, hence, support. On the other hand, intermediate densities of backfill, i.e. 1.7 to 1.8, might provide adequate support if the brittle yield criterion of backfill is not exceeded. Hence, a detailed investigation of backfill support function is required in the future work.

SECTION 6.0

6.0 DENISON-POTACAN 4.8 M X 4.8 M VIRGIN GROUND OPENING ANALYSES

6.1 ROOF DISPLACEMENTS

Following are the numerical modelling results for roof displacements for the 4.8 m x 4.8 m wide virgin ground opening.

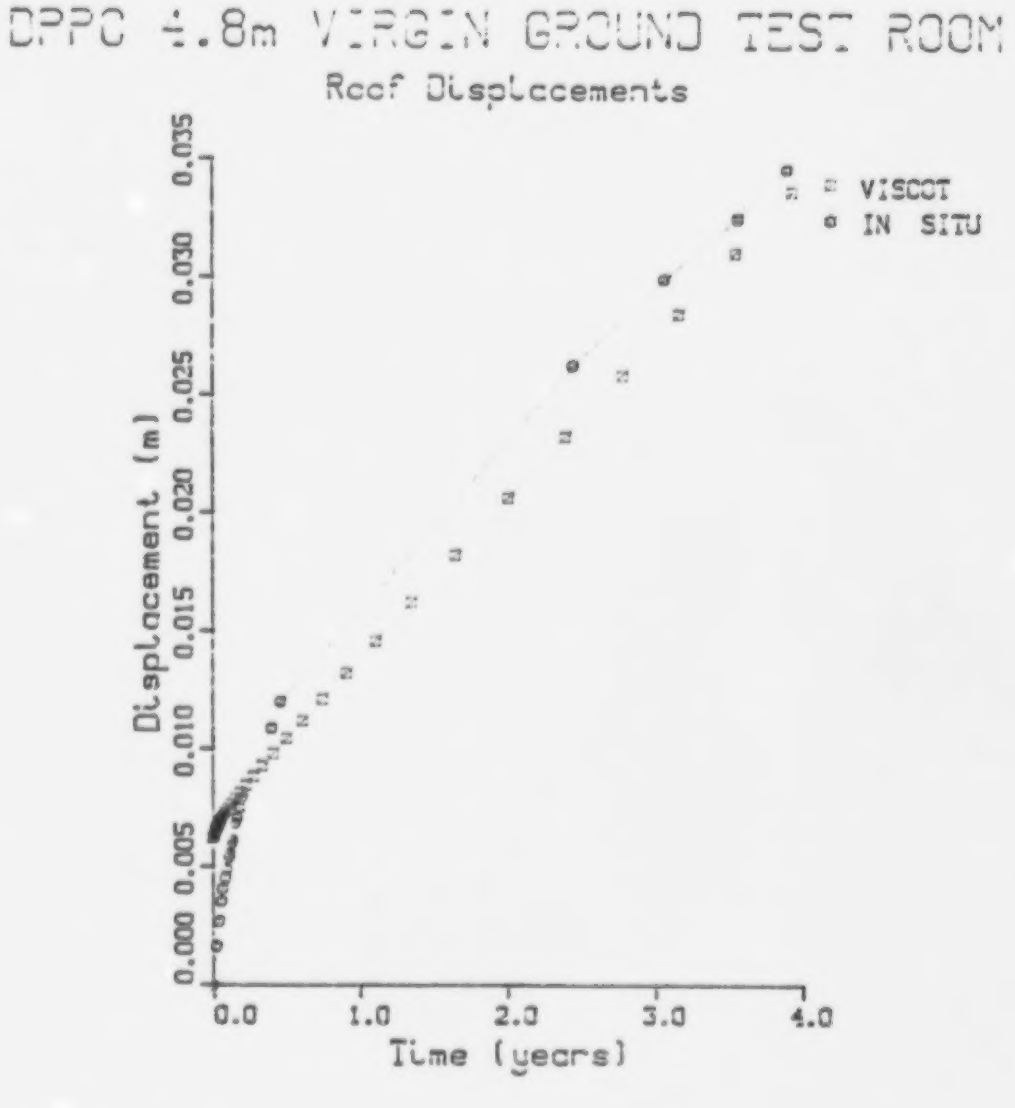
DPPC 4.8m VIRGIN GROUND TEST ROOM
Roof Displacements
VISCOT
IN SITU
Displacement (m)
0.000
0.005
0.010
0.015
0.020
0.025
0.030
0.035
Time (years)
0.0
1.0
2.0
3.0
4.0

FIGURE 6.1

6.2 WALL DISPLACEMENTS

Following are the numerical modelling results for wall displacements for the 4.8 m x 4.8 m wide virgin ground opening.

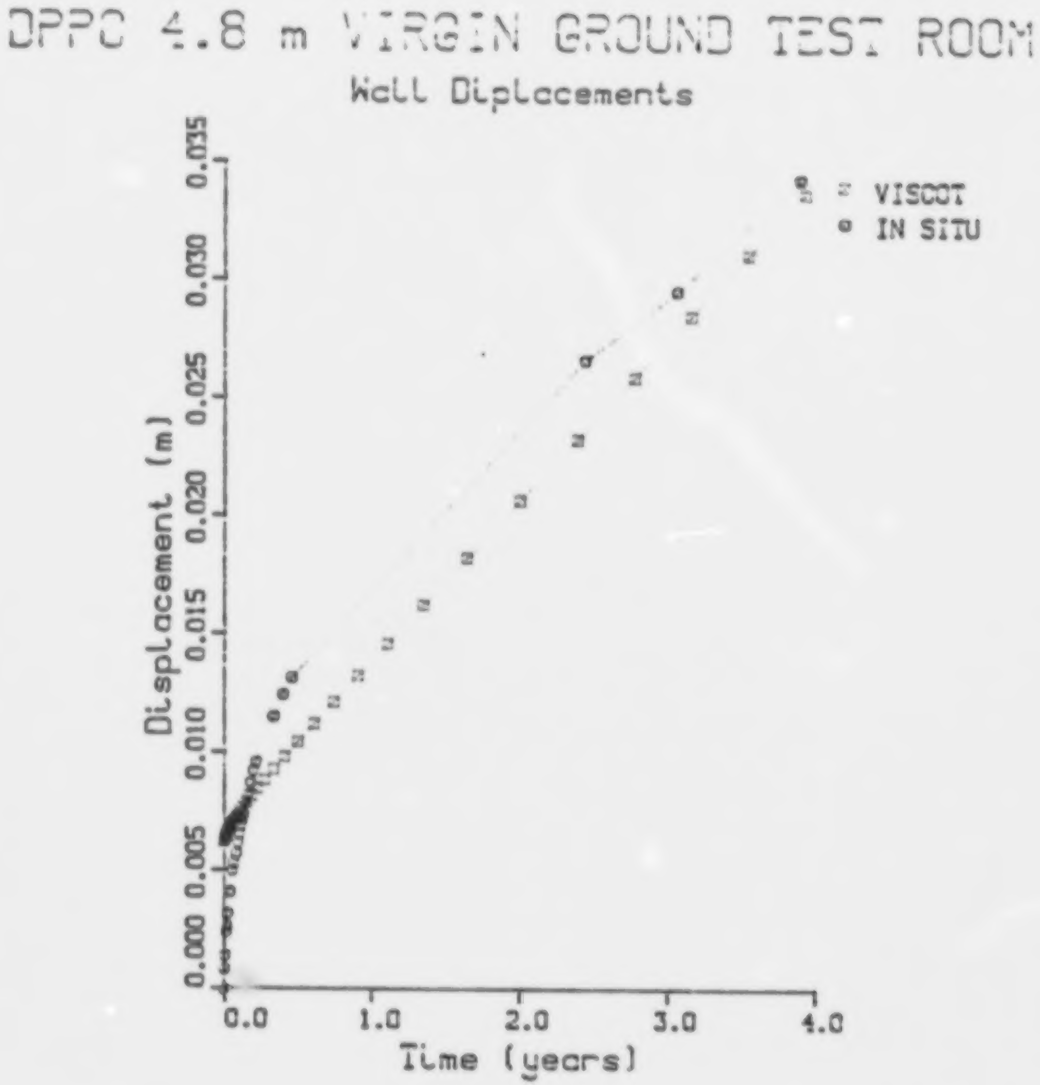
DPPC 4.8 m VIRGIN GROUND TEST ROOM
Wall Diplacements
Displacement (m)
0.000
0.005
0.010
0.015
0.020
0.025
0.030
0.035
Time (years)
0.0
1.0
2.0
3.0
4.0
VISCOT
IN SITU

FIGURE 6.2

6.3 SHEAR STRESS IN WALLS

Following are graphical summaries of the numerical modelling results for the shear stress with reference to distance from the centre of the pillar for the 4.8 m x 4.8 m wide virgin ground opening.

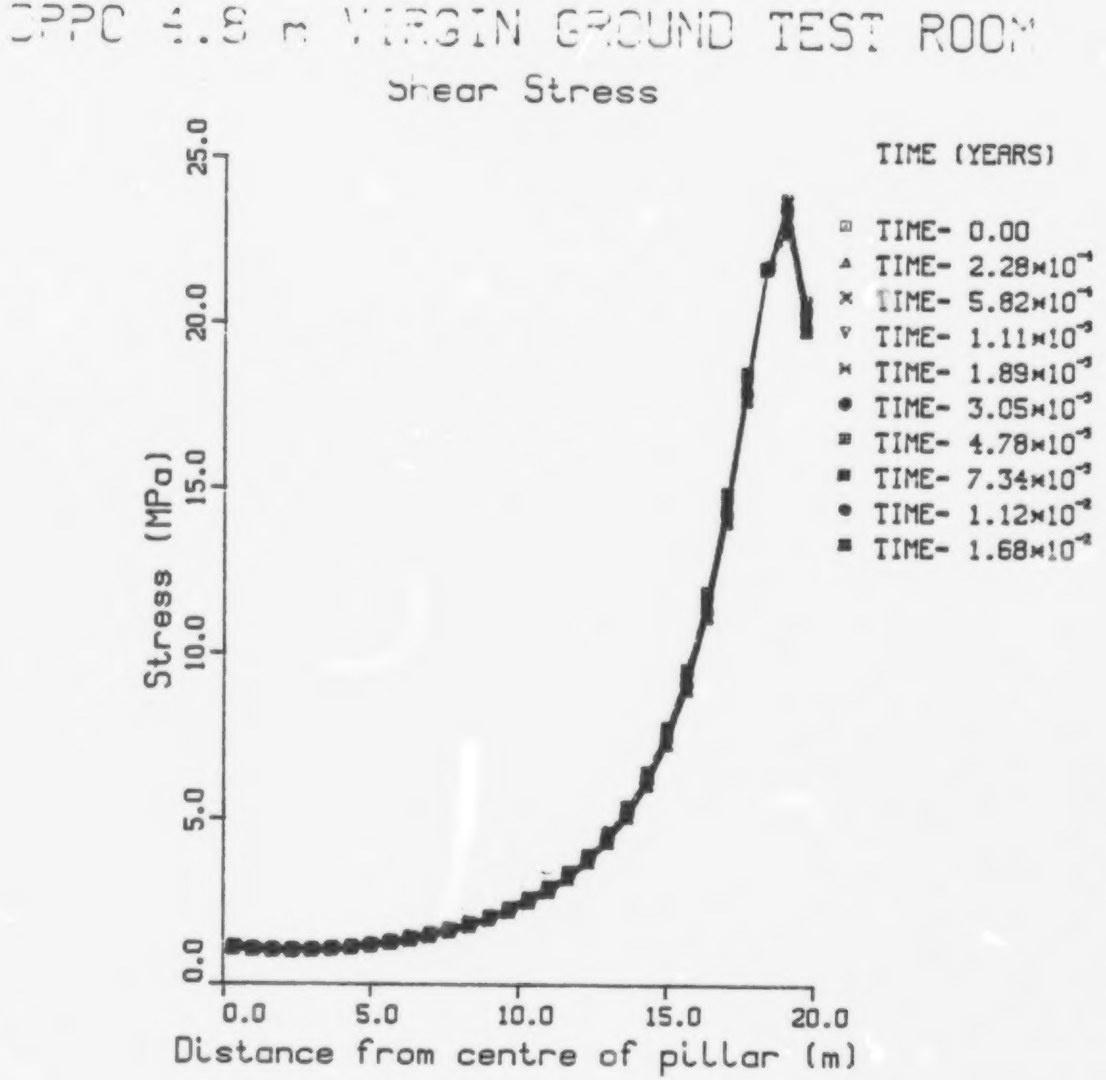
CPPC 4.8 m VIRGIN GROUND TEST ROOM
Shear Stress
Stress (MPa)
0.0
5.0
10.0
15.0
20.0
25.0
Distance from centre of pillar (m)
0.0
5.0
10.0
15.0
20.0
TIME (YEARS)
TIME- 0.00
TIME- 2.28×10⁻⁴
TIME- 5.82×10⁻⁴
TIME- 1.11×10⁻³
TIME- 1.89×10⁻³
TIME- 3.05×10⁻³
TIME- 4.78×10⁻³
TIME- 7.34×10⁻³
TIME- 1.12×10⁻²
TIME- 1.68×10⁻²

FIGURE 6.3

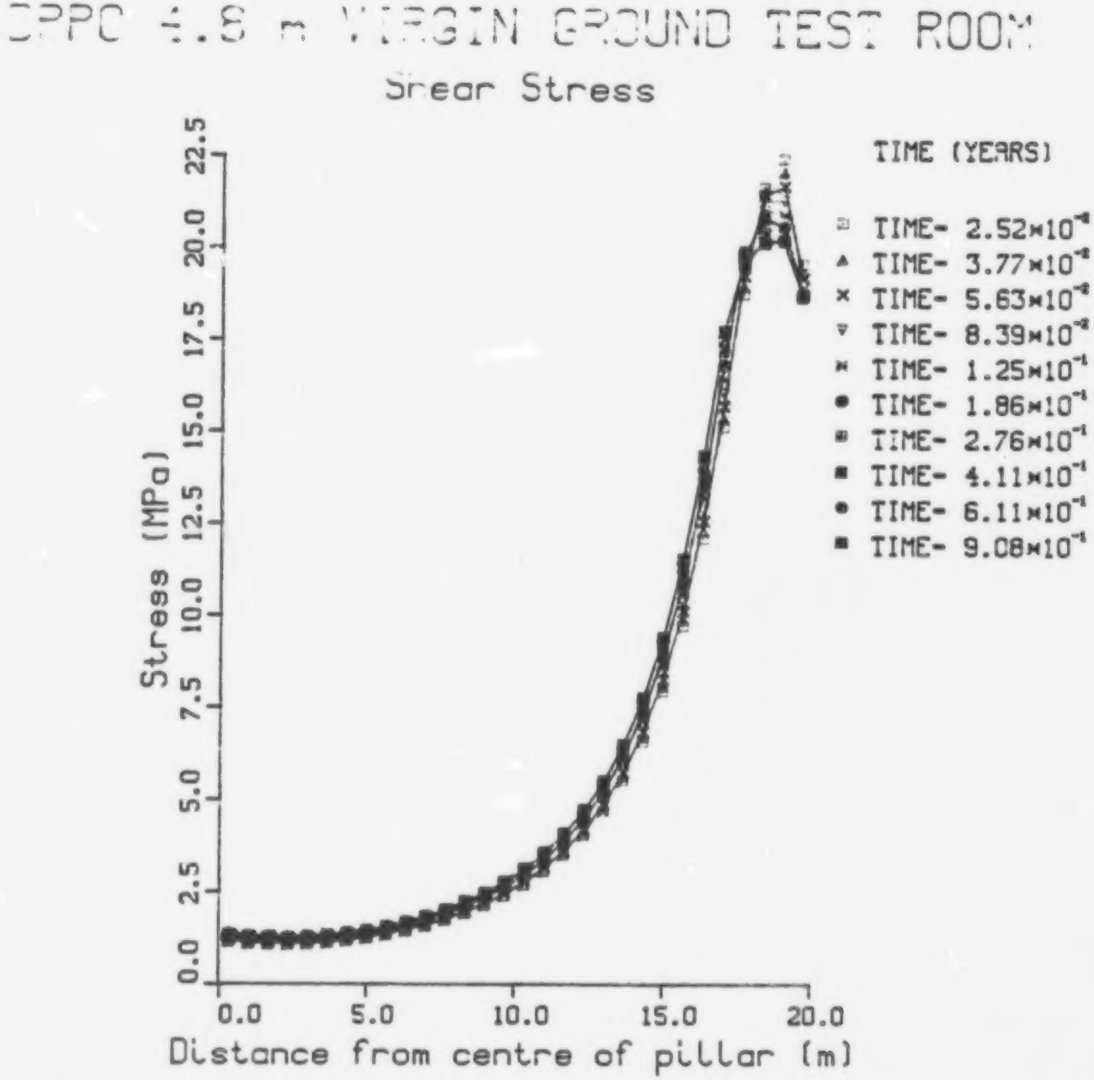
CPPC 4.8 m VIRGIN GROUND TEST ROOM
Shear Stress
Stress (MPa)
0.0
2.5
5.0
7.5
10.0
12.5
15.0
17.5
20.0
22.5
Distance from centre of pillar (m)
0.0
5.0
10.0
15.0
20.0
TIME (YEARS)
TIME- 2.52×10⁻²
TIME- 3.77×10⁻²
TIME- 5.63×10⁻²
TIME- 8.39×10⁻²
TIME- 1.25×10⁻¹
TIME- 1.86×10⁻¹
TIME- 2.76×10⁻¹
TIME- 4.11×10⁻¹
TIME- 6.11×10⁻¹
TIME- 9.08×10⁻¹

FIGURE 6.4

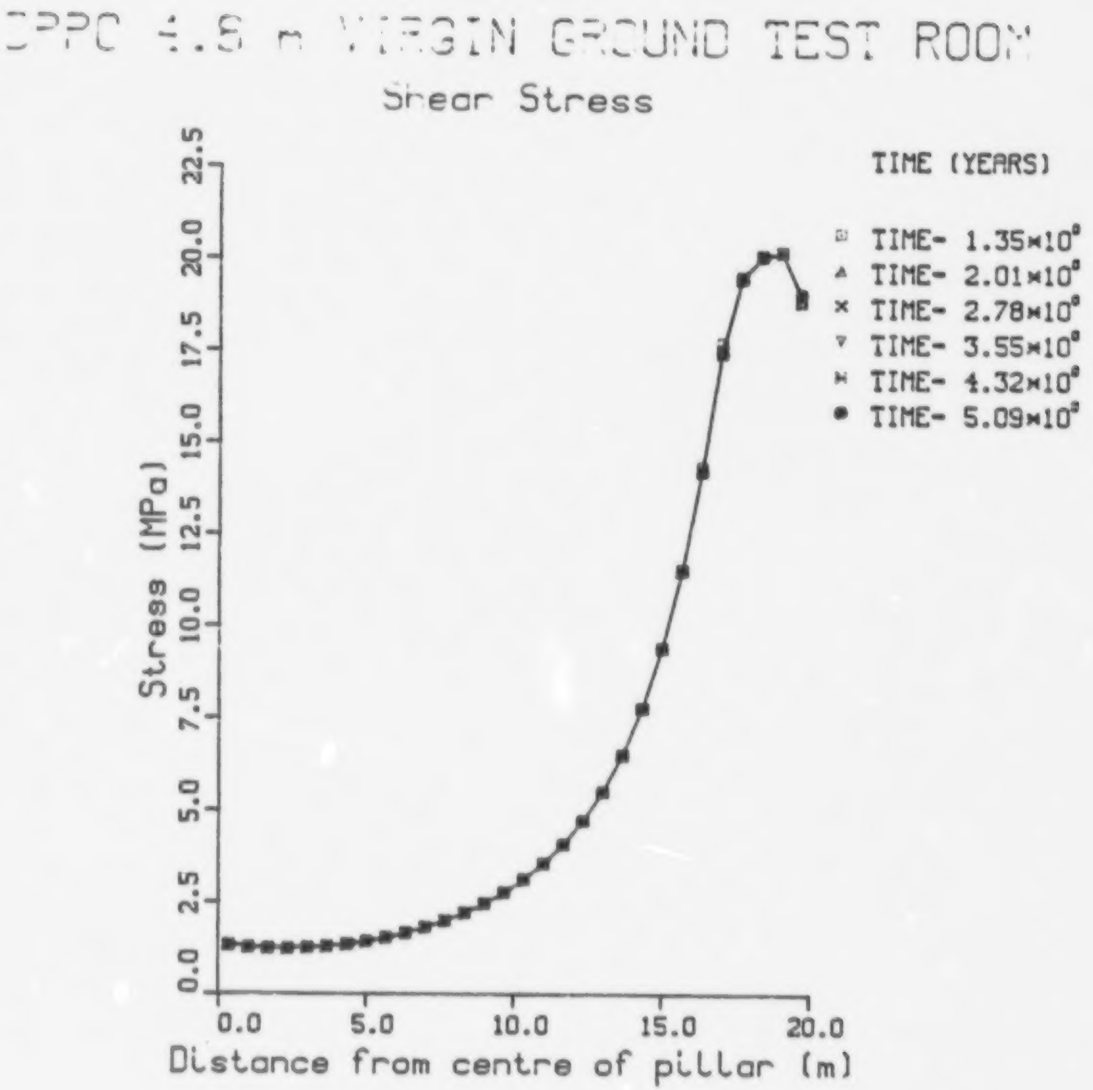
CPPC 4.5 m VIRGIN GROUND TEST ROOM
Shear Stress
Stress (MPa)
0.0
2.5
5.0
7.5
10.0
12.5
15.0
17.5
20.0
22.5
0.0
5.0
10.0
15.0
20.0
Distance from centre of pillar (m)
TIME (YEARS)
□ TIME- 1.35×10^{0}
▲ TIME- 2.01×10^{0}
× TIME- 2.78×10^{0}
▼ TIME- 3.55×10^{0}
⋈ TIME- 4.32×10^{0}
● TIME- 5.09×10^{0}

FIGURE 6.5

6.4 MAJOR PRINCIPAL STRESS IN WALLS

Following are graphical summaries of the numerical modelling results for the major (maximum) principal stress with reference to distance from the centre of the pillar for the 4.8 m x 4.8 m wide virgin ground opening.

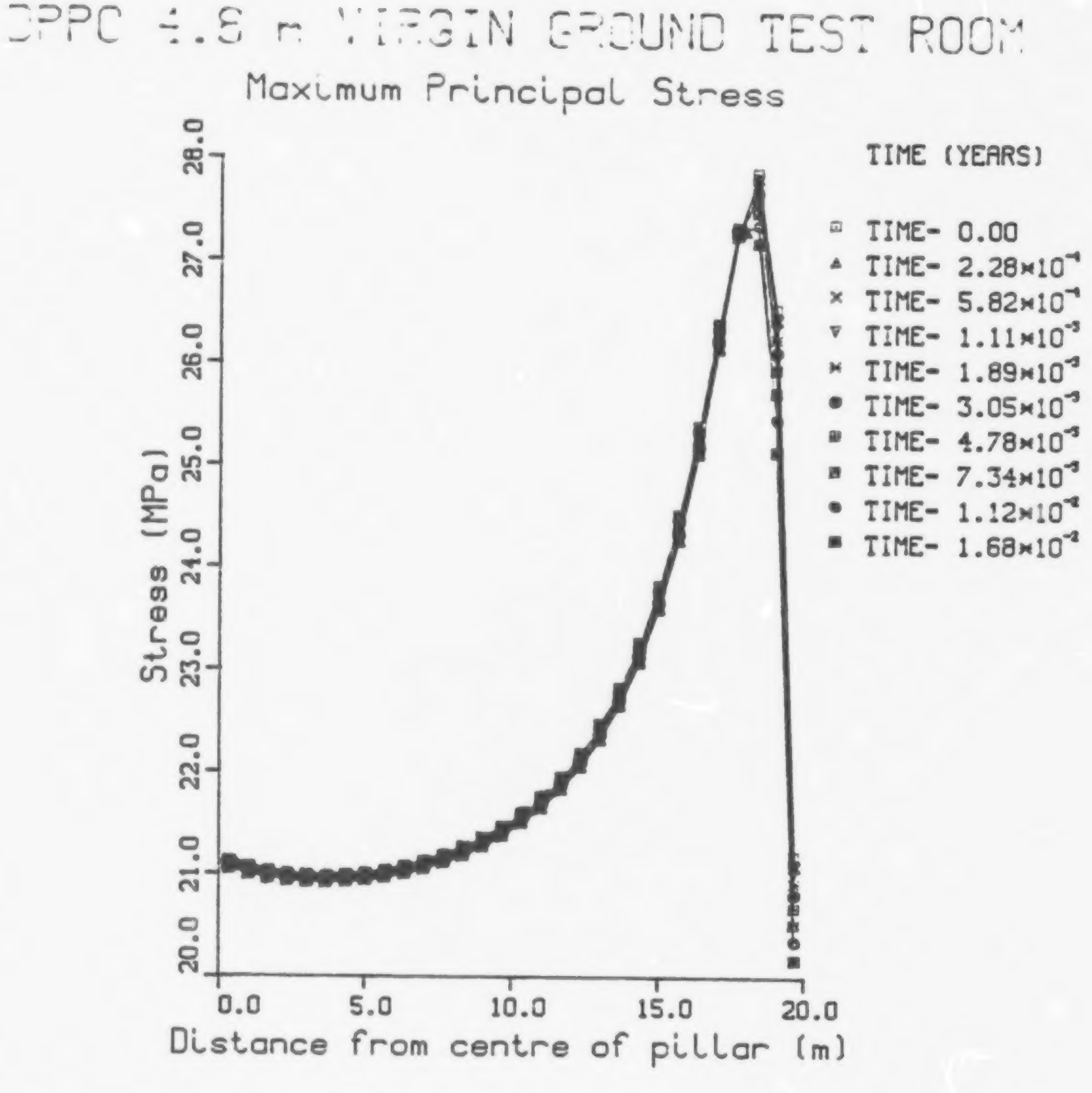
DPPC 4.8 m VIRGIN GROUND TEST ROOM
Maximum Principal Stress
Stress (MPa)
28.0
27.0
26.0
25.0
24.0
23.0
22.0
21.0
20.0
0.0
5.0
10.0
15.0
20.0
Distance from centre of pillar (m)
TIME (YEARS)
TIME- 0.00
TIME- 2.28×10⁻⁴
TIME- 5.82×10⁻⁴
TIME- 1.11×10⁻³
TIME- 1.89×10⁻³
TIME- 3.05×10⁻³
TIME- 4.78×10⁻³
TIME- 7.34×10⁻³
TIME- 1.12×10⁻²
TIME- 1.68×10⁻²

FIGURE 6.6

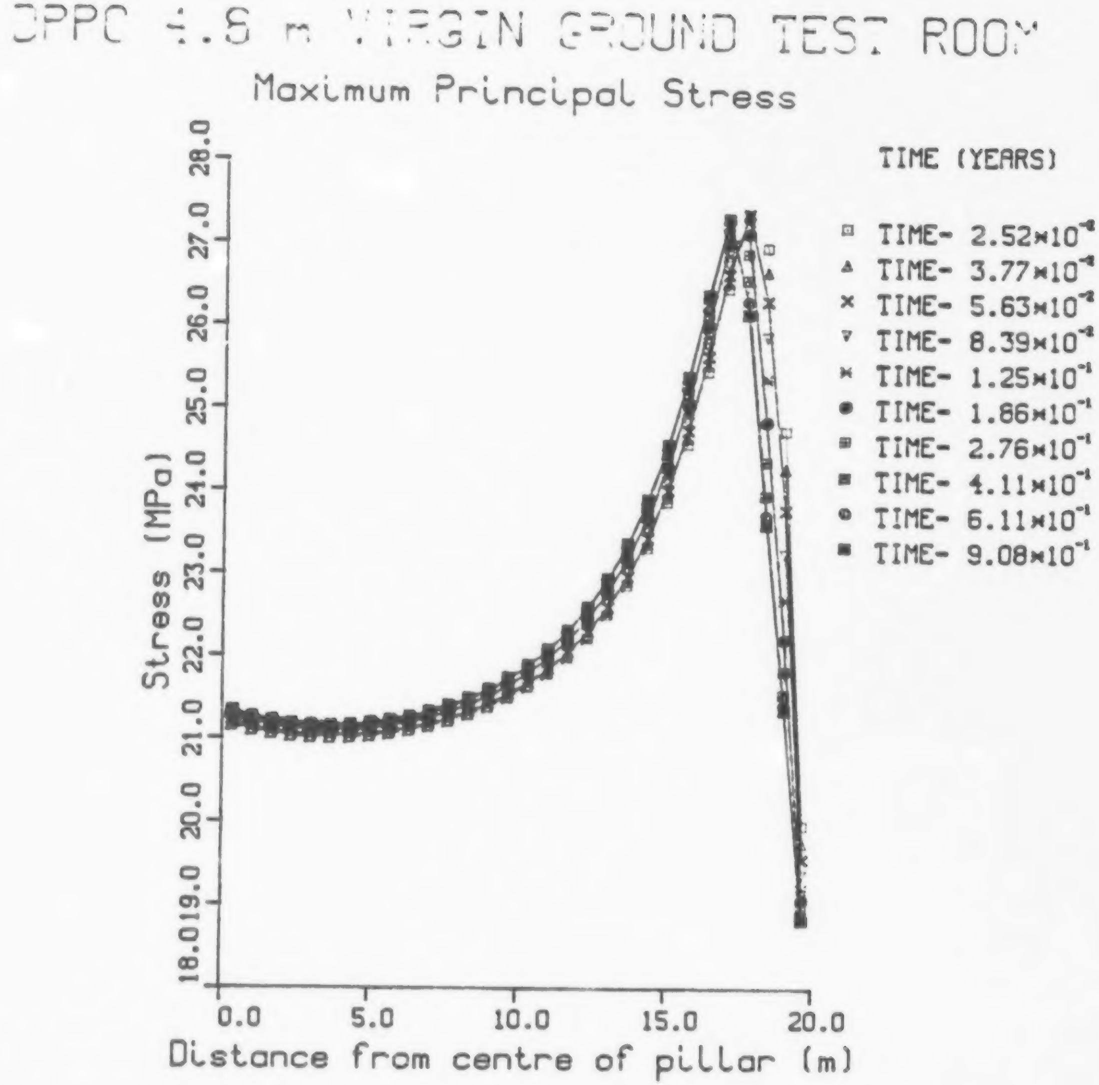
DPPC 4.8 m VIRGIN GROUND TEST ROOM
Maximum Principal Stress
TIME (YEARS)
TIME- 2.52×10⁻²
TIME- 3.77×10⁻²
TIME- 5.63×10⁻²
TIME- 8.39×10⁻²
TIME- 1.25×10⁻¹
TIME- 1.86×10⁻¹
TIME- 2.76×10⁻¹
TIME- 4.11×10⁻¹
TIME- 6.11×10⁻¹
TIME- 9.08×10⁻¹
Stress (MPa)
18.0
19.0
20.0
21.0
22.0
23.0
24.0
25.0
26.0
27.0
28.0
0.0
5.0
10.0
15.0
20.0
Distance from centre of pillar (m)

FIGURE 6.7

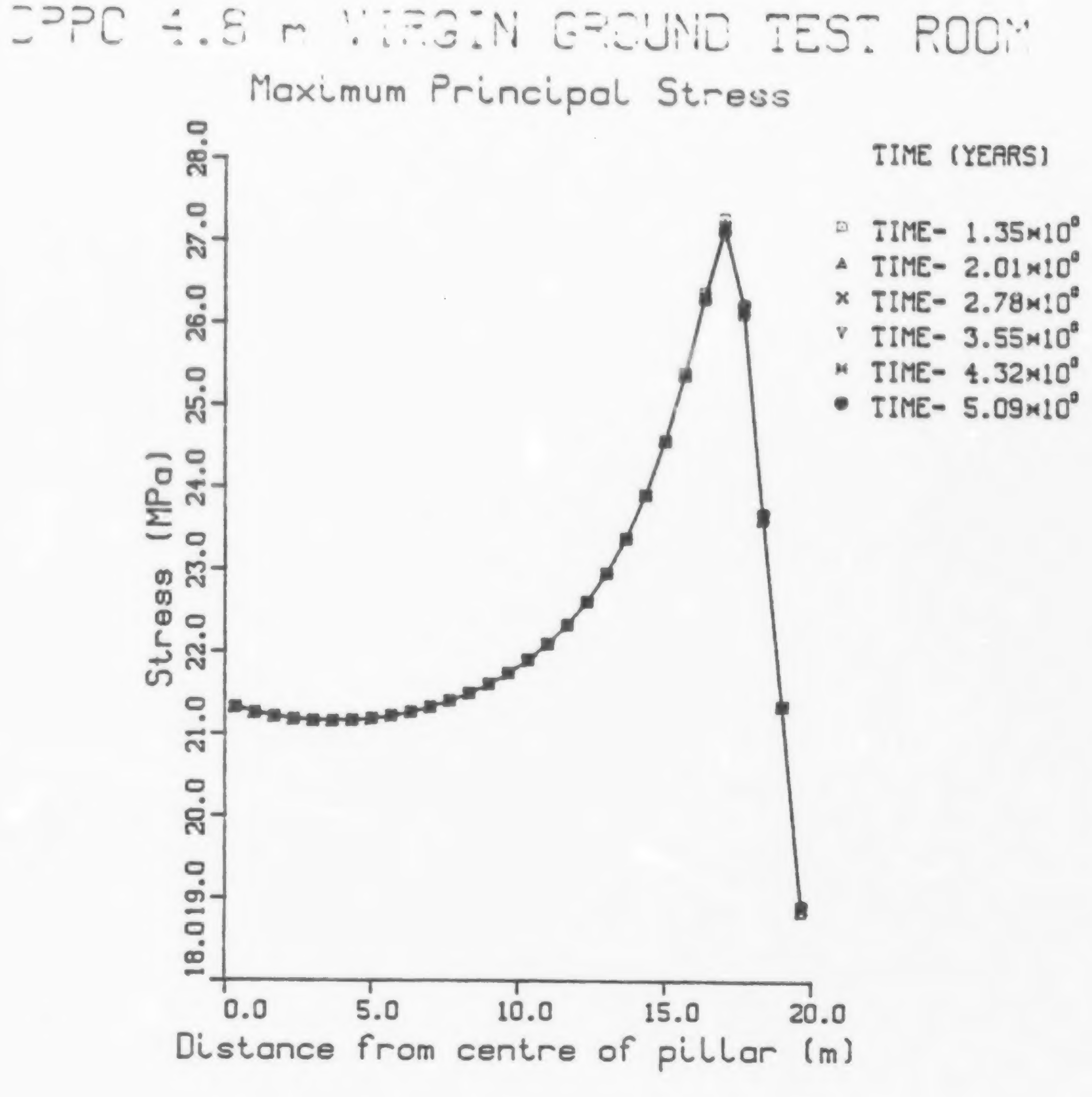
CPPC 4.8 m VIRGIN GROUND TEST ROOM
Maximum Principal Stress
Stress (MPa)
18.0
19.0
20.0
21.0
22.0
23.0
24.0
25.0
26.0
27.0
28.0
0.0
5.0
10.0
15.0
20.0
Distance from centre of pillar (m)
TIME (YEARS)
□ TIME- 1.35×10⁰
▲ TIME- 2.01×10⁰
× TIME- 2.78×10⁰
▼ TIME- 3.55×10⁰
⌘ TIME- 4.32×10⁰
● TIME- 5.09×10⁰

FIGURE 6.8

6.5 MINOR PRINCIPAL STRESS IN WALLS

Following are graphical summaries of the numerical modelling results for the minor (minimum) principal stress with reference to distance from the centre of the pillar for the 4.8 m x 4.8 m wide virgin ground opening.

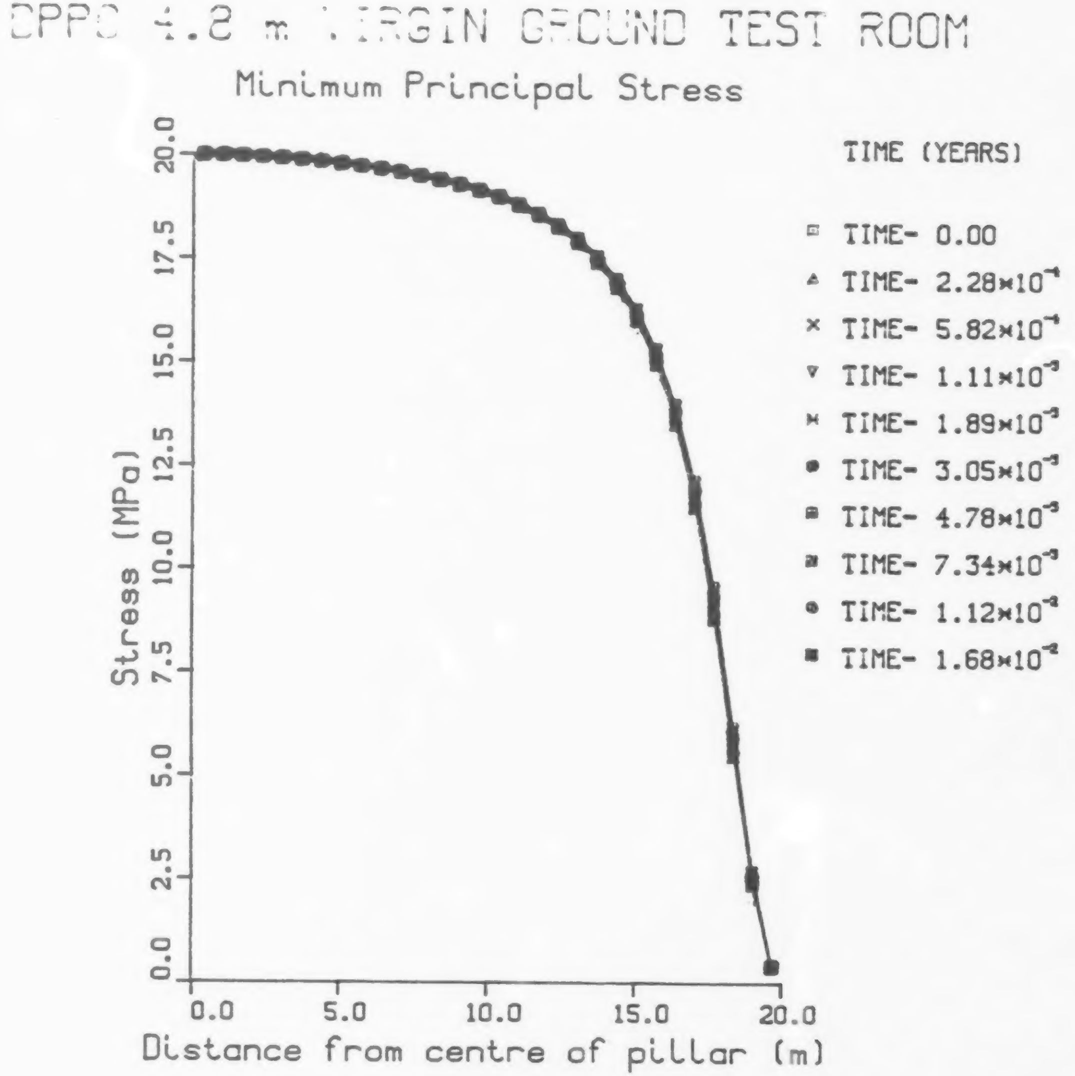CPPC 4.2 m VIRGIN GROUND TEST ROOM
Minimum Principal Stress
Stress (MPa)
0.0
2.5
5.0
7.5
10.0
12.5
15.0
17.5
20.0
Distance from centre of pillar (m)
0.0
5.0
10.0
15.0
20.0
TIME (YEARS)
TIME- 0.00
TIME- 2.28×10^{-4}
TIME- 5.82×10^{-4}
TIME- 1.11×10^{-3}
TIME- 1.89×10^{-3}
TIME- 3.05×10^{-3}
TIME- 4.78×10^{-3}
TIME- 7.34×10^{-3}
TIME- 1.12×10^{-2}
TIME- 1.68×10^{-2}

FIGURE 6.9

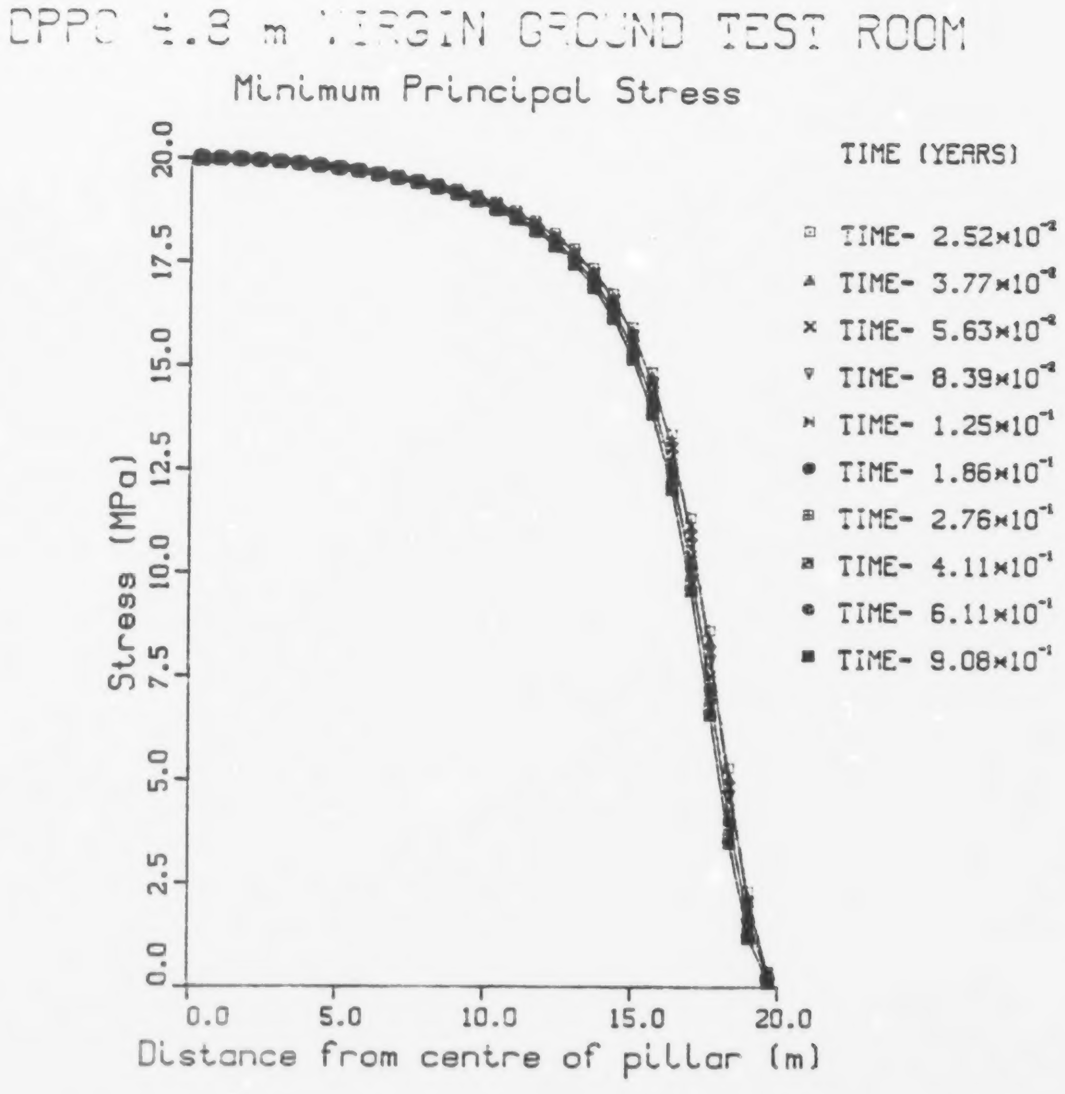
CPPC 4.8 m VIRGIN GROUND TEST ROOM
Minimum Principal Stress
Stress (MPa)
0.0
2.5
5.0
7.5
10.0
12.5
15.0
17.5
20.0
Distance from centre of pillar (m)
0.0
5.0
10.0
15.0
20.0
TIME (YEARS)
□ TIME- 2.52×10^{-2}
▲ TIME- 3.77×10^{-2}
× TIME- 5.63×10^{-2}
▼ TIME- 8.39×10^{-2}
⋈ TIME- 1.25×10^{-1}
● TIME- 1.86×10^{-1}
⊞ TIME- 2.76×10^{-1}
⊠ TIME- 4.11×10^{-1}
● TIME- 6.11×10^{-1}
■ TIME- 9.08×10^{-1}

FIGURE 6.10

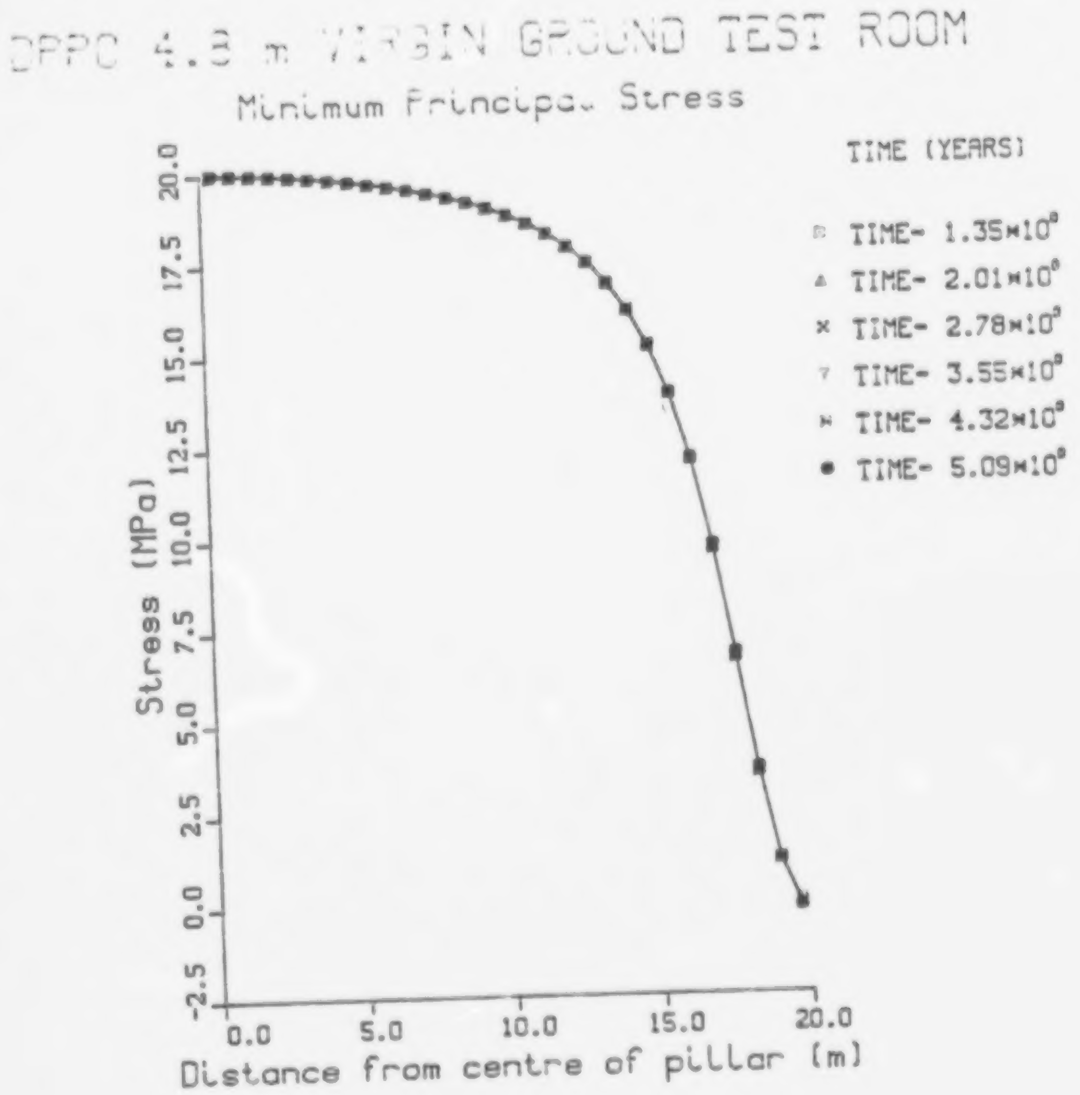
DPPC 4.8 m VIRGIN GROUND TEST ROOM
Minimum Principal Stress
TIME (YEARS)
TIME- 1.35×10^{0}
TIME- 2.01×10^{0}
TIME- 2.78×10^{0}
TIME- 3.55×10^{0}
TIME- 4.32×10^{0}
TIME- 5.09×10^{0}
Stress (MPa)
20.0
17.5
15.0
12.5
10.0
7.5
5.0
2.5
0.0
-2.5
0.0
5.0
10.0
15.0
20.0
Distance from centre of pillar (m)

FIGURE 6.11

6.6 DISPLACEMENT RATES DISTRIBUTION

Following are the numerical modelling results for displacement rates for the 4.8 m x 4.8 m wide virgin ground opening.

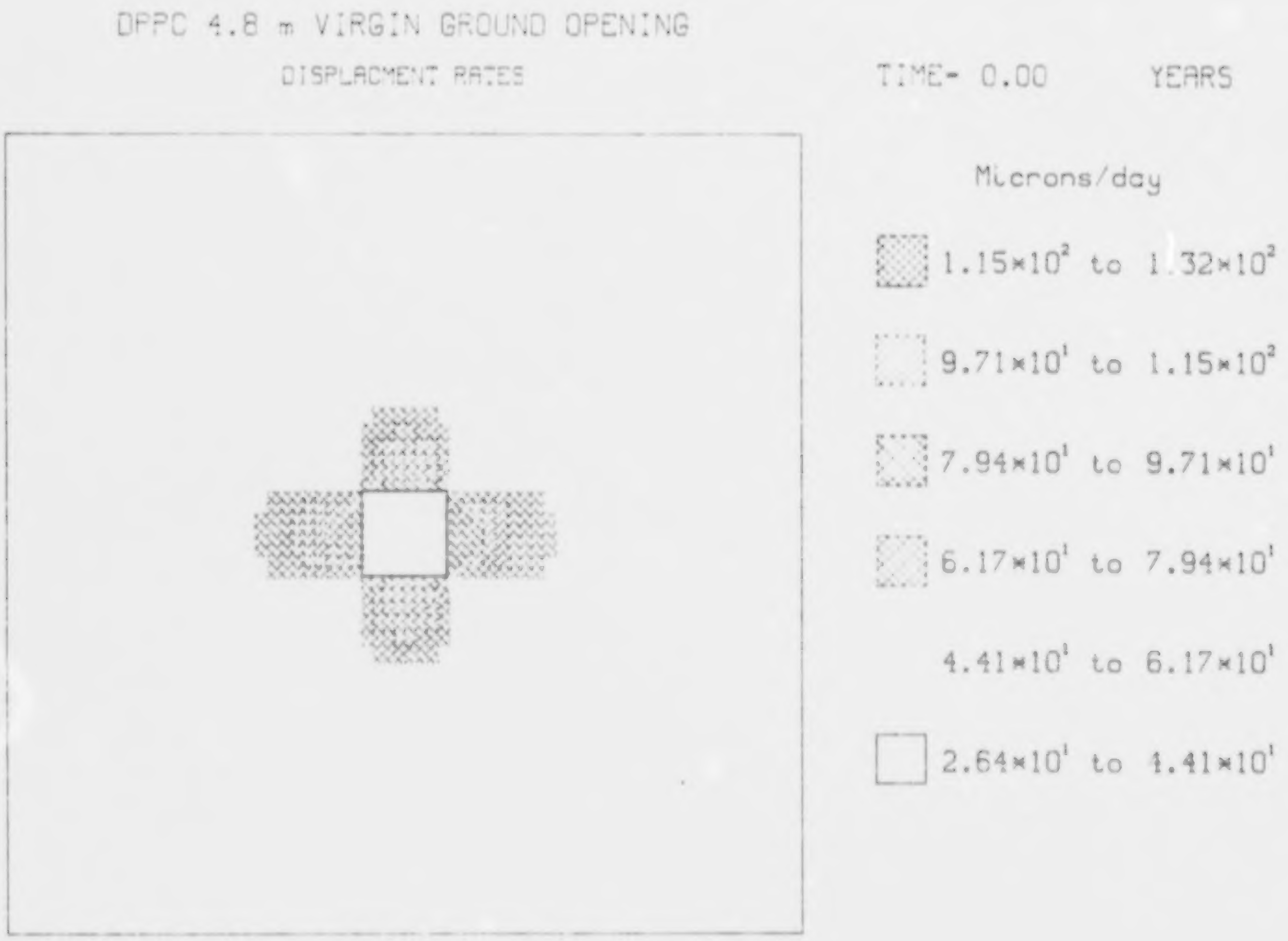
DPPC 4.8 m VIRGIN GROUND OPENING
DISPLACMENT RATES
TIME- 0.00 YEARS
Microns/day
1.15×10² to 1.32×10²
9.71×10¹ to 1.15×10²
7.94×10¹ to 9.71×10¹
6.17×10¹ to 7.94×10¹
4.41×10¹ to 6.17×10¹
2.64×10¹ to 4.41×10¹

FIGURE 6.12

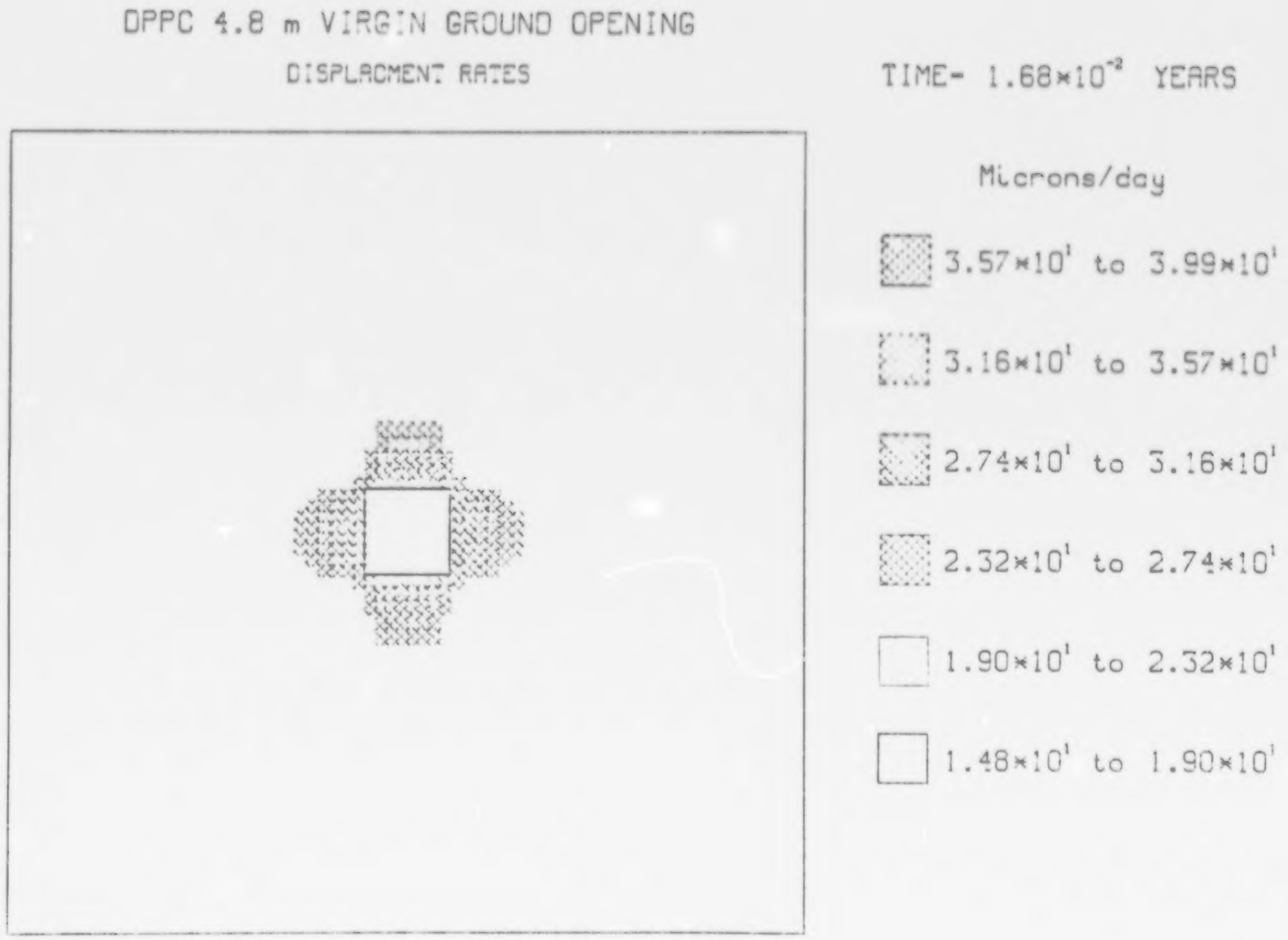
DPPC 4.8 m VIRGIN GROUND OPENING
DISPLACMENT RATES
TIME- 1.68×10⁻² YEARS
Microns/day
▩ 3.57×10¹ to 3.99×10¹
⬚ 3.16×10¹ to 3.57×10¹
▨ 2.74×10¹ to 3.16×10¹
▩ 2.32×10¹ to 2.74×10¹
☐ 1.90×10¹ to 2.32×10¹
☐ 1.48×10¹ to 1.90×10¹

FIGURE 6.13

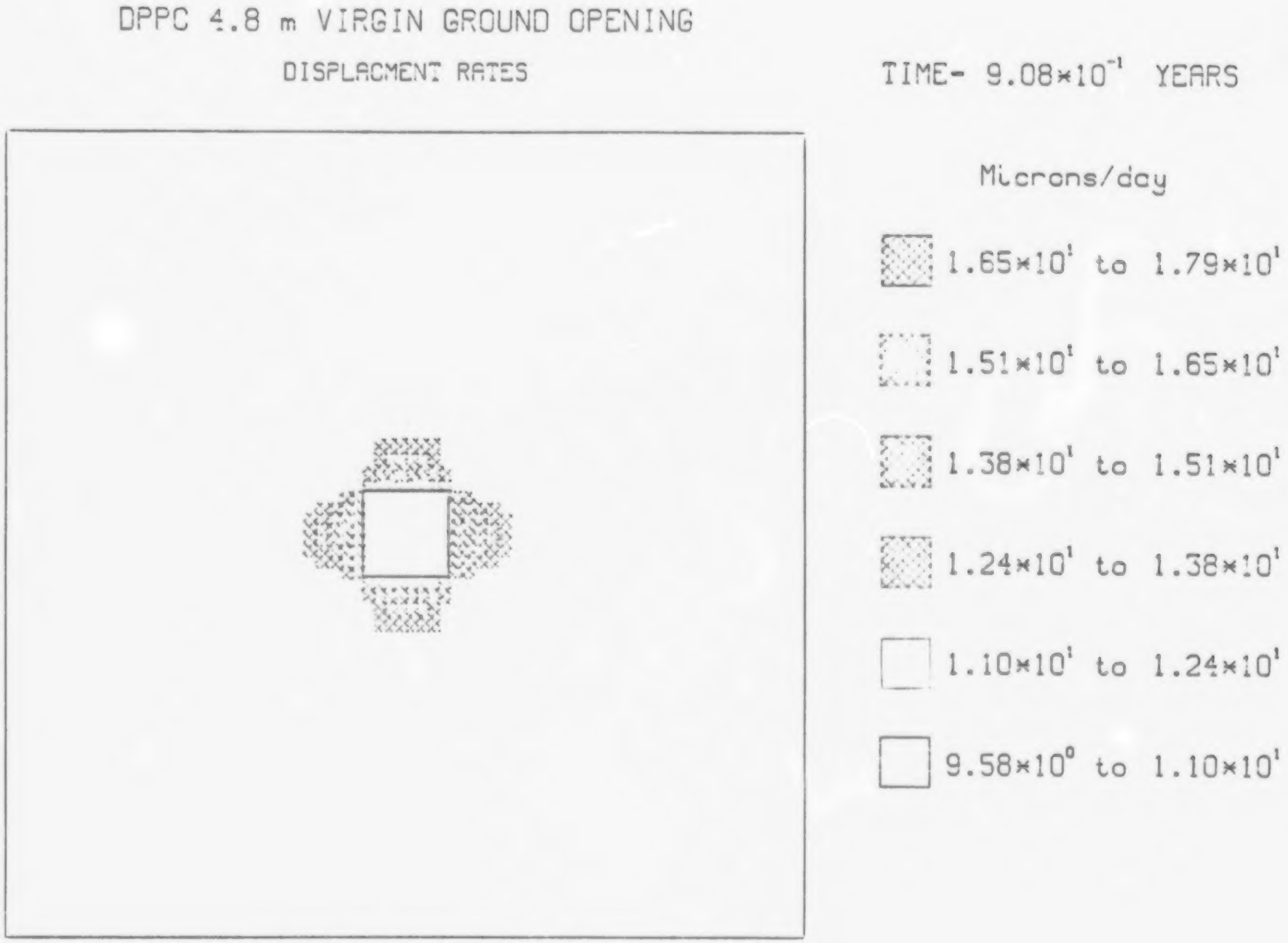

DPPC 4.8 m VIRGIN GROUND OPENING

DISPLACMENT RATES

FIGURE 6.14

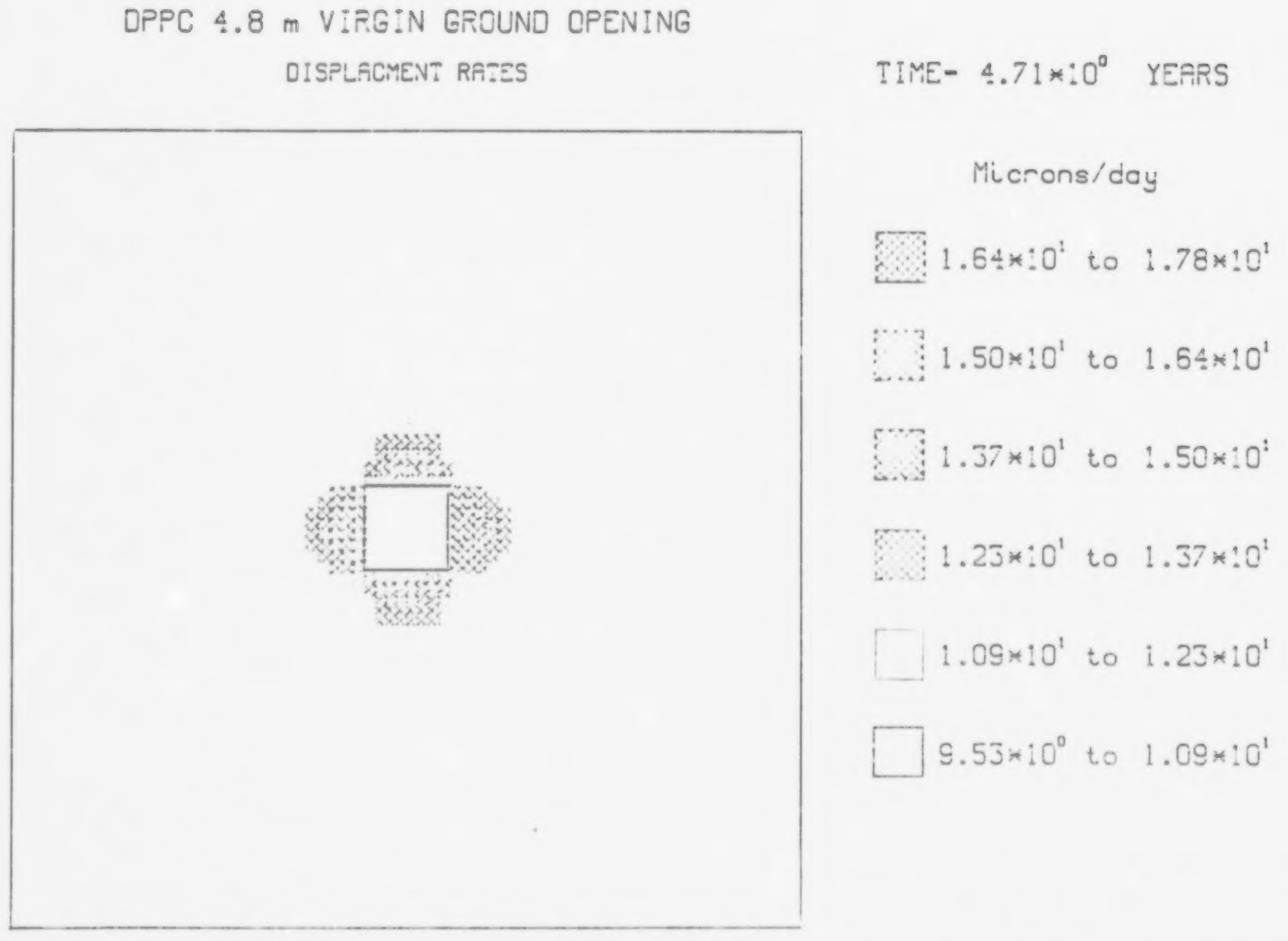DPPC 4.8 m VIRGIN GROUND OPENING
DISPLACMENT RATES
TIME- 4.71*10^0 YEARS
Microns/day
1.64*10^1 to 1.78*10^1
1.50*10^1 to 1.64*10^1
1.37*10^1 to 1.50*10^1
1.23*10^1 to 1.37*10^1
1.09*10^1 to 1.23*10^1
9.53*10^0 to 1.09*10^1

FIGURE 6.15

6.7 STRAIN RATE DISTRIBUTION

Following are the numerical modelling results for strain rates for the 4.8 m x 4.8m wide virgin ground opening.

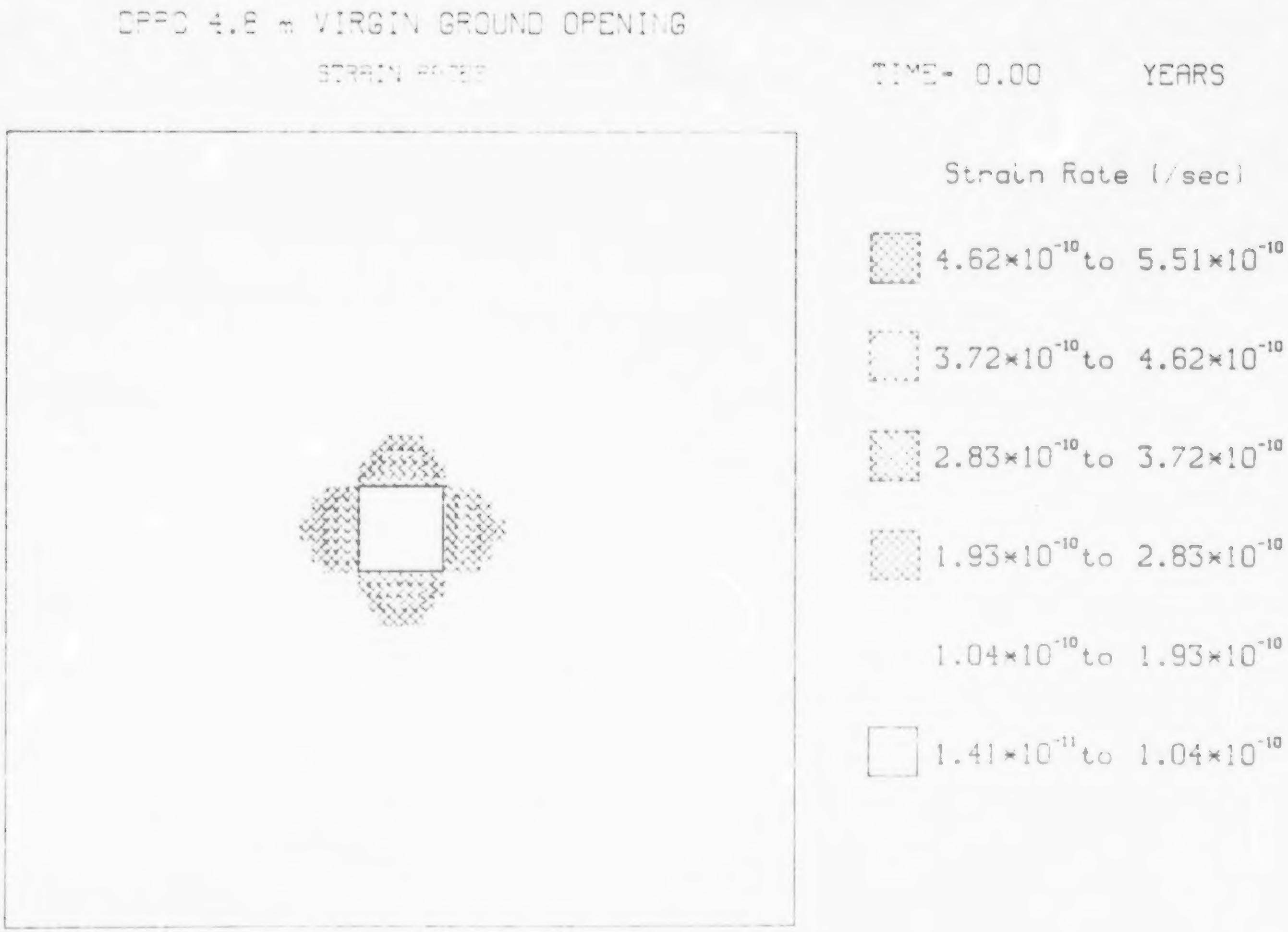
DPPC 4.8 m VIRGIN GROUND OPENING
STRAIN RATES
TIME- 0.00 YEARS
Strain Rate (/sec)
▨ 4.62×10^{-10} to 5.51×10^{-10}
▨ 3.72×10^{-10} to 4.62×10^{-10}
▨ 2.83×10^{-10} to 3.72×10^{-10}
▨ 1.93×10^{-10} to 2.83×10^{-10}
1.04×10^{-10} to 1.93×10^{-10}
☐ 1.41×10^{-11} to 1.04×10^{-10}

FIGURE 6.16

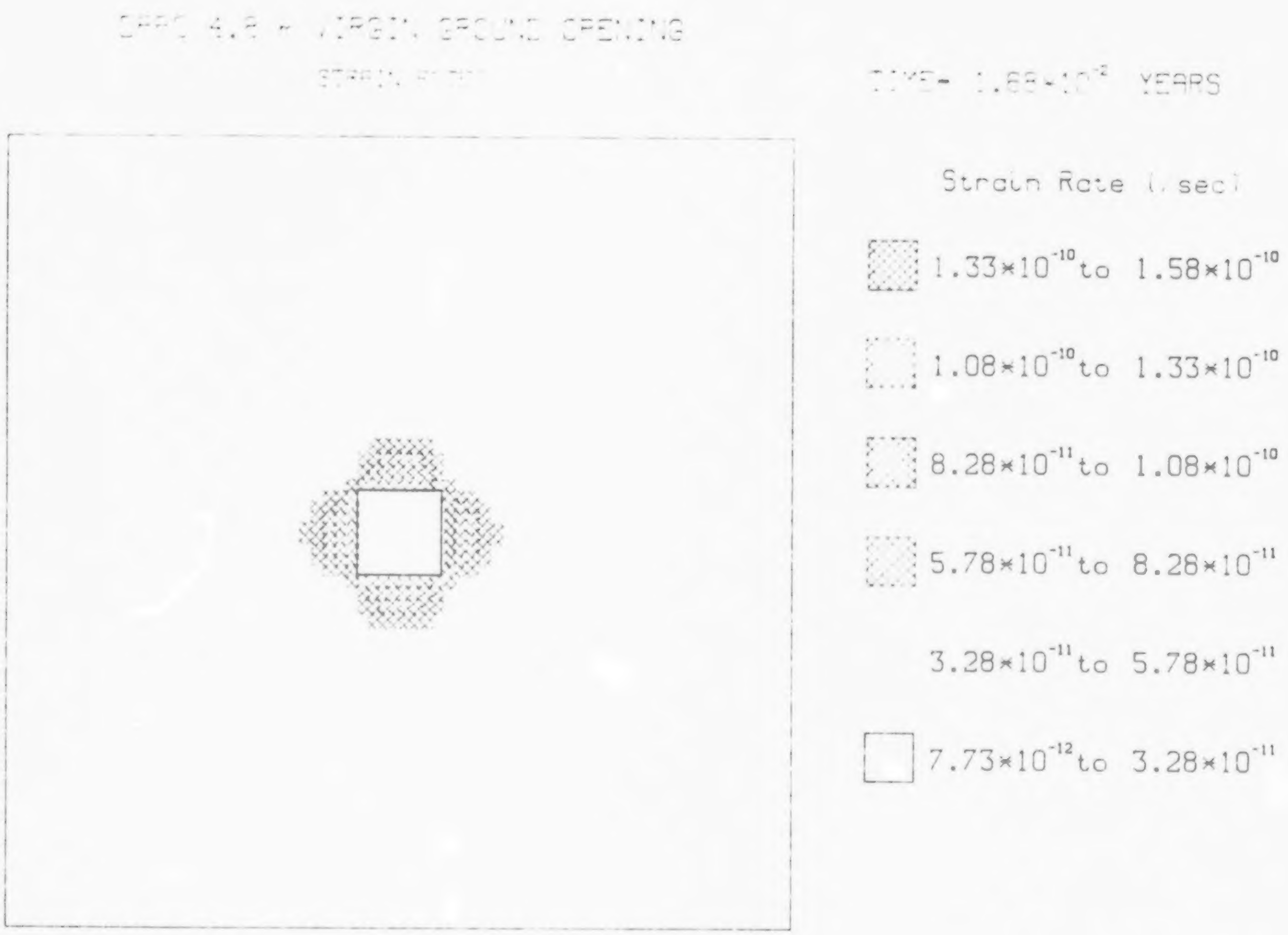
CARC 4.8 - VIRGIN GROUND OPENING
STRAIN RATE
TIME= 1.88×10⁻² YEARS
Strain Rate (/sec)
▨ 1.33×10⁻¹⁰ to 1.58×10⁻¹⁰
▨ 1.08×10⁻¹⁰ to 1.33×10⁻¹⁰
▨ 8.28×10⁻¹¹ to 1.08×10⁻¹⁰
▨ 5.78×10⁻¹¹ to 8.28×10⁻¹¹
3.28×10⁻¹¹ to 5.78×10⁻¹¹
☐ 7.73×10⁻¹² to 3.28×10⁻¹¹

FIGURE 6.17

DFPC 4.6 m VIRGIN GROUND OPENING

STRAIN RATES

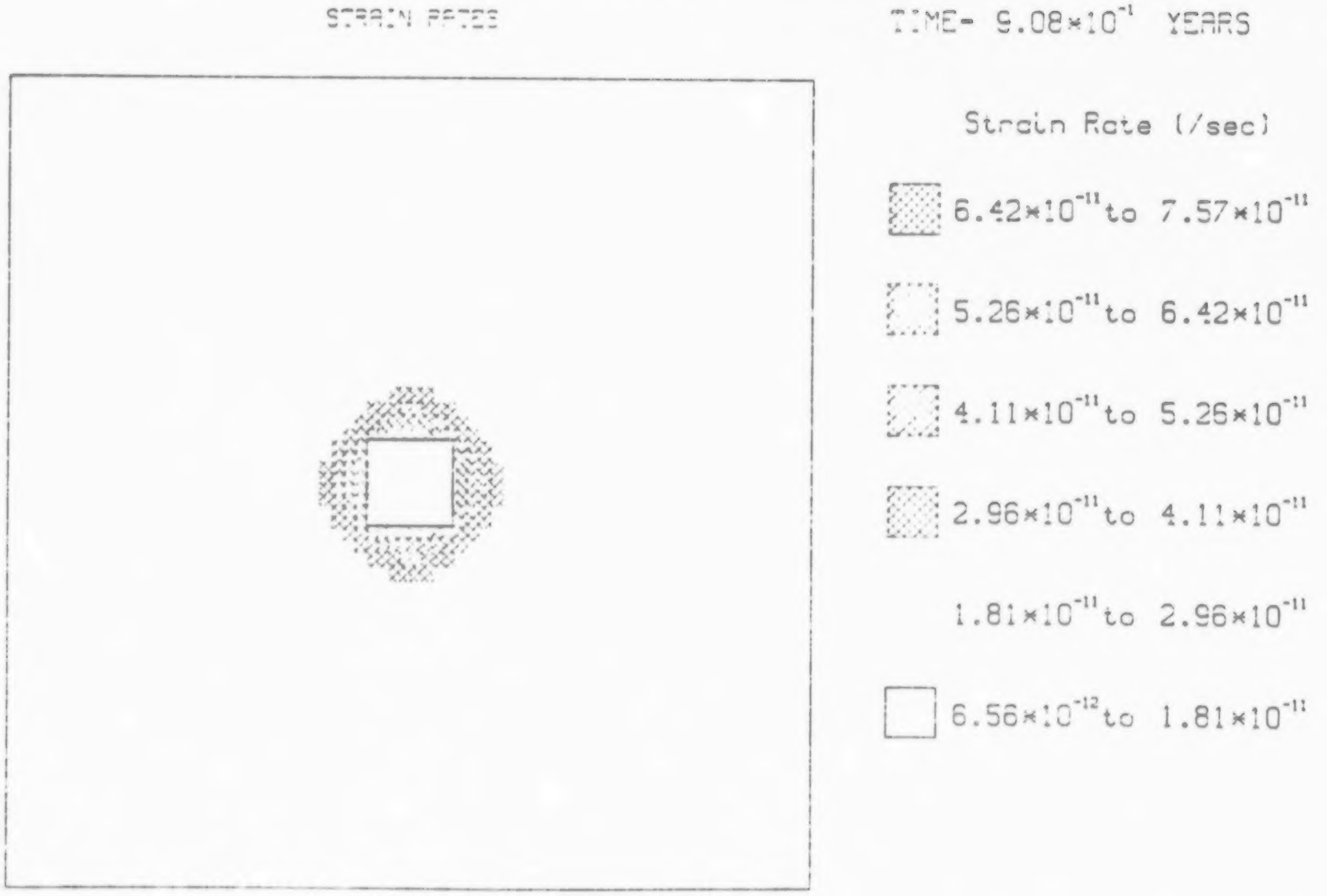

FIGURE 6.18

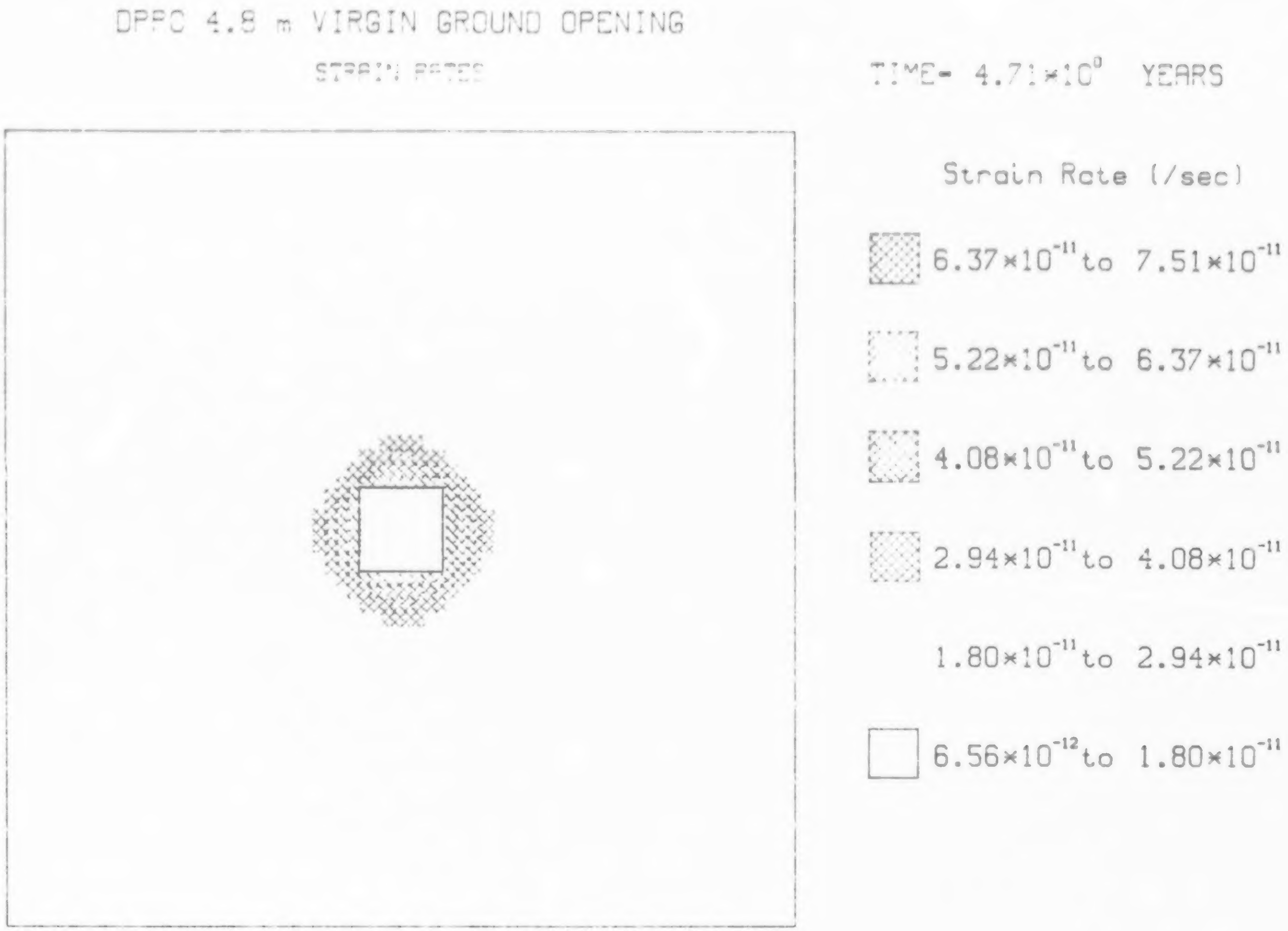
DPPC 4.8 m VIRGIN GROUND OPENING
STRAIN RATES
TIME- 4.71×10^0 YEARS
Strain Rate (/sec)
6.37×10^-11 to 7.51×10^-11
5.22×10^-11 to 6.37×10^-11
4.08×10^-11 to 5.22×10^-11
2.94×10^-11 to 4.08×10^-11
1.80×10^-11 to 2.94×10^-11
6.56×10^-12 to 1.80×10^-11

FIGURE 6.19

6.8 SHEAR STRESS DISTRIBUTION

Following are the numerical modelling results for shear stresses for 4.8 m x 4.8 m wide virgin ground opening.

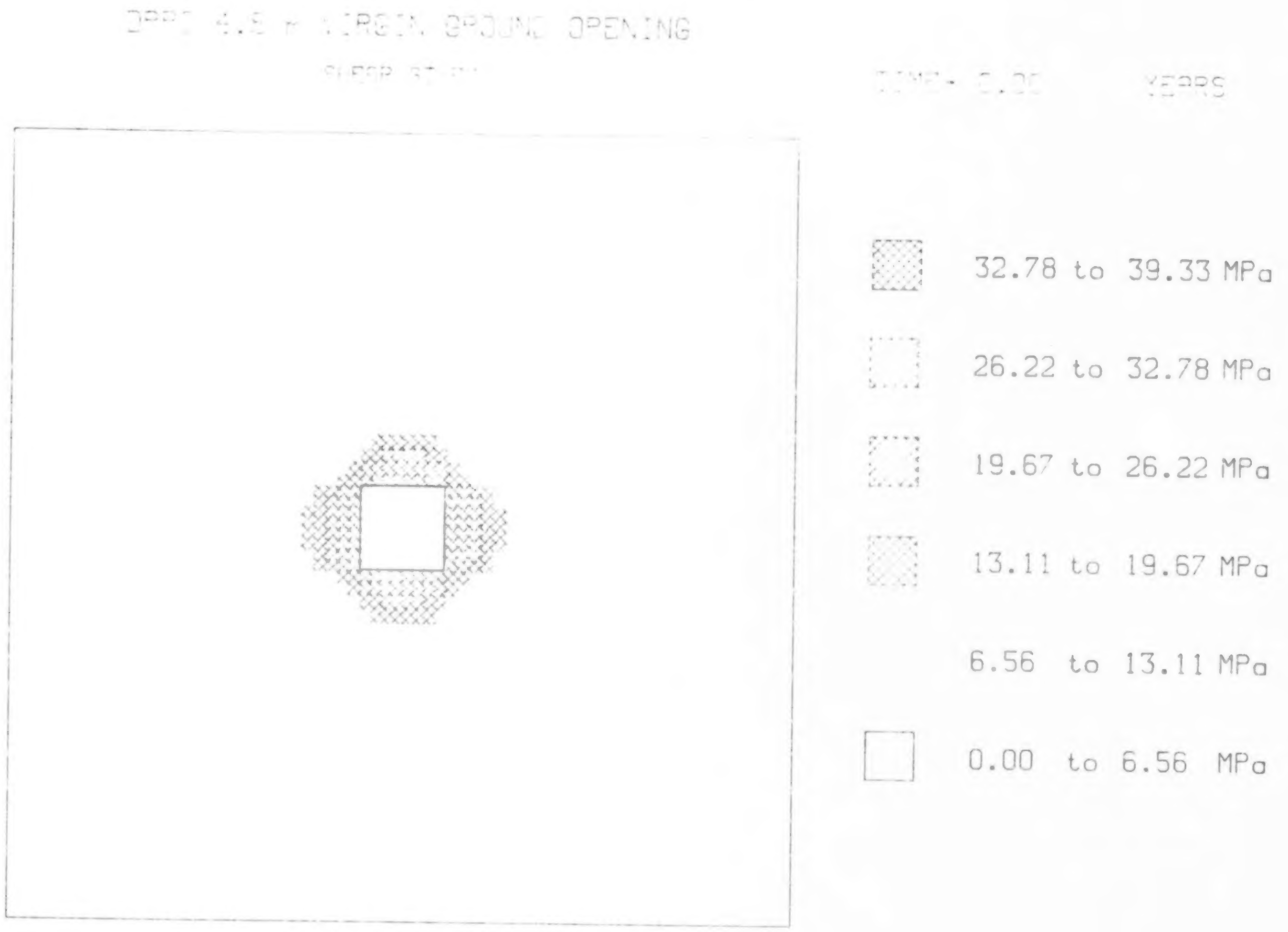
DRPC 4.5 m VIRGIN GROUND OPENING
SHEAR ST[illegible]
TIME= 0.00 YEARS
▨ 32.78 to 39.33 MPa
▨ 26.22 to 32.78 MPa
▨ 19.67 to 26.22 MPa
▨ 13.11 to 19.67 MPa
6.56 to 13.11 MPa
☐ 0.00 to 6.56 MPa

FIGURE 6.20

OPRC 4.8 – VIRGIN GROUND OPENING

SHEAR STRESS

TIME= 2.06×10^{-2} YEARS

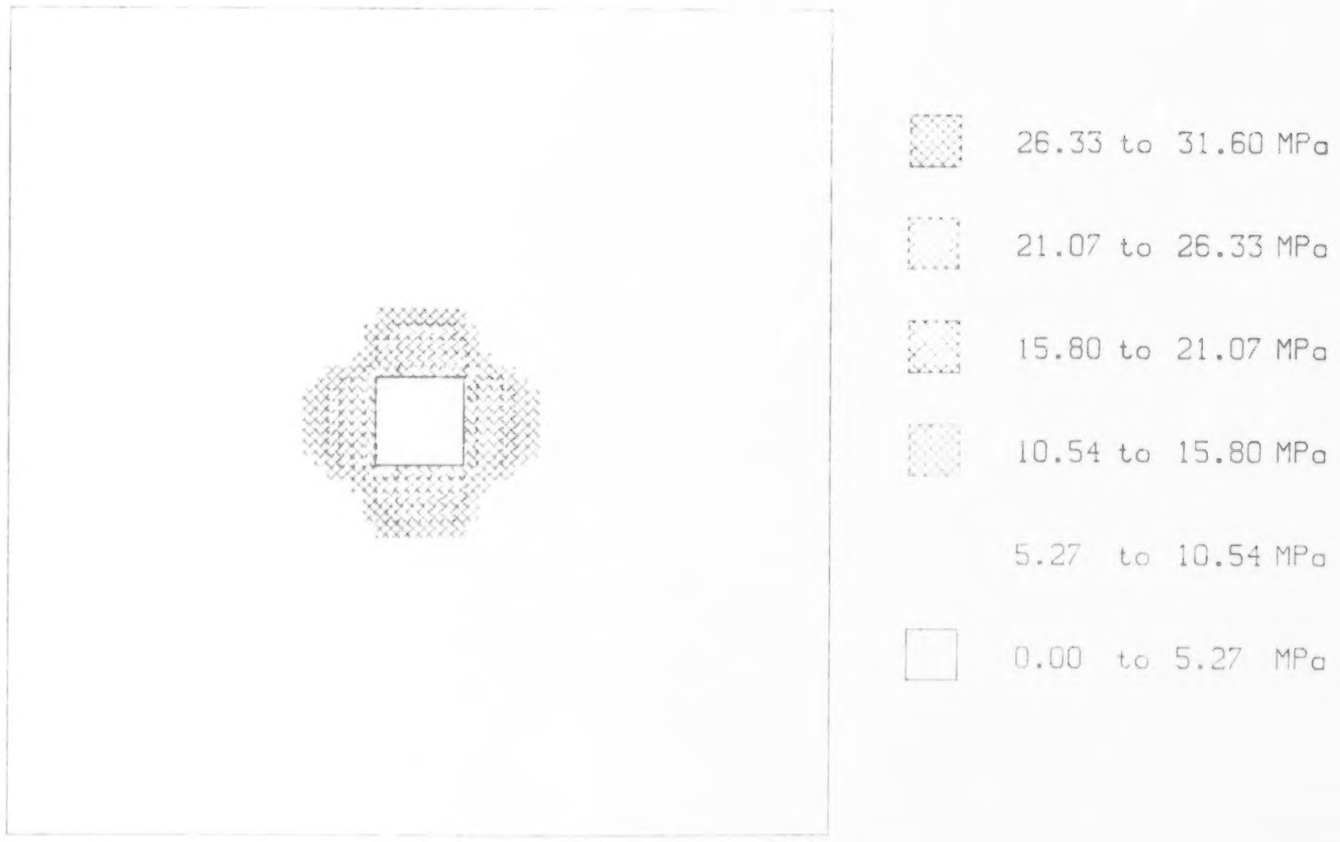

FIGURE 6.21

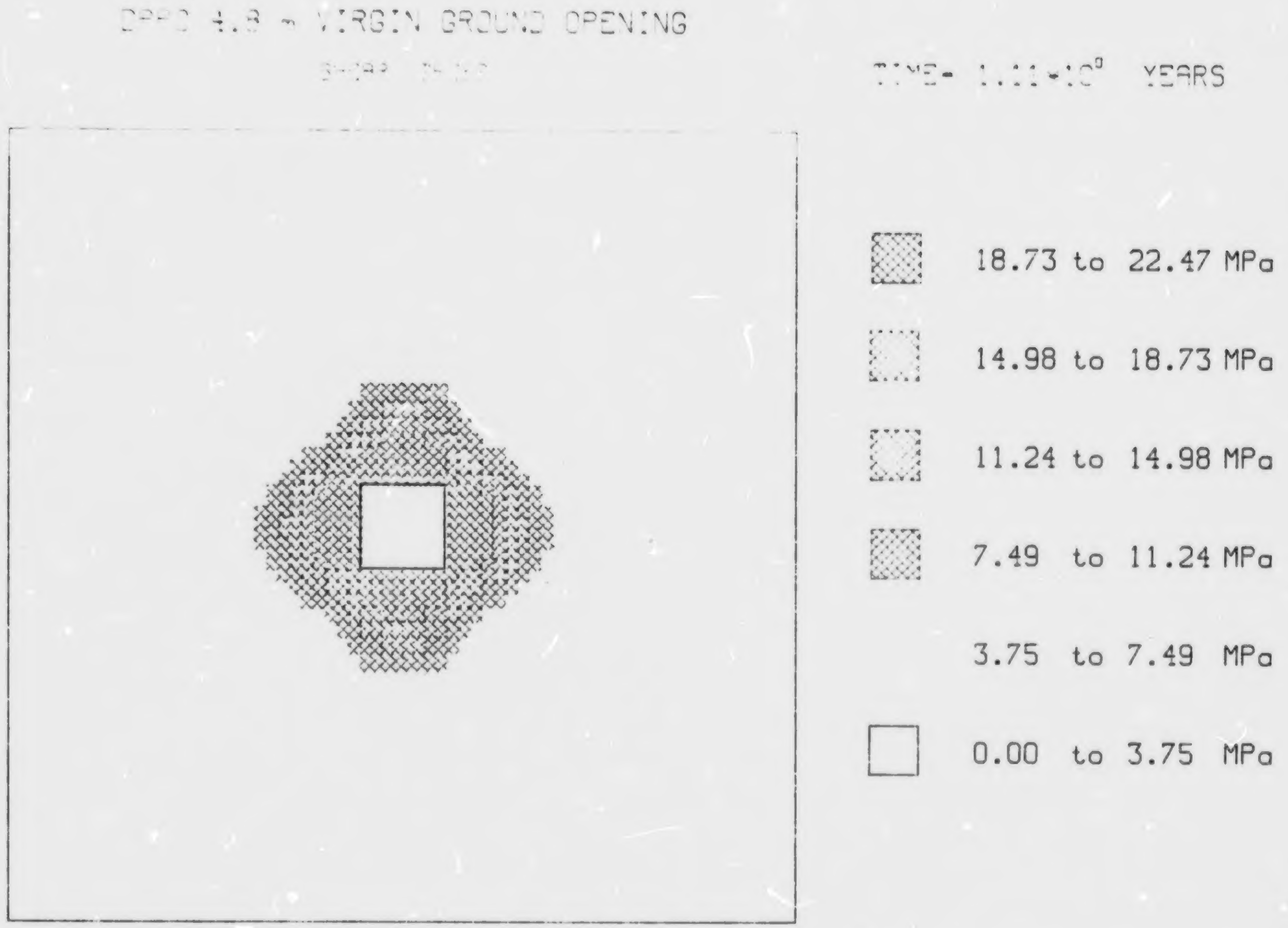
DPPC 4.8 - VIRGIN GROUND OPENING
[illegible]
TIME- 1.11*10^0 YEARS
▨ 18.73 to 22.47 MPa
▨ 14.98 to 18.73 MPa
▨ 11.24 to 14.98 MPa
▨ 7.49 to 11.24 MPa
3.75 to 7.49 MPa
☐ 0.00 to 3.75 MPa

FIGURE 6.22

DPPC 4.8 m VIRGIN GROUND OPENING

SHEAR STRESS

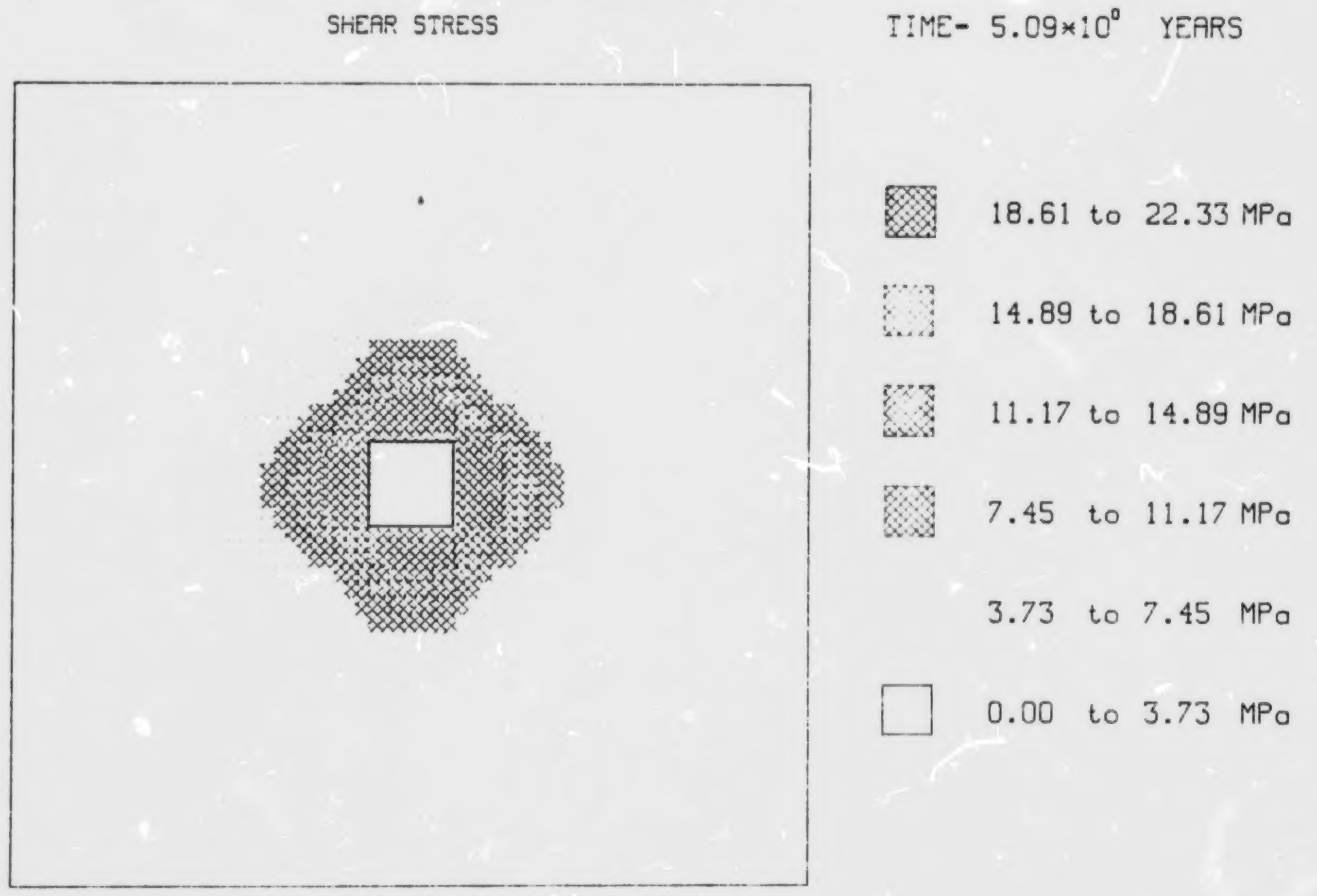

FIGURE 6.23

6.9 MAJOR PRINCIPAL STRESS DISTRIBUTION

Following are the numerical modelling results for major principal stresses for the 4.8 m x 4.8 m wide virgin ground opening.

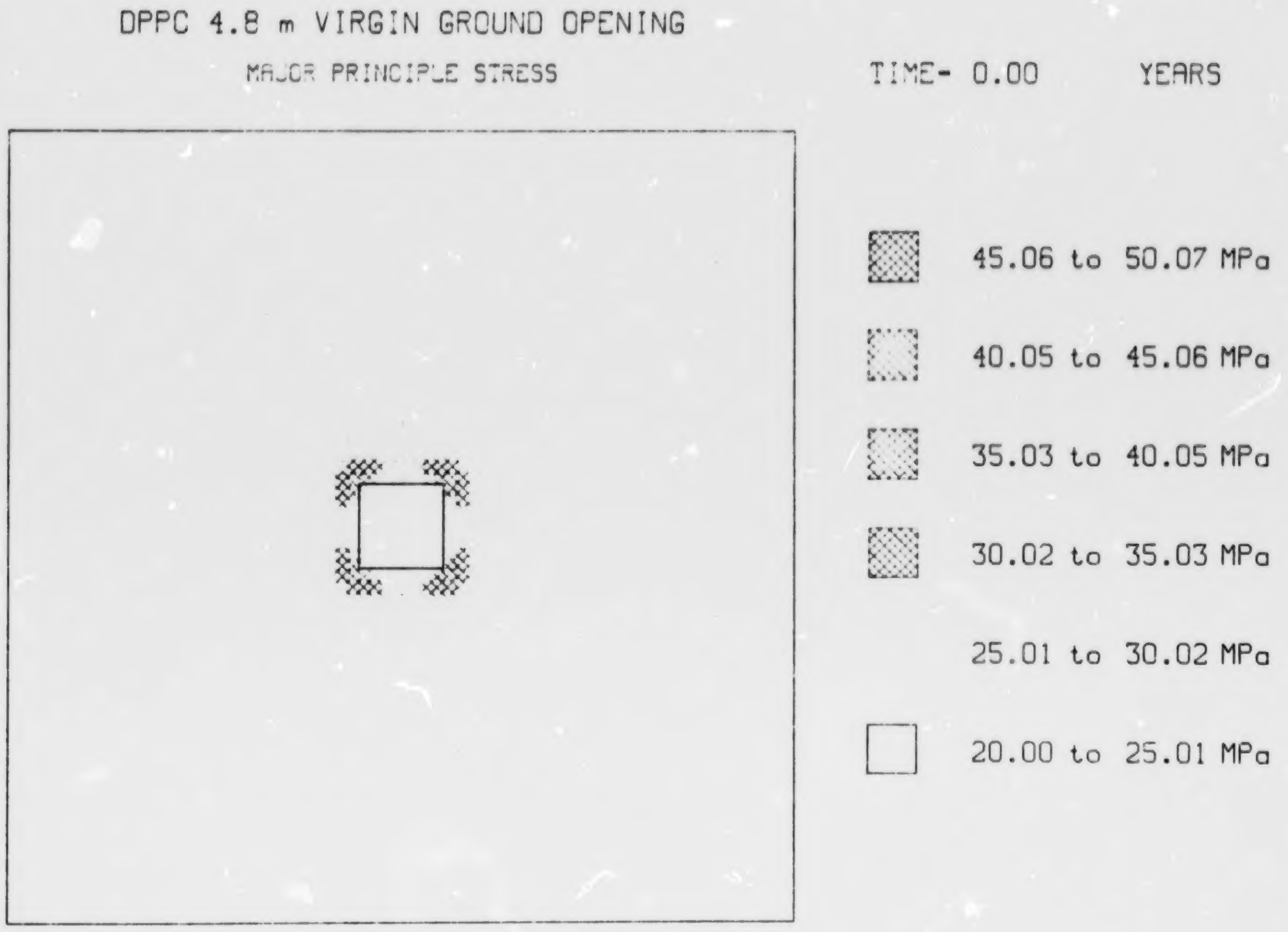
DPPC 4.8 m VIRGIN GROUND OPENING
MAJOR PRINCIPLE STRESS
TIME- 0.00 YEARS
45.06 to 50.07 MPa
40.05 to 45.06 MPa
35.03 to 40.05 MPa
30.02 to 35.03 MPa
25.01 to 30.02 MPa
20.00 to 25.01 MPa

FIGURE 6.24

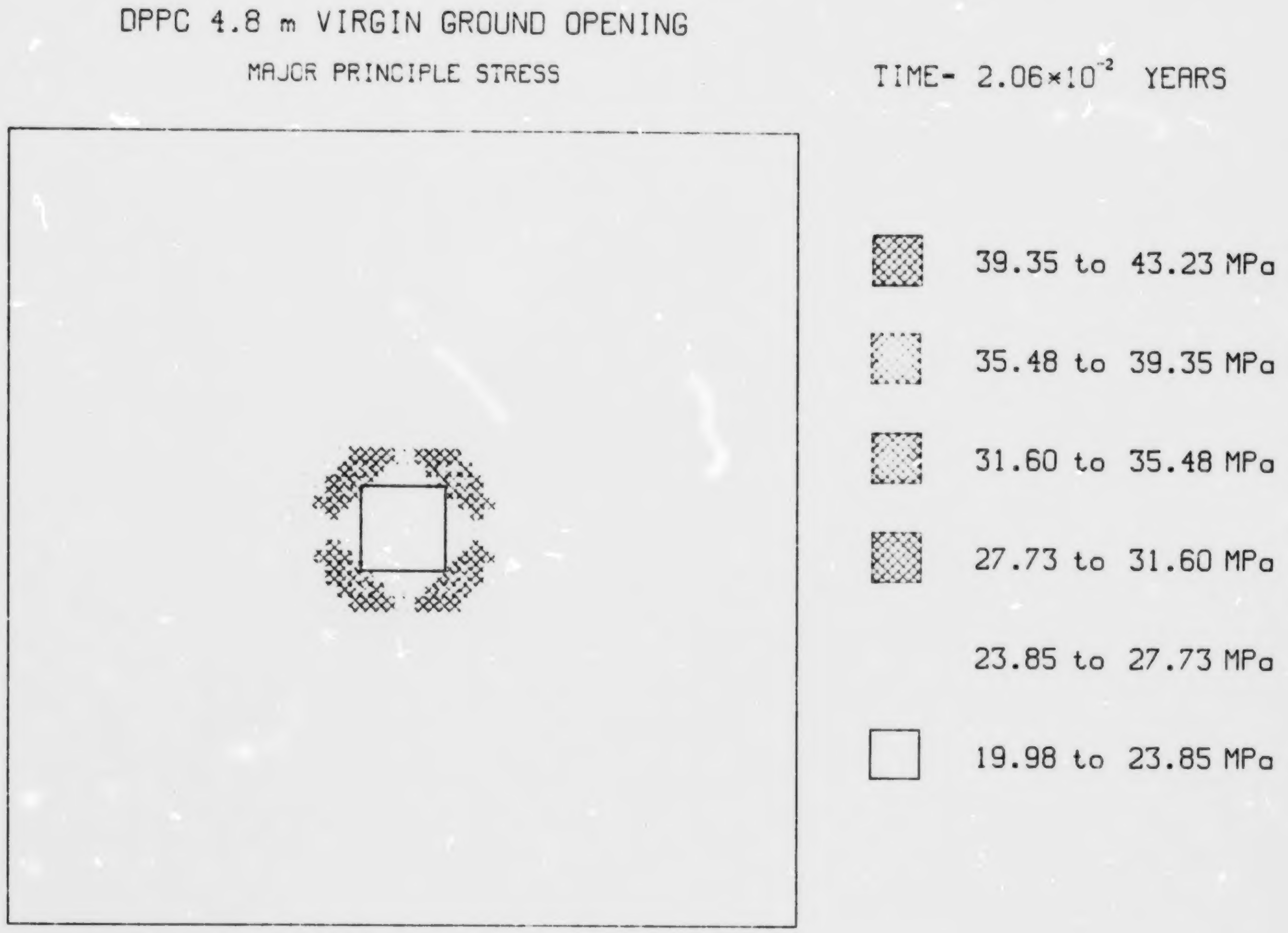
DPPC 4.8 m VIRGIN GROUND OPENING
MAJOR PRINCIPLE STRESS
TIME- 2.06×10^{-2} YEARS
39.35 to 43.23 MPa
35.48 to 39.35 MPa
31.60 to 35.48 MPa
27.73 to 31.60 MPa
23.85 to 27.73 MPa
19.98 to 23.85 MPa

FIGURE 6.25

DPPC 4.8 m VIRGIN GROUND OPENING

MAJOR PRINCIPLE STRESS

TIME- 1.11×10⁰ YEARS

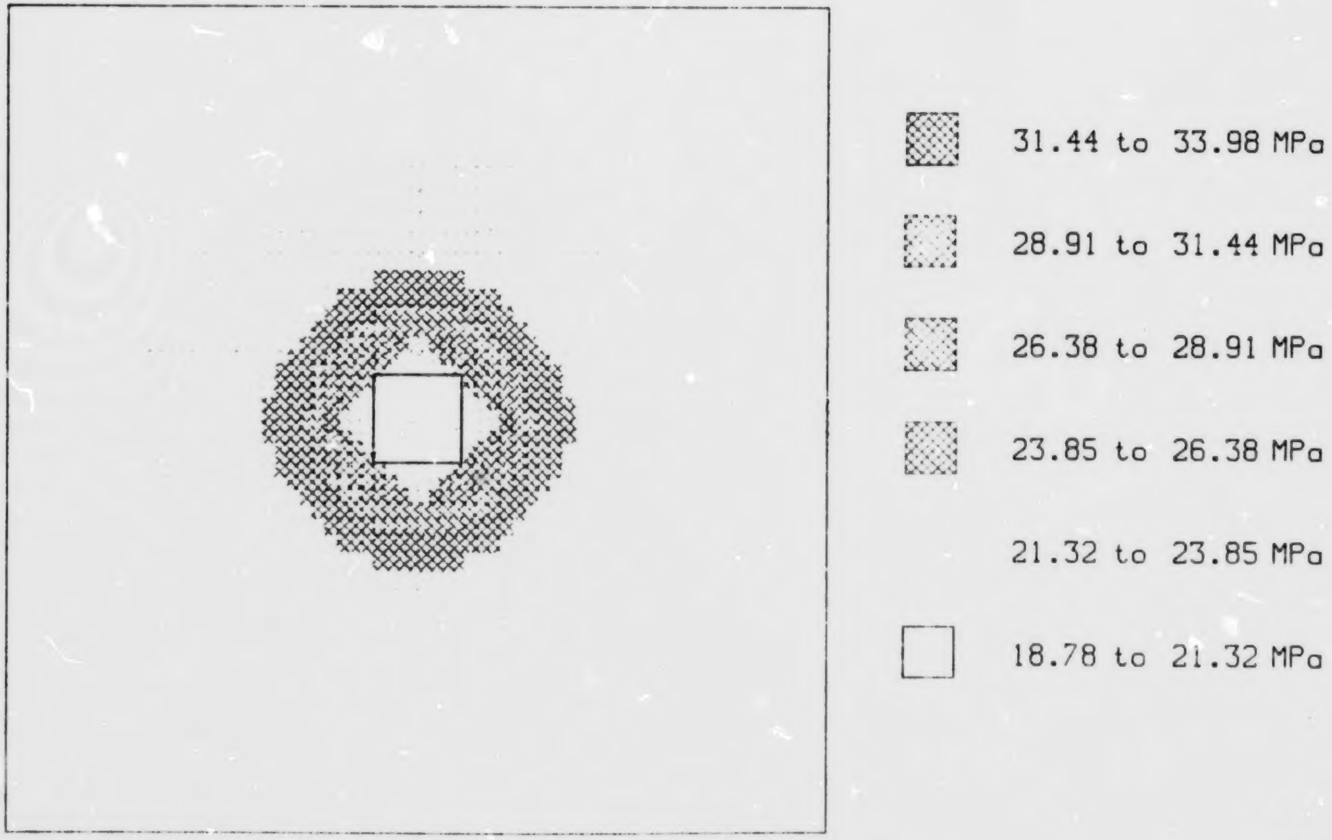

FIGURE 6.26

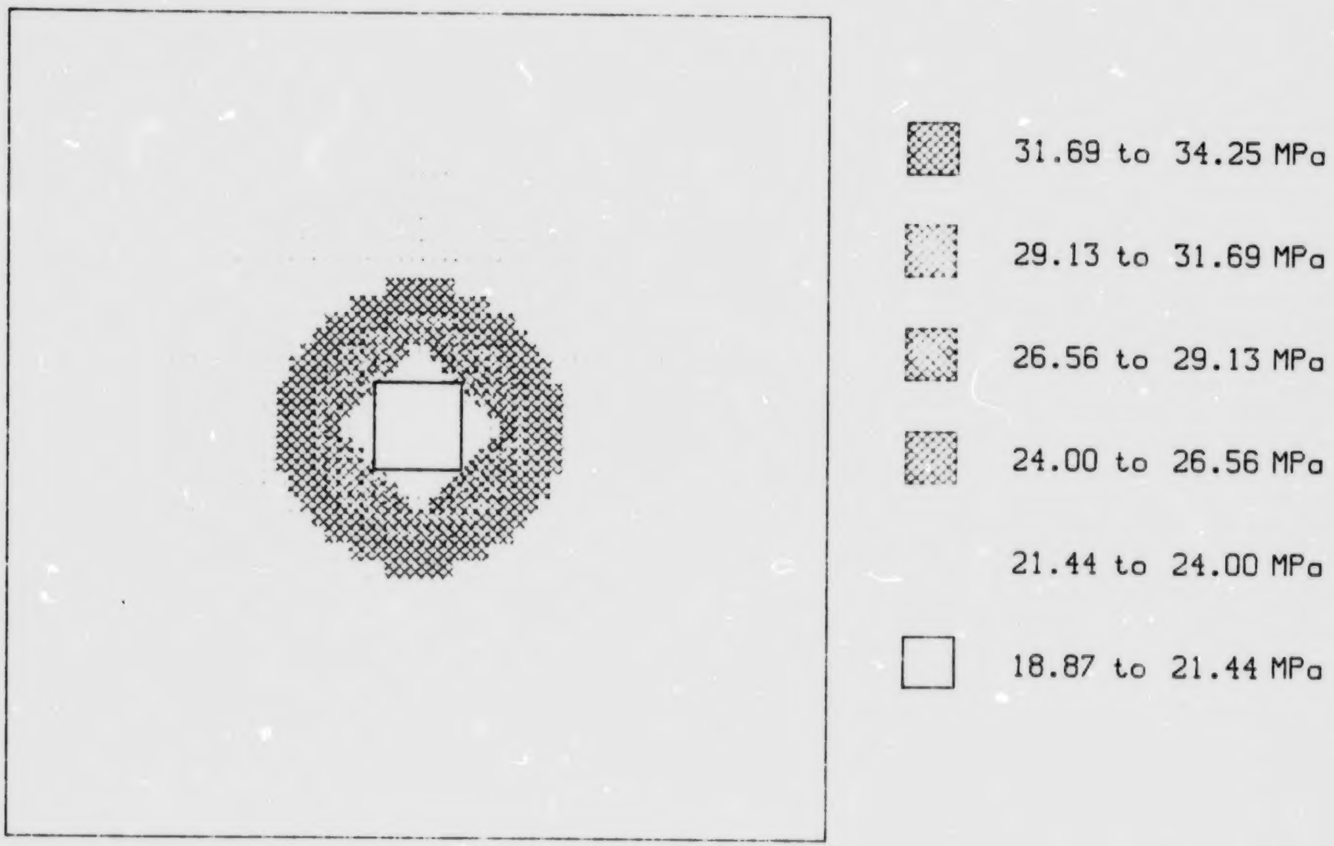

DPPC 4.8 m VIRGIN GROUND OPENING

MAJOR PRINCIPLE STRESS

TIME- 5.09×10^{0} YEARS

FIGURE 6.27

6.10 MINOR PRINCIPAL STRESS DISTRIBUTION

Following are the numerical modelling results for minor principal stresses for the 4.8 m x 4.8 m wide virgin ground opening.

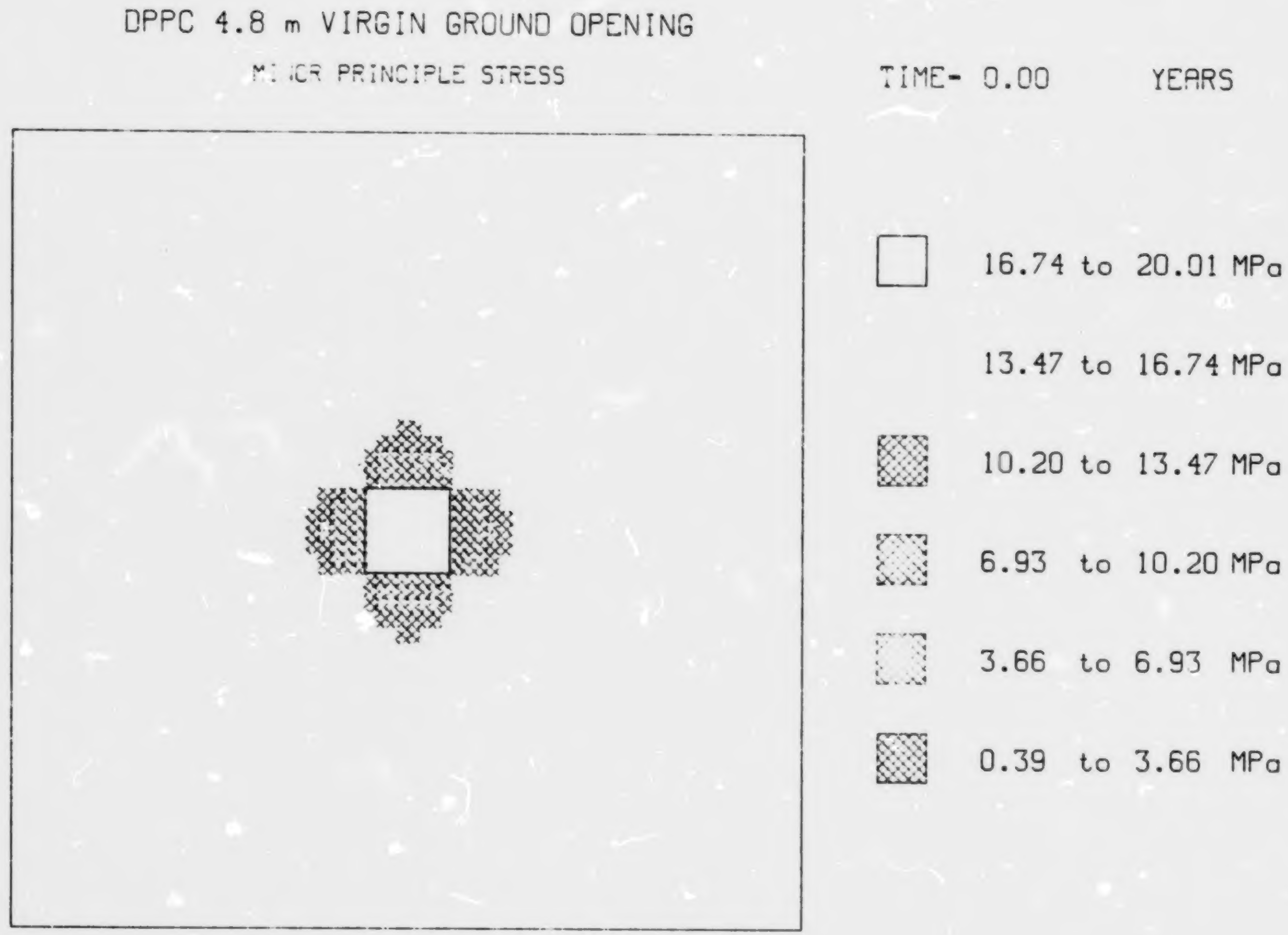
DPPC 4.8 m VIRGIN GROUND OPENING
MINOR PRINCIPLE STRESS
TIME- 0.00 YEARS
☐ 16.74 to 20.01 MPa
13.47 to 16.74 MPa
▩ 10.20 to 13.47 MPa
▨ 6.93 to 10.20 MPa
▧ 3.66 to 6.93 MPa
▩ 0.39 to 3.66 MPa

FIGURE 6.28

DPPC 4.8 m VIRGIN GROUND OPENING

MINOR PRINCIPLE STRESS

TIME- 2.06×10^{-2} YEARS

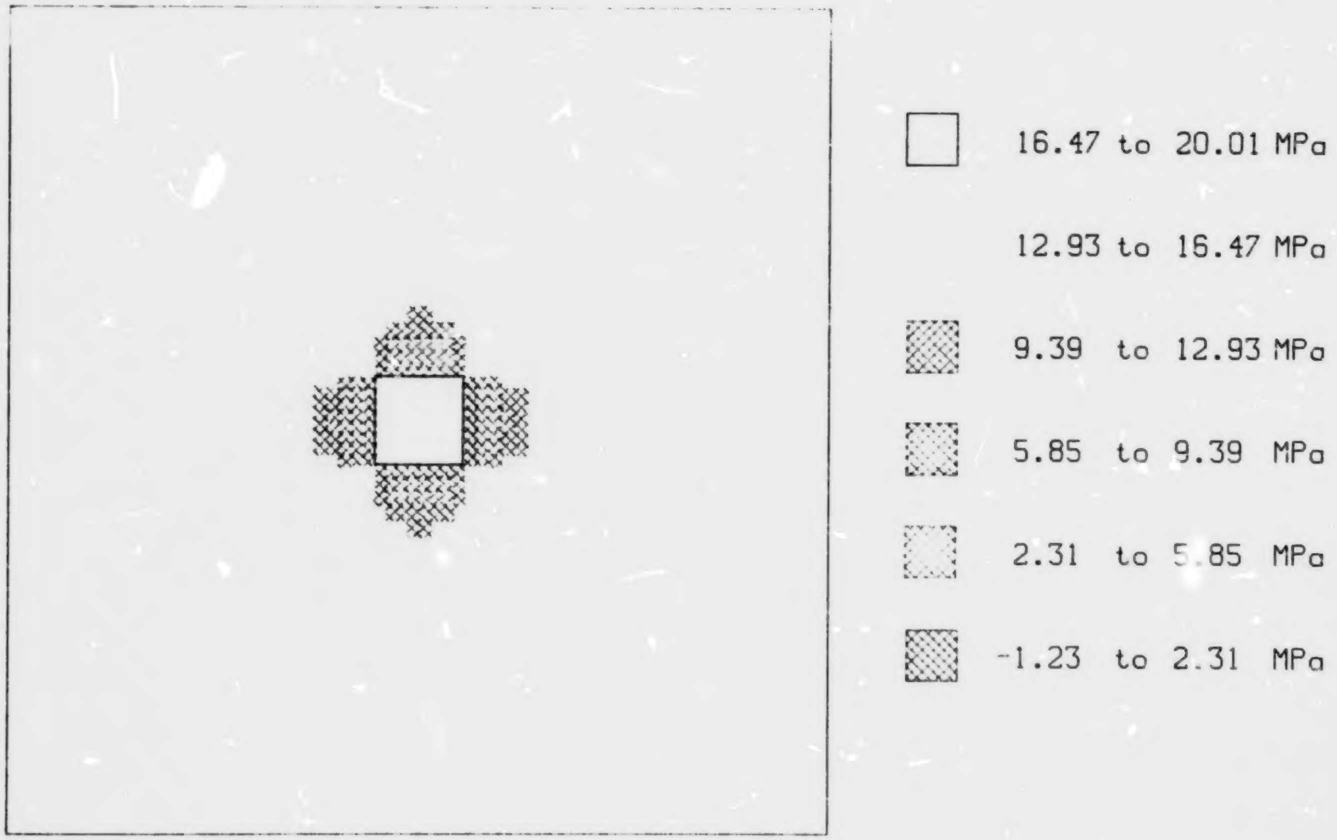

FIGURE 6.29

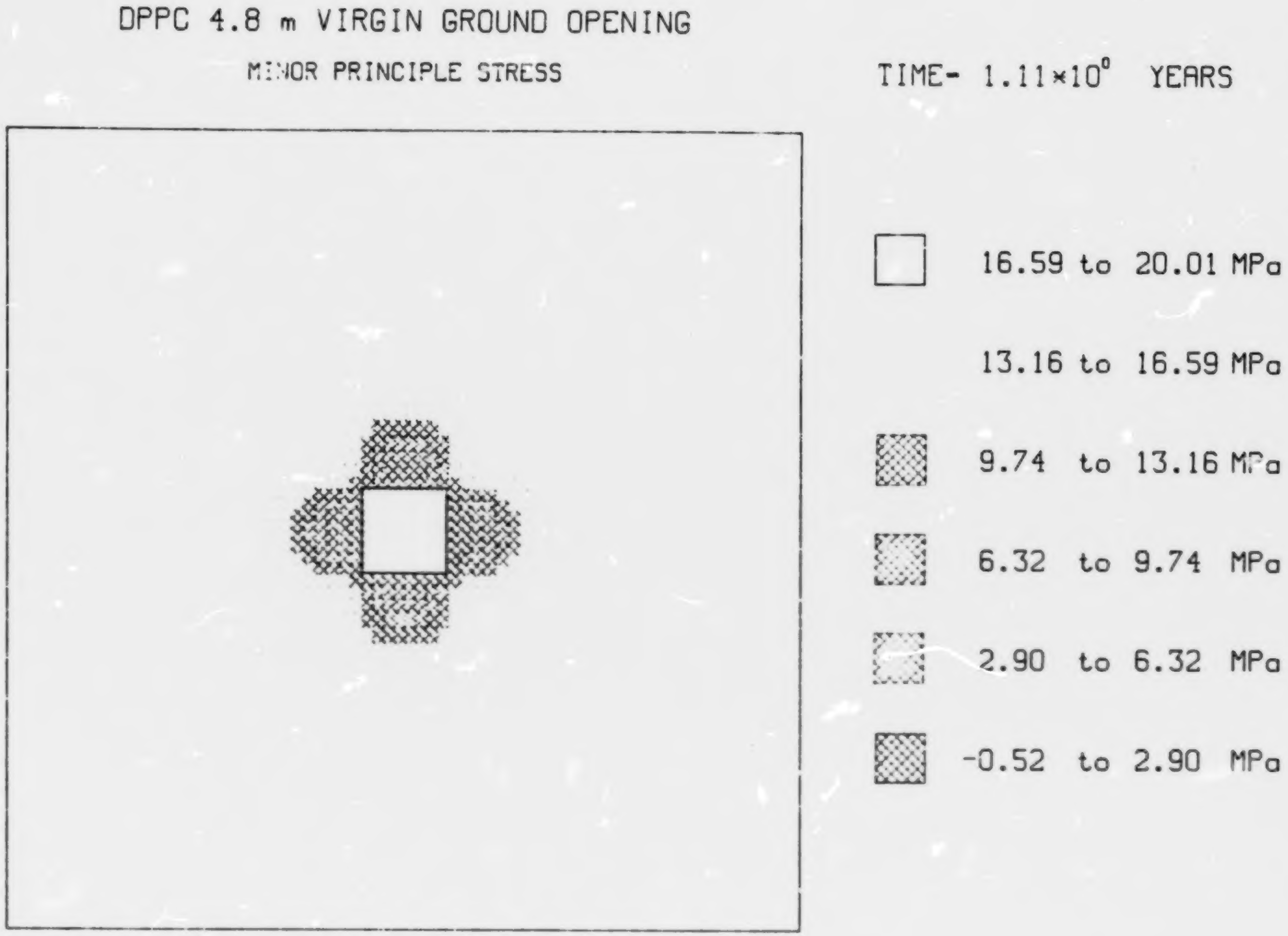
DPPC 4.8 m VIRGIN GROUND OPENING
MINOR PRINCIPLE STRESS
TIME- 1.11×10⁰ YEARS
16.59 to 20.01 MPa
13.16 to 16.59 MPa
9.74 to 13.16 MPa
6.32 to 9.74 MPa
2.90 to 6.32 MPa
-0.52 to 2.90 MPa

FIGURE 6.30

DPPC 4.8 m VIRGIN GROUND OPENING

MINOR PRINCIPLE STRESS

TIME- 5.09×10^{0} YEARS

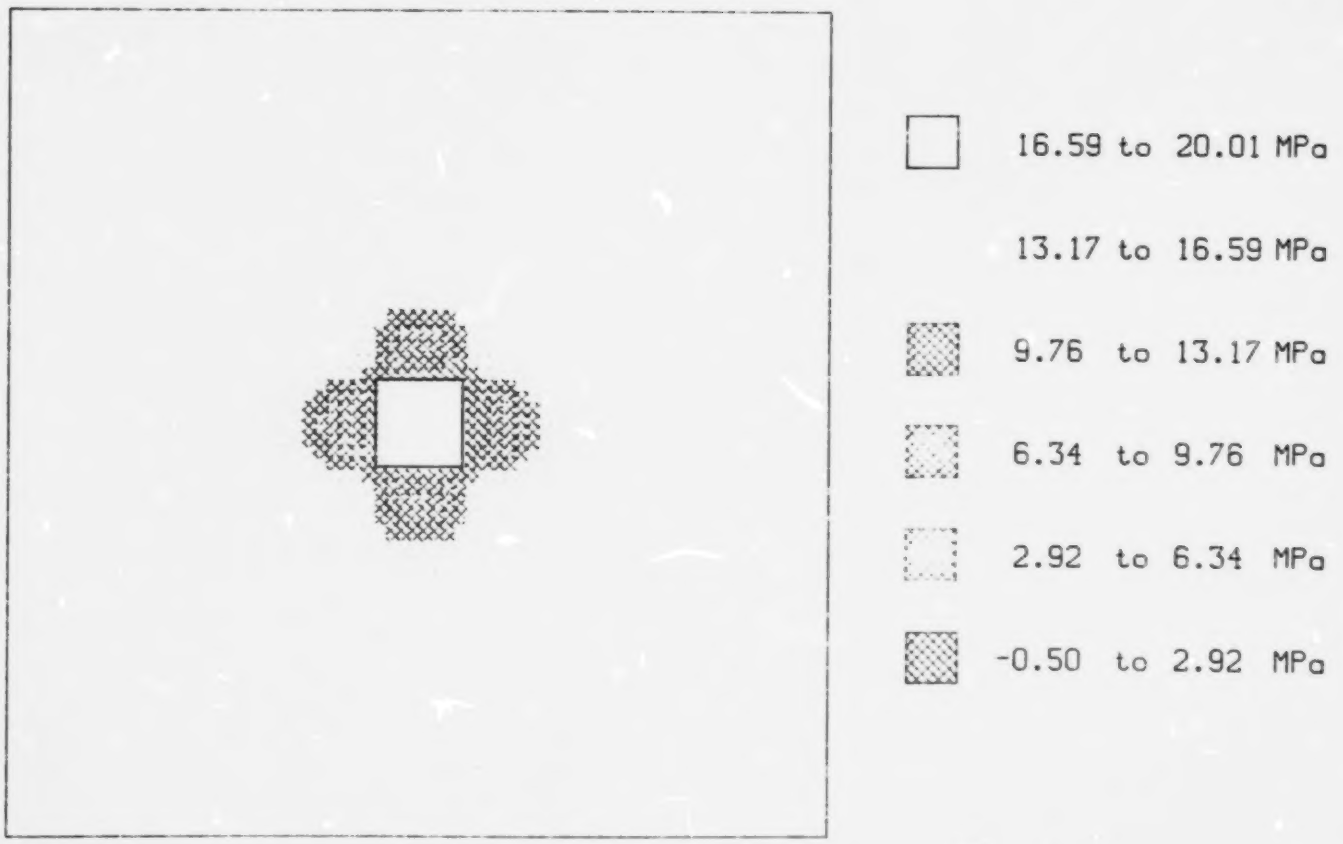

FIGURE 6.31

SECTION 7.0

7.0 DENISON-POTACAN 4 M X 42 M TEST STOPE, VIRGIN GROUND

7.1 ROOF DISPLACEMENTS

Following are the numerical modelling results for roof displacements for the 4 m x 42 m Test Stope, virgin ground opening.

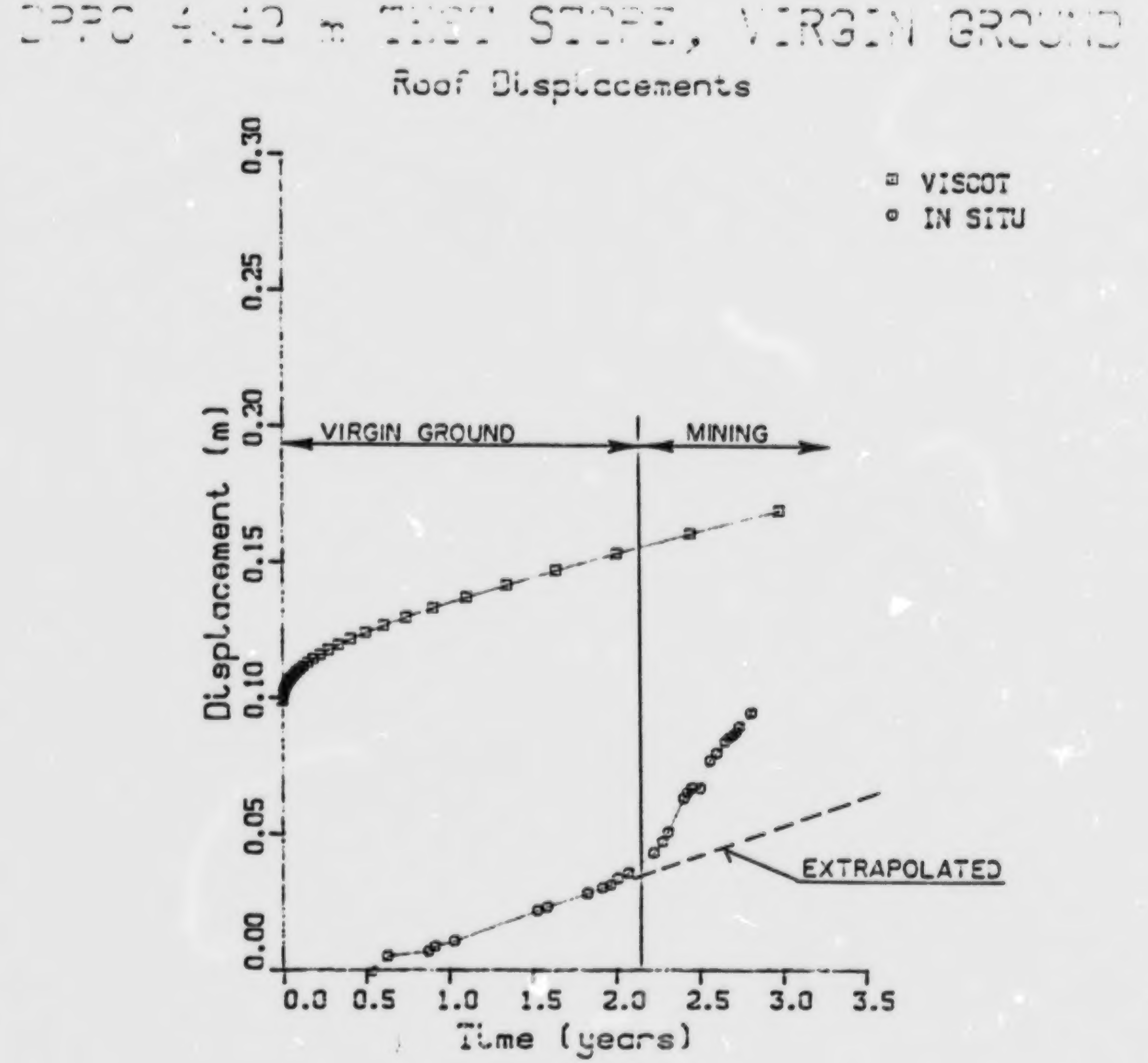
DPPC 4x42 m TEST STOPE, VIRGIN GROUND
Roof Displacements
VISCOT
IN SITU
VIRGIN GROUND
MINING
EXTRAPOLATED
Displacement (m)
0.00
0.05
0.10
0.15
0.20
0.25
0.30
Time (years)
0.0
0.5
1.0
1.5
2.0
2.5
3.0
3.5

FIGURE 7.1

7.2 WALL DISPLACEMENTS

Following are the numerical modelling results for wall displacements for the 4 m x 42 m Test Stope, virgin ground opening.

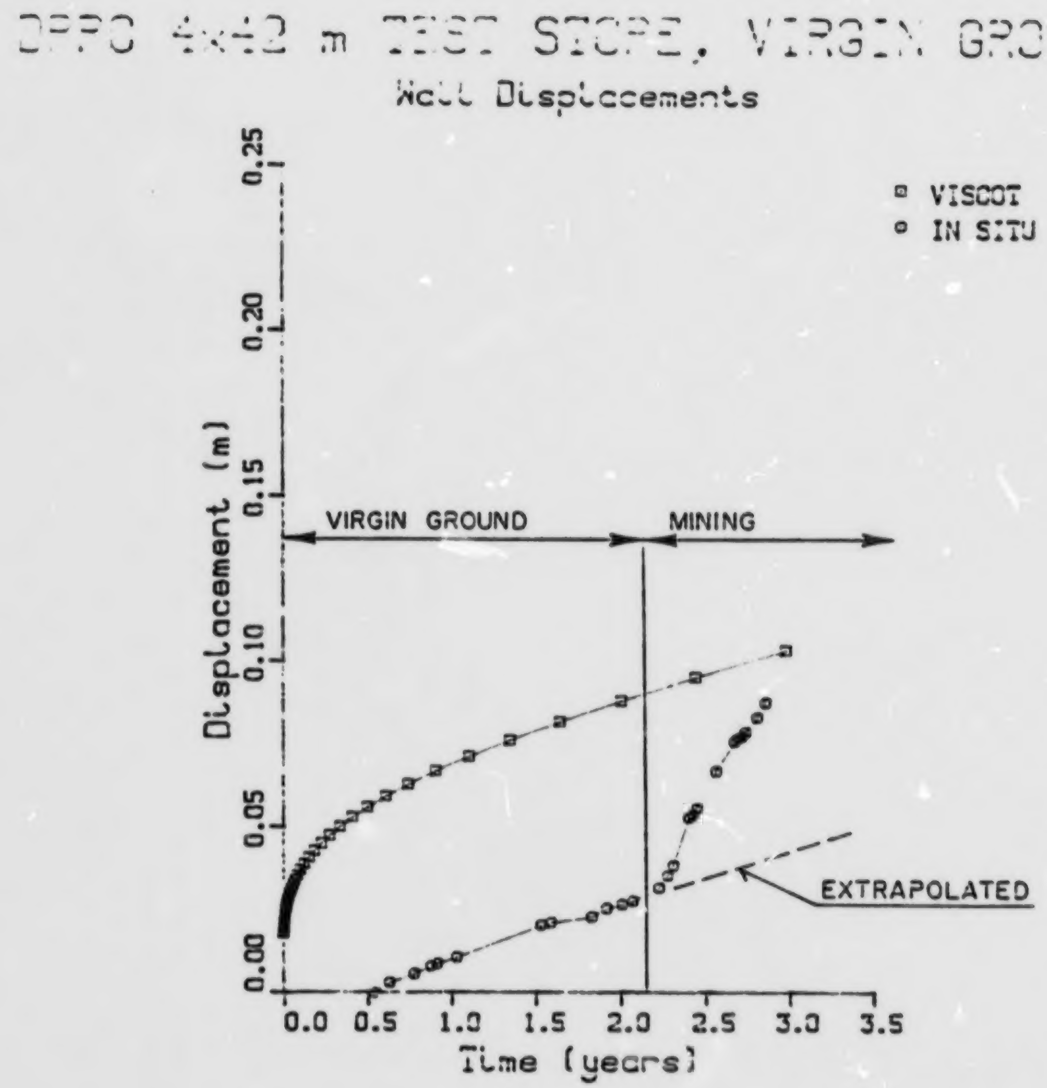
DPPC 4x42 m TEST STOPE, VIRGIN GROUND
Wall Displacements
VISCOT
IN SITU
VIRGIN GROUND
MINING
EXTRAPOLATED
Displacement (m)
0.00
0.05
0.10
0.15
0.20
0.25
Time (years)
0.0
0.5
1.0
1.5
2.0
2.5
3.0
3.5

FIGURE 7.2

7.3 STRAIN RATE DISTRIBUTION

Following are the numerical modelling results for strain rates for the 4 m x 42 m Test Stope, virgin ground opening.

DPPC 4x40 m TEST STOPE, VIRGIN GROUND

STRAIN RATES

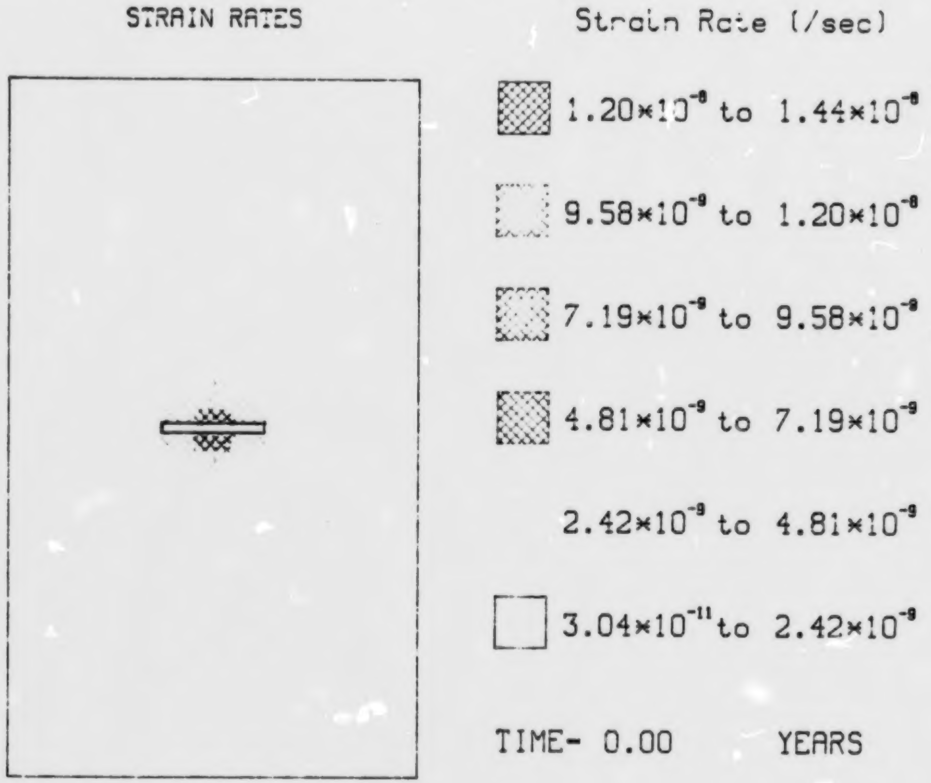

FIGURE 7.3

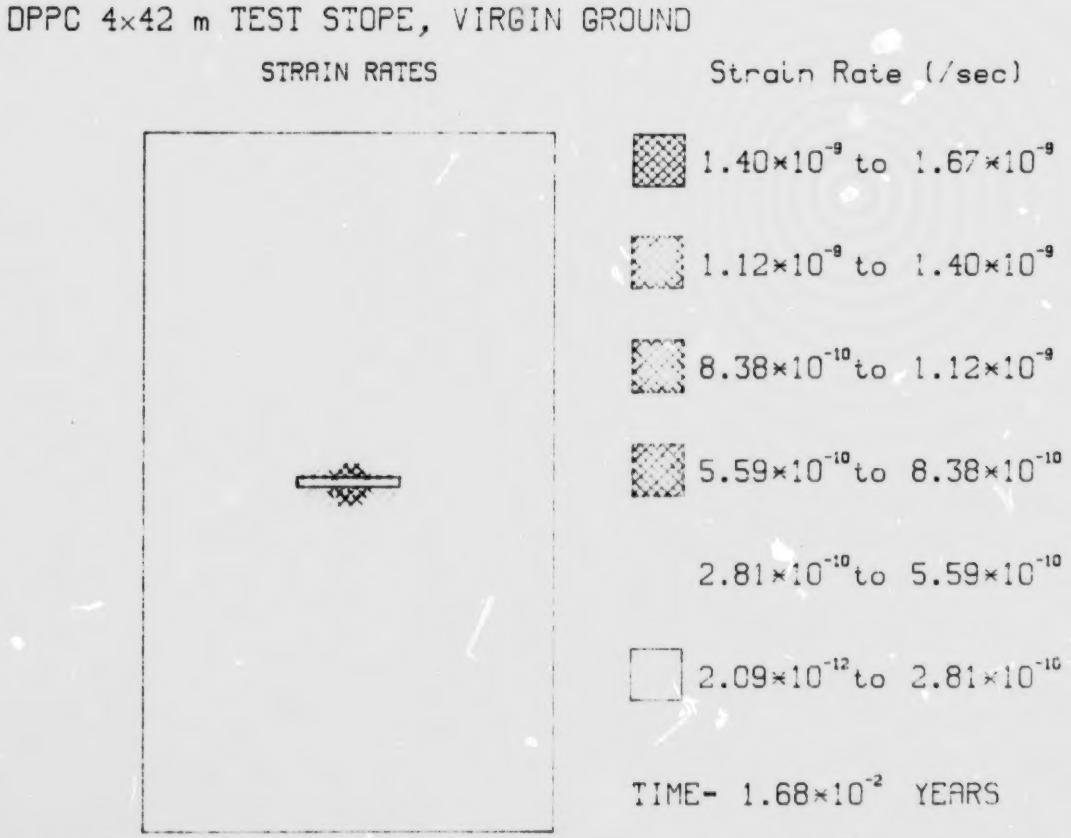
DPPC 4×42 m TEST STOPE, VIRGIN GROUND
STRAIN RATES
Strain Rate (/sec)
▩ 1.40×10⁻⁹ to 1.67×10⁻⁹
▨ 1.12×10⁻⁹ to 1.40×10⁻⁹
▨ 8.38×10⁻¹⁰ to 1.12×10⁻⁹
▩ 5.59×10⁻¹⁰ to 8.38×10⁻¹⁰
2.81×10⁻¹⁰ to 5.59×10⁻¹⁰
☐ 2.09×10⁻¹² to 2.81×10⁻¹⁰
TIME- 1.68×10⁻² YEARS

FIGURE 7.4

DPRC 4x42 m TEST STOPE, VIRGIN GROUND

STRAIN RATES

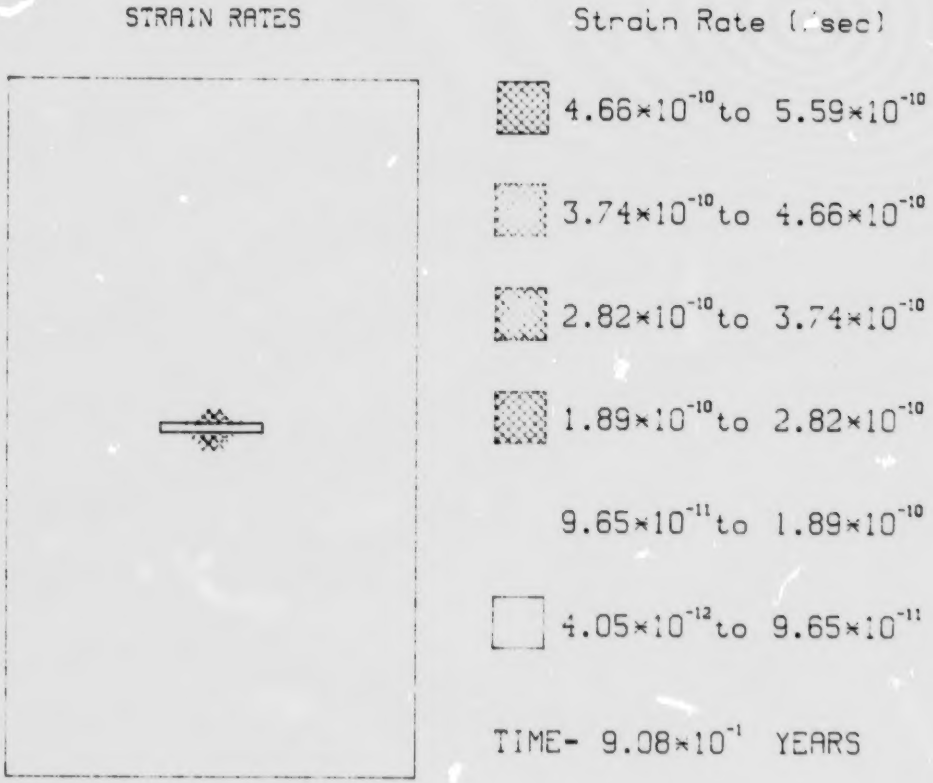

FIGURE 7.5

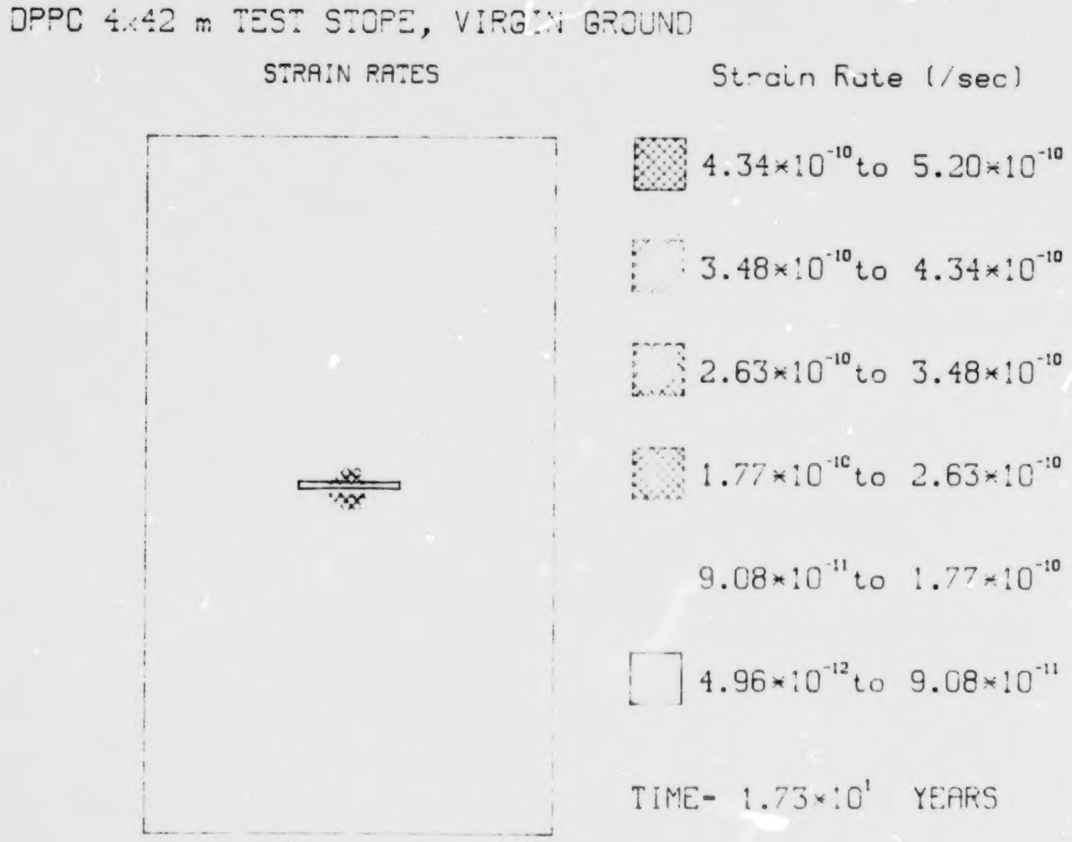
DPPC 4x42 m TEST STOPE, VIRGIN GROUND
STRAIN RATES
Strain Rate (/sec)
▩ 4.34×10^{-10} to 5.20×10^{-10}
▩ 3.48×10^{-10} to 4.34×10^{-10}
▩ 2.63×10^{-10} to 3.48×10^{-10}
▩ 1.77×10^{-10} to 2.63×10^{-10}
9.08×10^{-11} to 1.77×10^{-10}
☐ 4.96×10^{-12} to 9.08×10^{-11}
TIME- 1.73×10^{1} YEARS

FIGURE 7.6

7.4 SHEAR STRESS DISTRIBUTION

Following are the numerical modelling results for shear stresses for the 4 m x 42 m Test Stope, virgin ground opening.

DPPC 4x42 m TEST STOPE, VIRGIN GROUND

SHEAR STRESS

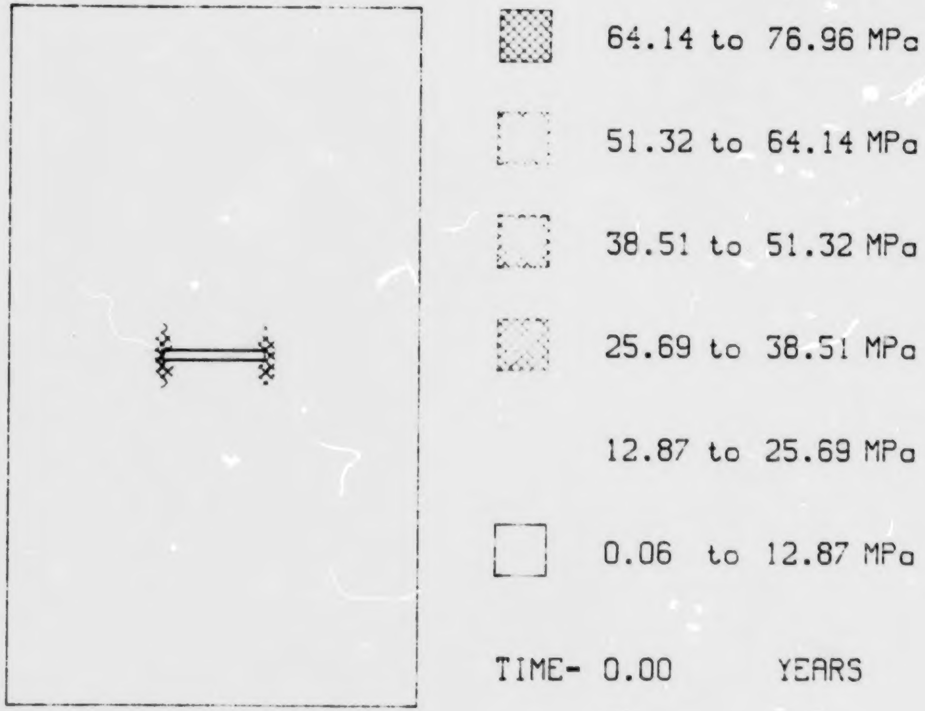

FIGURE 77

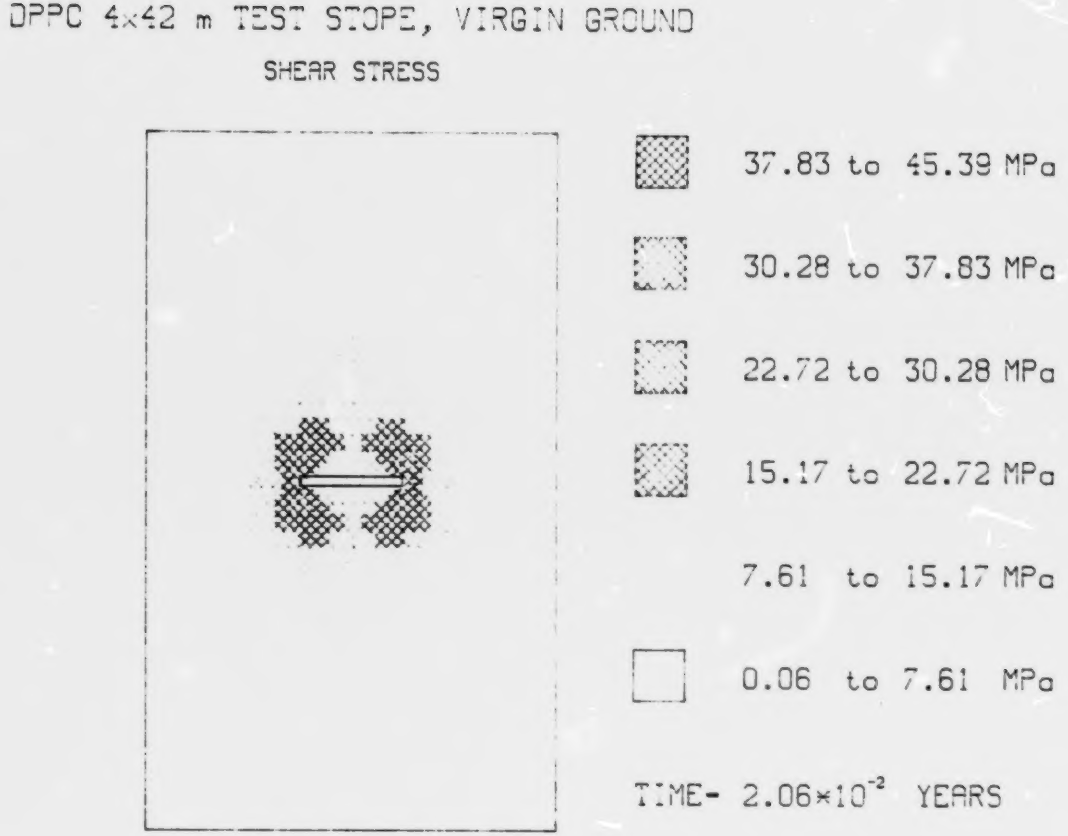
DPPC 4×42 m TEST STOPE, VIRGIN GROUND
SHEAR STRESS
37.83 to 45.39 MPa
30.28 to 37.83 MPa
22.72 to 30.28 MPa
15.17 to 22.72 MPa
7.61 to 15.17 MPa
0.06 to 7.61 MPa
TIME- 2.06×10^-2 YEARS

FIGURE 7.8

DPPC 4x42 m TEST STOPE, VIRGIN GROUND

SHEAR STRESS

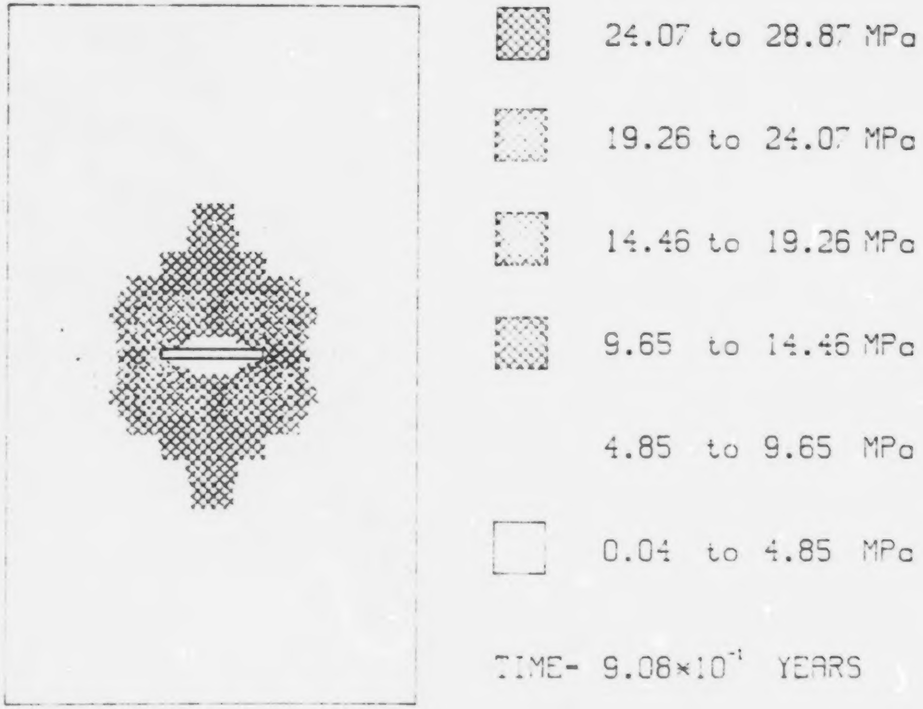

FIGURE 7.9

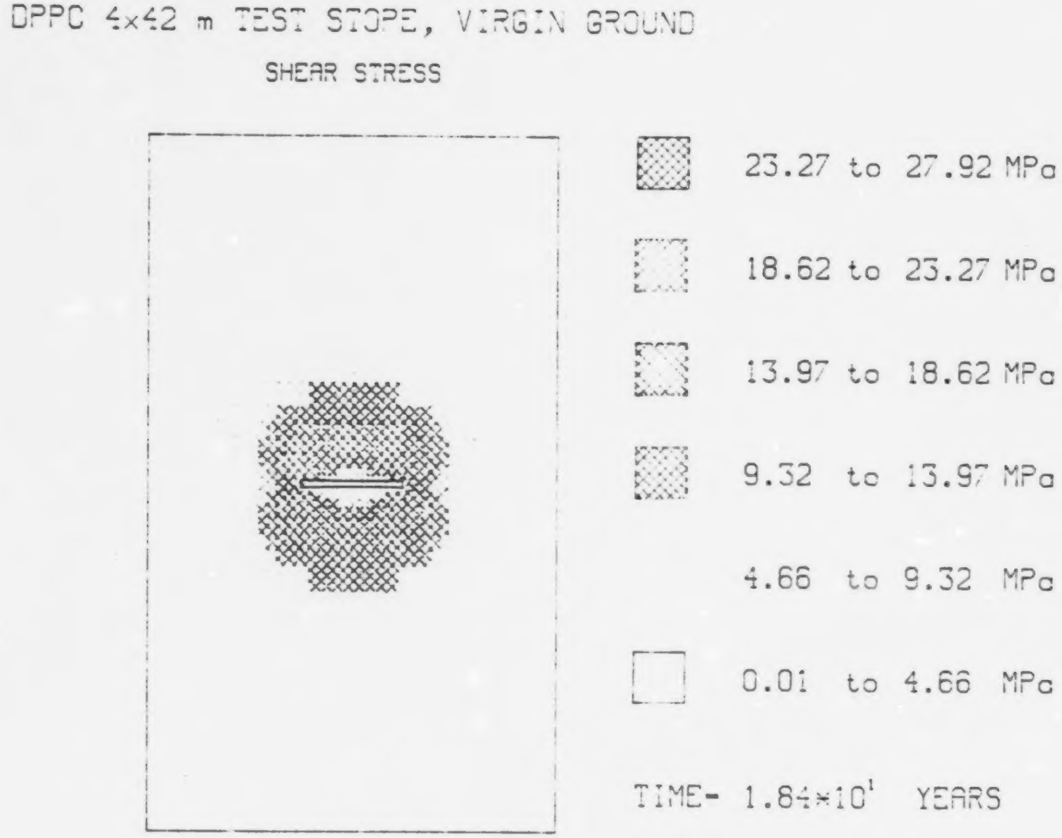
DPPC 4×42 m TEST STOPE, VIRGIN GROUND
SHEAR STRESS
23.27 to 27.92 MPa
18.62 to 23.27 MPa
13.97 to 18.62 MPa
9.32 to 13.97 MPa
4.66 to 9.32 MPa
0.01 to 4.66 MPa
TIME- 1.84×10¹ YEARS

FIGURE 7.10

7.5 MAJOR PRINCIPAL STRESS DISTRIBUTION

Following are the numerical modelling results for major principal stresses for the 4 m x 42 m Test Stope, virgin ground opening.

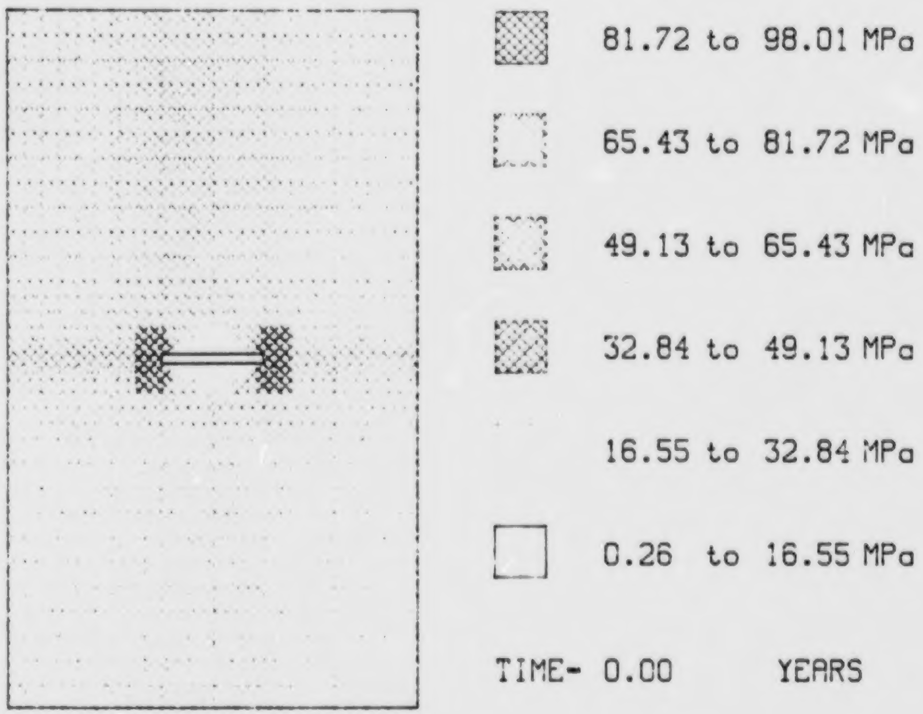

DPPC 4×42 m TEST STOPE, VIRGIN GROUND

MAJOR PRINCIPLE STRESS

FIGURE 7.11

LPPC 4 42 m TEST STOPE, VIRGIN GROUND

MAJOR PRINCIPLE STRESS

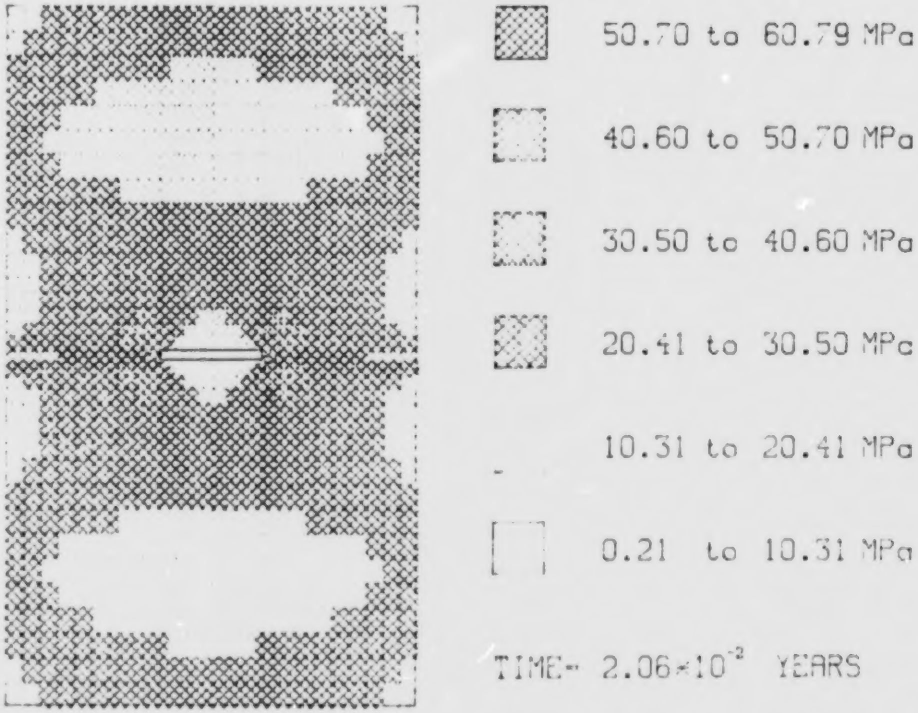

FIGURE 7.12

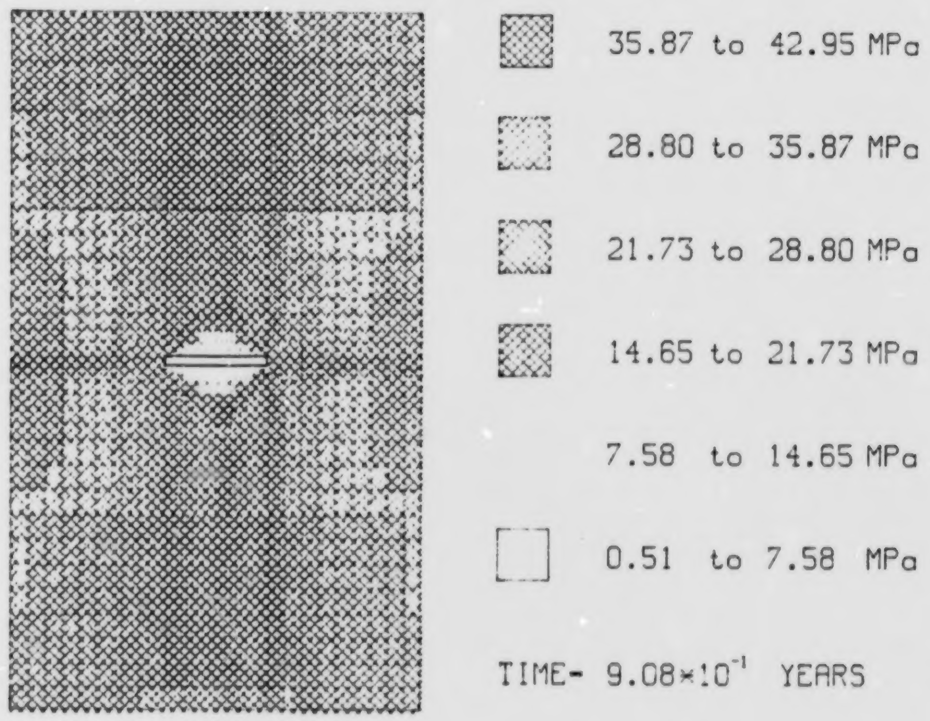

DPPC 4×42 m TEST STOPE, VIRGIN GROUND

MAJOR PRINCIPLE STRESS

FIGURE 7.13

DPPC 4×42 m TEST STOPE, VIRGIN GROUND

MAJOR PRINCIPLE STRESS

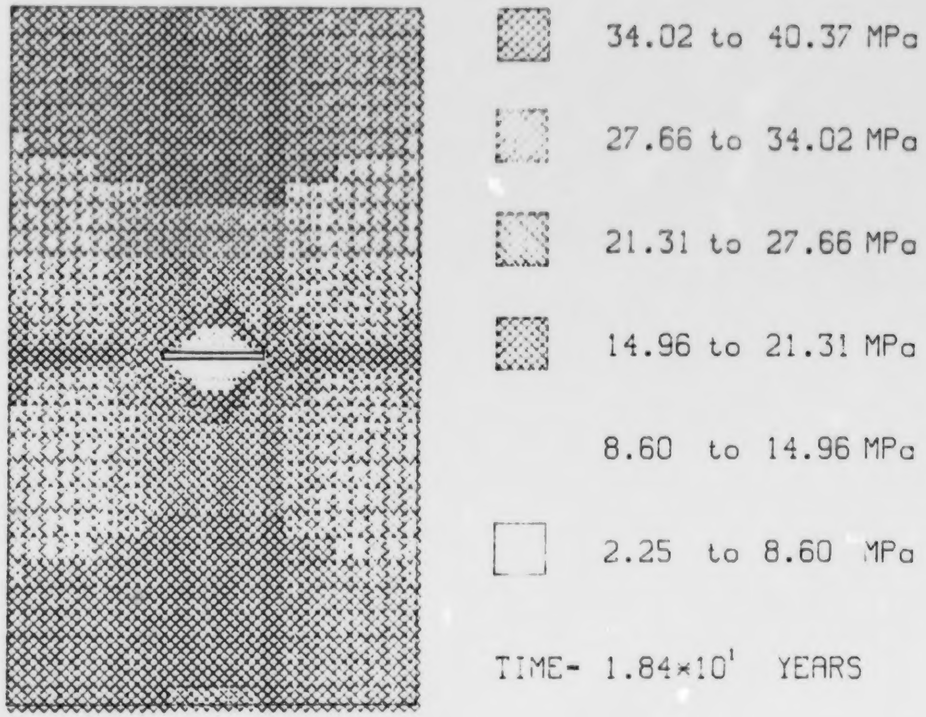

FIGURE 7.14

7.6 MINOR PRINCIPAL STRESS DISTRIBUTION

Following are the numerical modelling results for minor principal stresses for the 4 m x 42 m Test Stope, virgin ground opening.

DPPC 4×42 m TEST STOPE, VIRGIN GROUND

MINOR PRINCIPLE STRESS

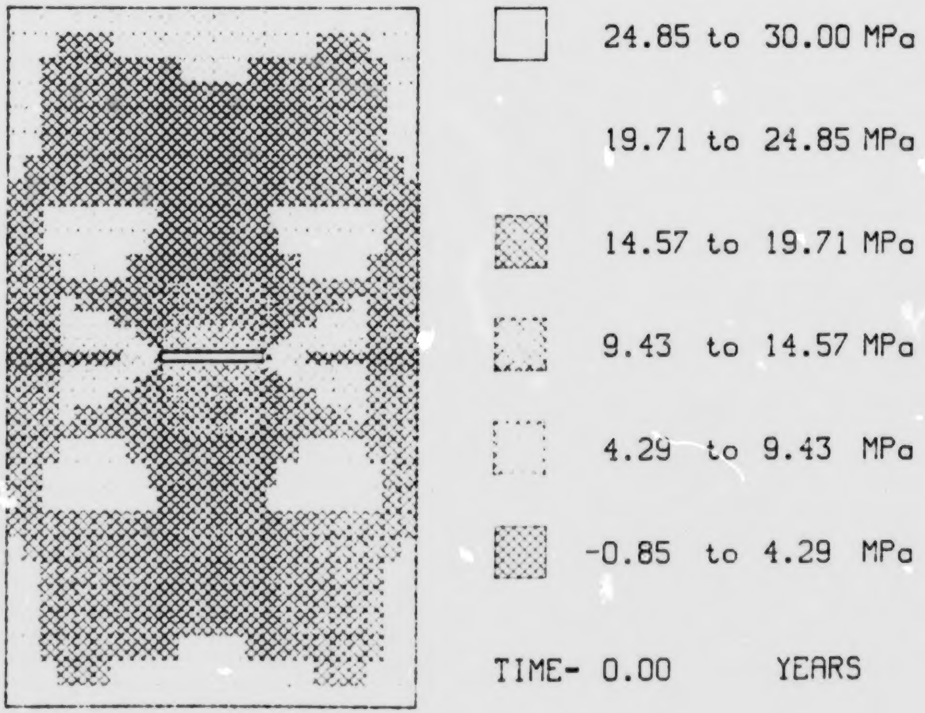

FIGURE 7.15

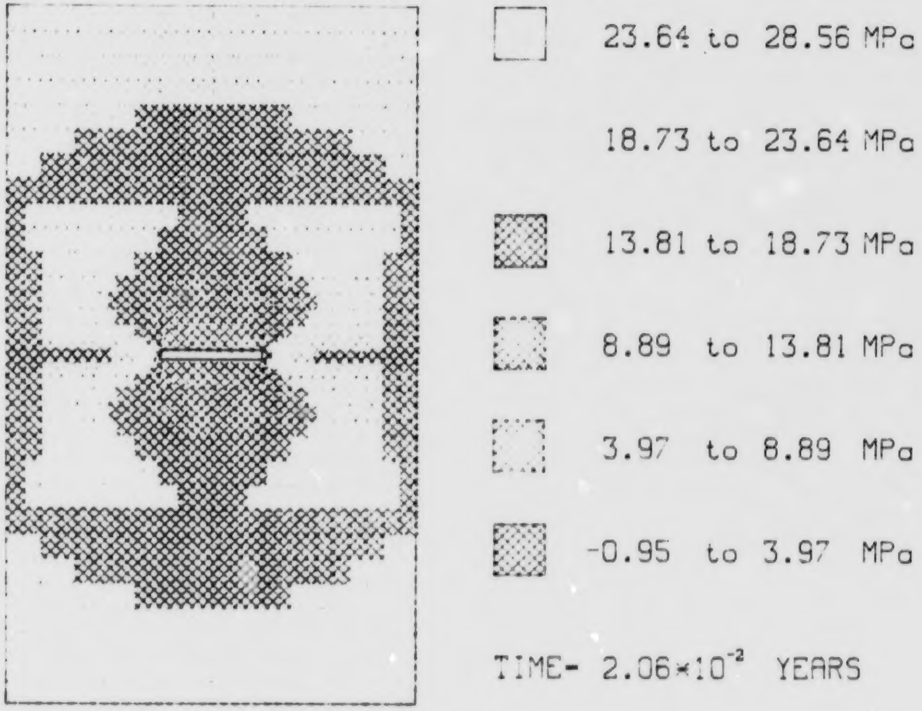

DPPC 4x42 m TEST STOPE, VIRGIN GROUND

MINOR PRINCIPLE STRESS

TIME- 2.06×10^{-2} YEARS

FIGURE 7.16

DPPC 4×42 m TEST STOPE, VIRGIN GROUND

MINOR PRINCIPLE STRESS

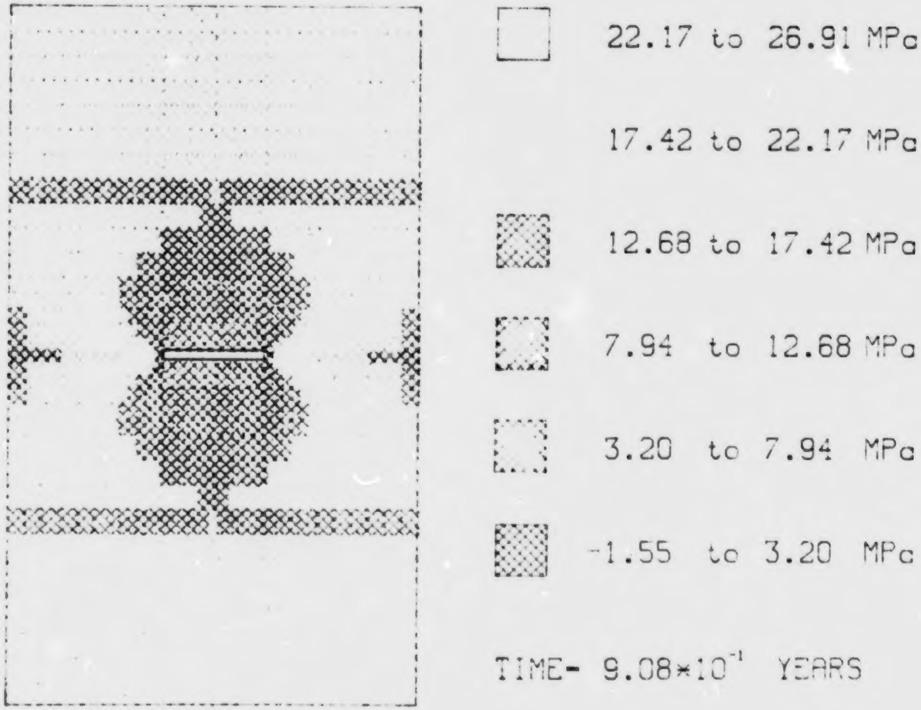

FIGURE 7.17

DPPC 4x42 m TEST STOPE, VIRGIN GROUND

MINOR PRINCIPLE STRESS

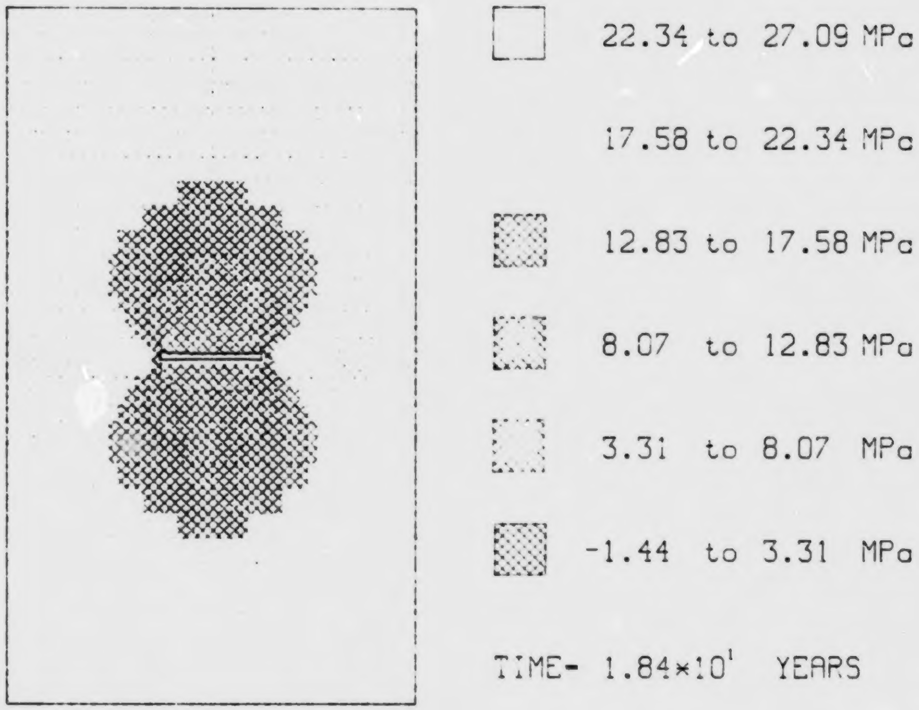

FIGURE 7.18

SECTION 8.0

8.0 DENISON-POTACAN 4 M X 42 M STOPE

8.1 ROOF DISPLACEMENTS

Following are the numerical modelling results for roof displacements for the 4 m x 42 m Stope. Note that throughout Section 8.0, all figure titles referring to 4 m x 42 m Test Stope should read 4 m x 42 m Mining Stope.

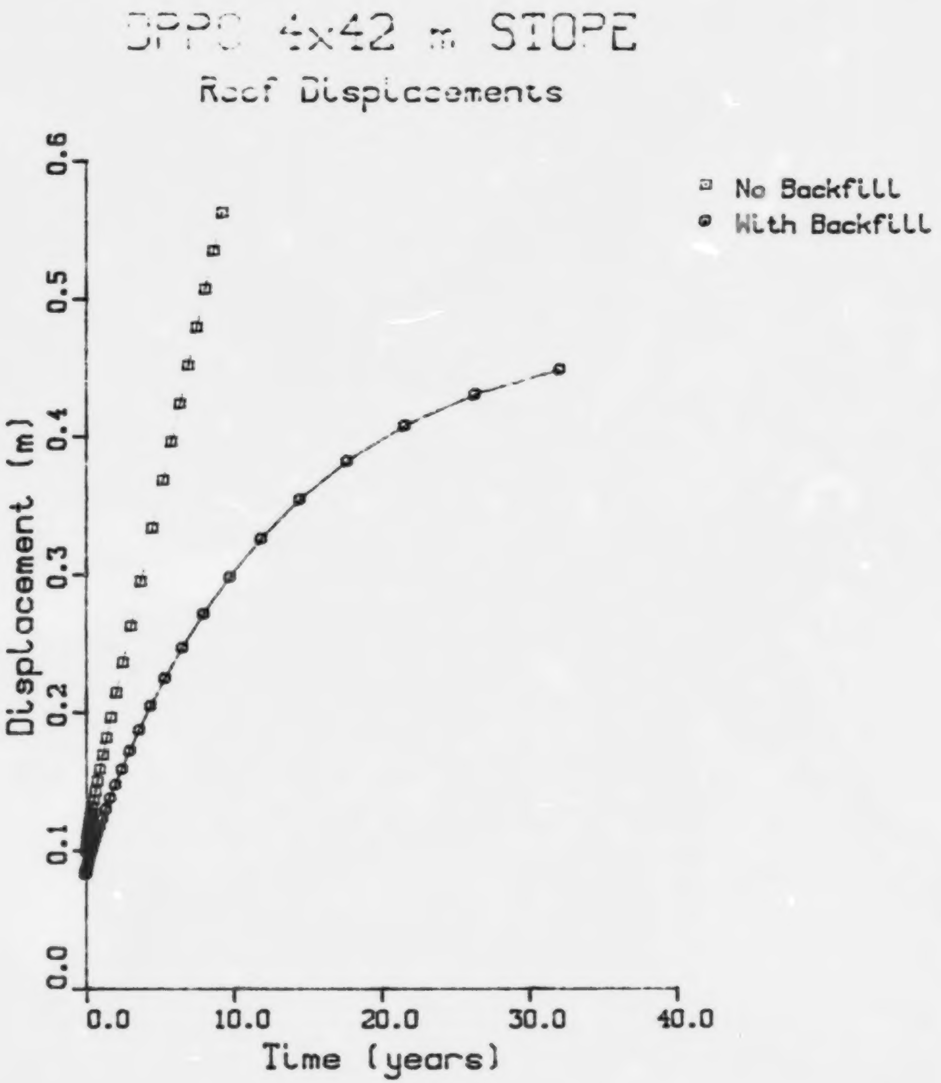
DPPC 4x42 m STOPE
Roof Displacements
No Backfill
With Backfill
Displacement (m)
0.0
0.1
0.2
0.3
0.4
0.5
0.6
Time (years)
0.0
10.0
20.0
30.0
40.0

FIGURE 8.1

8.2 WALL DISPLACEMENTS

Following are the numerical modelling results for wall displacements for the 4 m x 42 m Stope.

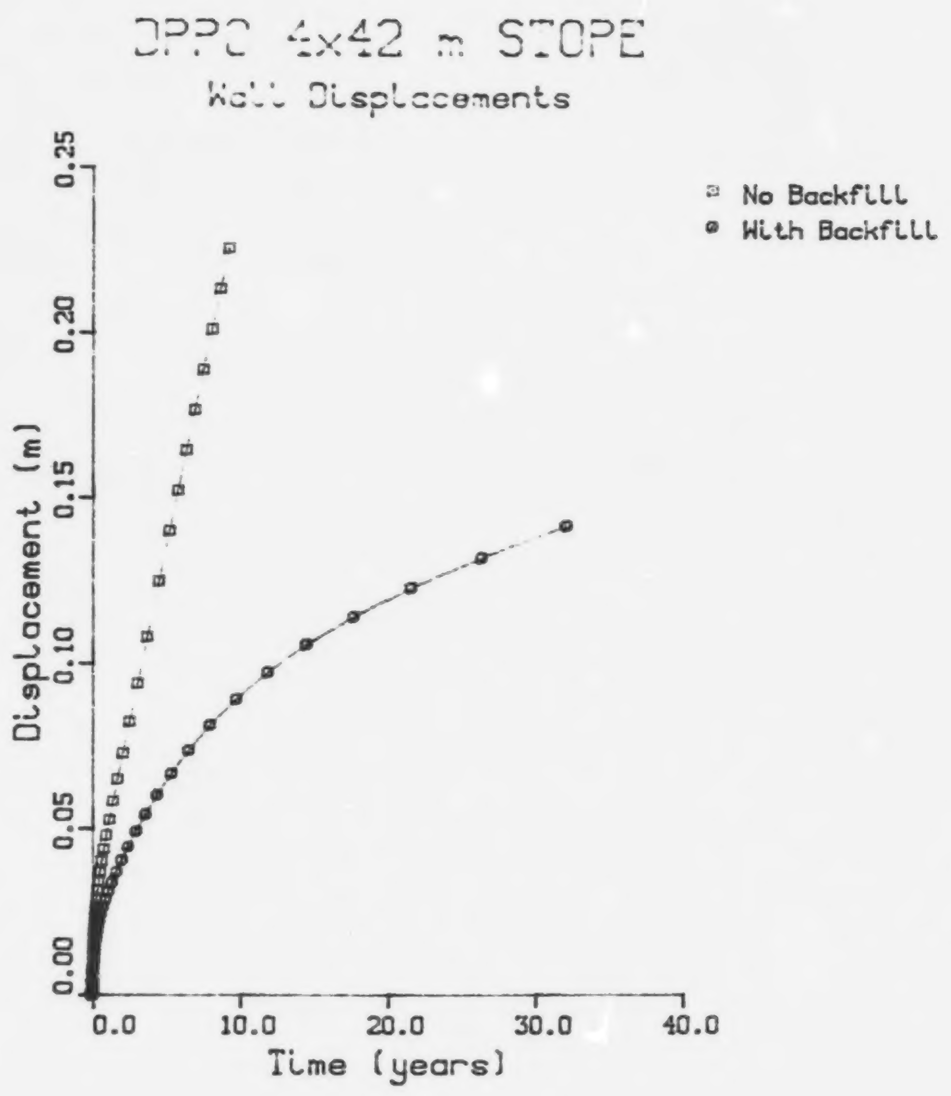
DPPC 4x42 m STOPE
Wall Displacements
Displacement (m)
0.00
0.05
0.10
0.15
0.20
0.25
Time (years)
0.0
10.0
20.0
30.0
40.0
No Backfill
With Backfill

FIGURE 8.2

8.3 MINOR PRINCIPAL STRESS IN WALLS

Following are graphical summaries of the numerical modelling results for the minor (minimum) principal stress with reference to distance from the centre of the pillar for the 4 m x 42 m Stope with backfill.

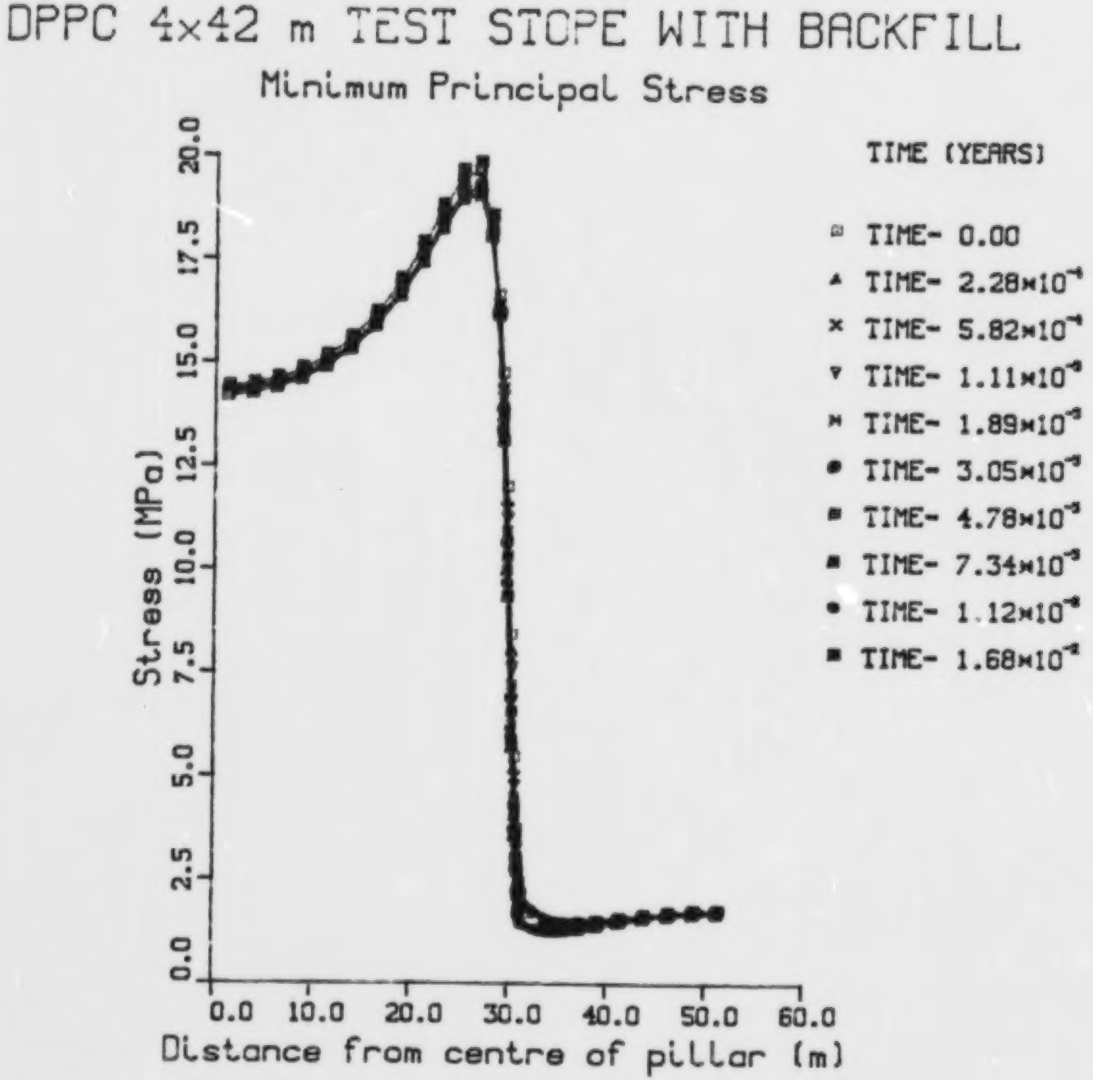
DPPC 4x42 m TEST STOPE WITH BACKFILL
Minimum Principal Stress
Stress (MPa)
0.0
2.5
5.0
7.5
10.0
12.5
15.0
17.5
20.0
Distance from centre of pillar (m)
0.0
10.0
20.0
30.0
40.0
50.0
60.0
TIME (YEARS)
TIME- 0.00
TIME- 2.28×10^{-4}
TIME- 5.82×10^{-4}
TIME- 1.11×10^{-3}
TIME- 1.89×10^{-3}
TIME- 3.05×10^{-3}
TIME- 4.78×10^{-3}
TIME- 7.34×10^{-3}
TIME- 1.12×10^{-2}
TIME- 1.68×10^{-2}

FIGURE 8.3

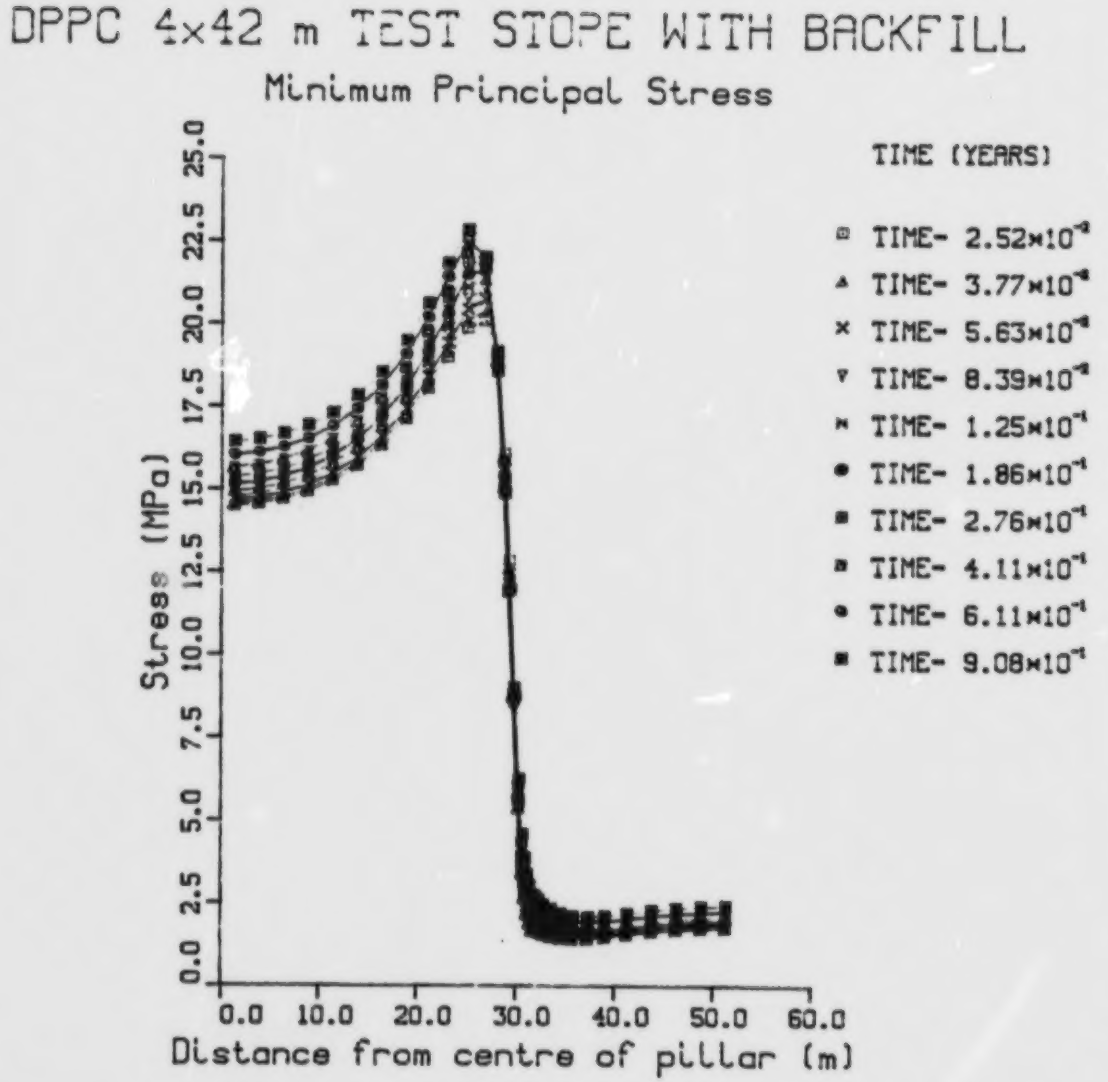

DPPC 4×42 m TEST STOPE WITH BACKFILL

Minimum Principal Stress

FIGURE 8.4

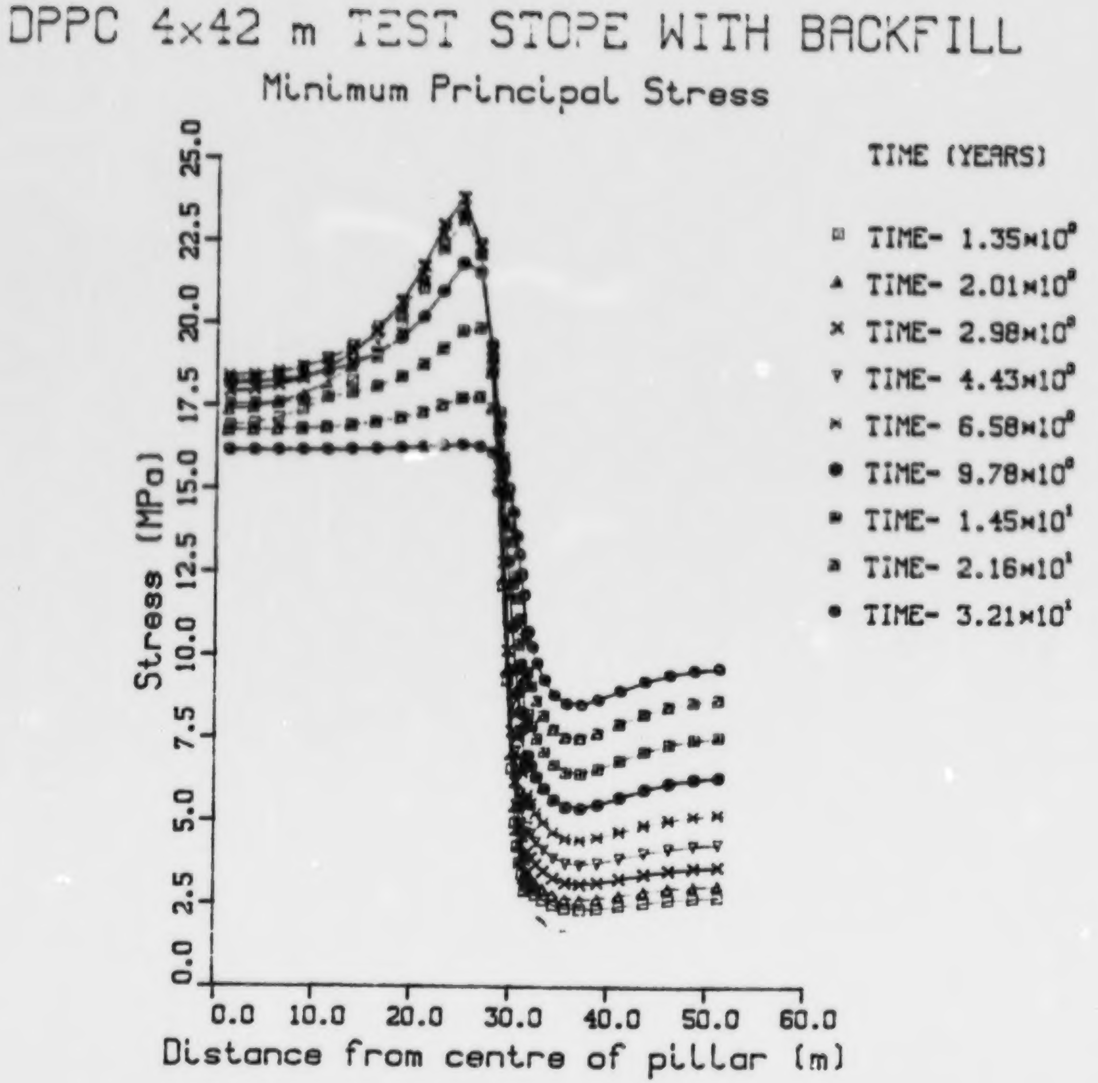
DPPC 4×42 m TEST STOPE WITH BACKFILL
Minimum Principal Stress
Stress (MPa)
0.0
2.5
5.0
7.5
10.0
12.5
15.0
17.5
20.0
22.5
25.0
Distance from centre of pillar (m)
0.0
10.0
20.0
30.0
40.0
50.0
60.0
TIME (YEARS)
⊡ TIME- 1.35×10⁰
▲ TIME- 2.01×10⁰
× TIME- 2.98×10⁰
▼ TIME- 4.43×10⁰
× TIME- 6.58×10⁰
● TIME- 9.78×10⁰
■ TIME- 1.45×10¹
■ TIME- 2.16×10¹
● TIME- 3.21×10¹

FIGURE 8.5

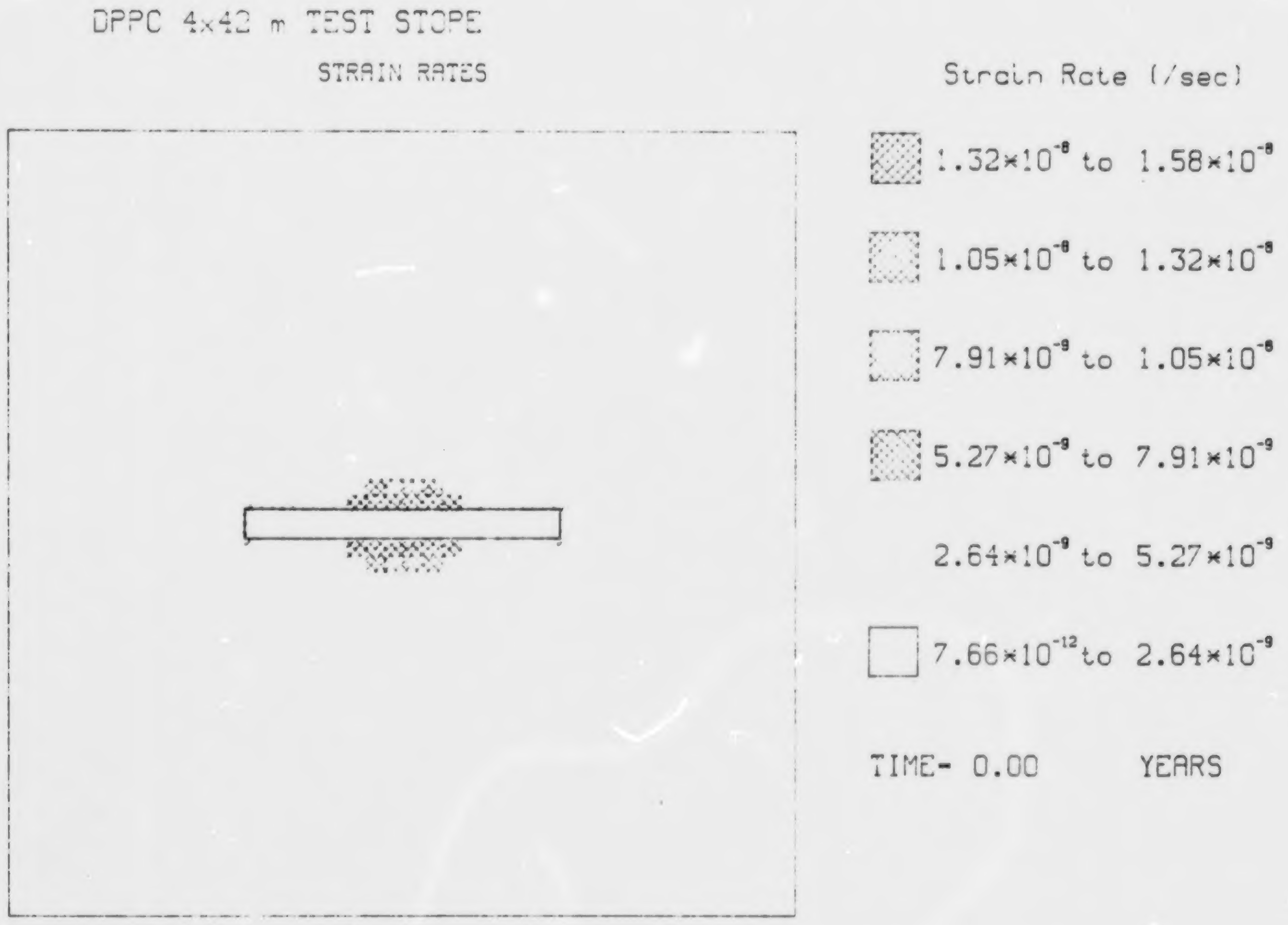
DPPC 4×42 m TEST STOPE
STRAIN RATES
Strain Rate (/sec)
1.32×10-8 to 1.58×10-8
1.05×10-8 to 1.32×10-8
7.91×10-9 to 1.05×10-8
5.27×10-9 to 7.91×10-9
2.64×10-9 to 5.27×10-9
7.66×10-12 to 2.64×10-9
TIME- 0.00 YEARS

FIGURE 8.6

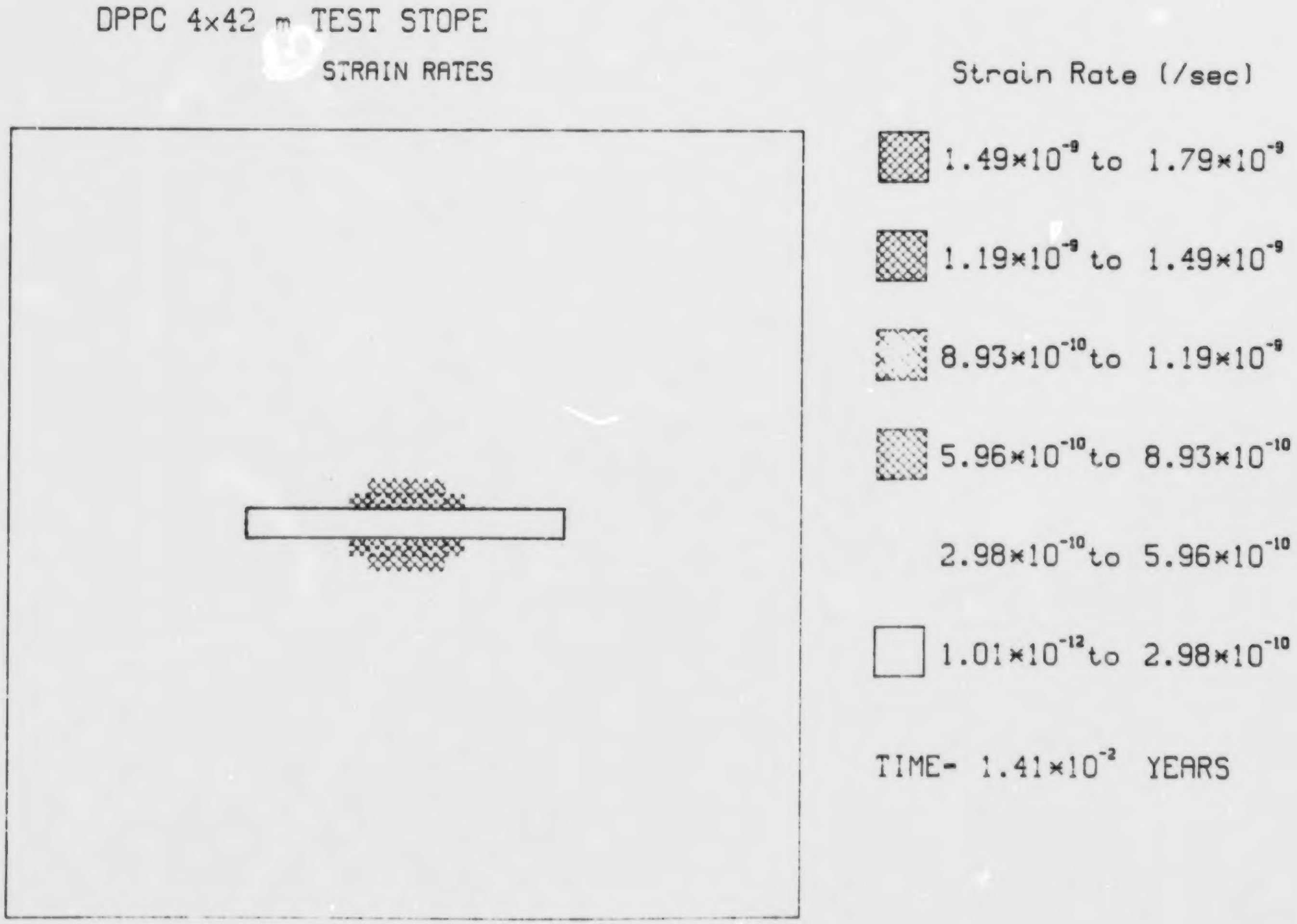
DPPC 4x42 m TEST STOPE
STRAIN RATES
Strain Rate (/sec)
▩ 1.49×10⁻⁹ to 1.79×10⁻⁹
▩ 1.19×10⁻⁹ to 1.49×10⁻⁹
▩ 8.93×10⁻¹⁰ to 1.19×10⁻⁹
▩ 5.96×10⁻¹⁰ to 8.93×10⁻¹⁰
2.98×10⁻¹⁰ to 5.96×10⁻¹⁰
☐ 1.01×10⁻¹² to 2.98×10⁻¹⁰
TIME- 1.41×10⁻² YEARS

FIGURE 8.7

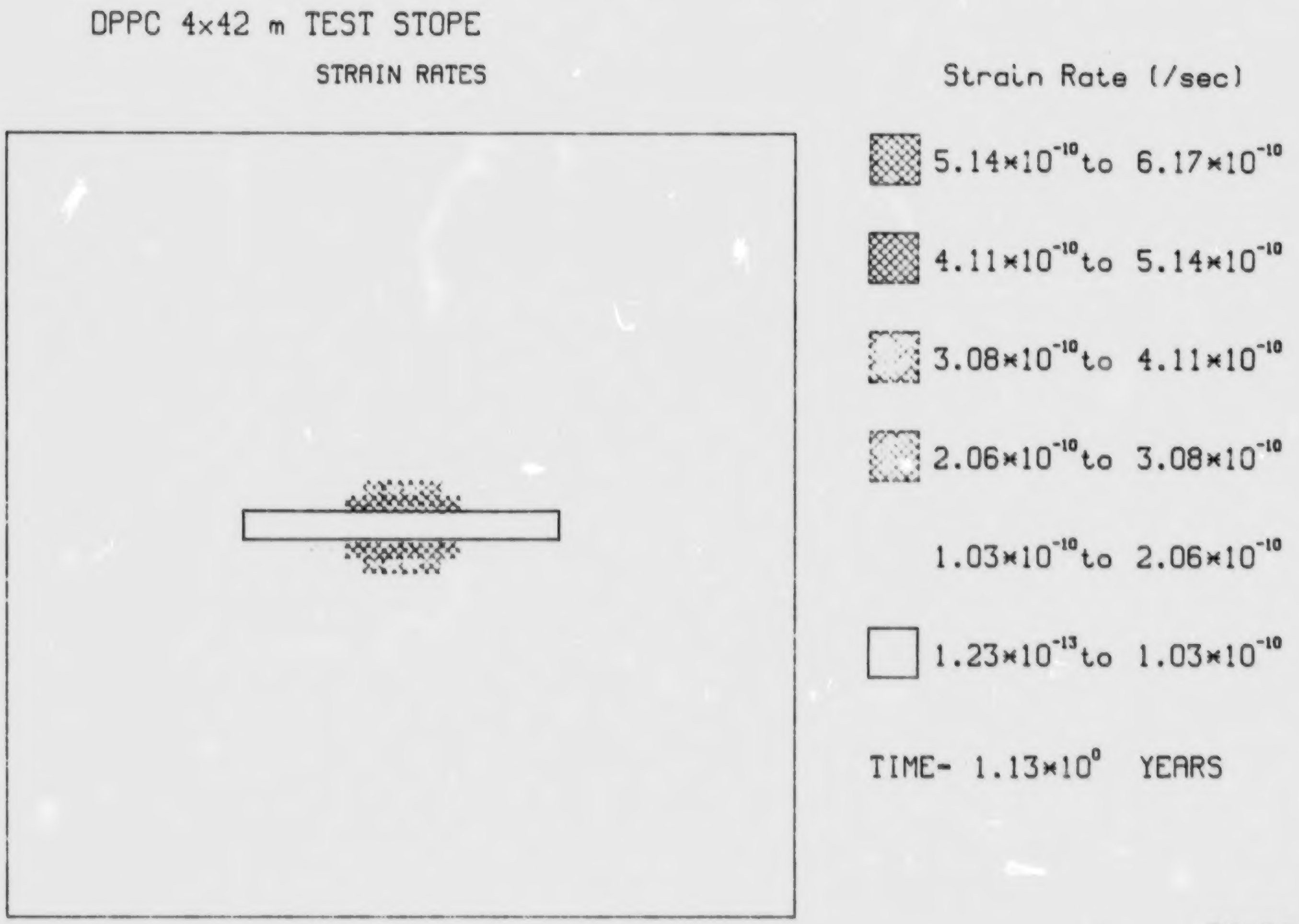
DPPC 4x42 m TEST STOPE
STRAIN RATES
Strain Rate (/sec)
▨ 5.14×10^{-10} to 6.17×10^{-10}
▨ 4.11×10^{-10} to 5.14×10^{-10}
▨ 3.08×10^{-10} to 4.11×10^{-10}
▨ 2.06×10^{-10} to 3.08×10^{-10}
1.03×10^{-10} to 2.06×10^{-10}
☐ 1.23×10^{-13} to 1.03×10^{-10}
TIME- 1.13×10^{0} YEARS

FIGURE 8.8

DPPC 4×42 m TEST STOPE

STRAIN RATES

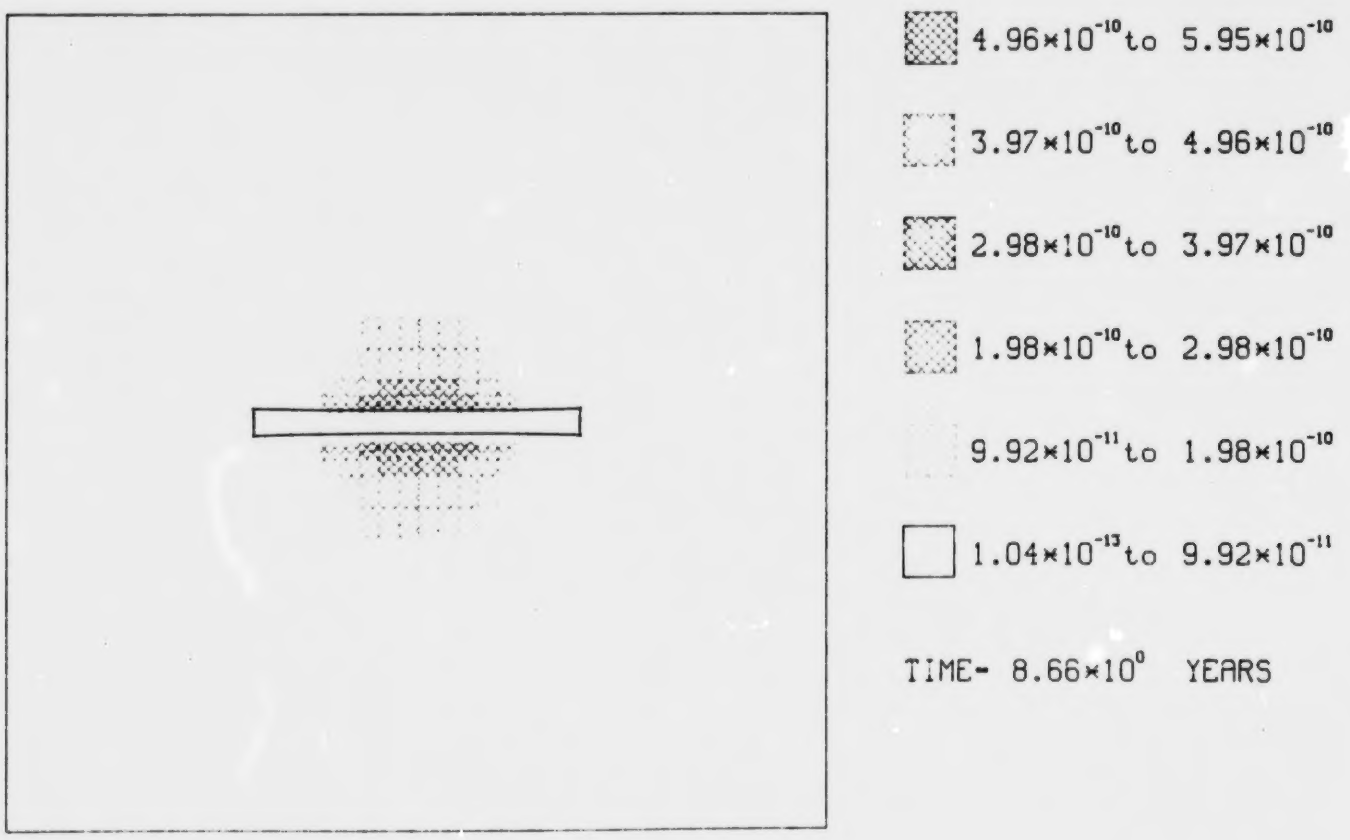

FIGURE 8.9

8.5 SHEAR STRESS DISTRIBUTION

Following are the numerical modelling results for the shear stress for the 4 m x 42 m Stope without backfill.

DPPC 4×42 m TEST STOPE

SHEAR STRESS

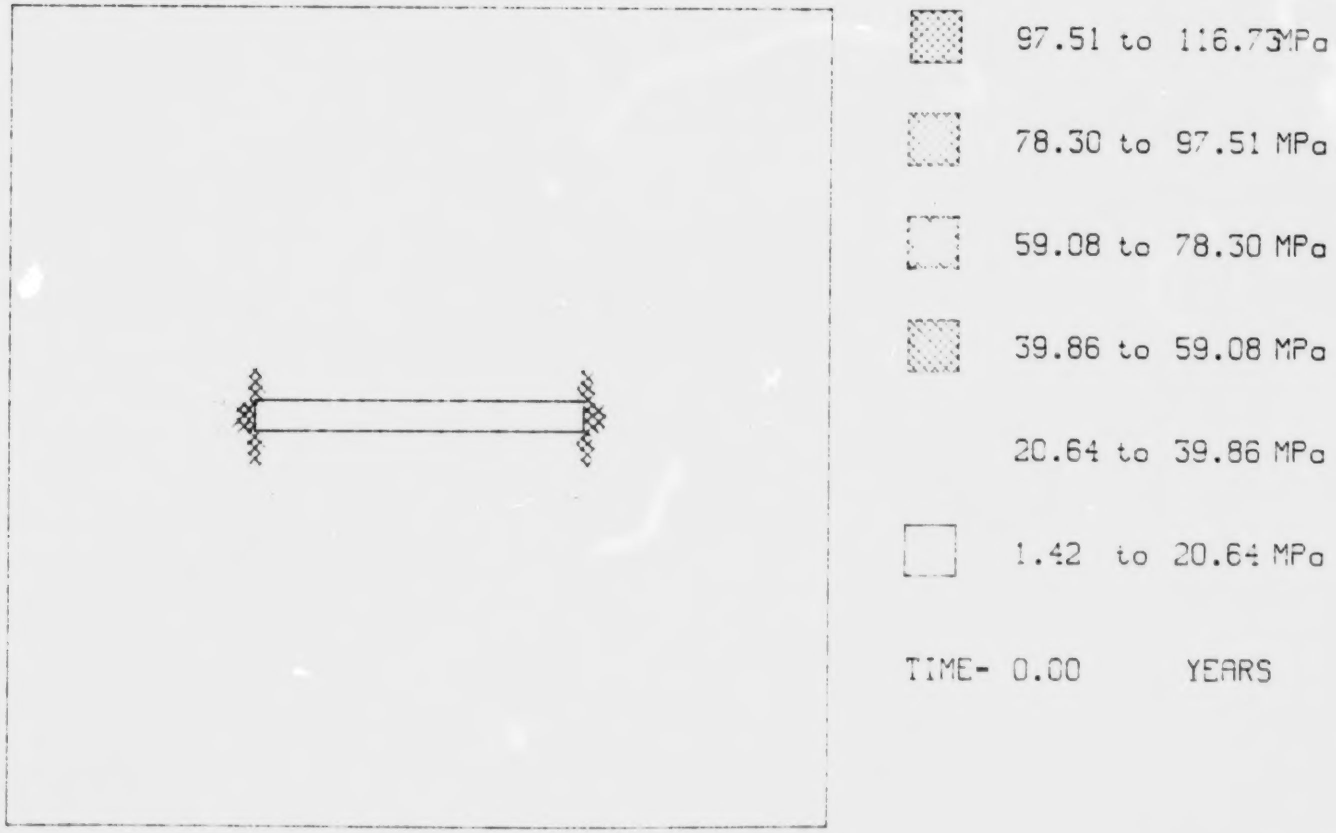

FIGURE 8.10

DPPC 4×42 m TEST STOPE

SHEAR STRESS

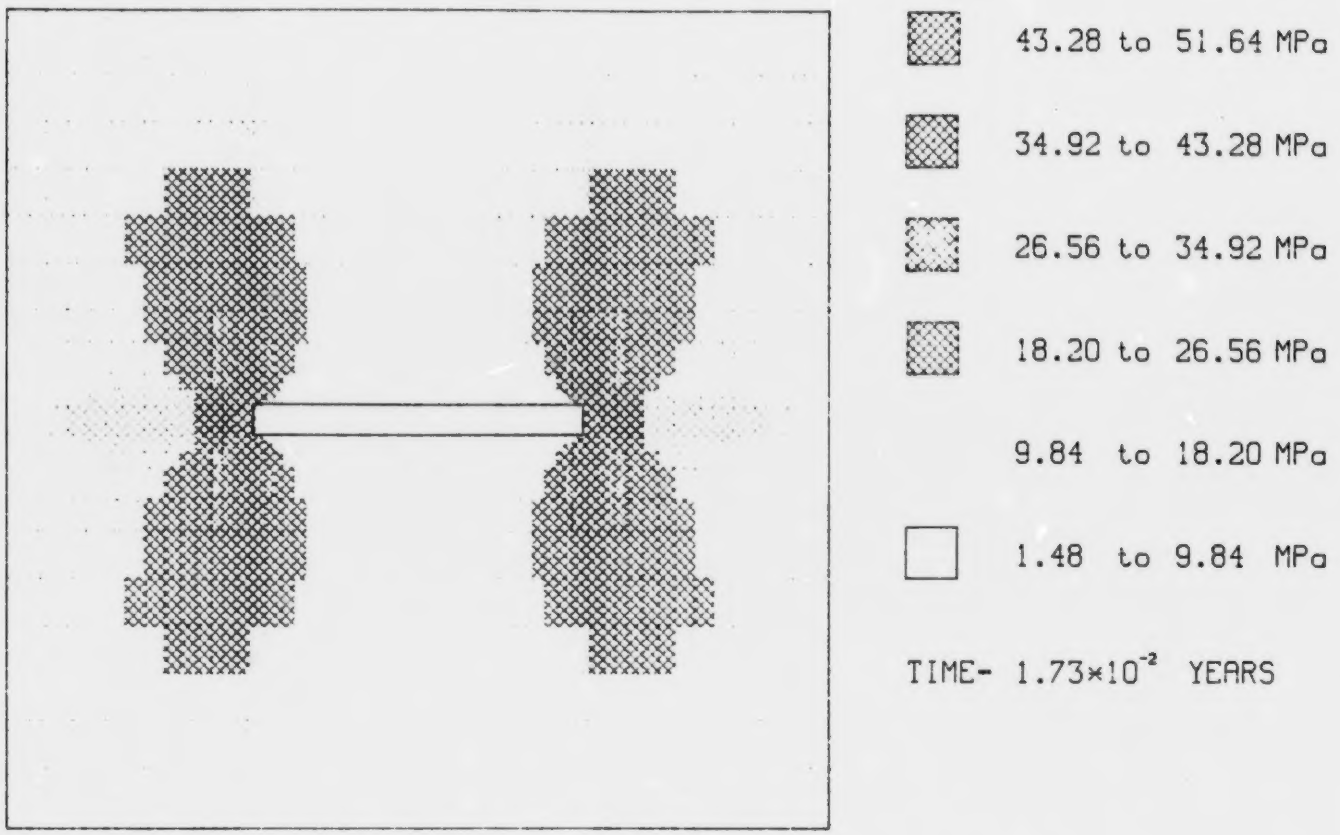

FIGURE 8.11

DPPC 4×42 m TEST STOPE

SHEAR STRESS

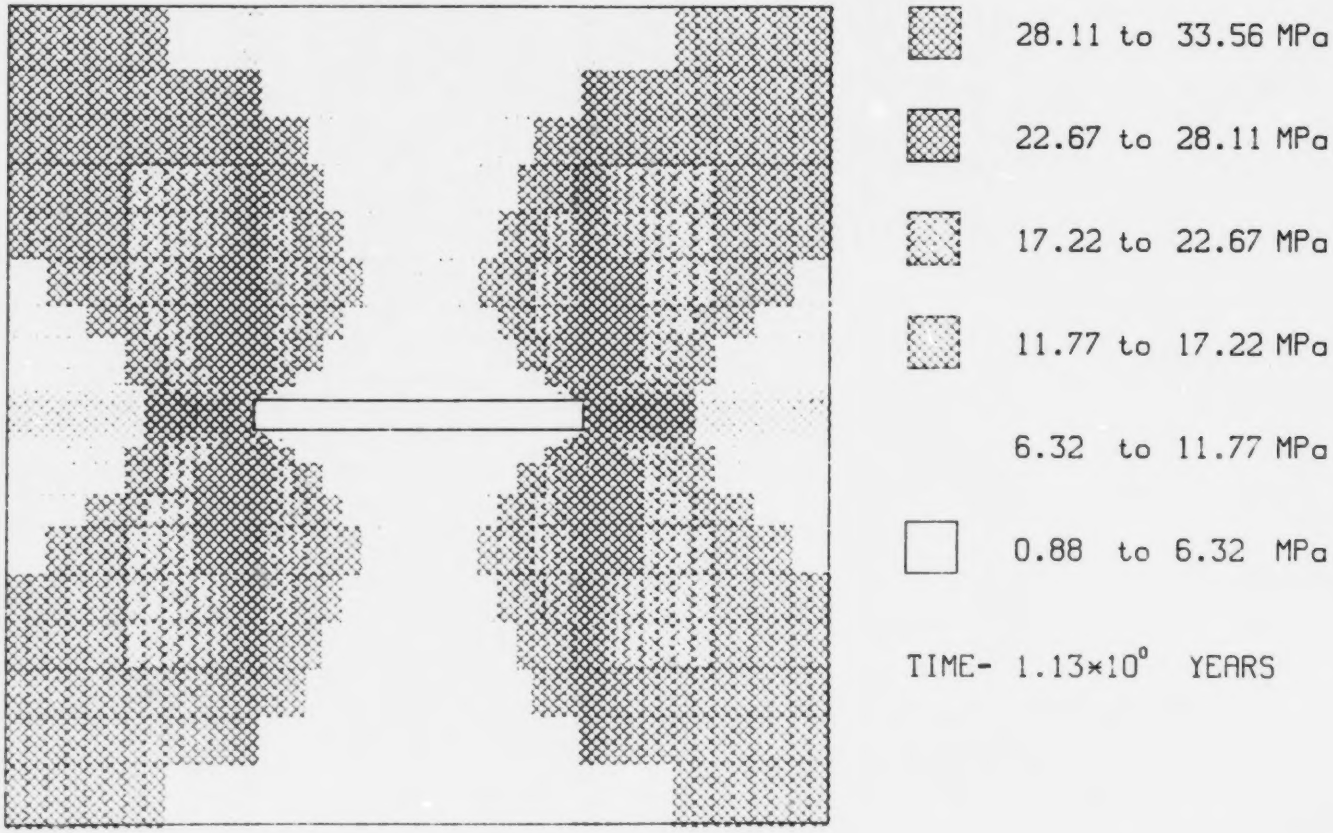

FIGURE 8.12

DPPC 4×42 m TEST STOPE

SHEAR STRESS

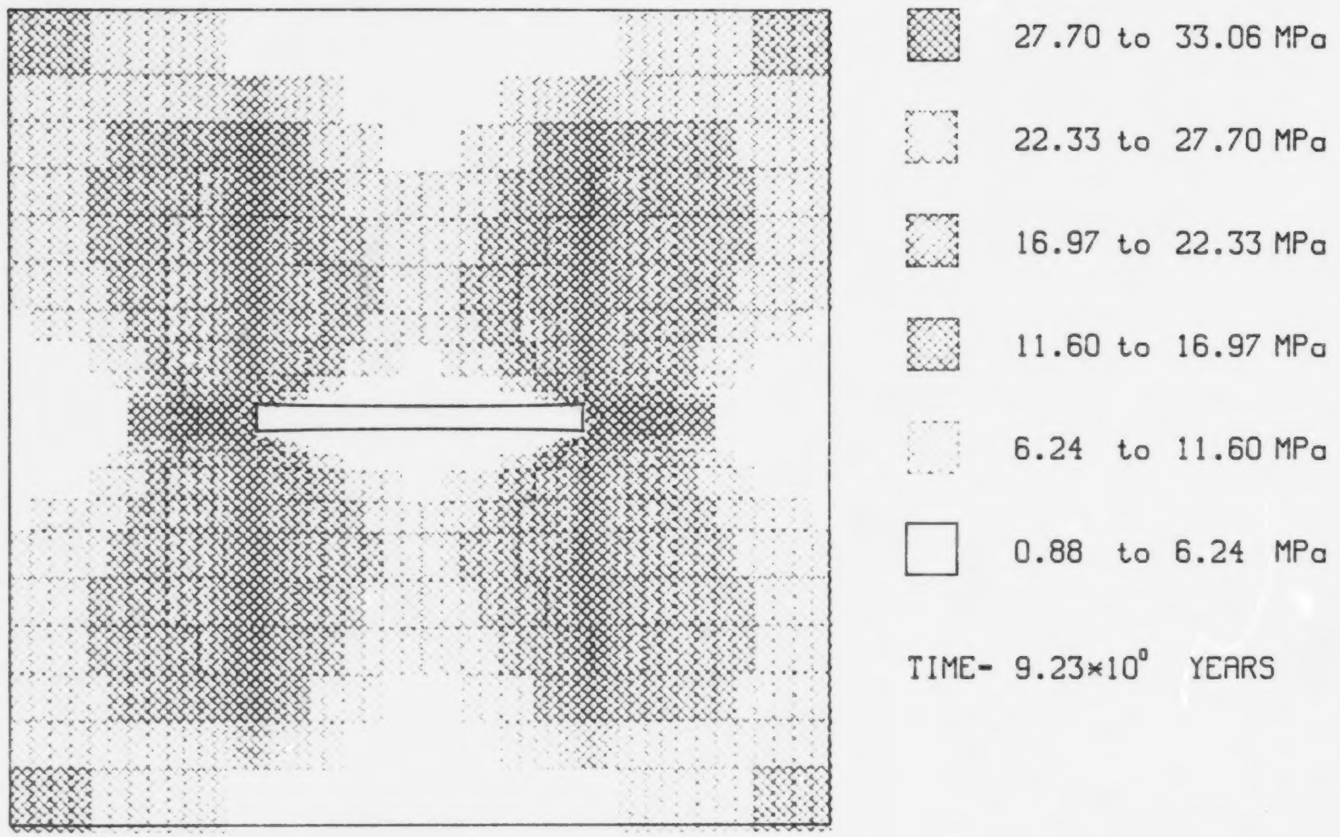

FIGURE 8.13

8.6 MAJOR PRINCIPAL STRESS DISTRIBUTION

Following are the numerical modelling results for major principal stress for the 4 m x 42 m Stope without backfill.

DPPC 4x42 m TEST STOPE

MAJOR PRINCIPLE STRESS

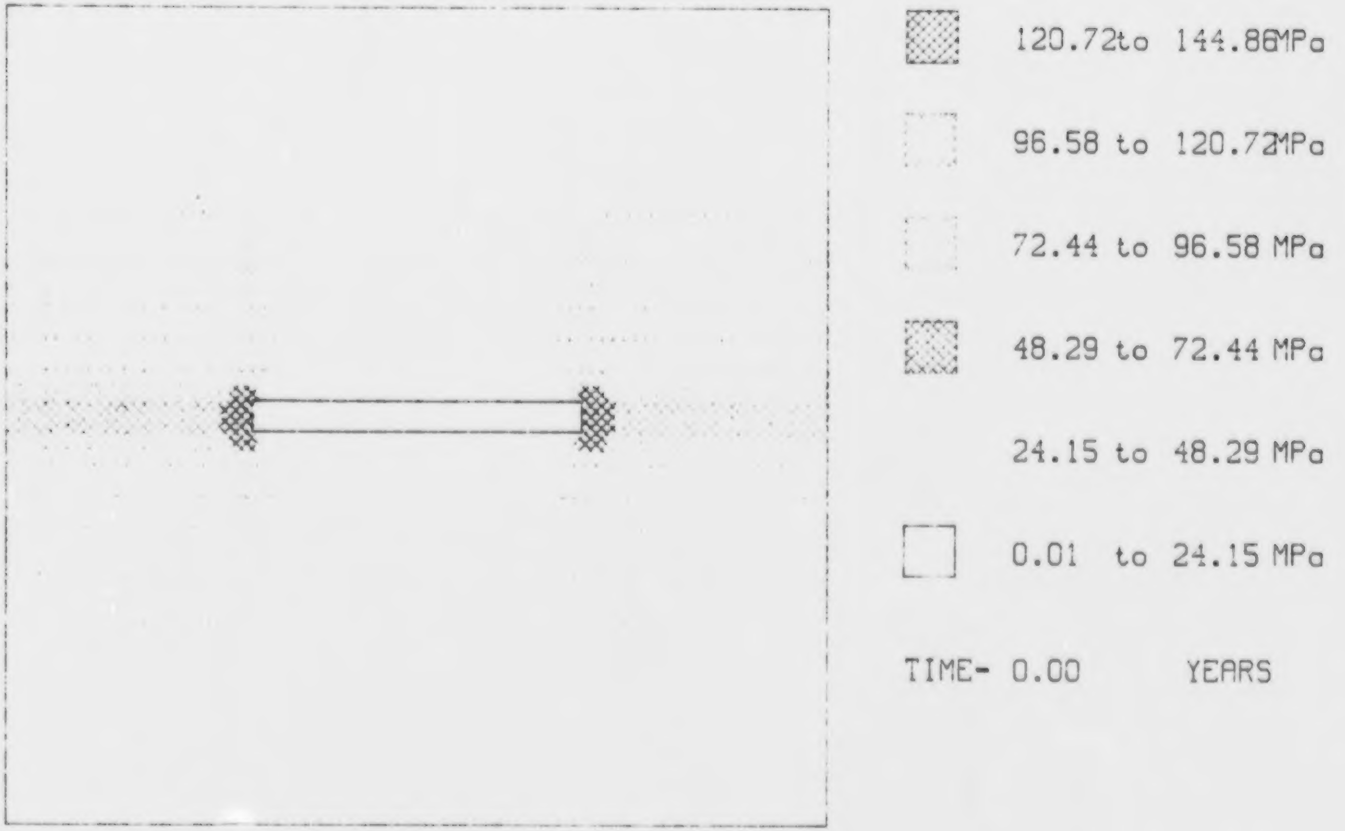

FIGURE 8.14

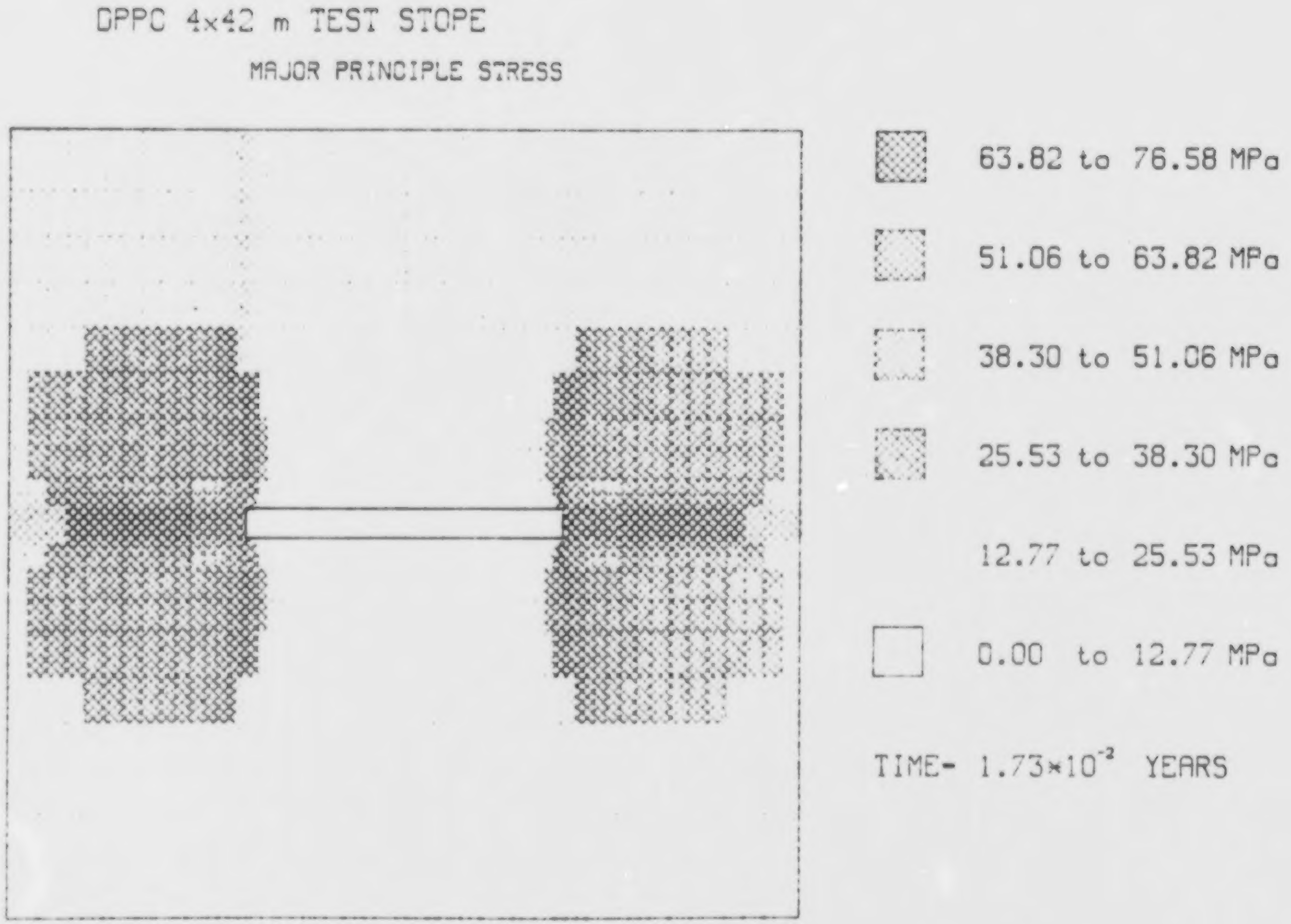
DPPC 4x42 m TEST STOPE
MAJOR PRINCIPLE STRESS
63.82 to 76.58 MPa
51.06 to 63.82 MPa
38.30 to 51.06 MPa
25.53 to 38.30 MPa
12.77 to 25.53 MPa
0.00 to 12.77 MPa
TIME- 1.73×10^-2 YEARS

FIGURE 8.15

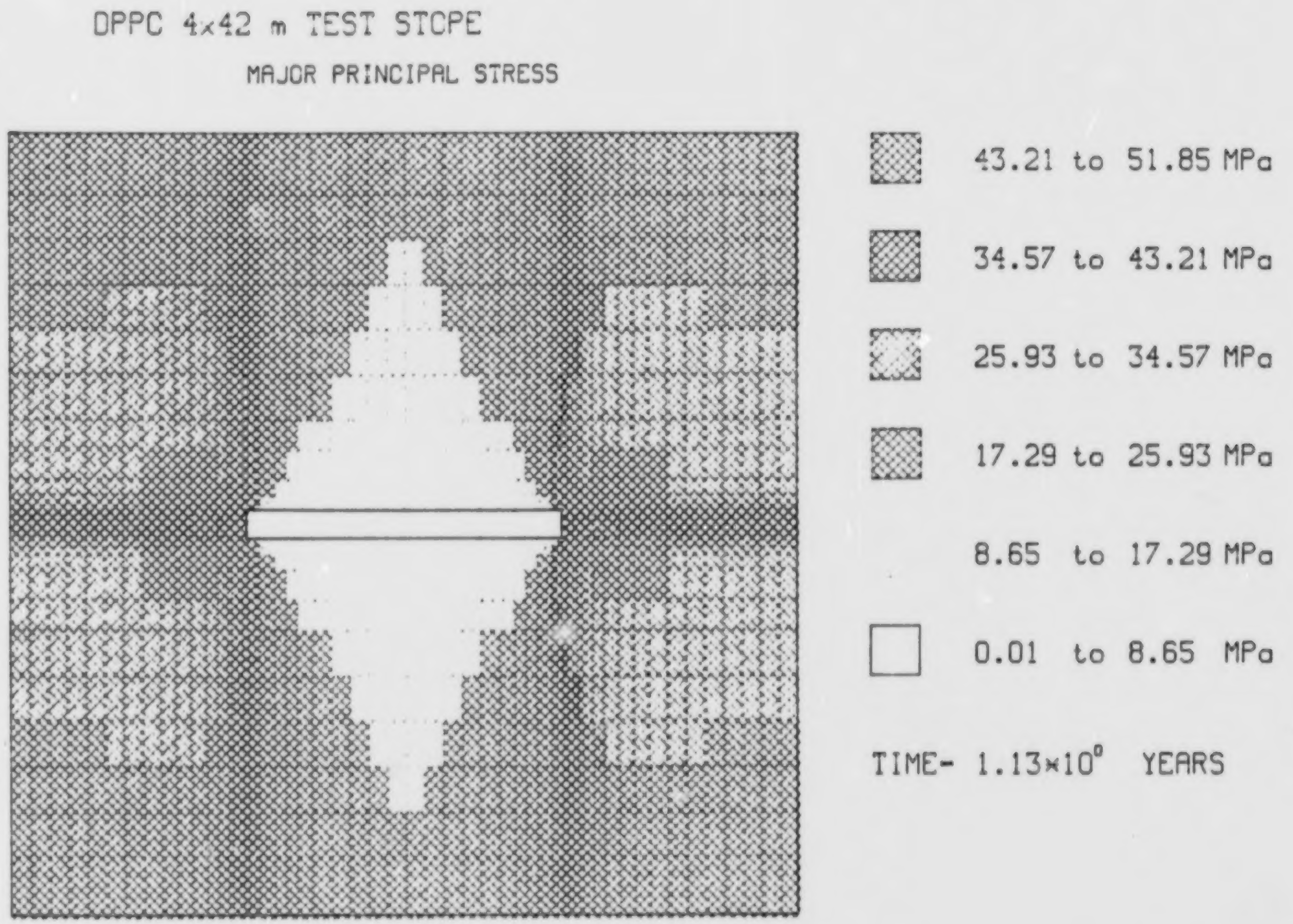
DPPC 4x42 m TEST STOPE
MAJOR PRINCIPAL STRESS
43.21 to 51.85 MPa
34.57 to 43.21 MPa
25.93 to 34.57 MPa
17.29 to 25.93 MPa
8.65 to 17.29 MPa
0.01 to 8.65 MPa
TIME- 1.13×10⁰ YEARS

FIGURE 8.16

DPPC 4×42 m TEST STOPE

MAJOR PRINCIPAL STRESS

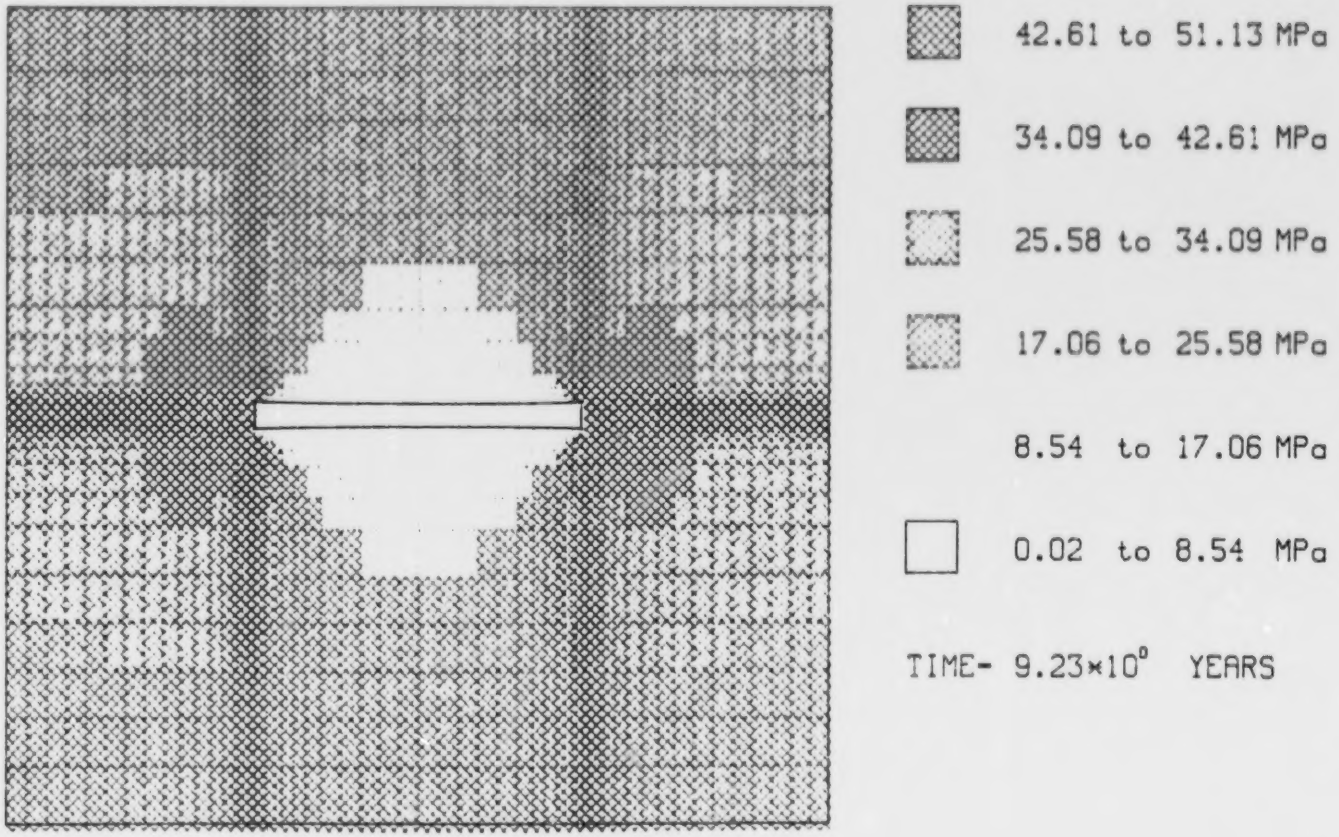

FIGURE 8.17

8.7 MINOR PRINCIPAL STRESS

Following are the numerical modelling results for the minor principal stress for the 4 m x 42 m Stope without backfill.

DPPC 4×42 m TEST STOPE

MINOR PRINCIPLE STRESS

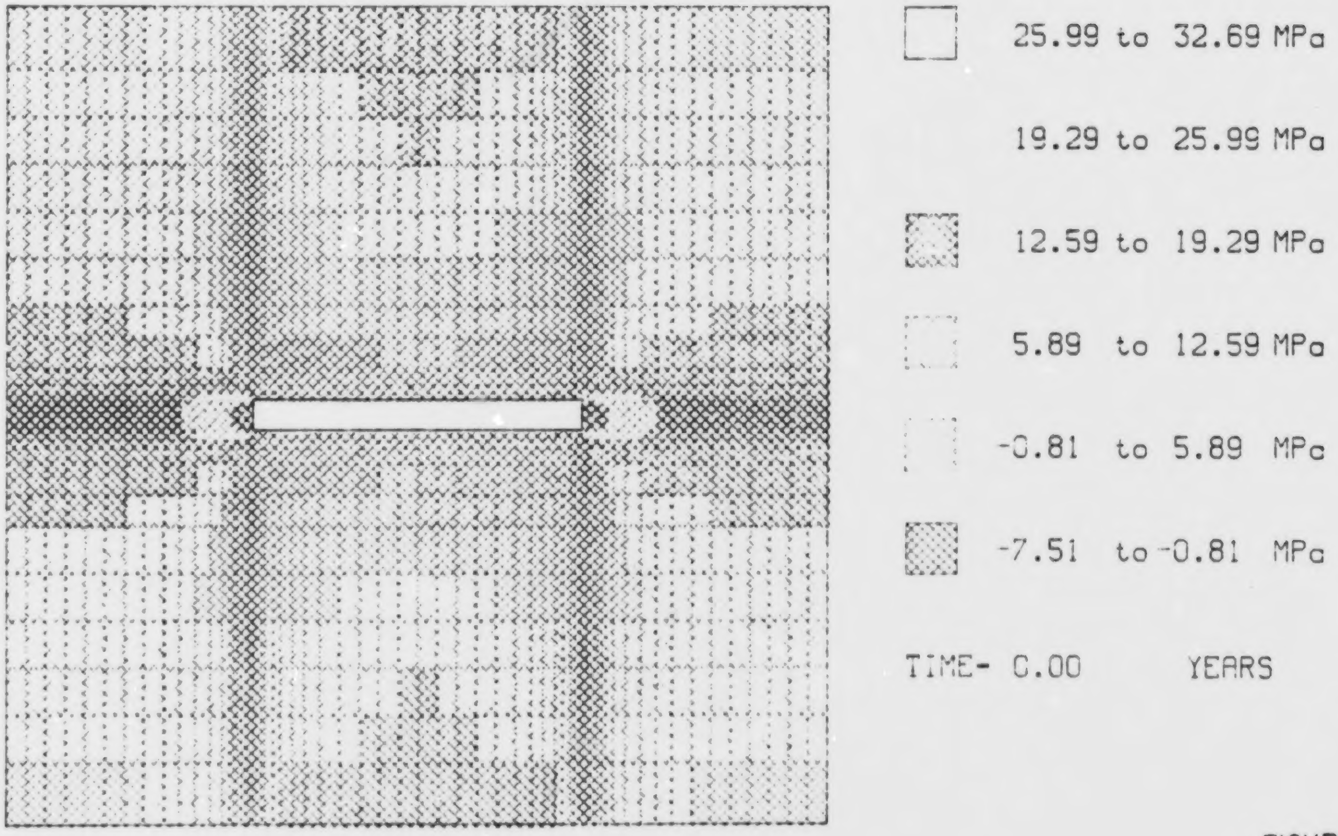

FIGURE 8.18

DPPC 4×42 m TEST STOPE

MINOR PRINCIPLE STRESS

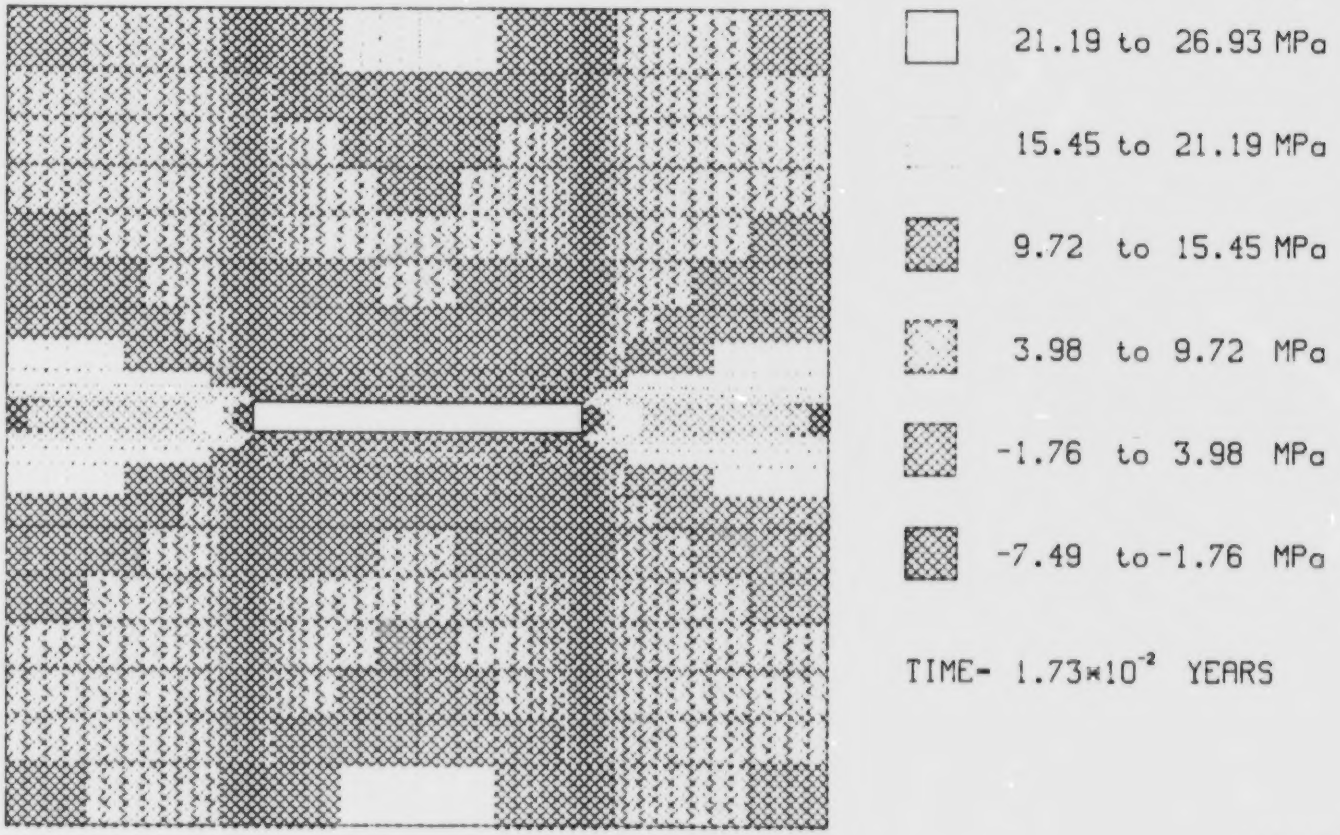

FIGURE 8.19

DPPC 4×42 m TEST STOPE

MINOR PRINCIPAL STRESS

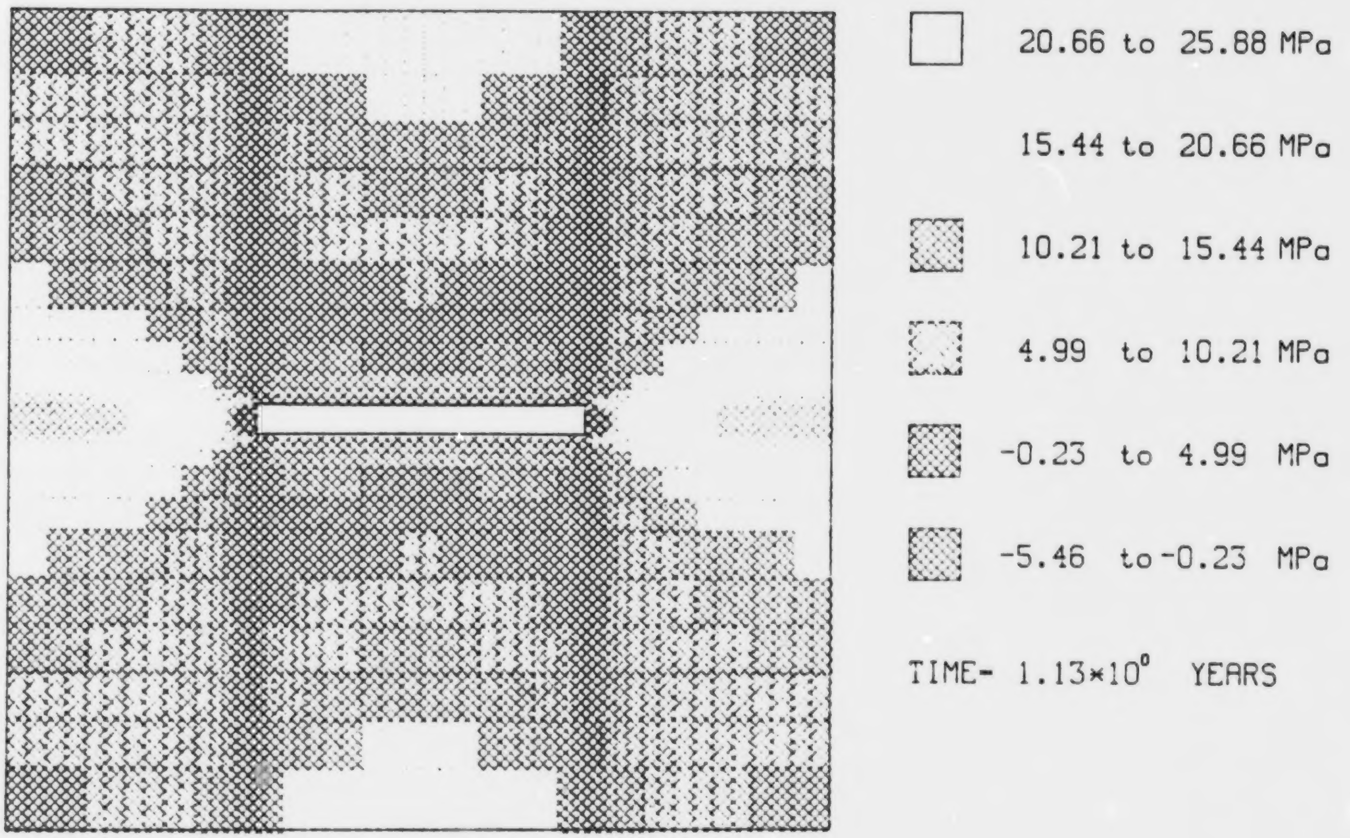

FIGURE 8.20

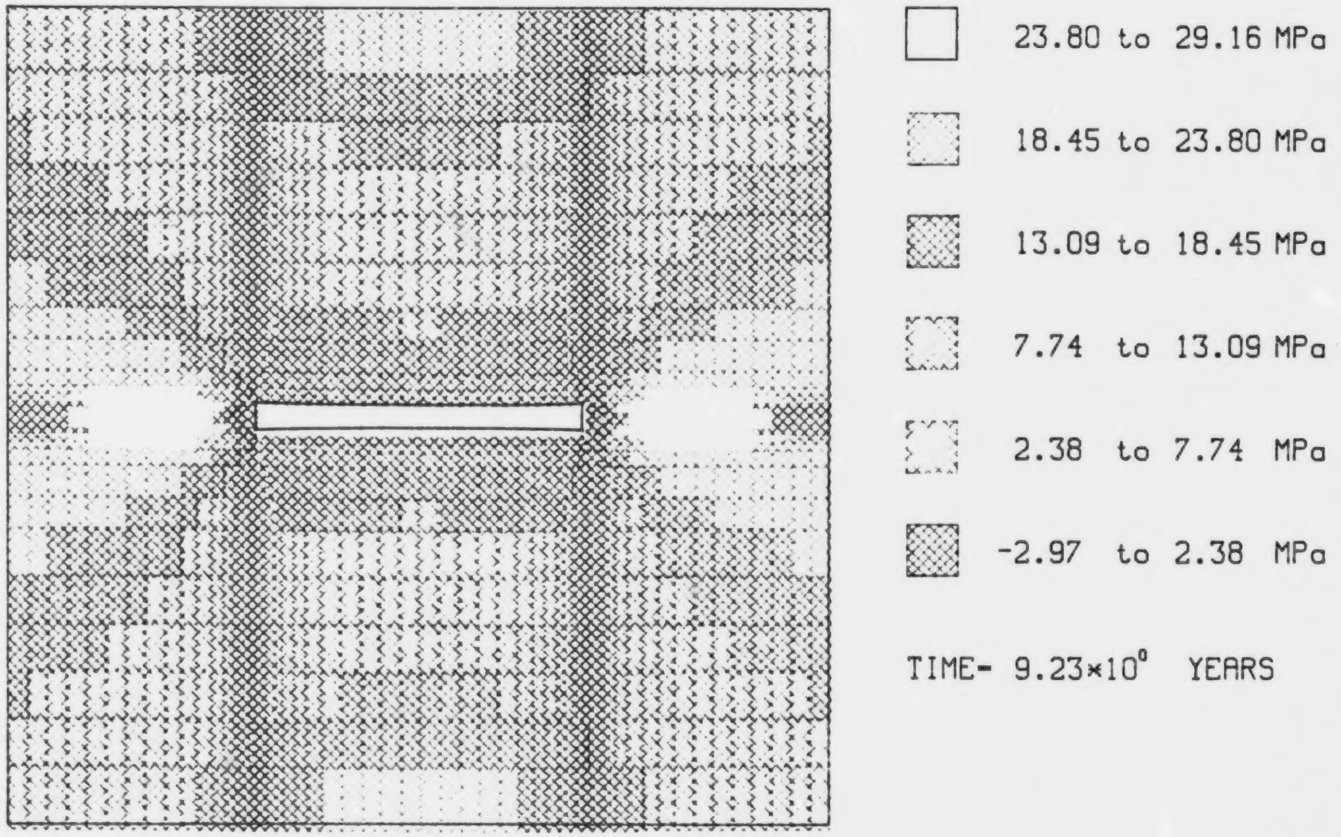

DPPC 4×42 m TEST STOPE

MINOR PRINCIPAL STRESS

FIGURE 8.21

SECTION 9.0

9.0 DENISON-POTACAN 12.5 M X 42 M STOPE

9.1 ROOF DISPLACEMENTS

Following are the numerical modelling results for roof displacements for the 12.5 m x 42 m stope.

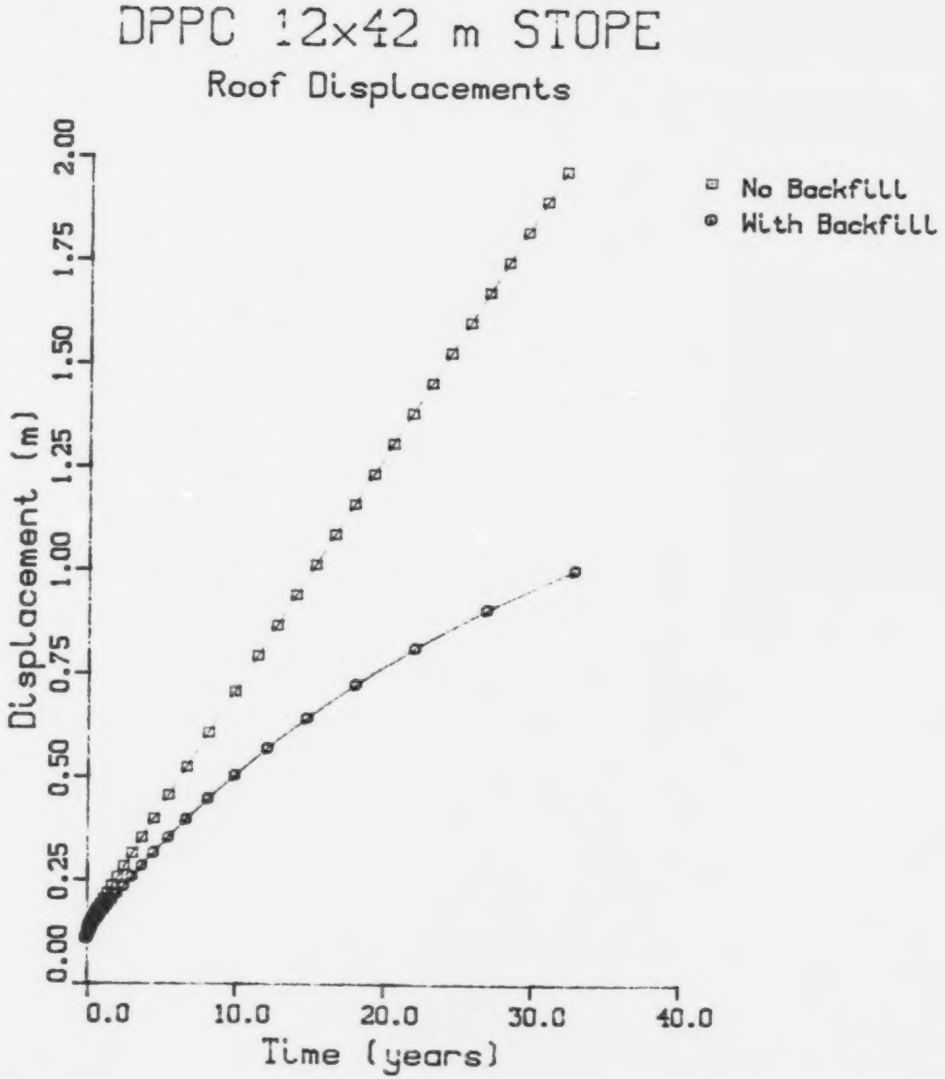
DPPC 12x42 m STOPE
Roof Displacements
No Backfill
With Backfill
Displacement (m)
0.00
0.25
0.50
0.75
1.00
1.25
1.50
1.75
2.00
Time (years)
0.0
10.0
20.0
30.0
40.0

FIGURE 9.1

9.2 WALL DISPLACEMENTS

Following are the numerical modelling results for wall displacements for the 12.5 m x 42 m stope.

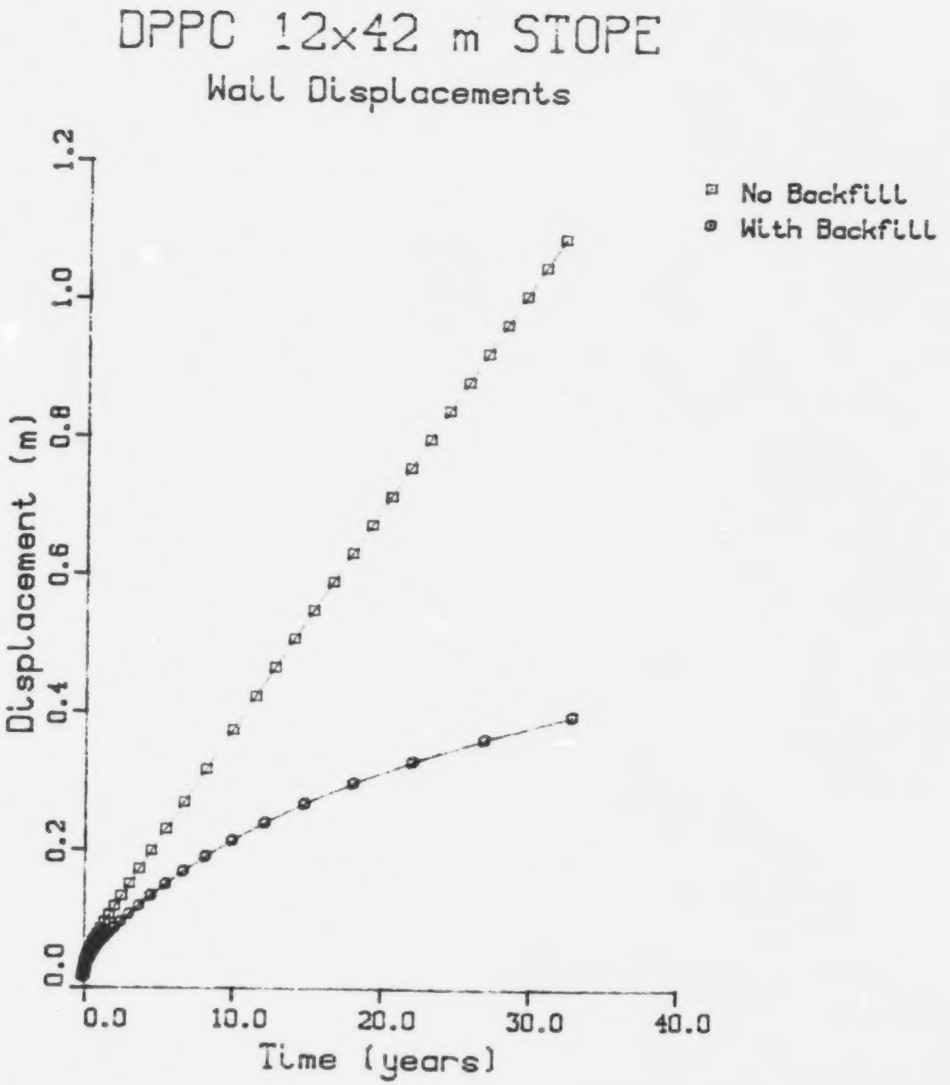
DPPC 12x42 m STOPE
Wall Displacements
Displacement (m)
0.0
0.2
0.4
0.6
0.8
1.0
1.2
Time (years)
0.0
10.0
20.0
30.0
40.0
No Backfill
With Backfill

FIGURE 9.2

9.3 MINOR PRINCIPAL STRESS IN WALLS

Following are graphical summaries of the numerical modelling results for the minor (minimum) principal stress with reference to distance from the centre of the pillar for the 12.5 m x 42 m Stope with backfill.

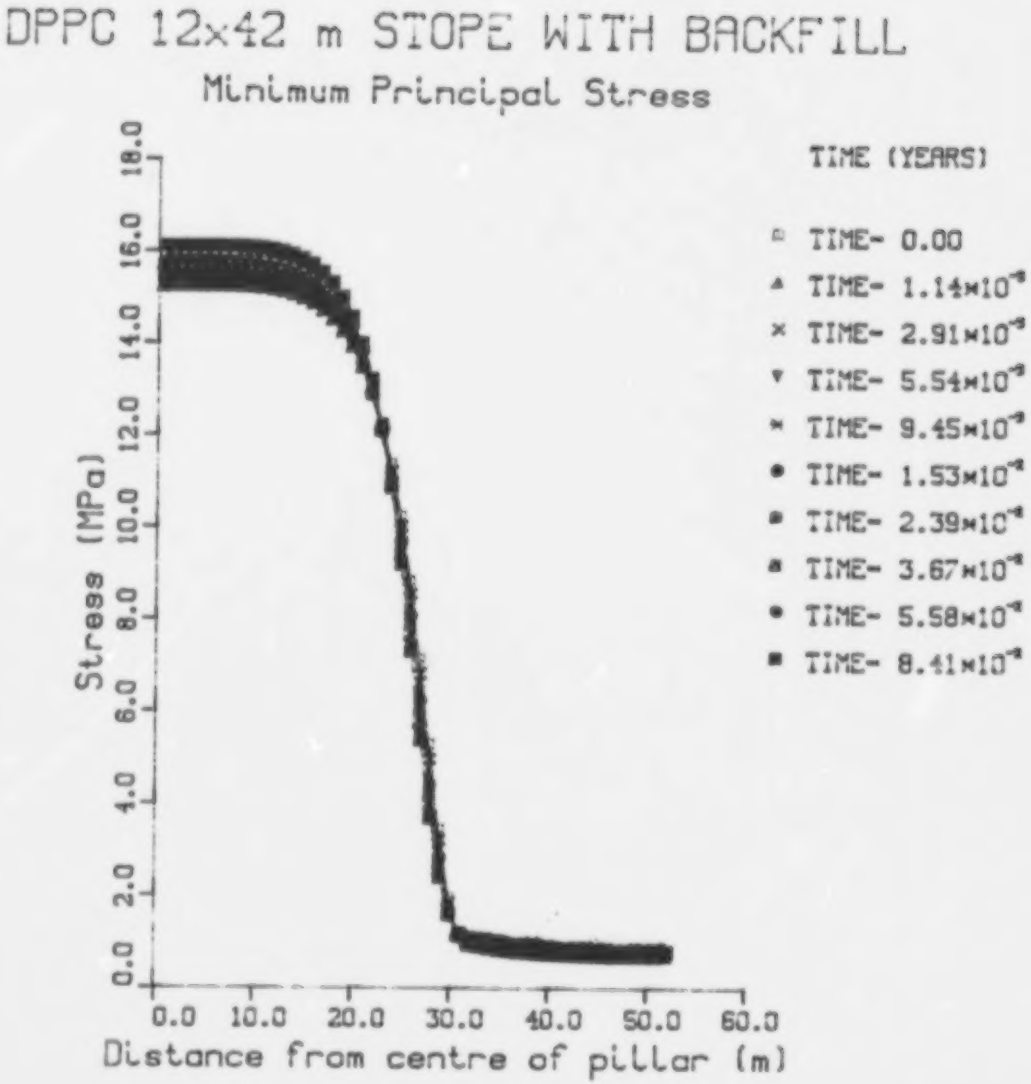
DPPC 12×42 m STOPE WITH BACKFILL
Minimum Principal Stress
Stress (MPa)
0.0
2.0
4.0
6.0
8.0
10.0
12.0
14.0
16.0
18.0
Distance from centre of pillar (m)
0.0
10.0
20.0
30.0
40.0
50.0
60.0
TIME (YEARS)
TIME- 0.00
TIME- 1.14×10^{-3}
TIME- 2.91×10^{-3}
TIME- 5.54×10^{-3}
TIME- 9.45×10^{-3}
TIME- 1.53×10^{-2}
TIME- 2.39×10^{-2}
TIME- 3.67×10^{-2}
TIME- 5.58×10^{-2}
TIME- 8.41×10^{-2}

FIGURE 9.3

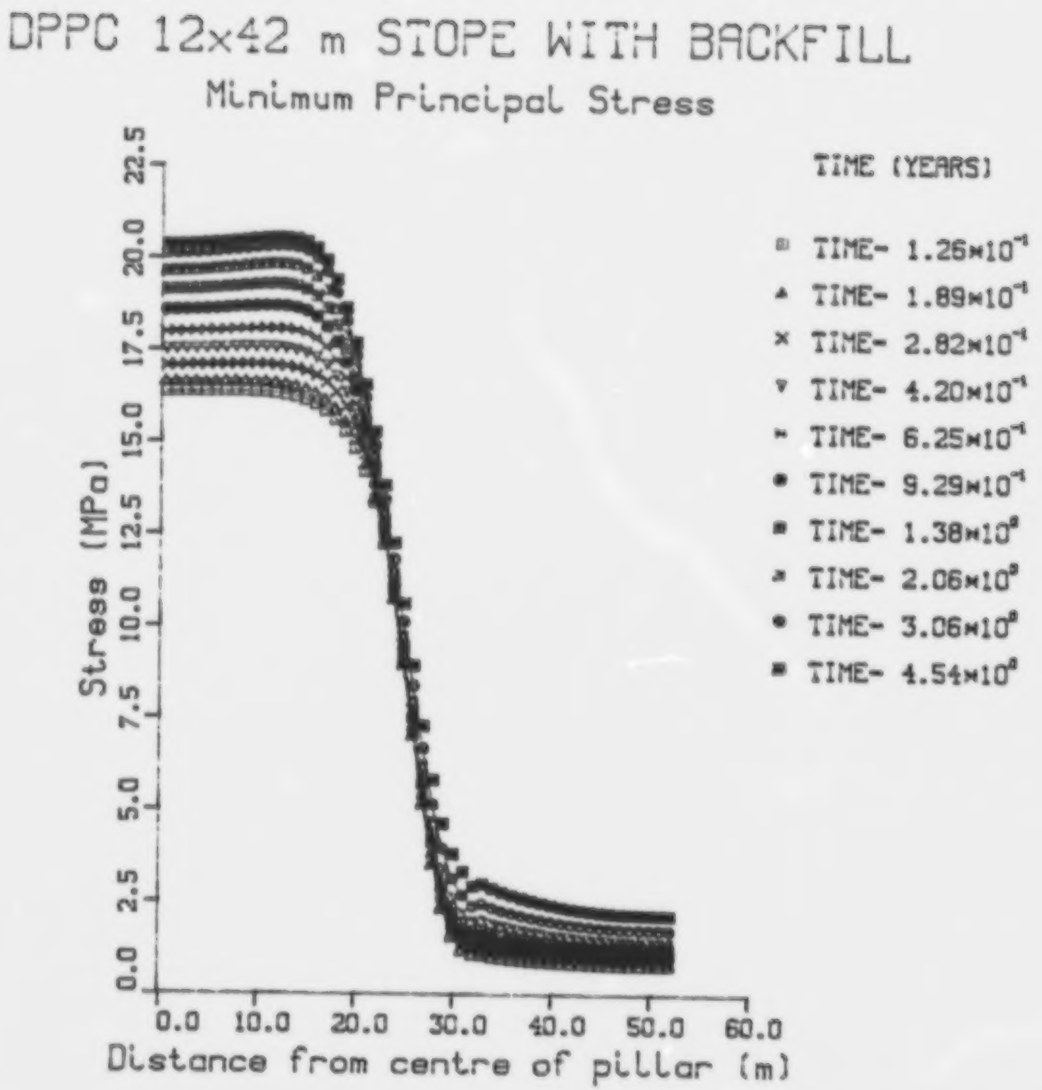
DPPC 12×42 m STOPE WITH BACKFILL
Minimum Principal Stress
Stress (MPa)
0.0
2.5
5.0
7.5
10.0
12.5
15.0
17.5
20.0
22.5
0.0
10.0
20.0
30.0
40.0
50.0
60.0
Distance from centre of pillar (m)
TIME (YEARS)
TIME- 1.26×10^{-1}
TIME- 1.89×10^{-1}
TIME- 2.82×10^{-1}
TIME- 4.20×10^{-1}
TIME- 6.25×10^{-1}
TIME- 9.29×10^{-1}
TIME- 1.38×10^{0}
TIME- 2.06×10^{0}
TIME- 3.06×10^{0}
TIME- 4.54×10^{0}

FIGURE 9.4

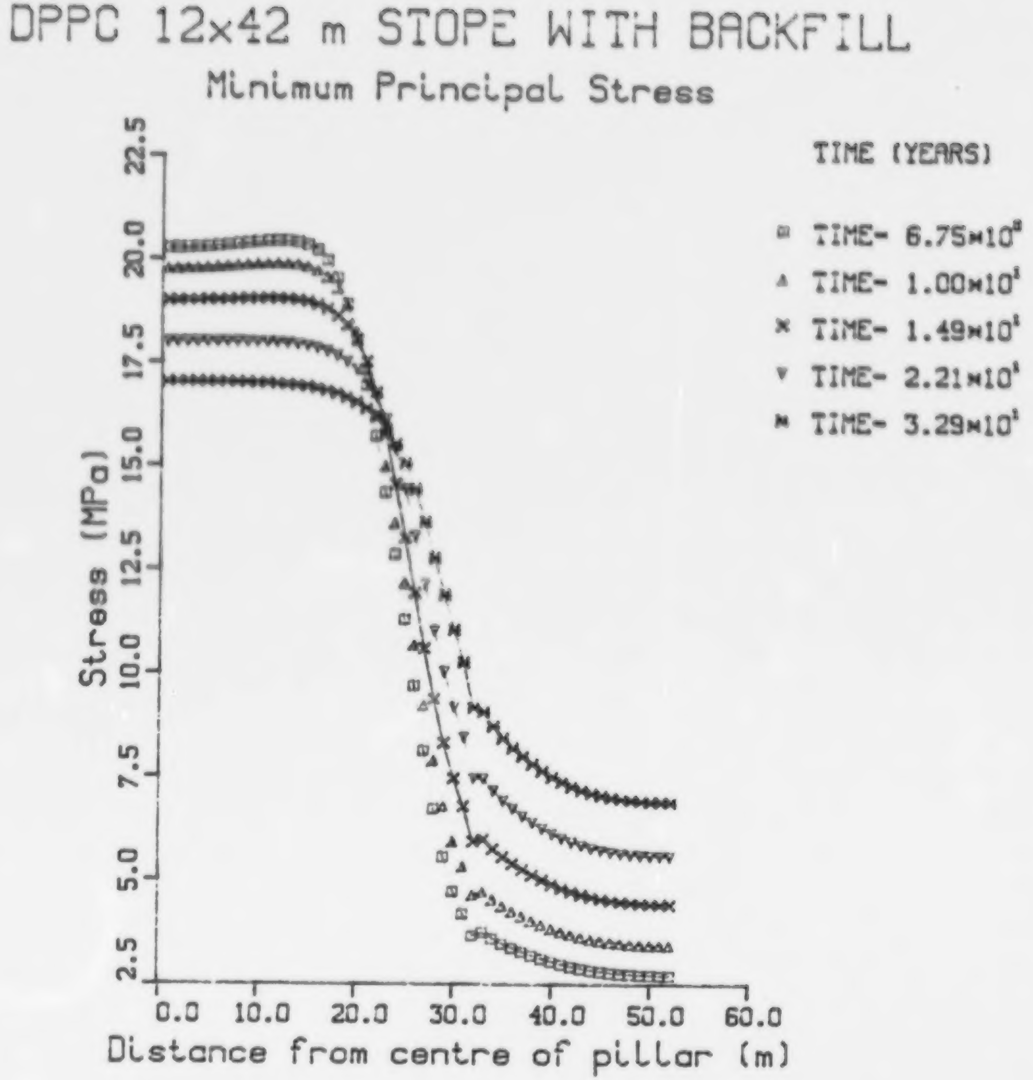
DPPC 12×42 m STOPE WITH BACKFILL
Minimum Principal Stress
TIME (YEARS)
TIME- 6.75×10^0
TIME- 1.00×10^1
TIME- 1.49×10^1
TIME- 2.21×10^1
TIME- 3.29×10^1
Stress (MPa)
2.5
5.0
7.5
10.0
12.5
15.0
17.5
20.0
22.5
0.0
10.0
20.0
30.0
40.0
50.0
60.0
Distance from centre of pillar (m)

FIGURE 9.5

9.4 STRAIN RATE DISTRIBUTION

Following are the numerical modelling results for strain rates for the 12.5 m x 42 m Stope without backfill.

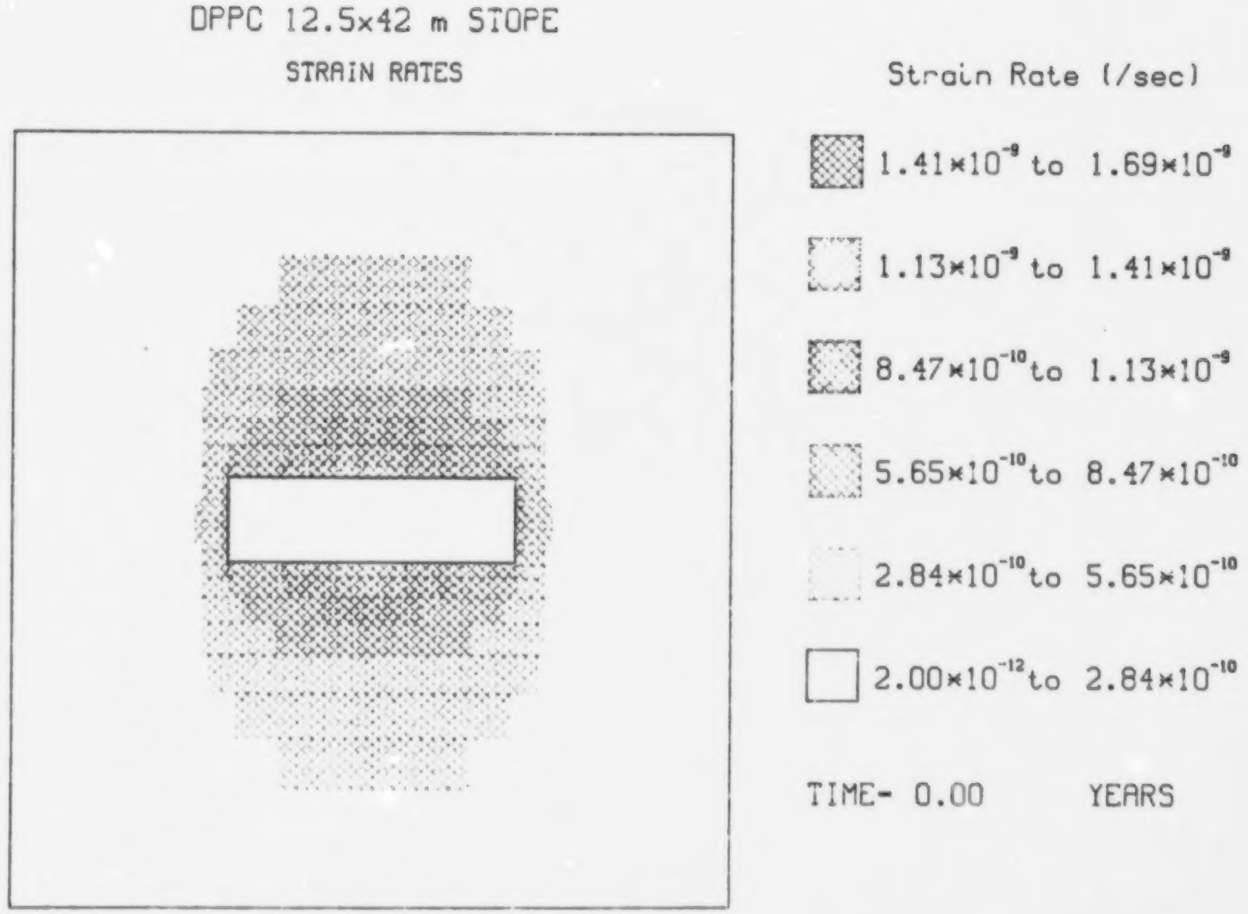
DPPC 12.5x42 m STOPE
STRAIN RATES
Strain Rate (/sec)
▩ 1.41×10^{-9} to 1.69×10^{-9}
▨ 1.13×10^{-9} to 1.41×10^{-9}
▩ 8.47×10^{-10} to 1.13×10^{-9}
▨ 5.65×10^{-10} to 8.47×10^{-10}
▨ 2.84×10^{-10} to 5.65×10^{-10}
☐ 2.00×10^{-12} to 2.84×10^{-10}
TIME- 0.00 YEARS

FIGURE 9.6

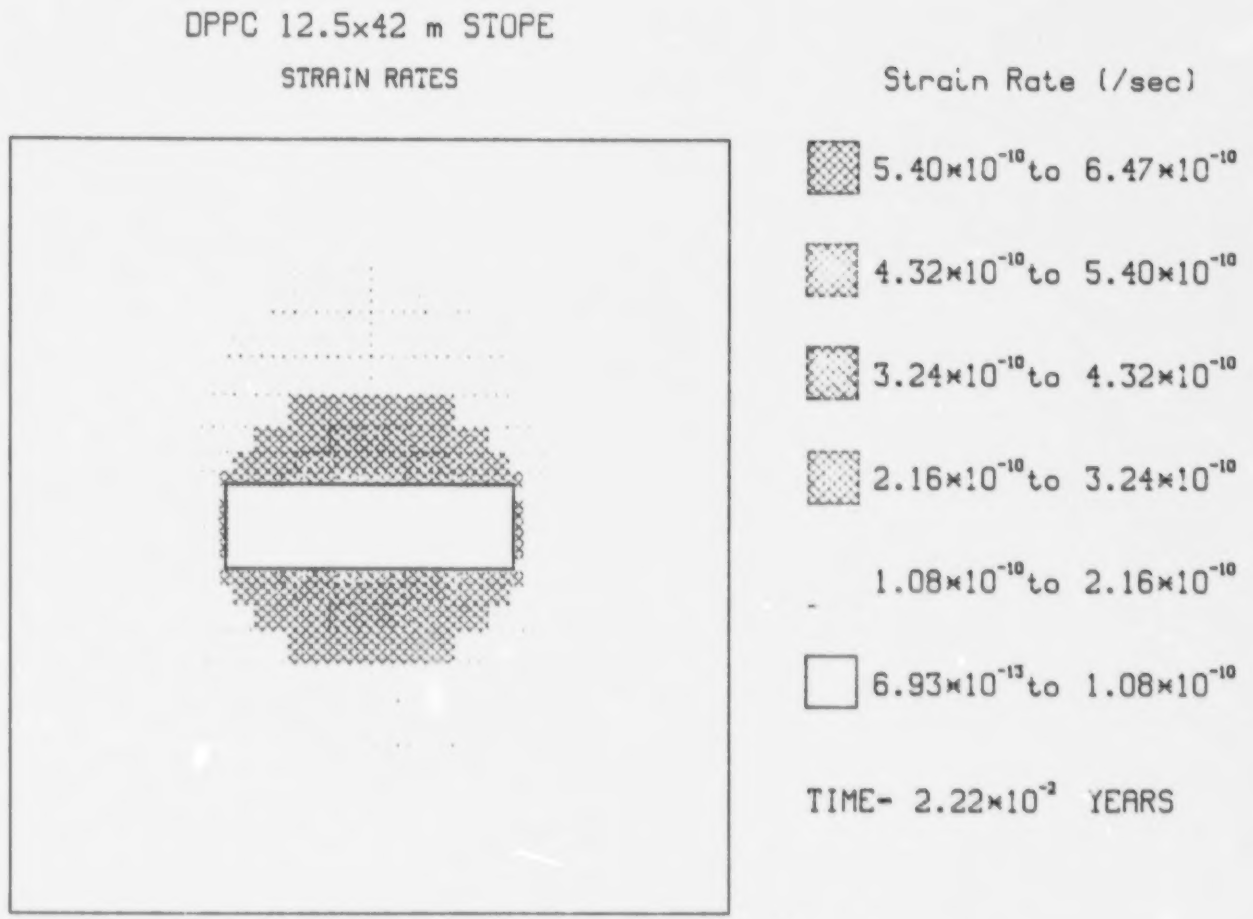
DPPC 12.5x42 m STOPE
STRAIN RATES
Strain Rate (/sec)
▨ 5.40×10^{-10} to 6.47×10^{-10}
▨ 4.32×10^{-10} to 5.40×10^{-10}
▨ 3.24×10^{-10} to 4.32×10^{-10}
▨ 2.16×10^{-10} to 3.24×10^{-10}
1.08×10^{-10} to 2.16×10^{-10}
☐ 6.93×10^{-13} to 1.08×10^{-10}
TIME- 2.22×10^{-2} YEARS

FIGURE 9.7

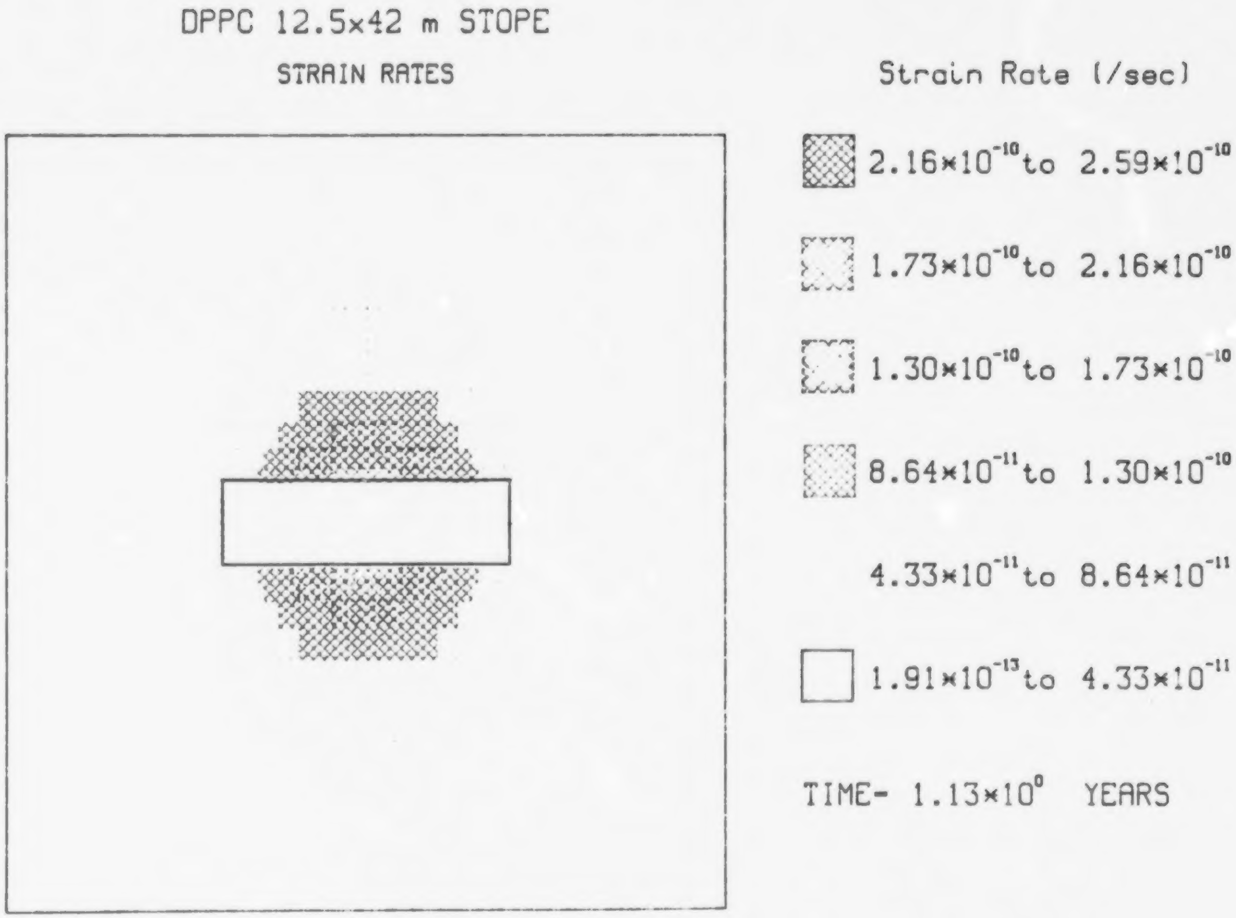
DPPC 12.5x42 m STOPE
STRAIN RATES
Strain Rate (/sec)
▩ 2.16×10^{-10} to 2.59×10^{-10}
▨ 1.73×10^{-10} to 2.16×10^{-10}
▨ 1.30×10^{-10} to 1.73×10^{-10}
▨ 8.64×10^{-11} to 1.30×10^{-10}
4.33×10^{-11} to 8.64×10^{-11}
☐ 1.91×10^{-13} to 4.33×10^{-11}
TIME- 1.13×10^{0} YEARS

FIGURE 9.8

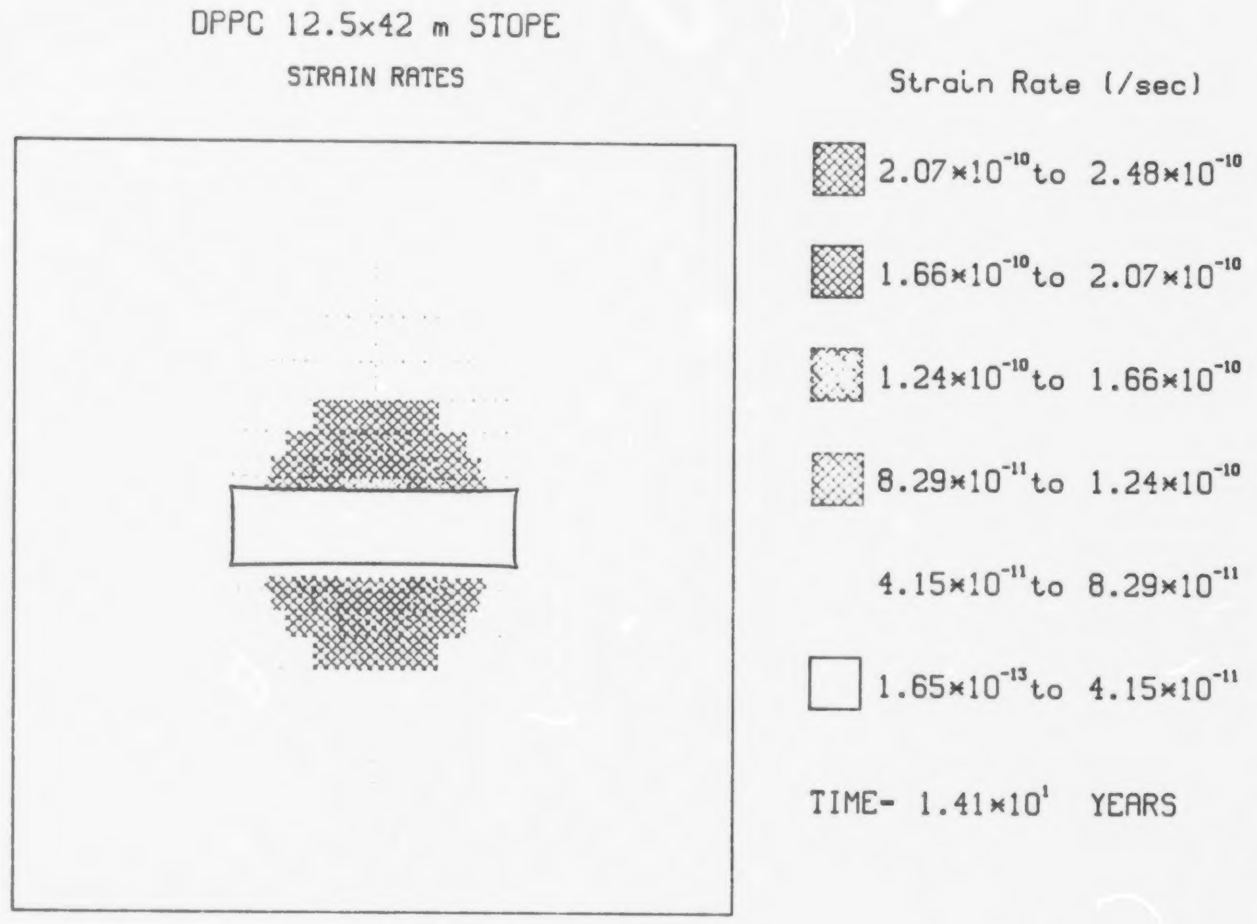
DPPC 12.5x42 m STOPE
STRAIN RATES
Strain Rate (/sec)
▩ 2.07×10⁻¹⁰ to 2.48×10⁻¹⁰
▩ 1.66×10⁻¹⁰ to 2.07×10⁻¹⁰
▨ 1.24×10⁻¹⁰ to 1.66×10⁻¹⁰
▨ 8.29×10⁻¹¹ to 1.24×10⁻¹⁰
4.15×10⁻¹¹ to 8.29×10⁻¹¹
☐ 1.65×10⁻¹³ to 4.15×10⁻¹¹
TIME- 1.41×10¹ YEARS

FIGURE 9.9

9.5 SHEAR STRESS DISTRIBUTION

Following are the numerical modelling results for shear stresses for 12.5 m x 42 m Stope without backfill.

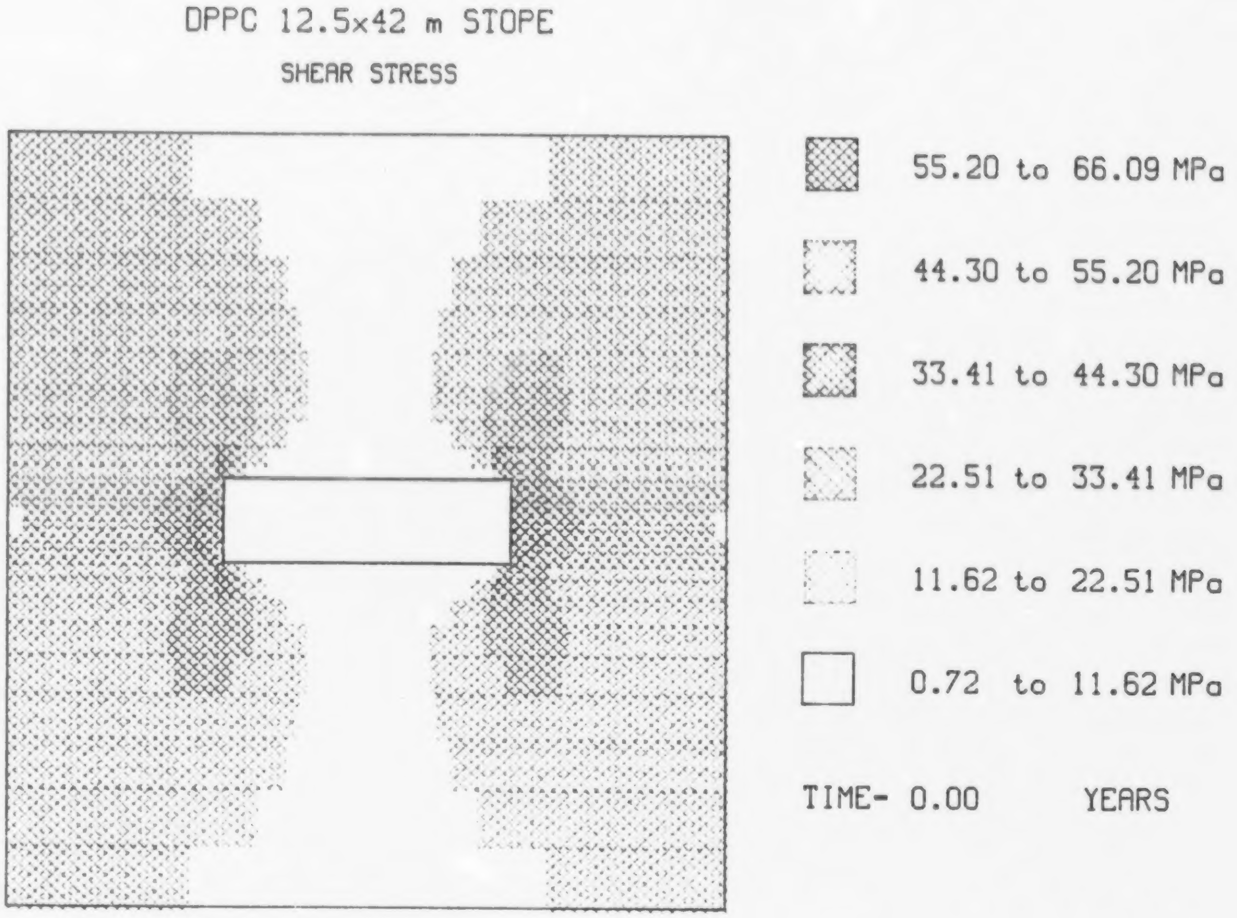
DPPC 12.5×42 m STOPE
SHEAR STRESS
55.20 to 66.09 MPa
44.30 to 55.20 MPa
33.41 to 44.30 MPa
22.51 to 33.41 MPa
11.62 to 22.51 MPa
0.72 to 11.62 MPa
TIME- 0.00 YEARS

FIGURE 9.10

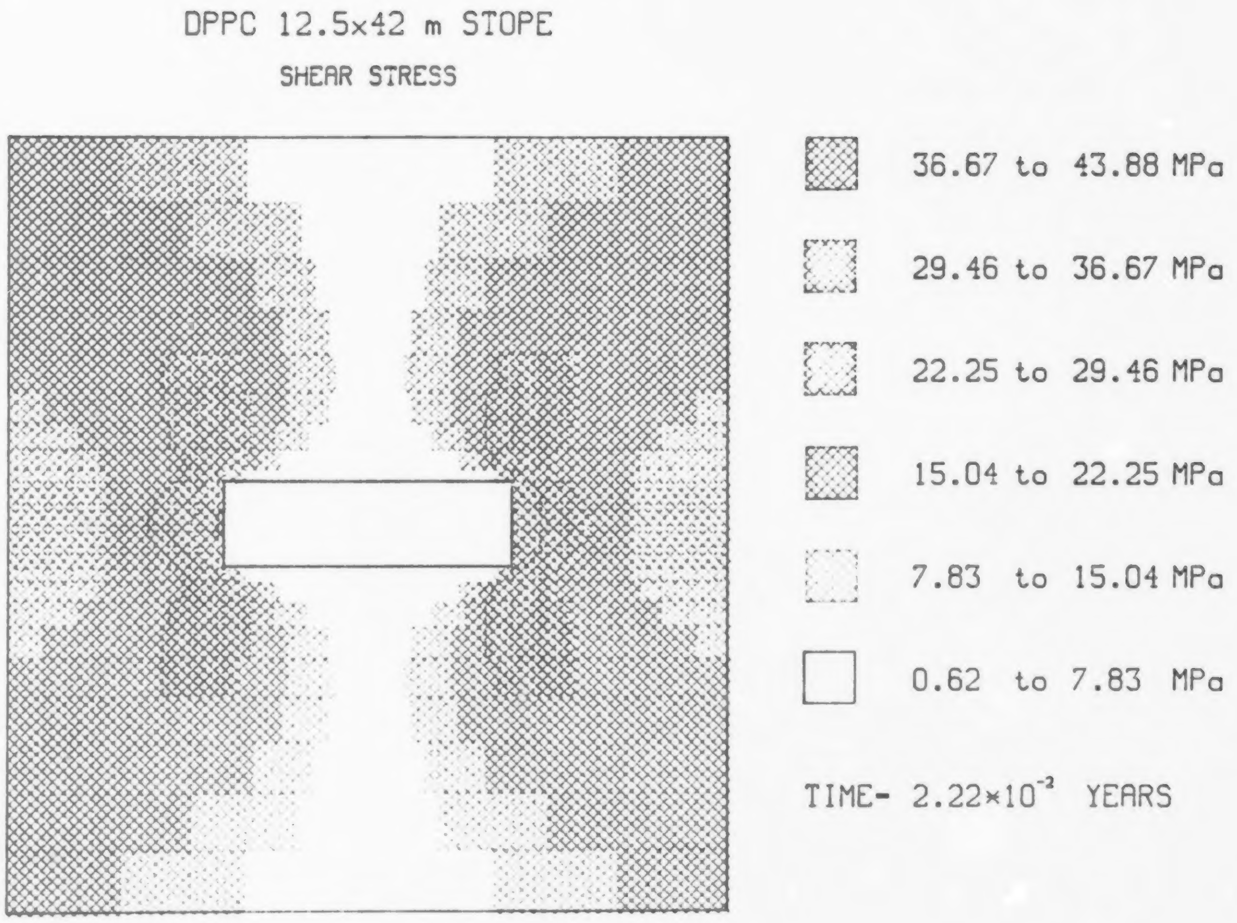
DPPC 12.5×42 m STOPE
SHEAR STRESS
36.67 to 43.88 MPa
29.46 to 36.67 MPa
22.25 to 29.46 MPa
15.04 to 22.25 MPa
7.83 to 15.04 MPa
0.62 to 7.83 MPa
TIME- 2.22×10⁻² YEARS

FIGURE 9.11

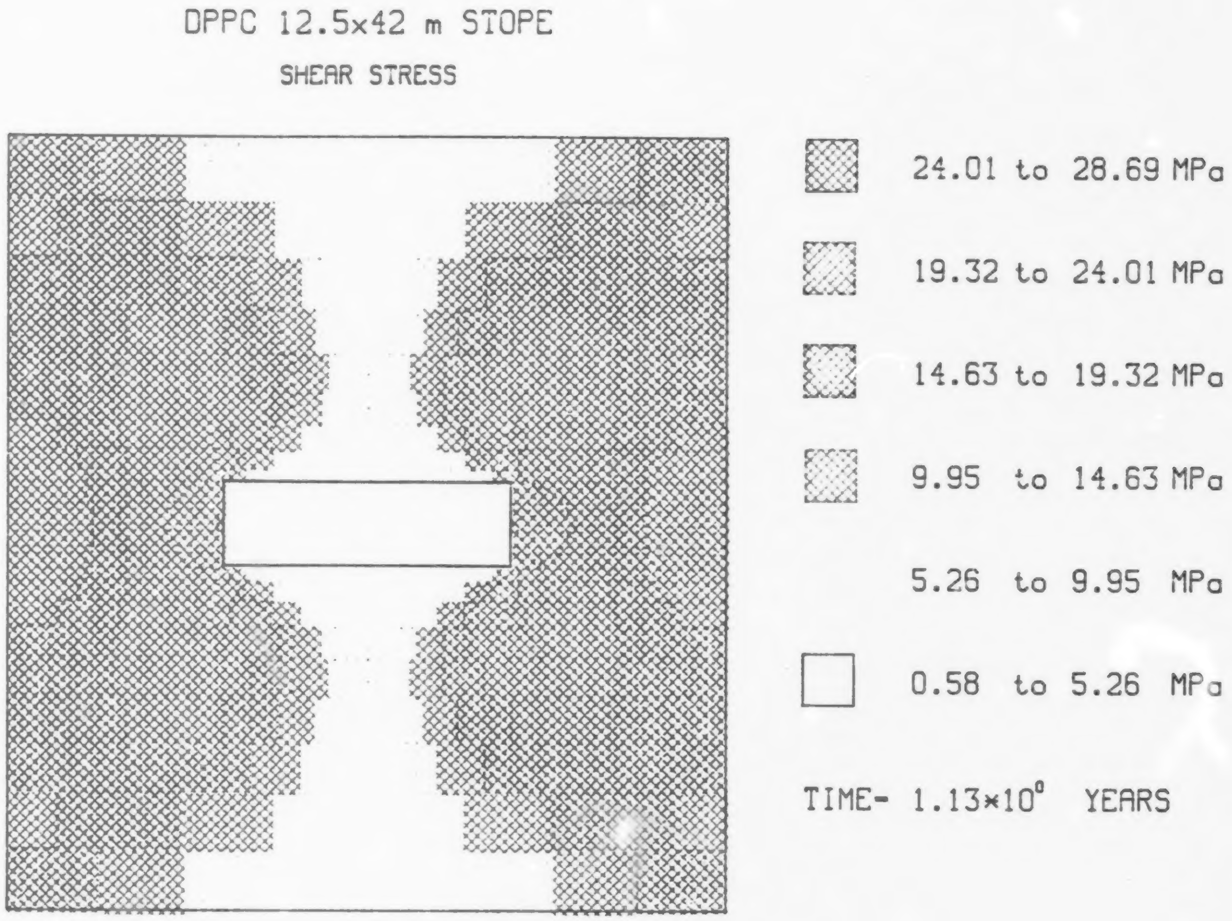
DPPC 12.5×42 m STOPE
SHEAR STRESS
24.01 to 28.69 MPa
19.32 to 24.01 MPa
14.63 to 19.32 MPa
9.95 to 14.63 MPa
5.26 to 9.95 MPa
0.58 to 5.26 MPa
TIME- 1.13×10⁰ YEARS

FIGURE 9.12

DPPC 12.5×42 m STOPE

SHEAR STRESS

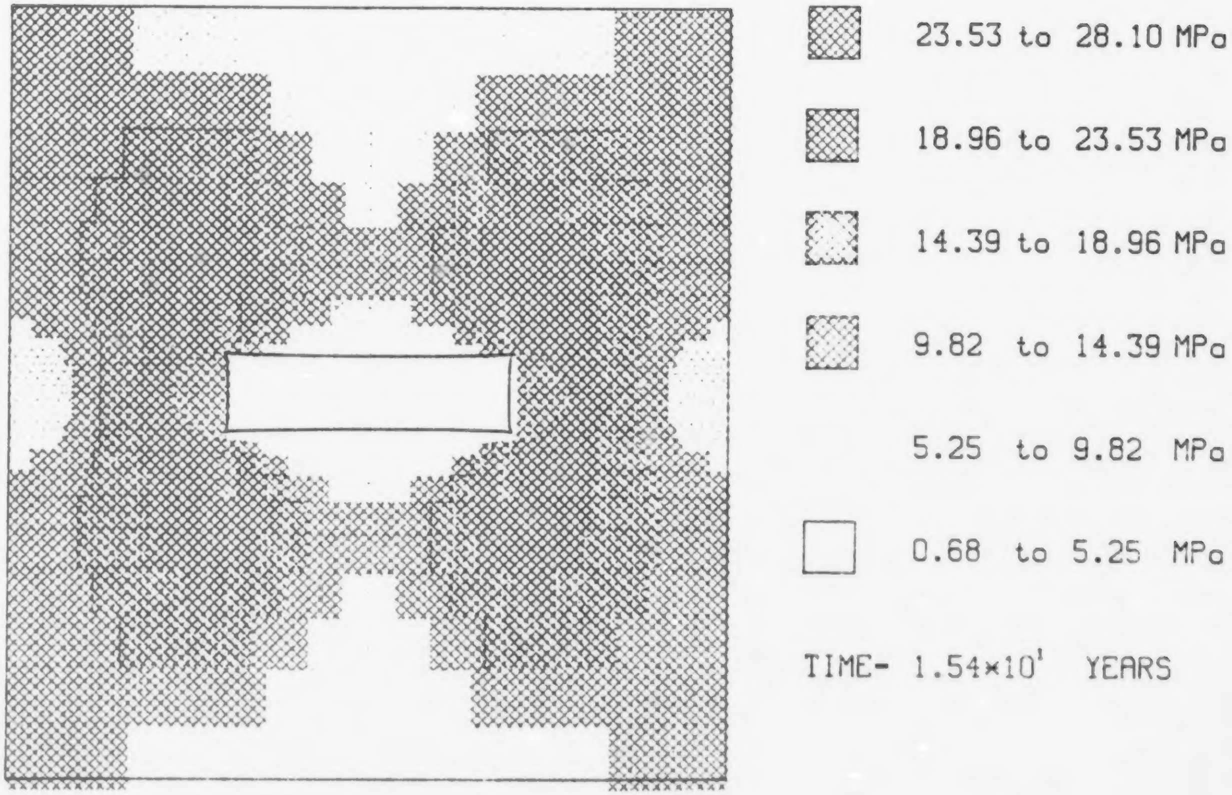

FIGURE 9.13

9.6 MAJOR PRINCIPAL STRESS DISTRIBUTION

Following are the numerical modelling results for major principal stresses for the 12.5 m x 42 m Stope without backfill.

DPPC 12.5x42 m STOPE

MAJOR PRINCIPAL STRESS

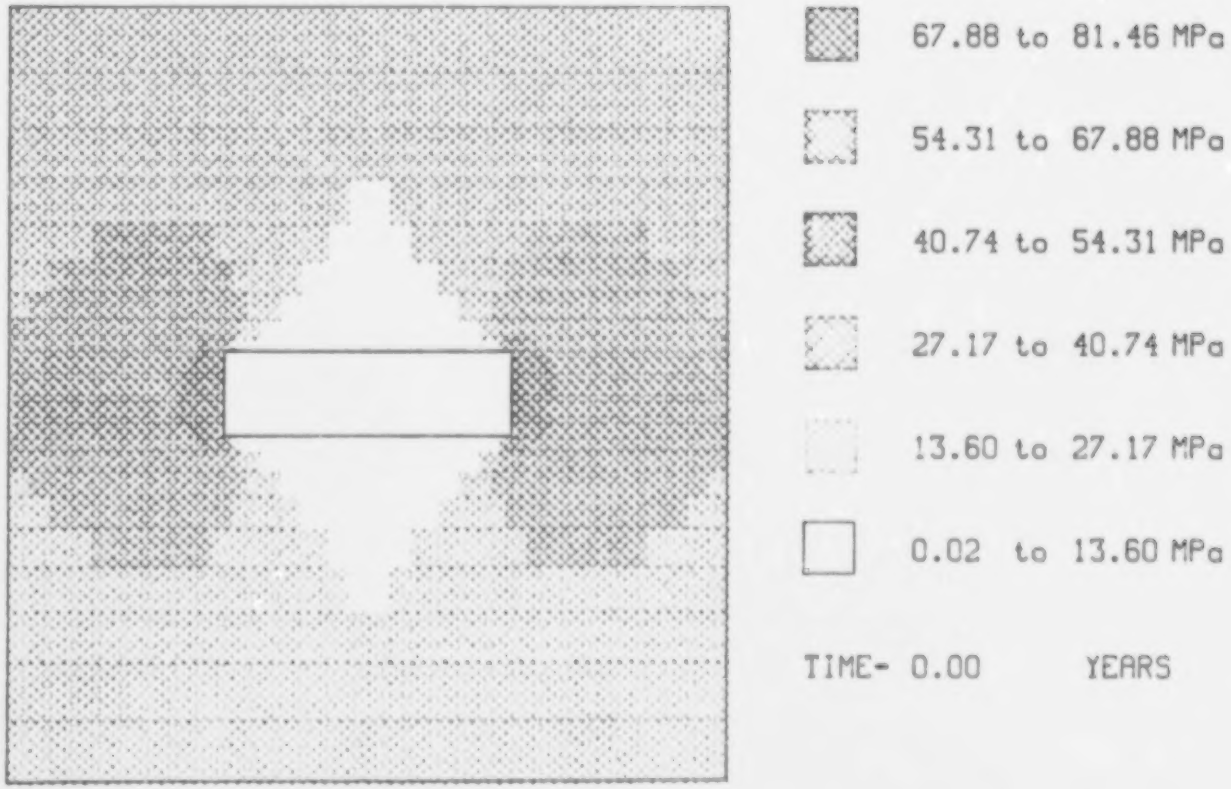

FIGURE 9.14

DPPC 12.5×42 m STOPE
MAJOR PRINCIPAL STRESS

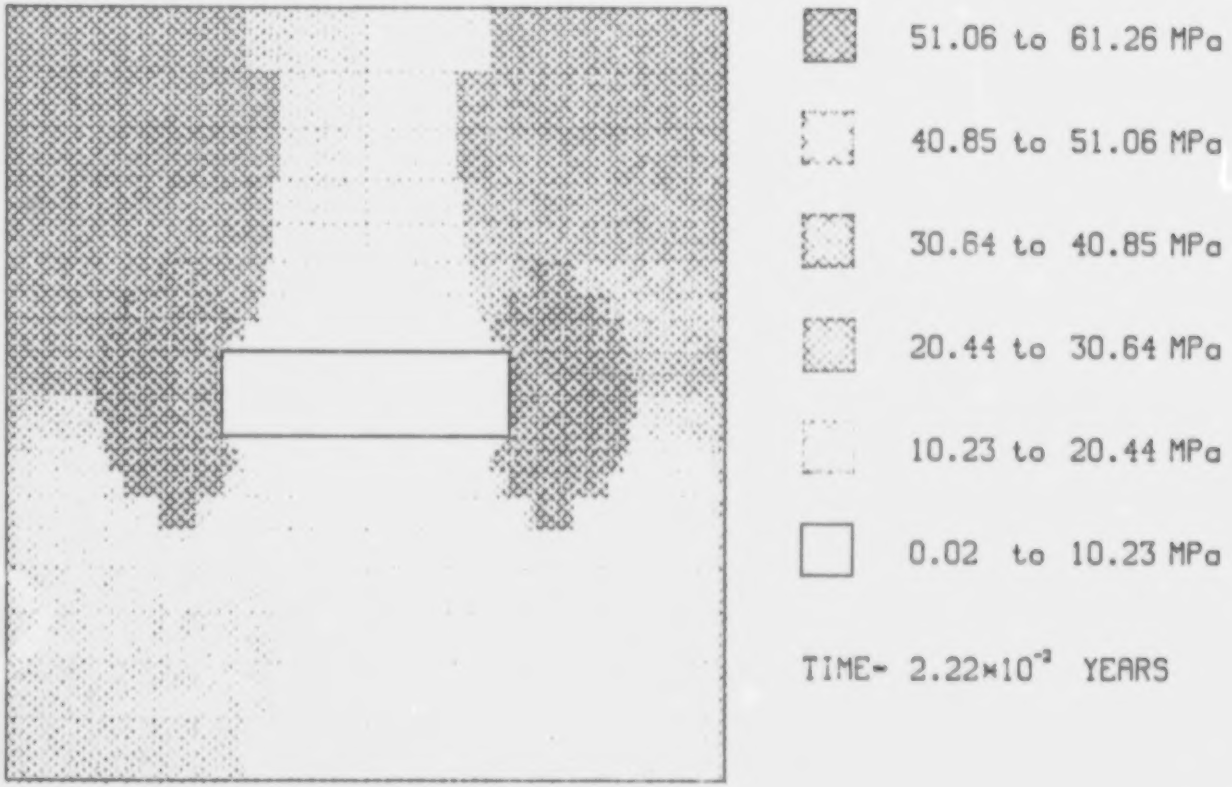

FIGURE 9.15

DPPC 12.5×42 m STOPE

MAJOR PRINCIPAL STRESS

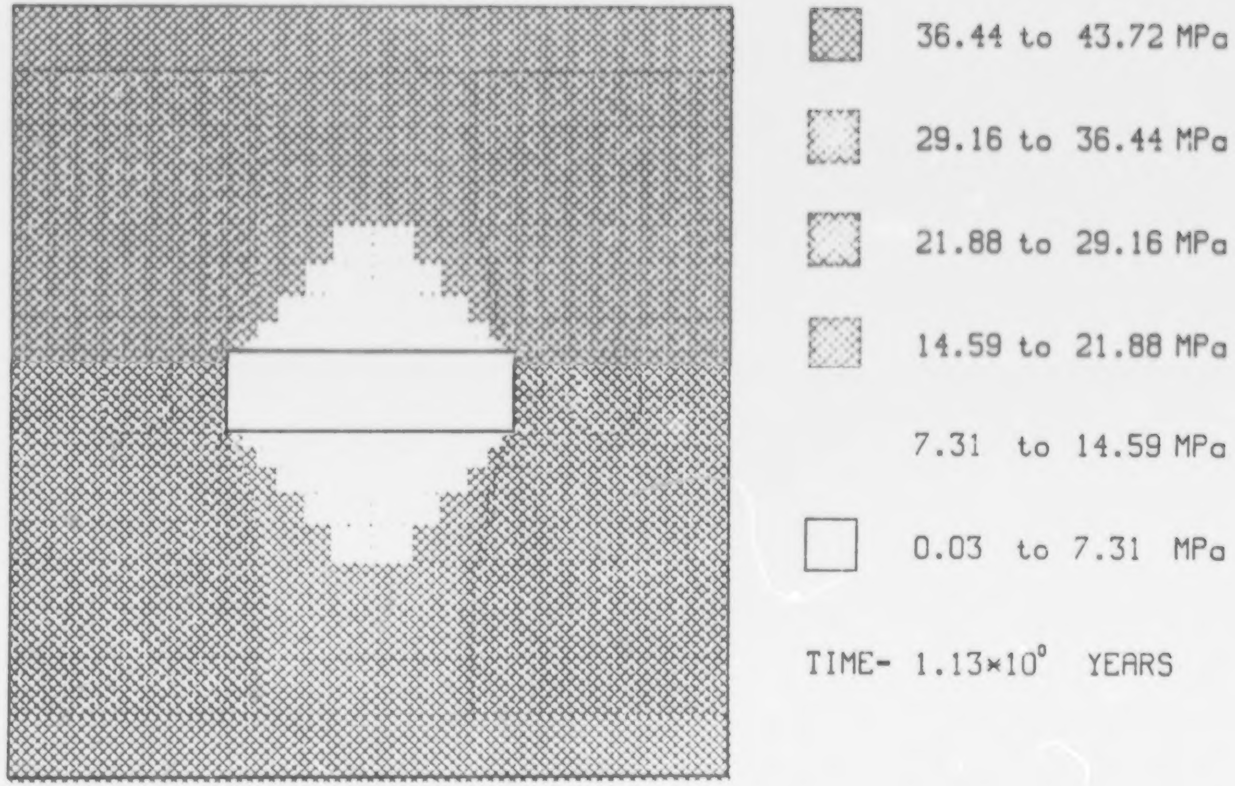

FIGURE 9.16

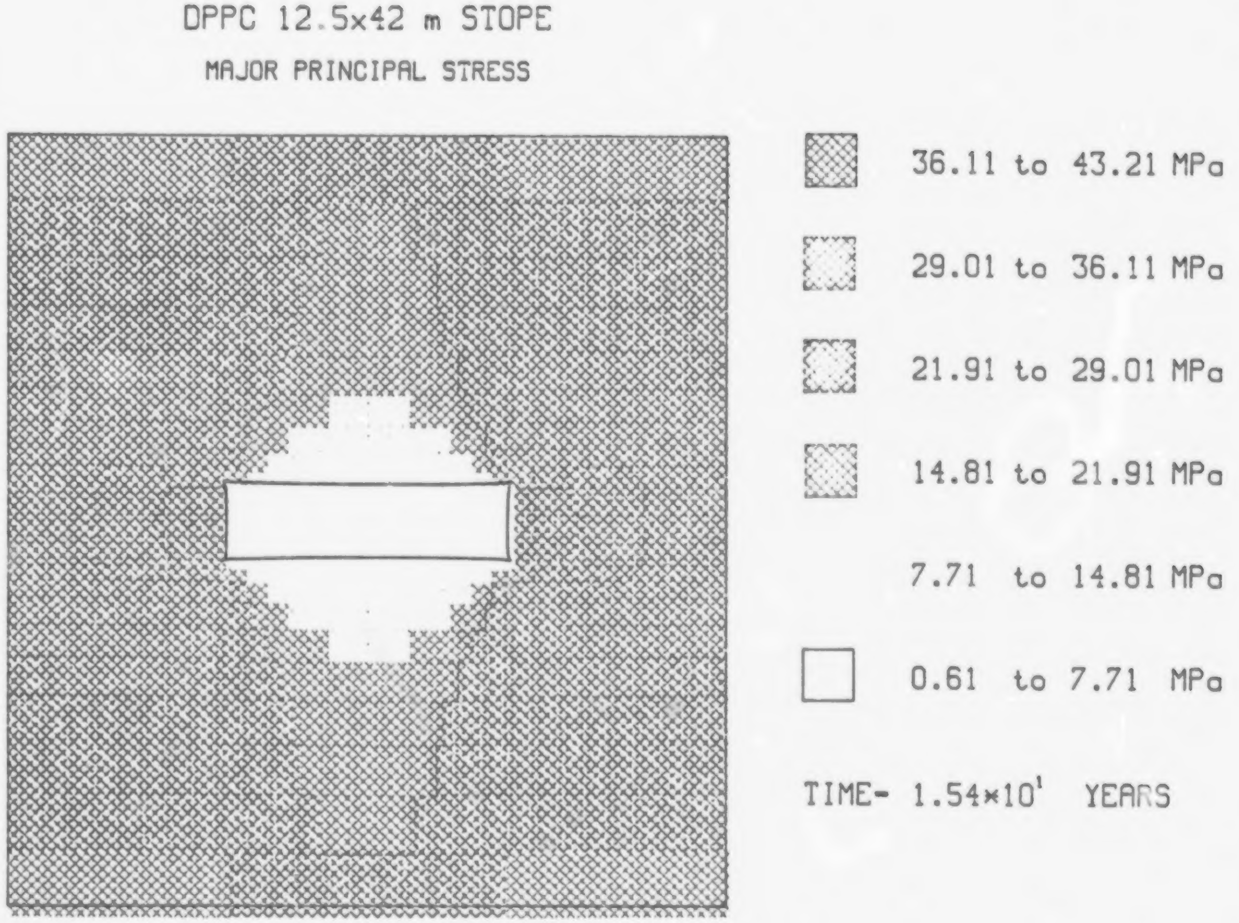
DPPC 12.5x42 m STOPE
MAJOR PRINCIPAL STRESS
36.11 to 43.21 MPa
29.01 to 36.11 MPa
21.91 to 29.01 MPa
14.81 to 21.91 MPa
7.71 to 14.81 MPa
0.61 to 7.71 MPa
TIME- 1.54*10¹ YEARS

FIGURE 9.17

9.7 MINOR PRINCIPAL STRESS

Following are the numerical modelling results for the minor principal stresses for the 12.5 m x 42 m Stope without backfill.

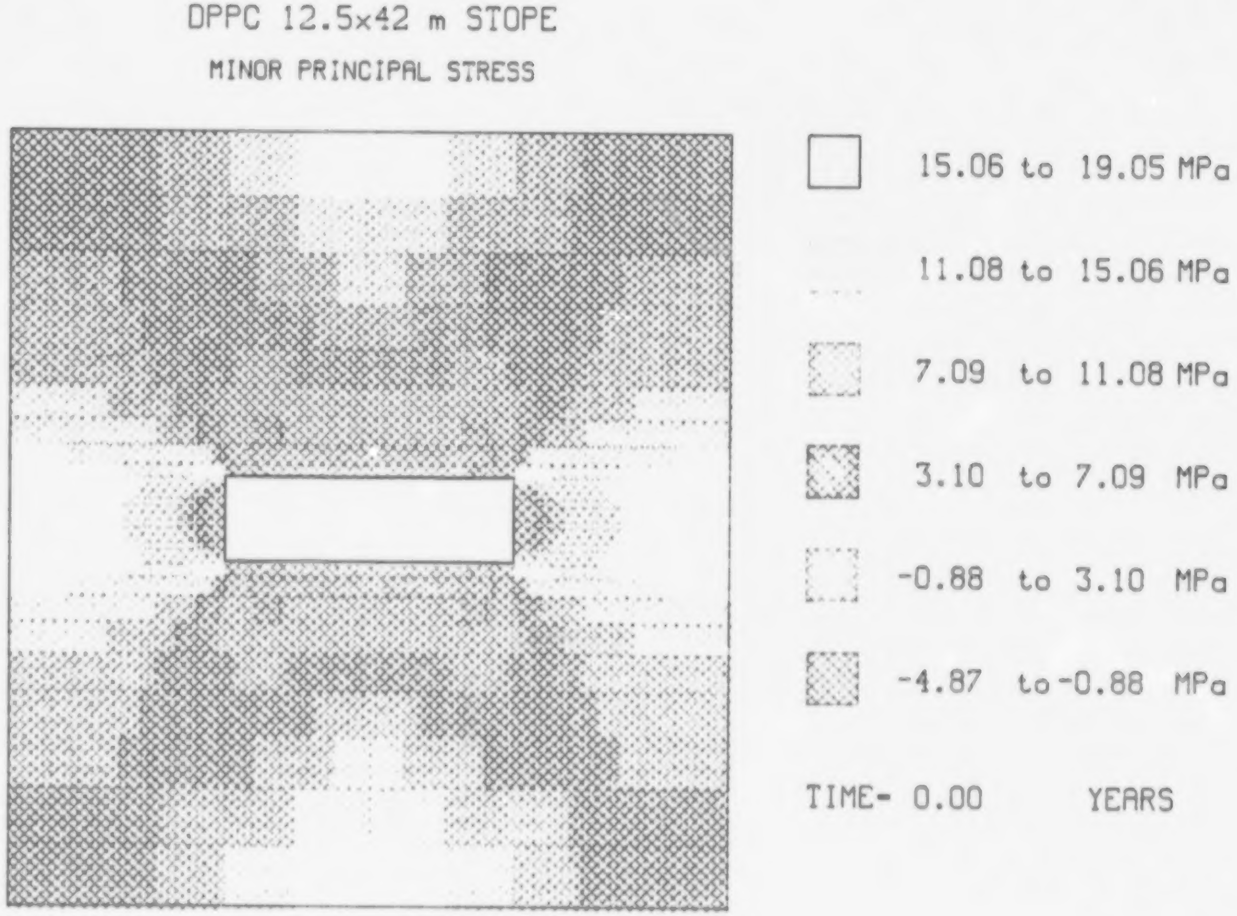
DPPC 12.5×42 m STOPE
MINOR PRINCIPAL STRESS
15.06 to 19.05 MPa
11.08 to 15.06 MPa
7.09 to 11.08 MPa
3.10 to 7.09 MPa
-0.88 to 3.10 MPa
-4.87 to -0.88 MPa
TIME- 0.00 YEARS

FIGURE 9.18

DPPC 12.5×42 m STOPE

MINOR PRINCIPAL STRESS

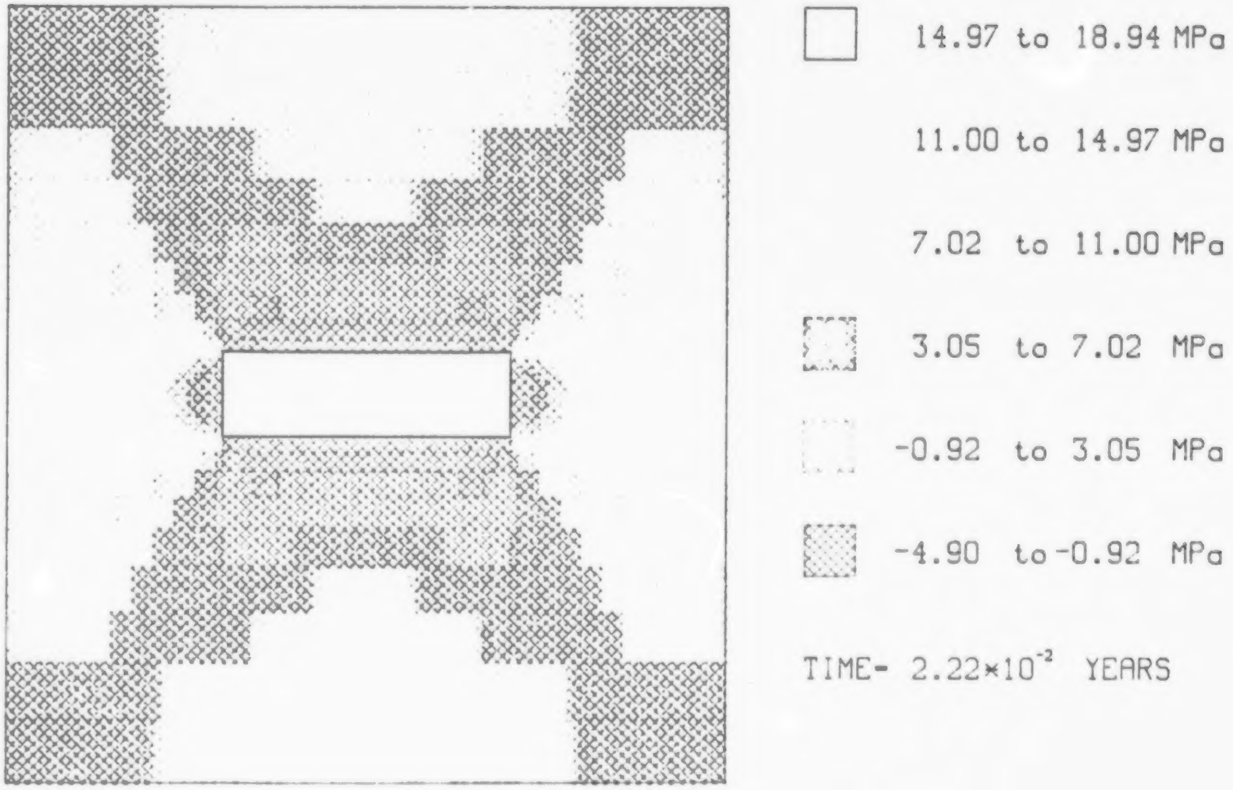

FIGURE 9.19

DPPC 12.5×42 m STOPE

MINOR PRINCIPAL STRESS

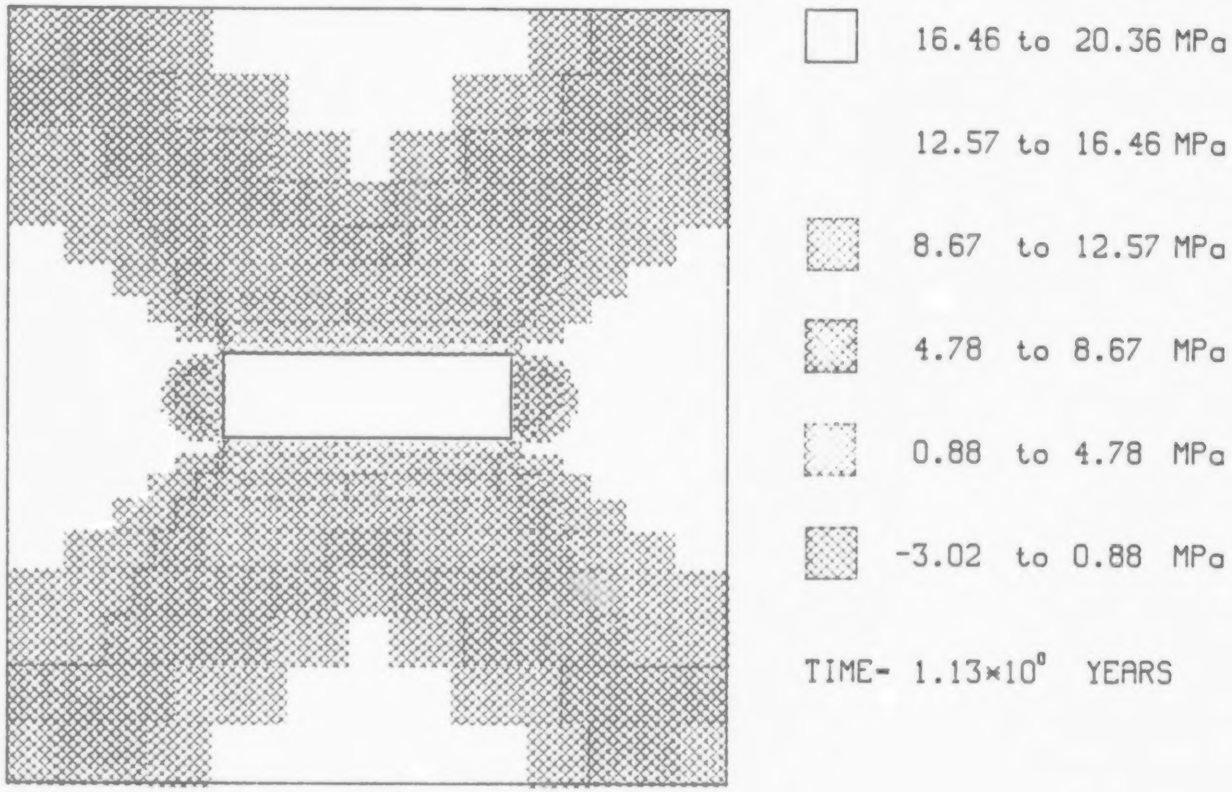

FIGURE 9.20

DPPC 12.5x42 m STOPE

MINOR PRINCIPAL STRESS

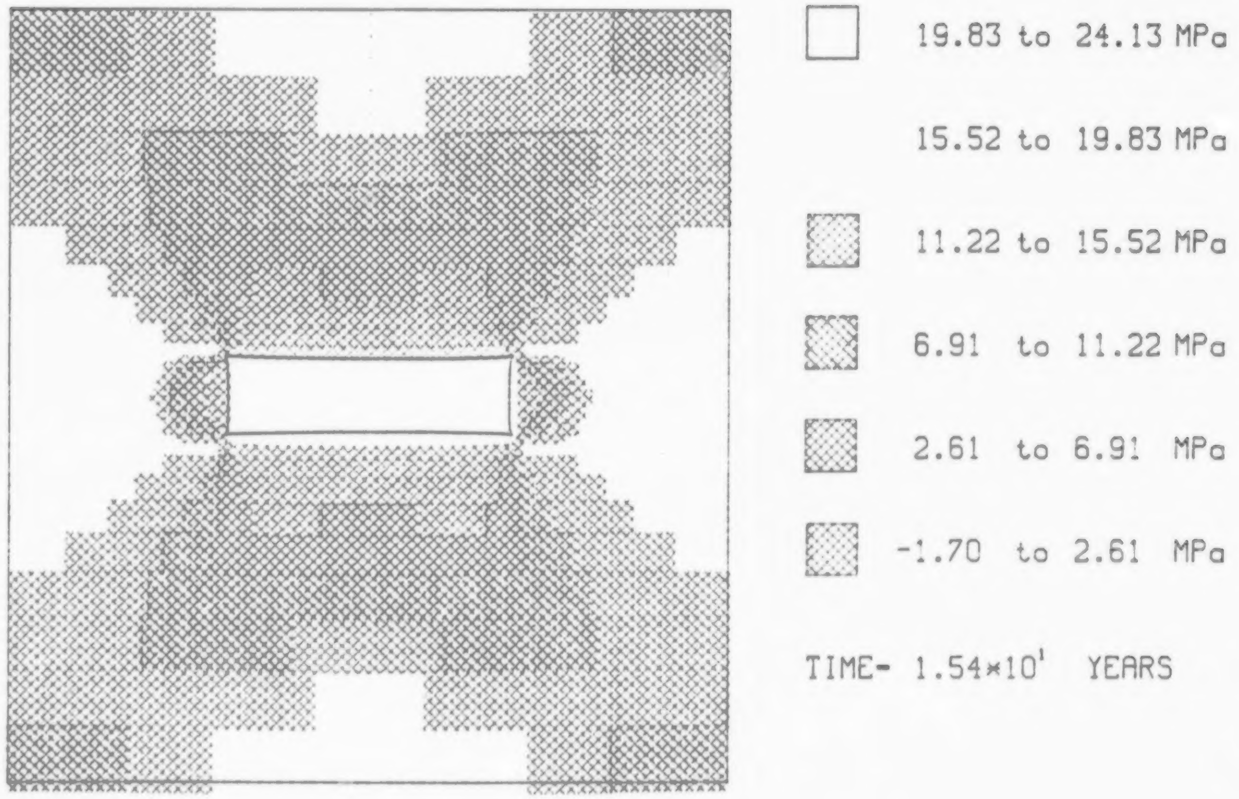

FIGURE 9.21

SECTION 10.0

10.0 DENISON-POTACAN 30 M X 42 M STOPE

10.1 ROOF DISPLACEMENTS

Following are the numerical modelling results for roof displacements for the 30 m x 42 m stope.

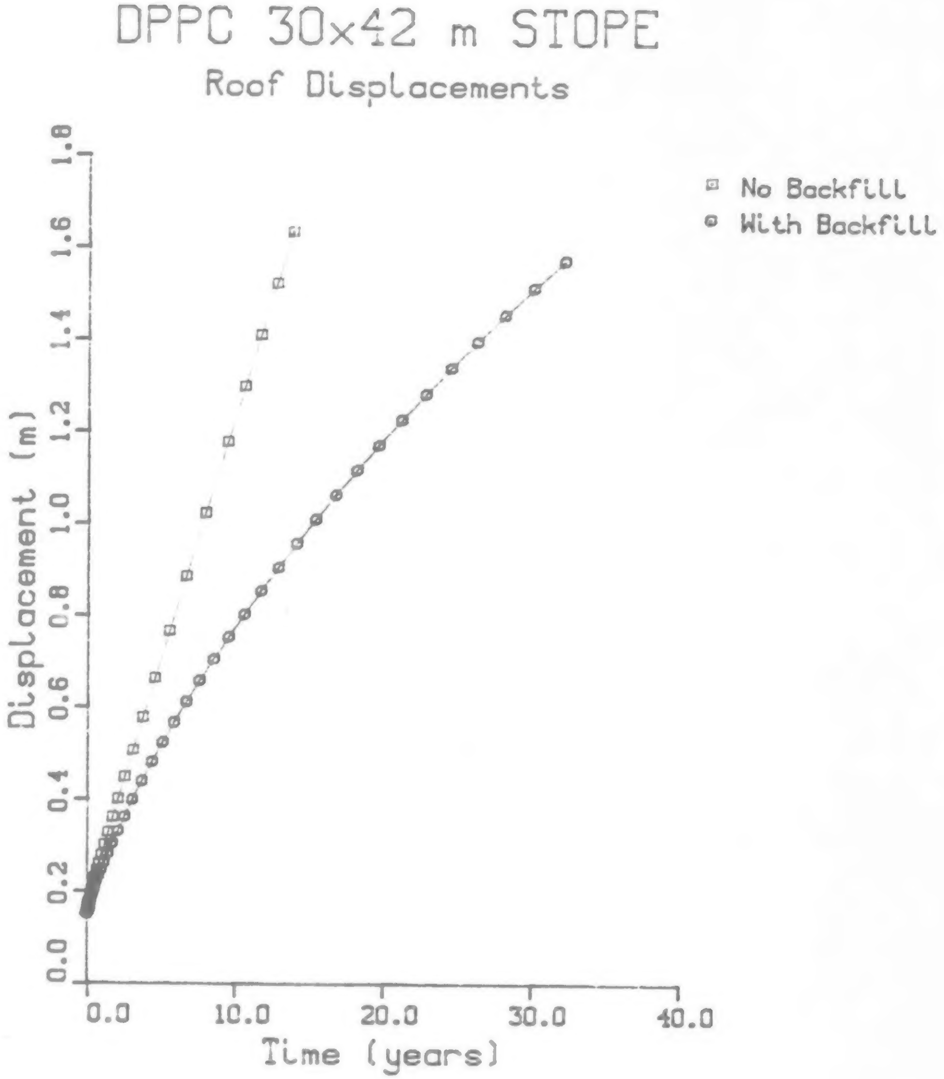
DPPC 30×42 m STOPE
Roof Displacements
No Backfill
With Backfill
Displacement (m)
0.0
0.2
0.4
0.6
0.8
1.0
1.2
1.4
1.6
1.8
Time (years)
0.0
10.0
20.0
30.0
40.0

FIGURE 10.1

10.2 WALL DISPLACEMENTS

Following are the numerical modelling results for wall displacements for the 30 m x 42 m stope.

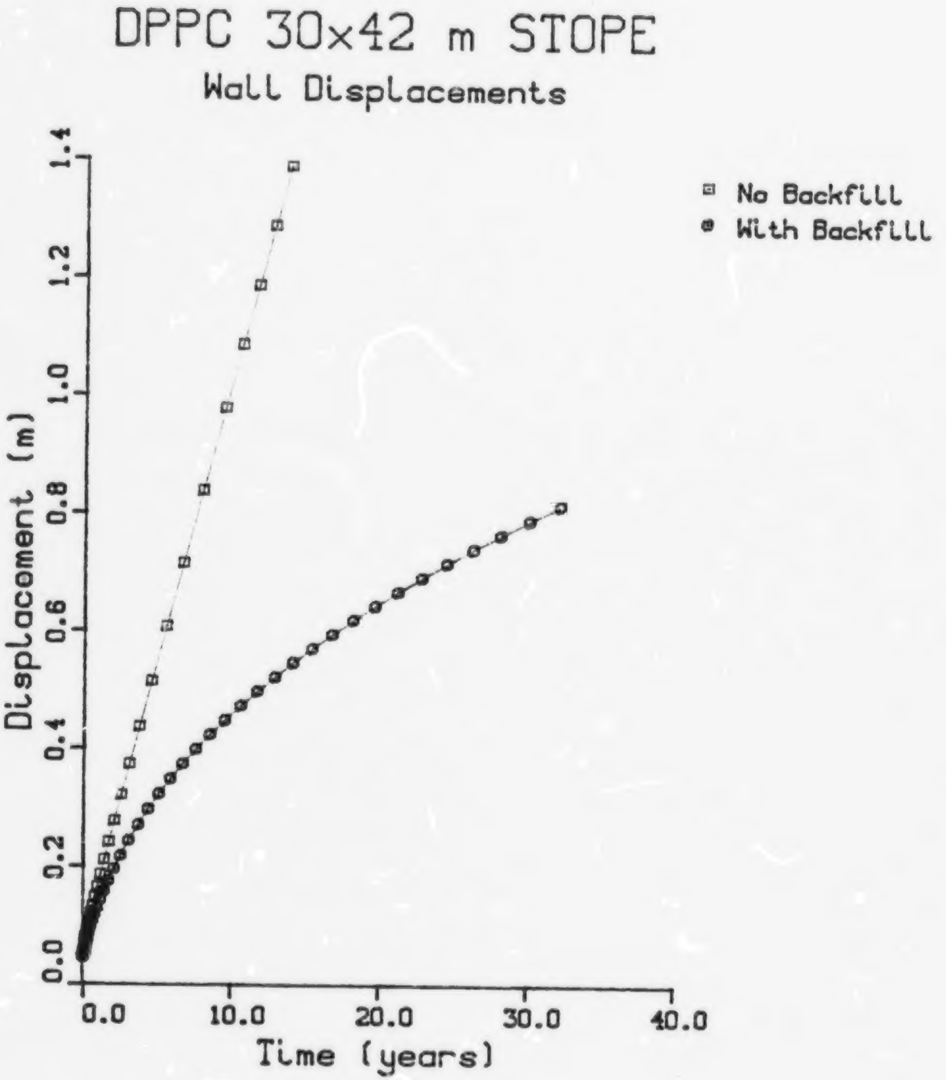
DPPC 30×42 m STOPE
Wall Displacements
Displacement (m)
0.0
0.2
0.4
0.6
0.8
1.0
1.2
1.4
Time (years)
0.0
10.0
20.0
30.0
40.0
No Backfill
With Backfill

FIGURE 10.2

10.3 MINOR PRINCIPAL STRESS IN WALLS

Following are graphical summaries of the numerical modelling results for the minor (minimum) principal stress with reference to distance from the centre of the pillar for the 12.5 m x 42 m Stope with backfill.

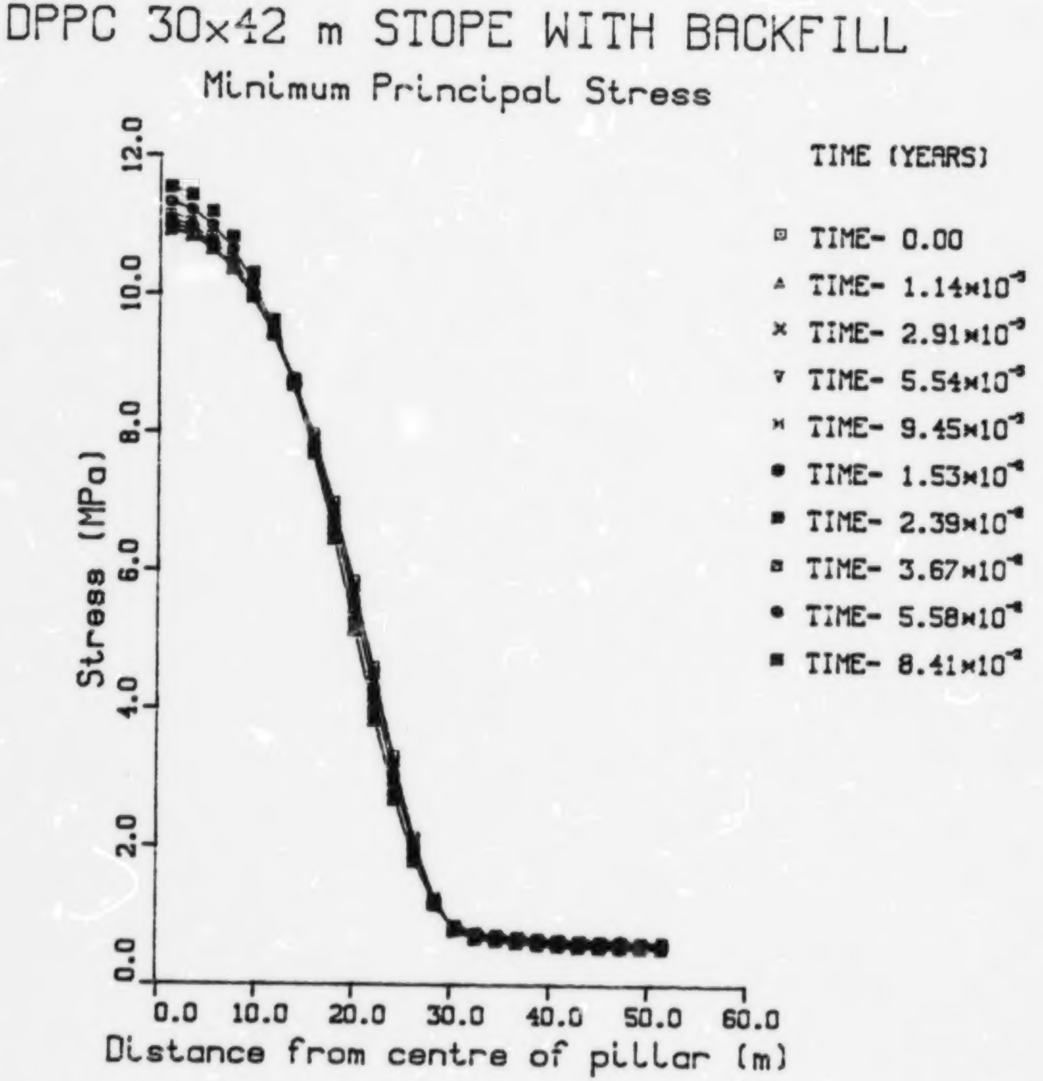
DPPC 30×42 m STOPE WITH BACKFILL
Minimum Principal Stress
Stress (MPa)
0.0
2.0
4.0
6.0
8.0
10.0
12.0
0.0
10.0
20.0
30.0
40.0
50.0
60.0
Distance from centre of pillar (m)
TIME (YEARS)
⊡ TIME- 0.00
▴ TIME- 1.14×10^{-3}
× TIME- 2.91×10^{-3}
▾ TIME- 5.54×10^{-3}
⋈ TIME- 9.45×10^{-3}
● TIME- 1.53×10^{-2}
■ TIME- 2.39×10^{-2}
▣ TIME- 3.67×10^{-2}
● TIME- 5.58×10^{-2}
■ TIME- 8.41×10^{-2}

FIGURE 10.3

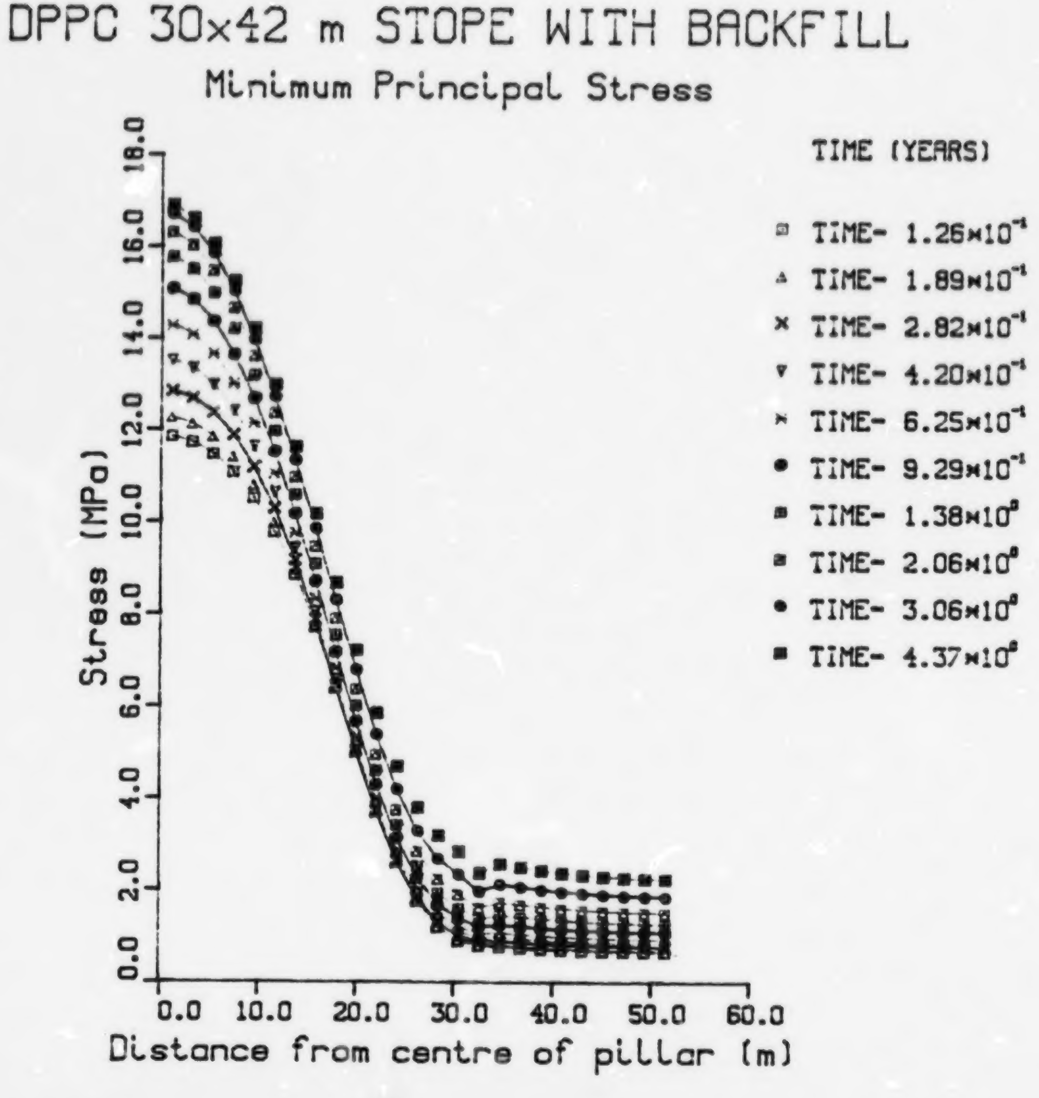
DPPC 30×42 m STOPE WITH BACKFILL
Minimum Principal Stress
TIME (YEARS)
TIME- 1.26×10⁻¹
TIME- 1.89×10⁻¹
TIME- 2.82×10⁻¹
TIME- 4.20×10⁻¹
TIME- 6.25×10⁻¹
TIME- 9.29×10⁻¹
TIME- 1.38×10⁰
TIME- 2.06×10⁰
TIME- 3.06×10⁰
TIME- 4.37×10⁰
Stress (MPa)
0.0
2.0
4.0
6.0
8.0
10.0
12.0
14.0
16.0
18.0
0.0
10.0
20.0
30.0
40.0
50.0
60.0
Distance from centre of pillar (m)

FIGURE 10.4

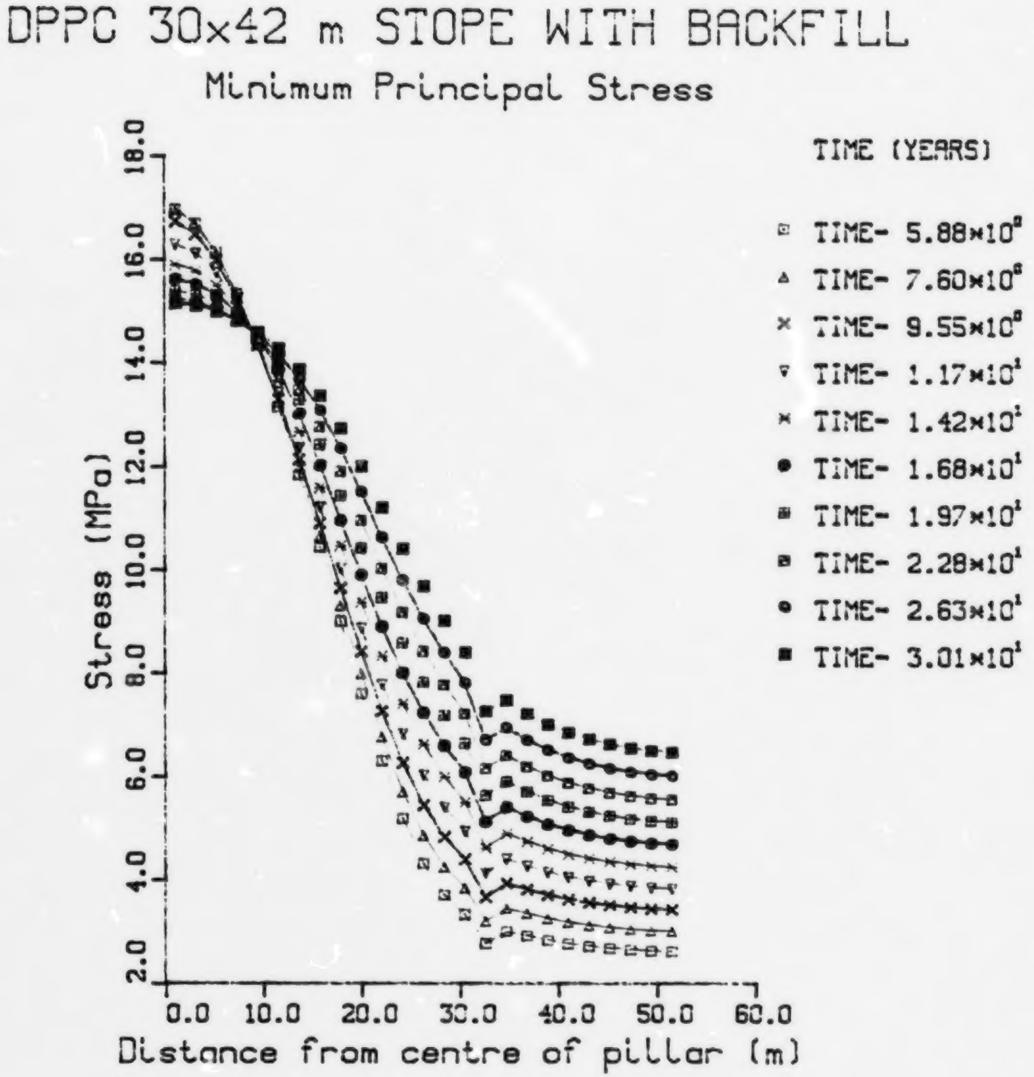
DPPC 30×42 m STOPE WITH BACKFILL
Minimum Principal Stress
Stress (MPa)
18.0
16.0
14.0
12.0
10.0
8.0
6.0
4.0
2.0
0.0
10.0
20.0
30.0
40.0
50.0
60.0
Distance from centre of pillar (m)
TIME (YEARS)
TIME- 5.88×10^0
TIME- 7.60×10^0
TIME- 9.55×10^0
TIME- 1.17×10^1
TIME- 1.42×10^1
TIME- 1.68×10^1
TIME- 1.97×10^1
TIME- 2.28×10^1
TIME- 2.63×10^1
TIME- 3.01×10^1

FIGURE 10.5

10.4 STRAIN RATE DISTRIBUTION

Following are the numerical modelling results for strain rates for the 30 m x 42 m Stope without backfill.

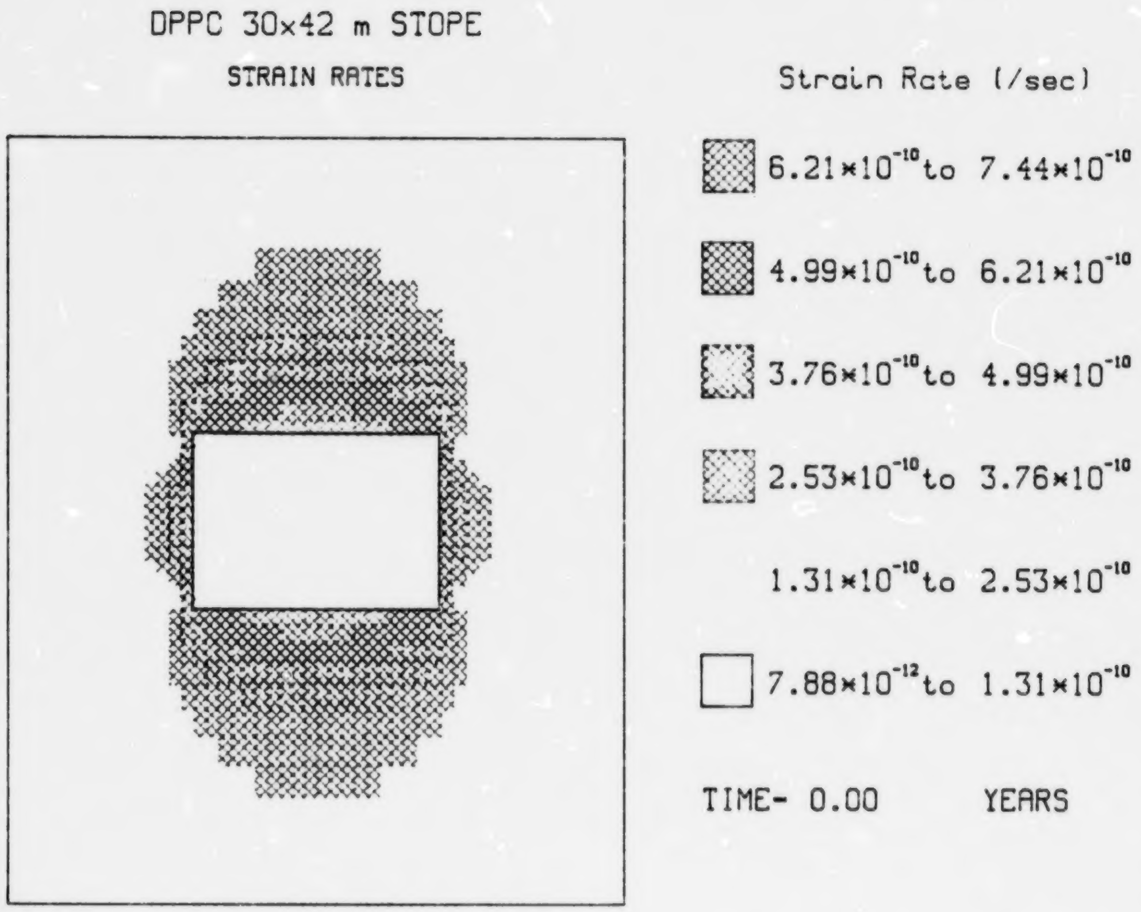
DPPC 30×42 m STOPE
STRAIN RATES
Strain Rate (/sec)
▨ 6.21×10^-10 to 7.44×10^-10
▨ 4.99×10^-10 to 6.21×10^-10
▨ 3.76×10^-10 to 4.99×10^-10
▨ 2.53×10^-10 to 3.76×10^-10
1.31×10^-10 to 2.53×10^-10
☐ 7.88×10^-12 to 1.31×10^-10
TIME- 0.00 YEARS

FIGURE 10.6

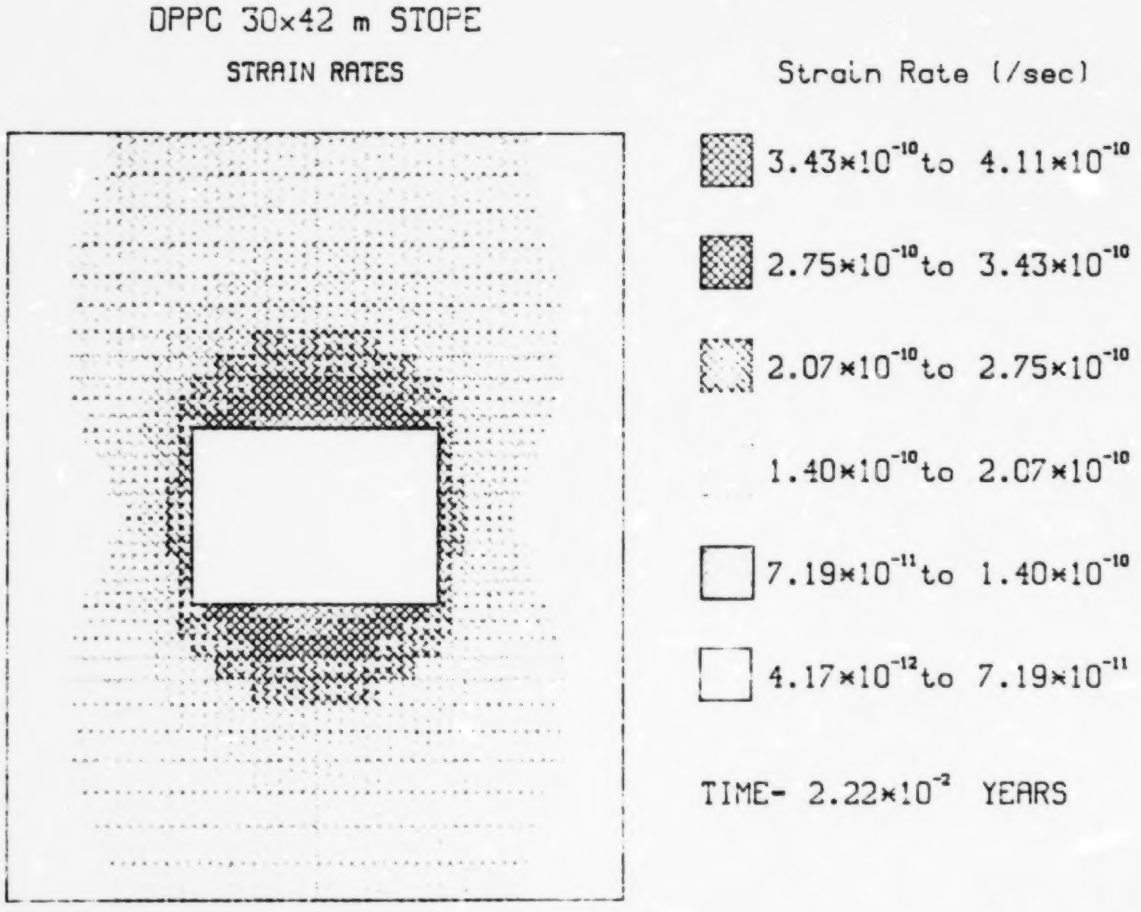

DPPC 30×42 m STOPE
STRAIN RATES
Strain Rate (/sec)
▩ 3.43×10^{-10} to 4.11×10^{-10}
▩ 2.75×10^{-10} to 3.43×10^{-10}
▨ 2.07×10^{-10} to 2.75×10^{-10}
1.40×10^{-10} to 2.07×10^{-10}
☐ 7.19×10^{-11} to 1.40×10^{-10}
☐ 4.17×10^{-12} to 7.19×10^{-11}
TIME- 2.22×10^{-2} YEARS

FIGURE 10.7

DPPC 30x42 m STOPE

STRAIN RATES

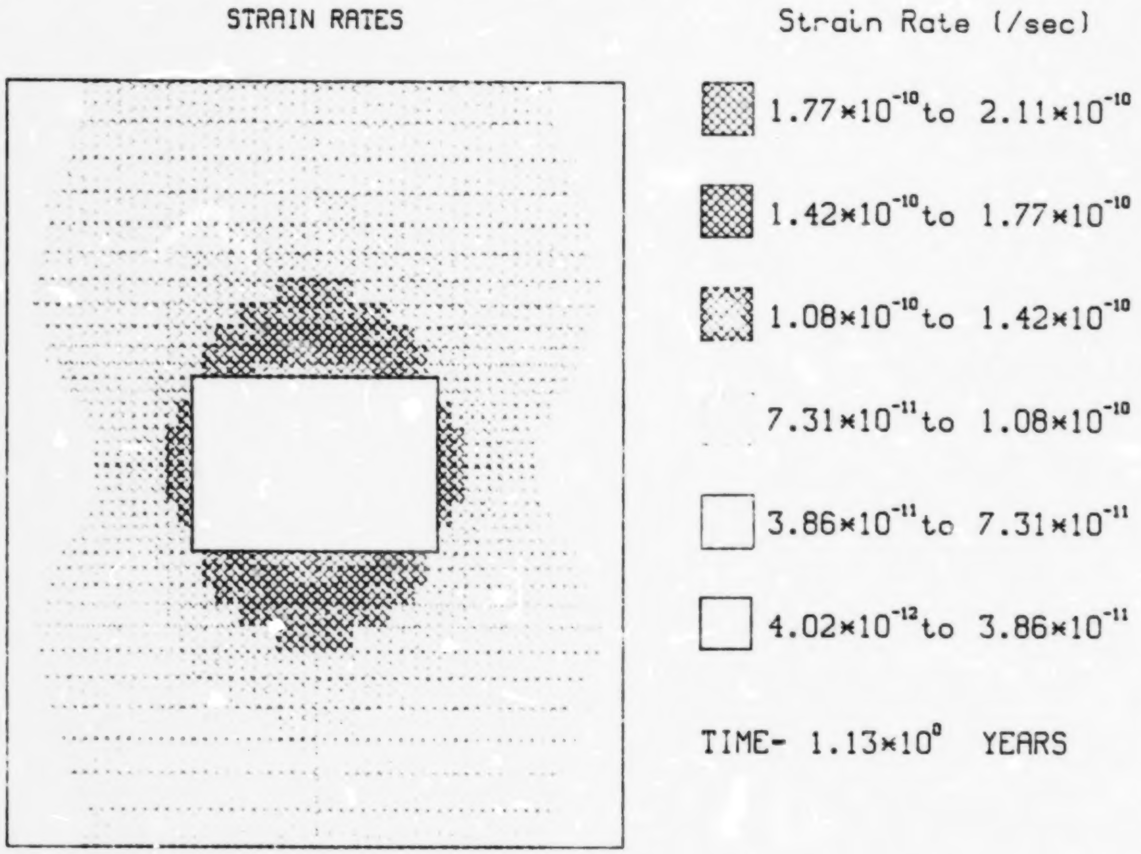

FIGURE 10.8

DPPC 30×42 m STOPE

STRAIN RATES

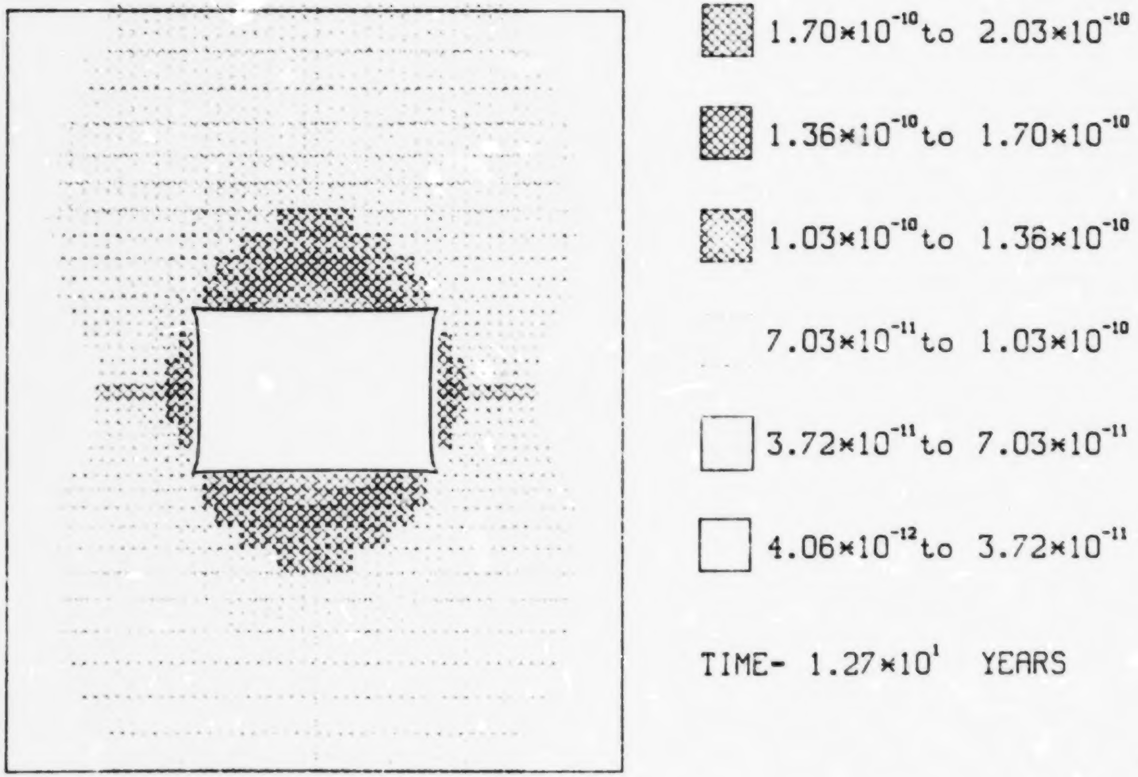

FIGURE 10.9

10.5 SHEAR STRESS DISTRIBUTION

Following are the numerical modelling results for shear stresses for the 30 m x 42 m Stope without backfill.

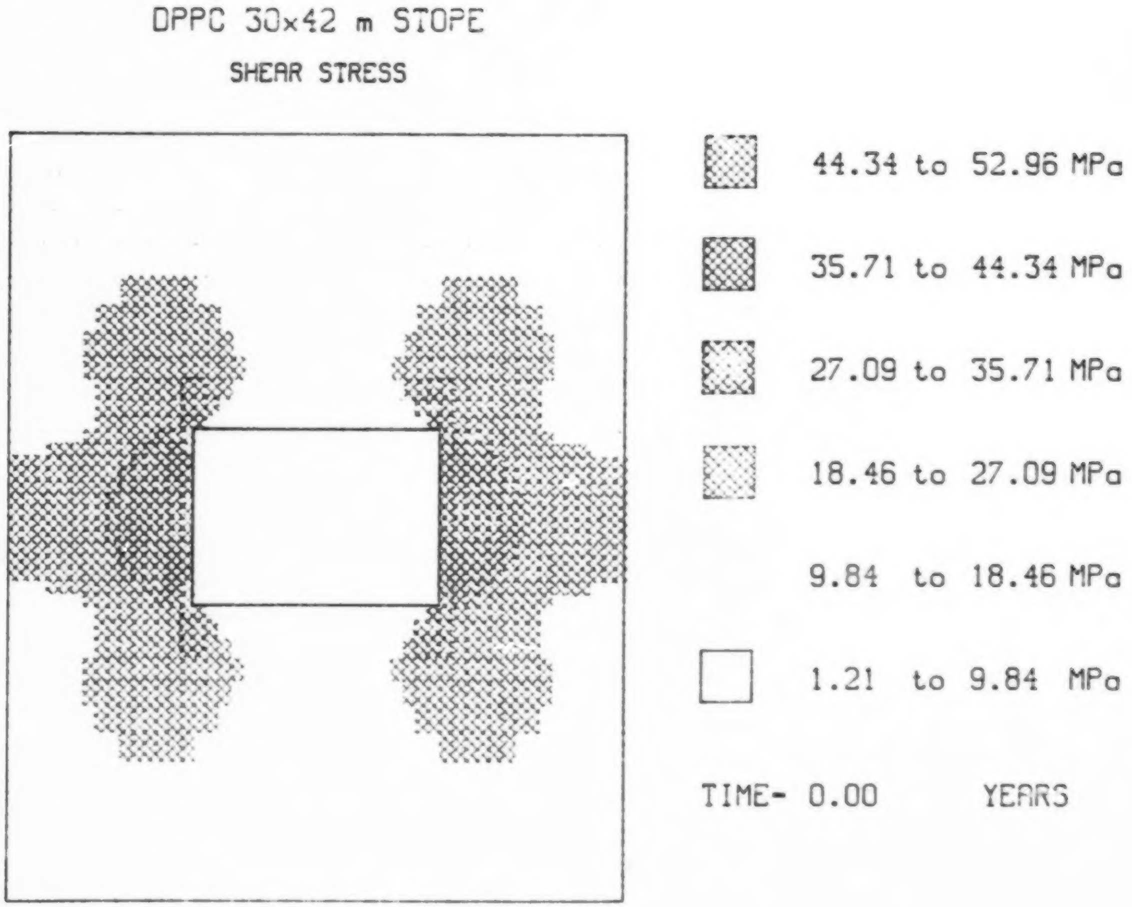
DPPC 30×42 m STOPE
SHEAR STRESS
44.34 to 52.96 MPa
35.71 to 44.34 MPa
27.09 to 35.71 MPa
18.46 to 27.09 MPa
9.84 to 18.46 MPa
1.21 to 9.84 MPa
TIME- 0.00 YEARS

FIGURE 10.10

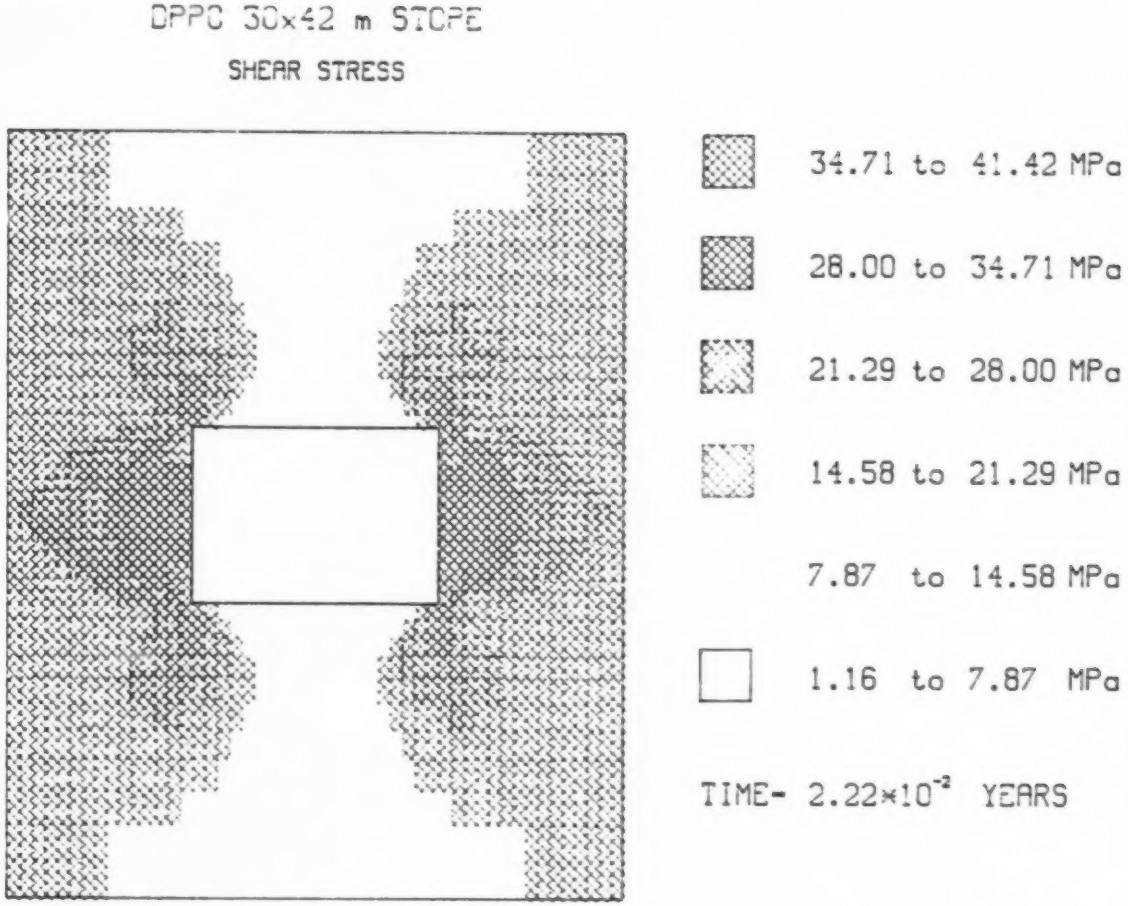
DPPC 30×42 m STOPE
SHEAR STRESS
34.71 to 41.42 MPa
28.00 to 34.71 MPa
21.29 to 28.00 MPa
14.58 to 21.29 MPa
7.87 to 14.58 MPa
1.16 to 7.87 MPa
TIME- 2.22×10⁻² YEARS

FIGURE 10.11

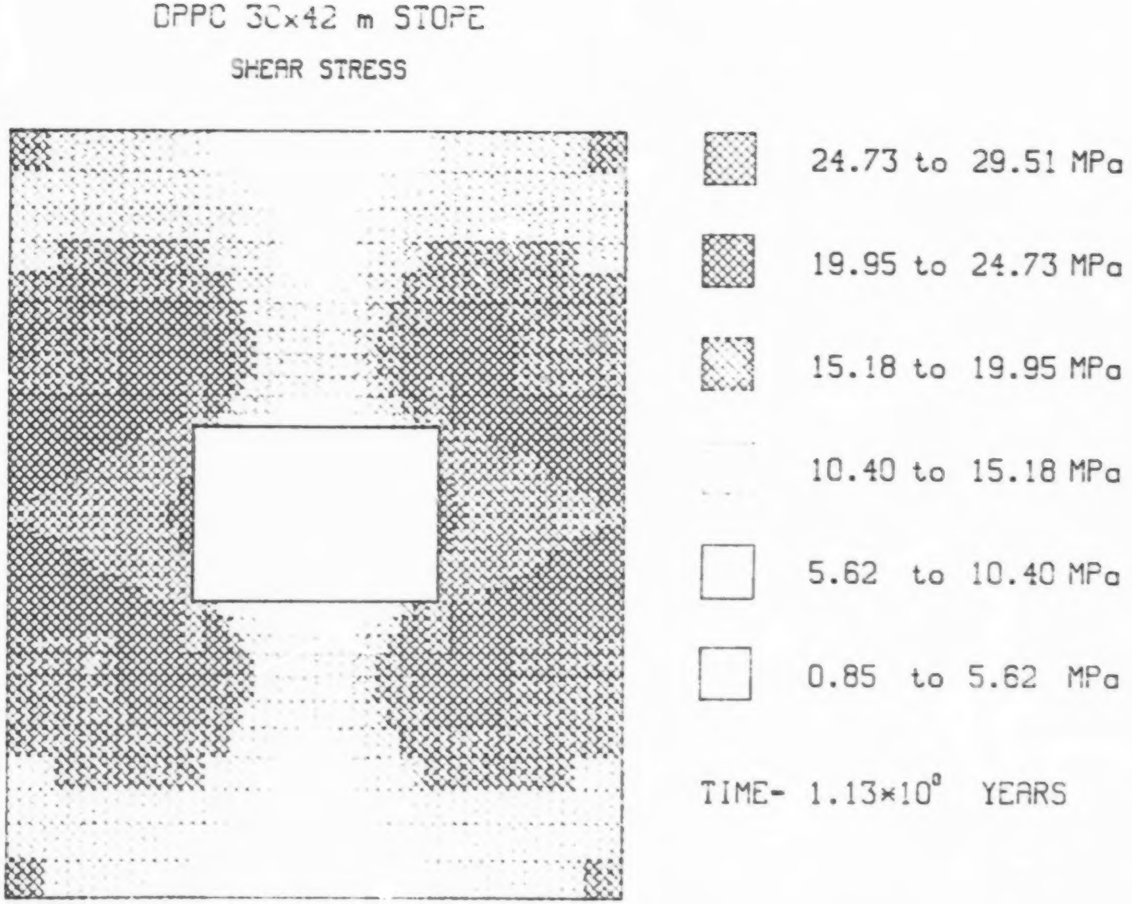
DPPC 30×42 m STOPE
SHEAR STRESS
24.73 to 29.51 MPa
19.95 to 24.73 MPa
15.18 to 19.95 MPa
10.40 to 15.18 MPa
5.62 to 10.40 MPa
0.85 to 5.62 MPa
TIME- 1.13×10⁰ YEARS

FIGURE 10.12

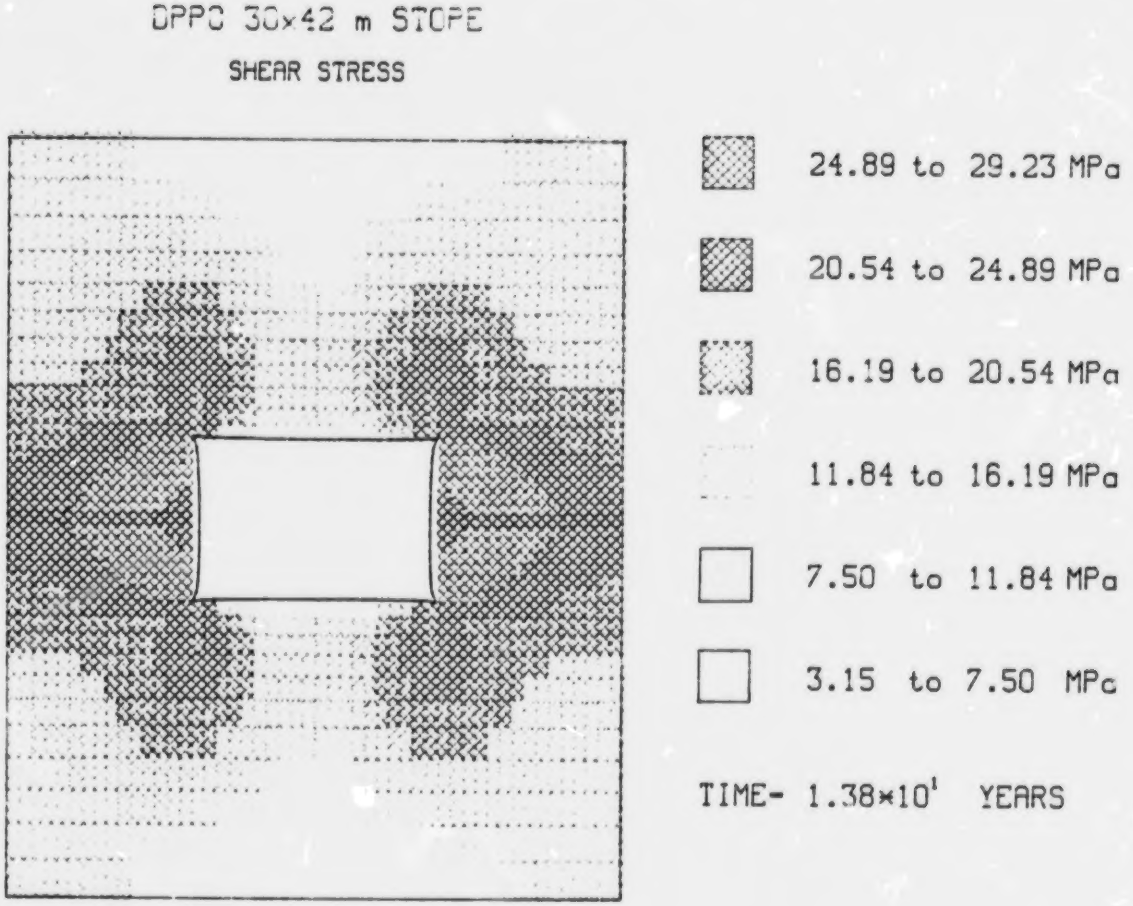
DPPC 30×42 m STOPE
SHEAR STRESS
24.89 to 29.23 MPa
20.54 to 24.89 MPa
16.19 to 20.54 MPa
11.84 to 16.19 MPa
7.50 to 11.84 MPa
3.15 to 7.50 MPa
TIME- 1.38×10¹ YEARS

FIGURE 10.13

10.6 MAJOR PRINCIPAL STRESS DISTRIBUTION

Following are the numerical modelling results for major principal stresses for the 30 m x 42 m Stope without backfill.

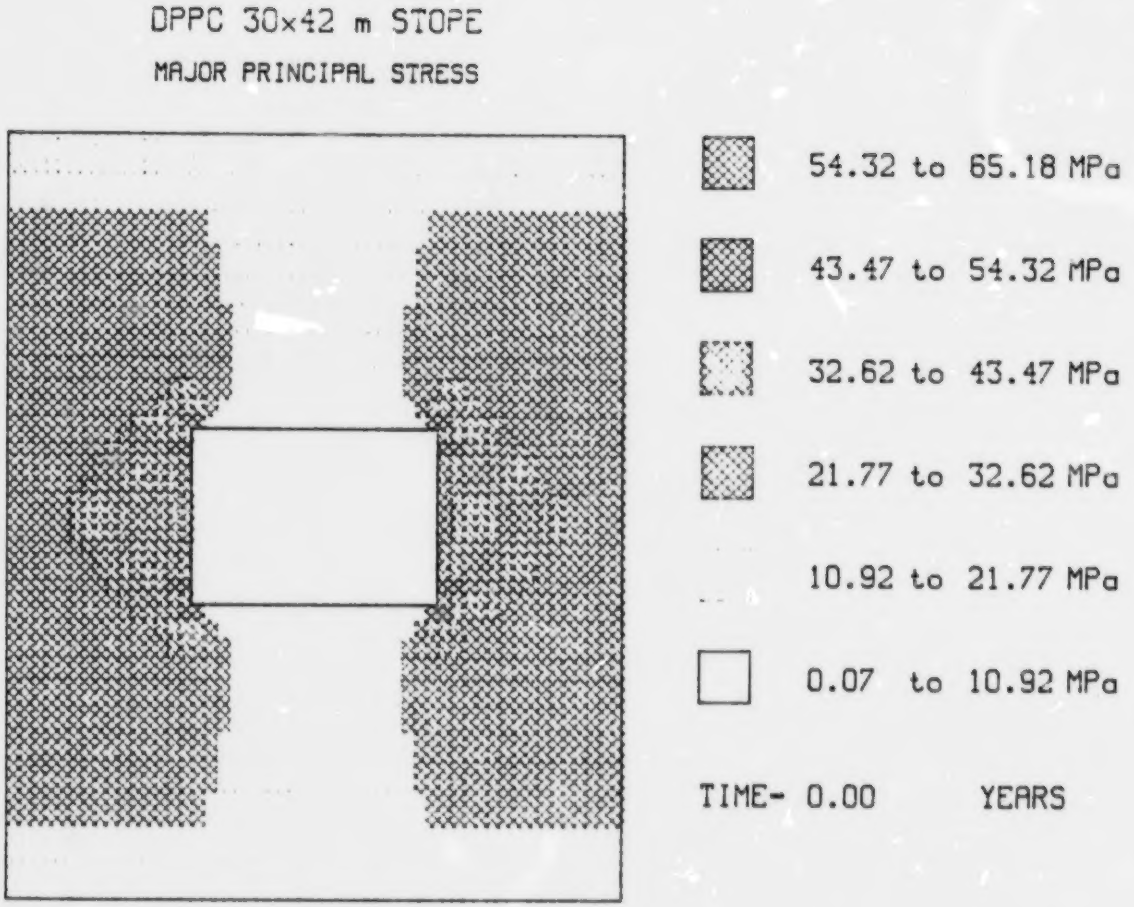

DPPC 30×42 m STOPE
MAJOR PRINCIPAL STRESS
54.32 to 65.18 MPa
43.47 to 54.32 MPa
32.62 to 43.47 MPa
21.77 to 32.62 MPa
10.92 to 21.77 MPa
0.07 to 10.92 MPa
TIME- 0.00 YEARS

FIGURE 10.14

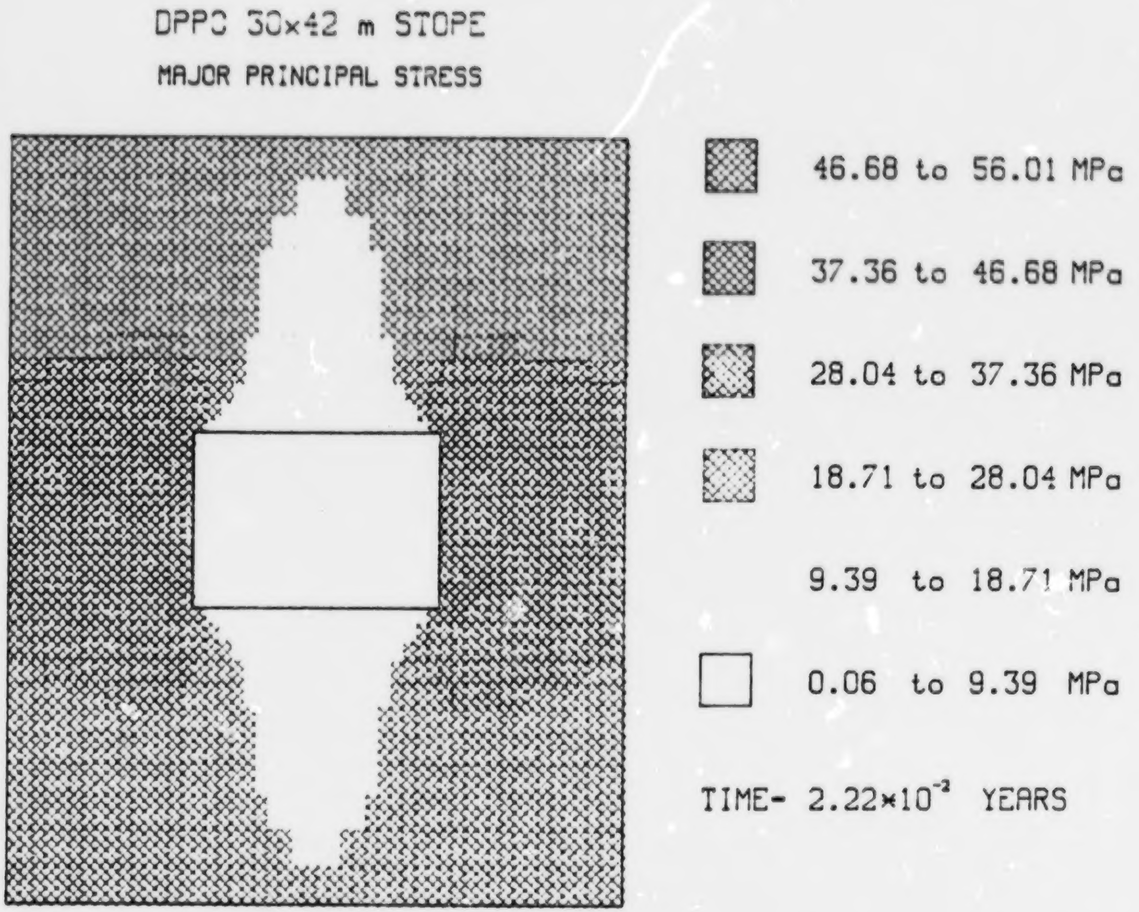
DPPC 30×42 m STOPE
MAJOR PRINCIPAL STRESS
▨ 46.68 to 56.01 MPa
▨ 37.36 to 46.68 MPa
▨ 28.04 to 37.36 MPa
▨ 18.71 to 28.04 MPa
9.39 to 18.71 MPa
☐ 0.06 to 9.39 MPa
TIME- 2.22×10^{-2} YEARS

FIGURE 10.15

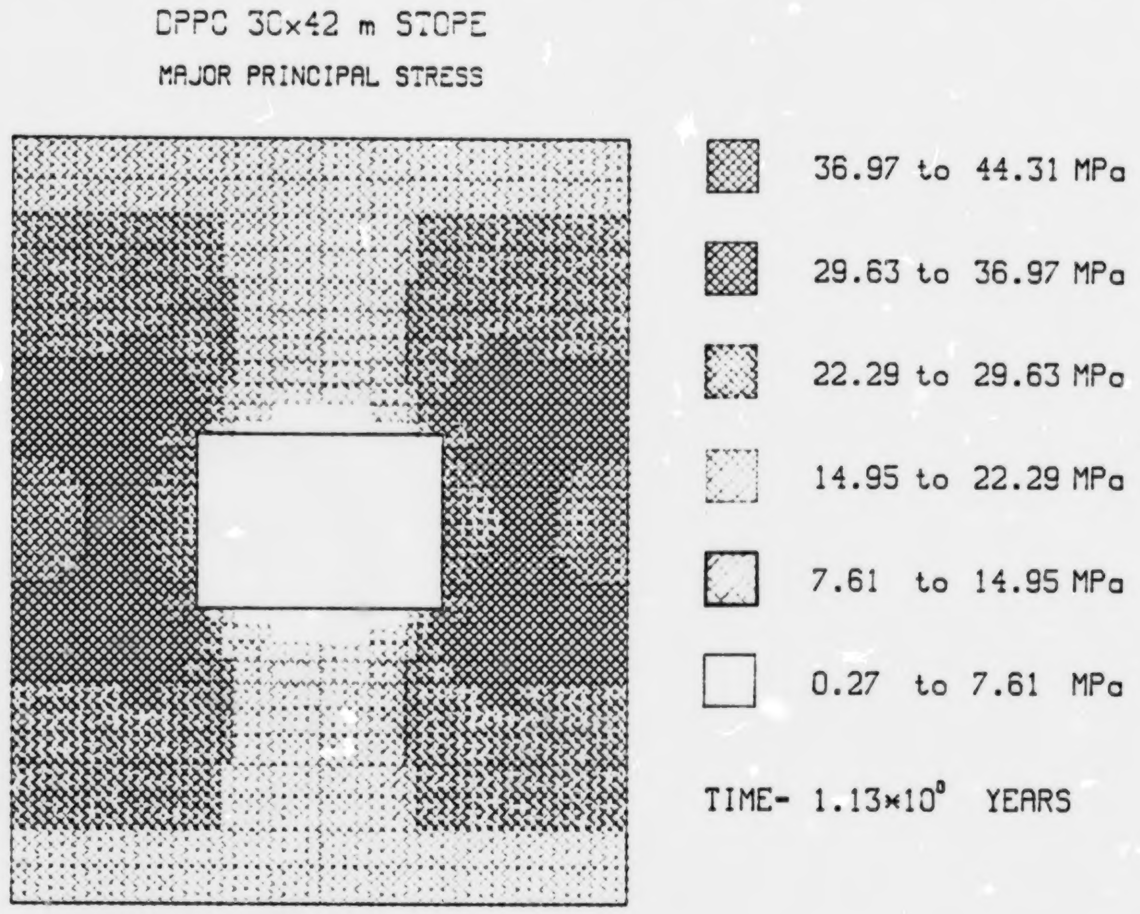
DPPC 30×42 m STOPE
MAJOR PRINCIPAL STRESS
36.97 to 44.31 MPa
29.63 to 36.97 MPa
22.29 to 29.63 MPa
14.95 to 22.29 MPa
7.61 to 14.95 MPa
0.27 to 7.61 MPa
TIME- 1.13×10⁰ YEARS

FIGURE 10.16

DPPC 30×42 m STOPE

MAJOR PRINCIPAL STRESS

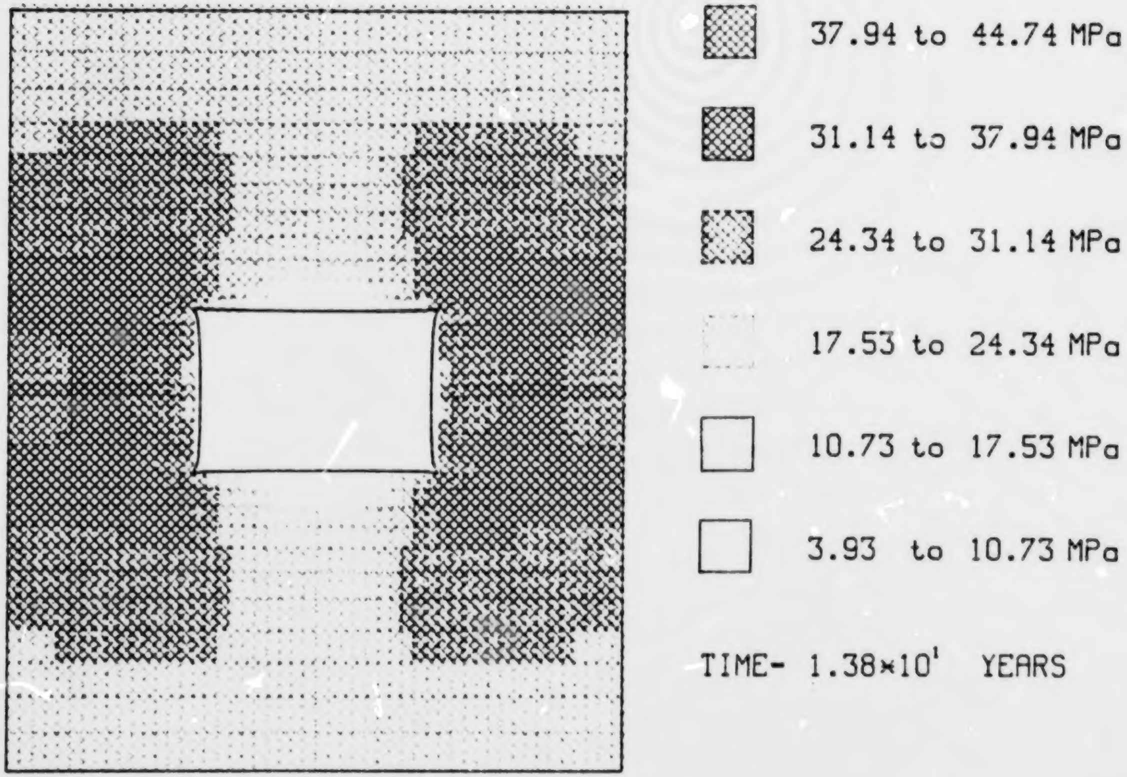

FIGURE 10.17

10.7 MINOR PRINCIPAL STRESS DISTRIBUTION

Following are the numerical modelling results for the minor principal stresses for the 30 m x 42 m Stope without backfill.

DPPC 30x42 m STOPE

MINOR PRINCIPAL STRESS

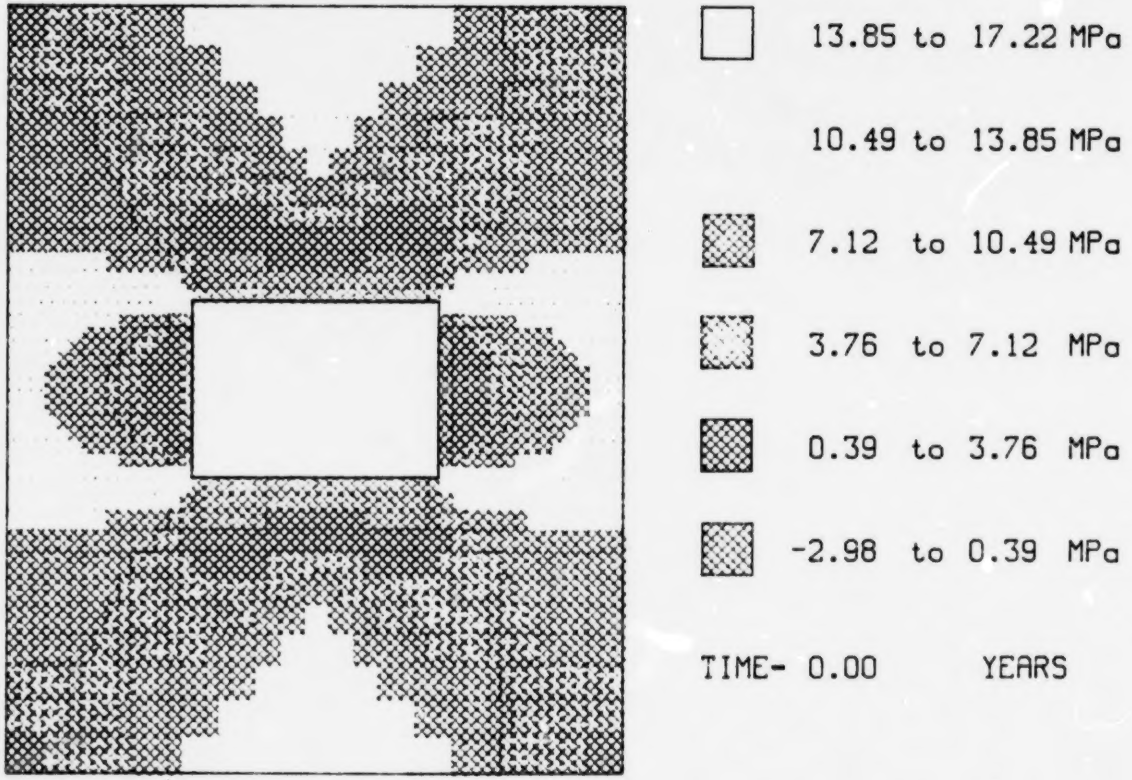

FIGURE 10.18

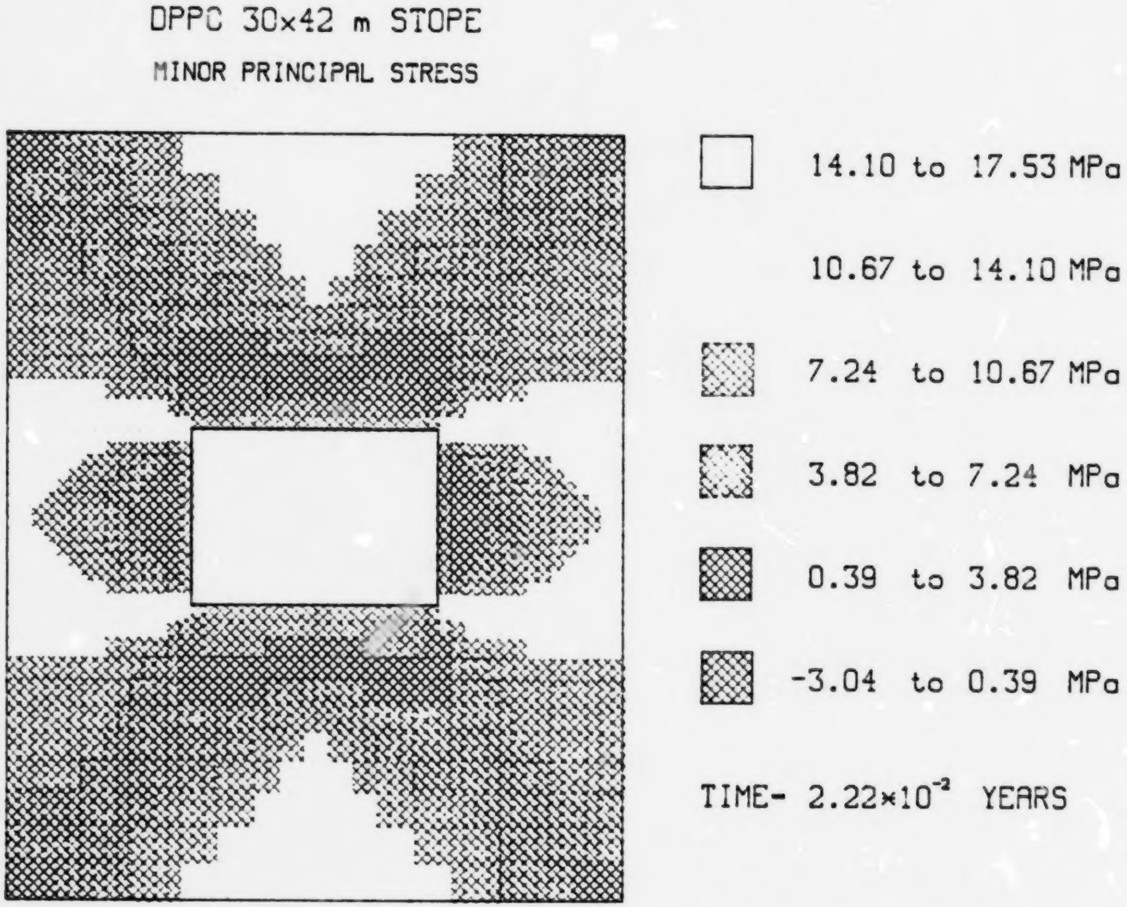
DPPC 30×42 m STOPE
MINOR PRINCIPAL STRESS
14.10 to 17.53 MPa
10.67 to 14.10 MPa
7.24 to 10.67 MPa
3.82 to 7.24 MPa
0.39 to 3.82 MPa
-3.04 to 0.39 MPa
TIME- 2.22×10⁻² YEARS

FIGURE 10.19

DPPC 30x42 m STOPE

MINOR PRINCIPAL STRESS

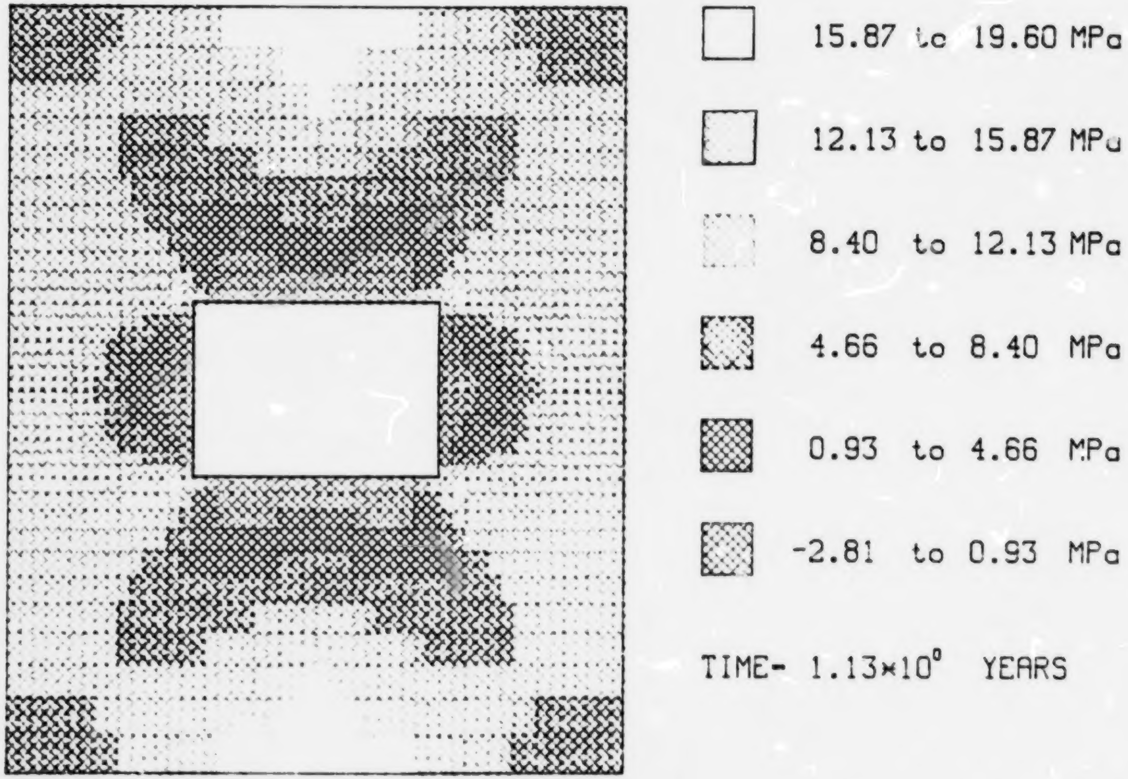

FIGURE 10.20

DPPC 30×42 m STOPE

MINOR PRINCIPAL STRESS

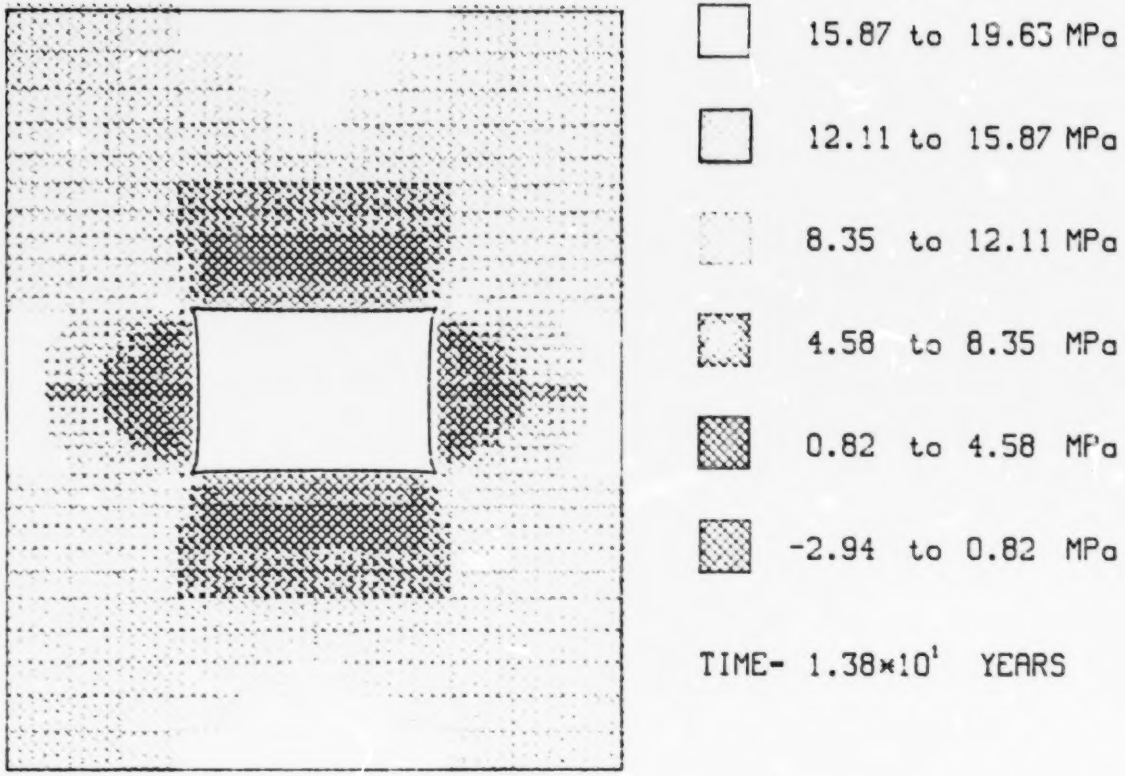

FIGURE 10.21

SECTION 11.0

11.0 APPROXIMATE CLOSED FORM SOLUTION ANALYSIS

11.1 ANALYTICAL MODEL

Prior to completion of numerical analysis, an approximate closed form solution analysis was used to estimate the behaviour of a typical mining layout. Two alternative stress distribution models were considered (Figure 11.1):

For Generally Plastic Substance:

$$\sigma_1 = \sigma_t = \frac{K}{\tan\rho}\left[\left(\frac{r}{a}\right)^n \frac{1+\sin\rho}{1-\sin\rho} - 1\right] \tag{1}$$

$$\sigma_3 = \sigma_r = \frac{K}{\tan\rho}\left[\left(\frac{r}{a}\right)^n - 1\right] \tag{2}$$

$$\tau = \frac{\sigma_1 - \sigma_3}{2} = \frac{Kn}{2\tan\rho}\left(\frac{r}{a}\right)^n \tag{3}$$

$$n = \frac{2\sin\rho}{1-\sin\rho} \qquad \rho \geqq 0 \tag{4}$$

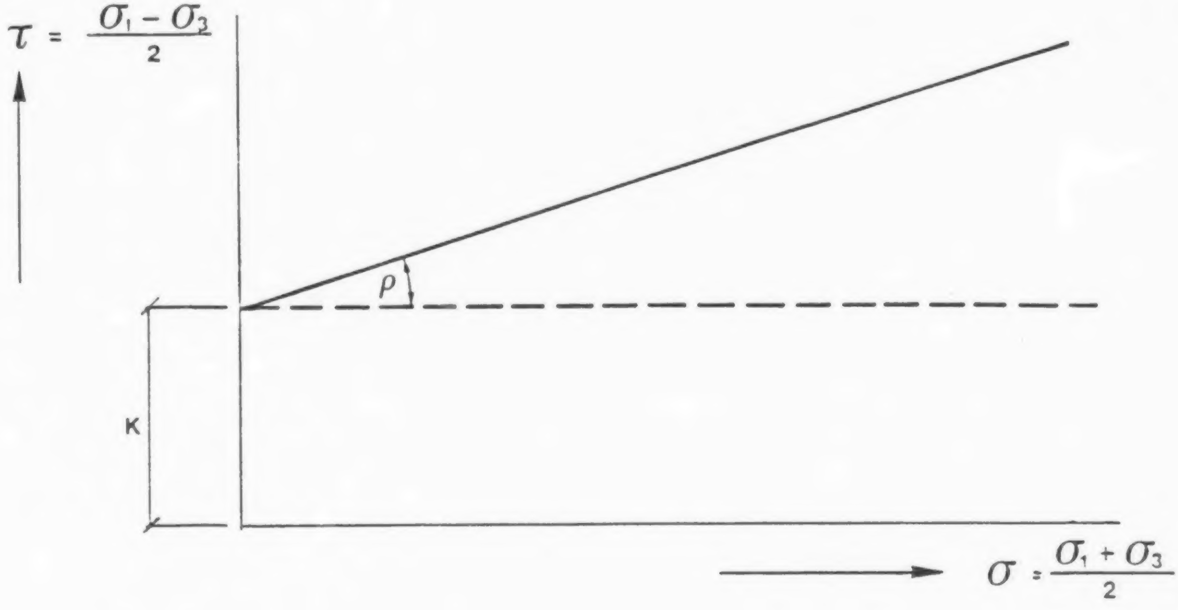

$\tau = \frac{\sigma_1 - \sigma_3}{2}$
ρ
K
$\sigma = \frac{\sigma_1 + \sigma_3}{2}$

GENERALLY PLASTIC SUBSTANCE

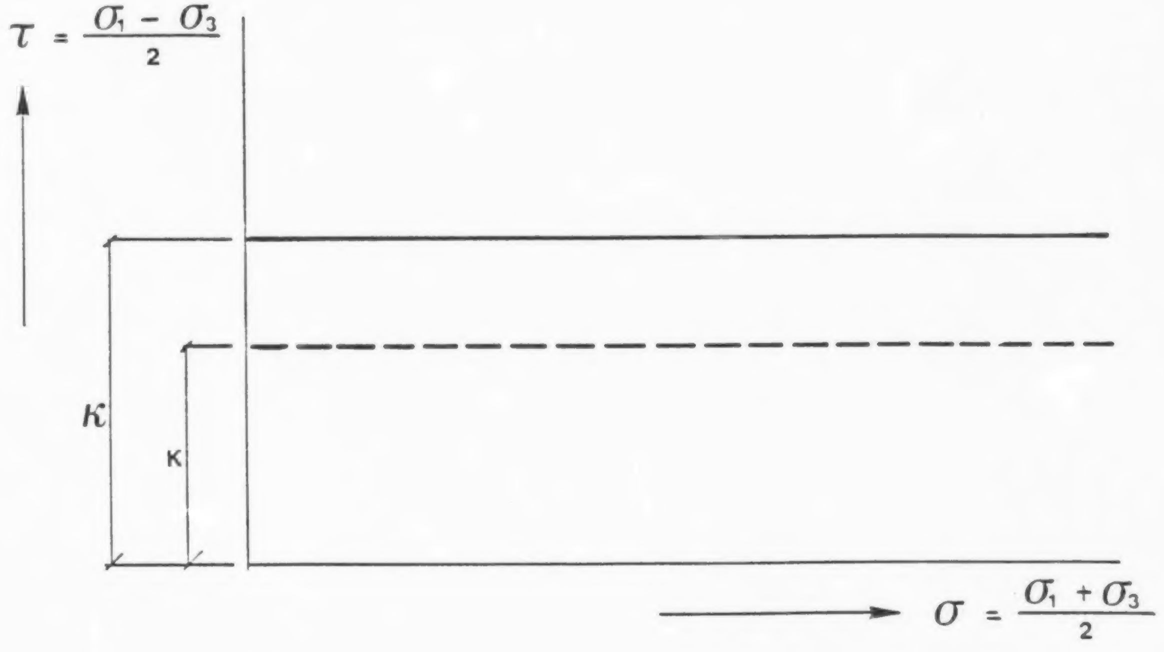

$\tau = \frac{\sigma_1 - \sigma_3}{2}$
K
K
$\sigma = \frac{\sigma_1 + \sigma_3}{2}$

IDEALLY PLASTIC SUBSTANCE

FIGURE 11.1

For Ideally Plastic Substance:

$$\sigma_1 = \sigma_t = 2\kappa \left(1 + \ln \frac{r}{a}\right) \qquad (5)$$

$$\sigma_3 = \sigma_r = 2\kappa \ \ln \frac{r}{a} \qquad (6)$$

$$\tau = \frac{\sigma_1 - \sigma_3}{2} = \kappa \qquad \kappa \geqq K \qquad (7)$$

The model of ideally plastic substance was adopted as more conservative, assuming " κ " to be an average shear stress within the viscoplastic zone.

11.2 GEOMETRY OF ACTIVE OPENING

Based on the observation of the test stope and other openings in salt rocks (Mraz and Dusseault, 1986), the following was used (Figure 11.2):

Major semiaxis $$d = \frac{1}{2}\left[\left(\sqrt{2} - 1\right) v + h\right] \qquad (8)$$

Minor semiaxis $$b = \frac{1}{2}\left[\left(\sqrt{2} - 1\right) h + v\right] \qquad (9)$$

Horizontal radius of curvature $$a = \frac{1}{\sqrt{2}} v \qquad (10)$$

Vertical radius of curvature $$a_v = \frac{1}{\sqrt{2}} h \qquad (11)$$

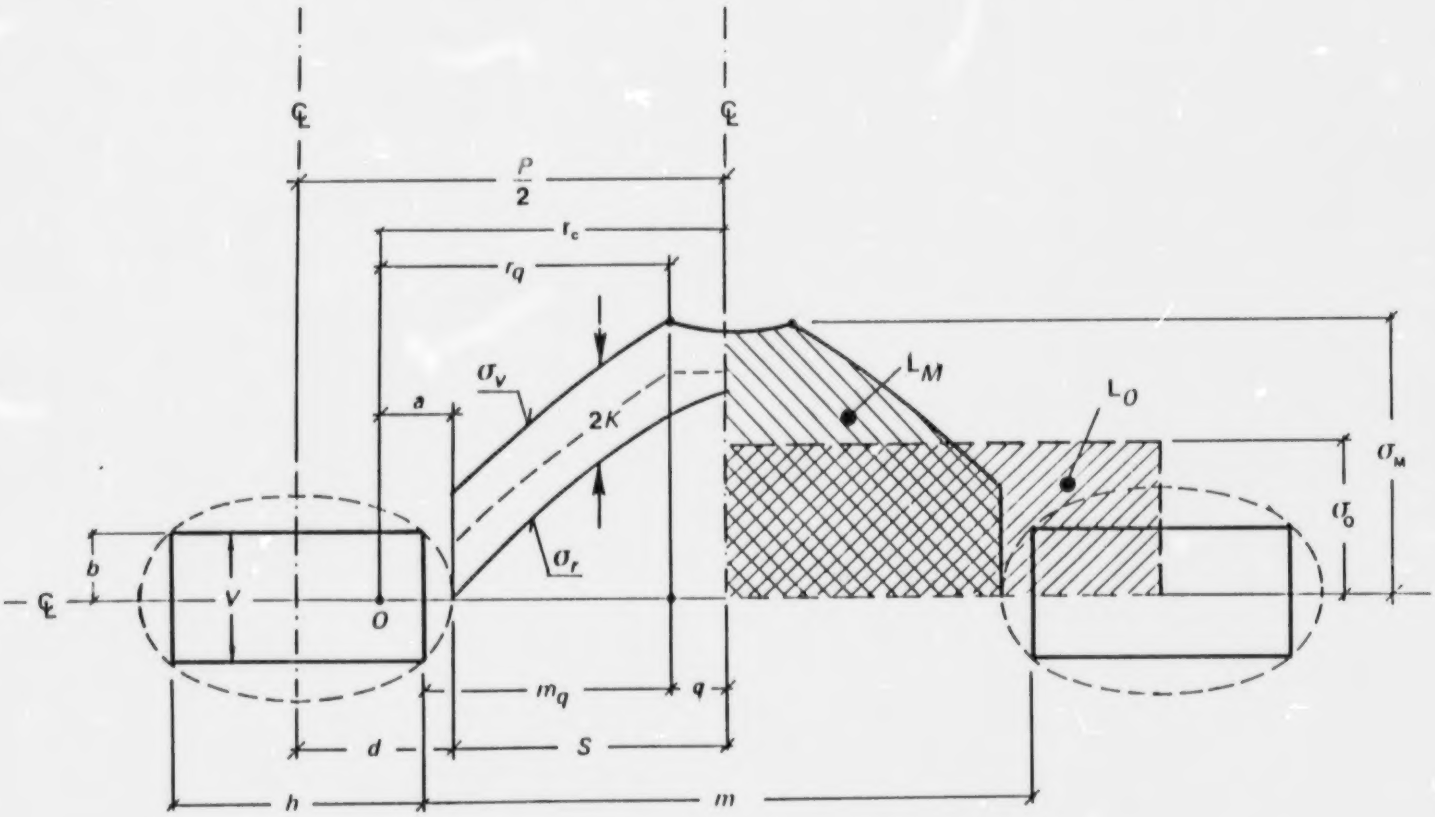

℄
℄
$\frac{P}{2}$
r_c
r_q
σ_v
2K
σ_r
L_M
L_O
σ_M
σ_o
a
b
V
O
℄
m_q
q
d
S
h
m

FIG.**11.2** LOAD EQUILIBRIUM IN PILLAR

Equilibrium Condition (Figure 11.2)

Lithostatic load $L_o = \sigma_o p$ (12)

σ = 20 MPa ..... Isotropic virgin stress as determined by 1983 overcoring tests in anhydrite

Pillar load, if $\kappa > K$, $q = o$

$$L_p = 2\int_a^{r_c} \sigma_t \, dr \qquad (13)$$

$$= 4\kappa \int_a^{r_c} \left(1 + \ln \frac{r}{a}\right) dr \qquad (14)$$

$$L_p = 4\kappa r_c \ln \frac{r_c}{a}$$

Pillar load, if $\kappa = K$, $q > o$

$$L_p = 4K r_q \ln \frac{r}{a} + 2\sigma_t q \qquad (15)$$

$$L_p = 4K \left[q + r_c \ln \frac{r_q}{a}\right]$$

Equilibrium $L_p = L_o$ (16)

Hence, if $q = o$

$$\kappa = \frac{\sigma_o P}{4 r_c \ln \frac{r_c}{a}} \qquad (17)$$

And, if $q > o$ and $\kappa = K$

$$\frac{\sigma_o}{4K} = \frac{q}{P} + \frac{r_c}{P} \ln \frac{r_c - q}{a} \qquad (18)$$

11.3 VIRGIN GROUND CLOSURE RATES

Assuming material behaviour as per equation (3) in Volume 4:

$$\frac{1}{2}(\sigma_1 - \sigma_3) = \kappa \qquad \begin{matrix} \kappa \leqq K \\ m = 1.0 \end{matrix} \qquad (19)$$

Displacement rates are

$$\dot{u} = \dot{u}_{VP} + \dot{u}_{VE} \qquad (20)$$

$$\dot{u}_{VP} = \int_{r_p}^{a} dr = -\dot{\epsilon}_K \, (r_p - a) \qquad \dot{\epsilon}_K = \text{CONSTANT} \qquad (21)$$

$$\dot{u}_{VE} = \dot{\epsilon}_K \int_{\infty}^{r_p} \left(\frac{\kappa}{K}\right)^m dr \qquad (22)$$

For viscoelastic stress distribution

$$\kappa = K \, \frac{r_p^2}{r^2} \qquad (23)$$

Hence

$$\dot{u}_{VE} = \dot{\epsilon}_K \, r_p^{2m} \int_{\infty}^{r_p} \frac{1}{r^{2m}} \, dr \qquad (24)$$

$$\dot{u}_{VE} = -\frac{1}{2m-1} \, \dot{\epsilon}_K \, r_p \qquad (25)$$

$\dot{u}_{VP}$ ... displacement rate in viscoplastic zone

$\dot{u}_{VE}$ ... displacement rate in viscoelastic zone

$\dot{\epsilon}_K$ ... Prandtl Strain Rate

K ... Prandtl Limit

m ... power law exponent for $\kappa \leqq K$

r_p ... boundary of viscoplastic zone

$\dot{u}$ ... displacement rate at boundary of active opening

Substituting into (20)

$$\dot{u} = -\dot{\epsilon}_K \left(\frac{2m}{2m-1} r_p - a \right) \tag{26}$$

Assuming the level of lateral stress

$$\sigma_2 = \frac{\sigma_1 + \sigma_3}{2} \tag{27}$$

From equations (5) and (6)

$$\sigma_2 = 2K \left(\frac{1}{2} + \ln \frac{r}{a} \right) \tag{28}$$

Hence, if $\sigma_2 = \sigma_0$ and $r = r_p$

$$r_p = a \exp \frac{1}{2} \left(\frac{\sigma_0}{K} - 1 \right) \tag{29}$$

Substituting (29) into (26)

$$\dot{u} = -\dot{\epsilon}_K \, a \left[\frac{2m}{2m-1} \exp \frac{1}{2} \left(\frac{\sigma_0}{K} - 1 \right) - 1 \right] \tag{30}$$

And taking $\sigma_0 = 20.0$ MPa

$K = 8.8$ MPa

$m = 1.0$

$$\dot{u} = -2.8 \, \dot{\epsilon}_K a \tag{31}$$

11.4 CLOSURE RATES IN MINING STOPES WITHOUT BACKFILL (FIGURE 11.2)

11.4.1 CLOSURE RATES AT AVERAGE SHEAR STRESS EQUAL TO K

As per Equation (3) in Volume 4

$$\dot{u} = \dot{u}_{VP} + \dot{u}_{VE}$$

From Equation (21), taking $r_p = r_q$

$$\dot{u}_{VP} = -\dot{\epsilon}_K (r_q - a) \qquad (32)$$

$$\dot{u}_{VE} = \dot{\epsilon}_K \, r_q^{2m} \int_{r_c}^{r_q} \frac{1}{r^{2m}} \, dr$$

$$\dot{u}_{VE} = -\frac{1}{2m-1} \, \dot{\epsilon}_K r_q \left[1 - \left(\frac{r_q}{r_c} \right)^{2m-1} \right] \qquad (33)$$

Taking $r_q = r_c - q$ and substituting into (20)

$$\dot{u} = -\dot{\epsilon}_K \left\{ r_c + \frac{r_c - q}{2m-1} \left[1 - \left(1 - \frac{q}{r_c} \right)^{2m-1} \right] - a - q \right\} \qquad (34)$$

Where q can be determined from Equation (18).

For $m = 1$, Equation (21) becomes

$$\dot{u} = -\dot{\epsilon}_K \left[r_c + (r_c - q) \frac{q}{r_c} - a - q \right] \qquad (35)$$

11.4.2 CLOSURE RATES AT AVERAGE SHEAR STRESS GREATER THAN K

Assuming power law in a normalized form to be a reasonable approximation

$$\dot{\epsilon}_{\kappa} = \dot{\epsilon}_{K}\left(\frac{\kappa}{K}\right)^{n} \qquad (36)$$

n ... power law exponent for $\kappa > K$
$\dot{\epsilon}_{\kappa}$ ... average strain rate at average stress $\kappa = K$

κ can be determined from Equation (17)

From Equation (21), taking $r_p = r_c$

$$\dot{u}_{VP} = -\dot{\epsilon}_{\kappa}(r_c - a) \qquad (37)$$

$$\dot{u}_{VE} = 0 \qquad (38)$$

$$\dot{u} = -\dot{\epsilon}_{K}(r_c - a)\left(\frac{\kappa}{K}\right)^{n}$$

11.4.3 COMPARISON WITH NUMERICAL ANALYSIS

Using equations applicable and the material properties used in numerical analysis, the results are compared in Table 11.1. Only wall closures are shown for simplicity.

Obviously, the accuracy of analytical solution decreases with increased width to height ratio. As well, the analytical prediction becomes highly conservative at increased shear stress.

TABLE 11.1

COMPARISON OF ANALYTICAL AND NUMERICAL PREDICTIONS OF STEADY STATE DISPLACEMENT RATES AT WALL

				STEADY STATE DISPLACEMENT RATES	
CASE	SITE	STRESS κ(Eq. 17) (MPa)	PILLAR CORE q(Eq. 18) (m)	ANALYTICAL PREDICTION $\dot{u}$(Eq.30 or 34) (μm/day)	NUMERICAL PREDICTION $\dot{u}$ (μm/day)
I	Test Room (4.8 m x 4.8 m virgin ground)	K	-	24.6	17.8
II	Test Stope (4 m x 42 m virgin ground)	K	–	20.5	52.1
III	4 m x 42 m Stope (40% extraction)	K	24.4	33.5	60.3
IV	12.5 m x 42 m Stope (40% extraction)	10.8	0	256.1	84.9

$K = 8.8$ MPa

$\dot{\epsilon}_K = 3 \times 10^{-11}\ s^{-1}$

$n = 1$, For $\kappa = K$

$n = 6$, For $\kappa > K$